THE UNIVERSITY OF CHICAGO

SYNTHESIS OF DOUBLY THREADED [3]ROTAXANES AND POLY[3]ROTAXANES THROUGH COMPONENT DESIGN

A DISSERTATION SUBMITTED TO

THE FACULTY OF THE DIVISION OF THE PHYSICAL SCIENCES

IN CANDIDACY FOR THE DEGREE OF

DOCTOR OF PHILOSOPHY

DEPARTMENT OF CHEMISTRY

BY

JERALD HERTZOG

CHICAGO, ILLINOIS

DECEMBER 2022

To my family.

TABLE OF CONTENTS

LISTS OF FIGURES

LIST OF SYMBOLS AND ABBREVIATIONS

° C	Degrees Celsius
δ (NMR)	NMR Chemical Shift
Å	Angstrom
Ar	Argon
Bip	2,6-bisbenzimidazolylpyridine
ca.	Circa
$CHCl_3$	Chloroform
COSY	Correlated Spectroscopy
d	Doublet
DB	Dumbbell
DCM	Dichloromethane
DMF	Dimethylformamide
DOSY	Diffusion Ordered Spectroscopy
HPLC	High Performance Liquid Chromotography
GPC	Gas Permeation Chromatography
K	Kelvin
kg/ mol	Kilograms Per Mole
LED	Light Emitting Diode
m	Multiplet
M–M	Metal–Metal (distance)
MALDI	Matrix-Assisted Laser Desorption/Ionization
MALS	Multi-Angle Light Scattering
MC	Macrocycle
MeOH	Methanol
mg	Milligram
MHz	Mega Hertz

M_n	Number Average Molar Mass
mM	Millimolar (molar^{-3})
mmol	Millimoles
mL	Milliliter
MSP	Metallosupramolecular Polymer
MW	Molecular Weight
NIR	Near Infrared Radiation
NOESY	Nuclear Overhauser Effect Spectroscopy
NMR	Nuclear Magnetic Resonance
oligo	Oligomer
PMT	Photomultiplier Tube
ppm	Parts Per Million
q	Quartet
RBF	Round-Bottom Flask
R_f	Retention Factor
RI	Refractive Index
rt	Room Temperature
s	Singlet
SEC	Size Exclusion Chromatography
TBAOH	Tetrabutylammonium Hydroxide
TEA	Triethylamine
TCPSC	Time-Correlated Single Photon Counting
t	Triplet
THF	Tetrahydrofuran
TMS	Tetramethylsilane
UV	Ultraviolet
VIS	Visible
wrt	With Respect To

ACKNOWLEDGEMENTS

First and foremost, I would like to thank my advisor Prof. Stuart Rowan for his unwavering support of me these past 6 years. This project was particularly difficult to get started, and we had multiple discussions about scrapping it all together. I am now so delighted to see where we have taken it and where this is all headed in terms of new interlocked polymers. Furthermore, I am grateful to everyone that troubleshooted with me for years on this project: Dr. Katie Herbert, Dr. Benjamin Rawe, Dr. Phillip Rauscher, Dr. Marissa Tranquilli, Laura Hart, Guancen Liu, Vincent Maddi, and Derek de Jong. I must give an extra nod to Vincent who I had the pleasure of mentoring as my undergraduate student for 3.5 years. He is a terrific scientist that I know is destined for great things. Beyond that I would like to thank every member of the Rowan Group for helping me move this study along. Stuart truly has assembled a fantastic group of chemists and engineers. This dissertation was also heavily aided by advice from facilities managers Dr. Philip Griffin, Dr. Justin Jureller, and Dr. Josh Kurutz, whose guidance made this work possible. Lastly, I must thank the members of my committee Prof. John Anderson and Prof. Dmitri Talapin for their advice and taking the time to learn about this project.

Outside of my academic acknowledgements I must thank my family. My parents John and Leigh Ann and brother Joey who have supported me since the beginning. In addition, I must thank my best friend and partner in everything Alyssa. She has shown me unconditional love and support during this PhD; without which it would not have been possible.

ABSTRACT

Mechanically interlocked polymers (MIPs) are polymeric materials that are made of individual monomeric components that are constrained in space using a mechanical bond as opposed to standard covalent methods. These materials have received increasing attention due to their wide range of applications and increased synthetic accessibility. Despite this, doubly threaded polyrotaxane materials, which are comprised of doubly threaded ring components connected by dumbbell components, have seen minimal synthetic success. These materials offer potential tunability parameters, synthetic control, and component interactions that are not possible with conventional singly threaded materials.

Recently in 2017, a poly(n)catenane derived entirely of interlocking rings was reported for the first time based on a doubly threaded metallosupramolecular polymer (MSP) template. It was then hypothesized that this MSP template could be used to access other classes of mechanically interlocking polymers besides the poly(n)catenane such as the doubly threaded poly[3]rotaxane. This dissertation is the initial synthetic work towards achieving this goal.

To do this, the representative monomeric interlocked component, a doubly threaded [3]rotaxane, had to first be well understood. Due to the doubly threaded nature, this study required larger rings than had been traditionally used in a rotaxane structure, and as such the stability of the complex became paramount. Three different sets of [3]rotaxanes that varied in stopper size, stopper arm length, and ring size were synthesized, characterized, and analyzed for their kinetic stability to dethreading. Of the parameters tested, ring size was the most influential on stability, and a fully stable [3]rotaxane could be realized with a 42-atom ring or smaller. The corresponding poly[3]rotaxanes were then synthesized and confirmed to have similar stability behavior. Based on this work, an entire range of doubly threaded interlocked polymers are now possible.

Chapter 1: The Synthesis of Rotaxane and Polyrotaxane Materials

-Chapter adapted from: Hart, L. F.*, Hertzog, J. E.*, Rauscher, P. M.*, Rawe, B. W.*, Tranquilli, M. M.*, and Rowan, S. J. *Nature Reviews Materials.* **2021**. *6*, 508-530.

1.1 Introduction to Rotaxanes

1.1.1 The Mechanical Bond

The mechanical bond is a unique bonding motif defined as an entanglement in space between multiple component parts such that they cannot be separated without breaking or distorting chemical bonds between atoms.[1] This gives the components the strength of a covalent bond without the added structural rigidity typically associated with it. Molecules containing these bonds are broadly referred to as mechanically interlocked molecules (MIMs), and the two most common classes are catenanes and rotaxanes (Fig 1.1).

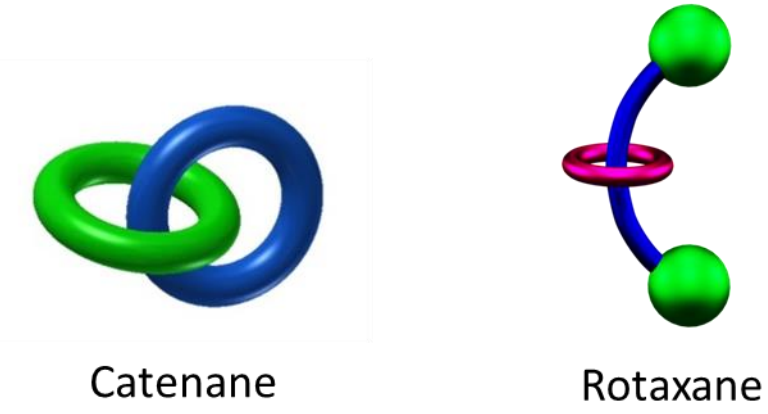

Fig 1.1 Cartoon representation of a catenane and a rotaxane.

Catenanes[2] are comprised of multiple interlocking ring components while rotaxanes[3] contain a ring component trapped between stopper groups on a dumbbell component. Rotaxanes specifically

have attracted significant attention and account for over 2/3 of all publications involving MIMs.[4] This popularity has resulted in their use in a wide range of applications including molecular machines, catalysis, molecular computing, and drug delivery, to name a few.[5–12] Specifically, their use as molecular machines and switches received international acclaim as a part of the 2016 Nobel Prize in chemistry awarded to Jean-Pierre Sauvage, Sir J. Fraser Stoddart and Bernard L. Feringa.[13–15]

1.1.2 Rotaxane Synthetic Methods

The simplest version of a rotaxane is a singly threaded [2]rotaxane (Fig 1.1) comprised of one ring component and one dumbbell component. The ring component is kinetically trapped between the stopper groups preventing it from dethreading. Three of the main synthetic pathways to make rotaxanes include stoppering, clipping, and active templating (Fig 1.2).[16]

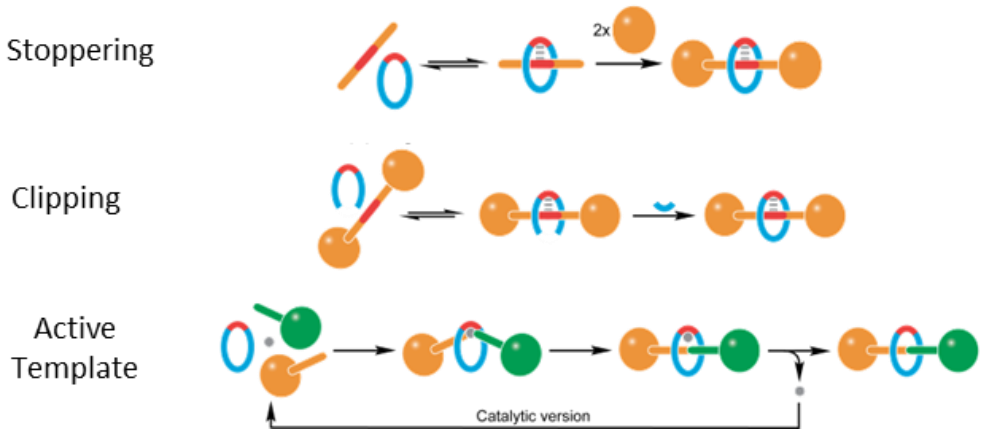

Fig 1.2 Common synthetic methods used to access rotaxanes, figure adapted from ref 16.[16]

Stoppering involves the addition of bulky stopper groups to a prethreaded supramolecular complex, clipping entails the ring closing of a single ring around another dumbbell component, and active metal templating catalyzes the addition of two half dumbbells inside the cavity of a macrocycle. Critical to the success of any of these synthetic methods is effective molecular

recognition between the components to ensure their proper orientation to form a rotaxane. Templating methods such as such as π-π stacking,[17] hydrogen bonding,[18] hydrophobic interactions,[19] anion recognition[20], and metal ion templating[21–23] have been used for such a purpose.

1.2 Polyrotaxane Materials

1.2.1 Polyrotaxane Architectures

With the advancement and development of polymer chemistry,[24] naturally chemists and engineers began to look to ways to incorporate the rotaxane motif into a polymeric backbone. A variety of ways have emerged to do this, and the main architectures that have been developed are shown in Figure 1.3.[25]

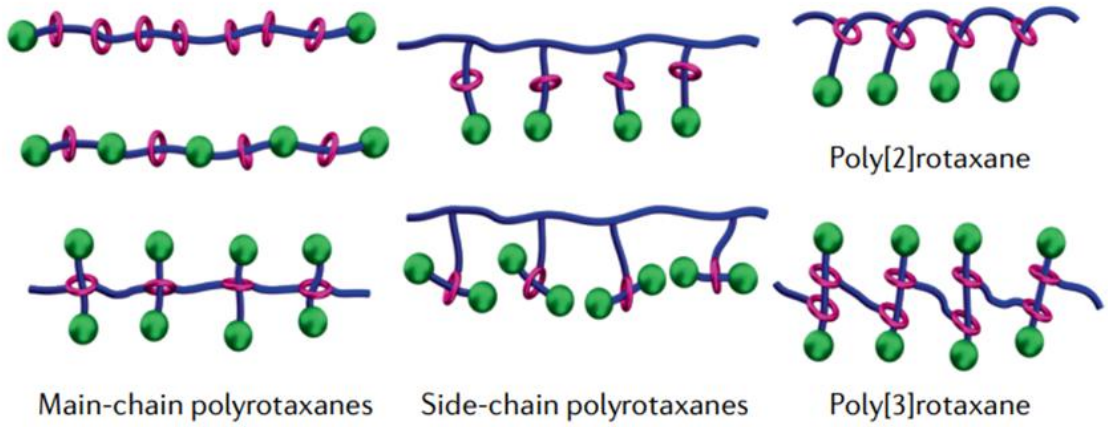

Fig 1.3 Selection of polyrotaxane architectures, figure adapted from ref 25.[25]

From this figure, three main types of architectures are seen that include non-topological main-chain, side-chain, and topological main-chain type polyrotaxanes.[26,27] Non-topological main-chain polyrotaxanes contain mechanical bonds in the main-chain of the polymer but these mechanical bonds are not an intrinsic part of the backbone (Fig 1.3 left), namely the polymer chain is threaded through one or more macrocycles. Side-chain polyrotaxanes have the rotaxane component attached

as a side chain to the polymer backbone (Fig 1.3 center) making these architectures most like conventional polymers. Topological main-chain polyrotaxanes contain mechanical bonds as an intrinsic part of the main-chain of the polymer (Fig 1.3 right, poly[2]rotaxanes and poly[3]rotaxanes) giving them unusually high levels of mobility and freedom relative to standard covalently bonded polymers. Although all of these architectures have been synthesized in some capacity,[26,28] it is perhaps the non-topological main-chain polyrotaxanes that have produced the most valuable insights into how such an interlocked architecture impacts material properties.

1.2.2 "Non-topological" Main-Chain Polyrotaxanes

As in traditional polymers, the chemistry and structure of the backbone plays a role in the behavior of polyrotaxanes. However, their properties are also impacted by the ring(s) and stopper(s) as well as the interactions between these interlocked components. These relationships have been most extensively characterized in non-topological main-chain polyrotaxanes (Fig 1.3 left), which were the first synthesized polyrotaxane architecture to be studied in detail. While the first report of a main-chain polyrotaxane was by Harrison and Harrison in 1967,[29] the field did not truly gain traction until 1992, when Wenz reported the threading of poly(iminooligomethylene)s through α-cyclodextrin (α-CD) rings[30] and Harada reported the simple and efficient threading of poly(ethylene glycol) (PEG) through α-CDs.[31] The PEG and α-CD pseudopolyrotaxane assembly is highly efficient and driven by a combination of hydrophobic interactions (between the polymer chain and the hydrophobic pocket of the CD) and hydrogen-bonding between adjacent CDs.[32] The polyrotaxane is formed when a stoppering reaction is used to "trap" the α-CD rings on the polymer backbone (Fig 1.4a).[33]

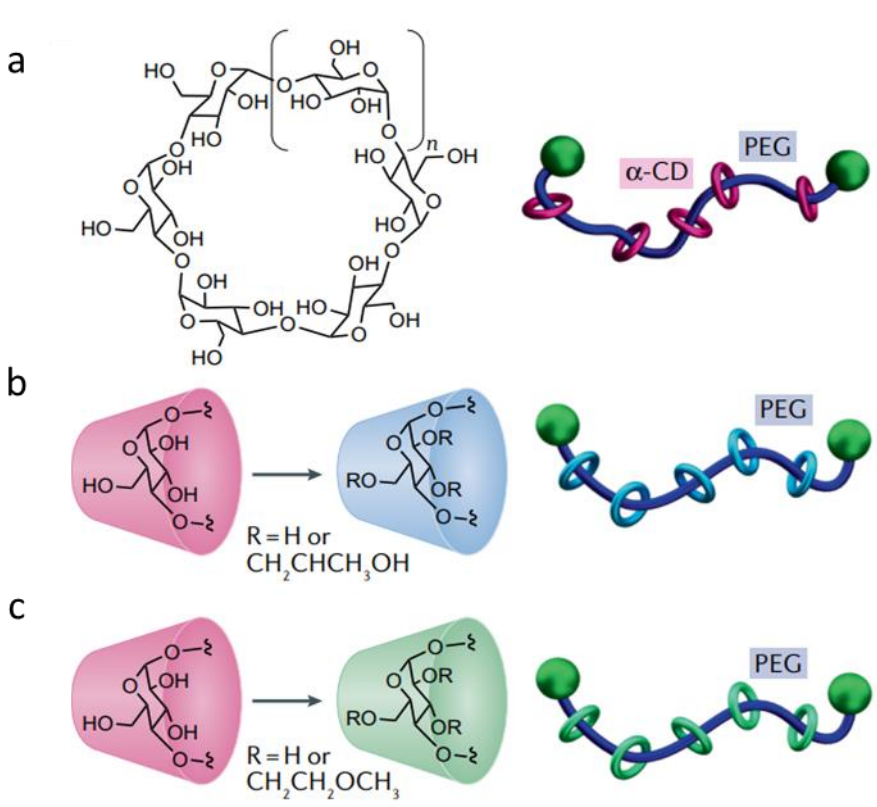

Fig 1.4 . a) Polyrotaxanes are often synthesized using cyclodextrin (top left), which is commercially available in three ring sizes, α, β and γ, where n=1, 2 or 3 anhydroglucopyranoside units. Main-chain polyrotaxane composed of poly(ethylene glycol) (PEG) threaded through α-CD (top right). b) Partial hydroxypropylation of α-CD is used to access a PEG-based polyrotaxane (middle). Partial methoxyethylation of α-CD is used to access a PEG-based polyrotaxane (bottom), figure adapted from ref 25.[25]

In addition to ease of synthesis, CDs are commonly used in polyrotaxanes as they are commercially available in three sizes that vary in the number of α-D-glucopyranoside units (Fig 1.4a, α-CD (n=1), β -CD (n=2), and γ -CD (n=3)). As such, CD-based polyrotaxanes are the most studied, producing valuable insights into polyrotaxane structure-property relationships.

In α-CD/PEG-based polyrotaxanes the CD rings play a significant role in the properties of the material. Hydrogen-bonding between the rings favors their aggregation on the polymer backbone resulting in semi-crystalline materials, limiting ring mobility along the polymer backbone.[34] However, these hydrogen bonds can be disrupted, either by introducing a hydrogen-

bond competing solvent or though partial hydroxypropylation or methoxyethylation of the CD rings, resulting in more soluble amorphous polyrotaxanes (Fig 1.4b,c) with enhanced ring mobility.[34,35] This translational mobility of the ring along the polymer chain is the most unique feature of polyrotaxanes. Numerous studies have focused on how this mobility and the resulting material properties are affected by parameters such as ring-backbone interactions, ring-ring interactions, polymer concentration, and ring coverage (calculated either as the number of rings per repeat unit or the percent coverage of the backbone by the rings).[36–40]

The mobility and placement of the rings are controlled, in part, by the inherent interactions between the ring and polymer backbone. For instance, the energy barrier resulting from attractive interactions between the CD and PEG backbone in α-CD/PEG-based polyrotaxanes leads to slower diffusion of the ring along the PEG backbone compared to un-threaded (free) CD.[38] Furthermore, the presence of the rings decreases the flexibility of the polymer with increasing ring coverage leading to stiffer polyrotaxanes.[32,41] The effect of ring-backbone interactions has also been studied in polyrotaxanes with rings other than CD, for instance, crown ethers. Early examples of polyrotaxanes based on crown ethers include those reported by Gibson in which the stopper groups are incorporated into the polymer backbone.[42–49] These polyrotaxanes were synthesized by copolymerizing an alkyl diol monomer and a bulky diol monomer with either diacid chloride monomers (to form polyesters) or diisocyanate monomers (forming polyurethanes) in the presence of a high concentration of [30]crown-10 rings. The sliding mobility of the crown ethers in the resulting polyrotaxanes are very different on account of their differing backbone chemistries. For the polyester based polyrotaxane, the crown ether rings can move freely between the stopper groups and so appear as broad range of peaks in the ^{1}H nuclear magnetic resonance (NMR) spectrum. In contrast, the polyurethanes based polyrotaxanes exhibit hydrogen-bonding between

the ring and the polymer backbone NH groups (in $CDCl_3$) which restricts ring mobility. In this case, the methylene groups of the crown ethers show a single sharper peak in the NMR spectrum. In a hydrogen-bond competing solvent (for example d^6-DMSO) the hydrogen bonding can be is "switched-off", increasing ring mobility and resulting in the methylenes appearing as a broad range of peaks in the ^1H NMR spectrum, similar to systems with no hydrogen bonding present.

This difference in ring mobility is also seen in the solid state properties of similar crown ether-based polyester and polyurethane polyrotaxanes.[42,46,48,49] The polyester polyrotaxanes exhibit two melting-to-crystallization transitions (as determined by differential scanning calorimetry (DSC)), suggesting that the rings are mobile enough to phase separate, allowing the rings and polymer chains to crystallize separately. In contrast, hydrogen-bonding in the polyurethanes results in a single-phase material that only exhibits one glass transition temperature (T_g).

The effect of ring mobility on a PR's solid-state properties can even been observed with just a single mobile ring present. For example, Takata and coworkers[50] synthesized macromolecular [2]rotaxanes using poly(δ-valerolactone) (PVL) with a single secondary ammonium binding site on the polymeric thread component (M_n *ca.* 2,300 $gmol^{-1}$) and [24]crown-8 as the ring (Fig 1.5a). The secondary ammonium site interacts favorably with the crown ether ring limiting its motion and allowing crystallization of the PVL segment. However, if the secondary amine is acetylated the hydrogen-bonding between the ring and thread is "switched-off" increasing ring mobility and disrupting crystallization resulting in an amorphous material (Fig 1.5b).[50]

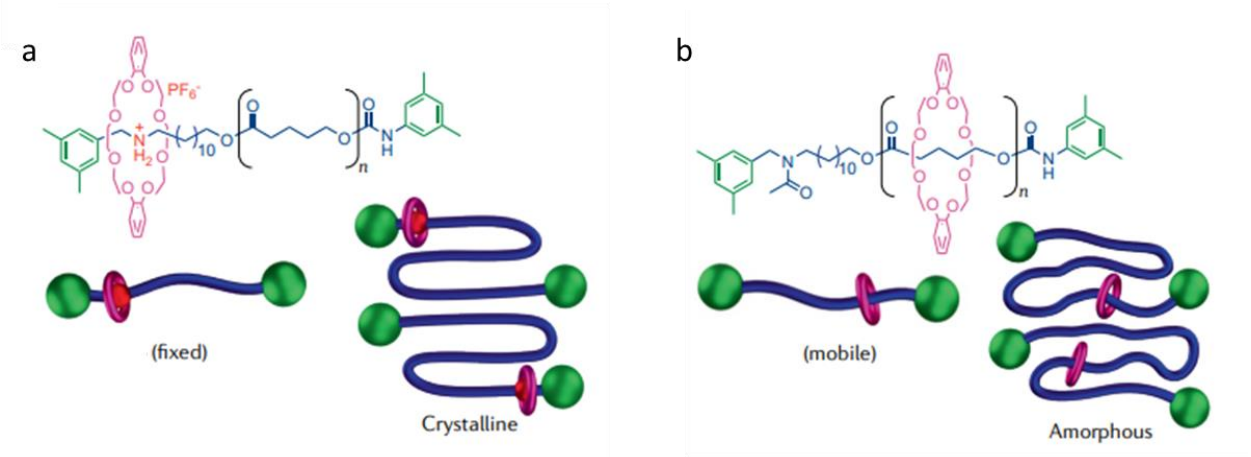

Fig 1.5 Chemical structure and crystallization behavior schematics of the a) ammonium-containing polyvalerolactone-based polyrotaxane with dibenzo[24]crown-8 and b) the related amine-protected polyrotaxane for comparison, figure adapted from ref 25.[25]

In addition to ring mobility, how the rings are distributed along the polymer backbone can also affect the solid-state properties. For example, Ito and coworkers[51] studied a poly(ethylene oxide)-*b*-poly(propylene oxide)-*b*-poly(ethylene oxide) (PEO−PPO−PEO) triblock main-chain polyrotaxane with either fully-functionalized hydroxypropyl-β-CDs (100% HP-β-CDs) or trimethylsilyl-functionalized hydroxypropyl-β-CDs (100% TMS-β-CDs) as the ring components. In the hydroxypropyl functionalized-β-CD systems, the β-CDs preferentially reside on the inner PPO block on account of more favorable hydrophobic interactions with PPO than PEO (Fig 1.6a).[52] The TMS functionalized β-CDs on the other hand, reside on the PEO end-blocks in order to shield the more polar PEO segments from the hydrophobic TMS-β-CD outer wall (Fig 1.6b).[50] In both polymers, the CDs form crystalline domains; however, the different positioning of the CDs along the polymer backbone results in drastically different mechanical properties. In the hydroxypropyl functionalized-β-CD systems, the concentration of the CDs on the central PPO block results in discrete crystalline assemblies and as a result the films exhibit fluid-like behaviour above T_g, as shown by dynamic mechanical analysis (DMA) (Fig 1.6a). Alternatively, in the TMS functionalized β-CD systems, the CDs are concentrated on the two PEO outer blocks so that the

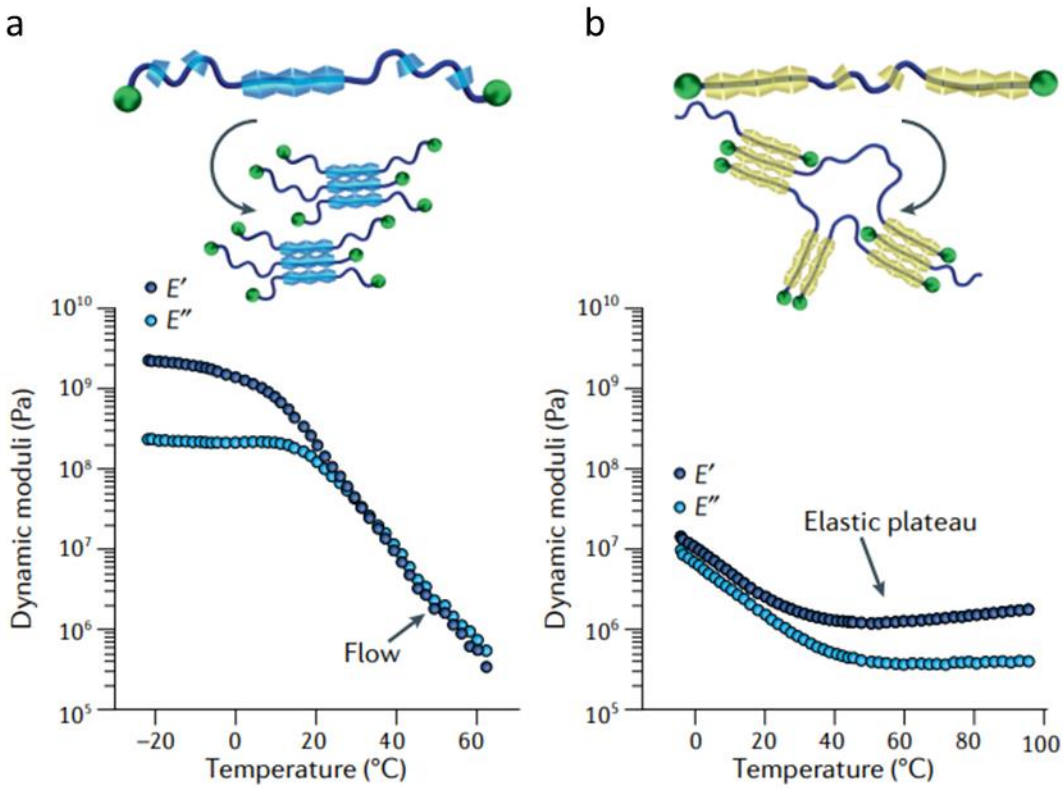

Fig 1.6 Cartoons showing the CD distribution, its proposed self-assembly and the temperature-sweep dynamic mechanical analysis data of a film of PEO−PPO−PEO triblock main-chain polyrotaxane with either a) fully-functionalized hydroxypropyl-β-CDs or b) trimethylsilyl-functionalized hydroxypropyl-β-CDs as the ring components, figure adapted from ref 25.[25]

crystalline CD domains are bridged by polymer chains, resulting in an elastic plateau even above T_g (Fig 1.6b).

CD-crystallization in polyrotaxanes has also been utilized by Ke and coworkers in 3D-printed cubic wood-pile lattices obtained from the chemical photo-crosslinking of main-chain pseudopolyrotaxanes.[53–55] In the resulting materials, the α-CDs hydrogen-bond into tubular arrays which form hexagonal crystalline domains that function as physical crosslinking sites.[53,54] The disruption and reformation of these physical crosslinks leads to a decrease and increase in moduli upon variation in pH (Fig 1.7a) or solvent (Fig 1.7b). Such shape-memory behavior combined with

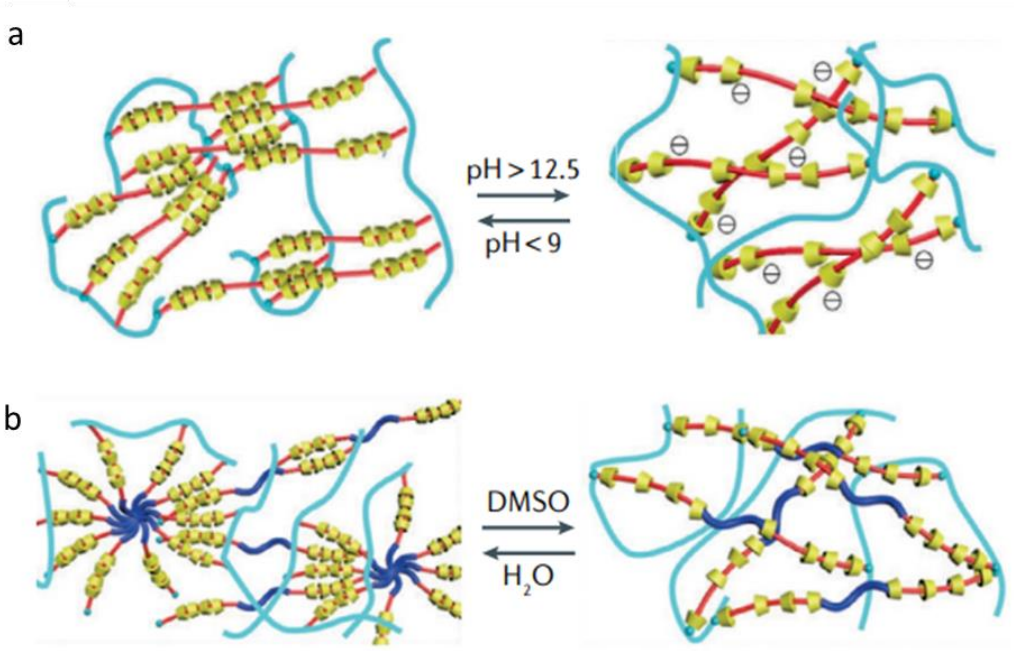

Fig 1.7 Cartoon showing the effect of a) pH or b) solvent change on the aggregation of threaded cyclodextrins (CDs) in a photocrosslinked polyrotaxane, figure adapted from ref 25.[25]

the lattice structure allows the material to actuate in a controlled manner, exemplified by the lifting of a coin upon reformation of the crystalline CD-domains.

All the films discussed so far were investigated above T_g (which allows movement of both polymer chains and rings), but polyrotaxanes may also have interesting properties in the glassy regime below T_g. However, as mentioned previously the rings in CD-based polyrotaxanes crystallize rather than vitrify. Crystallization can be inhibited by partial functionalization of the CD rings allowing access to polyrotaxane glasses. For example, consider a polyrotaxane containing a PEO backbone (M_n 20,000 gmol^{-1}) threaded through partially 2-methoxyethylated α-CD (46% hydroxy groups reacted and a CD to repeat unit ratio of 1:8 (25% coverage)). As the CDs comprise *ca.* 80 wt.% of the material there is a T_g at *ca.* 8 °C, comparable to the neat 2-methoxyethylated α-CDs (Fig 1.8a, top left). However, the polyrotaxane also exhibits a secondary relaxation (subrelaxation) at *ca.* −30 °C (Fig 1.8a, top right), close to the T_g of PEO (ca. −35 °C).

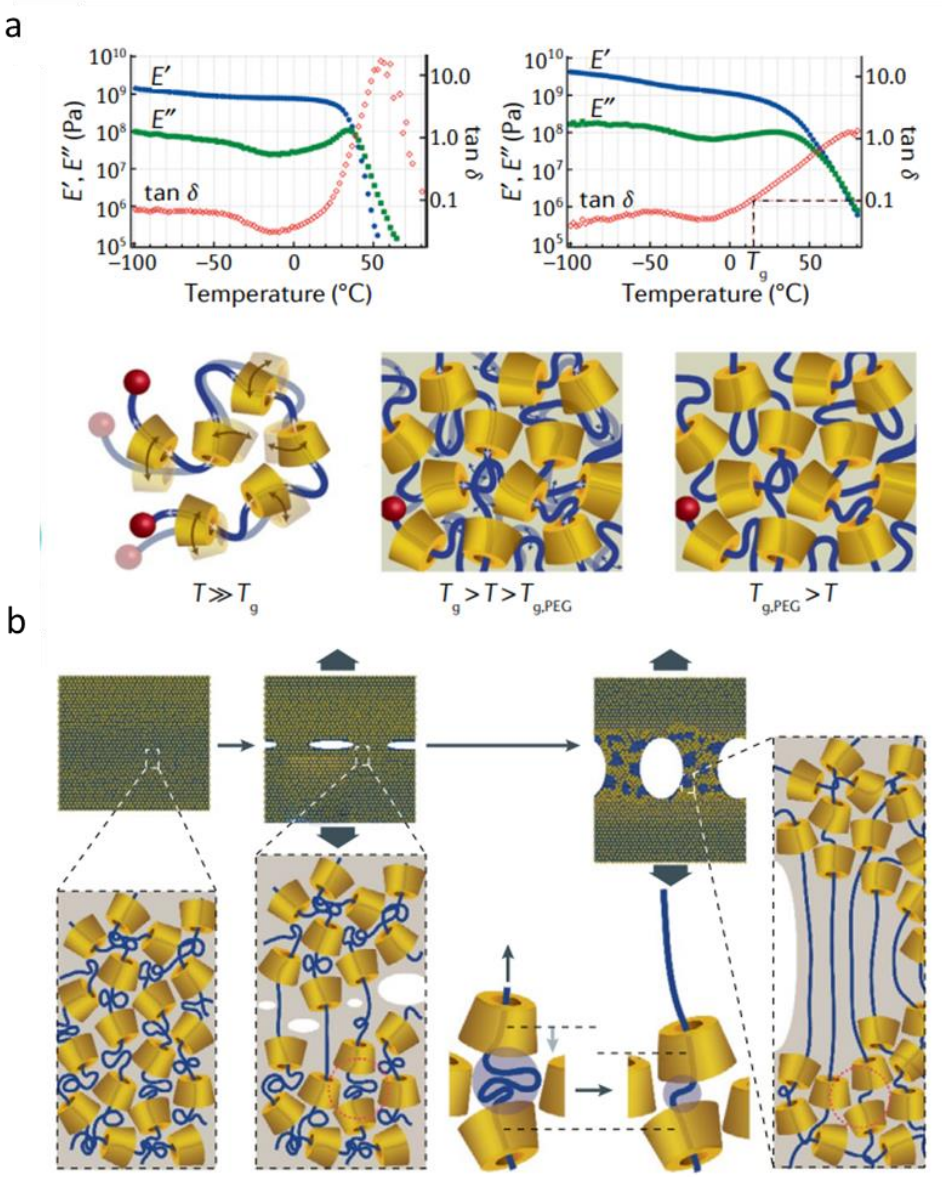

Fig 1.8 a) Temperature dependence of tensile storage modulus (E′), loss modulus (E″) and loss tangent (tan δ) of α-CD (46% methoxylated) glass (top left) and polyrotaxane glass (PEO backbone, 25% ring coverage, 46% methoxylated α-CD rings)) (top right). Cartoon showing the vitrification of CD rings highlighting the PEG chain mobility above $T_{g,PEG}$ (bottom). b) Scheme showing how the structure of a polyrotaxane glass changes during stress below the T_g: homogenous CD distribution before stress (left), fragmentation of CD framework (center), stress-induced translational motion of the threaded PEG chains (bottom right) and microscopic phase separation of PEG chains and CD framework (right), figure adapted from ref 25.[25]

Raising the temperature above this secondary relaxation reduces the modulus to about 1/3 of its value at −100 °C.[35] This subrelaxation is linked to the interlocked architecture and is consistent

with the PEG backbone sliding through the glassy CD framework (Fig 1.8a, bottom). As a result, these polyrotaxane glasses can be extremely ductile, as the polymer chains can slide through the rings at points of high stress allowing material deformation and resulting in enhanced toughness (Fig 1.8b).[56] Further research showed the polyrotaxanes could be tuned by changing either the amount of chemically-modified hydroxyl groups on the CD or the ring coverage. For instance, less "fragile" glass-formers with reduced T_g and less cooperative dynamics were obtained by increasing the chemical modification of the CDs, which mitigates ring-ring interactions,[57] while increased CD coverage results in an additional relaxation slightly above T_g, attributed to correlated motions of neighboring CDs on the polyrotaxane backbone.[58]

The encapsulation of a polymer by rings results in reduced interpolymer chain interactions and this concept has been utilized to access polyrotaxanes that can act a molecular wires.[59] Conjugated polymers have long been candidates for the development of molecular-scale wires; unfortunately, strong interchain interactions make it difficult to isolate single polymers and the conformational entropy of the polymer disfavors extended, straight chain configurations, limiting conjugation within the backbone.[60] Sheathing of a conjugated polymer with rings drastically improves its overall rigidity and "insulates" the threaded polymer chain. A number of conducting polymers have been investigated in such polyrotaxanes, including poly(phenylenevinylene),[61] polyfluorene,[62] poly(paraphenylene),[63] poly(diphenylenevinylene),[64] and, polythiophene[65] among others.[66] While the most common ring component in these polyrotaxanes is CD, other rings such as cyclophanes[67] and cucurbiturils[68] have been reported. Most studies on conjugated polyrotaxanes are focused on their optical properties. For example, CD-based conjugated polyrotaxanes exhibit sharper UV-Vis spectra, blue-shifted emission spectra, as well as higher quantum yields relative to the unthreaded conjugated polymer.[60,66] In these systems the rings separate the polymer chains

preventing aggregation (and quenching) and leading to longer life-time excited states. In addition, threaded rings cause increases in the persistence length of the backbone, stretching them out and resulting in more extended, near-planar conformations, important for enhancing the conjugation along the backbone.[60,69,70] For example, poly(4,4'-diphenylenevinylene) polyrotaxanes with varying β-CD ring coverage (between 0 and 82%) showed an increase in the electroluminescence quantum efficiency and solid-state photoluminescence with increasing coverage.[71] Ring size is also an important feature in these polyrotaxanes as systems with larger rings (for example, γ-CD vs. α-CD) exhibit greater fluorescence quenching by methylviologen in aqueous solution.[72] It was suggested that the larger rings have greater mobility along the polyrotaxane backbone allowing larger aggregate formation. Preliminary investigations into the electrical behaviour of these polyrotaxanes have shown that their conductivity can be orders of magnitude higher than the unthreaded conjugated backbone,[73] although investigations in this area are primarily focused on pseudopolyrotaxanes.[74,75] None-the-less such pseudo-polyrotaxane studies have shown that the hole mobility along a threaded poly(phenylene ethynylene) backbone can be similar to amorphous silicon, highlighting the potential of such MIPs as well-insulated organic semiconductors.[76,77]

Main-chain CD-polyrotaxanes have been investigated as functional biomaterials,[78–83] aided by the fact that α-CD and PEG are approved by the US FDA for drug use.[84] For instance, polyrotaxanes have been studied in the context of drug or gene delivery. For example, drugs can be covalently attached to the CD rings and selective removal of the stopper groups allows for controlled release.[78–81] For gene-delivery, CDs have been functionalized with cationic groups in order to form complexes with DNA or RNA. The mobility of the positively-charged CD rings on the polyrotaxanes allows them to form stronger complexes with the anionic nucleic acids than can be achieved with similarly-charged linear cationic polymers.[85,86] These complexes can enter the

cell where selective removal of the stopper groups results in decomplexation and delivery of the nucleic acid payload.[78–81]

The ring mobility in polyrotaxanes has also been used to enhance biological targeting of synthetic systems. In nature, multi-valency is commonly used to enhance the molecular recognition of weak ligand-receptor interactions,[87] however this usually requires that the individual binding sites are precisely arranged in space. When ligands are attached to the polyrotaxane rings the ring mobility (both translational and rotational) allows the ligands to arrange themselves to optimize the multivalent interactions.[82,83] Such polyrotaxane systems exhibit faster and more efficient multivalent binding to receptor proteins when compared to ligands tethered to standard covalent polymers (Fig 1.9).[88,89]

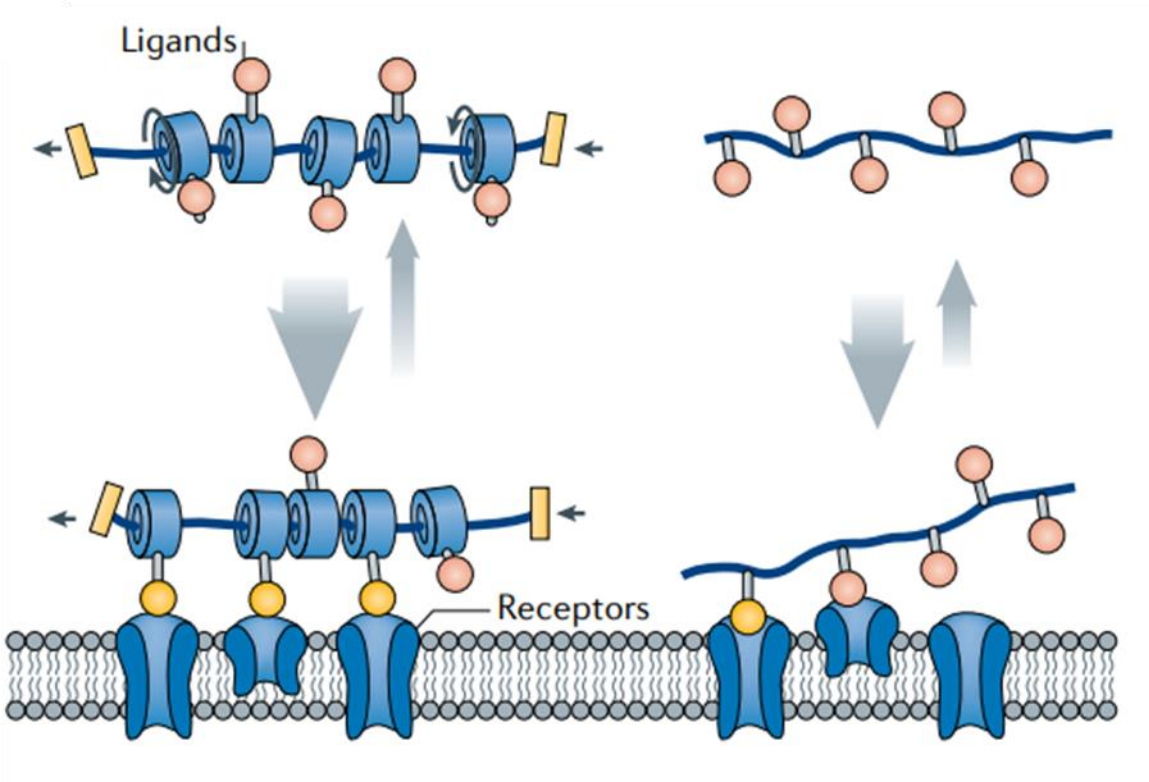

Fig 1.9 Cartoon highlighting the difference in multivalent binding of the more mobile ligands on polyrotaxane rings (left) versus them directly conjugated to a polymer backbone (right). Yellow ligands indicate successful ligand–receptor binding, figure adapted from ref 25.[25]

Building on the ability of MIMs to act as switches and machines[90,91] Polyrotaxane architectures are also garnering attention as polymer-based switches and machines.[92,93] For instance, Stoddart and coworkers developed polyrotaxane "foldamers" capable of concerted motion at the macromolecular scale.[93–96] These polyrotaxanes use π-stacking interactions between a cyclobis(paraquat-*p*-phenylene) ($CBPQT^{4+}$) rings and a 1,5-dioxynaphthalene backbone polymer (Fig 1.10a) to fold in a specific manner, which results in conformation that is ca. 15% shorter and 92% wider than the free backbone.[93] Single-molecule atomic force spectroscopy was used to observe the transition between folded and unfolded states under applied force and showed the polyrotaxanes could exert forces of up to 50 pN (under a load of 150 pN) during folding (Fig 1.10a).[97] Furthermore, π-stacking rupture events during extension can be observed with dynamic force spectroscopy confirming the folded structure.[98] These measurements also implied a rapid reformation of the folded structure as the interlocked structure prevents disassembly of the components. In addition, strides towards polyrotaxane machines have recently been made by Stoddart and coworkers through the synthesis of a high energy polyrotaxane through successive controlled pumping of $CBPQT^{4+}$ rings onto a polymeric chain (Fig 1.10b).[99–101] Each chain-end contains a viologen unit sandwiched between a pyridinium group (that acts as a Coulombic barrier) and an isopropyl group (acting as a steric speed bump).[99–101] Rings can be added to the polyrotaxane by reducing the viologen units and $CBPQT^{4+}$ ring allowing threading of the ring onto the viologen, driven by the formation of a trisradical tricationic association complex. Reoxidation then forces the ring over the isopropyl speed bump on account of Coulombic repulsions, resulting in a stable polyrotaxane. This ring-addition ratchet mechanism can be repeated to drive the controlled pumping of anywhere from 2 to 10 rings onto the polymer backbone. These polyrotaxanes are highly-charged, high-energy systems with the potential to perform work.

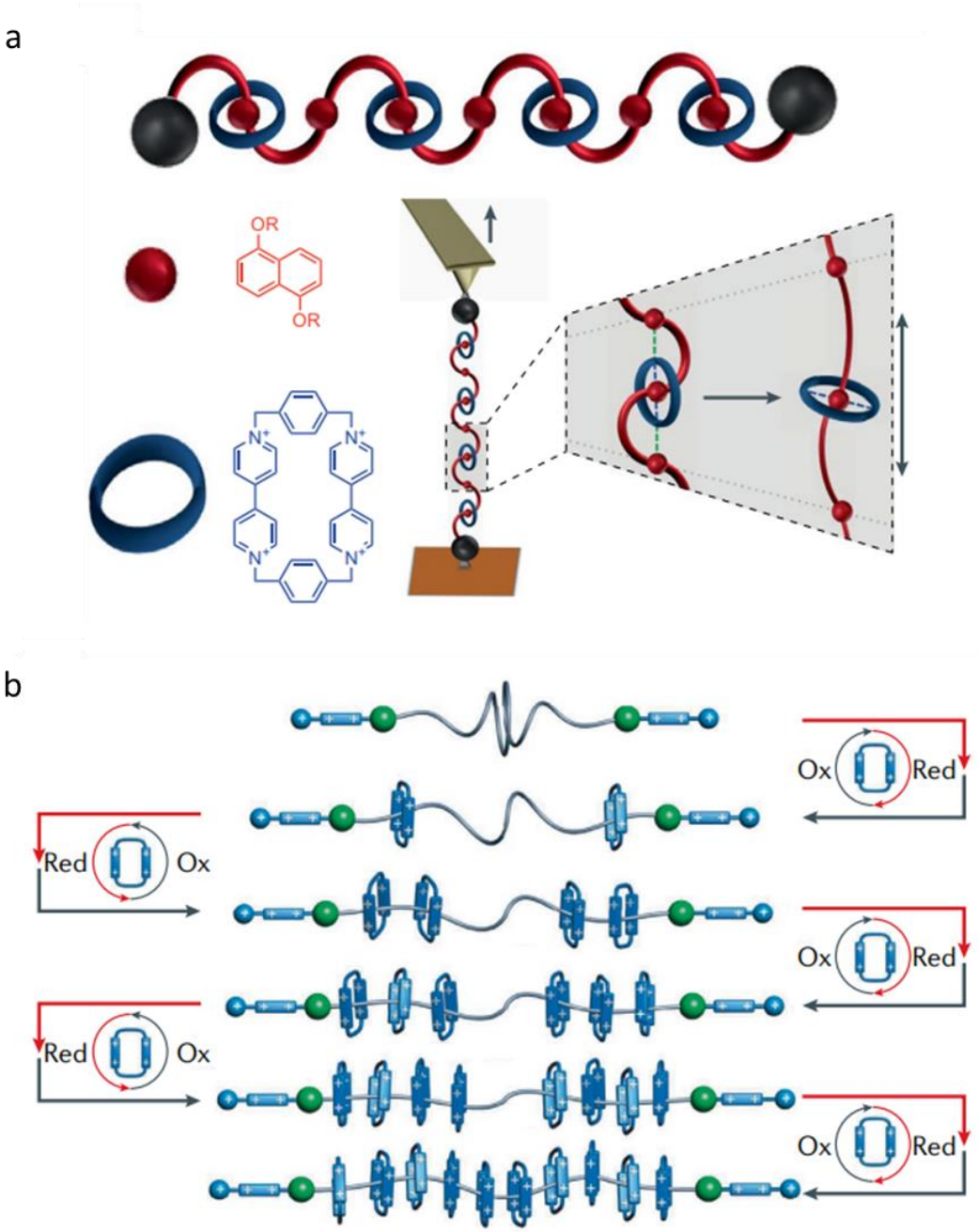

Fig 1.10 a) Cartoon image of folded structure of polyrotaxane made with blue cyclobis(paraquat-p-phenylene) (CBPQT) rings and red 1,5-dioxynaphthalene backbone polymer (top). Cartoon showing breaking of π-stacking between the CBPQT rings and naphthalene backbone in the foldamer during a single-molecule AFM experiment (bottom). b) Cartoon showing the stepwise addition of CBPQT rings (up to 10) onto a PEG backbone using chain-end redox-active molecular pumps, figure adapted from ref 25.[25]

Another application of main-chain polyrotaxanes is their use in slide-ring materials (SRMs). An alternative to covalent crosslinking is connecting the polymer chains through a

mechanical bond, for instance crosslinking main-chain polyrotaxanes by covalently linking their rings akin to a pulley (Fig 1.11a).[102]

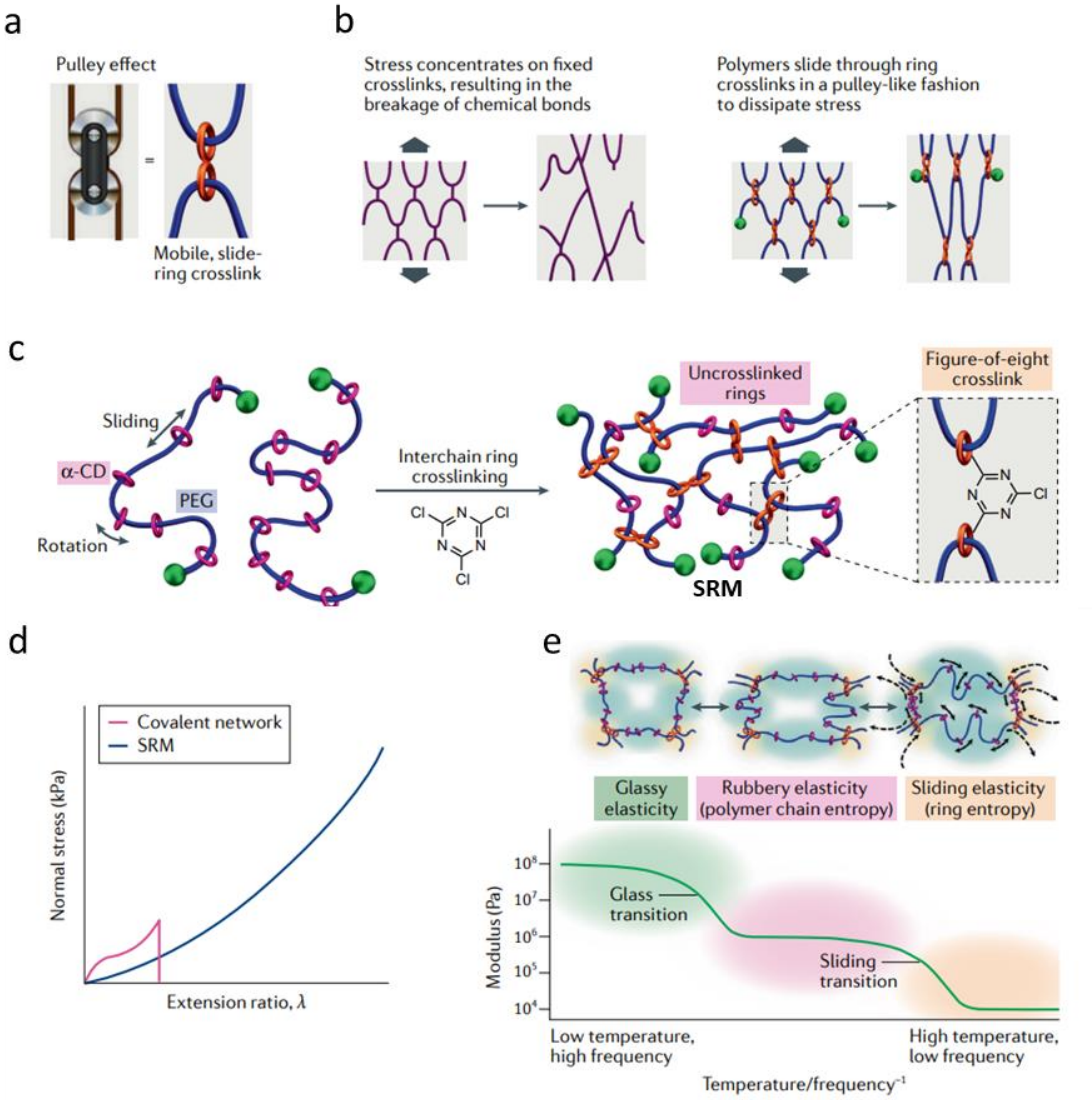

Fig 1.11 a) The pulley effect. b) The effects of strain on a FC network (left), short network strands tend to rupture under strain, and a SRM (right), where the pulley effect allows for dissipation of stress as polymer chains slide through the crosslinked rings in a cooperative manner, akin to a pulley system. c) Synthesis of a SRM via interchain ring crosslinking of hydroxy groups on the α-cyclodextrins (α-CDs). d) Schematic comparing the idealized tensile properties of figure-of-eight SRMs and conventional polymer networks with fixed crosslinks. e) Oscillatory shear rheology shows three plateaus: a glassy plateau (green), a rubber elasticity plateau (pink) and a high-temperature, low-frequency plateau (orange), referred to as sliding elasticity, wherein chain sliding and ring sliding occur simultaneously, figure adapted from ref 25.[25]

As the polymer chains are not fixed by permanent covalent bonds, the interlocked crosslinking site has the ability to slide along the polymer backbone, a process that can dramatically affect material properties. For example, in chemical gels, fixed (covalent) crosslinks (FCs) are not distributed evenly throughout the material and upon deformation, the shorter strands can rupture leading to mechanical failure (Fig 1.11b, left). On the other hand, mobile interlocked crosslinks allow polymer chains to slide through the network like a pulley system, allowing dissipation of stresses in a cooperative manner (Fig 1.11b, right). Such interlocked networks have been broadly classified as (SRMs) and the mobility of their crosslinks imbues them with new property profiles. The first and most studied class of SRMs incorporates interlocked crosslinks by covalently bonding rings from different polyrotaxanes, yielding "figure-of-eight" topological crosslinks. The quintessential example of a slide-ring material can be prepared by crosslinking the α-CD rings on standard α-CD/PEG-based polyrotaxanes (Fig 1.11c).[102] Importantly, this synthetic protocol results in both figure-of-eight crosslinks and residual uncrosslinked rings in the polymer network; the latter also plays a role in the properties of these SRMs (*vide infra*). This new class of polymer networks exhibits an impressive property profile as it can absorb 24,000 times its mass in water and extend to 24 times in length without hysteresis.[102–105] The interlocked crosslinking architecture also plays a significant role in the mechanical properties,[60] exemplified by the stress-strain behavior (Fig 1.11d). While fixed-crosslink networks exhibit the typical "S"-shaped curves, SRMs have a "J"-shaped profile with lower elastic (Young's) modulus and much greater strain-at-break. Furthermore, small-amplitude oscillatory shear rheology[106] on SRMs in DMSO revealed a time-dependent stress relaxation modulus with two distinct plateaus at low frequencies: the first was attributed to the typical rubbery modulus, while the second (lower) plateau is not observed in FC networks (Fig 1.11e). These unusual material properties have been utilized to develop scratch-

resistant coatings that have even been commercialized into cell phone cases and airplane coatings.[107]

1.2.3 Side-Chain Polyrotaxanes

Side-chain polyrotaxanes have a standard covalent polymeric backbone and consequently do not have the mechanical bond as a part of the polymer backbone (Fig 1.3 center) making these architectures most like conventional polymers. A significant amount of the work in this area is with polypseudorotaxanes in solution, but some work has extended to polyrotaxane systems with stoppers.[26,27] Most of this side-chain polyrotaxane work is synthetic in nature with cyclodextrin and crown ether being utilized as ring components.[26,27] Some notable examples with preliminary extension to materials include carbon nanotubes functionalized with *p*-phenyleneethynylene side-chain polyrotaxanes[108] and side-chain polyrotaxanes used for fluorescent[109] and photoregulated[110] switching. The fluorescent switching polyrotaxane systems are comprised of an azidohexyl methacrylate and butyl methacrylate copolymer functionalized with an alkyne-terminated bistable [2]rotaxane to form the side-chain poly[2]rotaxane.[109] Acid/base cycling using 1,8-diazabicyclo[5.4.0]undec-7-ene (DBU) and trifluoroacetic acid (TFA) switches the dibenzo[24]crown-8 macrocycle component between two separate protonated amine and methylated triazole stations (Fig 1.12a,b).[109] This shuttling is also accompanied by a large visual fluorescent change due to changes in the photoinduced electron transfer process of the rotaxane structure (Fig 1.12c).[109]

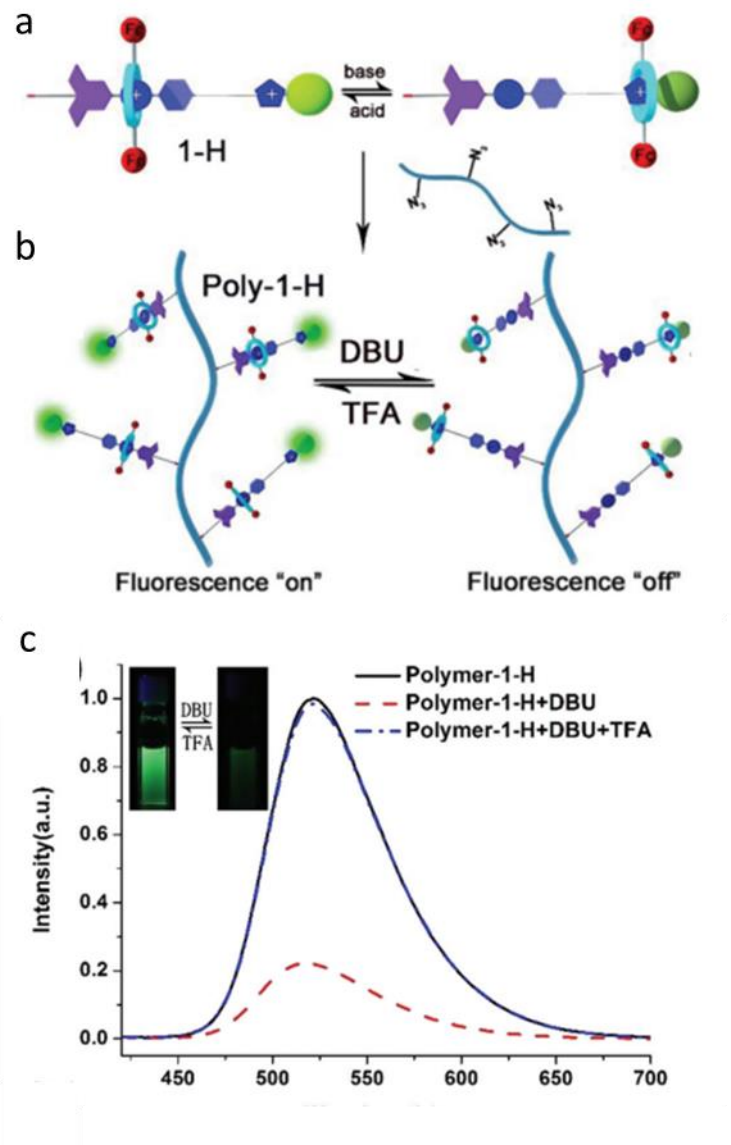

Fig 1.12 a) Scheme showing the relative shuttling movement of the rotaxane-type fluorescent switch upon acid/base cycling. (b) Scheme showing functionalization of this [2]rotaxane onto the backbone polymer and its switching upon acid/base cycling. c) Normalized fluorescence spectral changes of the polyrotaxane solution upon acid/base cycling with inset showing visual fluorescence change. Figure adapted from ref 109.[109]

1.2.4 Topological Main-Chain Polyrotaxanes

Topological main-chain polyrotaxanes contain mechanical bonds in the main-chain of the polymer (Fig 1.3 right, poly[2]rotaxanes and poly[3]rotaxanes) and they are an intrinsic part of the backbone giving them unusually high levels of mobility and freedom relative to standard

covalently bonded polymers making them attractive synthetic targets for chemists and engineers alike. The poly[2]rotaxane (Fig 1.3 right) is the simplest architecture in this class and has multiple synthetic examples using differing size crown ethers as the ring components.[27,111,112] Beyond synthetic procedures and initial structural characterization no material properties or related mechanical testing have been published on these materials.

Related to poly[2]rotaxanes are daisy-chain polymers that that incorporate cyclic dimeric daisy chain ([*c2*]daisy-chain) linkages. In this class of MIPs, the dimeric [*c2*]daisy-chain interlocked motif allows components to slide past each other and enables access to either contracted or expanded forms (Fig 1.13a cartoon).[113,114] Thus, the incorporation of such linkages into a polymer architecture offers a route to actuating or switchable materials which can undergo macroscopic changes based on molecular motion. Strides towards linear [c2]daisy-chain-containing polymers were made by Grubbs and Stoddart[115–118] who polymerized bifunctional [c2]daisy-chain monomers using either azide-alkyne cycloaddition or alkene metathesis chemistry. The resulting polymers (Fig 1.13a) could be switched between contracted and expanded forms by changing the pH of the solution. Subsequent efforts have focused on the design of network materials (either supramolecular[119–124] or covalent[125–127]) aimed at exploiting this molecular actuation in material systems. As an example, network [c2]daisy-chain (based on crown ether-ammonium recognition sites) gels[125] in acetonitrile have been developed to allow switchable swelling-deswelling behaviour with the addition of acid or base.

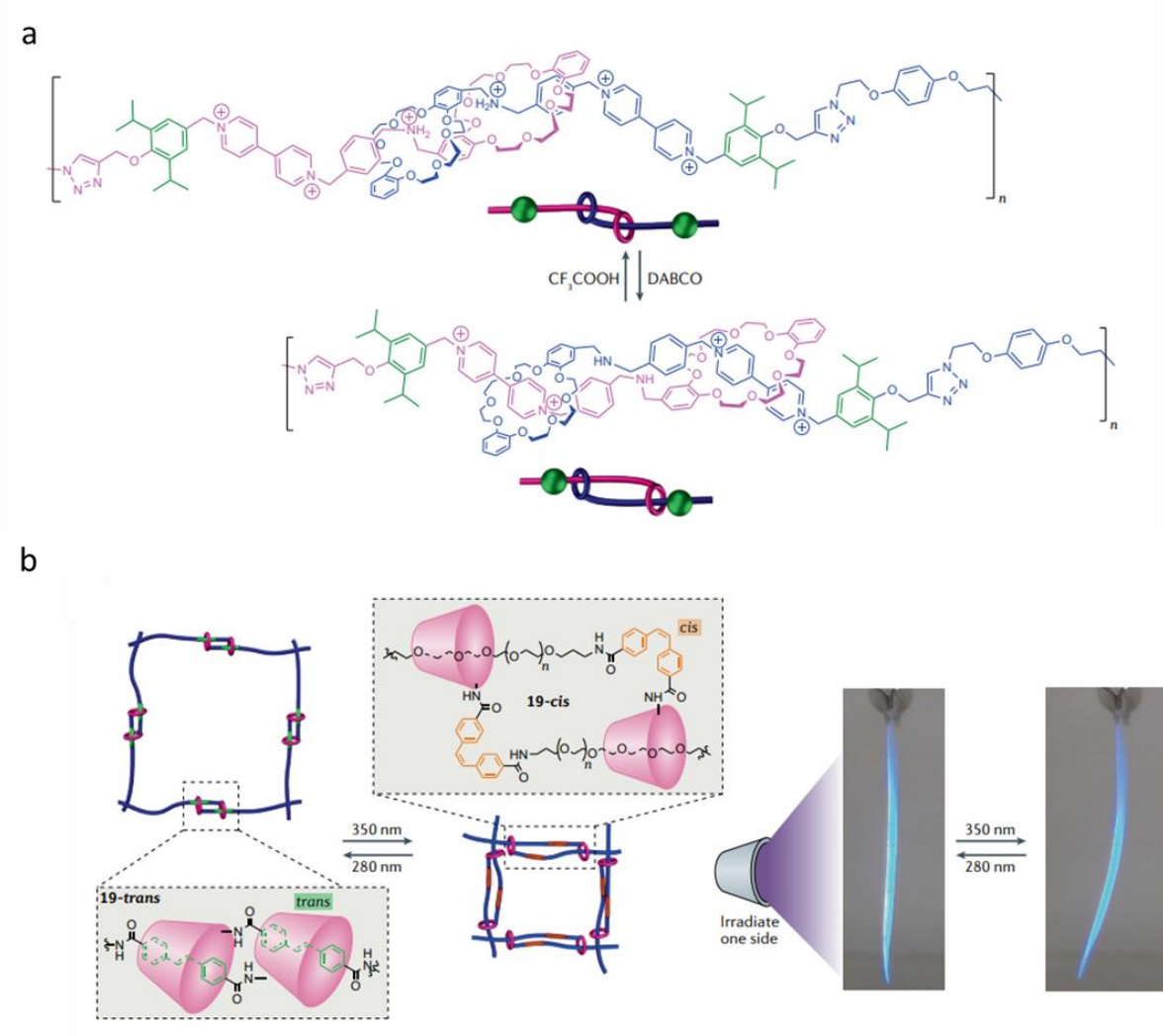

Fig 1.13 a) Structure of an acid–base switchable linear [c2]daisy-chain polymer, polymerized by alkyne–azide cycloaddition. Protonation of the secondary amines results in contraction of the polymer backbone, while deprotonation of the acidic form via addition of base reverts the polymer back to its expanded form. b) Stilbene-containing [c2] daisy-chain network polymer where the position of the α-cyclodextrin rings can be directed using ultraviolet light. Trans-stilbene binds strongly to the α-cyclodextrin rings, locking them in place. Irradiation with 350-nm light induces trans–cis isomerization, resulting in weaker binding and movement of the rings along the poly(ethylene glycol) backbone, causing the network structure to contract. The expanded structure can be recovered upon cis–trans isomerization with 280-nm light (left) which can be seen using a hydrogel hung via a clip (right), figure adapted from ref 25.[25]

UV-switchable [c2]daisy-chain networks have been prepared by reacting a four-armed PEG linker with a bifunctional [c2]daisy-chain monomer, comprised of α-CD and stilbene (Fig 1.13b left).[127] The photoresponsive stilbene is known to bind stronger with α-CD in its *trans* conformation. Switching between *cis* and *trans*, which can be achieved by irradiation, results in

the expansion (λ= 280 nm) or contraction (λ= 350 nm) of the network (Fig 1.13b right). This relatively rapid and robust photo-switching can result in UV-induced macroscopic bending of films by unidirectional irradiation of the material,[127] and such films have also been shown to lift objects 15 times their own weight. Related photo-responsive [c2]daisy-chain networks that use azobenzene rather than stilbene have also been reported.[126]

Main-chain poly[3]rotaxanes based on a singly threaded architecture with two rings (Fig 1.3 right) have been synthesized in a few notable cases.[111,128,129] Beyond initial synthesis and characterization no material properties or applications have been explored. In addition to the singly threaded poly[3]rotaxane, another poly[3]rotaxane architecture hypothetically exists, namely the doubly threaded poly[3]rotaxane (Fig 1.14).

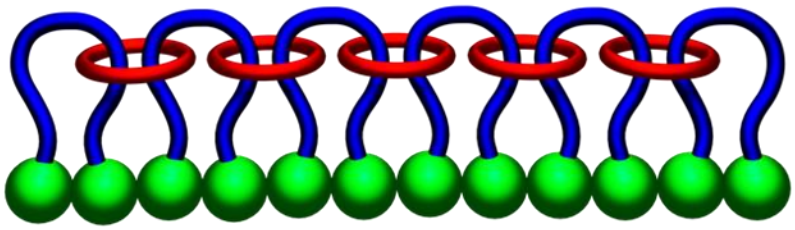

Fig 1.14 Cartoon showing doubly threaded poly[3]rotaxane architecture.

In this architecture each ring is threaded by two dumbbells, The doubly threaded poly[3]rotaxane continues to elude researchers and has never been synthetically reported in any capacity. This architecture should be a perfectly linear version of the SRMs discussed previously and may offer additional synthetic advantages and tunability parameters such as thread-thread interactions that are unique to the doubly threaded structure.

1.3 Conclusion

The mechanical bond is a unique bonding motif through space between differing interlocked components that gives the components the strength of a covalent bond without the added structural rigidity typically associated with it. This bond has been utilized to develop a number of differing MIMs including rotaxanes that have resulted in a wide range of applications with international attention.

The incorporation of the rotaxane motif into a polymeric backbone has resulted in a wide range of interlocked polymeric architectures. Many of them are still very early in synthetic development and have not been incorporated into actual materials. One specific class where extensive work has been done are non-topological main-chain polyrotaxanes (specifically those from CD and PEG). Research on these polyrotaxanes has resulted in their use in a wide range of functional polymeric materials that have been applied in areas such as molecular wires, drug/gene delivery, glassy materials, biological targeting, molecular machines, and more. Specifically, their incorporation into SRMs has resulted in commercialized scratch-resistant materials. Doubly threaded poly[3]rotaxanes remain an unmet synthetic challenge and may offer potential advantages to conventional materials such as easier synthetic pathways and additional tunability parameters. Current SRM materials are based on a movable "figure 8" cross-link that is synthesized from cross-linking singly threaded main-chain polyrotaxanes. The materials envisioned in this work contain a true doubly threaded cross-link which offers the unique potential to tune the inter-thread interactions as they move through each other. Systematically changing the thread backbone in ways such as increasing steric bulk or adding hydrogen bonding interactions offers additional ways to adjust the resultant material properties. The ability to implant specified reactive chemistry sites along the thread could lead to stretch-induced chemical reactivity in the interlocked polymers. In

addition, singly threaded macrocycles could be added in a straight forward and systematic manner to explore further the concepts of entropic elasticity introduced by Ito.[130] These represent just a few of the many benefits of accessing this doubly threaded architecture. As such, the focus of this thesis will be developing synthetic pathways towards doubly threaded poly[3]rotaxanes.

1.4 References

(1) Bruns, C. J.; Stoddart, J. F. *An Introduction to the Mechanical Bond*; 2010; Vol. 119.

(2) Wasserman, E. The Preparation of Interlocking Rings: A Catenane. *J. Am. Chem. Soc.* **1960**, *82* (16), 4433–4434. https://doi.org/10.1021/ja01501a082.

(3) Harrison, I. T.; Harrison, S. Synthesis of a Stable Complex of a Macrocycle and a Threaded Chain. *J. Am. Chem. Soc.* **1967**, *89* (22), 5723–5724.

(4) McGonigal, P. R. Multiply Threaded Rotaxanes. *Supramol. Chem.* **2018**, *30* (9), 782–794. https://doi.org/10.1080/10610278.2018.1433832.

(5) Erbas-Cakmak, S.; Leigh, D. A.; McTernan, C. T.; Nussbaumer, A. L. Artificial Molecular Machines. *Chem. Rev.* **2015**, *115* (18), 10081–10206. https://doi.org/10.1021/acs.chemrev.5b00146.

(6) Zhou, H. Y.; Han, Y.; Chen, C. F. PH-Controlled Motions in Mechanically Interlocked Molecules. *Mater. Chem. Front.* **2020**, *4* (1), 12–28. https://doi.org/10.1039/c9qm00546c.

(7) Dattler, D.; Fuks, G.; Heiser, J.; Moulin, E.; Perrot, A.; Yao, X.; Giuseppone, N. Design of Collective Motions from Synthetic Molecular Switches, Rotors, and Motors. *Chem. Rev.* **2020**, *120* (1), 310–433. https://doi.org/10.1021/acs.chemrev.9b00288.

(8) Fernandez, A.; Ferrando-Soria, J.; Pineda, E. M.; Tuna, F.; Vitorica-Yrezabal, I. J.; Knappke, C.; Ujma, J.; Muryn, C. A.; Timco, G. A.; Barran, P. E.; Ardavan, A.; Winpenny, R. E. P. Making Hybrid [n]-Rotaxanes as Supramolecular Arrays of Molecular Electron Spin Qubits. *Nat. Commun.* **2016**, *7*, 1–6. https://doi.org/10.1038/ncomms10240.

(9) Heath, J. R. Wires, Switches, and Wiring. A Route toward a Chemically Assembled Electronic Nanocomputer. *Pure Appl. Chem.* **2000**, *72* (1–2), 11–20. https://doi.org/10.1351/pac200072010011.

(10) Jamieson, E. M. G.; Modicom, F.; Goldup, S. M. Chirality in Rotaxanes and Catenanes. *Chem. Soc. Rev.* **2018**, *47* (14), 5266–5311. https://doi.org/10.1039/c8cs00097b.

(11) Lewis, J. E. M.; Galli, M.; Goldup, S. M. Properties and Emerging Applications of Mechanically Interlocked Ligands. *Chem. Commun.* **2017**, *53* (2), 298–312. https://doi.org/10.1039/C6CC07377H.

(12) Cotí, K. K.; Belowich, M. E.; Liong, M.; Ambrogio, M. W.; Lau, Y. A.; Khatib, H. A.; Zink, J. I.; Khashab, N. M.; Stoddart, J. F. Mechanised Nanoparticles for Drug Delivery.

Nanoscale **2009**, *1* (1), 16–39. https://doi.org/10.1039/b9nr00162j.

(13) Stoddart, J. F. Mechanically Interlocked Molecules (MIMs)-Molecular Shuttles, Switches, and Machines (Nobel Lecture). *Angew. Chemie Int. Ed.* **2017**, *56* (37), 11094–11125. https://doi.org/10.1002/anie.201703216.

(14) Sauvage, J.-P. From Chemical Topology to Molecular Machines (Nobel Lecture). *Angew. Chemie - Int. Ed.* **2017**, *56* (37), 11080–11093. https://doi.org/10.1002/anie.201702992.

(15) Feringa, B. L. The Art of Building Small: From Molecular Switches to Motors (Nobel Lecture). *Angew. Chemie Int. Ed.* **2017**, *56* (37), 11060–11078. https://doi.org/10.1002/anie.201702979.

(16) Hänni, K. D.; Leigh, D. A. The Application of CuAAC 'Click' Chemistry to Catenane and Rotaxane Synthesis. *Chem. Soc. Rev.* **2010**, *39* (4), 1240–1251. https://doi.org/10.1039/b901974j.

(17) Asakawa, M.; Ashton, P. R.; Ballardini, R.; Balzani, V.; Bělohradský, M.; Gandolfi, M. T.; Kocian, O.; Prodi, L.; Raymo, F. M.; Stoddart, J. F.; Venturi, M. The Slipping Approach to Self-Assembling [n]Rotaxanes. *J. Am. Chem. Soc.* **1997**, *119* (2), 302–310. https://doi.org/10.1021/ja961817o.

(18) Evans, N. H. Recent Advances in the Synthesis and Application of Hydrogen Bond Templated Rotaxanes and Catenanes. *European J. Org. Chem.* **2019**, No. 21, SI, 3320–3343. https://doi.org/10.1002/ejoc.201900081.

(19) Nepogodiev, S. A.; Stoddart, J. F. Cyclodextrin-Based Catenanes and Rotaxanes. *Chem. Rev.* **1998**, *98* (5), 1959–1976. https://doi.org/10.1021/cr970049w.

(20) Wisner, J. A.; Beer, P. D.; Drew, M. G. B.; Sambrook, M. R. Anion-Templated Rotaxane Formation. *J. Am. Chem. Soc.* **2002**, *124* (42), 12469–12476. https://doi.org/10.1021/ja027519a.

(21) Beves, J. E.; Blight, B. A.; Campbell, C. J.; Leigh, D. A.; McBurney, R. T. Strategies and Tactics for the Metal-Directed Synthesis of Rotaxanes, Knots, Catenanes, and Higher Order Links. *Angew. Chemie - Int. Ed.* **2011**, *50* (40), 9260–9327. https://doi.org/10.1002/anie.201007963.

(22) Lewis, J. E. M.; Beer, P. D.; Loeb, S. J.; Goldup, S. M. Metal Ions in the Synthesis of Interlocked Molecules and Materials. *Chem. Soc. Rev.* **2017**, *46* (9), 2577–2591. https://doi.org/10.1039/c7cs00199a.

(23) Inthasot, A.; Tung, S. Te; Chiu, S. H. Using Alkali Metal Ions to Template the Synthesis of Interlocked Molecules. *Acc. Chem. Res.* **2018**, *51* (6), 1324–1337. https://doi.org/10.1021/acs.accounts.8b00071.

(24) Jensen, W. B.; Thomas, R. The Origin of the Polymer Concept. *J. Chem. Educ.* **2004**, *81* (4), 2004.

(25) Hart, L. F.; Hertzog, J. E.; Rauscher, P. M.; Rawe, B. W.; Tranquilli, M. M.; Rowan, S. J. Material Properties and Applications of Mechanically Interlocked Polymers. *Nat. Rev. Mater.* **2021**, *6*, 508–530. https://doi.org/10.1038/s41578-021-00278-z.

(26) Huang, F. H.; Gibson, H. W. Polypseudorotaxanes and Polyrotaxanes. *Prog. Polym. Sci.* **2005**, *30* (10), 982–1018. https://doi.org/10.1016/j.progpolymsci.2005.07.003.

(27) Arunachalam, M.; Gibson, H. W. Recent Developments in Polypseudorotaxanes and Polyrotaxanes. *Prog. Polym. Sci.* **2014**, *39* (6), 1043–1073. https://doi.org/10.1016/j.progpolymsci.2013.11.005.

(28) Arunachalam, M.; Gibson, H. W. Recent Developments in Polypseudorotaxanes and Polyrotaxanes. *Prog. Polym. Sci.* **2014**, *39* (6), 1043–1073. https://doi.org/10.1016/j.progpolymsci.2013.11.005.

(29) Harrison, I. T.; Harrison, S. Synthesis of a Stable Complex of a Macrocycle and a Threaded Chain. *J. Am. Chem. Soc.* **1967**, *89* (22), 5723–5724. https://doi.org/10.1021/ja00998a052.

(30) Wenz, G.; Keller, B. Threading Cyclodextrin Rings on Polymer Chains. *Angew. Chem. Int.* **1992**, *31* (2), 197–199.

(31) Harada, A.; Li, J.; Kamachi, M. The Molecular Necklace: A Rotaxane Containing Many Threaded α-Cyclodextrins. *Nature* **1992**, *356* (March), 325–327.

(32) Fleury, G.; Brochon, C.; Schlatter, G.; Bonnet, G.; Lapp, A.; Hadziioannou, G. Synthesis and Characterization of High Molecular Weight Polyrotaxanes: Towards the Control over a Wide Range of Threaded α-Cyclodextrins. *Soft Matter* **2005**, *1* (5), 378–385. https://doi.org/10.1039/b510331b.

(33) Miyake, K.; Yasuda, S.; Harada, A.; Sumaoka, J.; Komiyama, M.; Shigekawa, H. Formation Process of Cyclodextrin Necklace−Analysis of Hydrogen Bonding on a Molecular Level. *J. Am. Chem. Soc.* **2003**, *125* (17), 5080–5085. https://doi.org/10.1021/ja026224u.

(34) Inomata, A.; Sakai, Y.; Zhao, C.; Ruslim, C.; Shinohara, Y.; Yokoyama, H.; Amemiya, Y.; Ito, K. Crystallinity and Cooperative Motions of Cyclic Molecules in Partially Threaded Solid-State Polyrotaxanes. *Macromolecules* **2010**, *43* (10), 4660–4666. https://doi.org/10.1021/ma100259t.

(35) Kato, K.; Mizusawa, T.; Yokoyama, H.; Ito, K. Polyrotaxane Glass: Peculiar Mechanics Attributable to the Isolated Dynamics of Different Components. *J. Phys. Chem. Lett.* **2015**, *6* (20), 4043–4048. https://doi.org/10.1021/acs.jpclett.5b01782.

(36) Mayumi, K.; Ito, K. Structure and Dynamics of Polyrotaxane and Slide-Ring Materials. *Polymer (Guildf).* **2010**, *51* (4), 959–967. https://doi.org/10.1016/j.polymer.2009.12.019.

(37) Zhao, C.; Domon, Y.; Okumura, Y.; Okabe, S.; Shibayama, M.; Ito, K. Sliding Mode of Cyclodextrin in Polyrotaxane and Slide-Ring Gel. *J. Phys. Condens. Matter* **2005**, *17* (31), S2841–S2846. https://doi.org/10.1088/0953-8984/17/31/009.

(38) Yasuda, Y.; Hidaka, Y.; Mayumi, K.; Yamada, T.; Fujimoto, K.; Okazaki, S.; Yokoyama, H.; Ito, K. Molecular Dynamics of Polyrotaxane in Solution Investigated by Quasi-Elastic Neutron Scattering and Molecular Dynamics Simulation: Sliding Motion of Rings on Polymer. *J. Am. Chem. Soc.* **2019**, *141*, 9655–9663.

(39) Yasuda, Y.; Toda, M.; Mayumi, K.; Yokoyama, H.; Morita, H.; Ito, K. Sliding Dynamics of Ring on Polymer in Rotaxane: A Coarse-Grained Molecular Dynamics Simulation Study. *Macromolecules* **2019**, *52* (10), 3787–3793. https://doi.org/10.1021/acs.macromol.9b00118.

(40) Mayumi, K.; Osaka, N.; Endo, H.; Yokoyama, H.; Sakai, Y.; Shibayama, M.; Ito, K. Concentration-Induced Conformational Change in Linear Polymer Threaded into Cyclic Molecules. *Macromolecules* **2008**, *41* (17), 6480–6485. https://doi.org/10.1021/ma801021g.

(41) Yamada, S.; Sanada, Y.; Tamura, A.; Yui, N.; Sakurai, K. Chain Architecture and Flexibility of α-Cyclodextrin/PEG Polyrotaxanes in Dilute Solutions. *Polym. J.* **2015**, *47* (6), 464–467. https://doi.org/10.1038/pj.2015.18.

(42) Gibson, H. W.; Liu, S.; Gong, C.; Ji, Q.; Joseph, E. Studies of the Formation of Poly(Ester Rotaxane)s from Diacid Chlorides, Diols, and Crown Ethers and Their Properties. *Macromolecules* **1997**, *30* (13), 3711–3727. https://doi.org/10.1021/ma961362n.

(43) Gong, C.; Gibson, H. W. Controlling Microstructure in Polymeric Molecular Shuttles: Solvent-Induced Localization of Macrocycles in Poly(Urethane/Crown Ether) Rotaxanes. *Angew. Chemie (International Ed. English)* **1997**, *36* (21), 2331–2333. https://doi.org/10.1002/anie.199723311.

(44) Shen, Y. X.; Xie, D.; Gibson, H. W. Polyrotaxanes Based on Polyurethane Backbones and Crown Ether Cyclics. 1. Synthesis. *J. Am. Chem. Soc.* **1994**, *116* (2), 537–548. https://doi.org/10.1021/ja00081a014.

(45) Gong, C.; Glass, T. E.; Gibson, H. W. Poly(Urethane/Crown Ether Rotaxane)s with Solvent Switchable Microstructures. *Macromolecules* **1998**, *31* (2), 308–313. https://doi.org/10.1021/ma970812o.

(46) Gong, C.; Ji, Q.; Subramaniam, C.; Gibson, H. W. Main Chain Polyrotaxanes by Threading Crown Ethers onto A Preformed Polyurethane: Preparation and Properties. *Macromolecules* **1998**, *31* (6), 1814–1818. https://doi.org/10.1021/ma9713116.

(47) Gong, C.; Gibson, H. W. Synthesis and Characterization of a Polyester/Crown Ether Rotaxane Derived from a Difunctional Blocking Group. *Macromolecules* **1996**, *29* (22), 7029–7033. https://doi.org/10.1021/ma960769p.

(48) Gong, C. G.; Gibson, H. W. Polyrotaxanes and Related Structures: Synthesis and Properties. *Curr. Opin. Solid State Mater. Sci.* **1997**, *2* (6), 647–652. https://doi.org/10.1016/S1359-0286(97)80004-6.

(49) Gong, C.; Gibson, H. W. Dethreading during the Preparation of Polyrotaxanes. *Macromol. Chem. Phys.* **1997**, *198* (7), 2321–2332. https://doi.org/10.1002/macp.1997.021980723.

(50) Chen, Z.; Aoki, D.; Uchida, S.; Marubayashi, H.; Nojima, S.; Takata, T. Effect of Component Mobility on the Properties of Macromolecular [2]Rotaxanes. *Angew. Chemie - Int. Ed.* **2016**, *55* (8), 2778–2781. https://doi.org/10.1002/anie.201510953.

(51) Uenuma, S.; Maeda, R.; Kato, K.; Mayumi, K.; Yokoyama, H.; Ito, K. Drastic Change of Mechanical Properties of Polyrotaxane Bulk: ABA-BAB Sequence Change Depending on

Ring Position. *ACS Macro Lett.* **2019**, *8* (2), 140–144. https://doi.org/10.1021/acsmacrolett.8b00896.

(52) Uenuma, S.; Maeda, R.; Takahashi, S.; Kato, K.; Yokoyama, H.; Ito, K. Self-Assembled Structure of Polyrotaxane Consisting of β-Cyclodextrin and Poly(Ethylene Oxide)-Block-Poly(Propylene Oxide)-Block-Poly(Ethylene Oxide) Triblock Copolymer in Bulk System. *Chem. Lett.* **2016**, *45* (8), 991–993. https://doi.org/10.1246/cl.160490.

(53) Lin, Q.; Li, L.; Tang, M.; Hou, X.; Ke, C. Rapid Macroscale Shape Morphing of 3D-Printed Polyrotaxane Monoliths Amplified from PH-Controlled Nanoscale Ring Motions. *J. Mater. Chem. C* **2018**, *6* (44), 11956–11960. https://doi.org/10.1039/c8tc02834f.

(54) Lin, Q.; Hou, X.; Ke, C. Ring Shuttling Controls Macroscopic Motion in a Three-Dimensional Printed Polyrotaxane Monolith. *Angew. Chemie - Int. Ed.* **2017**, *56* (16), 4452–4457. https://doi.org/10.1002/anie.201612440.

(55) Lin, Q.; Tang, M.; Ke, C. Thermo-Responsive 3D-Printed Polyrotaxane Monolith. *Polym. Chem.* **2020**, *11* (2), 304–308. https://doi.org/10.1039/c9py01510h.

(56) Kato, K.; Nemoto, K.; Mayumi, K.; Yokoyama, H.; Ito, K. Ductile Glass of Polyrotaxane Toughened by Stretch-Induced Intramolecular Phase Separation. *ACS Appl. Mater. Interfaces* **2017**, *9* (38), 32436–32440. https://doi.org/10.1021/acsami.7b10845.

(57) Kato, K.; Mizusawa, T.; Yokoyama, H.; Ito, K. Effect of Topological Constraint and Confined Motions on the Viscoelasticity of Polyrotaxane Glass with Different Interactions between Rings. *J. Phys. Chem. C* **2017**, *121* (3), 1861–1869. https://doi.org/10.1021/acs.jpcc.6b11362.

(58) Kato, K.; Ohara, A.; Yokoyama, H.; Ito, K. Prolonged Glass Transition Due to Topological Constraints in Polyrotaxanes. *J. Am. Chem. Soc.* **2019**, *141* (32), 12502–12506. https://doi.org/10.1021/jacs.9b06063.

(59) Cardin, D. J. Encapsulated Conducting Polymers. *Adv. Mater.* **2002**, *14* (8), 553–563. https://doi.org/10.1002/1521-4095(20020418)14:8<553::AID-ADMA553>3.0.CO;2-F.

(60) Mayumi, K.; Ito, K.; Kato, K. *Polyrotaxane and Slide-Ring Materials*; Monographs in Supramolecular Chemistry; Royal Society of Chemistry: Cambridge, 2015.

(61) Terao, J.; Tang, A.; Michels, J. J.; Krivokapic, A.; Anderson, H. L. Synthesis of Poly(Para-Phenylenevinylene) Rotaxanes by Aqueous Suzuki Coupling. *Chem. Commun.* **2004**, 56–57.

(62) Cacialli, F.; Wilson, J. S.; Michels, J. J.; Daniel, C.; Silva, C.; Friend, R. H.; Severin, N.; Samori, P.; Rabe, J. P.; O'connell, M. J.; Taylor, P. N.; Anderson, H. L. Cyclodextrin-Threaded Conjugated Polyrotaxanes as Insulated Molecular Wires with Reduced Interstrand Interactions. *Nat. Mater.* **2002**, *1* (3), 160–164. https://doi.org/10.1038/nmat750.

(63) Taylor, P. N.; O'Connell, M. J.; McNeill, L. A.; Hall, M. J.; Aplin, R. T.; Anderson, H. L. Insulated Molecular Wires: Synthesis of Conjugated Polyrotaxanes by Suzuki Coupling in Water. *Angew. Chemie - Int. Ed.* **2000**, *39* (19), 3456–3460. https://doi.org/10.1002/1521-3773(20001002)39:19<3456::AID-ANIE3456>3.0.CO;2-0.

(64) Michels, J. J.; O'Connell, M. J.; Taylor, P. N.; Wilson, J. S.; Cacialli, F.; Anderson, H. L. Synthesis of Conjugated Polyrotaxanes. *Chem. - A Eur. J.* **2003**, *9* (24), 6167–6176. https://doi.org/10.1002/chem.200305245.

(65) Van Den Boogaard, M.; Bonnet, G.; Van't Hof, P.; Wang, Y.; Brochon, C.; Van Hutten, P.; Lapp, A.; Hadziioannou, G. Synthesis of Insulated Single-Chain Semiconducting Polymers Based on Polythiophene, Polyfluorene, and β-Cyclodextrin. *Chem. Mater.* **2004**, *16* (23), 4383–4385. https://doi.org/10.1021/cm049665g.

(66) Frampton, M. J.; Anderson, H. L. Insulated Molecular Wires. *Angew. Chemie - Int. Ed.* **2007**, *46* (7), 1028–1064. https://doi.org/10.1002/anie.200601780.

(67) Ikeda, T.; Higuchi, M.; Kurth, D. G. From Thiophene [2]Rotaxane to Polythiophene Polyrotaxane. *J. Am. Chem. Soc.* **2009**, *131* (26), 9158–9159. https://doi.org/10.1021/ja902992c.

(68) Farcas, A.; Aubert, P. H.; Mohanty, J.; Lazar, A. I.; Cantin, S.; Nau, W. M. Molecular Wire Formation from Poly[2,7-(9,9-Dioctylfluorene)-Alt-(5,5′-Bithiophene/Cucurbit[7]Uril)] Polyrotaxane Copolymer. *Eur. Polym. J.* **2015**, *62*, 124–129. https://doi.org/10.1016/j.eurpolymj.2014.11.021.

(69) Belosludov, R. V.; Mizuseki, H.; Ichinoseki, K.; Kawazoe, Y. Theoretical Study on Inclusion Complex of Polyaniline Covered by Cyclodextrins for Molecular Device. *Jpn. J. Appl. Phys* **2002**, *41* (4 B), 2739–2741. https://doi.org/10.1143/JJAP.41.2739.

(70) Belosludov, R. V.; Sato, H.; Farajian, A. A.; Mizuseki, H.; Ichinoseki, K.; Kawazoe, Y. Molecular Enamel Wires for Electronic Devices: Theoretical Study. *Jpn. J. Appl. Phys.* **2003**, *42* (4 B), 2492–2494. https://doi.org/10.1143/jjap.42.2492.

(71) Brovelli, S.; Latini, G.; Frampton, M. J.; McDonnell, S. O.; Oddy, F. E.; Fenwick, O.; Anderson, H. L.; Cacialli, F. Tuning Intrachain versus Interchain Photophysics via Control of the Threading Ratio of Conjugated Polyrotaxanes. *Nano Lett.* **2008**, *8* (12), 4546–4551. https://doi.org/10.1021/nl802775a.

(72) Oddy, F. E.; Brovelli, S.; Stone, M. T.; Klotz, E. J. F.; Cacialli, F.; Anderson, H. L. Influence of Cyclodextrin Size on Fluorescence Quenching in Conjugated Polyrotaxanes by Methyl Viologen in Aqueous Solution. *J. Mater. Chem.* **2009**, *19* (18), 2846–2852. https://doi.org/10.1039/b821950h.

(73) Farcas, A.; Assaf, K. I.; Resmerita, A. M.; Sacarescu, L.; Asandulesa, M.; Aubert, P. H.; Nau, W. M. Cucurbit[7]Uril-Threaded Poly(3,4-Ethylenedioxythiophene): A Novel Processable Conjugated Polyrotaxane. *European J. Org. Chem.* **2019**, *2019* (21), 3442–3450. https://doi.org/10.1002/ejoc.201801724.

(74) Terao, J.; Tsuji, Y. New Synthetic Methods of π-Conjugated Inclusion Complexes with High Conductivity. *J. Incl. Phenom. Macrocycl. Chem.* **2014**, *80* (3–4), 165–175. https://doi.org/10.1007/s10847-014-0381-y.

(75) Grigoras, M.; Stafie, L. Electrically Insulated Molecular Wires. *Supramol. Chem.* **2010**, *22* (4), 237–248. https://doi.org/10.1080/10610270903410496.

(76) Terao, J.; Tanaka, Y.; Tsuda, S.; Kambe, N.; Taniguchi, M.; Kawai, T.; Saeki, A.; Seki, S.

Insulated Molecular Wire with Highly Conductive π-Conjugated Polymer Core. *J. Am. Chem. Soc.* **2009**, *131* (50), 18046–18047. https://doi.org/10.1021/ja908783f.

(77) Terao, J.; Wadahama, A.; Matono, A.; Tada, T.; Watanabe, S.; Seki, S.; Fujihara, T.; Tsuji, Y. Design Principle for Increasing Charge Mobility of π-Conjugated Polymers Using Regularly Localized Molecular Orbitals. *Nat. Commun.* **2013**, *4*, 1691. https://doi.org/10.1038/ncomms2707.

(78) Wankar, J.; Kotla, N. G.; Gera, S.; Rasala, S.; Pandit, A.; Rochev, Y. A. Recent Advances in Host–Guest Self-Assembled Cyclodextrin Carriers: Implications for Responsive Drug Delivery and Biomedical Engineering. *Adv. Funct. Mater.* **2020**, 1909049.

(79) Tamura, A.; Yui, N. Threaded Macromolecules as a Versatile Framework for Biomaterials. *Chem. Commun.* **2014**, *50* (88), 13433–13446. https://doi.org/10.1039/C4CC03709J.

(80) Li, J. J.; Zhao, F.; Li, J. Polyrotaxanes for Applications in Life Science and Biotechnology. *Appl. Microbiol. Biotechnol.* **2011**, *90* (2), 427–443. https://doi.org/10.1007/s00253-010-3037-x.

(81) Loethen, S.; Kim, J.-M.; Thompson, D. H. Biomedical Applications of Cyclodextrin Based Polyrotaxanes. *Polym. Rev.* **2007**, *47* (3), 383–418. https://doi.org/10.1080/15583720701455145.

(82) Arisaka, Y.; Yui, N. Polyrotaxane-Based Biointerfaces with Dynamic Biomaterial Functions. *J. Mater. Chem. B* **2019**, *7* (13), 2123–2129. https://doi.org/10.1039/C9TB00256A.

(83) Yui, N.; Ooya, T. Molecular Mobility of Interlocked Structures Exploiting New Functions of Advanced Biomaterials. *Chem. Eur. J.* **2006**, *12* (26), 6730–6737. https://doi.org/10.1002/chem.200600370.

(84) Patel, P.; Pol, A.; Jain, R.; Dandekar, P. Cyclodextrin Polyrotaxanes: Drug and Nucleic Acid Delivery. In *Encyclopedia of Biomedical Polymers and Polymeric Biomaterials*; Mishra, M., Ed.; CRC press: Boca Raton, 2015.

(85) Ooya, T.; Yamashita, A.; Kurisawa, M.; Sugaya, Y.; Maruyama, A.; Yui, N. Effects of Polyrotaxane Structure on Polyion Complexation with DNA. *Sci. Technol. Adv. Mater.* **2004**, *5* (3), 363–369. https://doi.org/10.1016/j.stam.2003.12.014.

(86) Ooya, T.; Choi, H. S.; Yamashita, A.; Yui, N.; Sugaya, Y.; Kano, A.; Maruyama, A.; Akita, H.; Ito, R.; Kogure, K.; Harashima, H. Biocleavable Polyrotaxane-Plasmid DNA Polyplex for Enhanced Gene Delivery. *J. Am. Chem. Soc.* **2006**, *128* (12), 3852–3853. https://doi.org/10.1021/ja055868+.

(87) Mammen, M.; Choi, S.-K.; Whitesides, G. M. Polyvalent Interactions in Biological Systems: Implications for Design and Use of Multivalent Ligands and Inhibitors. *Angew. Chem. Int.* **1998**, *37* (20), 2754–2794. https://doi.org/10.1002/chin.199909293.

(88) Seo, J.-H.; Kakinoki, S.; Inoue, Y.; Yamaoka, T.; Ishihara, K.; Yui, N. Inducing Rapid Cellular Response on RGD-Binding Threaded Macromolecular Surfaces. *J. Am. Chem. Soc.* **2013**, *135* (15), 5513–5516. https://doi.org/10.1021/ja400817q.

(89) Ooya, T.; Eguchi, M.; Yui, N. Supramolecular Design for Multivalent Interaction: Maltose Mobility along Polyrotaxane Enhanced Binding with Concanavalin A. *J. Am. Chem. Soc.* **2003**, *125* (43), 13016–13017. https://doi.org/10.1021/ja034583z.

(90) Sluysmans, D.; Stoddart, J. F. The Burgeoning of Mechanically Interlocked Molecules in Chemistry. *Trends Chem.* **2019**, *1* (2), 185–197. https://doi.org/10.1016/j.trechm.2019.02.013.

(91) Berná, J.; Leigh, D. A.; Lubomska, M.; Mendoza, S. M.; Pérez, E. M.; Rudolf, P.; Teobaldi, G.; Zerbetto, F. Macroscopic Transport by Synthetic Molecular Machines. *Nat. Mater.* **2005**, *4* (9), 704–710. https://doi.org/10.1038/nmat1455.

(92) Sun, X.; Amabilino, D. B.; Ashton, P. R.; Parsons, I. W.; Fraser Stoddart, J.; Tolley, M. S. Towards the Self-Assembly of Polyrotaxanes. *Macromol. Symp.* **1994**, *77* (1), 191–207. https://doi.org/10.1002/masy.19940770123.

(93) Zhang, W.; Dichtel, W. R.; Stieg, A. Z.; Benitez, D.; Gimzewski, J. K.; Heath, J. R.; Stoddart, J. F. Folding of a Donor-Acceptor Polyrotaxane by Using Noncovalent Bonding Interactions. *Proc. Natl. Acad. Sci.* **2008**, *105* (18), 6514–6519. https://doi.org/10.1073/pnas.0711072105.

(94) Zhu, Z.; Bruns, C. J.; Li, H.; Lei, J.; Ke, C.; Liu, Z.; Shafaie, S.; Colquhoun, H. M.; Stoddart, J. F. Synthesis and Solution-State Dynamics of Donor–Acceptor Oligorotaxane Foldamers. *Chem. Sci.* **2013**, *4* (4), 1470–1483. https://doi.org/10.1039/c3sc00015j.

(95) Basu, S.; Coskun, A.; Friedman, D. C.; Olson, M. A.; Benítez, D.; Tkatchouk, E.; Barin, G.; Yang, J.; Fahrenbach, A. C.; Goddard, W. A.; Stoddart, J. F. Donor-Acceptor Oligorotaxanes Made to Order. *Chem. - A Eur. J.* **2011**, *17* (7), 2107–2119. https://doi.org/10.1002/chem.201001822.

(96) Zhu, Z.; Li, H.; Liu, Z.; Lei, J.; Zhang, H.; Botros, Y. Y.; Stern, C. L.; Sarjeant, A. A.; Stoddart, J. F.; Colquhoun, H. M. Oligomeric Pseudorotaxanes Adopting Infinite-Chain Lattice Superstructures. *Angew. Chemie Int. Ed.* **2012**, *51* (29), 7231–7235. https://doi.org/10.1002/anie.201202513.

(97) Sluysmans, D.; Hubert, S.; Bruns, C. J.; Zhu, Z.; Stoddart, J. F.; Duwez, A. S. Synthetic Oligorotaxanes Exert High Forces When Folding under Mechanical Load. *Nat. Nanotechnol.* **2018**, *13* (3), 209–213. https://doi.org/10.1038/s41565-017-0033-7.

(98) Sluysmans, D.; Devaux, F.; Bruns, C. J.; Stoddart, J. F.; Duwez, A.-S. Dynamic Force Spectroscopy of Synthetic Oligorotaxane Foldamers. *Proc. Natl. Acad. Sci.* **2018**, *115* (38), 9362–9366. https://doi.org/10.1073/pnas.1712790115.

(99) Pezzato, C.; Nguyen, M. T.; Cheng, C.; Kim, D. J.; Otley, M. T.; Stoddart, J. F. An Efficient Artificial Molecular Pump. *Tetrahedron* **2017**, *73* (33), 4849–4857. https://doi.org/10.1016/j.tet.2017.05.087.

(100) Qiu, Y.; Zhang, L.; Pezzato, C.; Feng, Y.; Li, W.; Nguyen, M. T.; Cheng, C.; Shen, D.; Guo, Q. H.; Shi, Y.; Cai, K.; Alsubaie, F. M.; Astumian, R. D.; Stoddart, J. F. A Molecular Dual Pump. *J. Am. Chem. Soc.* **2019**, *141* (44), 17472–17476. https://doi.org/10.1021/jacs.9b08927.

(101) Qiu, Y.; Song, B.; Pezzato, C.; Shen, D.; Liu, W.; Zhang, L.; Feng, Y.; Guo, Q.-H.; Cai, K.; Li, W.; Chen, H.; Nguyen, M. T.; Shi, Y.; Cheng, C.; Dean Astumian, R.; Li, X.; Fraser Stoddart, J. A Precise Polyrotaxane Synthesizer. *Science (80-.).* **2020**, *368* (June), 1247–1253.

(102) Okumura, Y.; Ito, K. The Polyrotaxane Gel: A Topological Gel by Figure-of-Eight Cross-Links. *Adv. Mater.* **2001**, *13* (7), 485–487. https://doi.org/doi:10.1002/1521-4095(200104)13:7<485::AID-ADMA485>3.0.CO;2-T.

(103) Ito, K. Slide-Ring Materials Using Topological Supramolecular Architecture. *Curr. Opin. Solid State Mater. Sci.* **2010**, *14* (2), 28–34. https://doi.org/10.1016/j.cossms.2009.08.005.

(104) Neal, E. A.; Goldup, S. M. Chemical Consequences of Mechanical Bonding in Catenanes and Rotaxanes: Isomerism, Modification, Catalysis and Molecular Machines for Synthesis. *Chem. Commun.* **2014**, *50* (40), 5128–5142. https://doi.org/10.1039/C3CC47842D.

(105) Karino, T.; Okumura, Y.; Ito, K.; Shibayama, M. SANS Studies on Spatial Inhomogeneities of Slide-Ring Gels. *Macromolecules* **2004**, *37* (16), 6177–6182. https://doi.org/10.1021/ma049598b.

(106) Kato, K.; Yasuda, T.; Ito, K. Viscoelastic Properties of Slide-Ring Gels Reflecting Sliding Dynamics of Partial Chains and Entropy of Ring Components. *Macromolecules* **2013**, *46* (1), 310–316. https://doi.org/10.1021/ma3021135.

(107) Noda, Y.; Hayashi, Y.; Ito, K. From Topological Gels to Slide-Ring Materials. *J. Appl. Polym. Sci.* **2014**, *131* (15), 40509. https://doi.org/10.1002/app.40509.

(108) Kang, W. Y.; Jeong, S. Y.; Lee, S.; Park, J. S. Supramolecular Complexes of Carbon Nanotubes with Cyclodextrin-Incorporated Side-Chain Polyrotaxanes. *Mater. Lett.* **2013**, *93*, 203–206. https://doi.org/10.1016/j.matlet.2012.11.082.

(109) Cao, Z. Q.; Luan, Z. L.; Zhang, Q.; Gu, R. R.; Ren, J.; Qu, D. H. An Acid/Base Responsive Side-Chain Polyrotaxane System with a Fluorescent Signal. *Polym. Chem.* **2016**, *7* (10), 1866–1870. https://doi.org/10.1039/c5py01944c.

(110) Hu, J.; Hashidzume, A.; Harada, A. Photoregulated Switching of the Recognition Site of α-Cyclodextrin in a Side Chain Polyrotaxane Bearing Two Recognition Sites Linked with Oligo(Ethylene Glycol). *Macromol. Chem. Phys.* **2011**, *212* (10), 1032–1038. https://doi.org/10.1002/macp.201100029.

(111) Lee, Y. G.; Koyama, Y.; Yonekawa, M.; Takata, T. Synthesis of Main-Chain-Type Polyrotaxanes by New Click Polymerization Using Homoditopic Nitrile N -Oxides via Rotaxanation-Polymerization Protocol. *Macromolecules* **2010**, *43* (9), 4070–4080. https://doi.org/10.1021/ma100262g.

(112) Kohsaka, Y.; Konishi, G.; Takata, T. Synthesis of a Main Chain-Type Polyrotaxane Consisting of Poly(Crown Ether) and Sec-Ammonium Salt Axle and Its Application to Polyrotaxane Network. *Polym. J.* **2007**, *39* (8), 861–873. https://doi.org/10.1295/polymj.PJ2007030.

(113) Rotzler, J.; Mayor, M. Molecular Daisy Chains. *Chem. Soc. Rev.* **2013**, *42* (1), 44–62.

https://doi.org/10.1039/c2cs35217f.

(114) Bruns, C. J.; Stoddart, J. F. Rotaxane-Based Molecular Muscles. *Acc. Chem. Res.* **2014**, *47* (7), 2186–2199. https://doi.org/10.1021/ar500138u.

(115) Clark, P. G.; Day, M. W.; Grubbs, R. H. Switching and Extension of a [C2]Daisy-Chain Dimer Polymer. *J. Am. Chem. Soc.* **2009**, *131* (38), 13631–13633. https://doi.org/10.1021/ja905924u.

(116) Fang, L.; Hmadeh, M.; Wu, J.; Olson, M. A.; Spruell, J. M.; Trabolsl, A.; Yang, Y. W.; Elhablrl, M.; Albrecht-Gary, A. M.; Stoddart, J. F. Acid-Base Actuation of [C2]Daisy Chains. *J. Am. Chem. Soc.* **2009**, *131* (20), 7126–7134. https://doi.org/10.1021/ja900859d.

(117) Hmadeh, M.; Fang, L.; Trabolsi, A.; Elhabiri, M.; Albrecht-Gary, A. M.; Stoddart, J. F. On the Thermodynamic and Kinetic Investigations of a [C2]Daisy Chain Polymer. *J. Mater. Chem.* **2010**, *20* (17), 3422–3430. https://doi.org/10.1039/b924273b.

(118) Guidry, E. N.; Li, J.; Stoddart, J. F.; Grubbs, R. H. Bifunctional [C2]Daisy-Chains and Their Incorporation into Mechanically Interlocked Polymers. *J. Am. Chem. Soc.* **2007**, *129* (29), 8944–8945. https://doi.org/10.1021/ja0725100.

(119) Mariani, G.; Goujon, A.; Moulin, E.; Rawiso, M.; Giuseppone, N.; Buhler, E. Integration of Molecular Machines into Supramolecular Materials: Actuation between Equilibrium Polymers and Crystal-like Gels. *Nanoscale* **2017**, *9* (46), 18456–18466. https://doi.org/10.1039/c7nr04251e.

(120) Goujon, A.; Mariani, G.; Lang, T.; Moulin, E.; Rawiso, M.; Buhler, E.; Giuseppone, N. Controlled Sol-Gel Transitions by Actuating Molecular Machine Based Supramolecular Polymers. *J. Am. Chem. Soc.* **2017**, *139* (13), 4923–4928. https://doi.org/10.1021/jacs.7b00983.

(121) Xia, D.; Xue, M. A Supramolecular Polymer Gel with Dual-Responsiveness Constructed by Crown Ether Based Molecular Recognition. *Polym. Chem.* **2014**, *5* (19), 5591–5597. https://doi.org/10.1039/c4py00590b.

(122) Bruns, C. J.; Stoddart, J. F. Supramolecular Polymers: Molecular Machines Muscle Up. *Nat. Nanotechnol.* **2013**, *8* (1), 9–10. https://doi.org/10.1038/nnano.2012.239.

(123) Zhao, Y. L.; Zhang, R. Q.; Minot, C.; Hermann, K.; Van Hove, M. A. Revealing Highly Unbalanced Energy Barriers in the Extension and Contraction of the Muscle-like Motion of a [C2]Daisy Chain. *Phys. Chem. Chem. Phys.* **2015**, *17* (28), 18318–18326. https://doi.org/10.1039/c5cp00315f.

(124) Du, G.; Moulin, E.; Jouault, N.; Buhler, E.; Giuseppone, N. Muscle-like Supramolecular Polymers: Integrated Motion from Thousands of Molecular Machines. *Angew. Chemie - Int. Ed.* **2012**, *51* (50), 12504–12508. https://doi.org/10.1002/anie.201206571.

(125) Goujon, A.; Lang, T.; Mariani, G.; Moulin, E.; Fuks, G.; Raya, J.; Buhler, E.; Giuseppone, N. Bistable [C2] Daisy Chain Rotaxanes as Reversible Muscle-like Actuators in Mechanically Active Gels. *J. Am. Chem. Soc.* **2017**, *139* (42), 14825–14828. https://doi.org/10.1021/jacs.7b06710.

(126) Iwaso, K.; Takashima, Y.; Harada, A. Fast Response Dry-Type Artificial Molecular Muscles with [C2]Daisy Chains. *Nat. Chem.* **2016**, *8* (6), 625–632. https://doi.org/10.1038/nchem.2513.

(127) Ikejiri, S.; Takashima, Y.; Osaki, M.; Yamaguchi, H.; Harada, A. Solvent-Free Photoresponsive Artificial Muscles Rapidly Driven by Molecular Machines. *J. Am. Chem. Soc.* **2018**, *140* (49), 17308–17315. https://doi.org/10.1021/jacs.8b11351.

(128) Jiang, Y.; Guo, J. Bin; Chen, C. F. A Bifunctionalized [3]Rotaxane and Its Incorporation into a Mechanically Interlocked Polymer. *Chem. Commun.* **2010**, *46* (30), 5536–5538. https://doi.org/10.1039/c0cc00999g.

(129) Sato, T.; Takata, T. Synthesis and Characterization of Poly[3]Rotaxane through the Mizoroki-Heck Coupling Polymerization of Divinyl-Functionalized [3]Rotaxane. *Polym. J.* **2009**, *41* (6), 470–476. https://doi.org/10.1295/polymj.PJ2008298.

(130) Mayumi, K.; Tezuka, M.; Bando, A.; Ito, K. Mechanics of Slide-Ring Gels: Novel Entropic Elasticity of a Topological Network Formed by Ring and String. *Soft Matter* **2012**, *8* (31), 8179–8183. https://doi.org/10.1039/c2sm25508a.

Chapter 2: Initial [3]Rotaxane Attempts Using Thiol-ene Click Chemistry

2.1 Introduction

As indicated in Chapter 1, the main goal of this thesis is to develop synthetic methods towards the doubly threaded poly[3]rotaxane architecture. Synthesizing interlocked polymers can require complex characterization procedures and be difficult to prove in some cases. Previously in the Rowan group, an interlocked poly[n]catenane[1,2] was synthesized for the first time by first synthesizing a related [3]catenane[3] and then developing the polymeric synthesis based on the understanding learned from the small molecule [3]catenane. Based on this work, a similar approach to the doubly threaded poly[3]rotaxane using an interlocked "monomer" will be taken. First, a doubly threaded [3]rotaxane using a ditopic macrocycle will be synthesized and fully characterized (Fig 2.1a).

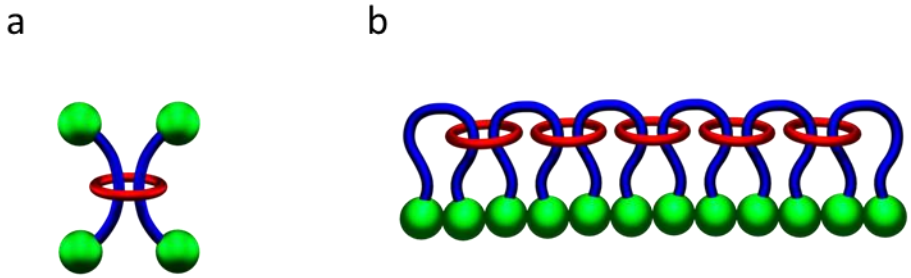

Fig 2.1 Cartoon representation of a) [3]Rotaxane and b) Poly[3]rotaxane.

A detailed physical understanding of the [3]rotaxane with full characterization with then be targeted. The use of the [3]rotaxane allows the stoppering conditions and component sizes to be optimized with the small molecule before moving onto the more complex polymeric architecture.

Synthesizing a doubly threaded [3]rotaxane with a ditopic macrocycle is not a trivial task. While rotaxanes are the most popular example of MIMs, this is due to the significant amount of

work on singly threaded [2]rotaxanes comprised of one macrocycle and one dumbbell component.[4] Threading two dumbbells within the same macrocyclic cavity to form a [3]rotaxane has proven far more challenging synthetically[5] and thus their reported syntheses are much more limited.[6–13] In addition, all of the rings used in these [3]rotaxanes are monotopic and thus not useful for extending to any polymeric structure. This is mainly the result of the difficulty in accessing large rings in rotaxane synthesis as synthetic efforts targeted at accessing rotaxanes with bigger rings have revealed that even relatively small increases in macrocycle size (a few atoms) necessitate dramatic increases in stopper group size.[14,15] Use of accessing a larger ditopic ring is critical for incorporation into polymers. Thus, ensuring proper component size match between stopper group and macrocycle size will be of paramount importance for the desired [3]rotaxane to be realized.

2.2 Component Synthesis and Design

While a variety of supramolecular templating methods have been utilized to synthesize rotaxanes (such as π-π stacking,[16] hydrogen bonding,[17] hydrophobic interactions,[18] and anion recognition[19]), it is metal ion templating[20–22] that has proven to be one of the most popular and highest yielding routes for accessing doubly threaded [3]rotaxanes. A range of ligands have been explored to access mechanically interlocked structures,[21] and the terdentate ligand, 2,6-bis(*N*-alkyl-benzimidazolyl)pyridine (Bip), will be used in this entire thesis as it has a number of attractive features including a flexible and scalable synthesis combined with the ability to tailor its solubility by altering its *N*-alkyl moeities.[23] In addition, Bip binds with transition metals (Zn^{2+} and Fe^{2+}) in an octahedral manner (Fig 2.2) which has been shown to successfully direct the doubly threaded templated assembly of [3]catenanes[3] and poly[n]catenanes making it a perfect candidate for the proposed synthesis.[1]

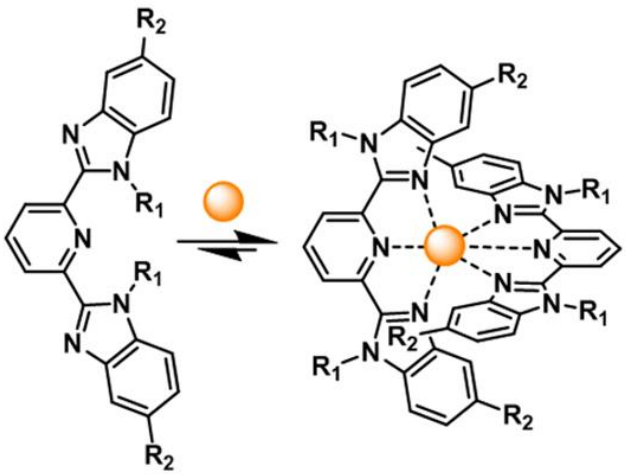

Fig 2.2 Chemical structure of the Bip ligand and its 2:1 binding assembly with transition metal ions.

Initial choice for the macrocycle component was based on previous polycatenane work in the group[1] and thus the 68 atom ring (**2.1**) was synthesized and used for initial [3]rotaxane studies in this chapter. A rather uncontrolled Williamson ether ring closing reaction using the Bip ligand **2.2**[23] and Tetraethylene glycol ditosylate in dilute conditions afforded **2.1** in 20% isolated yield from its cyclical and linear byproducts (Fig 2.3, see Experimental for full details).[1]

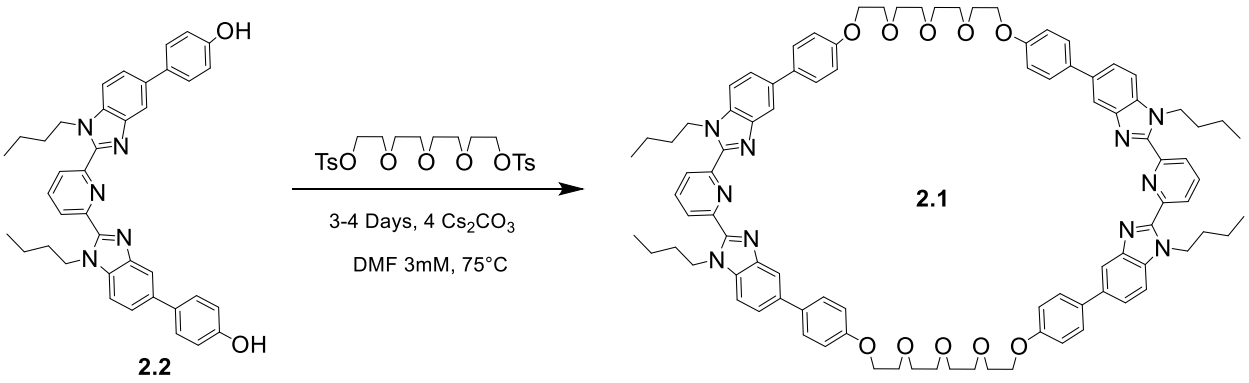

Fig 2.3 Scheme showing synthesis and chemical structure of 68 atom macrocycle component **2.1**.

The thread component was also derived from Bip, but this component was monotopic in order to ensure one thread would bind with each side of the ditopic macrocycle upon metal addition to form the desired pseudo[3]rotaxane. Standard Williamson ether reaction conditions on **2.2**[23] end

functionalized both ends of the Bip ligand with an alkene group providing the thread molecule (**2.3**) in 75% yield, and its structure was confirmed via ^{1}H-NMR spectroscopy (Fig 2.4) and MALDI-TOF MS (See Experimental for full details).

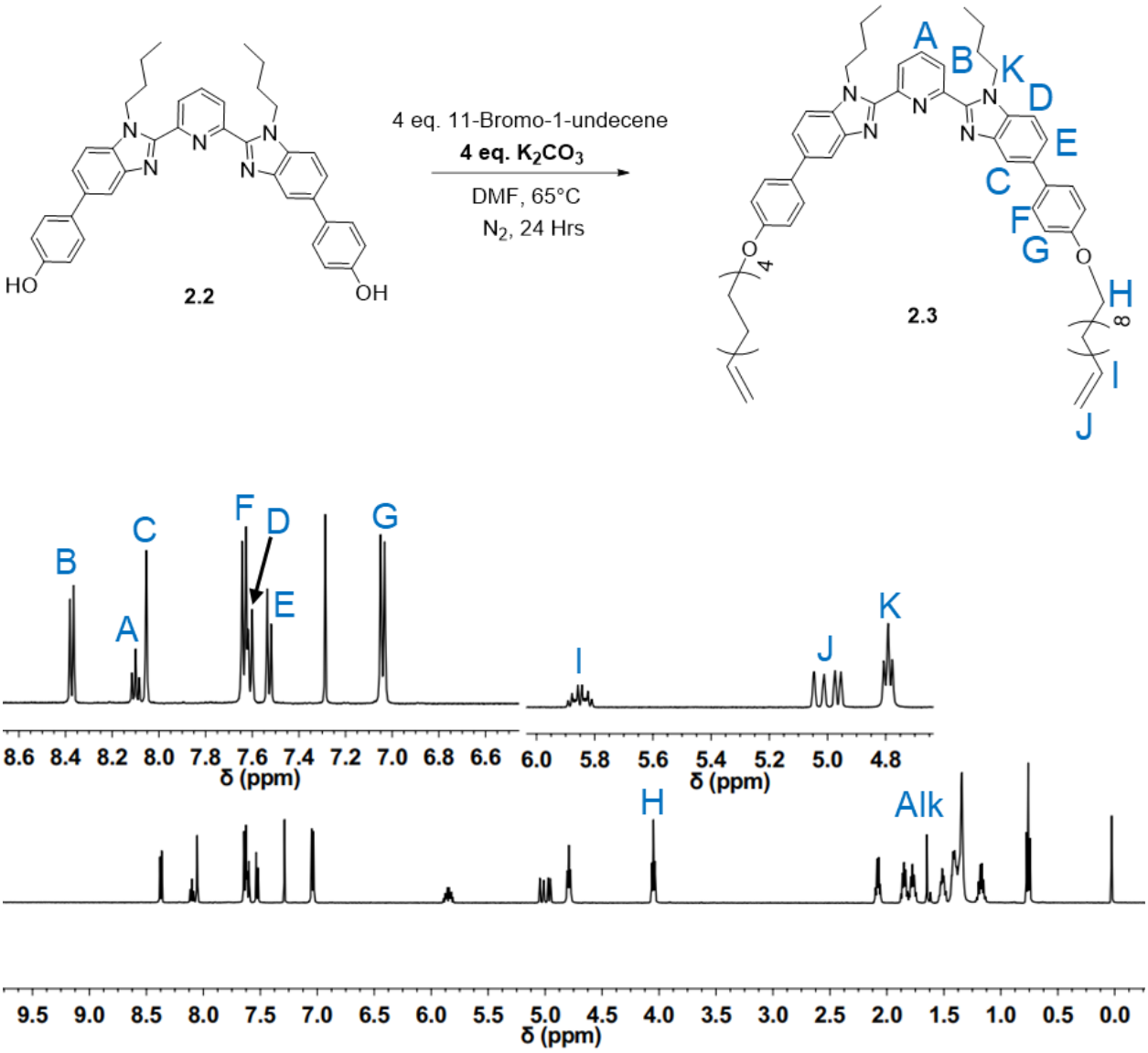

Fig 2.4 Figure showing synthesis of thread component **2.3** and its full ^{1}H-NMR spectrum (500 MHz, $CDCl_3$, 25°C).

As the starting thread and macrocycle components were decided, the last to determine was the stopper group component. The two most important parameters associated with this decision are what specific chemistry will be used for attachment and what size should it be to prevent dethreading of the large macrocycle. For size, the triaryl stoppering group **2.4** (Fig 2.5) was synthesized in two steps. First, a Grignard reaction using 1-bromo-4-*tert*-butylbenzene and diethyl carbonate gave **2.5** which was subsequently reacted with phenol in a Friedel-Crafts reaction to give **2.4.** This stopper group was specifically chosen as it is analogous in size to the largest stopper groups used in other reported doubly threaded systems and thus seemed to be a reasonable starting point for this study.[10,11]

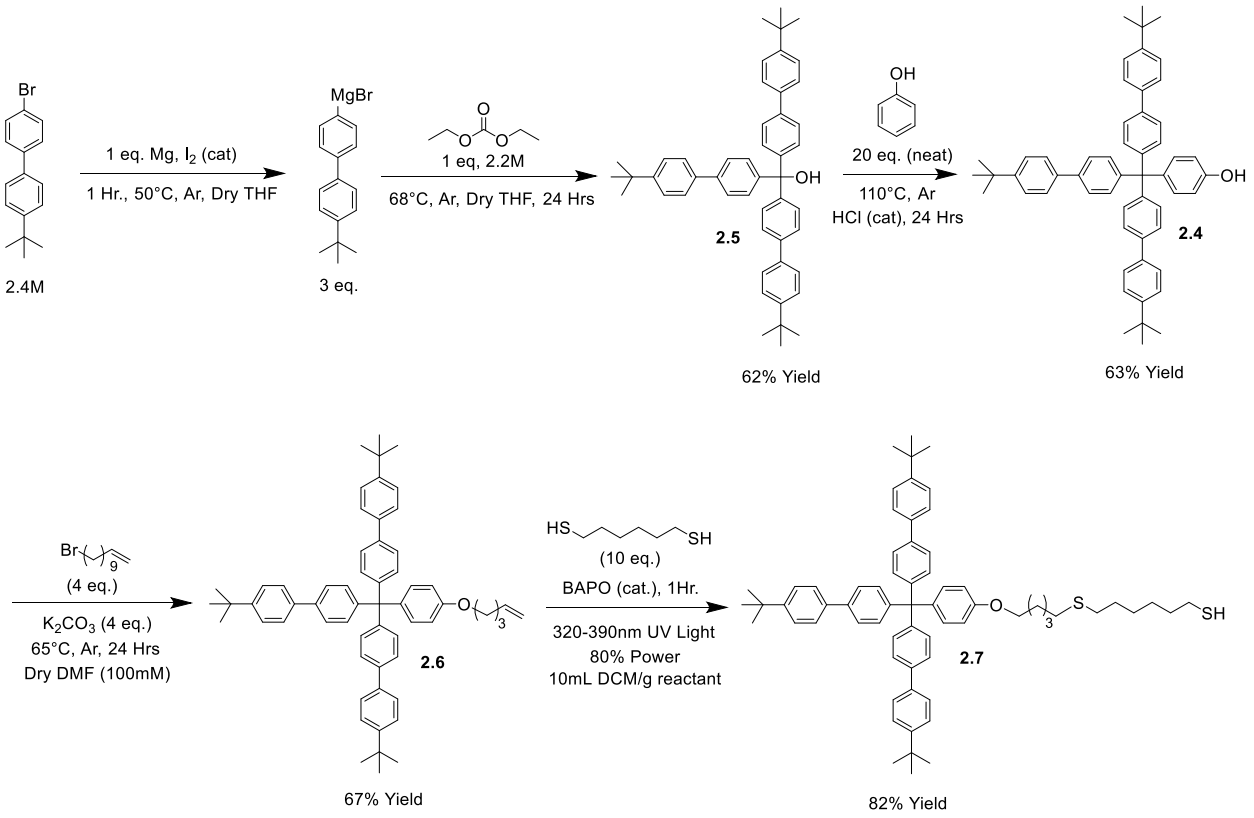

Fig 2.5 Scheme showing full synthesis of thiol terminated stopper group **2.7** from commercially available starting reagents.

Next, the specific stoppering chemistry was decided. As the thread (**2.3**) component is alkene terminated, a reasonable chemistry to start with is thiol-ene click chemistry.[24] This chemistry brings together a thiol and alkene in high yield with little to no side products and thus serves as a good starting point for initial [3]rotaxane studies. In two steps the stopper group **2.4** was alkene terminated via Williamson ether conditions (**2.6**) and then consequently thiol terminated via standard photoinitiated conditions to yield **2.7** (Fig 2.5) and its structure was confirmed via ^{1}H-NMR spectroscopy (Fig 2.6) and MALDI-TOF MS (See Experimental for full details).

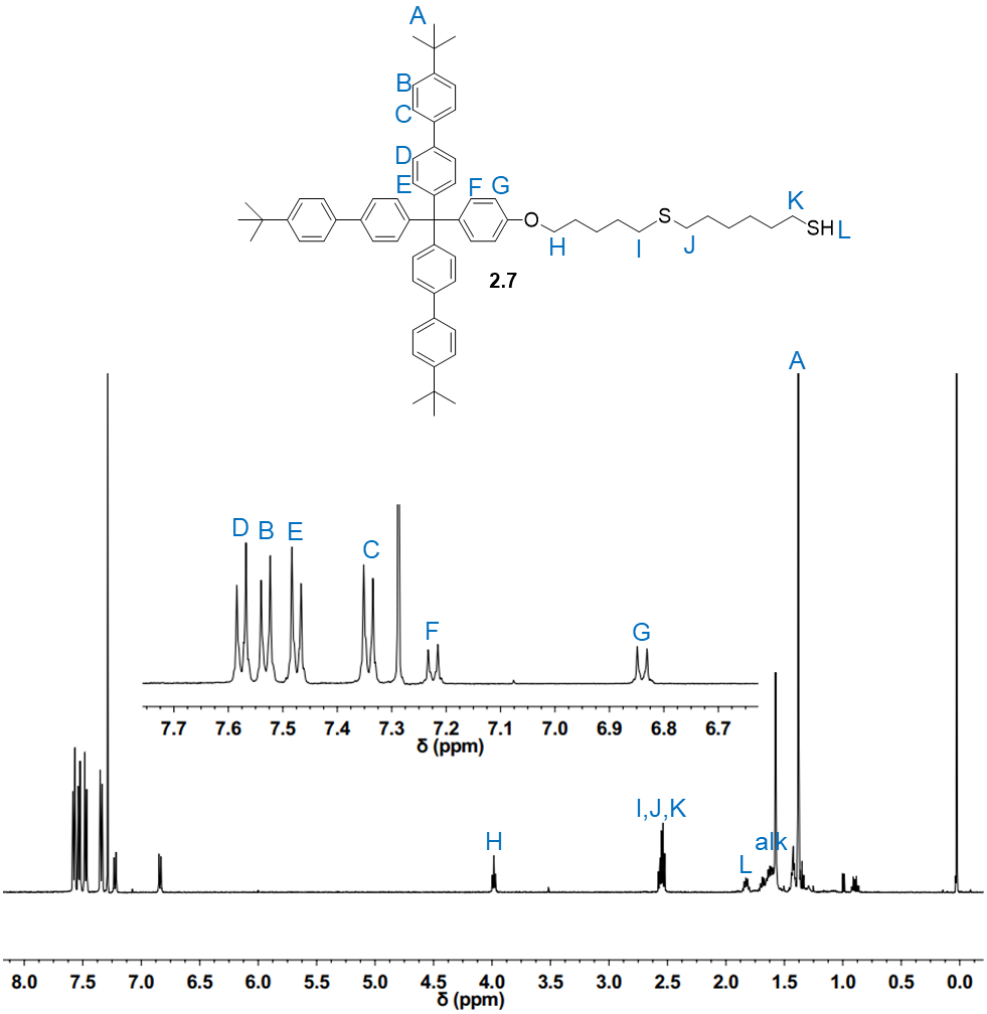

Fig 2.6 Full ^{1}H-NMR spectrum (500 MHz, $CDCl_3$, 25°C) and chemical structure of **2.7.**

2.3 Pseudo[3]rotaxane Assembly and Initial Stoppering Efforts

For the doubly threaded [3]rotaxane to be synthesized in high yield, an efficient way to template the pseudo[3]rotaxane must be used. Bip has been shown to template doubly threaded architectures in a passive metal templated manner using Fe(II) or Zn(II)[1,3] and thus a modified procedure based on this literature precedent using the macrocycle component **2.1** and the thread component **2.3** was used. The formation of pseudo[3]rotaxane **2.1**:**2.3**$_2$:Zn(II)$_2$ (Fig 2.7) from the free macrocycle and thread upon zinc(II) addition was carefully monitored using proton nuclear magnetic spectroscopy (^{1}H NMR).

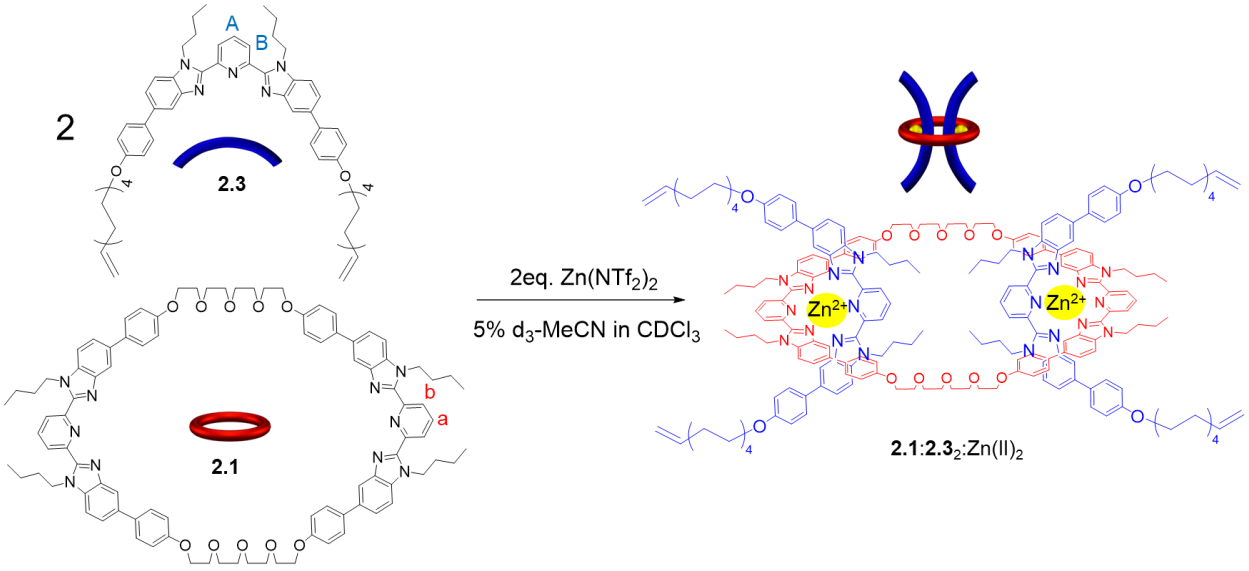

Fig 2.7 Scheme showing assembly of **2.1**:**2.3**$_2$:Zn(II)$_2$ from **2.1** and **2.3** upon zinc addition.

First, a 2:1 solution of **2.3**:**2.1** was made and analyzed via ^{1}H NMR spectroscopy to ensure proper stoichiometry. Integration of the labeled meta-pyridinyl peaks (Fig 2.7 for labels) confirmed the appropriate ratio (Fig 2.8).

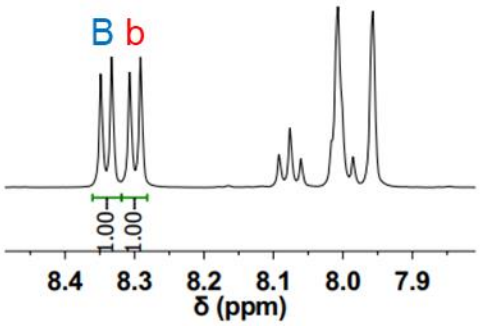

Fig 2.8 Partial ^{1}H-NMR spectrum (500 MHz, $CDCl_3$, 25°C) with integrations of a 2:1 solution of **2.3**:**2.1**, ^{1}H labels in Fig 2.7.

This 2:1 ratio before adding exactly 2 equivalents of metal is critical to maximize the enthalpic gain of the pseudo[3]rotaxane relative to any other possible products to ensure accurate templating. 2 equivalents of $Zn(NTf_2)_2$ were then added resulting in significant downfield shifting of the labeled pyridinyl peaks (See Fig 2.7 for labels) in the ^{1}H-NMR spectrum (Fig 2.9).

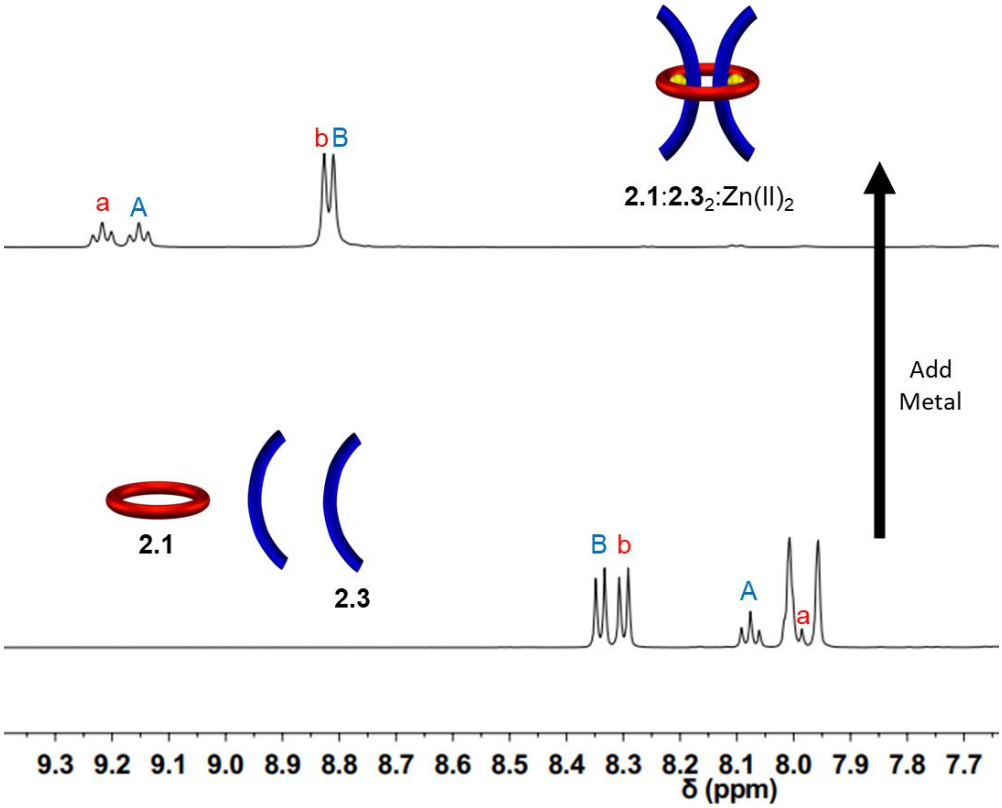

Fig 2.9 Partial ^{1}H-NMR overlay (500 MHz, 25°C) of **2.1**:**2.3**$_2$:$Zn(II)_2$ (top, 5% d_3-MeCN in $CDCl_3$) and a 2:1 solution of **2.3**:**2.1** (bottom, $CDCl_3$).

The observed downfield shifting (Fig 2.9) is consistent with previously published doubly threaded Bip complexes.[1,3] In addition, the fact that a single peak is seen for each assignable proton in the pseudo[3]rotaxane is consistent with the overall high symmetry expected in the pseudo[3]rotaxane complex.

With the alkene terminated pseudo[3]rotaxane **2.1**:**2.3**$_2$:Zn(II)$_2$ and the thiol terminated stopper group **2.7** in hand, efforts were then turned to stoppering the pseudo[3]rotaxane. A photo-initiated procedure using thiol-ene click chemistry modified from literature[24] developed in collaboration with a previous group graduate, Dr. Katie Herbert, was used (Fig 2.10).

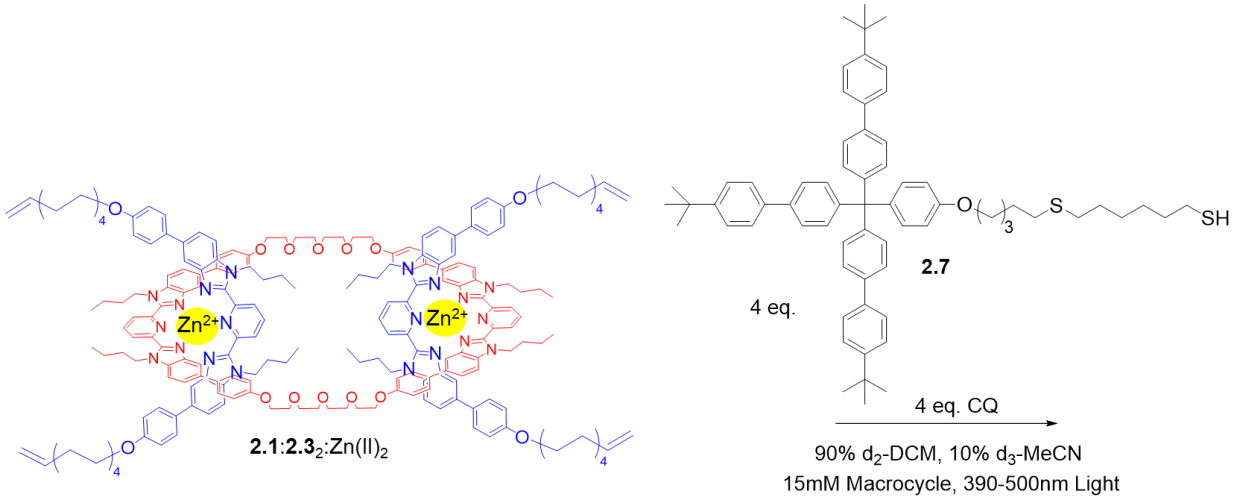

Fig 2.10 Scheme showing proposed stoppering of **2.1**:**2.3**$_2$:Zn(II)$_2$ with **2.7** using thiol-ene click conditions.

Camphorquinone was chosen as the photo-initiator due to its useful absorbance in the region of 390-500nm (**2.1**:**2.3**$_2$:Zn(II)$_2$ absorbs in the typical 320-390nm wavelength[25] and leads to decomplexation upon irradation). Briefly, a solution of **2.1**:**2.3**$_2$:Zn(II)$_2$, CQ, and **2.7** was stirred in a 90% DCM/10% MeCN solution in an NMR tube that was irradiated with 390-500nm for one hour, analyzed via ^{1}H-NMR spectroscopy, and then allowed to react further under irradiation overnight. ^{1}H-NMR acquisition was then repeated the next day (after 16 hours total of irradiation

time). ^{1}H-NMR is useful for monitoring the thiol-ene click reaction as the two multiplets corresponding to the alkene functionality labeled “I” and “J” in Figure 2.4 are particularly diagnostic and free of any other peaks. Careful monitoring of these peaks shows that after 1 hour they are consumed approximately 30% relative to starting integrations, and after 16 hours consumed ~40%, but ~60% of the original alkene functionality still remains (Fig 2.11).

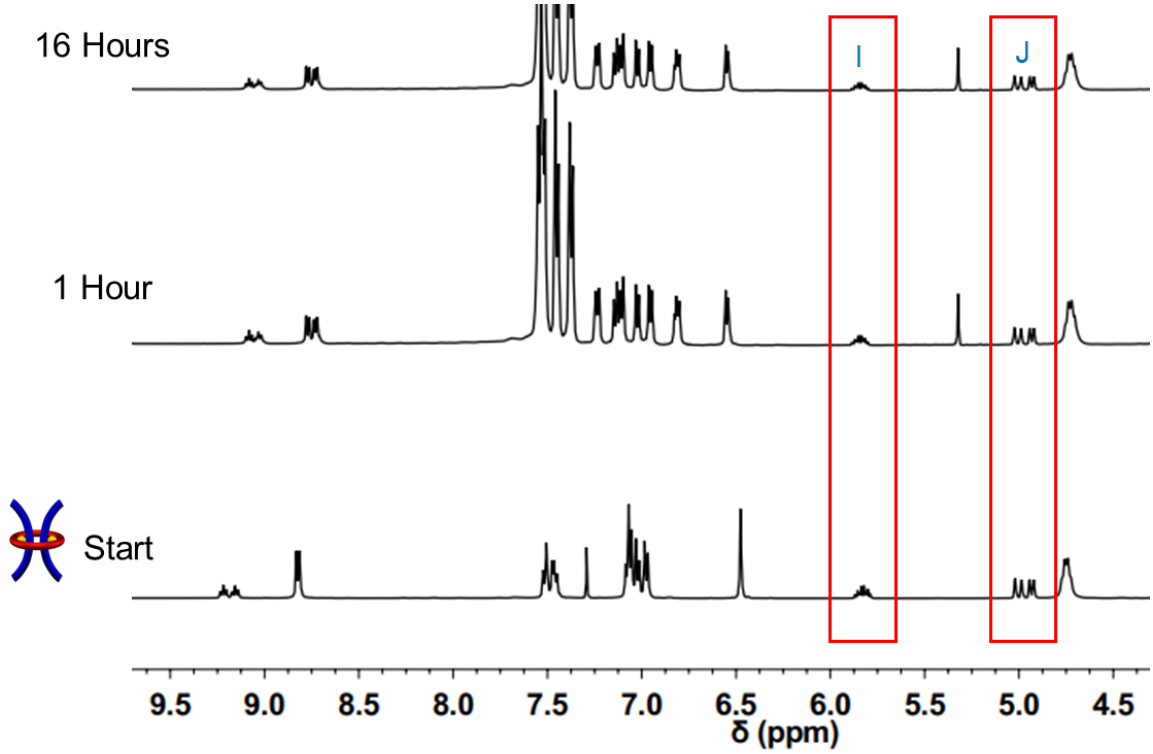

Fig 2.11 Partial ^{1}H-NMR overlay (500 MHz, 25°C, 5% d_3-MeCN in $CDCl_3$) of stoppering of **2.1**:**2.3**$_2$:Zn(II)$_2$ with **2.7** at the start (bottom) after 1 hour irradiation (middle) and 16 hours of irradiation (top).

As this is nowhere near quantitative (or even above 75% that would hypothetically be needed to consider at least adding four stopper groups to some of the pseudo[3]rotaxane), rotaxane formation is not feasible using these stoppering conditions. Attempts to increase conversion by changing photoinitiator amount, concentration, and irradiation power all were met with negligible or small conversion increases.

2.4 Attempts Using Alternative Initiation Source

As quantitative alkene conversion could not be achieved with photo-initiated conditions, efforts were then turned towards alternative means for initiating the reaction in hopes this could increase the conversion. The low temperature thermal initiator 2,2'-Azobis(4-methoxy-2,4-dimethylvaleronitrile) (commonly called V-70) was seen as a viable option as the pseudo[3]rotaxane complex was shown to be stable at the moderate temperature (35 °C) needed for activation (Fig 2.12a top).

a

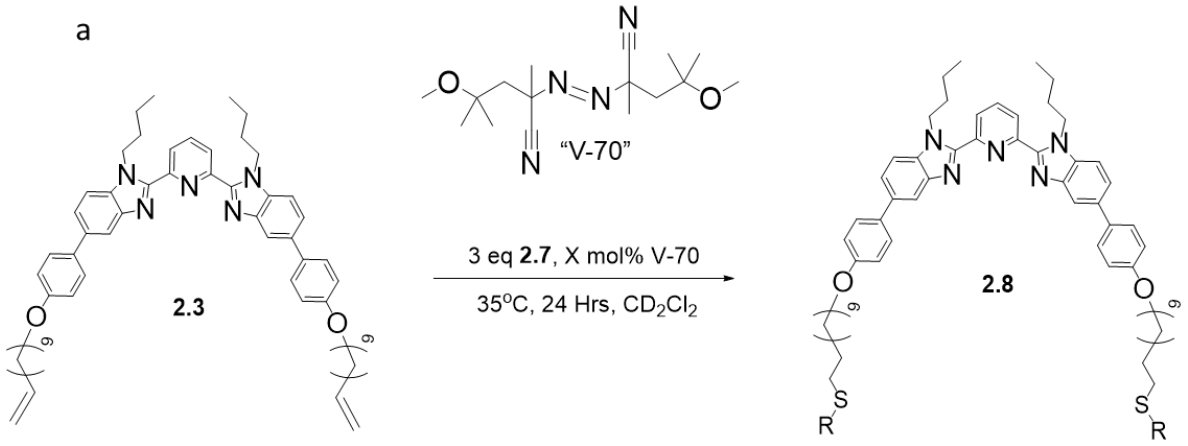

b

Amount of V-70	Alkene Conversion
0.1 mol %	6%
1 mol %	50%
10 mol %	61%
50 mol %	95%
1 equiv to Bip	98%
2 equiv to Bip	100%

Fig 2.12 a) Scheme showing stoppering control reaction of **2.3** with **2.7** using varying amounts of V-70, and b) table summarizing alkene conversion calculated using ^{1}H-NMR analysis of the reacted **2.3** using varying V-70 amounts.

First, a control reaction was done using standard thiol-ene click conditions[24] on the free thread (**2.3**) to see what initiator loading would be necessary to achieve quantitative alkene conversion (Fig 2.12a). The V-70 amount was varied from 0.1 mol% to 2 full molar equivalents (with respect to Bip), and the alkene conversion could be easily quantified from ^{1}H-NMR integration relative to the starting material and the obtained values are summarized in Figure 2.12b. As can be seen two full molar equivalents of V-70 relative to Bip are necessary to see quantitative alkene conversion in the free thread. As a note, this is a significantly higher initiator amount than is typically used in the literature for similar thiol-ene click reactions,[24] but nonetheless these conditions were then carried over to the pseudo[3]rotaxane **2.1**:**2.3**$_2$:Zn(II)$_2$.

2.1:**2.3**$_2$:Zn(II)$_2$ was let stir overnight in dichloromethane at 35°C with 4 equivalents of V-70 and 6 equivalents of **2.7** as the stopper group component (Fig 2.13).

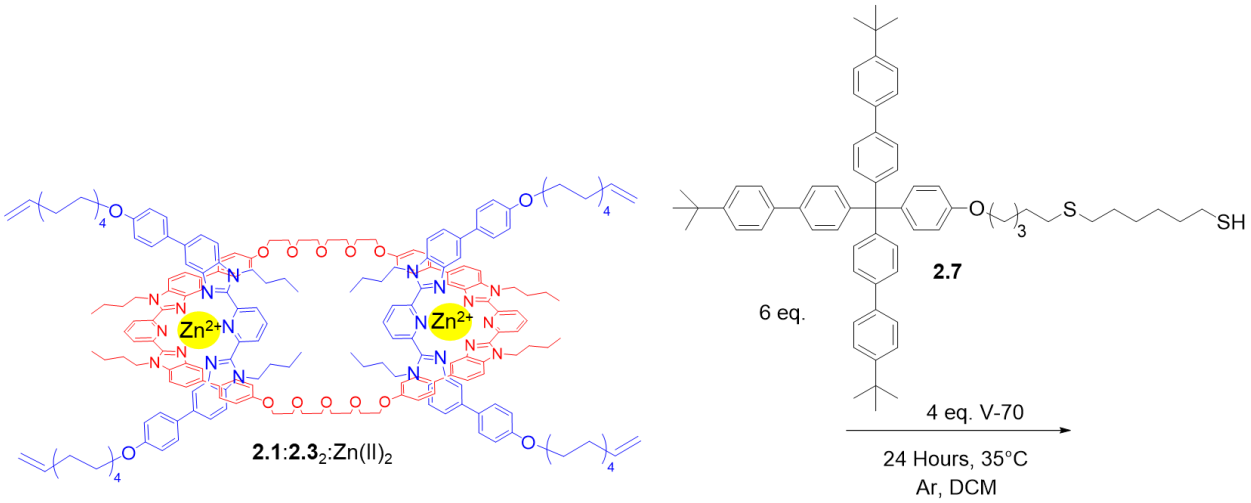

Fig 2.13 Scheme showing stoppering of **2.1**:**2.3**$_2$:Zn(II)$_2$ with **2.7** using V-70 as initiator.

A small condenser was used to ensure the reaction did not run dry. After 24 hours, ^{1}H-NMR spectroscopy of the crude sample showed that alkene peaks were still present in a significant amount (Fig 2.14).

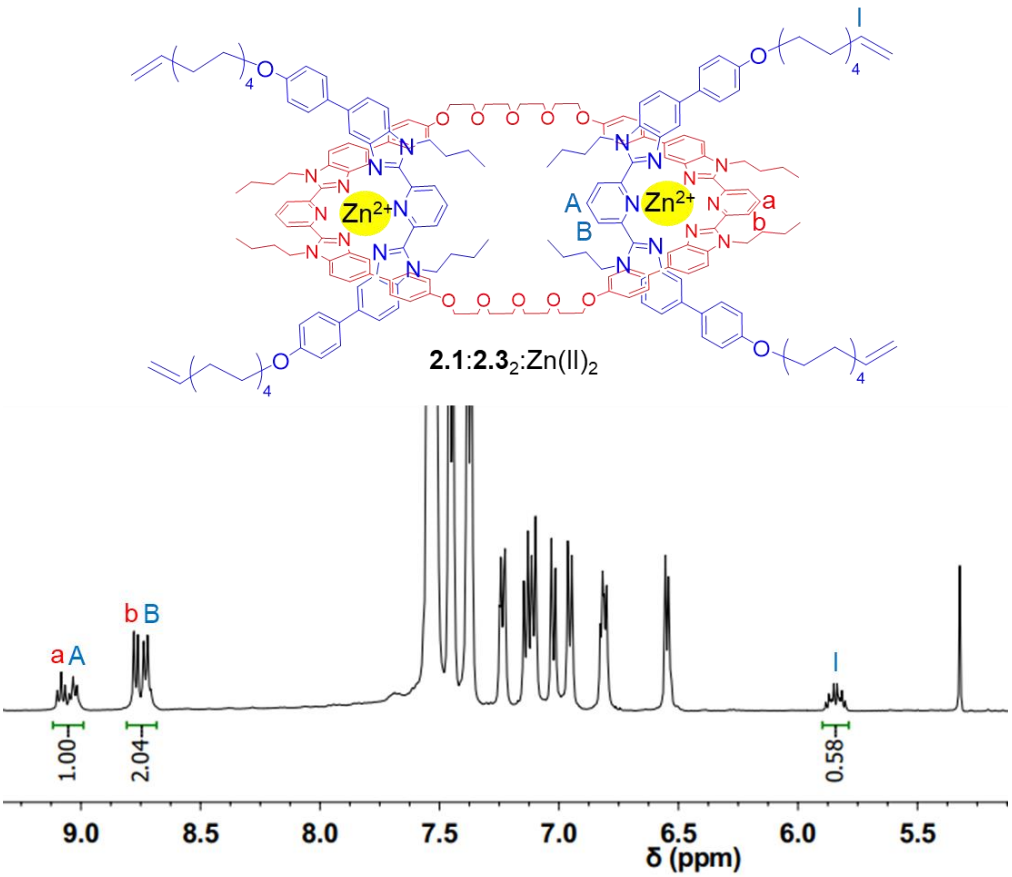

Fig 2.14 Partial ^{1}H-NMR spectrum (500 MHz, 25°C, 5% d_3-MeCN in $CDCl_3$) of stoppering of **2.1**:**2.3**$_2$:Zn(II)$_2$ with **2.7** using V-70 as initiator and 24 hours of reaction time, ^{1}H-labels at top of figure.

Specifically, only ~45% of the alkene peaks initially present in **2.1**:**2.3**$_2$:Zn(II)$_2$ had reacted after 24 hours. Further reaction time did not see any drastic increases in conversion. In addition, further attempts at higher temperatures using V-70 or any related azo initiators resulted in decomplexation of the pseudo[3]rotaxane. All in all, no thiol-ene click conditions using either thermal or photo initiation were able to achieve quantitative stoppering of the pseudo[3]rotaxane **2.1**:**2.3**$_2$:Zn(II)$_2$.

2.5 Conclusion and Future Directions

In this chapter initial synthetic efforts towards a doubly threaded [3]rotaxane using a ditopic macrocycle derived from a Bip framework have been described. Using a metal-templated approach, a pseudo[3]rotaxane was successfully formed using a ditopic macrocycle and two Bip

containing threads. The threads were alkene terminated in order to allow stopper group attachment. Stoppering attempts using a large bulky triaryl group that contained a thiol end group using various thiol-ene click conditions revealed that quantitative attachment was not possible. Further optimization attempts showed that with the free thread full attachment of the thiol stopper could be achieved at high initiator amounts, but these results did not correlate to any of the metalated complexes. A working hypothesis is that the metalated Bip complex is too much of a radical trap for a radical-initiated chemical reaction to ever proceed in the conversion needed to effectively stopper a rotaxane. Thus, future work based on this should look into stoppering reactions that do not utilize a radical based mechanism, such as azide-alkyne cycloaddition.

2.6 Experimental

2.6.1 Materials and Methods

Materials. All reagents were purchased from Sigma-Aldrich unless otherwise stated. All chemicals were used as received without further purification unless otherwise stated. Solvents for chromatography were purchased from Fisher-Scientific. Deuterated solvents were purchased from ACROS Organics. 4-Bromo-4'-tert-butylbiphenyl was purchased from TCI chemicals. *p*-Toluenesulfonyl chloride was purchased from Alfa Aesar. 2,6-bisbenzimidazolylpyridine ligands[23] was prepared following literature procedures. Tetrahydrofuran (THF) was dried over sodium and benzophenone. Dichloromethane was distilled over calcium hydride before use. Dimethylformamide (DMF) was dried with activated molecular sieves before use. Thin layer chromatography plates (1000 micron) were purchased from Analtech.

Matrix Assisted Laser Desorption/Ionization Mass Spectrometry (MALDI-MS). MALDI-TOF was measured by a Bruker Ultraflextreme MALDI-TOF-TOF spectrometer in linear

(or reflectance) mode using dithranol as matrix and sodium trifluoroacetate or silver trifluoroacetate as ionizer (or no ionizer).

Nuclear Magnetic Resonance Spectroscopy (NMR). Room Temperature Nuclear Magnetic Resonance Spectroscopy was performed using a Bruker Ascend Avance III 500 MHz spectrometer, a Bruker Avance II+ 500 MHz spectrometer, or a Bruker DRX 400 MHz spectrometer at the University of Chicago NMR facilities. ^{1}H NMR spectra were referenced to the residual protonated solvent signal and ^{13}C{^{1}H} NMR spectra were referenced to the deuterated solvent carbon resonance signal.

2.6.2 Synthesis 2.2[1]

Procedure adapted from literature.[1,23] 2,5-dibromonitrobenzene (50g, 178mmol) was combined with 1-butylamine (150mL) in a 500 mL round bottom flask equipped with stir bar and a waterless

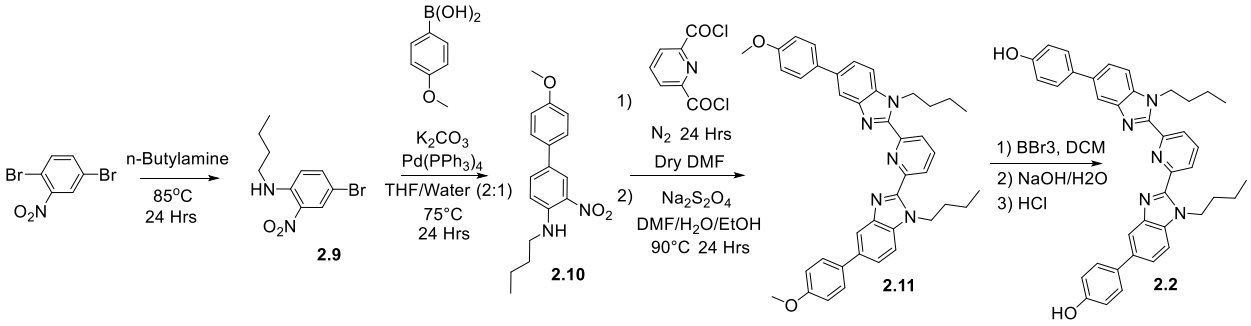

condenser. The solution was heated to 85°C and stirred for 24 hours. The resulting orange solution was precipitated in 1L of ice water followed by an addition of 2 M HCl to neutralize the pH (~7). The precipitate was collected via filtration and recrystallized in cold methanol to yield **2.9** in 90% yield. ^{1}H-NMR (500 MHz, $CDCl_3$) δ 8.34 (d, *J* = 2.4 Hz, 1H), 8.06 (s, 1H), 7.51 (dd, *J* = 9.2, 2.4 Hz, 1H), 6.79 (d, *J* = 9.2 Hz, 1H), 3.37 – 3.27 (m, 2H), 1.74 (p, *J* = 7.2 Hz, 2H), 1.50 (h, *J* = 7.4 Hz, 2H), 1.01 (t, *J* = 7.3 Hz, 3H). ^{13}C-NMR (126 MHz, $CDCl_3$) δ 144.66, 139.03, 132.14, 129.06, 115.68, 106.26, 43.02, 31.04, 20.34, 13.90. MALDI-MS: 295.2 ([M]+Na^+).

Procedure adapted from literature.[1,23] **2.9** (30g, 109.8 mmol) was added to a 1L round bottom flask containing 4-methoxyphenylboronic acid (16.9 g, 110.9 mmol,) potassium carbonate (138.2 g, 440 mmol), tetrahydrofuran (360mL) and deionized water (180mL). The flask was equipped with a stir bar and condenser and purged with argon for 30 minutes. After 30 minutes, of tetrakis(triphenylphosphine) palladium[0] catalyst (0.64 g, 0.55 mmol) was added, then the reaction was heated to 75 °C and stirred for 24 hours under inert atmosphere. The resulting red solution was cooled to room temperature and the organic layer was collected using a separation funnel. Washed the organic layer 2X with 150mL deionized water. The residual solvent in the organic layer was removed via rotary evaporation and **2.10** was recrystallized from cold acetonitrile (yield = 85%). ^{1}H-NMR (500 MHz, $CDCl_3$) δ 8.38 (s, 1H), 8.08 (s, 1H), 7.68 (d, *J* = 9.0 Hz, 1H), 7.51 – 7.46 (m, 2H), 7.00 – 6.95 (m, 2H), 6.93 (d, *J* = 9.0 Hz, 1H), 3.85 (s, 3H), 3.40 – 3.29 (m, 2H), 1.75 (p, *J* = 7.3 Hz, 2H), 1.53 – 1.46 (m, 2H), 1.00 (t, *J* = 7.4 Hz, 3H). ^{13}C-NMR (126 MHz, $CDCl_3$) δ 159.14, 144.61, 134.88, 131.99, 131.62, 128.17, 127.38, 123.96, 114.48, 114.46, 55.49, 42.98, 31.21, 20.38, 13.91. MALDI-MS: 323.3 ([M]+Na^+).

Procedure adapted from literature.[1,23] **2.10 (**20g, 78 mmol) was combined with 2,6-pyridinecarbonyl dicholoride (8g, 39 mmol) in a 1L round bottom flask with stir bar and flushed with argon for 15 minutes. Anhydrous dimethylformamide (DMF, 200mL) was cannulated into the flask and the solution was stirred for 24 hours. Next, a solution of sodium hydrosulfite (33g, 188 mmol, saturated in 5:1 vol/vol solution of deionized H_2O/ethanol) and an additional 100 mL of DMF were added to the flask followed by the addition of a waterless condenser to the top neck of the flask. The setup was flushed again with argon. The system was heated to 90°C and stirred for 24 hours. After 24 hours, the solution was cooled to room temperature and refrigerated overnight (ca. 20 hours). The resulting precipitate was collected via vacuum filtration then

triturated in chloroform. The filtrate was dried using rotary evaporation and the product was recrystallized from chloroform/acetonitrile to yield **2.11** in 70% yield. ^{1}H-NMR (500 MHz, $CDCl_3$) δ 8.35 (d, *J* = 7.8 Hz, 2H), 8.07 (t, *J* = 7.9 Hz, 1H), 8.03 (d, *J* = 1.5 Hz, 2H), 7.64 – 7.61 (m, 4H), 7.58 (dd, *J* = 8.4, 1.7 Hz, 2H), 7.50 (d, *J* = 8.4 Hz, 2H), 7.04 – 7.01 (m, 4H), 3.88 (s, 6H), 1.79 – 1.71 (m, 4H), 1.19 – 1.11 (m, 4H), 0.73 (t, *J* = 7.4 Hz, 6H). ^{13}C-NMR (126 MHz, $CDCl_3$) δ 159.05, 150.85, 150.14, 143.56, 138.30, 136.30, 135.63, 134.45, 128.53, 125.66, 123.25, 118.23, 114.43, 110.60, 55.51, 44.91, 32.32, 20.03, 13.66. MALDI-MS: 636.4 ([M]+H^+).

Procedure adapted from literature.[1,23] **2.11** (10g) was added to dicholoromethane (DCM, 150mL) in a 500 mL round bottom flask with stir bar. The solution was flushed with argon and cooled to 0 °C using an ice bath. While stirring the solution vigorously, 10 mL of boron tribromide were injected into the flask slowly. (*CAUTION: boron tribromide is extremely reactive with water, consult SDS.*) The solution was allowed to warm to room temperature with constant stirring over the next 24 hours. The reaction was added to a 2L beaker containing 1L of 1M NaOH solution and stirred until the mixture was yellow in color. Using 1M HCl, the mixture was neutralized (pH = 7) causing a product to visibly crash out of solution, and this solid was collected via vacuum filtration. The crude product was recrystallized in chloroform/methanol mixture to yield **2.2** in 89% yield. ^{1}H-NMR (500 MHz, DMSO-d_6) δ 10.32 (s, 2H), 9.20 – 9.15 (m, 2H), 9.10 – 9.05 (m, 1H), 8.75 (d, *J* = 1.6 Hz, 2H), 8.58 (d, *J* = 8.5 Hz, 2H), 8.43 – 8.37 (m, 6H), 7.74 – 7.68 (m, 4H), 5.62 (t, *J* = 7.2 Hz, 4H), 2.50 (p, *J* = 7.4 Hz, 4H), 1.90 (h, *J* = 7.4 Hz, 4H), 1.48 (t, *J* = 7.4 Hz, 6H). ^{13}C-NMR (126 MHz, DMSO-d_6) δ 156.71, 150.08, 149.55, 142.92, 138.74, 135.34, 135.15, 131.65, 127.95, 125.27, 122.36, 116.60, 115.70, 111.32, 54.88, 44.06, 31.69, 19.15, 13.20. MALDI-MS: 608.4 ([M]+H^+).

2.6.3 Synthesis of 2.1

Procedure adapted from literature.[1] A 2-necked 1 L RBF was charged with **2.2** (1.19 g, 1.95 mmol), Cs_2CO_3 (2.6 g, 7.8 mmol, 4 eq.) and DMF (440 mL) under an Ar atmosphere. The mixture was

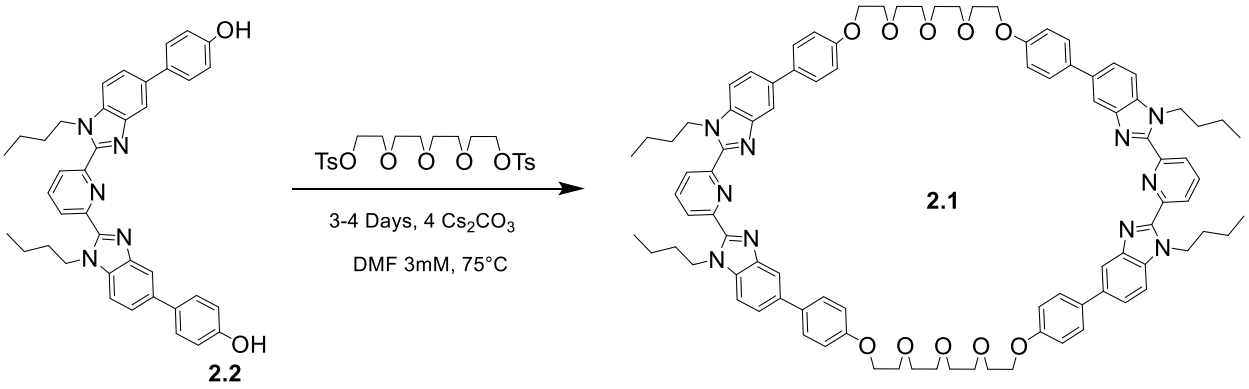

2.2

heated to 75 °C and stirred while a DMF (220 mL) solution of ditosylated tetraethylene glycol (0.98g, 1.95 mmol) was added dropwise (at an approximate rate of one drop every 10 s) over 3 d. When all the solution was added the reaction was stirred for a further 24 h at 75 °C. After this time (total reaction time 4 d) the reaction mixture was cooled to RT and the solvent was removed under reduced pressure. The residue was washed in hot $CHCl_3$ (4 × 100 mL) and the insoluble material (salts) was removed by filtration. The filtrate was collected and the solvent removed under reduced pressure. The resulting material was purified using column chromatography (TEA treated silica gel, chloroform/methanol gradient as eluent) followed by recrystallization (chloroform/methanol mixture) to yield white crystals of **2.1** in 20% yield. ^{1}H-NMR (500 MHz, $CDCl_3$) δ 8.30 (d, *J* = 7.8 Hz, 4H), 8.02 –53 7.96 (6H), 7.52 – 7.48 (m, 8H), 7.39 (dd, *J* = 8.4, 1.7 Hz, 4H), 7.27 (d, *J* = 8.4 Hz, 4H), 7.00 – 6.94 (m, 8H), 4.56 (t, *J* = 7.3 Hz, 8H), 4.14 – 4.11 (m, 8H), 3.93 – 3.90 (m, 8H), 3.79 – 3.76 (m, 8H), 3.74 (dt, *J* = 6.0, 2.0 Hz, 8H), 1.60 – 1.52 (m, 8H), 1.01 – 0.91 (m, 8H), 0.59 (t, *J* = 7.4 Hz, 12H). ^{13}C-NMR (126 MHz, $CDCl_3$) δ 158.16, 150.49, 150.01, 143.35, 138.05,

135.97, 135.40, 134.18, 128.26, 125.50, 123.11, 117.86, 115.02, 110.45, 70.91, 69.79, 67.65, 44.58, 32.07, 19.74, 13.54, 13.45. MALDI MS: 1553.1 ([M]+Na^+).

2.6.3 Synthesis of 2.3

2.2 (1g, 1.64mmol) and K_2CO_3 (9.10 g, ~4eq) were added to a 100mL RBF which was purged

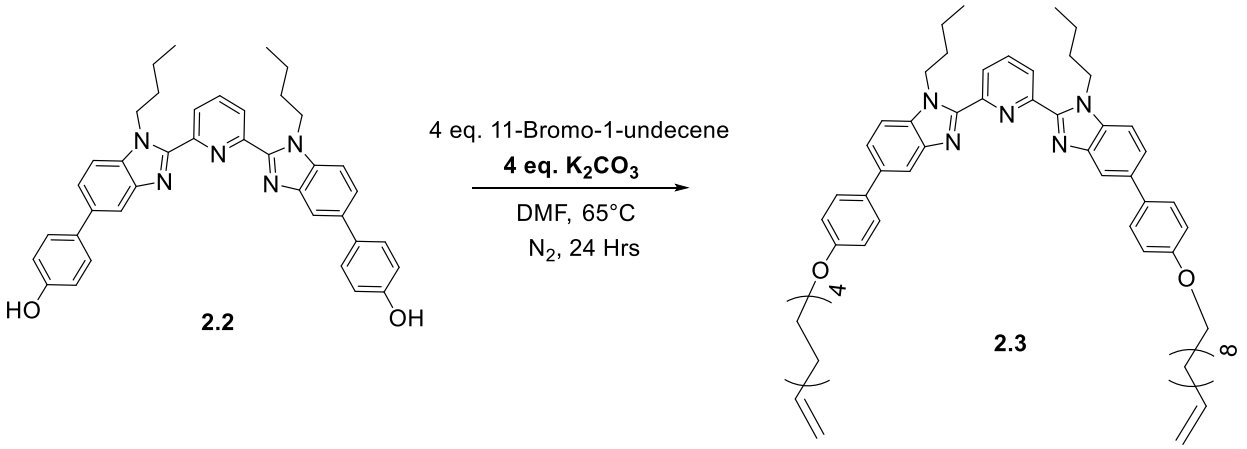

with N_2. To this mixture was added DMF (26 mL) and11-bromo-1-undecene (1.52 g, 4 eq.). The subsequent mixed was stirred at 65°C for 24 h. After this time the solvent was removed under reduced pressure leaving a yellow residue. This residue was washed with chloroform (4 × 150 mL) and filtered. The filtrate was collected and the solvent removed under reduced pressure. The resulting material was purified using column chromatography (TEA treated silica gel, chloroform to 5% methanol in chloroform gradient as eluent, followed by recrystallization (chloroform/methanol mixture) to yield off-white crystals of **2.3** in 70% yield. ^{1}H NMR (500 MHz, $CDCl_3$) δ 8.35 (d, *J* = 7.8Hz, 2H), 8.03 (t, *J* = 7.9Hz, 1H), 8.00 (s, 2H), 7.62-7.57 (m, 6H), 7.51 (d, *J* = 7.2Hz, 2H), 7.02-6.98 (m, 4H), 5.85 (m, 2H), 4.97 (m, 4H), 4.78 (q, *J* = 7.2 Hz, 4H), 4.04 (t, 4H), 2.06 (m, 4H), 1.81 (m, 4H), 1.76 (m, 4H), 1.48 (m, 4H), 1.30 (m, 8H), 1.12 (m, 4H), 0.72 (t, *J* =7.2 Hz, 6H). MALDI MS: 913.2 ([M]+H^+).

2.6.4 Synthesis of 2.7

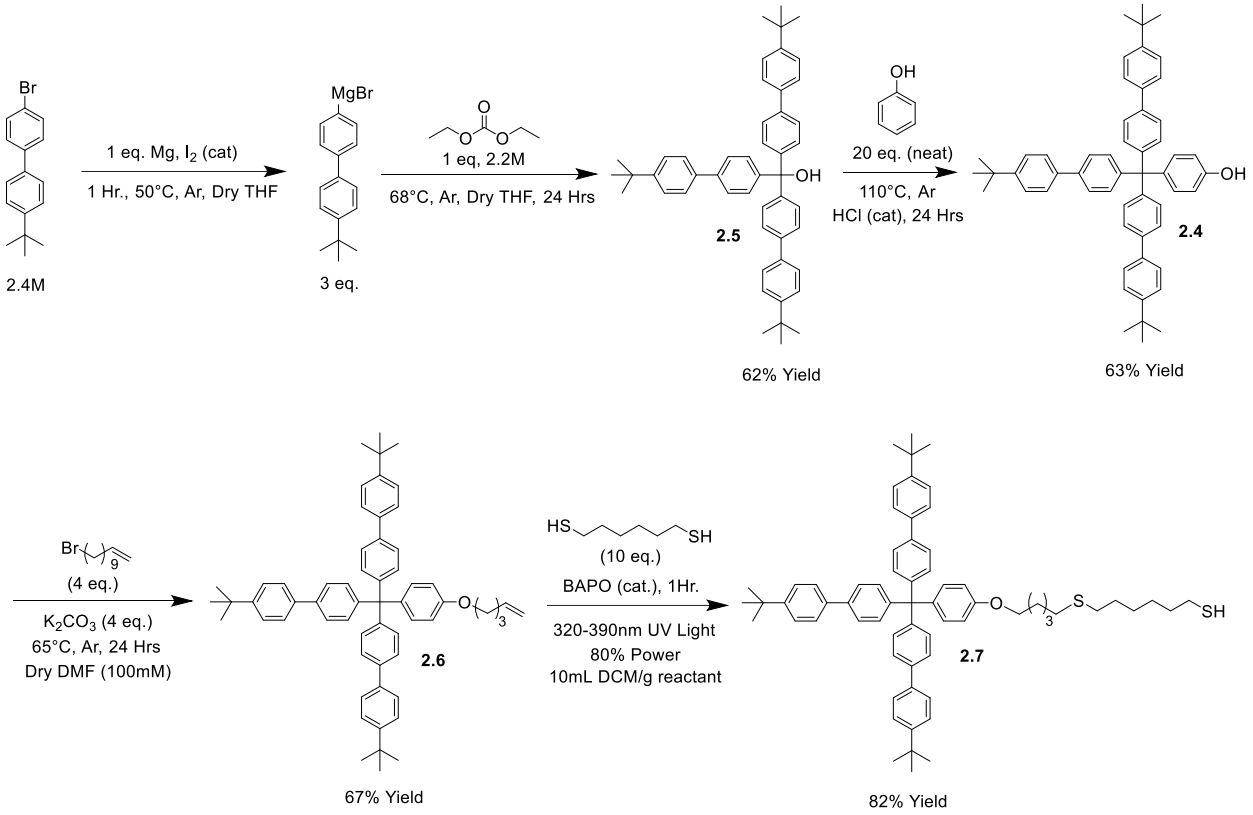

Synthetic work for thiol stopper group done in collaboration with Dr. Katie Herbert and Dr. Eric Bruckner. An oven dried 3-neck 500 mL RBF was charged with Mg turnings (1.67 g, 68.6 mmol), I_2(10 mg) and THF (30 mL) under an Ar atmosphere and stirred at 50 °C. A solution of 4-bromo-4'-tert-butylbiphenyl (13.21 g 45.7 mmol) in THF (60mL) was prepared in an addition funnel and added to the RBF over 15 min. Once the bromide was completely added the reaction was stirred under reflux for an additional 90 min. After this time the reaction mixture was cooled to RT and a solution of diethyl carbonate (1.85 mL, 15.2 mmol) in THF (7 mL) was added. The reaction was then heated under reflux for 18 h. After this time the reaction was cooled to RT, quenched with 1M HCl (60 mL) and filtered. To the filtrate was added hexanes (2 × 75 mL) and H_2O (50 mL). The organic layer was washed with brine (2 × 200 mL), dried with $MgSO_4$ and subsequently concentrated under reduced pressure to yield an off-white solid, **2.5**, in a 71% yield. ^{1}H-NMR (500

MHz, $CDCl_3$) δ 7.59-7.55 (d overlap, J = 8.4 Hz, 12H), 7.47 (d, J = 8.4 Hz, 6H), 7.43 (d, J = 8.4 Hz, 6H), 1.37 (s, 27H). $^{13}C\{^1H\}$ NMR (126 MHz, $CDCl_3$) δ 150.47, 145.70, 140.10, 137.86, 128.46, 126.87, 126.69, 125.86, 81.88, 34.68, 31.52. MALDI-MS: 679.6 ($[M]+Na^+$) and 639.7 ($[M] – OH^-$).

To an argon filled 100 mL RBF was added **2.5** (4.50 g, 6.8 mmol), phenol (14 mL of an 89% phenol solution in H_2O) and conc. HCl (1mL, 12M). The reaction mixture was stirred and heated at 110 °C for 22 h. The reaction mixture was subsequently cooled to RT, diluted with toluene (~200 mL) and washed with 1x200mL 1M NaOH followed by 2x200mL H_2O. Dried organic phase over magnesium sulfate and removed solvent under reduced pressure resulting in a yellow crude solid. Boiled solid in 200mL hexanes and filtered (3 times) resulting in an off-white solid, **2.4**, in 79% yield. ^1H NMR (500 MHz, $CDCl_3$) δ 7.55 (d, *J* = 8.5 Hz, 6H), 7.51 (d, *J* = 8.5 Hz, 6H), 7.45 (d, *J* = 8.5 Hz, 6H), 7.32 (d, *J* = 8.5 Hz, 6H), 7.18 (d, *J* = 8.8 Hz, 2H), 6.77 (d, *J* = 8.8 Hz, 2H), 4.73 (s, 1H), 1.37 (s, 27H). $^{13}C\{^1H\}$ NMR (126 MHz, $CDCl_3$) δ 153.64, 150.30, 145.91, 139.41, 138.54, 137.83, 132.59, 131.58, 126.73, 126.07, 125.82, 114.47, 63.79, 34.67, 31.52. MALDI-MS: 841.1 ($[M]+Ag^+$).

2.4 (0.5g, 0.68mmol) was reacted with 0.63 g (4 eq., 2.72 mmol, 0.60 mL) 5-bromo-1-pentene (0.63g, 2.72 mmol) and potassium carbonate (0.38g, 2.72 mmol) in DMF (0.10 M) at 65°C under argon atmosphere. All reactants were placed in a round bottom flask (equipped with stir bar and condenser). The system was then flushed with argon and reacted at 65°C for 24 hours while stirring. Upon completion of the reaction, the product was extracted with DCM and washed with deionized water. Solvent was removed through rotary evaporation and excess heptane was added to facilitate the removal of DMF. Product was further purified through silica gel column chromatography with a 5:2 solution of hexane/DCM to obtain **2.6** in 80% yield. ^1H-NMR (500

MHz $CDCl_3$ δ 7.55 (*d*, 6H), 7.50 (*d*, 6H), 7.45 (*d*, 6H), 7.30 (*d*, 6H), 7.20 (*d*, 2H), 6.82 (*d*, 2H), 5.86 (*m*, 1H), 5.07 (*d*, 1H), 5.00 (*d*, 1H), 3.97 (*t*, 2H), 2.24 (*m*, 2H), 1.88 (*m*, 2H), 1.35 (*s*, 27H). MALDI-MS: 909.1 ([M]+Ag^+).

2.6 (100mg, 174.3 μmol) and 1,6-hexanedithiol (262mg, 17.4 mmol) were dissolved in 14.4 mL (10 mL/g) DCM in a 25 mL round bottom flask equipped with a stir bar. A catalytic quantity of the photoinitiator BAPO (Phenylbis(2,4,6-trimethylbenzoyl)phosphine oxide) was added to the mixture. The flask was capped with a balloon and exposed to high intensity UV light (320-390 nm, 50 mW/cm^2) for 1 hour. The product was precipitated in cold (-18°C) hexanes overnight and **2.7** was isolated via vacuum filtration in 75% yield. ^{1}H-NMR (500 MHz $CDCl_3$ δ 7.54 (*d*, 6H), 7.49 (*d*, 6H), 7.44 (*d*, 6H), 7.31 (*d*, 6H), 7.19 (*d*, 2H), 6.80 (*d*, 2H), 3.95 (*t*, 2H), 2.49-2.54 (m, 6H), 1.79 (*m*, 2H), 1.50-1.67 (m, 9H), 1.39 (*m*, 3H), 1.35 (*s*, 27H). MALDI-MS (973.5, [M]+Na^+).

2.7 References

(1) Wu, Q.; Rauscher, P. M.; Lang, X.; Wojtecki, R. J.; De Pablo, J. J.; Hore, M. J. A.; Rowan, S. J. Poly[n]Catenanes: Synthesis of Molecular Interlocked Chains. *Science (80-.).* **2017**, *358* (6369), 1434–1439. https://doi.org/10.1126/science.aap7675.

(2) Tranquilli, M. M.; Wu, Q.; Rowan, S. J. Effect of Metallosupramolecular Polymer Concentration on the Synthesis of Poly[n]Catenanes . *Chem. Sci.* **2021**. https://doi.org/10.1039/d1sc02450g.

(3) Wojtecki, R. J.; Wu, Q.; Johnson, J. C.; Ray, D. G.; Korley, L. S. T. J.; Rowan, S. J. Optimizing the Formation of 2,6-Bis(N-Alkyl-Benzimidazolyl)Pyridine-Containing [3]Catenates through Component Design. *Chem. Sci.* **2013**, *4* (12), 4440–4448. https://doi.org/10.1039/c3sc52082j.

(4) Xue, M.; Yang, Y.; Chi, X.; Yan, X.; Huang, F. Development of Pseudorotaxanes and Rotaxanes: From Synthesis to Stimuli-Responsive Motions to Applications. *Chem. Rev.* **2015**, *115* (15), 7398–7501. https://doi.org/10.1021/cr5005869.

(5) McGonigal, P. R. Multiply Threaded Rotaxanes. *Supramol. Chem.* **2018**, *30* (9), 782–794. https://doi.org/10.1080/10610278.2018.1433832.

(6) Klotz, E. J. F.; Claridge, T. D. W.; Anderson, H. L. Homo- and Hetero-[3]Rotaxanes with

Two π-Systems Clasped in a Single Macrocycle. *J. Am. Chem. Soc.* **2006**, *128* (48), 15374–15375. https://doi.org/10.1021/ja0665139.

(7) Prikhod'ko, A. I.; Durola, F.; Sauvage, J. P. Iron(II)-Templated Synthesis of [3]Rotaxanes by Passing Two Threads through the Same Ring. *J. Am. Chem. Soc.* **2008**, *130* (2), 448–449. https://doi.org/10.1021/ja078216p.

(8) Prikhod'ko, A. I.; Sauvage, J. P. Passing Two Strings through the Same Ring Using an Octahedral Metal Center as Template: A New Synthesis of [3]Rotaxanes. *J. Am. Chem. Soc.* **2009**, *131* (19), 6794–6807. https://doi.org/10.1021/ja809267z.

(9) Cheng, H. M.; Leigh, D. A.; Maffei, F.; McGonigal, P. R.; Slawin, A. M. Z.; Wu, J. En Route to a Molecular Sheaf: Active Metal Template Synthesis of a [3]Rotaxane with Two Axles Threaded through One Ring. *J. Am. Chem. Soc.* **2011**, *133* (31), 12298–12303. https://doi.org/10.1021/ja205167e.

(10) Yamashita, Y.; Mutoh, Y.; Yamasaki, R.; Kasama, T.; Saito, S. Synthesis of [3]Rotaxanes That Utilize the Catalytic Activity of a Macrocyclic Phenanthroline-Cu Complex: Remarkable Effect of the Length of the Axle Precursor. *Chem. - A Eur. J.* **2015**, *21* (5), 2139–2145. https://doi.org/10.1002/chem.201405090.

(11) Hayashi, R.; Mutoh, Y.; Kasama, T.; Saito, S. Synthesis of [3]Rotaxanes by the Combination of Copper-Mediated Coupling Reaction and Metal-Template Approach. *J. Org. Chem.* **2015**, *80* (15), 7536–7546. https://doi.org/10.1021/acs.joc.5b01120.

(12) Danon, J. J.; Leigh, D. A.; McGonigal, P. R.; Ward, J. W.; Wu, J. Triply Threaded [4]Rotaxanes. *J. Am. Chem. Soc.* **2016**, *138* (38), 12643–12647. https://doi.org/10.1021/jacs.6b07733.

(13) Movsisyan, L. D.; Franz, M.; Hampel, F.; Thompson, A. L.; Tykwinski, R. R.; Anderson, H. L. Polyyne Rotaxanes: Stabilization by Encapsulation. *J. Am. Chem. Soc.* **2016**, *138* (4), 1366–1376. https://doi.org/10.1021/jacs.5b12049.

(14) Saito, S.; Nakazono, K.; Takahashi, E.; April, R. V. Template Synthesis of [2] Rotaxanes with Large Ring Components and Tris (Biphenyl) Methyl Group as the Blocking Group . The Relationship between the Ring Size and the Stability of the Rotaxanes Our Recent Interest in the Chemistry of Rotaxanes Prompte. *J. Org. Chem.* **2006**, *71* (19), 7477–7480.

(15) Saito, S.; Takahashi, E.; Wakatsuki, K.; Inoue, K.; Orikasa, T.; Sakai, K.; Yamasaki, R.; Mutoh, Y.; Kasama, T. Erratum: Synthesis of Large [2]Rotaxanes. the Relationship between the Size of the Blocking Group and the Stability of the Rotaxane (Journal of Organic Chemistry (2013) 8 (3553-3560)DOI: 10.1021/Jo302800t). *J. Org. Chem.* **2013**, *78* (11), 5816. https://doi.org/10.1021/jo4010052.

(16) Asakawa, M.; Ashton, P. R.; Ballardini, R.; Balzani, V.; Bělohradský, M.; Gandolfi, M. T.; Kocian, O.; Prodi, L.; Raymo, F. M.; Stoddart, J. F.; Venturi, M. The Slipping Approach to Self-Assembling [n]Rotaxanes. *J. Am. Chem. Soc.* **1997**, *119* (2), 302–310. https://doi.org/10.1021/ja961817o.

(17) Evans, N. H. Recent Advances in the Synthesis and Application of Hydrogen Bond Templated Rotaxanes and Catenanes. *European J. Org. Chem.* **2019**, No. 21, SI, 3320–

3343. https://doi.org/10.1002/ejoc.201900081.

(18) Nepogodiev, S. A.; Stoddart, J. F. Cyclodextrin-Based Catenanes and Rotaxanes. *Chem. Rev.* **1998**, *98* (5), 1959–1976. https://doi.org/10.1021/cr970049w.

(19) Wisner, J. A.; Beer, P. D.; Drew, M. G. B.; Sambrook, M. R. Anion-Templated Rotaxane Formation. *J. Am. Chem. Soc.* **2002**, *124* (42), 12469–12476. https://doi.org/10.1021/ja027519a.

(20) Beves, J. E.; Blight, B. A.; Campbell, C. J.; Leigh, D. A.; McBurney, R. T. Strategies and Tactics for the Metal-Directed Synthesis of Rotaxanes, Knots, Catenanes, and Higher Order Links. *Angew. Chemie - Int. Ed.* **2011**, *50* (40), 9260–9327. https://doi.org/10.1002/anie.201007963.

(21) Lewis, J. E. M.; Beer, P. D.; Loeb, S. J.; Goldup, S. M. Metal Ions in the Synthesis of Interlocked Molecules and Materials. *Chem. Soc. Rev.* **2017**, *46* (9), 2577–2591. https://doi.org/10.1039/c7cs00199a.

(22) Inthasot, A.; Tung, S. Te; Chiu, S. H. Using Alkali Metal Ions to Template the Synthesis of Interlocked Molecules. *Acc. Chem. Res.* **2018**, *51* (6), 1324–1337. https://doi.org/10.1021/acs.accounts.8b00071.

(23) McKenzie, B. M.; Miller, A. K.; Wojtecki, R. J.; Johnson, J. C.; Burke, K. A.; Tzeng, K. A.; Mather, P. T.; Rowan, S. J. Improved Synthesis of Functionalized Mesogenic 2,6-Bisbenzimidazolylpyridine Ligands. *Tetrahedron* **2008**, *64* (36), 8488–8495. https://doi.org/10.1016/j.tet.2008.05.075.

(24) Hoyle, C. E.; Bowman, C. N. Thiol-Ene Click Chemistry. *Angew. Chemie - Int. Ed.* **2010**, *49* (9), 1540–1573. https://doi.org/10.1002/anie.200903924.

(25) Rowan, S. J.; Beck, J. B. Metal-Ligand Induced Supramolecular Polymerization: A Route to Responsive Materials. *Faraday Discuss.* **2005**, *128*, 43–53. https://doi.org/10.1039/b403135k.

Chapter 3: Metastable Doubly Threaded [3]Rotaxanes With Varying Stopper Size

-Chapter adapted from: Hertzog, J.E., Maddi, V. J., Hart, L. F., Rawe, B. W., Rauscher, P. M., Herbert, K. M., Bruckner, E. P., de Pablo, J. J., and Rowan, S. J. *Chemical Science.* **2022**, *13*, *5333-5344.*

3.1 Introduction

Even after multiple decades of research, mechanically interlocked molecules (MIMs) continue to inspire chemists and engineers alike on account of their unique interlocked structure and properties.[1–5] Specifically, the synthesis and study of rotaxanes, which are interlocked molecules comprised of dumbbell and ring components, account for over two thirds of all publications involving MIMs.[6,7] This popularity, which is in part a result of their synthetic accessibility, has resulted in their use in a wide range of applications that include molecular machines, catalysis, molecular computing, and drug delivery, to name a few.[8–15] The simplest and most-investigated version of a rotaxane is the singly threaded [2]rotaxane comprised of one macrocycle component kinetically trapped between the large stopper groups of the dumbbell-like component.[16,17] However, as the field continues to grow, there is increasing interest in looking towards higher order rotaxanes[6,18] (containing more rings, more dumbbells, or both) and their corresponding mechanically interlocked polymers (MIPs).[19,20] This has led to complex architectures capable of advanced function such as molecular elevators,[21,22] artificial molecular muscles,[23,24] molecular pulleys,[25] and more.[9] In addition, polyrotaxane-based materials, such as slide-ring gels,[26,27] have attracted great interest on account of their unique property profiles which have, for example, been commercialized into scratch-resistant coatings.[28] In these materials (and

MIPs more broadly), macrocycle size variation has emerged as an important design parameter[19,29–31] with preliminary studies indicating that fluorescence quenching[32] and viscoelastic relaxation dynamics[33] can be tuned by controlling the size of the ring component. As such, there is interest in accessing interlocked polymeric systems with larger rings for further tunability. However, in the literature there appears to be an upper boundary in the size of the macrocycles (around 40 atoms) that are used to synthesize the majority of rotaxane-like structures.

Synthetic efforts targeted at accessing rotaxanes with bigger rings have revealed that even relatively small increases in macrocycle size necessitate dramatic increases in stopper group size.[34,35] Furthermore, investigations into the interlocked stability of rotaxanes have shown that depending on the relative size of the stopper and ring,[36–41] some of these interlocked structures are in fact environmentally-dependent metastable rotaxanes,[42] in which the macrocycle is able to slowly slip over the stoppering moiety resulting in the non-interlocked components. Controlling environmental conditions such as temperature, pH, and solvent polarity combined with this unique feature of metastable rotaxanes has been utilized in controlled release applications.[43–45] Furthermore, metastable rotaxanes have been employed in the development of molecular pumps,[46–49] chemical protection,[50–52] modifiable molecular containers,[53] and bacterial imaging probes.[54]

All of the rotaxane materials discussed above are based on singly-threaded architectures. Threading multiple dumbbells within the same macrocyclic cavity offers the unique ability to ensure their close spatial proximity allowing for their physical and optical properties to be influenced.[6] However, doubly threaded [3]rotaxanes have proven extremely challenging from a synthetic standpoint[6] leading to only limited exploration of the corresponding MIPs and higher order rotaxanes.[55–58] As larger macrocycles are typically required to incorporate multiple threads,

the difficulty, at least in part, stems from ensuring that the stopper size is large enough to stabilize the interlocked architecture. For example, work by Leigh and coworkers showed that it was possible to access a stable [3]rotaxane with a 38 atom macrocycle, however changing the ring size by just one atom (to 39 atoms) resulted in no isolatable interlocked product.[59] As a result, molecular doubly threaded [3]rotaxanes where both threads exist in a single ring have seen limited high yielding syntheses with reported isolated yields between 6-70%.[59–66] In addition, the largest reported macrocycle size used to access such a [3]rotaxane is 41 atoms and the resulting interlocked compound exhibited slow slippage in solution ($t_{1/2}$ ~ 1 week at 298K in dichloromethane).[62] With the goal of accessing multiply threaded higher ordered MIMs and MIPs (doubly threaded poly[3]rotaxanes in particular) and developing a better understanding of how to control the stability (and therefore utility) of such structures, reported in this chapter are studies aimed at targeting doubly threaded metastable [3]rotaxanes with a large 46 atom macrocycle and similar thread components to Chapter 2 (Fig 3.1) derived from the same Bip framework.

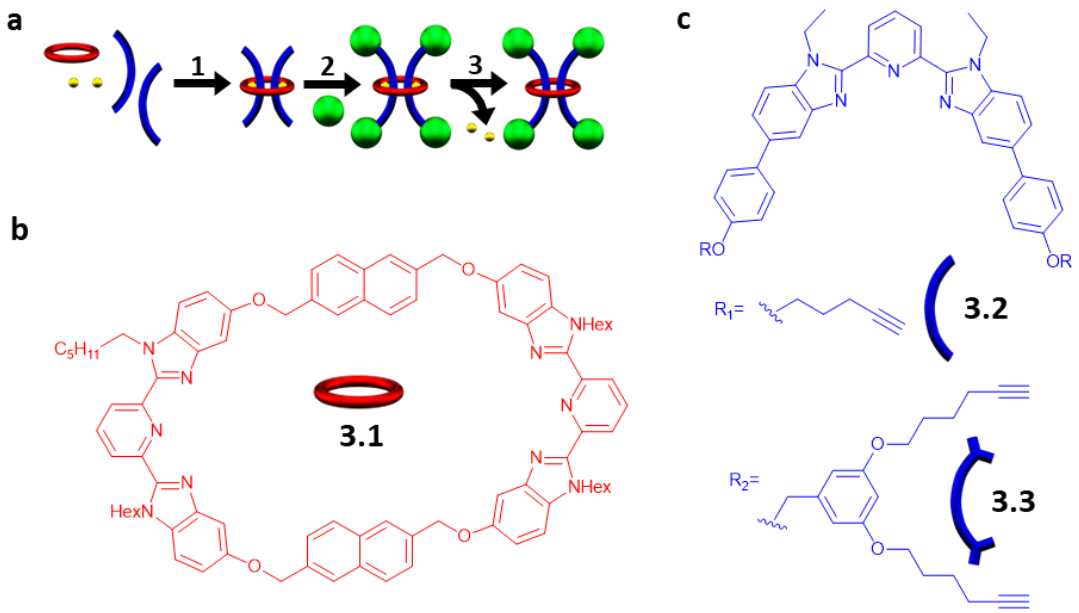

Fig 3.1 a) Cartoon scheme of the doubly threaded [3]rotaxane synthesis that involves metalation of the components with Fe(II) (Step 1) followed by addition of the stopper group (Step 2) and finally demetallation (Step 3). b) Chemical structure of the Bip containing 46 atom macrocycle **3.1** and c) thread components **3.2** and **3.3**.

3.2 Component Synthesis and Design

Metal-directed self-assembly of the macrocycle with two thread-like components followed by stoppering and demetallation was used to access the [3]rotaxanes (Fig 3.1). Initial studies in Chapter 2 used a large 68 atom macrocycle that was solely based on previous poly[n]catenane work in the group. As noted in the introduction of this chapter, 68 atoms is significantly larger than any macrocycle used in rotaxane synthesis and the successful stabilization of this macrocycle with stopper groups is most likely extremely difficult. As such, this chapter focuses on a 46 atom ring based on the same Bip framework that is larger than what has been reported in literature (but to a more reasonable extent). A Williamson ether ring closing reaction using a hexyl-substituted Bip ligand (**3.4**) and 2,6-bis(bromomethyl)naphthalene in dilute conditions yielded the macrocycle **3.1** in 20-25% yield (Figure 3.2).

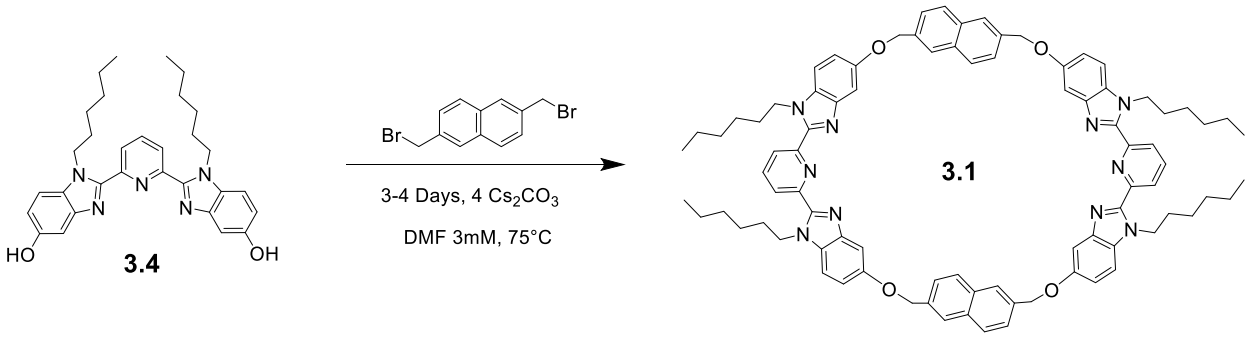

Fig 3.2 Scheme showing synthesis of 46 atom macrocycle component **3.1**.

The *N*-hexyl substituted Bip ligand was chosen to aid solubility of the macrocycle. The rigidity present in the macrocycle was designed to prevent both Bip ligands in **3.1** binding to the same metal ion and ensure that the only way for these ligands to form 2:1 Bip:metal complexes is in the presence of the threads. This was confirmed by a UV metal titration of **3.1** which clearly shows visible absorption changes upon metal addition to **3.1** at 378nm until 2 metal equivalents (relative to **3.1**) are reached (Fig 3.3). Further metal addition results in negligible absorption increase.

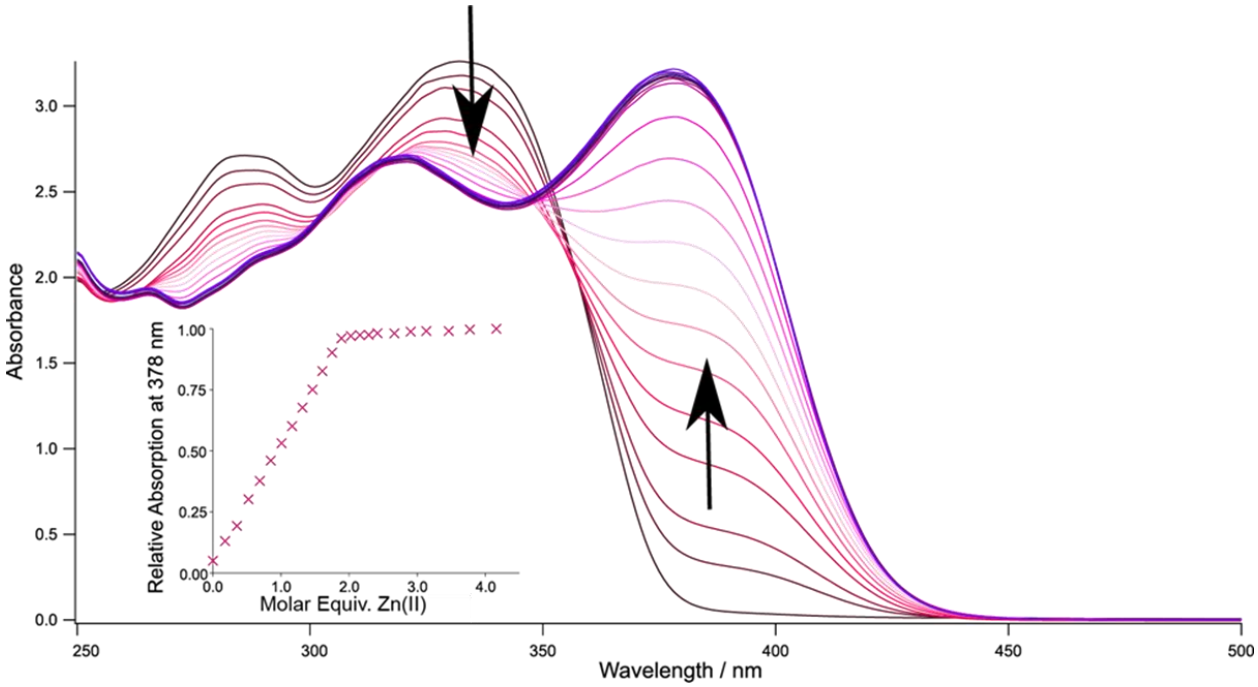

Fig 3.3 UV/Vis titration of **3.1** with Zn(II), inset shows absorbance at 378nm.

The linear thread components (**3.2** and **3.3**, Figure 3.1) are similarly derived from Bip but are monotopic in order to ensure one thread each can bind with both ligands in **3.1**. In addition, **3.2** and **3.3** are derived from an *N*-ethyl substituted Bip ligand (as opposed to Hexyl in **3.1**) to minimize steric repulsion between the thread molecules when both are bound within macrocycle. Briefly, **3.2** is made in one step from the hydroxyl terminated Bip ligand **3.5** via standard Williamson Ether conditions to yield **3.2** (Fig 3.4) which is alkyne terminated in order to allow azide-alkyne cycloaddition[67,68] as the stoppering chemistry. A second thread molecule (**3.3**) was also synthesized that contained double the amount of end alkyne groups as **3.2**. 3,5-Dihydroxybenzyl alcohol was reacted with 6-chloro-1-hexyne under Williamson ether conditions to yield **3.6** which was chlorinated at the benzyl alcohol position to give **3.7** (Fig 3.4). The Bip ligand **3.5** was then reacted with **3.7** under standard Williamson ether conditions to give the second thread molecule **3.3** (Fig 3.4). The synthesis of these two different thread molecules will allow differing amounts of stopper group to be attached.

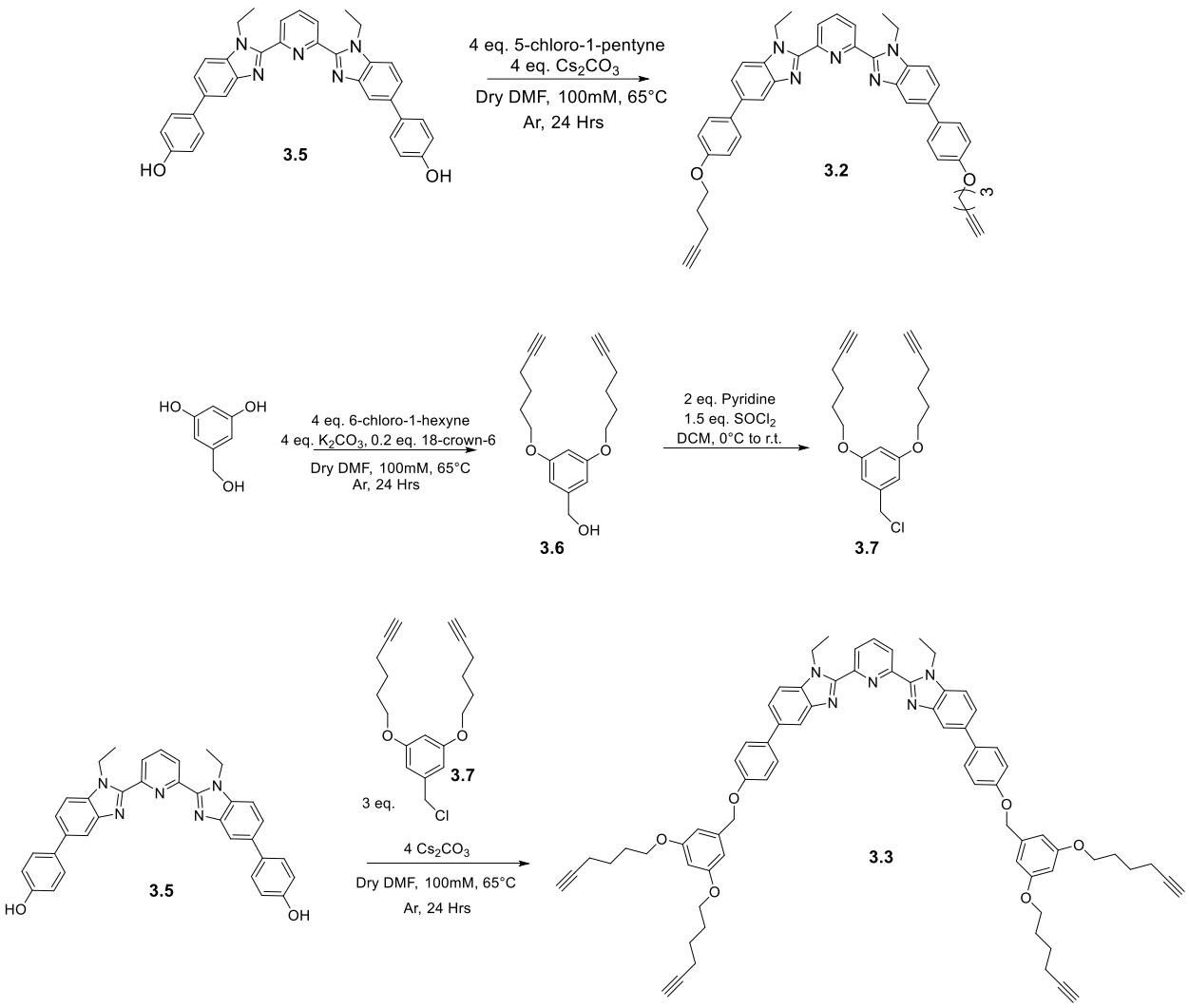

Fig 3.4 Scheme showing synthesis of thread components **3.2** and **3.3.**

Two different size stopper groups were synthesized in order to see how large of a stopper group would be needed to keep the 46 atom ring **3.1** stable (Fig 3.5). Both were end functionalized with an azide to react with the alkyne terminated thread components using azide-alkyne cycloaddition[67,68] chemistry. Briefly, stopper group **2.4** (synthetic details in chapter 2) was reacted with 2-(2-chloroethoxy)ethanol under Williamson ether conditions to yield **3.8**. The terminal hydroxyl group on **3.8** was then converted to a tosylate to yield **3.9** which could be further functionalized to yield the azide terminated **3.10**. in order to form a second, larger stopper, the tosylate end functionalized stopper **3.9** was reacted with the phenolic OH groups in 3,5-

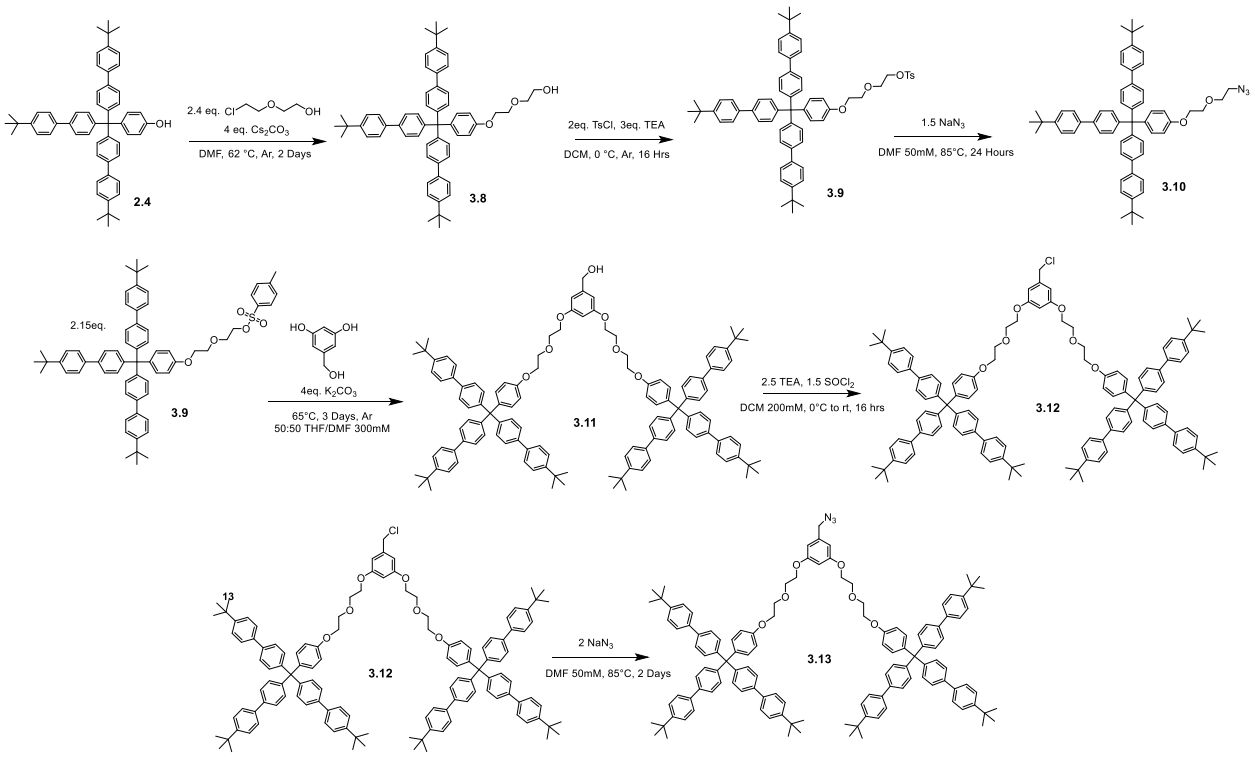

Fig 3.5 Scheme showing synthesis of azide-terminated stopper group components **3.10** and **3.13.**

dihydroxybenzyl alcohol to yield **3.11**. The benzylic hydroxyl group could then be chlorinated (**3.12**) and then finally azidated to yield the azide teriminated "double stopper" **3.13**.

3.3 Assembly of Pesudo[3]rotaxanes

With all of the components for [3]rotaxane assembly in hand, and following the synthetic strategy in Figure 3.1a, initial studies focused on the self-assembly of the ditopic macrocycle **3.1** with thread **3.2** to yield the doubly threaded pseudo[3]rotaxane **3.1:3.2**$_2$**:**Fe(II)$_2$ via metal-templating (Fig 3.6).

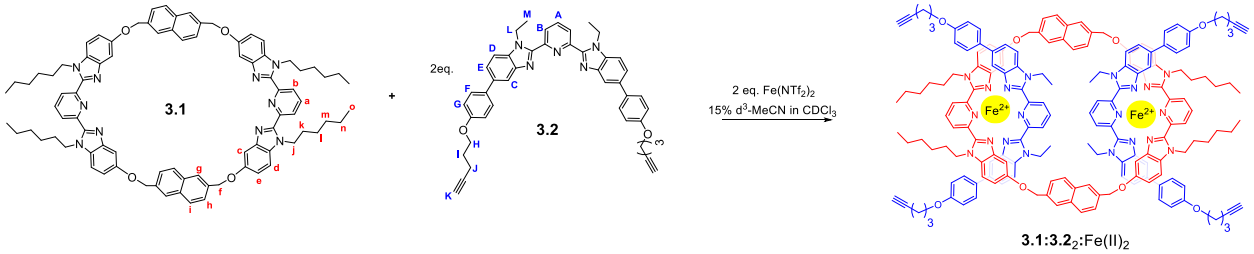

Fig 3.6 Scheme showing formation of **3.1:3.2**$_2$**:**Fe(II)$_2$ from its components**.**

It is important that the doubly threaded pseudo[3]rotaxane self-assembles efficiently upon metal ion addition for the [3]rotaxane to be formed in high yield. Fe(II) ions have been shown to have a high binding constant with Bip ($>10^{10}M^{-2}$)[69] and were therefore employed as the templating agent. Initially, a 2:1 solution of **3.2** and **3.1** in $CDCl_3$ was prepared utilizing ^{1}H-NMR spectroscopy to ensure a 2:1 stoichiometry (Fig 3.7 bottom). Upon addition of $Fe(NTf_2)_2$ to the 2:1 solution an

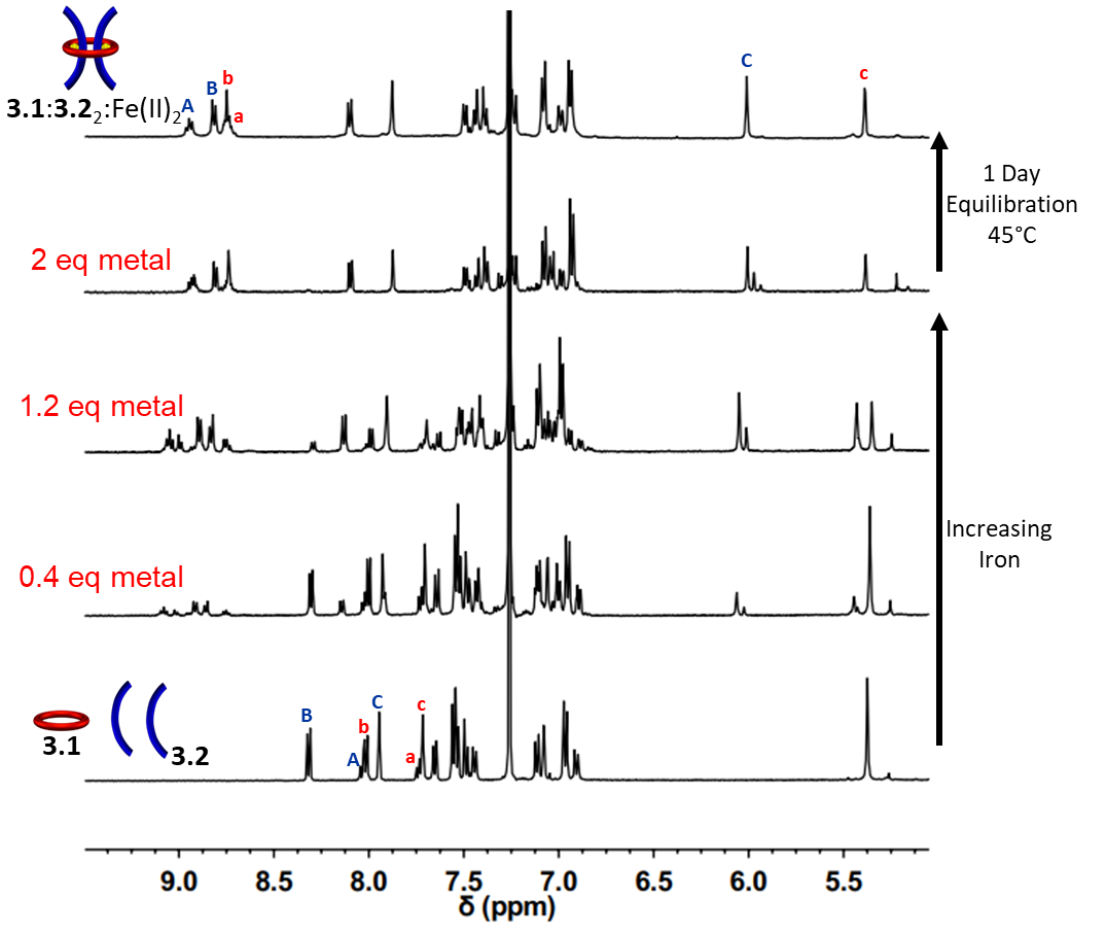

Fig 3.7 Partial ^{1}H-NMR overlay (500 MHz, 25°C, Solvent: 0, 3, 9, 15, 15% d_3-MeCN in $CDCl_3$ increasing upwards) of metal addition and 1 day equilibration. ^{1}H assignments in Fig 3.6.

instantaneous color change from colorless to dark purple is observed, indicative of the newly formed Bip-Fe(II) complexes. Monitoring the metalation by ^{1}H-NMR spectroscopy revealed the appearance of new signals corresponding to the metal ion complexed species and a concomitant decrease in the peak intensities that correspond to unbound **3.1** and **3.2**. The metal ions were

titrated into the sample until no free Bip signals were observed (ca. 2 equiv., Fig 3.7) and the mixture was equilibrated for 1 day at 45 °C. After equilibration, the ^{1}H-NMR spectrum simplified and, using previously published ^{1}H NMR spectra of doubly threaded metal-templated Bip complexes,[70–72] it is possible to assign each resonance peak to a given proton in the complex (Fig 3.8).

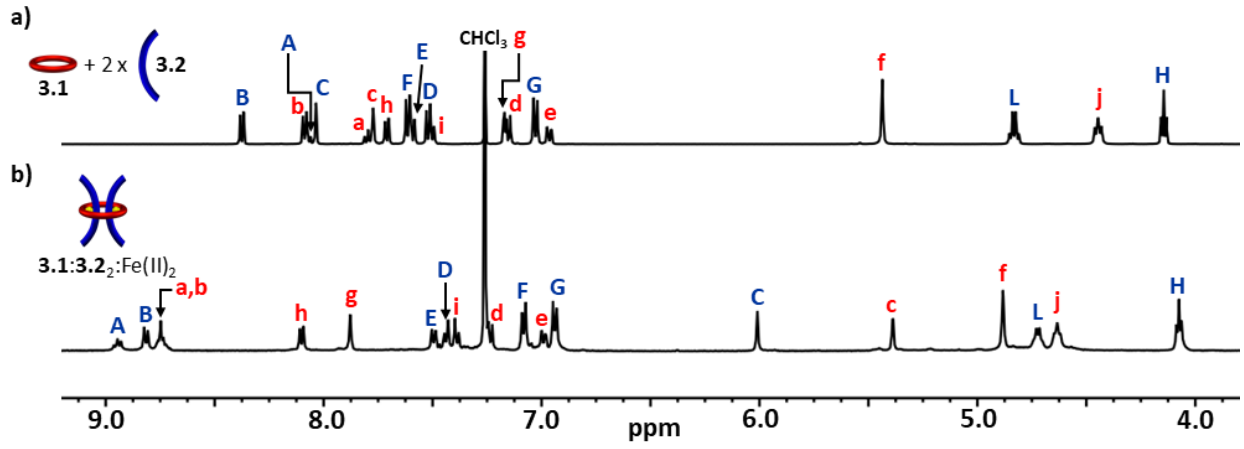

Fig 3.8 Partial ^{1}H-NMR overlay of (a) 2:1 mixture of **3.2**:**3.1** (500 MHz, 25 °C, $CDCl_3$) and (b) **3.1**:**3.2**$_2$:Fe(II)$_2$ (500 MHz, 25 °C, 15% d_3-MeCN in $CDCl_3$) after equilibration for 1 day at 45 °C. See Figure 3.6 for the corresponding ^{1}H assignments.

Similar observations were made using **3.1** with **3.3** following a similar metalation procedure to form a second doubly threaded pseudo[3]rotaxane **3.1**:**3.3**$_2$:Fe(II)$_2$ (Fig 3.9).

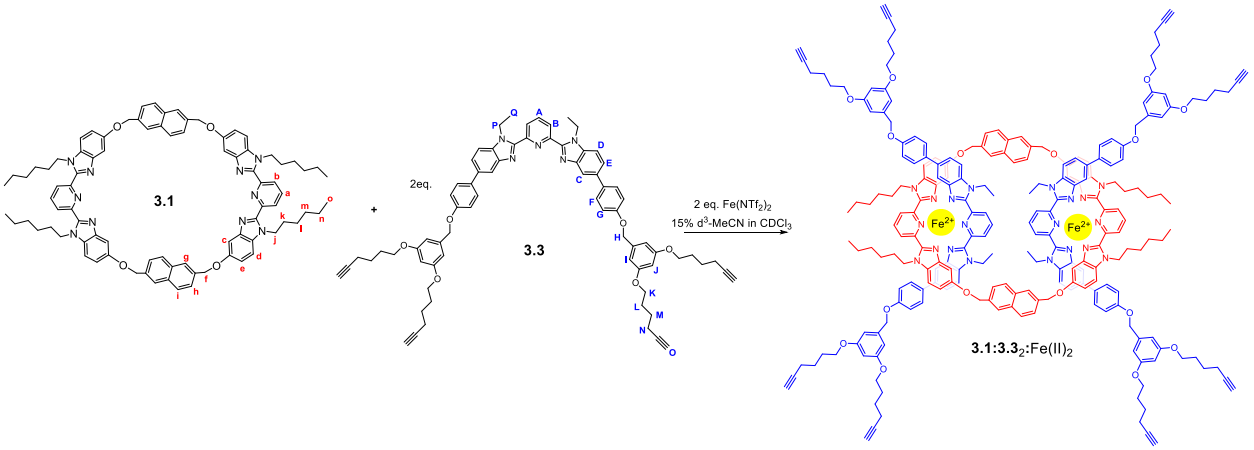

Fig 3.9 Scheme showing formation of **3.1**:**3.3**$_2$:Fe(II)$_2$ from its components.

Addition of two equivalents of iron(II) to an exact 2:1 mixture of **3.3**:**3.1** followed by a 2 day equilibration period at 45°C saw similar ^{1}H-NMR shifting to the results discussed above for **3.1**:**3.3**$_2$:Fe(II)$_2$ (Fig 3.10).

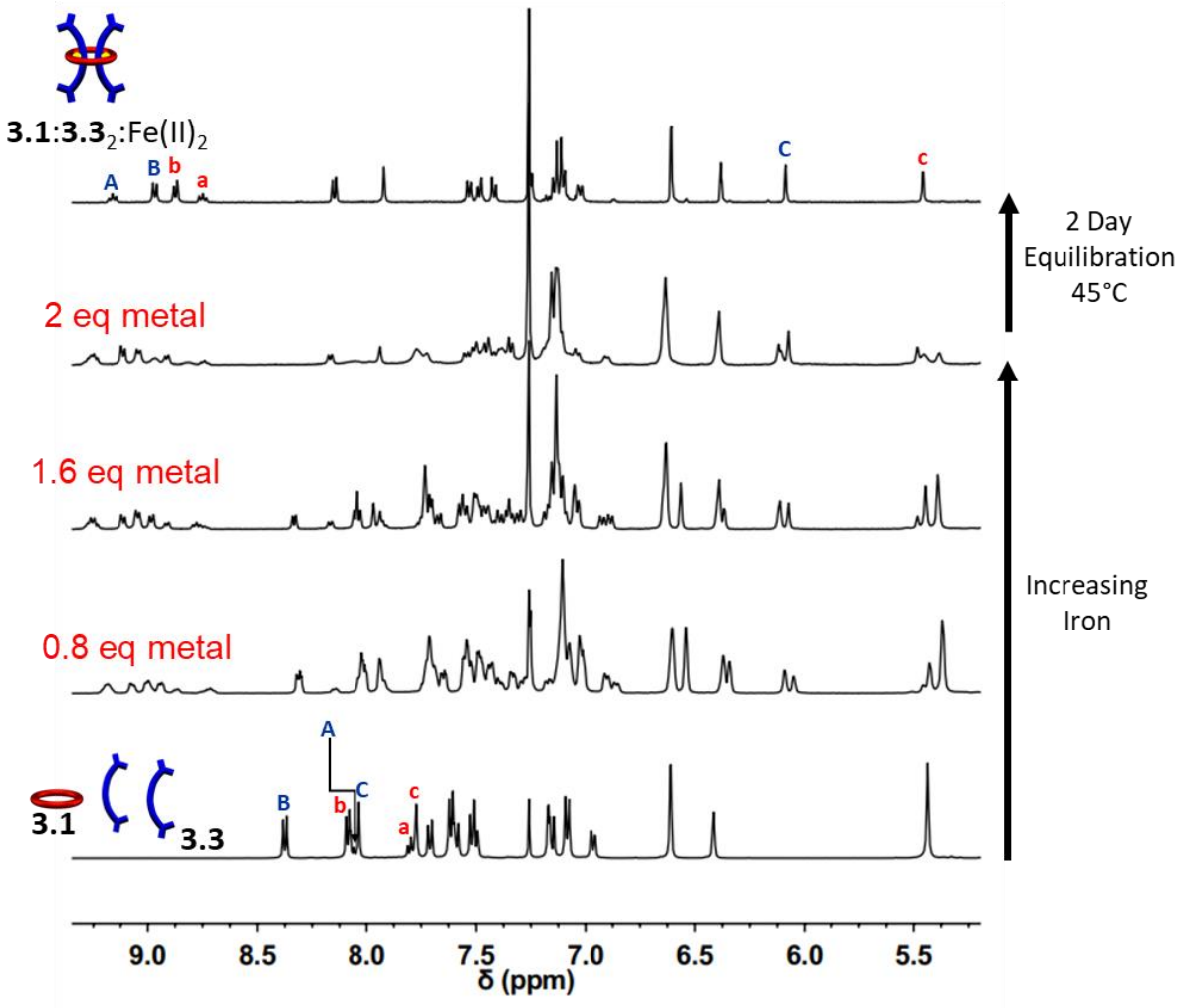

Fig 3.10 Partial ^{1}H-NMR overlay (500 MHz, 25°C, Solvent: 0, 6, 12, 15, 15% d_3-MeCN in $CDCl_3$ increasing upwards) of metal addition and equilibration of 2:1 mixture of **3.3**:**3.1**. ^{1}H assignments from Fig 3.9.

After equilibration, the ^{1}H-NMR spectrum simplified and, using previously published ^{1}H-NMR spectra of doubly threaded metal-templated Bip complexes,[70–72] it is possible to assign each resonance peak to a given proton in the complex **3.1**:**3.3**$_2$:Fe(II)$_2$ (Fig 3.11).

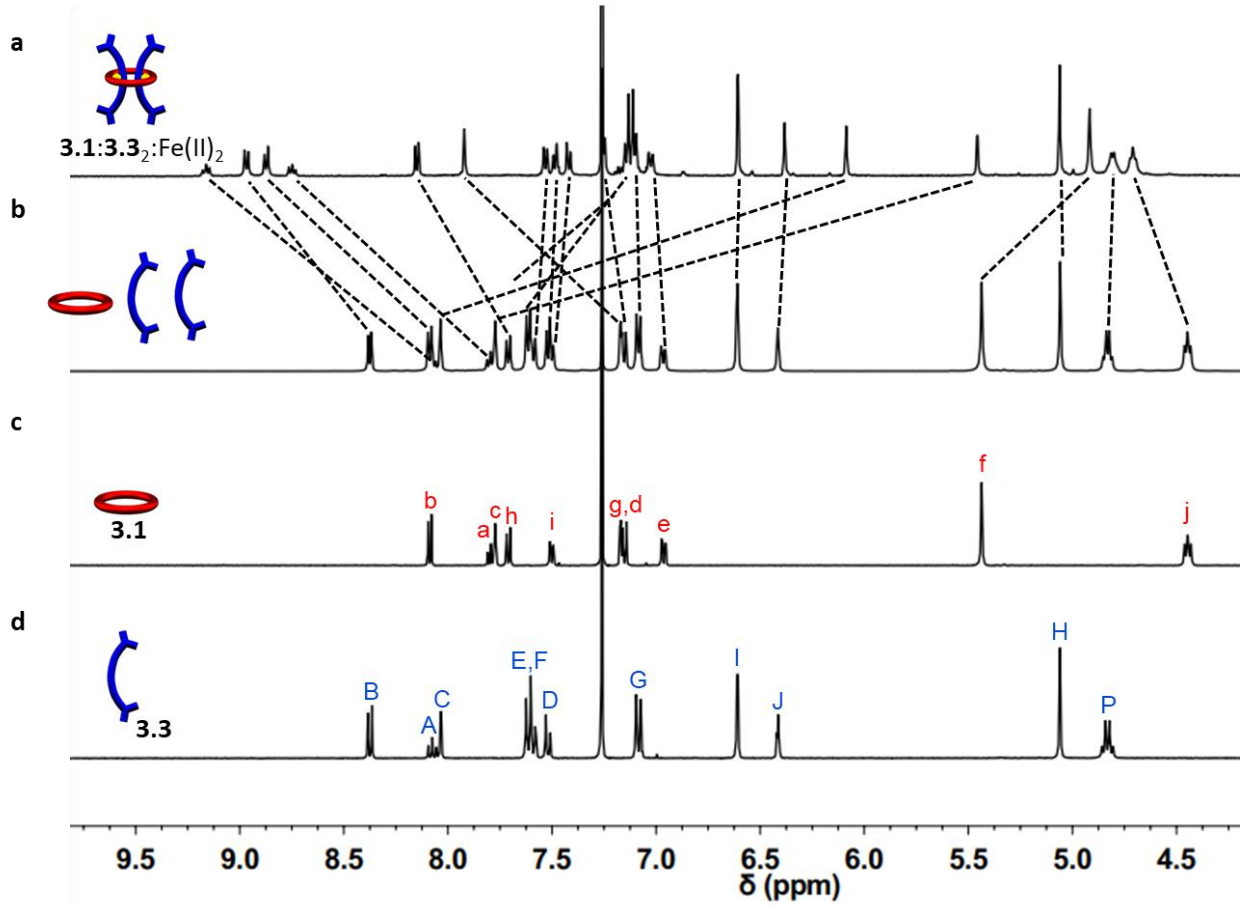

Fig 3.11 Partial ^{1}H-NMR overlay (500 MHz, 25°C)of a) **3.1:3.3$_2$:**Fe(II)$_2$ (15% d$_3$-MeCN in $CDCl_3$), b) 2:1 mixture of **3.3**:**3.1** ($CDCl_3$), c) **3.1** ($CDCl_3$) and d) **3.3** ($CDCl_3$). ^{1}H assignments from Fig 3.9.

3.4 Stoppering Efforts and [3]Rotaxane Characterization

A macrocycle the size of **3.1** had not be used to access a [3]rotaxane before, and as such a key goal of this chapter was to explore different stoppering groups to see what would allow access to isolatable [3]rotaxanes with such a large ring. Initial experiments focused on using the tris(biphenyl)methyl derivative **3.10** as the stoppering moiety (Fig 3.5) as it is analogous in size to the largest stopper groups used in other reported doubly threaded systems.[64,65] To prepare the [3]rotaxanes, a modified literature procedure[61,62] was employed. **3.1**:**3.2**$_2$:Fe(II)$_2$ was stirred in a biphasic (DCM/H_2O) mixture of **3.10** (6 equiv.), $Cu(SO_4)\cdot 5H_2O$ (1 equiv.), and sodium ascorbate

(10 equiv.) overnight at room temperature (Fig 3.12, see experimental for full details including the synthesis of the free dumbbell **3.14**).

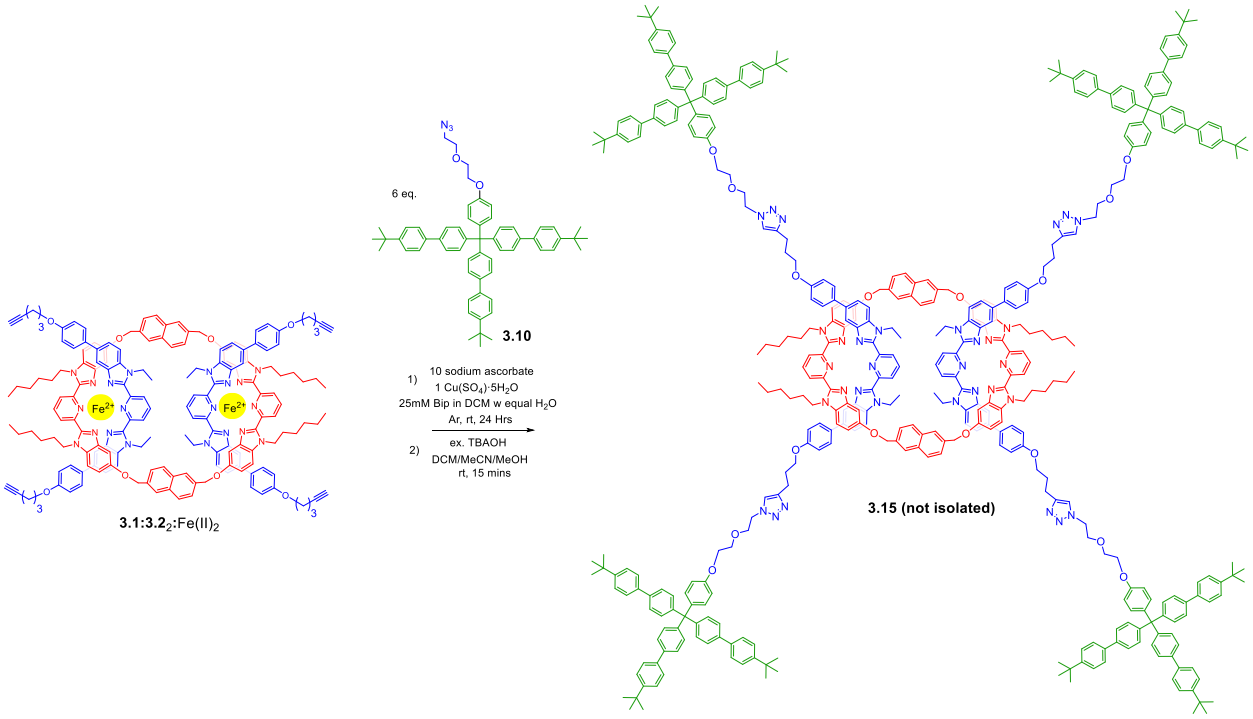

Fig 3.12 Attempted stoppering and demetallation of doubly threaded [3]rotaxane **3.15** (not isolated).

Facile demetallation of the system was achieved using tetrabutylammonium hydroxide as confirmed by a rapid color change of the solution from purple to off-white. The demetallated product was isolated and analyzed immediately. Comparison of the crude demetallated ^{1}H-NMR spectrum relative to the starting components confirmed quantitative consumption of the alkyne signal in **3.2**, and if the ^{1}H NMR spectrum is taken as soon as possible after demetallation (~4 mins), very small signals, upfield from the noninterlocked components, were observed (Fig 3.13) that rapidly disappear within a couple of minutes.

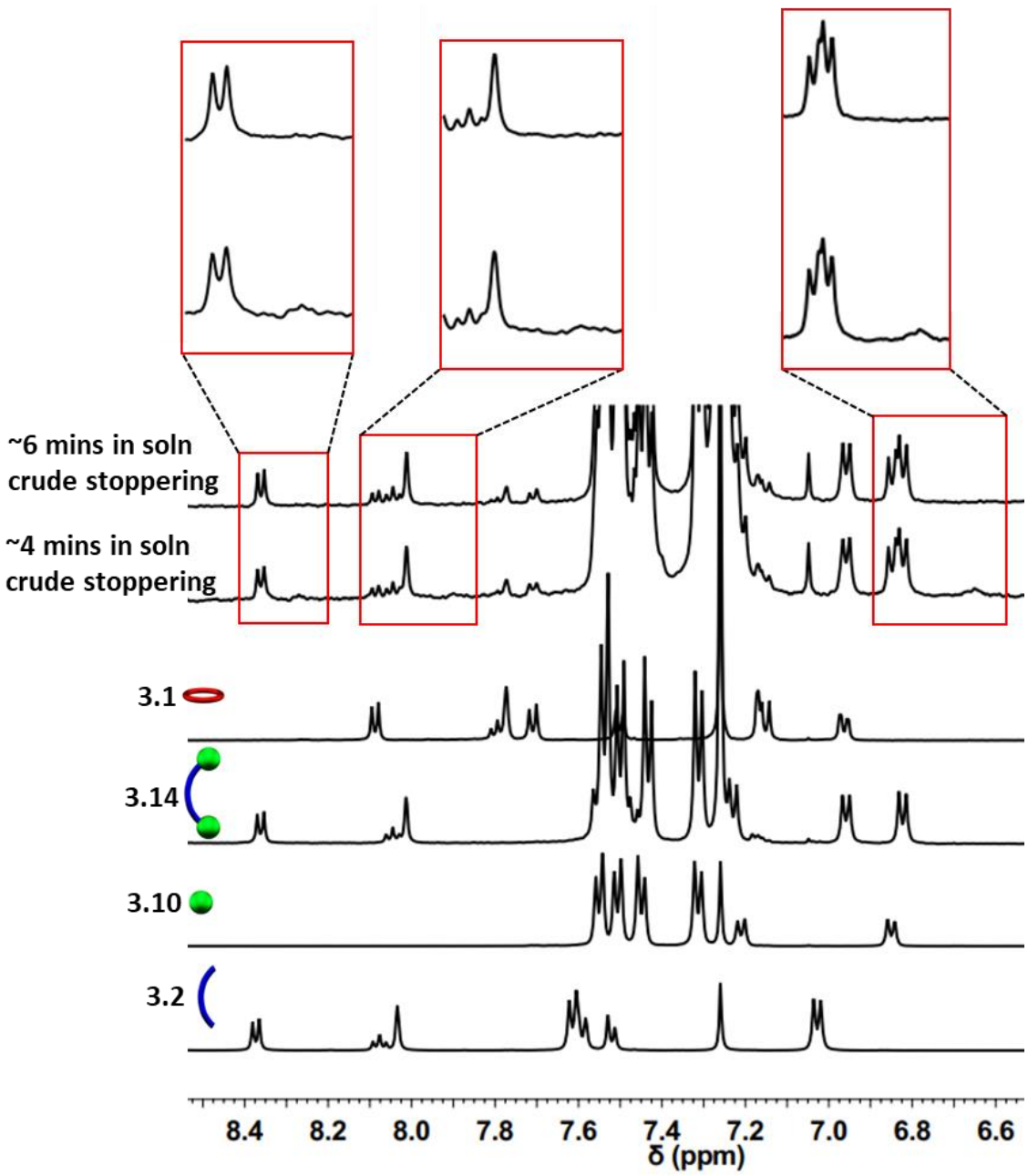

Fig 3.13 Partial ^{1}H-NMR overlay (500 MHz, 25°C, $CDCl_3$) of the demetallated crude reaction mixture from the stoppering of **3.1**:**3.2**$_2$:Fe(II)$_2$ with **3.10**. Top two NMR spectra correspond to crude reaction mixture at indicated time in solution. Bottom four spectra correspond to indicated components and starting materials for comparison.

The presence of such upfield shifted peaks imply these protons are in a more shielded environment, and would be consistent with an interlocked structure.[70–72] A MALDI-TOF MS spectrum (Fig

3.14) of the reaction mixture recorded after 6 minutes in solution confirmed only the presence of **3.1** and **3.14**, with no signals indicative of [3]rotaxane **3.15**.

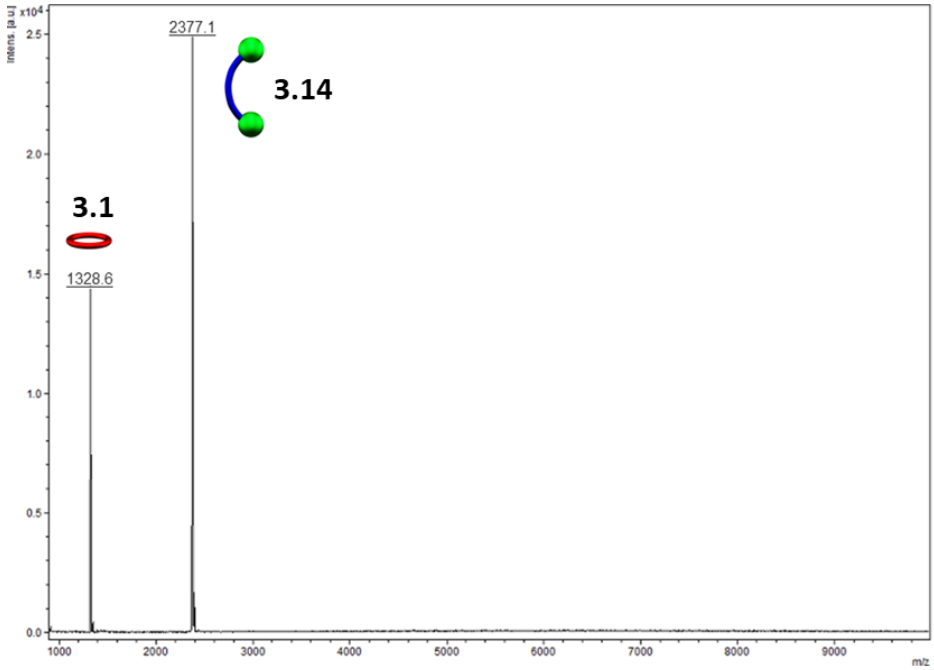

Fig 3.14 MALDI-TOF analysis (Dithranol, no salt) of the of the demetallated crude reaction mixture from the stoppering of **3.1**:**3.2**$_2$:Fe(II)$_2$ with **3.10**.

Any further attempts to optimize the synthesis and isolate **3.15** were unsuccessful and thus, while the doubly threaded [3]rotaxane **3.15** may have been initially formed, these stopper groups are not large enough to prevent the rapid dethreading of the large macrocycle **3.1** upon demetallation implying **3.10** is not a viable option for stopper group.

While it was not possible to isolate **3.15**, this result is perhaps not particularly surprising on account of the large size of the ring. As such, efforts turned to exploring [3]rotaxanes featuring the same macrocycle **3.1** and thread **3.2** but with the larger stopper group **3.13** using the same azide/alkyne cycloaddition conditions and demetallation procedure (Fig 3.15) described previously (See experimental for full synthetic details including the synthesis of the free dumbbell **3.16**).

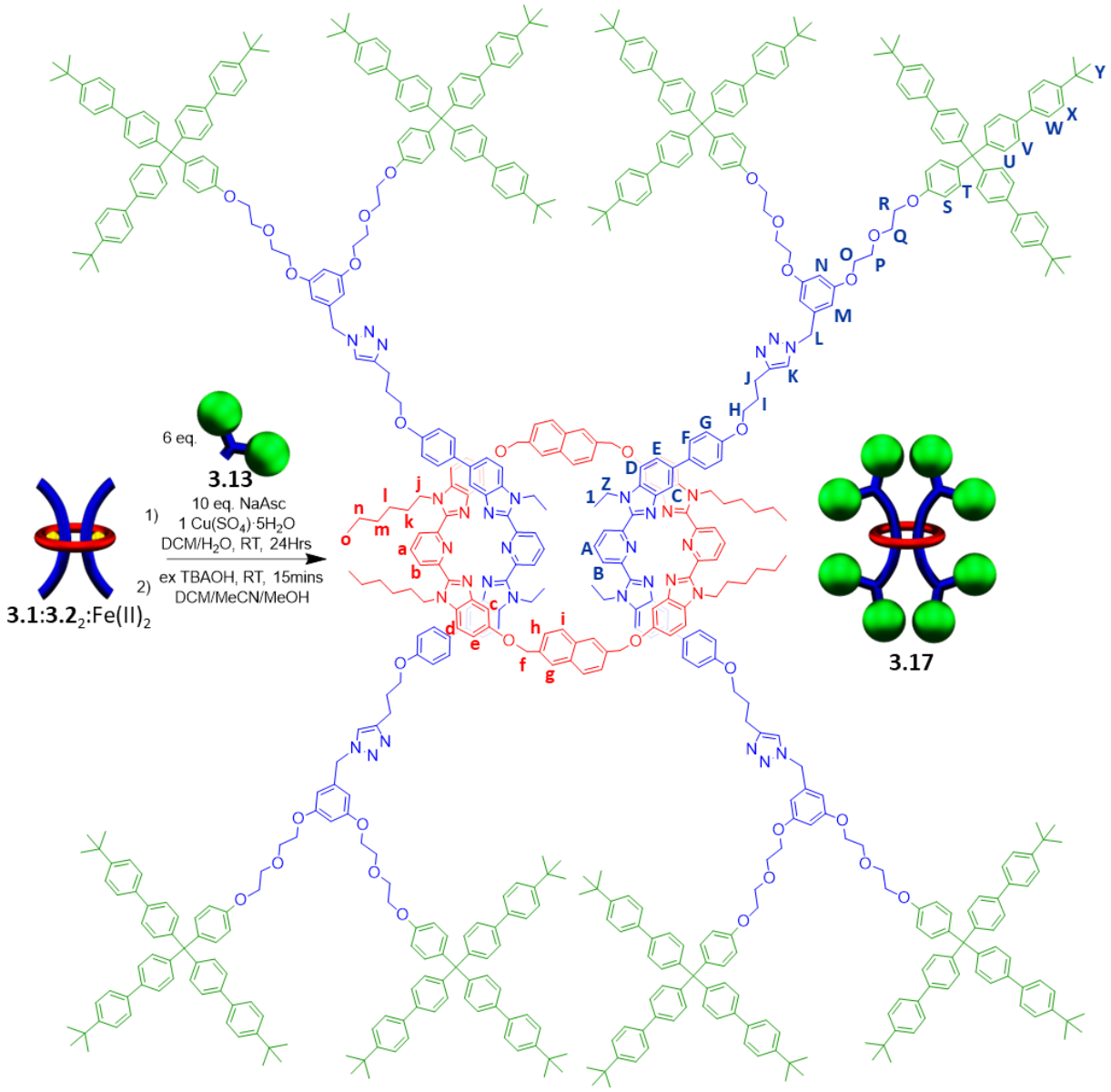

Fig 3.15 Scheme showing synthesis and chemical structure of doubly threaded [3]rotaxane **3.17**.

Similar to what was observed in the crude reaction mixture of the attempted synthesis of **3.15**, the ^{1}H-NMR analysis of the crude (demetallated) reaction mixture of the targeted synthesis of **3.17** revealed the presence of new signals that are shifted upfield (on average about 0.15 ppm) from the noninterlocked components. (Fig 3.16, interlocked peaks outlined in red).

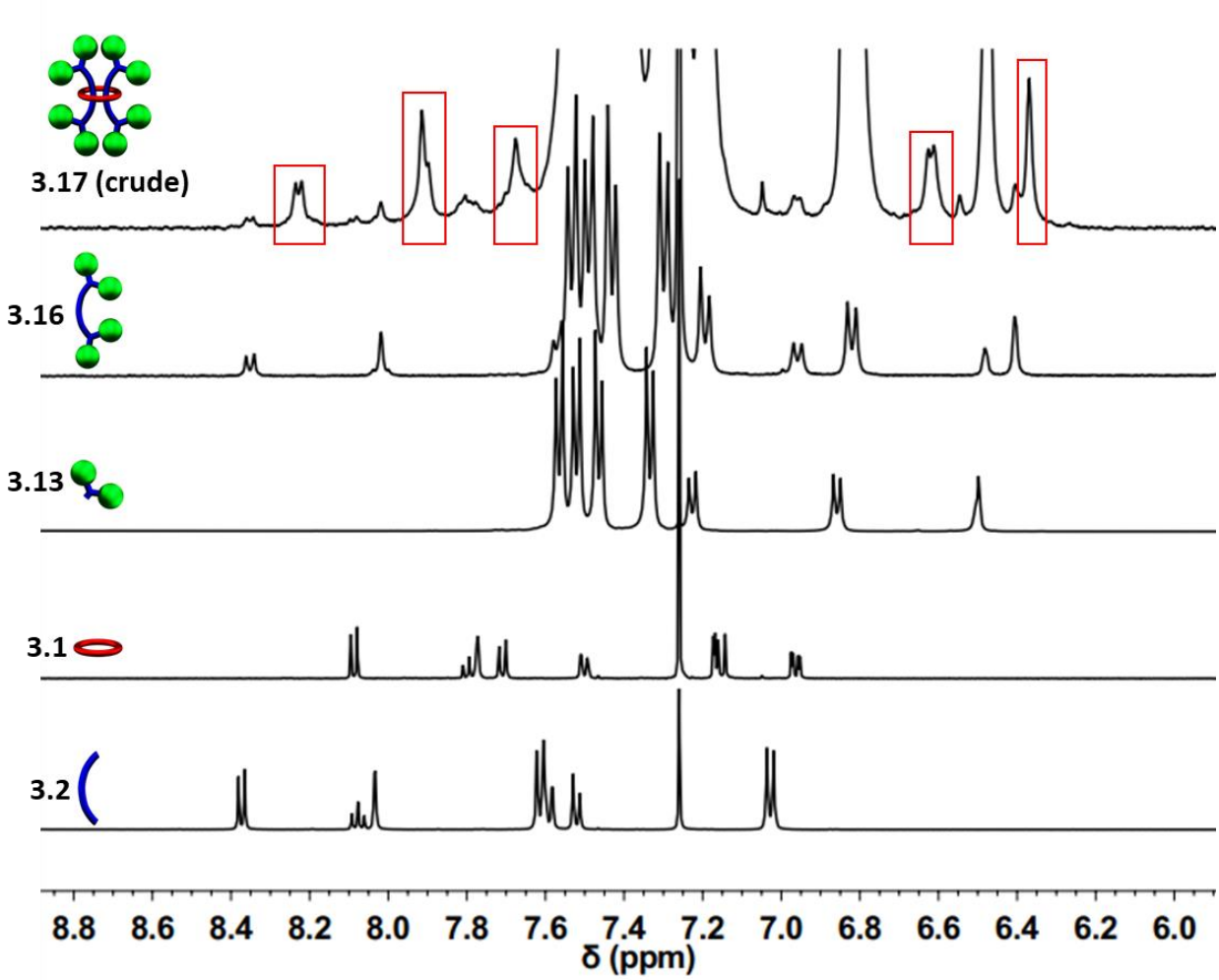

Fig 3.16 Partial ^{1}H-NMR overlay (500 MHz, 25°C, $CDCl_3$) of crude **3.17** overlayed with starting materials and components, interlocked product outlined in red.

In addition, no unreacted **3.2** was detected. Thin layer chromatography (silica, 6% MeOH in $CHCl_3$) confirmed a new single lower R_f product had been formed relative to the noninterlocked components. Preparative thin layer chromatography was then used to separate the lower R_f product in 75% isolated yield from its noninterlocked byproducts. Utilizing a variety of 1D and 2D NMR techniques (COSY, HSQC, HMBC) combined with comparison to the free macrocyclic and dumbbell components, **3.1** and **3.16**, the ^{1}H and ^{13}C-NMR spectra of **3.17** could be fully assigned. See Figures 3.17-3.20 on the next four pages for the corresponding NMR spectra.

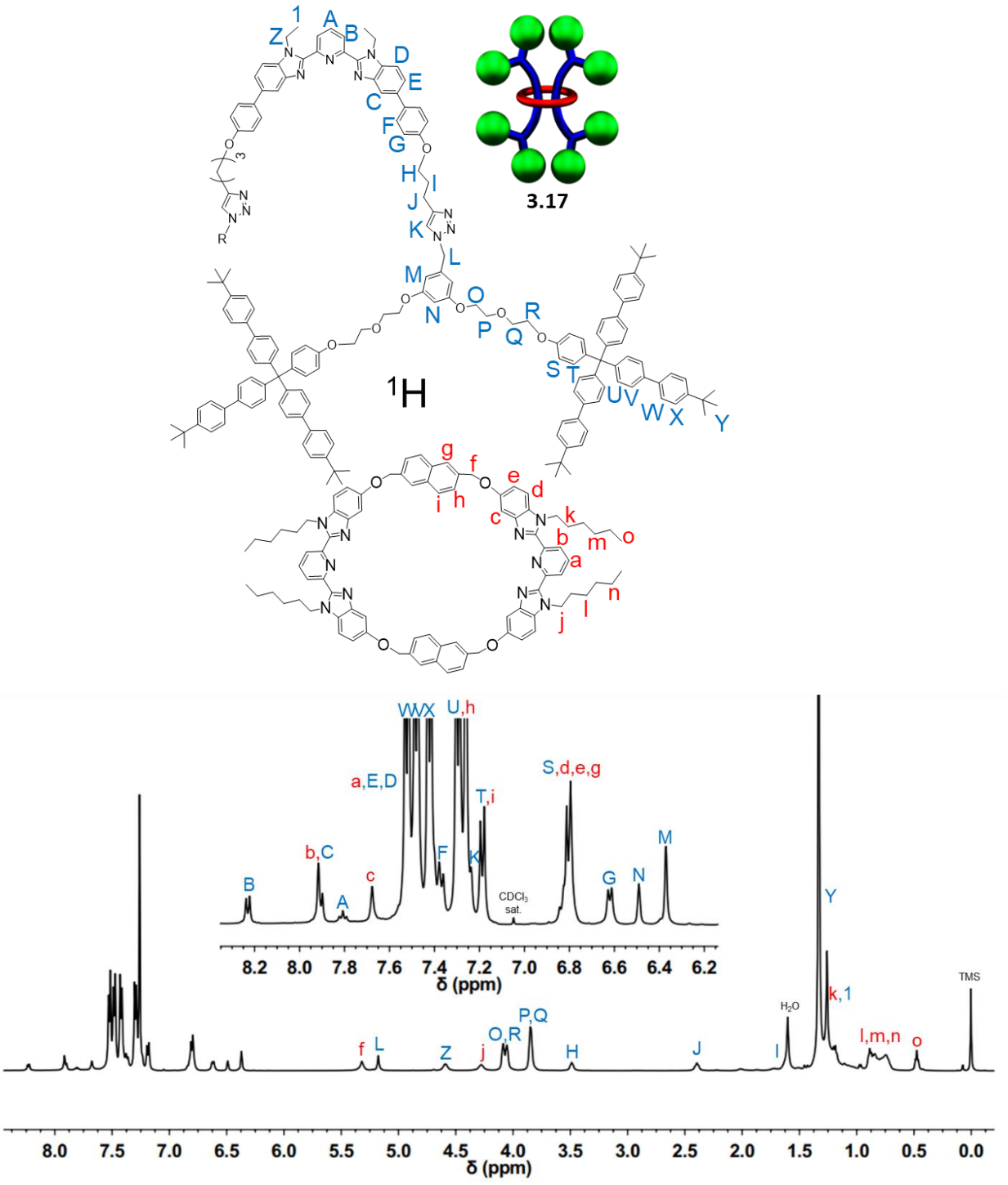

Fig 3.17 Full ^{1}H-NMR (500 MHz, 25°C, $CDCl_3$) of doubly threaded [3]rotaxane **3.17**. Peak assignments correspond to those given at top of figure.

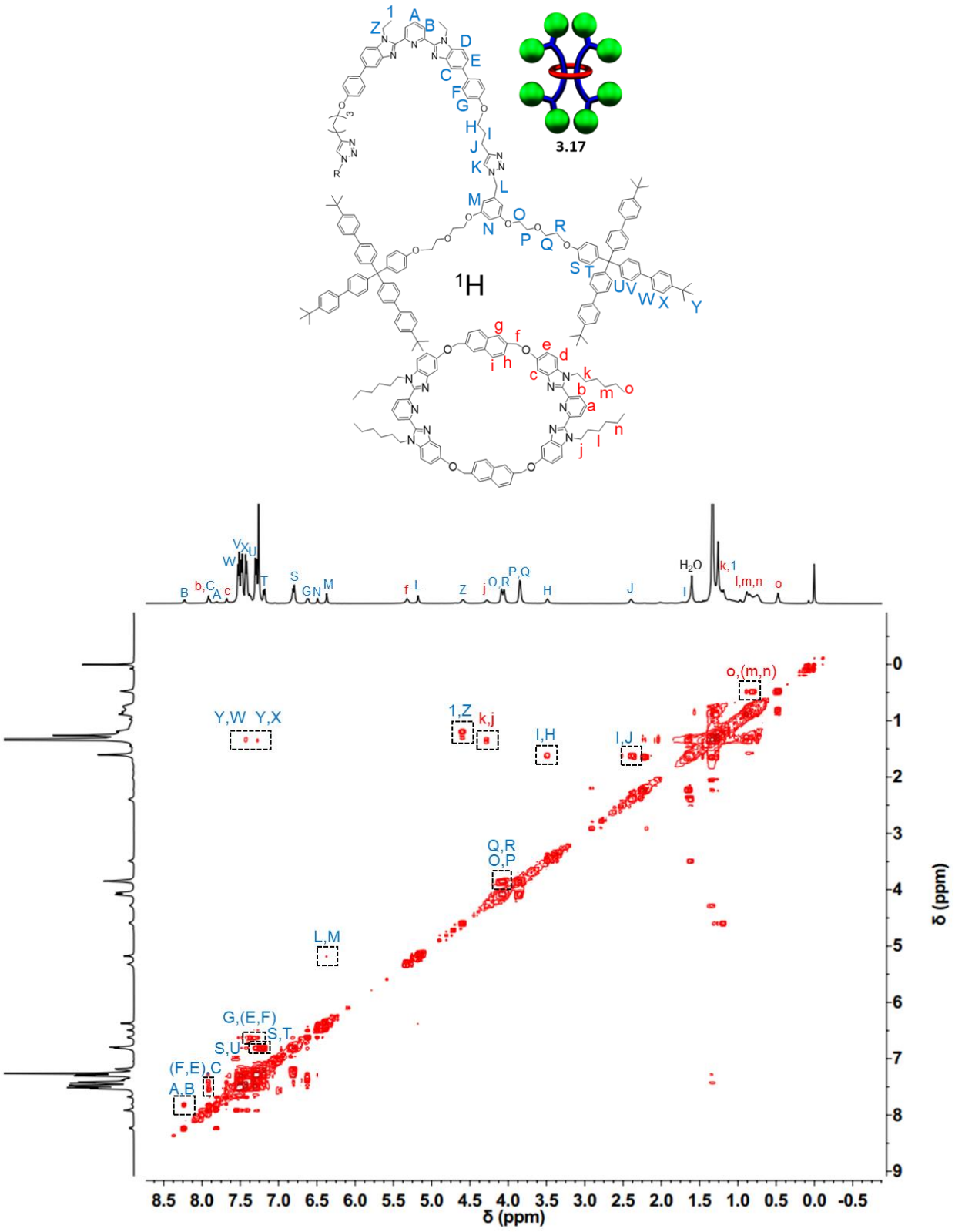

Fig 3.18 Full ^{1}H-^{1}H COSY NMR spectrum (500 MHz, 25°C, $CDCl_3$) of doubly threaded [3]rotaxane **3.17**. Peak assignments correspond to those given at top of figure.

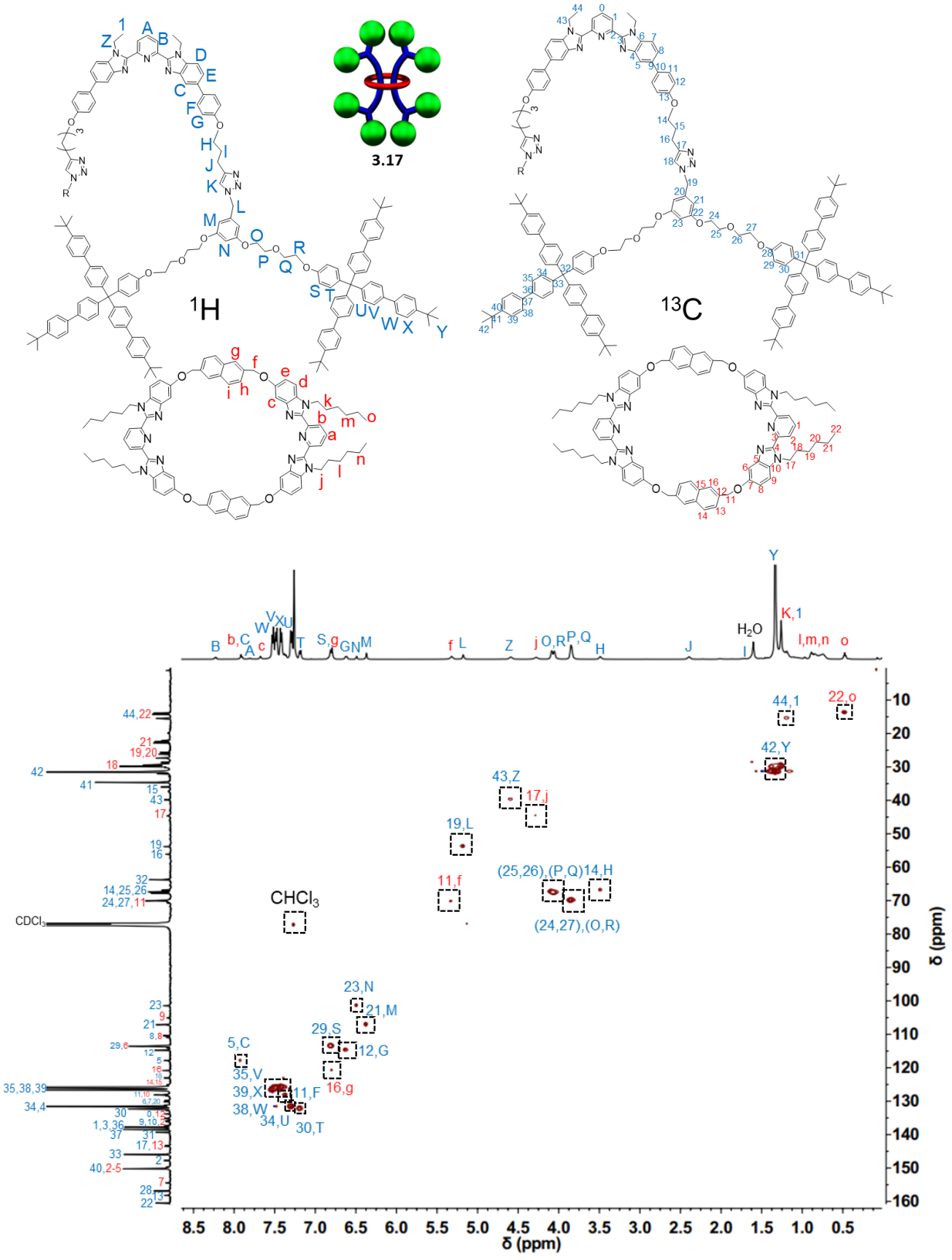

Fig 3.19 Full ^{1}H-^{13}C HSQC (5mM, 500 MHz, 25°C, $CDCl_3$) of **3.17**. Full ^{13}C and select ^{1}H annotations correspond to those at top of figure.

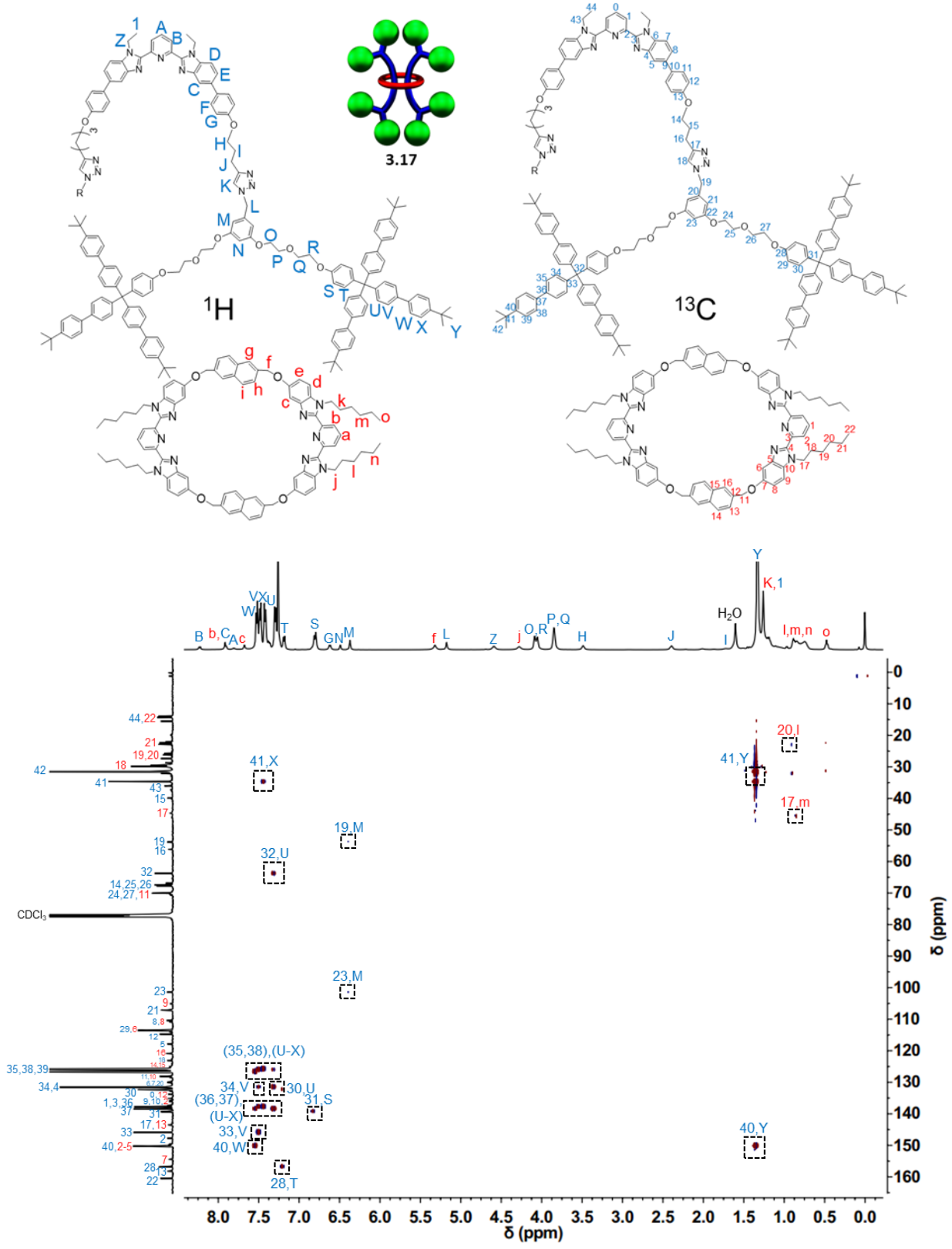

Fig 3.20 Full ^{1}H-^{13}C HMBC (5mM, 500 MHz, 25°C, $CDCl_3$) of **3.17**. Full ^{13}C and select ^{1}H annotations correspond to those at top of figure.

Figure 3.21 shows the diagnostic aromatic region of the ^{1}H NMR of the [3]rotaxane **3.17** relative to the free components **3.1** and **3.16** revealing upfield shifting of the interlocked structure.

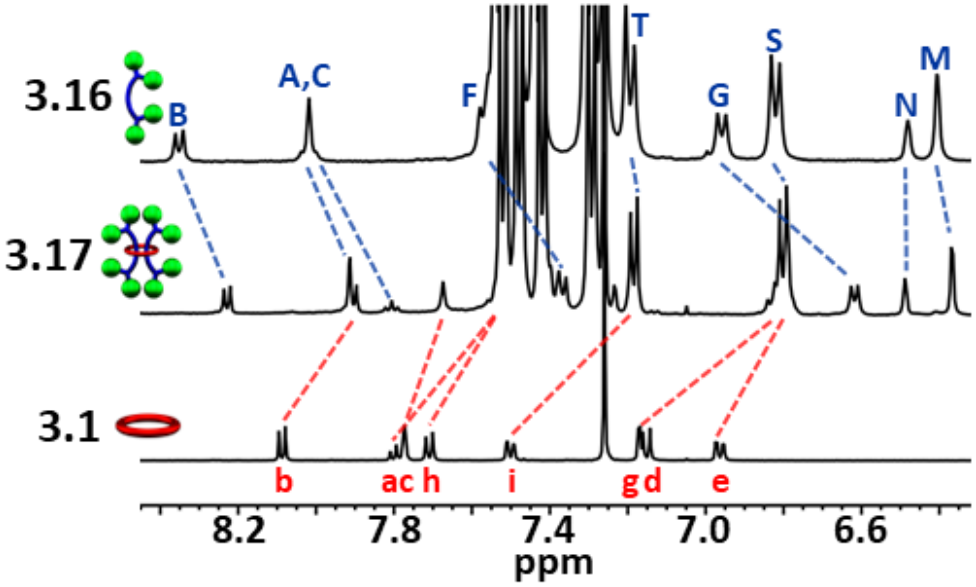

Fig 3.21 Partial aromatic ^{1}H-NMR overlay (500mHz, 25°C, $CDCl_3$) of **3.16** (top), **3.17** (middle), and **3.1** (bottom), ^{1}H assignments in Fig 3.20.

MALDI-TOF MS of purified **3.17** (Fig 3.22a) shows a high molecular weight peak ($(M+H^+)$ m/z: 9782) that is consistent with the targeted [3]rotaxane. Additional lower molecular weight peaks ($(M+H^+)$ m/z: 5554, 4226, 2402) are also observed which are consistent with the expected fragmentation pattern of the doubly threaded interlocked structure. Breaking open the macrocycle in **3.17** results in free dumbbell ($(M+H^+)$ m/z: 4226) while fragmentation of a single dumbbell gives the [2]rotaxane ($(M+H^+)$ m/z: 5554) and fragmented dumbbell ($(M+H^+)$ m/z: 2402) peaks. The high molecular weight peak was further examined using reflectance mode MALDI-TOF to access the mass distribution of **3.17**. The obtained isotopic distribution displays a clear match to the expected distribution from **3.17** based on its chemical composition ($C_{676}H_{696}N_{32}O_{32}$ $(M+H^+)$) giving further evidence for the doubly threaded [3]rotaxane **3.17** (Fig 3.22a expansion).

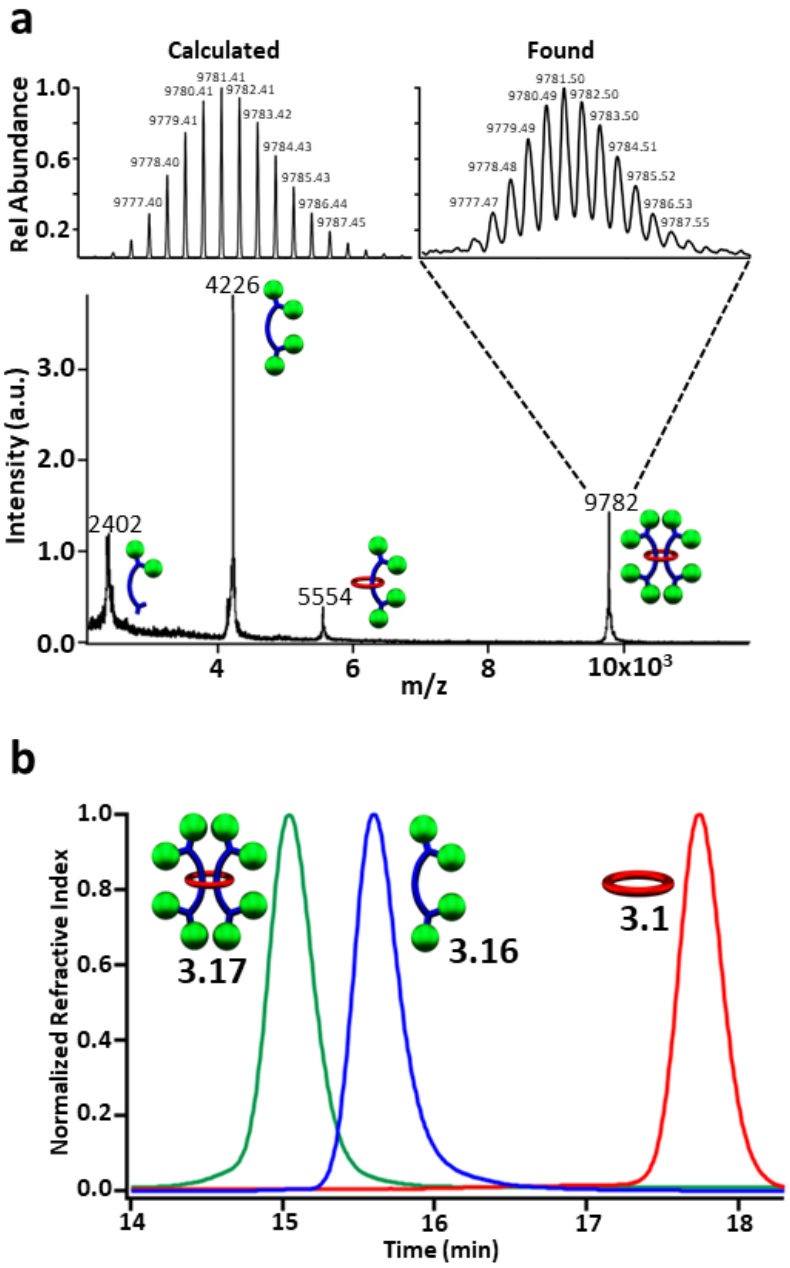

Fig 3.22 a) MALDI-TOF MS of **3.17** with expansion showing isotopic distribution of the 9782 m/z peak ($C_{676}H_{696}N_{32}O_{32}$ (MH^+)), and b) GPC chromatogram of (3:1 THF:DMF) purified **3.17**, **3.16**, and **3.1** at 25°C.

To confirm that **3.17** was one interlocked molecule free of its noninterlocked components, size exclusion chromatography was employed. GPC analysis using RI detection shows a single peak for **3.17** with a clear decrease in retention time relative to **3.16** and **3.1** (Fig 3.22b) as would be expected for the larger doubly threaded architecture.

The close proximity of the interlocked components in **3.17** was demonstrated using ^{1}H-^{1}H NOESY NMR experiments carried out at 278K in order to slow the intermolecular motions of the components. At this temperature, 10 different intercomponent NOEs could be identified in **3.17** (Fig 3.23a-b and 3.24) that were not present in a separately prepared 2:1 mixture of the dumbbell **3.16** and macrocycle **3.1** at the same concentration (Fig 3.25). NOEs typically arise from distances <5.0Å[73] and as such the presence of 10 different intercomponent NOEs confirms that the components of **3.17** are indeed interlocked and is the best proof of interlocked structure given in this chapter. It is interesting to note that there are NOE interactions between **3.1** and the entire length of the dumbbell component within **3.17** suggesting that there is some free mobility of the ring along the dumbbell (Fig 3.23a-b). To better understand how these NOE interactions might occur, all-atom molecular dynamics simulations were conducted to help explore possible rotaxane conformations that could explain the observed NOE signals (Fig 3.23c, molecular simulations conducted by collaborators Dr. Phillip M. Rauscher and Vincent J. Maddi). The simulations show that the macrocycle typically assumes a position near a stopper group of one dumbbell and in the middle of the other (as shown in Fig 3.23c). It is worth pointing out that such conformations are consistent with the majority of the NOEs observed (1, 2, 4, 5, 6, 8, 9, and 10) and give further backing to the confirmation of the interlocked structure.

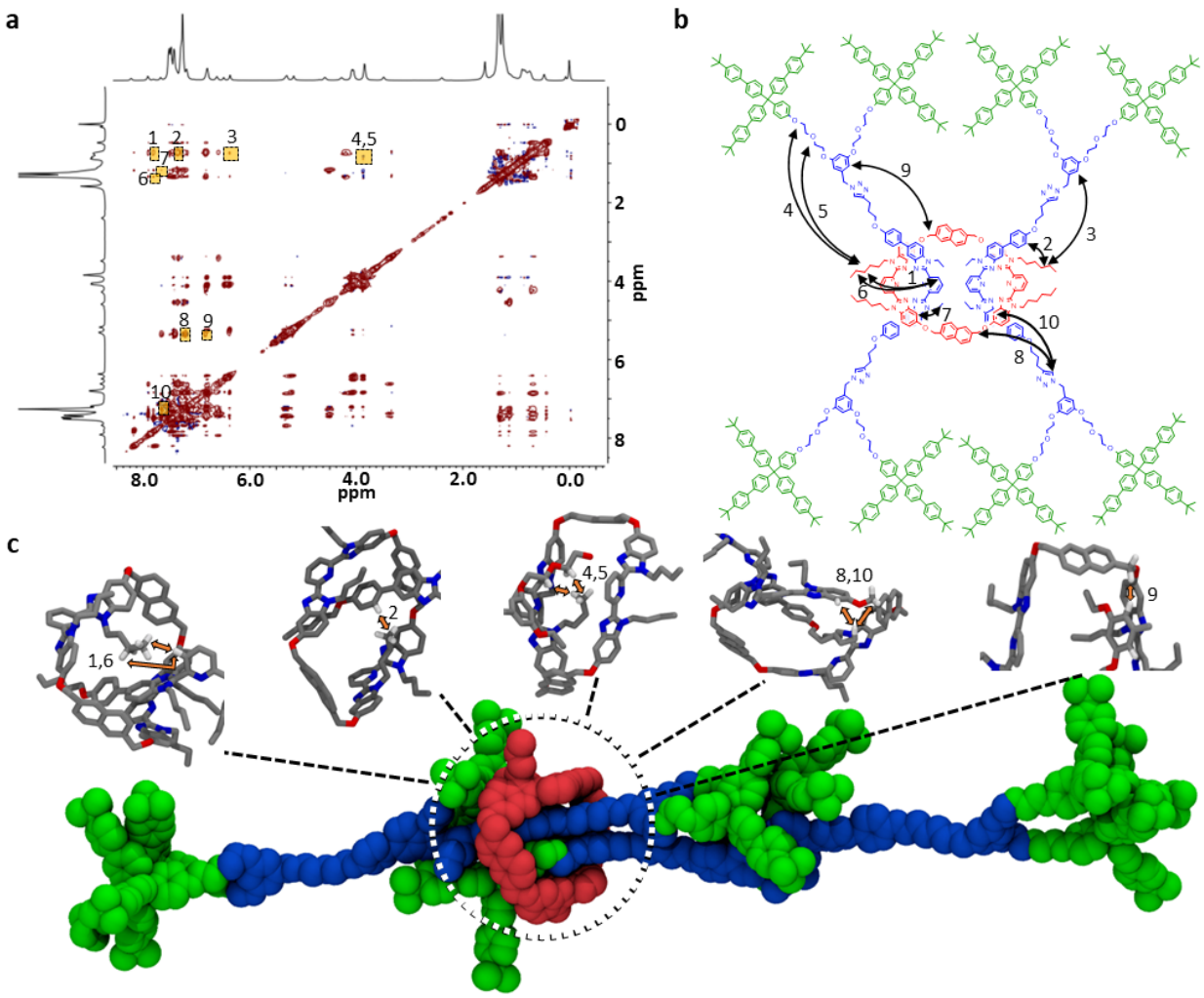

Fig 3.23 a) Full ^{1}H-^{1}H NOESY NMR spectrum (500 MHz, $CDCl_3$) of **3.17** at 278K. b) Schematic diagram showing labeled intercomponent NOEs of **3.17**. c) All-atom implicit-solvent model renders of **3.17** showing how NOEs 1, 2, 4, 5, 6, 8, 9, and 10 could arise. In the upper panel, molecular segments are colored according to atom type (gray = Carbon, blue = Nitrogen, red = Oxygen, white = Hydrogen). In the bottom panel, the various rotaxane components are colored in accordance with the rest of the figures (red = ring, blue = thread, green = stopper(s)).

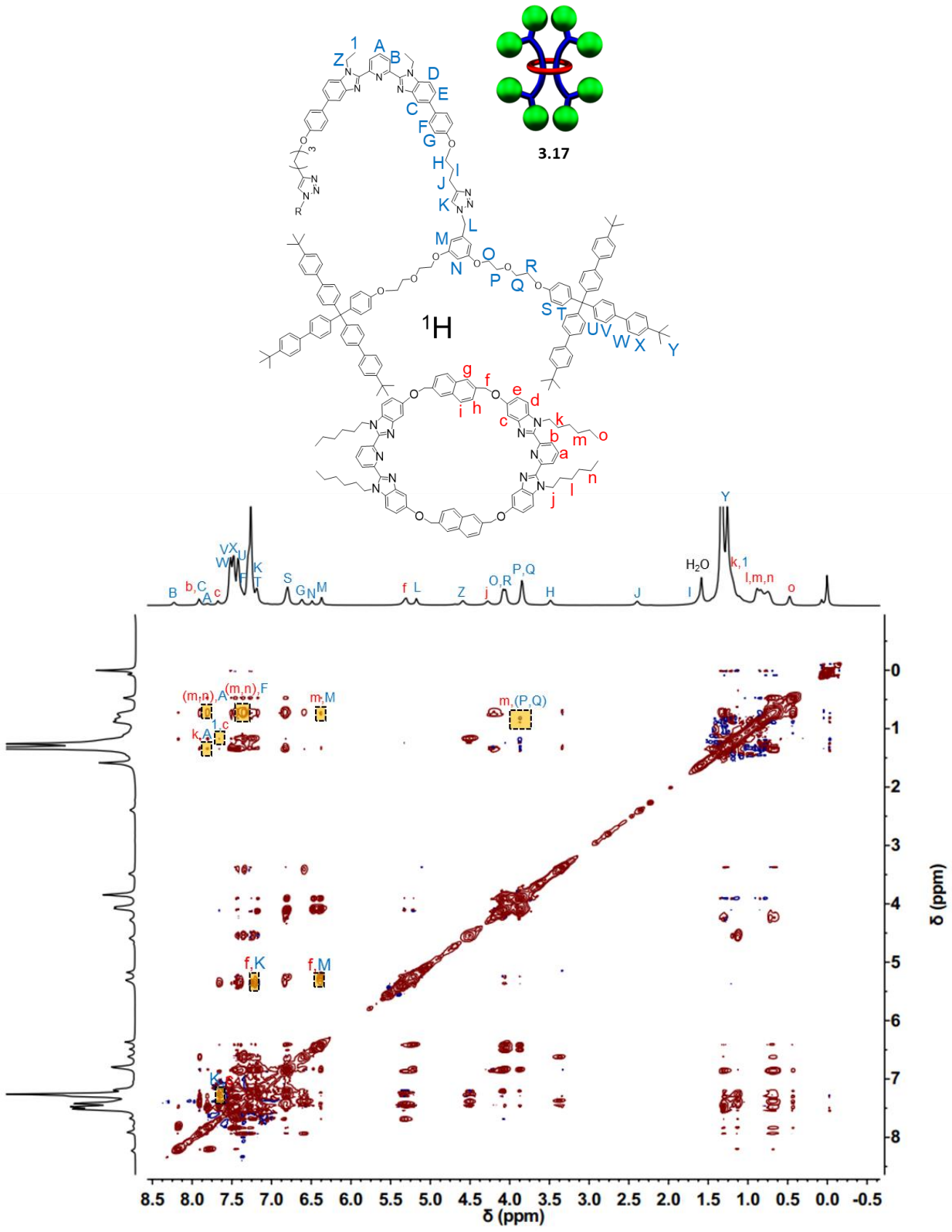

Fig 3.24 Full ^{1}H-^{1}H NOESY NMR spectrum (500 MHz, 5°C, $CDCl_3$) of doubly threaded [3]rotaxane **3.17**. Peak assignments correspond to those given at top of figure.

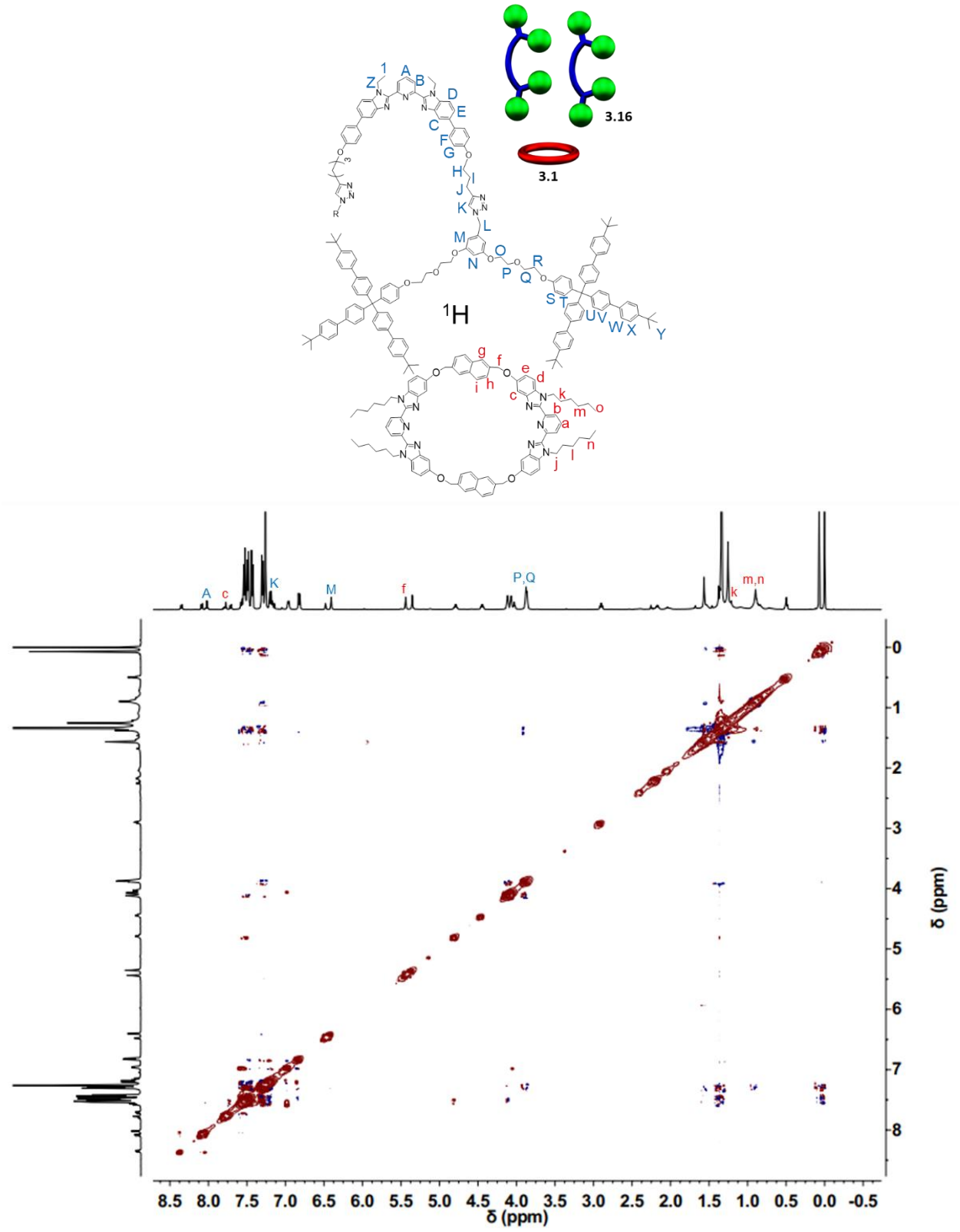

Fig 3.25 Full ^{1}H-^{1}H NOESY NMR spectrum (500 MHz, 5°C, $CDCl_3$) a 2:1 solution of **3.16**:**3.1**. Peak assignments correspond to those given at top of figure.

During the NMR analysis of **3.17**, an interesting observation was made. Specifically, after being allowed to sit in solution overnight during ^{13}C-NMR acquisition, small trace signals were observed in the ^{1}H-NMR spectrum that correspond to free dumbbell and macrocycle. As a consequence of this observation and the large size of **3.1**, it was hypothesized that even with the larger stopper group **3.13**, very slow slippage may be occurring in solution and that the [3]rotaxane **3.17** is in fact metastable. As such, the doubly threaded [3]rotaxane **3.19** (Fig 3.26) was targeted.

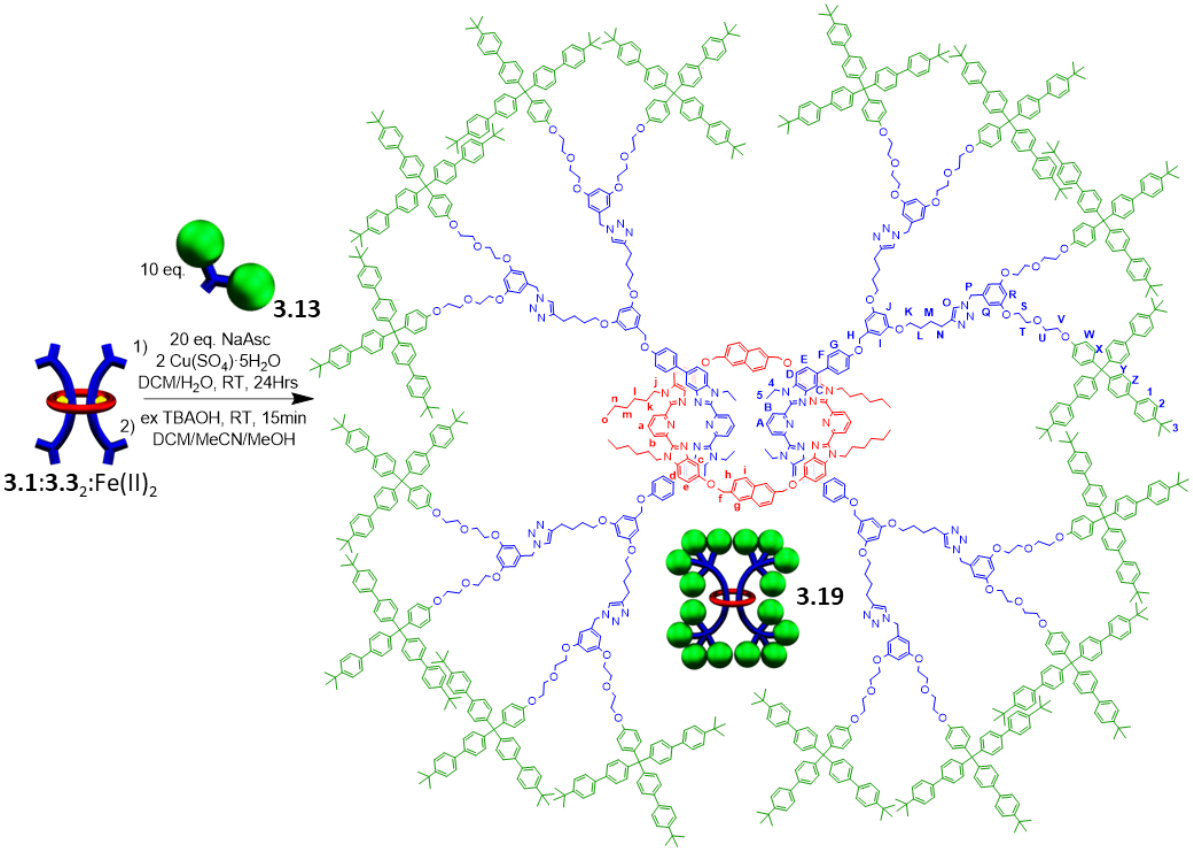

Fig 3.26 Scheme showing synthesis and chemical structure of doubly threaded [3]rotaxane **3.19**.

In order to access such a structure, the doubly threaded pseudo[3]rotaxane **3.1**:**3.3**$_2$:Fe(II)$_2$ (which contains the thread component **3.3** with two alkyne moieties on each end group and was discussed above), was stoppered with **3.13** and demetallated using similar conditions to those used to synthesize **3.17** (See experimental for full synthetic details including the synthesis of the free

dumbbell **3.18**). ^{1}H-NMR analysis of the crude product again revealed new upfield shifted signals from the noninterlocked components with a small amount (ca. 25%) of noninterlocked byproduct observed (See Fig 3.27, interlocked peaks outlined in red) and thin layer chromatography (silica, 5% MeOH in $CHCl_3$) confirmed a new single lower R_f product had been formed relative to the noninterlocked components.

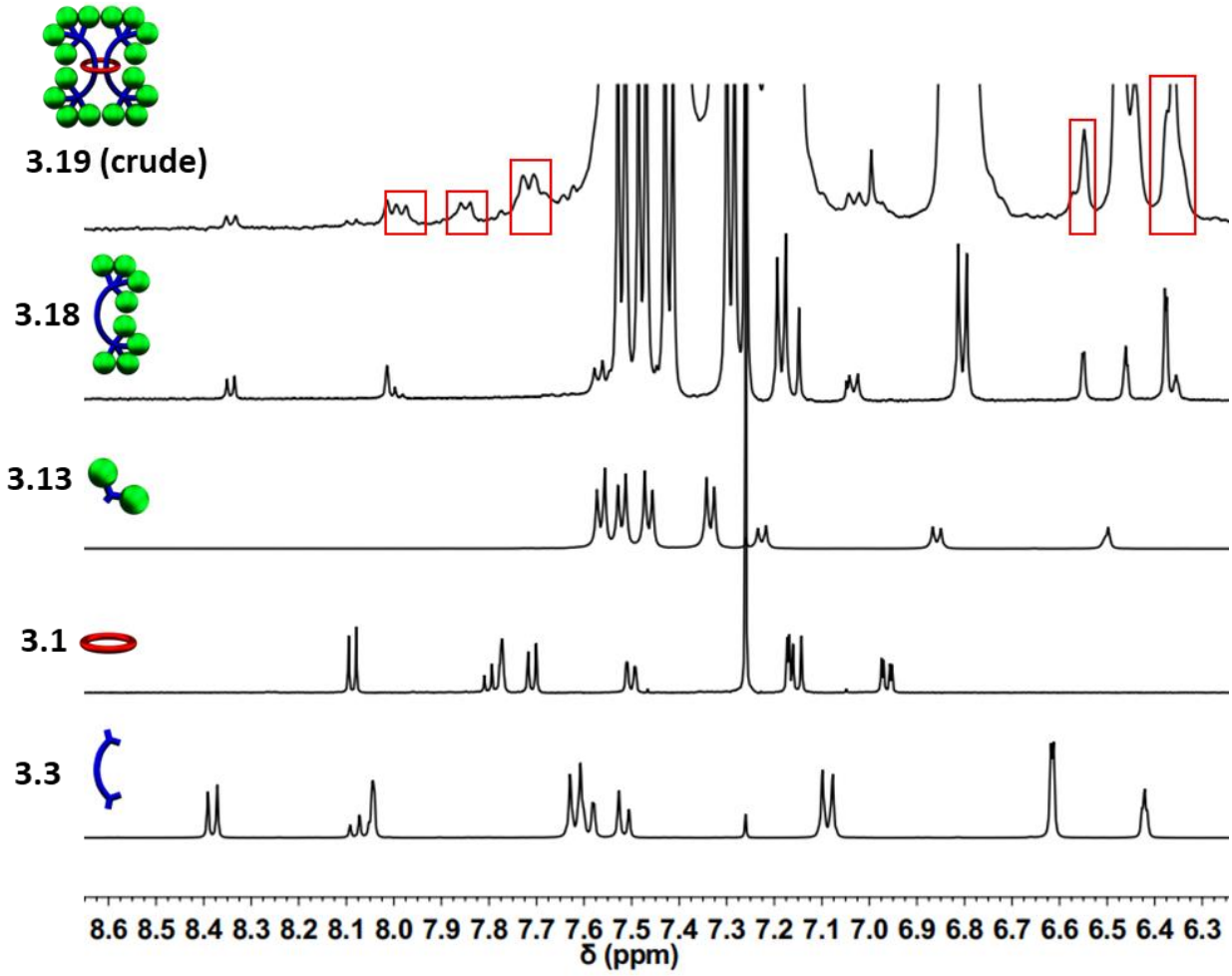

Fig 3.27 Partial ^{1}H-NMR overlay (500 MHz, 25°C, $CDCl_3$) of crude **3.19** compared to starting materials and free components.

Preparative thin layer chromatography was used to isolate this new product in 65% yield. The entire ^{1}H-NMR spectrum of **3.19** could be assigned by comparison to the spectra of **3.1**, **3.17**, and **3.18** combined with ^{1}H-^{1}H COSY of **3.19** (See Fig 3.28-29).

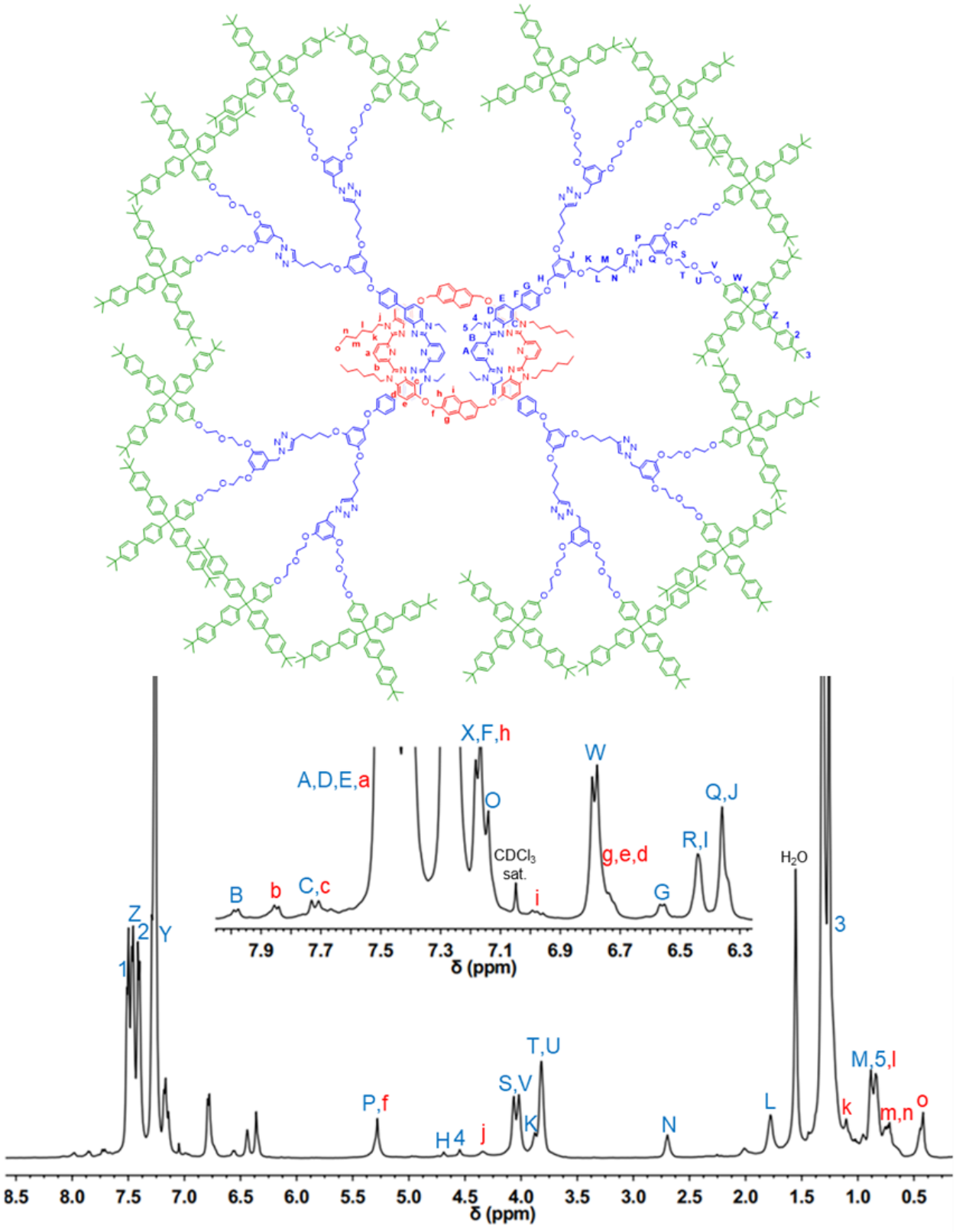

Fig 3.28 Full ^{1}H-NMR (500 MHz, 25°C, $CDCl_3$) of doubly threaded [3]rotaxane **3.19**.

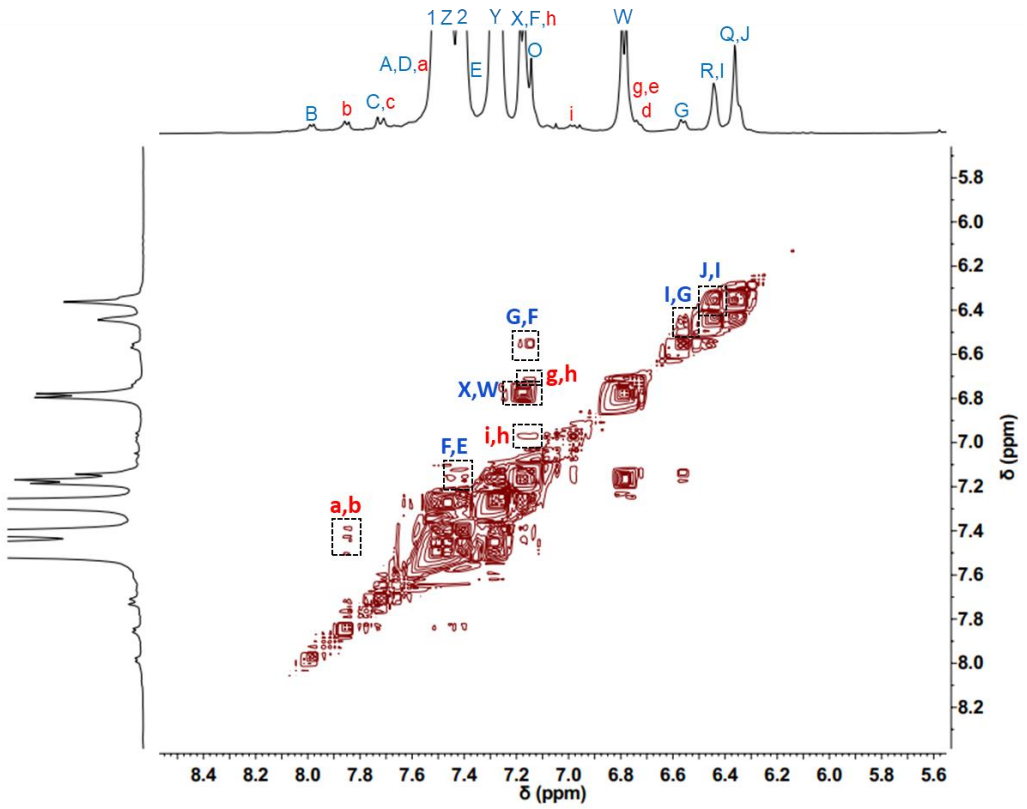

Fig 3.29 Partial ^{1}H-^{1}H COSY (5mM, 500 MHz, 25°C, $CDCl_3$) of doubly threaded [3]rotaxane **3.19**. Peak assignments correspond to those given in Figure 3.28.

Fig 3.30a shows the diagnostic ^{1}H-NMR aromatic region which reveals an average upfield shift of 0.3ppm was observed for the aromatic resonances of **3.19** compared to its noninterlocked components **3.18** and **3.1**. It is interesting to note this upfield shift is significantly larger than what was observed for the [3]rotaxane **3.17**. Further characterization was then obtained and MALDI-TOF MS of purified **3.19** shows the expected fragmentation pattern of the interlocked structure (Fig 3.30b). Furthermore, GPC analysis using RI detection shows a clear decrease in retention time of **3.19** relative to its noninterlocked components **3.18** and **3.1** (Fig 3.30c) and the [3]rotaxane **3.17** (Fig 3.30d) as expected. All in all, this characterization confirms the structure of the doubly threaded [3]rotaxane **3.19**.

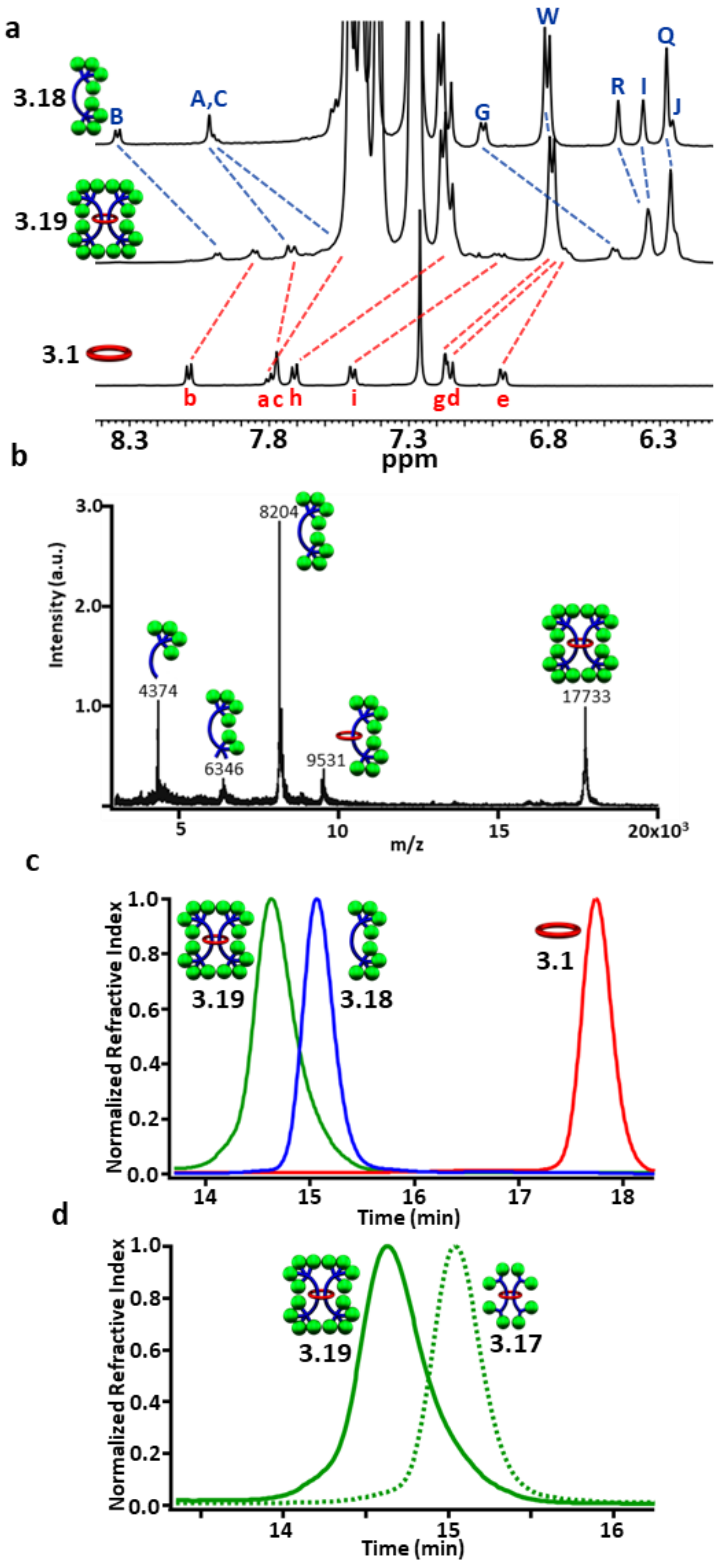

Fig 3.30 a) Partial aromatic ^{1}H-NMR (500mHz, 25°C, $CDCl_3$) overlay of **3.18** (top), **3.19** (middle), and **3.1** (bottom). b) Maldi-TOF MS (Dithranol, no salt) of purified **3.19**. c) GPC chromatogram of (3:1 THF:DMF as eluent) purified **3.19**, **3.18**, and **3.1** at 298K**.** d) GPC chromatogram of (3:1 THF:DMF as eluent) purified and **3.19** and **3.17** at 298K.

3.5 [3]Rotaxane Stability Studies in Solution

While the [3]rotaxane **3.15** was not stable enough to be isolated, both [3]rotaxanes **3.17** and **3.19** were isolatable and stable enough to withstand chromatography conditions. None-the-less, as mentioned above the [3]rotaxane **3.17** appeared to be metastable. Thus, it was decided to explore the lifetime solution stability of both [3]rotaxanes **3.17** and **3.19** in more detail. To this end freshly purified solutions of **3.17** and **3.19** were monitored via ^{1}H NMR spectroscopy at room temperature (25°C, $CDCl_3$, 1mM [3]R) for six weeks. Interestingly in both cases, the upfield shifted protons assigned to the rotaxane slowly decreased in intensity and were replaced with new signals identical to those of the corresponding free dumbbell and macrocycle (Fig 3.31) indicative of both compounds undergoing a slow slippage process (**3.17** half-life ($t_{1/2}$) of ca. 5 weeks, **3.19** half-life ($t_{1/2}$) of ca. 6 months).

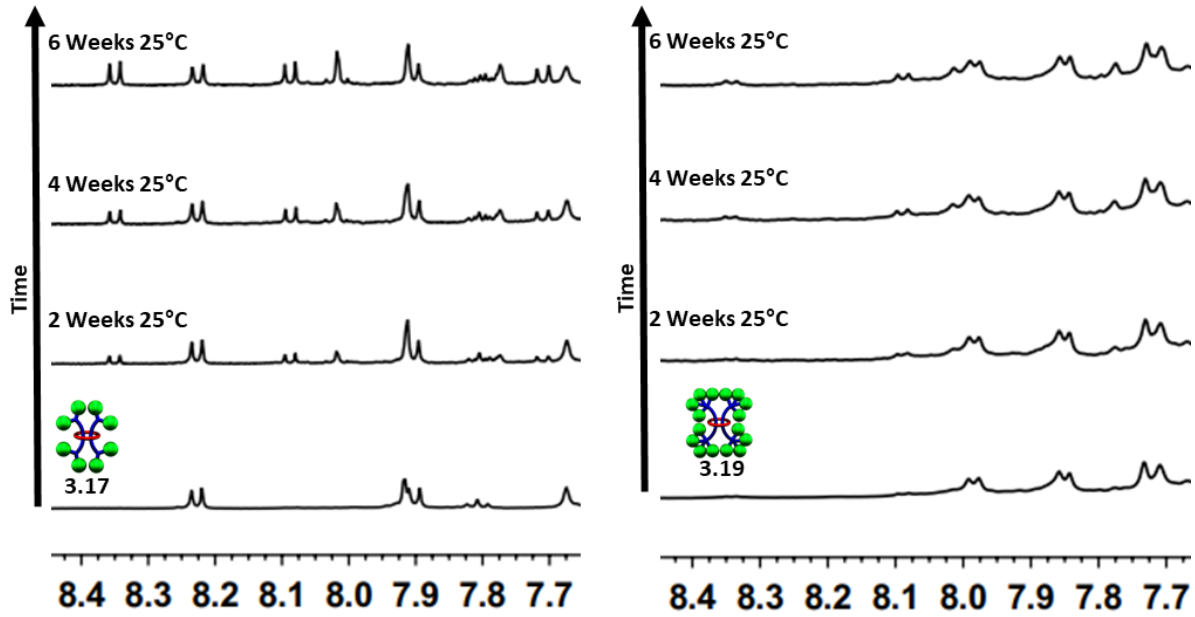

Fig 3.31 Partial ^{1}H-NMR overlay (1mM, 500 MHz, 25°C, $CDCl_3$) of initial room temperature slippage observations of **3.17** (left) and **3.19** (right).

In order to obtain more detailed information on the stability of these metastable double threaded [3]rotaxanes, a full kinetic study was carried out on freshly purified solutions of **3.17** and **3.19** in $CDCl_3$ (1mM [3]R).[62] Both solutions were monitored at 35 °C for one week followed by 40 °C for another week, and finally 45 °C for a final week with their ^{1}H-NMR spectra recorded at regular time intervals (Fig3.32a-d). This process was repeated in triplicate for both rotaxanes and the concentration of remaining [3]rotaxane in solution could easily be determined from integration of the ^{1}H-NMR spectra at each timepoint (See the Experimental for full details and the corresponding slippage spectra). Standard kinetic analysis revealed the slippage process followed first-order kinetics dependent on the concentration of the [3]rotaxane (i.e., rate of slippage = k_1[rotaxane], Fig 3.33a-b) with the indicated half-lives (Figure 3.33c).

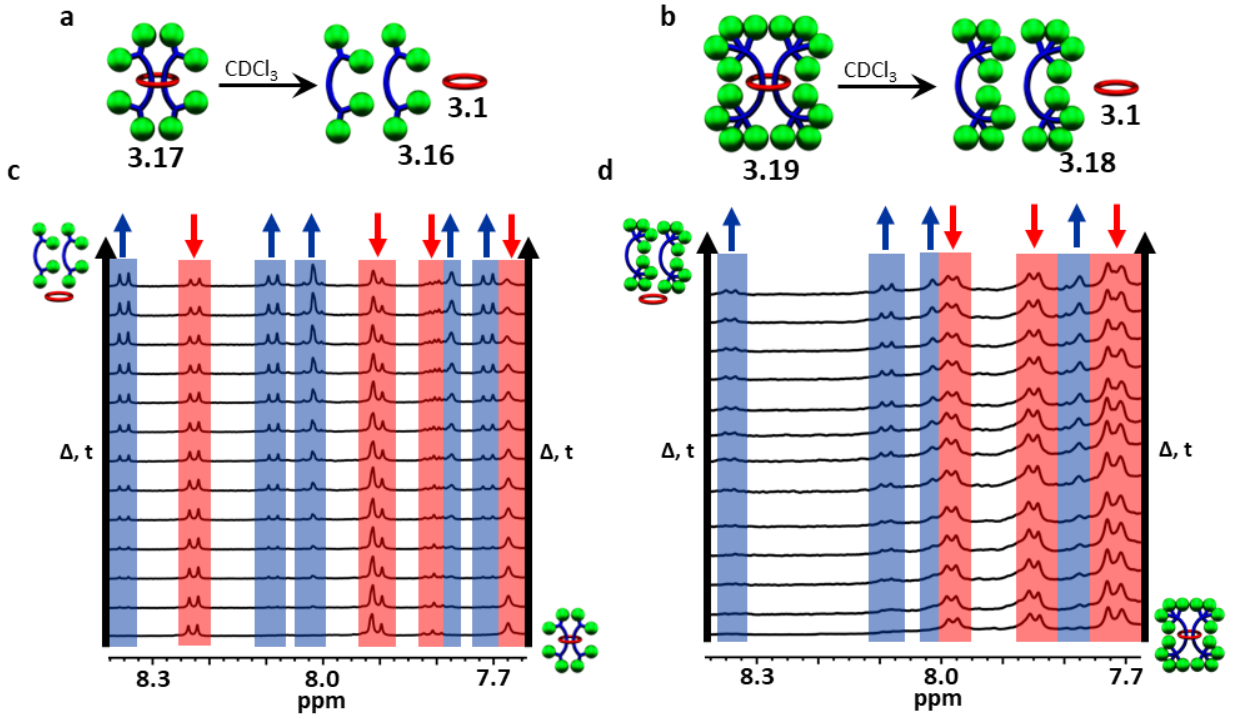

Fig 3.32 a) Scheme illustrating slippage process of **3.17.** b) Scheme illustrating slippage process of **3.19.** c) Partial ^{1}H-NMR overlay (500mHz, $CDCl_3$) of 3-week slippage experiment of **3.17.** d) Partial ^{1}H-NMR overlay (500mHz, $CDCl_3$) of 3-week slippage experiment of **3.19.**

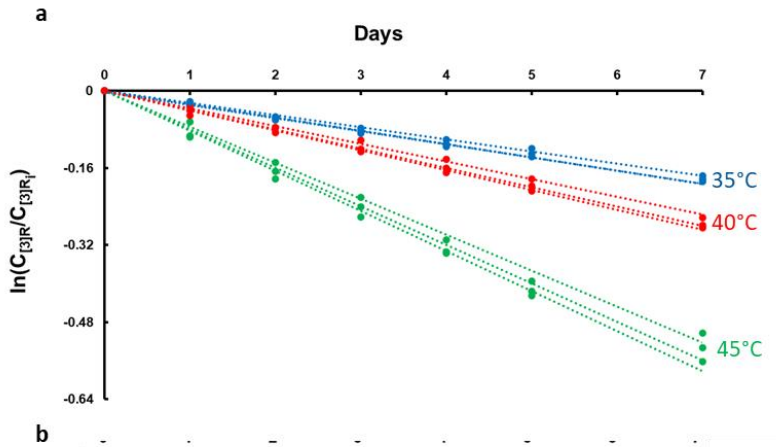

c

[3]R	$t_{1/2}$ (days, 308K)	$t_{1/2}$ (days, 313K)	$t_{1/2}$ (days, 318K)
3.17	27 ± 1	17 ± 1	8.5 ± 2
3.19	86 ± 3	49 ± 3	21 ± 2

Fig 3.33 Kinetic first-order plot of three trials of slippage of at three different temperatures of a) **3.17**, b) **3.19**, and c) obtained kinetic parameters of the slippage of **3.17** and **3.19.**

In addition to NMR spectroscopy, GPC was used to confirm that the only new products obtained after the 3-week slippage experiments of **3.17** and **3.19** were the corresponding free dumbbell and macrocycle (Fig 3.34). One important observation from both of these studies is that no singly threaded [2]rotaxane intermediate was observed during any of the slippage trials done which suggests that any of the corresponding singly threaded [2]rotaxanes using **3.1** are not stable on any appreciable timescale. This makes sense as it can be expected that the presence of one dumbbell trapped within the macrocycle helps to hinder slippage of the second dumbbell.

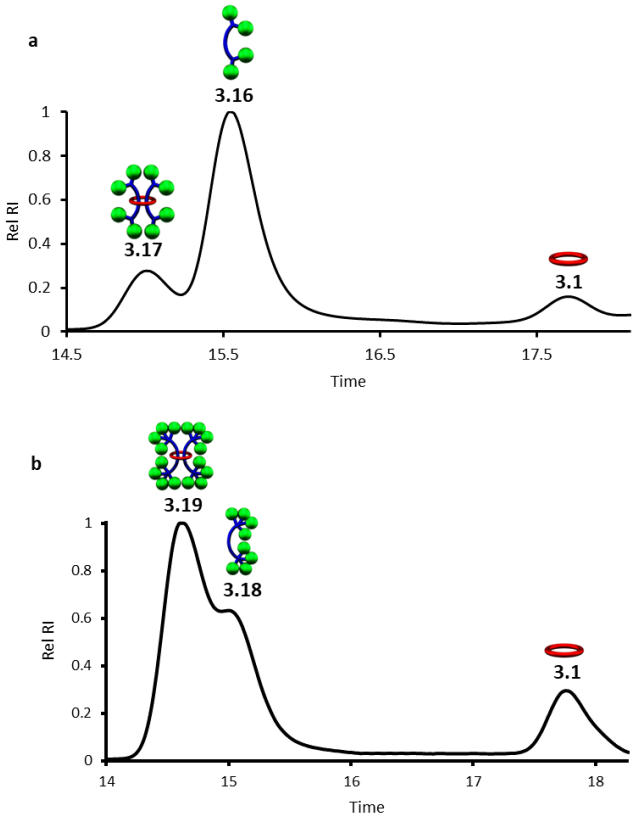

Fig 3.34 GPC (3:1 THF:DMF as eluent, 25°C) trace of a) **3.17**, and b) **3.19** after the 3-week slippage experiment.

Standard Arrhenius and Eyring analysis provided the thermodynamic parameters to both slippage processes (Fig 3.35a-d). Direct comparison to other rotaxane systems in literature is difficult as such data is not typically reported. However, it is worthwhile noting that the activation energy of the slippage process in both **3.17** (98±4 kJ/mol) and **3.19** (112±5 kJ/mol) are very high compared to the only other doubly threaded [3]rotaxane for which such data is available (35±3 kJ/mol)[62] and is consistent with the very slow slippage process observed in these systems (Fig 3.35e). Comparing **3.19** to **3.17** shows that while effectively doubling the number of the tris(*p*-*t*-butylbiphenyl)methyl moieties on the stopper group does not prevent slippage, it does result in an increase in the energy barrier to dethreading and a dramatic increase in the lifetime stability of the [3]rotaxane ($t_{1/2}$ of 5 weeks vs. 6 months at room temperature).

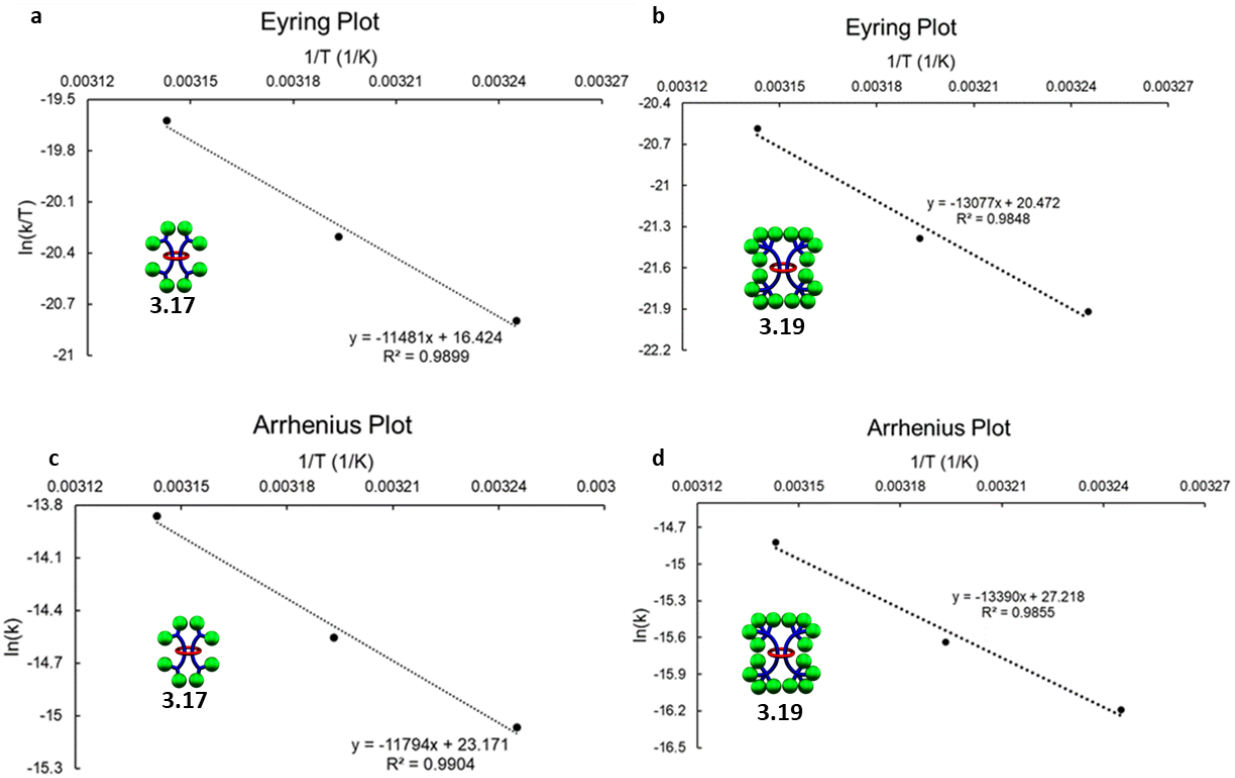

e

[3]R	E_a (kJ/mol)	$\Delta H^{\ddagger}$ (kJ/mol)	$\Delta S^{\ddagger}$ (J/mol*K)	$\Delta G^{\ddagger 298K}$ (kJ/mol)
3.17	98 ± 4	95 ± 3	-61 ± 8	113 ± 6
3.19	112 ± 5	108 ± 5	-30 ± 10	120 ± 10

Fig 3.35 Eyring plot of the slippage of a) **3.17**, and b) **3.19**. Arrhenius plot of the slippage of c) **3.17**, and d) **3.19**. e) Obtained thermodynamic parameters of slippage processes of **3.17** and **3.19**.

3.6 Conclusions

In conclusion, the successful assembly, stoppering, and demetallation of Bip-containing doubly threaded [3]rotaxanes using one of the largest macrocycles reported to date (46 atoms) has been achieved in good yield. On account of the large size of the macrocycle in these interlocked species, all of the [3]rotaxanes synthesized were found to be metastable and that by tuning the number of tris(*p*-*t*-butylbiphenyl)methyl moieties present in the stoppering unit it was possible to vary their stability with their half-life varying from < 1 minute (one tris(*p*-*t*-butylbiphenyl)methyl moiety) to ca. 6 months (four tris(*p*-*t*-butylbiphenyl)methyl moieties) at room temperature. In fact, two of these metastable [3]rotaxanes were stable enough to withstand column chromatography and

allow a full suite of characterization experiments, ^{1}H-^{1}H-NOESY, DOSY, GPC, and MALDI-MS, to confirm their assigned interlocked structure. The extremely slow slippage of [3]rotaxanes **3.17** and **3.19** is especially intriguing as it opens the door to the development of a range of relatively long lived metastable materials. For example, the utilization of such metastable doubly threaded rotaxanes may allow access to polyrotaxane networks/slide ring gels whose degradation rate can be controlled or are able to be reprocessed. In particular, this thesis will build on this framework for progress towards doubly threaded [3]rotaxanes and poly[3]rotaxanes.

3.7 Experimental

3.7.1 Materials and Methods

Materials. All reagents were purchased from Sigma-Aldrich unless otherwise stated. All chemicals were used as received without further purification unless otherwise stated. Solvents for chromatography were purchased from Fisher-Scientific. Deuterated solvents and 3,5-dihydroxybenzyl alcohol were purchased from ACROS Organics. 4-Bromo-4'-tert-butylbiphenyl was purchased from TCI chemicals. *p*-Toluenesulfonyl chloride was purchased from Alfa Aesar. Iron(II) bistriflimide[74] and 2,6-bisbenzimidazolylpyridine ligands[75] were prepared following literature procedures. Tetrahydrofuran (THF) was dried over sodium and benzophenone. Dichloromethane was distilled over calcium hydride before use. Dimethylformamide (DMF) was dried with activated molecular sieves before use. Thin layer chromatography plates (1000 micron) were purchased from Analtech.

Matrix Assisted Laser Desorption/Ionization Mass Spectrometry (MALDI-MS). MALDI-TOF was measured by a Bruker Ultraflextreme MALDI-TOF-TOF spectrometer in linear

(or reflectance) mode using dithranol as matrix and sodium trifluoroacetate or silver trifluoroacetate as ionizer (or no ionizer).

Nuclear Magnetic Resonance Spectroscopy (NMR). Room Temperature Nuclear Magnetic Resonance Spectroscopy was performed using a Bruker Ascend Avance III 500 MHz spectrometer, a Bruker Avance II+ 500 MHz spectrometer, or a Bruker DRX 400 MHz spectrometer at the University of Chicago NMR facilities. ^{1}H NMR spectra were referenced to the residual protonated solvent signal and $^{13}C\{^{1}H\}$ NMR spectra were referenced to the deuterated solvent carbon resonance signal.

NMR Slippage Kinetic Experiments. Kinetic experiments were performed in Shigemi Tubes purchased from Wilmad-Labglass in $CDCl_3$ (1mM) using a Bruker AVANCE III HD 500 MHz spectrometer at the NMR facilities at the University of Chicago.

Gel Permeation Chromatography (GPC). GPC measurements were performed utilizing the Soft Matter Characterization Facility at the University of Chicago. Measurements were conducted at 25°C using 3:1 THF:DMF as eluent (flow rate = 1 mL/min), using a Shimadzu autosampler, Shimadzu HPLC LC20-AD pump, 2 Agilent PLgel 5 um MIXED-D + guard SEC columns, and a Wyatt Optilab T-rEX differential refractive index detector.

UV-Vis Spectrometry. UV-Vis spectrometry was measured using a Shimadzu UV-3600 Plus UV-Vis-NIR spectrophotometer and a 1 cm width quartz cuvette.

3.7.2 Synthesis of 3.4

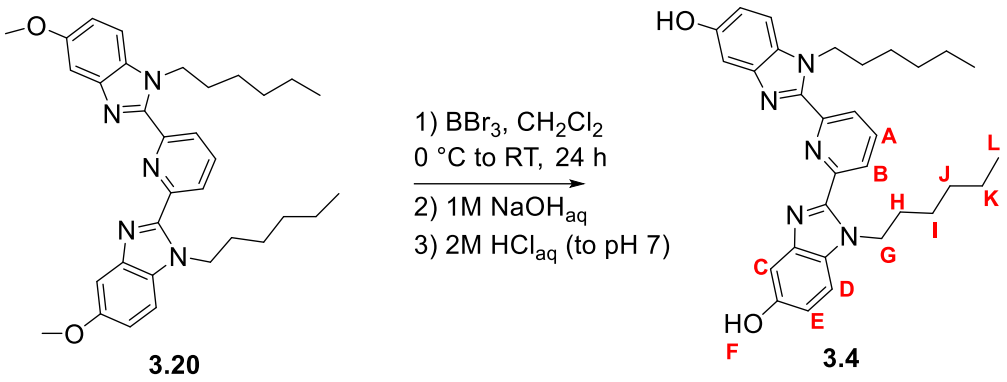

A 500mL RBF flask was purged with Ar and charged with **3.20**[75] (14 g, 25.9 mmol), a stir bar and DCM (250 mL). The mixture was stirred, cooled to 0 °C and BBr_3 (15 mL, 39.6 g, 158 mmol) was added dropwise over 5 min resulting in a deep red colored mixture. The reaction was warmed to RT and stirred for a total of 24 h. The reaction mixture was poured slowly into a 4L beaker containing 1M aq. NaOH (1.5 L) and vigorously stirred until the color changed from red to yellow. The pH of the suspension was then adjusted to 7 using a 2M aq HCl solution. Upon reducing the pH of the solution, a pale yellow precipitate formed, which was subsequently collected by vacuum filtration and purified by recrystallization (chloroform/methanol) to yield **3.4**, a white solid, in 79% yield. ^{1}H NMR (500 MHz, DMSO-d_6) δ 9.19 (s, 2H, F), 8.22 (d, J = 8.8 Hz, 2H, B), 8.16 (t, J = 8.8 Hz, 1H, A), 7.48 (d, J = 8.7 Hz, 2H, E), 7.04 (s, 2H, C), 6.84 (dd, J = 8.7, 2.3 Hz, 2H, D), 4.68 (t, J = 7.3 Hz, 4H, G), 1.62 (t, J = 7.2 Hz, 4H, H), 1.01-0.93 (m, 12H, I+J+K), 0.55 (m, 6H, L). ^{13}C{^{1}H} NMR (126 MHz, DMSO-d_6) δ 153.57, 149.70, 149.46, 143.27, 138.41, 130.01, 124.76, 113.47, 111.13, 103.68, 45.69, 30.45, 29.46, 25.50, 21.83, 13.52. MALDI-MS: 619.7 ([M]+Ag^+).

3.7.3 Synthesis of Macrocycle Component 3.1

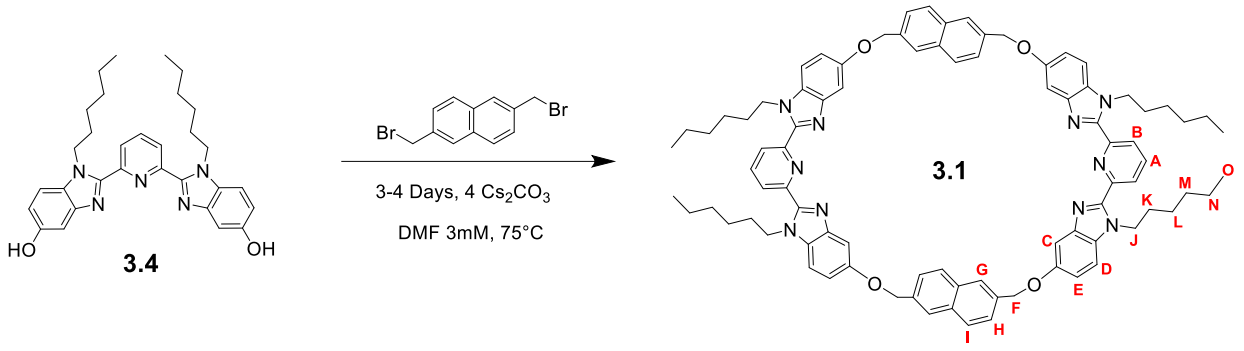

A 2-necked 1 L RBF was charged with **3.4** (1.0 g, 1.95 mmol), Cs_2CO_3 (2.6 g, 7.8 mmol, 4 eq.) and DMF (440 mL) under an Ar atmosphere. The mixture was heated to 75 °C and stirred while a DMF (220 mL) solution of 2,6-bis(bromomethyl)naphthalene (0.61, 1.95 mmol) was added dropwise (at an approximate rate of one drop every 10 s) over 3 d. When all the solution was added the reaction was stirred for a further 24 h at 75 °C. After this time (total reaction time 4 d) the reaction mixture was cooled to RT and the solvent was removed under reduced pressure. The residue was washed in hot $CHCl_3$ (4 × 100 mL) and the insoluble material (salts) was removed by filtration. The filtrate was collected and the solvent removed under reduced pressure. The resulting material was purified using column chromatography (TEA treated silica gel, chloroform/methanol gradient as eluent) followed by recrystallization (chloroform/methanol mixture) to yield white crystals of **3.1** in 26% yield. ^{1}H NMR (500 MHz, $CDCl_3$) δ 8.08 (d, *J* = 8.0 Hz, 4H, B), 7.79 (t, *J* = 8.0 Hz, 2H, A), 7.77 (s, 4H, C), 7.71 (d, *J* = 8.5 Hz, 4H, H), 7.50 (d, *J* = 8.5 Hz, 4H, I), 7.16 (m, 8H, G+D), 6.96 (dd, *J* = 8.9, 2.4 Hz, 4H, E), 5.44 (s, 8H, F), 4.44 (t, *J* = 7.5 Hz, 8H, J), 1.52 (m, 8H, K), 0.89 (m, 24H, L+M+N), 0.49 (m, 12H, O). ^{13}C{^{1}H} NMR (126 MHz, $CDCl_3$) δ 154.48, 150.17, 149.83, 143.29, 137.70, 135.42, 132.90, 131.19, 128.49, 125.66, 125.23, 124.99, 114.88, 110.73, 104.80, 70.46, 44.85, 31.15, 30.04, 26.32, 22.41, 13.77. MALDI-MS: 1435.9 ([M]+Ag^+).

3.7.4 Synthesis of 3.5

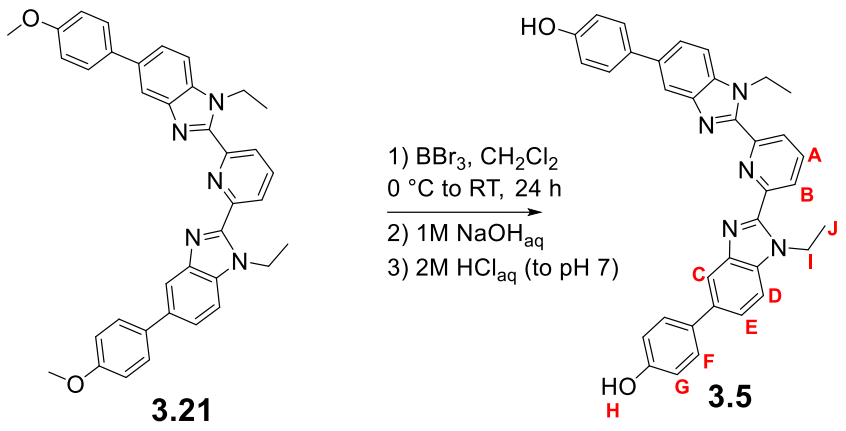

The deprotection of compound **3.21**[75] was performed in a similar way to **3.20** above, to give compound **3.5** as a pale white solid in a 90 % yield. ^{1}H NMR (400 MHz, DMSO-d_6) δ 9.67 (s, 2H, H), 8.38 (d, J = 7.8 Hz, 2H, B), 8.20 (t, J=7.8 Hz, 1H, A), 7.92 (s, 2H, C), 7.71 (d, J = 8.5 Hz, 2H, D), 7.56 (m, 6H, E+F), 6.97-6.86 (m, 4H, G), 4.83 (q, J = 7.1 Hz, 4H, I), 1.30 (t, J = 7.1 Hz, 6H, J). ^{13}C {^{1}H} NMR (101 MHz, DMSO-d_6) δ 156.88, 149.63, 149.59, 143.04, 138.65, 135.45, 134.82, 131.54, 127.91, 125.50, 122.41, 116.58, 115.79, 111.25, 15.39. MALDI-MS: 552.1 ([M]+H^{+}).

3.7.5 Synthesis of Thread Component 3.2

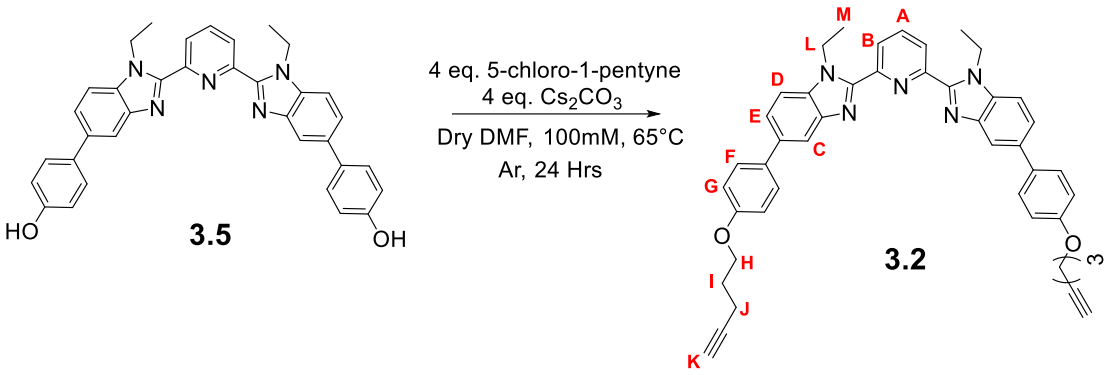

3.5 (2g, 3.62mmol) and Cs_2CO_3 (4.73 g, 14.5mmol, 4eq) were added to a 100mL RBF which was purged with Ar. To this mixture was added DMF (36 mL) and 5-chloro-1-pentyne (1.48 g, 1.53 mL, 14.5 mmol, 4 eq.). The subsequent mixed was stirred at 65°C for 24 h. After this time the solvent was removed under reduced pressure leaving a yellow residue. This residue was washed with chloroform (4 × 150 mL) and filtered. The filtrate was collected and the solvent removed under reduced pressure. The resulting material was purified using column chromatography (TEA treated silica gel, chloroform to 5% methanol in chloroform gradient as eluent, followed by recrystallization (chloroform/methanol mixture) to yield off-white crystals of **3.2** in 72% yield. ^{1}H NMR (500 MHz, $CDCl_3$) δ 8.37 (d, *J* = 7.9Hz, 2H, B), 8.08 (t, *J* = 7.9Hz, 1H, A), 8.03 (s, 2H, C), 7.65-7.56 (m, 6H, E+F), 7.52 (d, *J* = 8.4 Hz, 2H, D), 7.06-6.99 (m, 4H, G), 4.83 (q, *J* = 7.2 Hz, 4H, L), 4.14 (t, *J* = 6.1 Hz, 4H, H), 2.45 (m, 4H, J), 2.09-2.01 (m, 4H, I), 1.99 (t, *J* =2.6 Hz, 2H, K), 1.40 (t, *J* =7.2 Hz, 6H, M). ^{13}C{^{1}H} NMR (126 MHz, $CDCl_3$) δ 158.33, 150.48, 150.09, 143.63, 138.22, 136.32, 135.26, 134.45, 128.50, 125.79, 123.27, 118.21, 115.02, 110.45, 83.61, 69.03, 66.35, 40.05, 28.34, 15.62, 15.33. MALDI-MS: 684.3 ([M]+Na^+).

3.7.6 Synthesis of 3.7

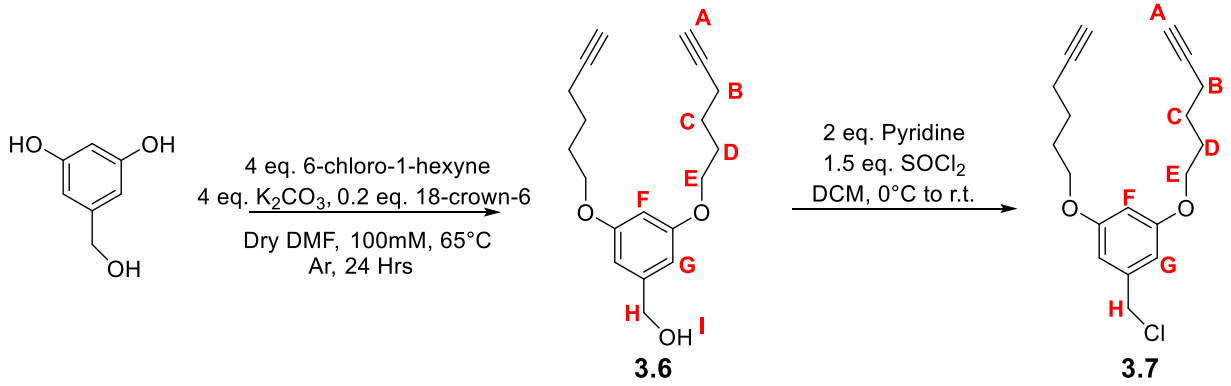

3,5-Dihydroxybenzyl alcohol (2.0g, 14.2mmol), K_2CO_3 (7.89g, 57mmol), and 18-crown-6 (0.75g, 2.8mmol) were added to a 100mL RBF. The reaction chamber was purged with

argon and DMF (28.5mL) was added via cannula. The reaction mixture was heated to 65°C and 6-chloro-1-hexyne (4.6mL, 57mmol) was injected via syringe. The reaction mixture was allowed to stir at 65°C overnight and the following day cooled to room temperature. The reaction mixture was diluted with 75mL ether and washed 1x100mL 1M NaOH and 2x100mL H_2O. The organic layer was isolated and the solvent was removed under vacuum to yield a yellow oil that was purified via column chromatography (25% hexanes in chloroform to pure chloroform gradient) to yield **3.6** as a light yellow oil in 70% yield. ^{1}H NMR (400 MHz, $CDCl_3$) δ 6.50 (bs, 2H, G), 6.37 (bs, 1H, F), 4.61 (d, *J* = 5.9 Hz, 2H, H), 3.97 (t, *J* = 6.8 Hz, 4H, E), 2.27 (td, *J* = 7.0, 2.6 Hz, 4H, B), 1.97 (t, *J* = 2.6 Hz, 2H, A), 1.90 (m, 4H, D), 1.71 (m, 4H, C). ^{13}C NMR (101 MHz, $CDCl_3$) δ 160.40, 143.40, 105.17, 100.58, 84.18, 68.79, 67.41, 65.32, 28.31, 25.10, 18.21. MALDI-MS: 322.9 ([M]+Na^+).

3.6 (2.05g, 6.8mmol) was added to a 100mL RBF with stir bar followed pyridine (1.10mL, 13.6mmol). The reaction chamber was purged with argon and DCM (27.3ml) was added via cannula. The reaction mixture was cooled to 0°C and $SOCl_2$ (0.74mL, 10.2mmol) was injected dropwise. The reaction mixture was allowed to stir overnight and slowly warm to room temperature. 50mL H_2O and 25mL DCM were then added to the crude reaction mixture and the organic layer was isolated, washed 3 x 75mL H_2O/brine, dried over magnesium sulfate and finally solvent was removed under vacuum. Column chromatography (50% hexanes in chloroform to pure chloroform gradient) gave **3.7** as a colorless oil in 62% yield. ^{1}H NMR (400 MHz, $CDCl_3$) δ 6.52 (bd, *J* = 2.2 Hz, 2H, G), 6.39 (bt, *J* = 2.2 Hz, 1H, F), 4.50 (s, 2H, H), 3.97 (t, *J* = 6.8 Hz, 4H, E), 2.28 (td, *J* = 7.0, 2.6 Hz, 4H, B), 1.97 (t, *J* = 2.6 Hz, 2H, A), 1.90 (m, 4H, D), 1.72 (m, 4H, C). ^{13}C NMR (101 MHz, $CDCl_3$) δ 160.37, 139.49, 107.06, 101.37, 84.32, 68.82, 67.46, 46.45, 28.28, 25.09, 18.22. MALDI-MS: 341.1 ([M]+Na^+).

3.7.7 Synthesis of Thread Component 3.3

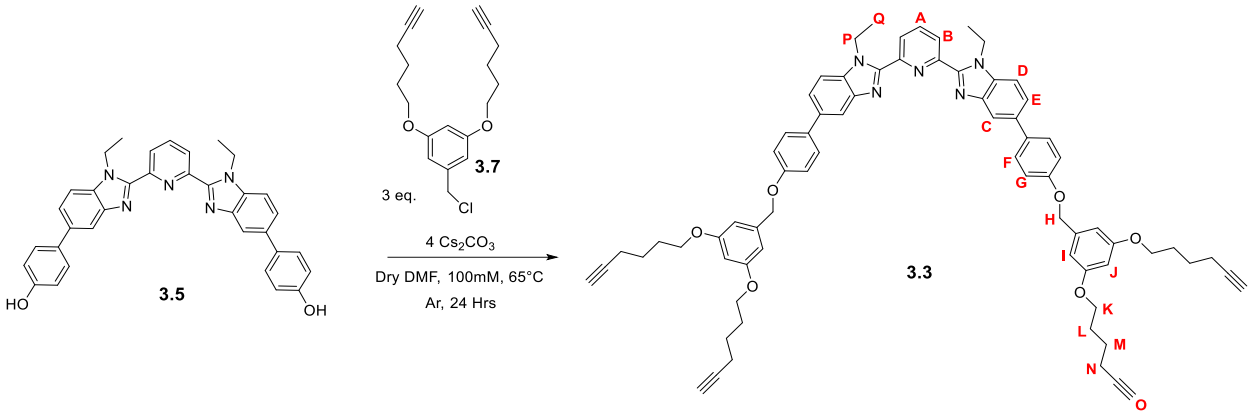

3.5 (253mg, 0.45mmol) were added to a 25mL RBF followed by **3.7** (440mg, 1.35mmol) and Cs_2CO_3 (600mg, 1.8mmol, 4eq.). The reaction chamber was purged with Ar and DMF (4.6mL) was syringed into reaction vessel. The reaction mixture was allowed to stir under Ar at 65°C for 24 hours. Solvent was then removed under vacuum and the crude solid was boiled in chloroform and consequently filtered (4x50mL). The filtrate was collected and the solvent was removed under reduced pressure. The resulting material was purified using column chromatography (TEA treated silica gel, chloroform to 5% methanol in chloroform gradient) followed by recrystallization (chloroform/methanol mixture) to yield **3.3** as off-white crystals in 90% yield. ^{1}H NMR (400 MHz, $CDCl_3$) δ 8.38 (d, *J* = 7.8Hz, 2H, B), 8.08 (t, *J* = 7.8Hz, 1H, A), 8.05 (s, 2H, C), 7.66-7.57 (m, 6H, D+E), 7.52 (d, *J* = 8.4 Hz, 2H, F), 7.09 (d, *J* = 8.7 Hz, 4H, G), 6.62 (bd, *J* = 2.2 Hz, 4H, I), 6.42 (bt, *J* = 2.2 Hz, 2H, J), 5.06 (s, 4H, H), 4.83 (q, *J* = 7.2 Hz, 4H, P), 4.00 (t, *J* = 6.2 Hz, 8H, K), 2.28 (td, *J* = 7.0, 2.6 Hz, 8H, N), 1.98 (t, *J* = 2.6 Hz, 4H, O), 1.96-1.87 (m, 8H, L), 1.79-1.68 (m, 8H, M), 1.40 (t, *J* = 7.2 Hz, 6H, Q). ^{13}C NMR (101 MHz, $CDCl_3$) δ 160.52, 158.21, 150.49, 150.08, 143.63, 139.49, 138.23, 136.26, 135.29, 134.67, 128.51, 125.80, 123.28, 118.22, 115.38, 110.46, 105.81, 100.89, 84.20, 70.24, 68.80, 67.47, 40.06, 28.36, 25.16, 18.27, 15.62. MALDI-MS: 1,224.4 ([M]+Ag^+).

3.7.8 Synthesis of 3.8

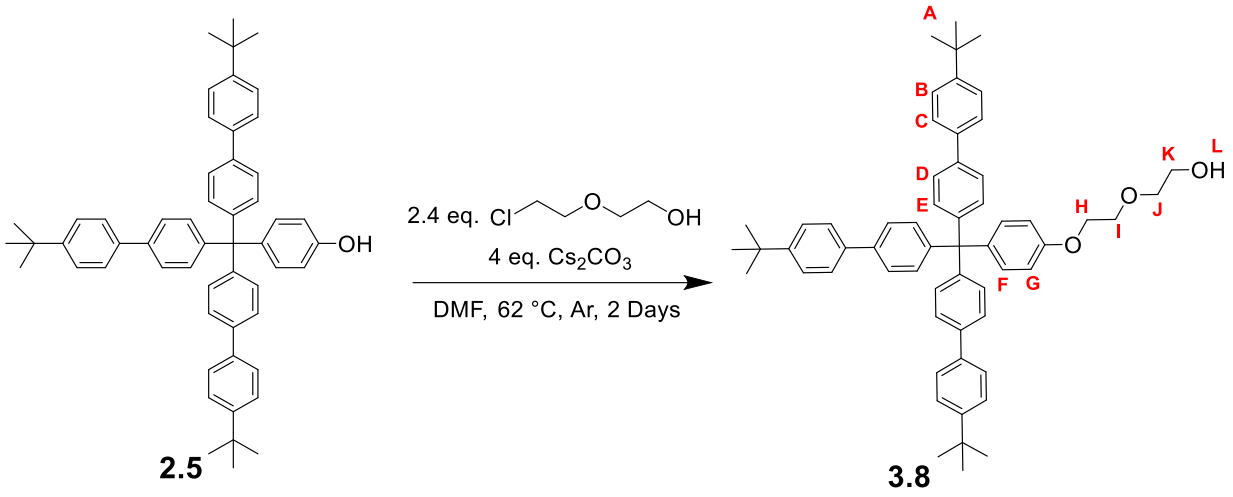

A 200 mL RBF was charged with **2.5** (5.0 g, 6.8 mmol), Cs_2CO_3 (8.9 g, 27 mmol, 4eq.) and DMF (68 mL, reaction concentration 100 mM) in an argon atmosphere. The reaction was stirred and 2-(2-chloroethoxy)ethanol (0.86 mL, 8.2mmol, 1.2eq.) was added dropwise and the reaction was heated at 62 °C for 18 h. A further portion of 2-(2-chloroethoxy)ethanol (0.86 mL, 8.2mmol, 1.2eq) was added and the reaction was stirred for a further 24 h. The reaction was cooled to RT and the volatiles were removed under vacuum. To the resulting off-white solid was added hot $CHCl_3$ (3 × 250 mL) and insoluble material was removed by filtration. The solvent was removed from the filtrate under reduced pressure resulting in an off-white residue. Purification of desired product **3.8** was achieved by column chromatography (silica gel, eluent gradient of 100 % $CHCl_3$ to 95:5 $CHCl_3$:MeOH) followed by recrystallization (chloroform/hexane layering). 89% yield. ^{1}H NMR (500 MHz, $CDCl_3$) δ 7.55 (d, *J* = 8.5 Hz, 6H, D), 7.50 (d, *J* = 8.5 Hz, 6H, B), 7.45 (d, *J* = 8.5 Hz, 6H, E), 7.31 (d, *J* = 8.5 Hz, 6H, C), 7.21 (d, *J* = 8.9 Hz, 2H, F), 6.85 (d, *J* = 8.9 Hz, 2H, G), 4.14 (m, 2H, K), 3.88 (m, 2H, H), 3.76 (m, 2H, J), 3.68 (m, 2H, I), 2.10 (t, *J* = 6.2 Hz, 1H, L), 1.35 (s, 27H, A). ^{13}C{^{1}H} NMR (126 MHz, $CDCl_3$) δ 156.81, 150.28, 145.90, 139.50, 138.52, 137.82,

132.39, 131.57, 126.72, 126.06, 125.80, 113.56, 72.68, 69.84, 67.40, 63.78, 61.94, 34.65, 31.50. MALDI-MS: 929.1 ([M]+Ag^+).

3.7.9 Synthesis of 3.9

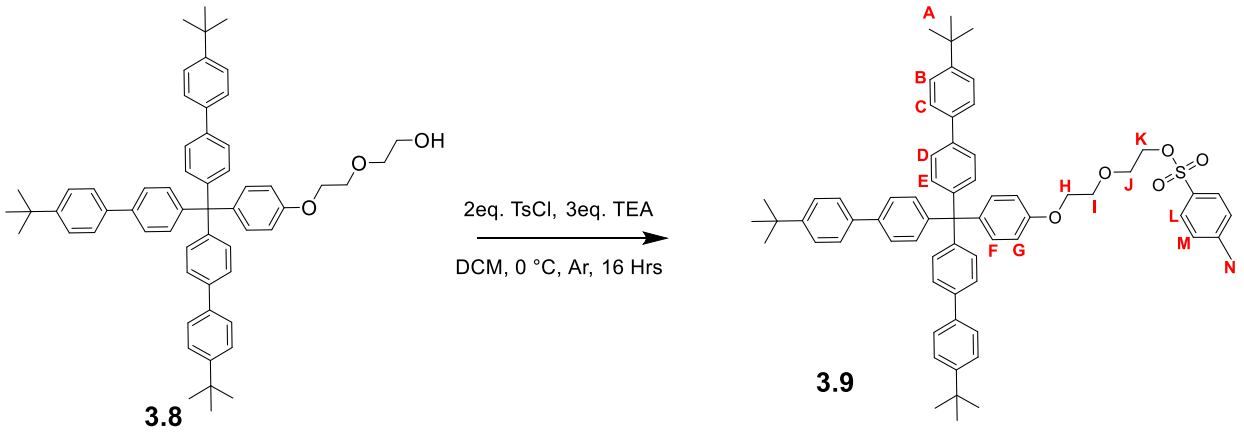

A 100 mL RBF was charged with **3.8** (5 g, 6.08 mmol), *p*-toluenesulfonyl chloride (2.30 g, 12.2 mmol, 2 eq.) and DCM (41 mL, reaction conc. = 150 mM). The reaction was stirred, cooled with an ice bath and NEt_3 (2.55 mL, 18.2 mmol, 3 eq.) was added dropwise and the reaction was allowed to warm to RT. After 18 h the reaction mixture was diluted with 40mL CH_2Cl_2 and H_2O (100 mL) was added. The organic layer was removed and dried with $MgSO_4$, filtered and the solvent reduced under reduced pressure. The resulting material was purified using column chromatography (silica gel, eluent gradient 1:1 hexanes:$CHCl_3$ to 95:5 $CHCl_3$:MeOH followed by precipitation (chloroform/hexane layering) to yield **3.9** as a white solid in 78% yield. ^{1}H NMR (500 MHz, $CDCl_3$) δ 7.79 (d, *J* = 8.3Hz, 2H, M), 7.55 (d, *J* = 8.5 Hz, 6H, D), 7.51 (d, *J* = 8.5 Hz, 6H, B), 7.45 (d, *J* = 8.5 Hz, 6H, E), 7.31 (d, *J* = 8.5 Hz, 6H, C), 7.28 (d, *J* = 8.3 Hz, 2H, L), 7.21 (d, *J* = 8.9 Hz, 2H, F), 6.85 (d, *J* = 8.9 Hz, 2H, G) 4.19 (m, 2H, K), 4.03 (m, 2H, H), 3.77 (m, 4H, I+J), 2.37 (s, 3H, N), 1.35 (s, 27H, A). ^{13}C{^{1}H} NMR (126 MHz, $CDCl_3$) δ 156.76, 150.26, 145.88, 144.87,

139.42, 138.49, 137.78, 133.06, 132.34, 131.55, 129.91, 128.10, 126.69, 126.05, 125.80, 113.50, 69.98, 69.38, 68.96, 67.34, 63.76, 34.63, 31.49, 21.72. MALDI-MS: 1083.5 ([M]+Ag^+).

3.7.10 Synthesis of Stopper Component 3.10

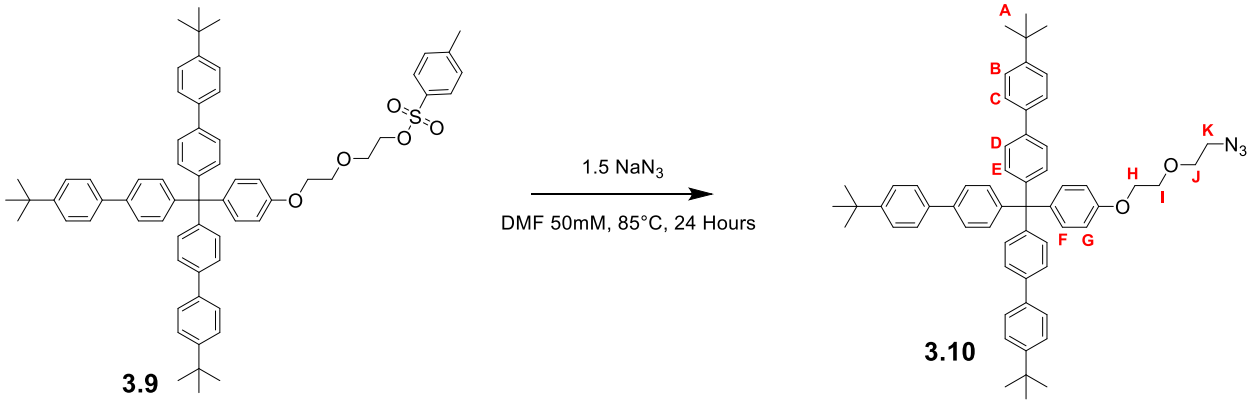

An Ar-filled 50 mL RBF was charged with **3.9** (400 mg, 0.41 mmol), NaN_3 (40 mg, 1.15 mmol, 1.5 eq.) and DMF (8.2 mL, reaction concentration 50 mM). The reaction mixture was heated at 85 °C and stirred for 18 h. After this time the solvent was removed under reduced pressure resulting in an off-white solid that was washed with hot $CHCl_3$ (4 × 15 mL) and filtered. The filtrate was collected and the solvent removed under reduced pressure resulting in an off-white residue. Purification using column chromatography (standard silica gel, eluent gradient 1:3 $CHCl_3$:Hexanes to 100 % $CHCl_3$) resulted in a white solid, **3.10**, in 90% yield. ^{1}H NMR (500 MHz, $CDCl_3$) δ 7.55 (d, *J* = 8.2 Hz, 6H, D), 7.51 (d, *J* = 8.2 Hz, 6H, B), 7.45 (d, *J* = 8.2 Hz, 6H, E), 7.31 (d, *J* = 8.2 Hz, 6H, C), 7.21 (d, *J* = 8.6 Hz, 2H, F), 6.85 (d, *J* = 8.6 Hz, 2H, G), 4.15 (t, *J* = 4.8 Hz, 2H, H), 3.87 (t, *J* = 4.8 Hz, 2H, I), 3.75 (t, *J* = 5.0 Hz, 2H, J), 3.42 (t, *J* = 5.0 Hz, 2H, K), 1.36 (s, 27H, A). ^{13}C{^{1}H} NMR (101 MHz, $CDCl_3$) δ 156.85, 150.27, 145.93, 139.43, 138.51, 137.83, 132.37, 131.58, 126.72, 131.58, 126.72, 126.05, 125.81, 113.59, 70.36, 69.95, 67.46, 63.79, 50.86, 34.66, 31.51. MALDI-MS: 954.1 ([M]+Ag^+) and 926.2 ([M]+Ag^+ -N_2).

3.7.11 Synthesis of 3.11

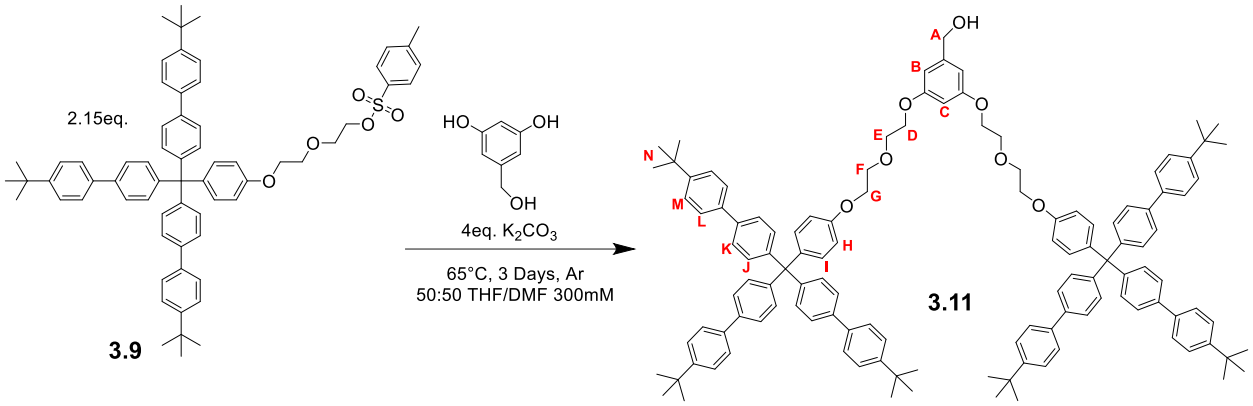

An Ar-filled 100 mL RBF was charged with **3.9** (4.5g, 4.6mmol, 2.15eq.), K_2CO_3 (1.18 g 8.5mmol, 4eq.) and 3,5-dihydroxybenzyl alcohol (300 mg, 2.1mmol, 1eq.). To the reaction vessel was added THF/DMF (1:1 ratio, 15 mL) and the reaction was stirred at 65 °C for 3 d. The solvent was cooled to RT and the solvent was removed under vacuum. To the resulting off-white solid was added hot $CHCl_3$ (4 × 200 mL) and the insoluble material was removed by filtration. The filtrate was collected and the solvent removed under reduced pressure. The resulting material was purified using column chromatography (silica gel, eluent gradient of 12:88 ethyl acetate:hexanes to 7:3 $CHCl_3$:hexanes to $CHCl_3$.) followed by recrystallization (chloroform/methanol layering) resulting in **3.11** as a white solid in 50% yield. ^{1}H NMR (500 MHz, $CDCl_3$) δ 7.54 (d, *J* = 8.5 Hz, 12H, K), 7.49 (d, *J* = 8.5 Hz, 12H, M), 7.44 (d, *J* = 8.5 Hz, 12H, J), 7.30 (d, *J* = 8.5 Hz, 12H, L), 7.19 (d, *J* = 8.9 Hz, 4H, I), 6.83 (d, *J* = 8.9 Hz, 4H, H), 6.53 (d, *J* = 2.2 Hz, 2H, B), 6.44 (t, *J* = 2.3 Hz, 1H, C), 4.58 (d, *J* = 6.3 Hz, 2H, A), 4.13 (m, 8H, D+G), 3.90 (m, 8H, E+F), 1.35 (s, 54H, N). ^{13}C{^{1}H} NMR (126 MHz, $CDCl_3$) δ 160.46, 157.25, 150.72, 146.39, 144.26, 139.56, 138.71, 137.89, 132.44, 131.70, 126.87, 126.35, 126.13, 113.89, 105.63, 100.81, 70.22, 67.96, 65.32, 64.07, 60.65, 34.80, 31.49, 14.42. MALDI-MS: 1854.6 ([M]+Ag^+).

3.7.12 Synthesis of 3.12

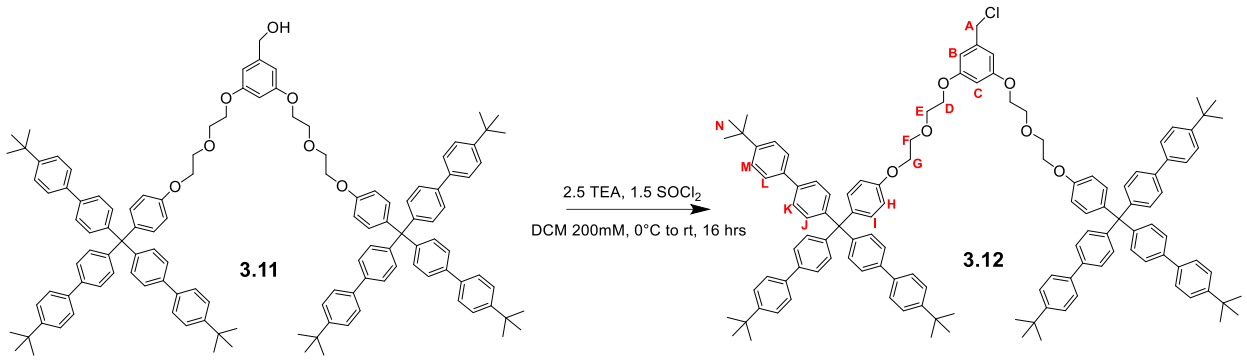

A 5 mL RBF was charged with **3.11** (0.24 g, 0.14 mmol) and purged with Ar. CH_2Cl_2 (0.7 mL) was added to the reaction vessel, which was subsequently cooled to 0°C. The solution was vigorously stirred while NEt_3 (48 µL, 0.35 mmol, 2.5 eq.) and $SOCl_2$ (15 µL, 0.21mmol, 1.5eq.) were added dropwise. The reaction mixture was stirred at RT for a total of 18 h before dilution with additional CH_2Cl_2 (25 mL). The resulting mixture was washed with H_2O (2 × 25 mL) and sat. $NaHCO_3$ (1 × 25 mL). The organic layer was dried with $MgSO_4$, filtered and the solvent was removed under reduced pressure resulting in an off-white residue. Purification by column chromatography (SiO_2, eluent gradient from 1:3 $CHCl_3$:hexanes to 100% $CHCl_3$) followed by recrystallization (chloroform/methanol layering) resulted in the isolation of **3.12** as a white solid in 80% yield. ^{1}H NMR (500 MHz, $CDCl_3$) δ 7.57 (d, *J* = 8.5 Hz, 12H, K), 7.52 (d, *J* = 8.5 Hz, 12H, M), 7.46 (d, *J* = 8.5 Hz, 12H, J), 7.33 (d, *J* = 8.5 Hz, 12H, L), 7.23 (d, *J* = 8.9 Hz, 4H, I), 6.86 (d, *J* = 8.9 Hz, 4H, H), 6.57 (d, *J* = 2.2 Hz, 2H, B), 6.49 (t, *J* = 2.2 Hz, 1H, C), 4.47 (s, 2H, A), 4.15 (m, 8H, D+G), 3.94 (m, 8H, E+F), 1.37 (s, 54H, N). ^{13}C{^{1}H} NMR (126 MHz, $CDCl_3$) δ 160.15, 156.90, 150.27, 145.94, 139.57, 139.35, 138.50, 137.83, 132.35, 131.59, 126.72, 126.05, 125.81, 113.60, 107.64, 101.81, 70.10, 69.97, 67.76, 67.48, 63.79, 46.40, 34.66, 31.51. MALDI-MS: 1873.0 ([M]+Ag^+).

3.7.13 Synthesis of Stopper Component 3.13

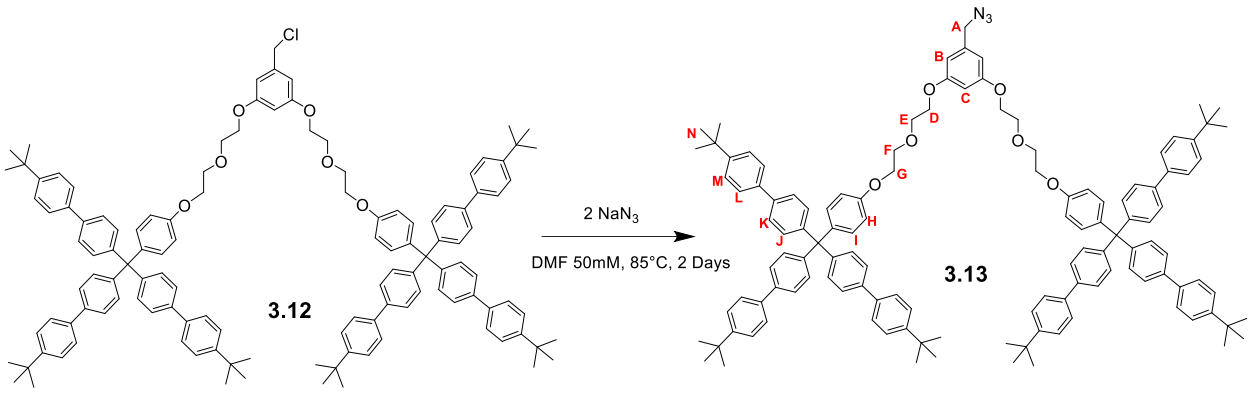

An Ar-purged 10 mL RBF was charged with **3.12** (0.24 g, 0.14mmol) NaN_3 (9mg, 0.14 mmol, 1eq.) and DMF (2.7 mL, reaction conc = 50 mM). The reaction was stirred for 18h at 85 °C and another portion of NaN_3 (9 mg, 0.14 mmol) was added, and the reaction was stirred for a further 18 h (total reaction time 36 h). The solvent was then removed under reduced pressure and the mixture washed with hot $CHCl_3$ (4 × 15 mL) and filtered. The filtrate was collected and the solvent removed under reduced pressure resulting in an off-white residue. Purification of **5** was achieved using column chromatography (silica gel, eluent gradient of 12:88 to 20:80 ethyl acetate:hexanes followed by 7:3 $CHCl_3$:hexanes to 100% $CHCl_3$) resulting in a white solid **3.13** in 72% yield. ^{1}H NMR (500 MHz, $CDCl_3$) δ 7.56 (d, *J* = 8.4 Hz, 12H, K), 7.52 (d, *J* = 8.4 Hz, 12H, M), 7.46 (d, *J* = 8.4 Hz, 12H, J), 7.33 (d, *J* = 8.4 Hz, 12H, L), 7.23 (d, *J* = 8.9 Hz, 4H, I), 6.86 (d, *J* = 8.9 Hz, 4H, H), 6.50 (bs, 3H, B+C), 4.23 (s, 2H, A), 4.15 (m, 8H, D+G), 3.93 (m, 8H, E+F), 1.37 (s, 54H, N). ^{13}C{^{1}H} NMR (126 MHz, $CDCl_3$) δ 160.29, 156.88, 150.26, 145.92, 139.33, 138.49, 137.82, 137.63, 132.34, 131.58, 126.72, 126.05, 125.80, 113.57, 107.15, 101.53, 70.09, 69.96, 67.72, 67.45, 63.77, 54.92, 34.65, 31.50. MALDI-MS: 1879.5 ([M]+Ag^+) and 1851.9 ([M]+Ag^+ -N_2).

3.7.14 Assembly of 3.1:3.2$_2$:Fe(II)$_2$

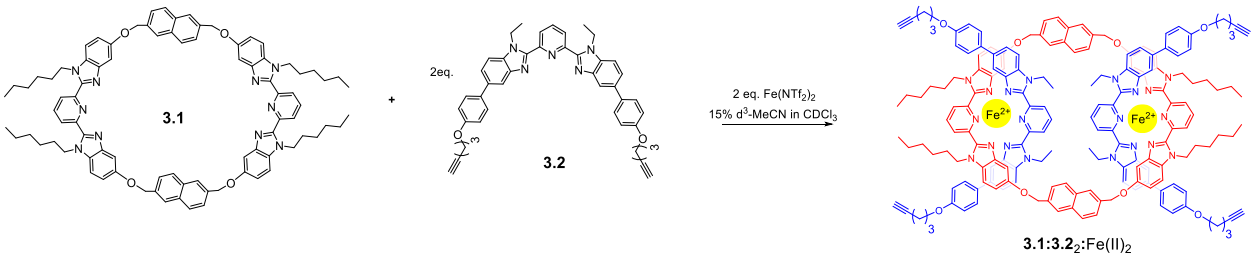

Dissolved 20.2mg of **3.1** in 1.5mL $CDCl_3$**.** Titrated thread stock solution (30mM) of **3.2** into solution of **3.1** until an exact 2:1 (**3.2**:**3.1**) ratio was formed (done by monitoring both the N-CH_2 peaks on the alkyl groups of the bip ligands). The mixture was then diluted to a total volume to 3mL $CDCl_3$ (5 mM **3.1**). A stock solution of $Fe(NTF_2)_2$ (30mM in 2:1 $CDCl_3$:d_3-MeCN) was added until no free Bip peak appeared at ~2 equiv. of metal ion. The solvent was removed under vacuum resulting in a dark purple solid that was redissolved in 2mL dry 15% MeCN in $CHCl_3$, bubbled with argon for 1 min, and allowed to stir under Ar at 45°C for 1 day to allow equilibration. Solvent was then removed under vacuum and ^{1}H-NMR was recorded using 15% d_3-MeCN in $CDCl_3$.

3.7.15 Assembly of 3.1:3.3$_2$:Fe(II)$_2$

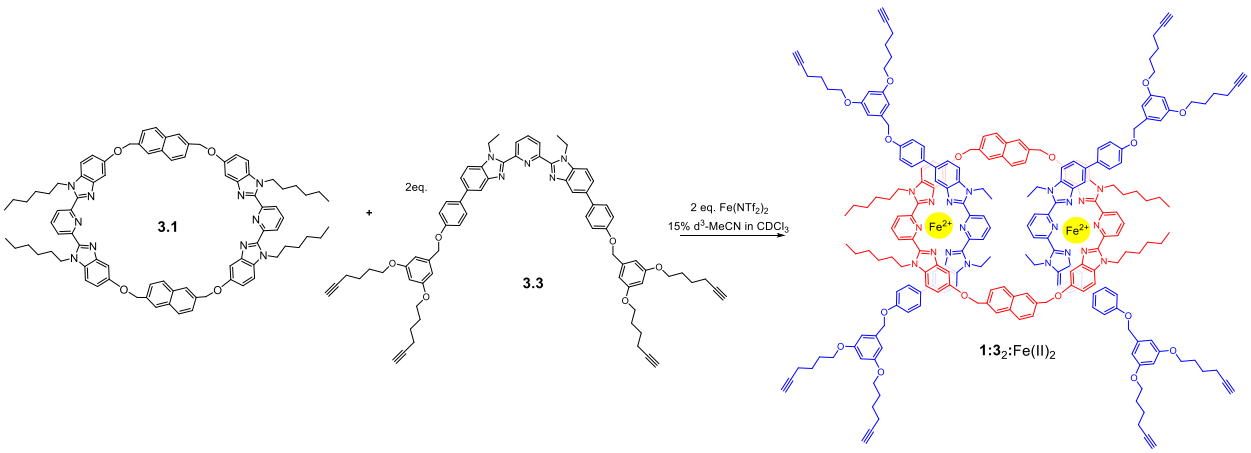

Dissolved 26.5mg of **3.1** in 1.5mL $CDCl_3$**.** Titrated thread stock solution (30mM) of **3.3** into solution of **3.1** until an exact 2:1 (**3.3**:**3.1**) ratio was formed (done by monitoring both the N-CH_2 peaks on the alkyl groups of the bip ligands). The mixture was then diluted to a total volume to 4mL $CDCl_3$ (5 mM **3.1**). A stock solution of $Fe(NTF_2)_2$ (30mM in 2:1 $CDCl_3$:d_3-MeCN) was added

until no free Bip peak appeared at ~2 equiv. of metal ion. The solvent was removed under vacuum resulting in a dark purple solid that was redissolved in 2mL dry 15% MeCN in $CHCl_3$, bubbled with argon for 1 min, and allowed to stir under Ar at 45°C for 2 days to allow equilibration. Solvent was then removed under vacuum and ^{1}H-NMR was recorded using 15% d_3-MeCN in $CDCl_3$.

3.7.16 Synthesis of Dumbbell Component 3.14

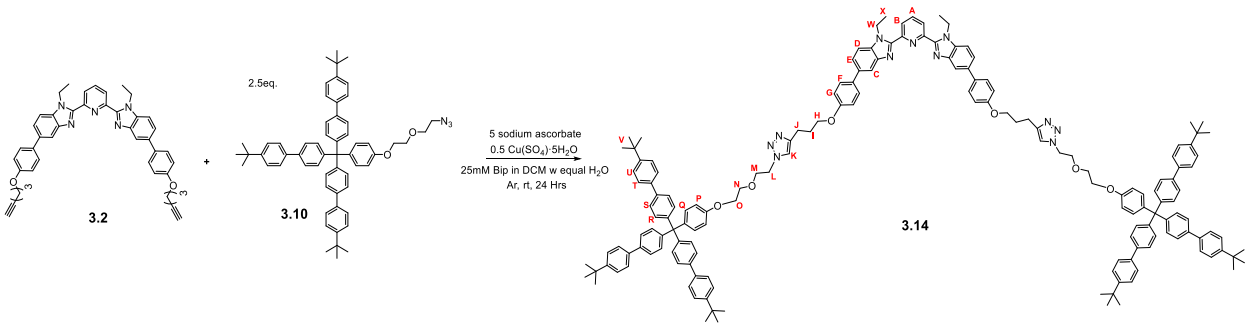

3.10 (45 mg, 0.053mmol, 2.5eq.), **3.2** (14.5 mg, 0.021 mmol) and sodium ascorbate (20.9 mg, 0.1 mmol, 5 eq) were added to a 4mL glass vial purged with Ar. To this mixture was added CH_2Cl_2 (0.90 mL, conc of **3.2** = 25 mM), H_2O (0.8 mL), and 100µL of an aqueous stock solution of $Cu(SO_4)\cdot 5H_2O$ (100 mM, 0.010mmol, 0.5eq, (25 mol% per alkyne)). The reaction was stirred vigorously for 18 h at RT. After this time the reaction mixture was diluted with CH_2Cl_2 and H_2O (10 mL each). The organic layer was taken and washed with H_2O (2 × 5 mL). Removal of the organic solvent resulted in a light brown crude solid, which was purified using preparative thin layer chromatography (SiO_2, eluent = 95:5 $CHCl_3$:MeOH) followed by recrystallization (chloroform/methanol layering) to result in a white solid, **3.14** in 86% yield. ^{1}H NMR (500 MHz, $CDCl_3$) δ 8.36 (d, *J* = 7.9Hz, 2H, B), 8.06-8.01 (m, 3H, A+C), 7.57– 7.45 (m, 34H, S+U+D+E+F+K), 7.43 (d, *J* = 8.5 Hz, 12H, R), 7.31 (d, *J* = 8.5 Hz, 12H, T), 7.23 (d, *J* = 8.9 Hz, 4H, Q), 6.96 (d, *J* = 8.7 Hz, 4H, G), 6.82 (d, *J* = 8.9 Hz, 8H, P), 4.80 (q, *J* = 7.2 Hz, 4H, W), 4.54 (t, *J* = 5.0 Hz, 4H, H), 4.08 (m, 4H, L), 4.03 (t, *J* = 6.2 Hz, 4H, O), 3.93 (t, *J* = 5.0 Hz, 4H, N),

3.80 (m, 4H, M), 2.92 (t, *J* = 7.5 Hz, 4H, J), 2.19 (m, 4H, I), 1.37 (t, *J* =7.2 Hz, 6H, X), 1.34 (s, 54H, V). $^{13}C\{^{1}H\}$ NMR (126 MHz, $CDCl_3$) δ 158.45, 156.79, 156.74, 150.48, 150.32, 150.10, 147.29, 145.89, 143.64, 139.61, 138.54, 138.26, 137.79, 136.39, 135.26, 134.33, 132.44, 131.57, 128.50, 126.72, 126.08, 125.83, 123.33, 122.42, 118.22, 115.02, 113.52, 110.46, 69.97, 67.26, 67.08, 63.80, 50.33, 40.08, 34.67, 31.50, 29.86, 22.33, 15.64. MALDI-MS: 2,484.2 ([M]+Ag^+).

3.7.17 Attempted Synthesis of [3]Rotaxane 3.15

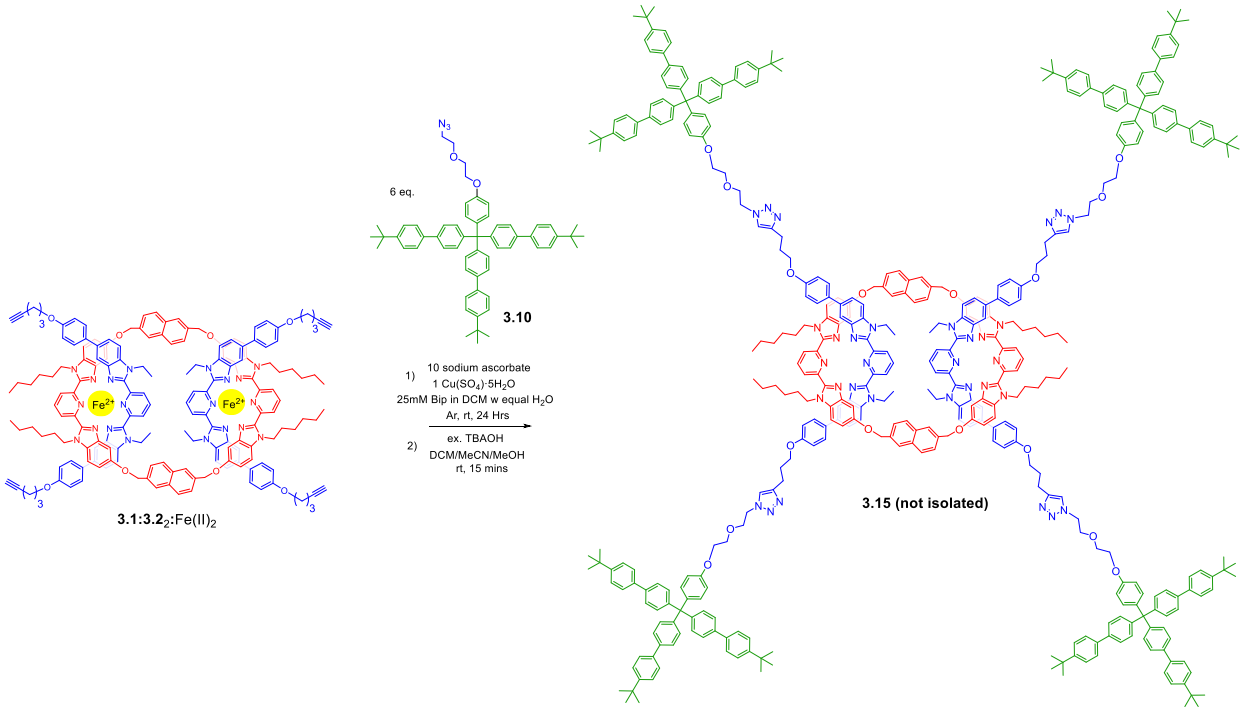

3.1:3.2$_2$: Fe(II)$_2$ (8.2 mg, 0.0021mmol), **3.10** (10.6 mg, 0.012 mmol, 6eq) and sodium ascorbate (4.1 mg, 0.021 mmol, 10 eq) were added to a 4mL glass vial purged with Ar. To this mixture was added CH_2Cl_2 (0.34 mL, conc of alkyne = 25 mM), H_2O (0.24 mL), and 100μL of an aqueous stock solution of $Cu(SO_4)\cdot 5H_2O$ (21 mM, 0.0021mmol, 1eq, (25 mol% per alkyne)). The reaction was stirred vigorously for 18 h at RT. After this time the reaction mixture was diluted with CH_2Cl_2 and H_2O (5 mL each). The organic layer was taken and washed with H_2O (2 × 5 mL). Removal of the organic solvent resulted in a purple solid that was washed 3x with 5mL of 10% chloroform in

hexanes to help remove leftover stopper group. The crude purple solid was redissolved in 5mL of 50:50 dichloromethane and acetonitrile and stirred slowly at room temperature. 2mL of tetrabutylammonium hydroxide solution (1M in MeOH) were added dropwise to the stirring solution resulting in a rapid color change from purple to light brown and precipitation of demetallated product. After 15 minutes of stirring an offwhite solid was filtered off and washed with methanol (2x 10mL). The frit was then washed with 2mL of $CDCl_3$ to redissolve the demetallated product and transferred to an NMR tube for analysis.

3.7.18 Synthesis of Dumbbell Component 3.16

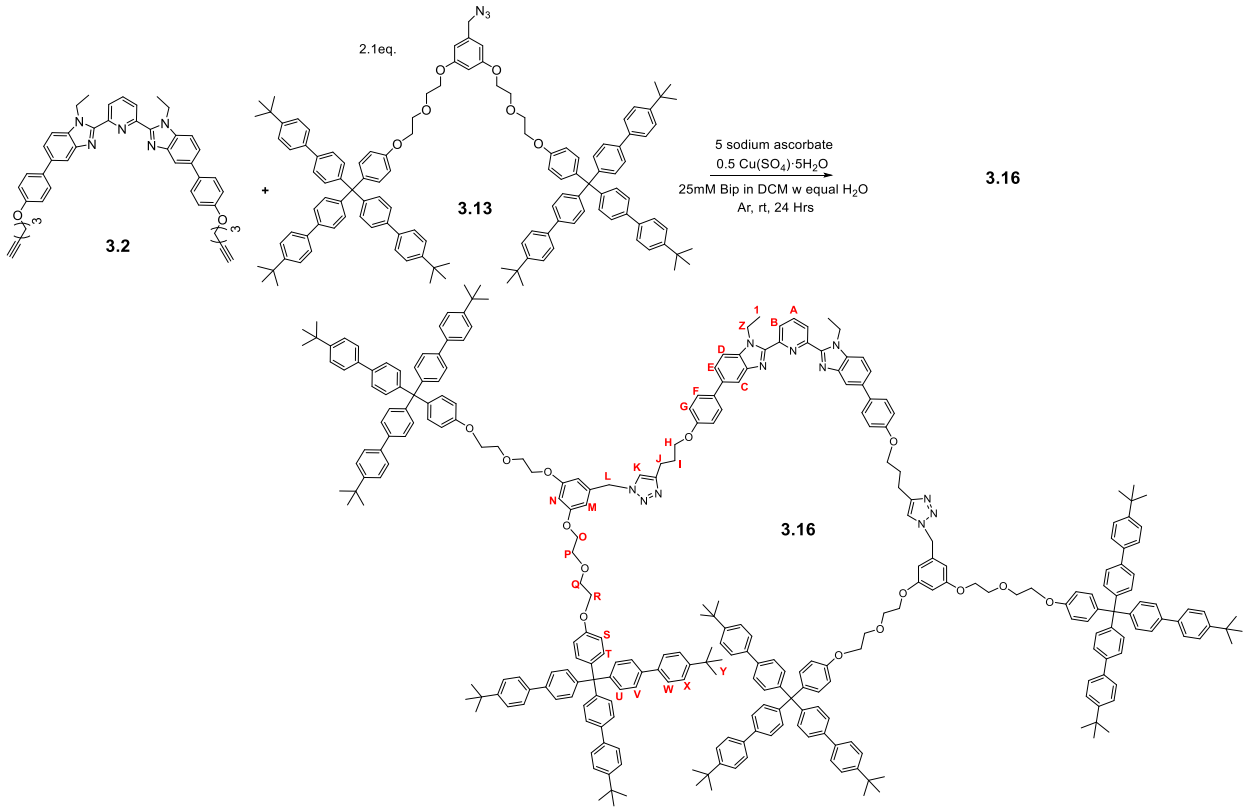

3.13 (60 mg, 0.034mmol, 2.1eq.), **3.2** (11 mg, 0.016 mmol) and sodium ascorbate (16 mg, 0.08 mmol, 5 eq) were added to a 4mL glass vial purged with Ar. To this mixture was added CH_2Cl_2 (0.63 mL, conc of **3.2** = 25 mM), H_2O (0.53 mL), and 100µL of an aqueous stock solution of $Cu(SO_4)\cdot 5H_2O$ (80 mM, 0.008mmol, 0.5eq, (25mol% per alkyne)). The reaction was stirred

vigorously for 18 h at RT. After this time the reaction mixture was diluted with CH_2Cl_2 and H_2O (10 mL each). The organic layer was taken and washed with H_2O (2 × 5 mL). Removal of organic solvent resulted in a light brown crude solid, which was purified using preparative thin layer chromatography (SiO_2, eluent = 95:5 $CHCl_3$:MeOH) followed by recrystallization (chloroform/methanol layering) resulting in a white solid, **3.16** in 88% yield. ^{1}H NMR (500 MHz, $CDCl_3$) δ 8.36 (d, *J* = 7.9Hz, 2H, B), 8.02 (m, 3H, A+C), 7.58 – 7.48 (m, 56H, V+X+D+E+F), 7.43 (d, *J* = 8.2 Hz, 24H, U), 7.30 (d, *J* = 8.2 Hz, 24H, W), 7.21 (s, 2H, K), 7.19 (d, *J* = 8.5 Hz, 8H, T), 6.96 (d, J = 8.3 Hz, 4H, G), 6.82 (d, *J* = 8.5 Hz, 8H, S), 6.48 (s, 2H, N), 6.40 (d, *J* = 2.2 Hz, 4H, M), 5.35 (s, 4H, L), 4.79 (q, *J* = 7.2 Hz, 4H, Z), 4.12-4.02 (m, 20H, O+R+H), 3.89-3.85 (m, 16H, P+Q), 2.90 (t, *J* = 7.2 Hz, 4H, J), 2.17 (t, *J* = 7.1 Hz, 4H, I), 1.37 (t, *J* =7.2 Hz, 6H, 1), 1.34 (s, 108H, Y). ^{13}C{^{1}H} NMR (126 MHz, $CDCl_3$) δ 160.51, 158.40, 156.88, 150.49, 150.28, 150.09, 147.86, 145.92, 143.65, 139.36, 138.50, 138.25, 137.81, 137.05, 136.38, 135.26, 134.34, 132.35, 131.58, 128.51, 126.71, 126.52, 126.05, 125.81, 123.32, 121.05, 118.22, 115.00, 113.57, 110.47, 107.14, 101.66, 70.10, 69.91, 67.76, 67.44, 67.10, 63.77, 54.17, 40.07, 34.66, 31.50, 29.03, 22.41, 15.64. MALDI-MS: 4,334.9 ([M]+Ag^+).

3.7.19 Synthesis of [3]Rotaxane 3.17

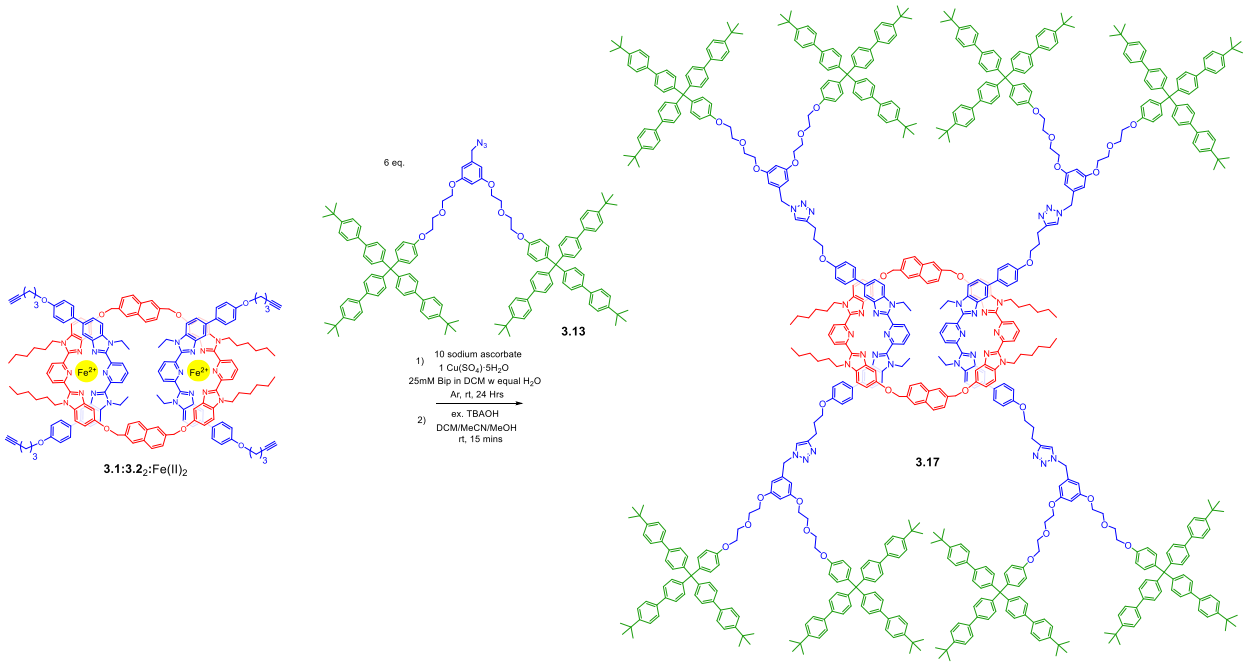

3.1:3.2$_2$:Fe(II)$_2$ (20.0 mg, 0.0051mmol), **3.13** (54.2 mg, 0.030 mmol, 6eq) and sodium ascorbate (10.1 mg, 0.051 mmol, 10 eq) were added to a 4mL glass vial purged with Ar. To this mixture was added CH_2Cl_2 (0.82 mL, conc of alkyne = 25 mM), H_2O (0.72 mL), and 100µL of an aqueous stock solution of $Cu(SO_4)\cdot 5H_2O$ (51mM, 0.0051mmol, 1eq, (25mol% per alkyne)). The reaction was stirred vigorously for 18 h at RT. The reaction mixture was then diluted with CH_2Cl_2 and H_2O (5 mL each). The organic layer was collected and washed with H_2O (2 × 5 mL). Removal of organic solvent resulted in a purple solid that was washed 3x with 5mL of 10% chloroform in hexanes to help remove leftover stopper group. The crude purple solid was redissolved in 5mL of 50:50 dichloromethane and acetonitrile and stirred slowly at room temperature. 1mL of tetrabutylammonium hydroxide solution (1M in MeOH) was added dropwise to the stirring solution resulting in a rapid color change from purple to light brown and precipitation of demetallated product. After 15 minutes of stirring, an off-white solid was filtered off and washed

with methanol (2x 10mL). The frit was then washed with 5mL of $CHCl_3$ to redissolve the demetallated product and washed once with 5mL water. Solvent was removed under reduced pressure resulting in an off-white residue. Purification of **3.17** was achieved using preparative thin layer chromatography (SiO_2, eluent = 94:6 $CHCl_3$:MeOH, lowest Rf band taken (R_f=0.1-0.3) as [3]R product, macrocycle byproduct R_f=0.4, dumbbell byproduct R_f=0.65-0.75) followed by precipitation from cold methanol to result in an off-white solid, **3.17** in 75% isolated yield. ^{1}H NMR (500 MHz, $CDCl_3$) δ 8.22 (d, *J* = 7.8Hz, 4H), 7.96-7.88 (m, 8H), 7.81 (t, *J* = 7.8Hz, 2H), 7.67 (s, 4H), 7.55-7.45 (m, 106H), 7.42 (d, *J* = 8.5 Hz, 48H), 7.37 (d, *J* = 8.9 Hz, 8H), 7.31-7.28 (m 52H), 7.24 (s, 2H), 7.21-7.15 (m, 20H), 6.86-6.75 (m, 28H), 6.62 (d, *J* = 8.6 Hz, 8H), 6.49 (s, 4H), 6.37 (d, *J* = 2.0 Hz, 8H), 5.32 (bs, 4H), 5.18 (s, 4H), 4.59 (bq, *J* = 7.2 Hz, 8H), 4.27 (bt, 8H) 4.12-4.00 (m, 32H), 3.90-3.78 (m, 32H), 3.48 (bt, 8H), 2.39 (bt, 8H), 1.62 (bt, 8H), 1.36 (m, 8H), 1.33 (s, 216H), 1.18 (t, *J* = 7.2H, 12H), 0.90-0.70 (m, 24H), 0.47 (t, *J* = 6.9Hz, 12H). ^{13}C{^{1}H} NMR (126 MHz, $CDCl_3$) δ 160.48, 158.19, 156.85, 154.42, 150.25, 150.18, 150.09, 149.90, 149.66, 147.73, 145.90, 143.50, 143.28, 139.32, 138.47, 137.95, 137.79, 137.33, 136.13, 135.82, 135.13, 133.80, 132.76, 132.33, 131.56, 131.27, 130.14, 130.05, 129.87, 128.40, 128.12, 126.70, 126.04, 125.80, 125.33, 125.08, 123.08, 120.84, 117.85, 114.74, 114.06, 113.54, 110.90, 110.41, 107.11, 105.06, 101.44, 70.71, 70.06, 69.90, 67.73, 67.38, 66.88, 63.75, 56.12, 53.83, 44.65, 39.86, 36.04, 34.64, 31.49, 29.84, 27.34, 26.17, 22.37, 15.52, 13.91. MALDI-MS: 9,782.2 ([M]+H^+), 5,554.5 ([M]+H^+-DB(**3.16**)), 4,226.7 ([M]+H^+-MC(**3.1**)-DB(**3.16**)).

3.7.20 Synthesis of Dumbbell Component 3.18

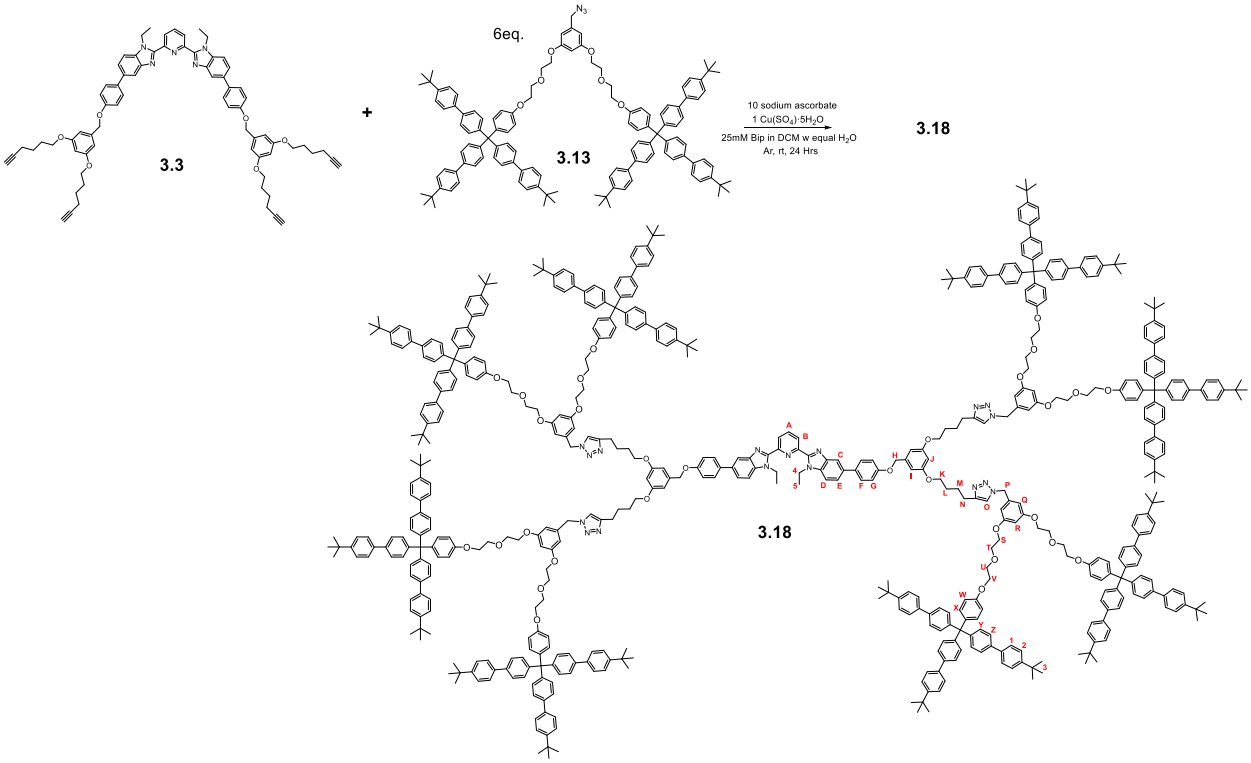

3.13 (51mg, 0.028mmol, 6eq.) was added to a 4mL glass vial followed by **3.3** (5.3mg, 0.0047mmol), sodium ascorbate (9.3mg, 0.047mmol, 10eq.), and the reaction chamber was purged with Ar. 200µL DCM (25mM **3**), 100µL H_2O, and finally 100µL of stock $Cu(SO_4)\cdot 5H_2O$ in H_2O solution (1.2mg, 0.0047mmol, 1.0eq, (25mol% per alkyne)) were added to reaction mixture. The reaction mixture was left to stir overnight and then diluted with 10mL DCM and 10mL H_2O. The organic layer was isolated and washed with 2x5mL H_2O before the organic solvent was removed under reduced pressure resulting in a light brown crude solid. The solid was purified using preparative thin layer chromatography (5% MeOH in $CHCl_3$ as eluent) followed by recrystallization (chloroform/methanol layering) resulting in **3.18** as white solid in 82% yield. ^{1}H NMR (500 MHz, $CDCl_3$) δ 8.34 (d, *J* = 7.9Hz, 2H, A), 8.01 (m, 3H, B+C), 7.57 (d, *J* = 8.6 Hz, 4H, F), 7.56 – 7.44 (m, 100H, D+E+Z+2), 7.42 (d, *J* = 8.4 Hz, 48H, Y), 7.28 (d, *J* = 8.4 Hz, 48H, 1), 7.18 (d, *J* = 8.9 Hz, 16H, X), 7.15 (s, 4H, O), 7.04 (d, *J* = 8.3 Hz, 4H, G), 6.80 (d, *J* = 8.9 Hz,

16H, W), 6.55 (bd, *J* = 1.8 Hz, 4H, I), 6.46 (bt, *J* = 2.2 Hz, 4H, *J* R), 6.38 (bd, = 2.2 Hz, 8H, Q), 6.34 (bt, *J* = 1.8 Hz, 2H, J), 5.31 (s, 8H, P), 4.97 (s, 4H, H), 4.77 (q, *J* = 7.1 Hz, 4H, 4 J), 4.09 (t, *J* = 5.6 Hz, 16H, V), 4.05 (q, *J* = 5.6 Hz, 16H, S), 3.92 (bt, *J* = 6.9 Hz, 8H, K), 3.89-3.81 (m, 32H, T+U), 2.72 (t, *J* = 6.9 Hz, 8H, N), 1.79 (bs, 16H, L+M), 1.34 (s, 216H, 3), 0.88 (t, *J* =7.2 Hz, 6H, 5). ^{13}C NMR (126 MHz, $CDCl_3$) δ 160.52, 160.49, 158.26, 156.87, 150.47, 150.27, 150.09, 148.43, 145.92, 143.64, 139.40, 139.35, 138.49, 137.80, 137.13, 136.32, 135.29, 134.63, 132.34, 131.57, 130.16, 129.87, 128.52, 126.71, 126.04, 125.81, 123.33, 120.83, 118.23, 115.37, 113.58, 110.48, 107.07, 105.85, 101.63, 100.85, 70.25, 70.08, 69.90, 67.74, 67.43, 63.77, 54.09, 40.07, 34.65, 31.50, 29.85, 28.93, 26.05, 25.56, 15.63. MALDI-MS: 8,197.3 ([M]+Na^+).

3.7.21 Synthesis of [3]Rotaxane 3.19

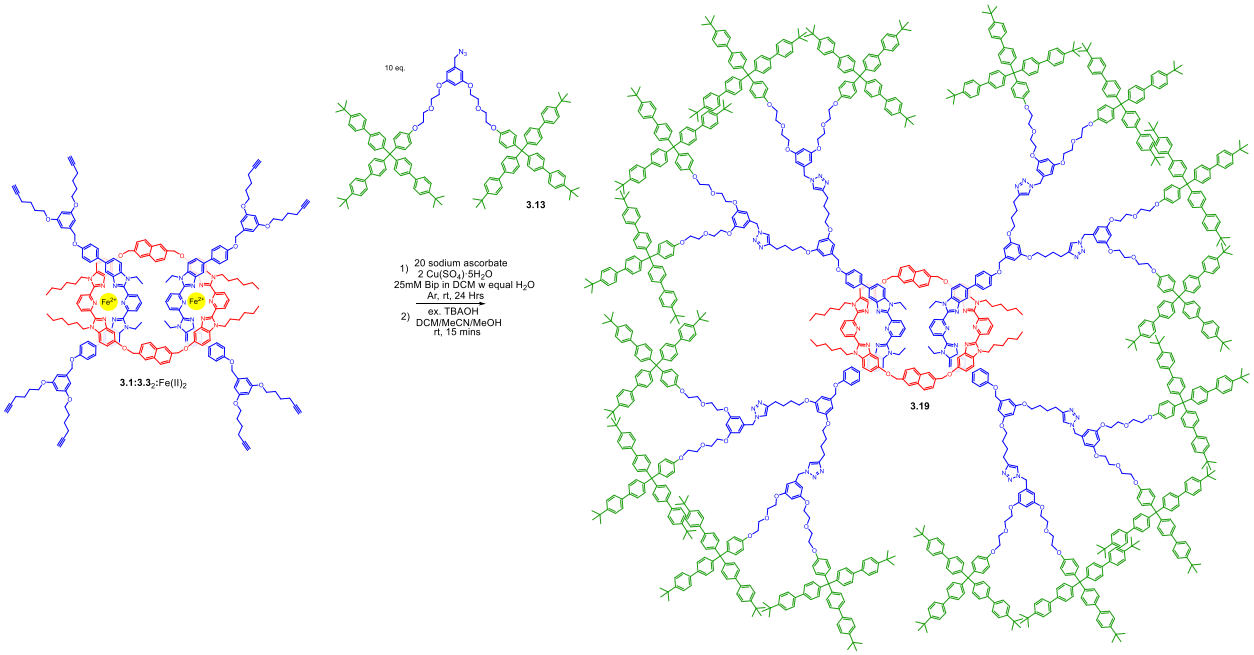

3.1:**3.3**$_2$:Fe(II)$_2$ (17.2 mg, 0.0036mmol), **5** (63.5 mg, 0.036 mmol, 10eq) and sodium ascorbate (13.8 mg, 0.036 mmol, 10 eq) were added to a 4mL glass vial purged with Ar. To this mixture was added CH_2Cl_2 (0.62 mL, conc of alkyne = 25 mM), H_2O (0.52 mL), and 100μL of an aqueous

stock solution of $Cu(SO_4)\cdot 5H_2O$ (72mM, 0.0072mmol, 2eq, (25mol% per alkyne)). The reaction was stirred vigorously for 18 h at RT. After this time the reaction mixture was diluted with CH_2Cl_2 and H_2O (5 mL each). The organic layer was taken and washed with H_2O (2 × 5 mL). Removal of the organic solvent resulted in a purple solid that was washed 3x with 5mL of 10% chloroform in hexanes to help remove leftover stopper group. The crude purple solid was redissolved in 5mL of 50:50 dichloromethane and acetonitrile and stirred slowly at room temperature. 1mL of tetrabutylammonium hydroxide solution (1M in MeOH) was added dropwise to the stirring solution resulting in a rapid color change from purple to light brown and precipitation of the demetallated product. After 15 minutes of stirring, the off-white solid was filtered off and washed with methanol (2x 10mL). The frit was then washed with 5mL of $CHCl_3$ to redissolve the demetallated product and washed once with 5mL water. Solvent was removed under reduced pressure resulting in an off-white residue. Purification of **3.19** was achieved using preparative thin layer chromatography (SiO_2, eluent = 94:6 $CHCl_3$:MeOH, lowest Rf band taken (R_f=0.15-0.3) as [3]R product, macrocycle byproduct R_f=0.35, dumbbell byproduct R_f=0.70-0.80) followed by precipitation from cold methanol resulting in an off-white solid, **3.19** in 65% isolated yield. ^{1}H NMR (500 MHz, $CDCl_3$) δ 7.98 (bd, *J* = 8.5 Hz, 4H), 7.85 (bd, *J* = 8.4 Hz, 4H), 7.73 (s, 4H), 7.69 (s, 4H), 7.53-7.32 (m, 308H), 7.29 (d, *J* = 8.2 Hz, 96H), 7.20-7.14 (m, 52H), 6.98 (bd, 4H), 6.82-6.74 (m, 44H), 6.56 (bd, *J* = 8.4 Hz, 8H), 6.46-6.40 (m, 16H), 6.38-6.31 (m, 20H), 5.36-5.25 (m, 24H), 4.7(bd, 8H), 4.55 (bd, 8H), 4.36 (bd, 8H), 4.10-3.97 (m, 64H), 3.94-3.78 (m, 80H), 2.70 (m, 16H), 1.72 (m, 16H), 1.36 (s, 512H), 1.28 (bt, 8H), 0.96-0.72 (m, 52H), 0.46 (bt, 12H). MALDI-MS: 17,733.2 ([M]+H^+), 9,531.5 ([M]+H^+-DB(**3.18**)), 8,203.1 ([M]+H^+-MC(**3.1**)-DB(**3.18**)).

3.7.22 Kinetic Slippage Experimental Details

Kinetic experiments were modeled after work by Sauvage and coworkers.[62] A 1mM sample of fresh **3.17** was prepared in a 5 mm Bruker Shigemi NMR tube. This tube was placed in an oil bath at 35°C and the ^{1}H-NMR spectrum was recorded every 24 hours for 5 days and then after another 48 hours for a seventh day. The tube was then heated to 40°C and the same ^{1}H-NMR acquisition process was repeated. The tube was then heated to 45°C and the same ^{1}H-NMR acquisition process was repeated. In total, the [3]rotaxane was heated for three weeks. This process was repeated in triplicate. The resulting kinetic data was analyzed according to the following method. The downfield doublet corresponding to the proton labeled B in the dumbbell of the [3]rotaxane (Fig 3.22) was used to determine the amount of [3]R left in each sample as the shift between free and interlocked species was diagnostic and clean of other peaks. The free B doublet is in the region 8.34-8.38ppm and the interlocked B doublet is in the region 8.21-8.25ppm. Let C_0 be the initial concentration of [3]rotaxane and C be the concentration of [3]rotaxane at timepoint *t*. The absolute integral intensity of B that is interlocked ($I_{3[R]}$) divided by the sum of the absolute integral intensities of B that is free and interlocked ($I_{DB} + I_{3[R]}$) multiplied by 100% gives the percent of [3]R remaining in the sample. Dividing this percent rotaxane remaining by the initial rotaxane percent present is equivalent to C/C_0 for each timepoint of slippage. Following first-order kinetics and standard Eyring/Arrhenius methods the thermodynamic and kinetic parameters were determined. See Fig 3.36-3.39 for the appropriate spectra. Experimental protocol for **3.19** was similar to **3.17** above. A 1mM sample of fresh **3.19** was prepared in a 5 mm Bruker Shigemi NMR tube. This tube was placed in an oil bath at 35°C and the ^{1}H-NMR spectrum was recorded after 2 days, 4 days, 5 days, and 7 days. The tube was then heated to 40°C and the same ^{1}H-NMR acquisition process was repeated. The tube was then heated to 45°C and the same ^{1}H-NMR

acquisition process was repeated. In total, the [3]rotaxane was heated for three weeks. This process was repeated in triplicate. The resulting kinetic data was analyzed following a similar procedure to **3.17** above. The downfield doublets corresponding to the proton labeled B in the free dumbbell (**3.18**) and b of the [3]rotaxane **3.19** (Fig 3.30a) was used to determine the amount of [3]R left in each sample as the shift between free and interlocked species was diagnostic and clean of other peaks. The free B doublet was in the region 8.32-8.37ppm and the interlocked b doublet was in the region 7.82-7.88ppm. See Fig 3.40 for appropriate spectra.

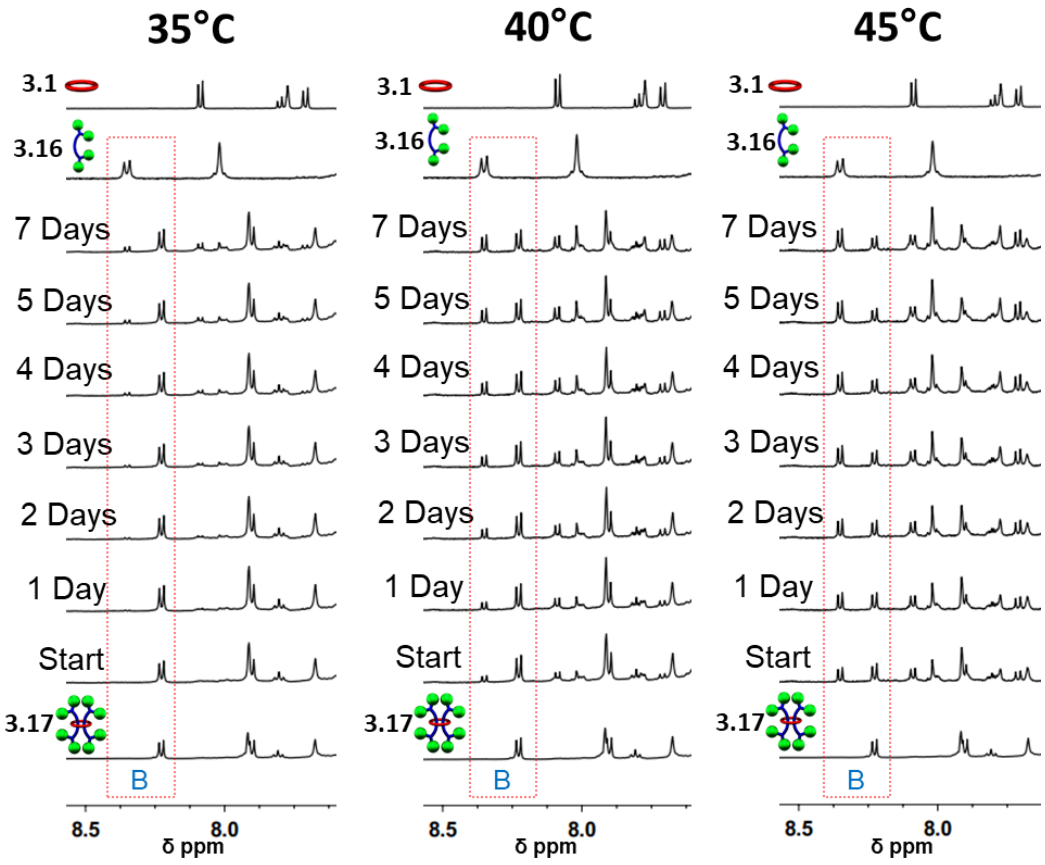

Fig 3.36 Partial ^{1}H-NMR overlay (1mM, 500 MHz, $CDCl_3$, 25°C) of trial 1 of slippage experiments of **3.17**.

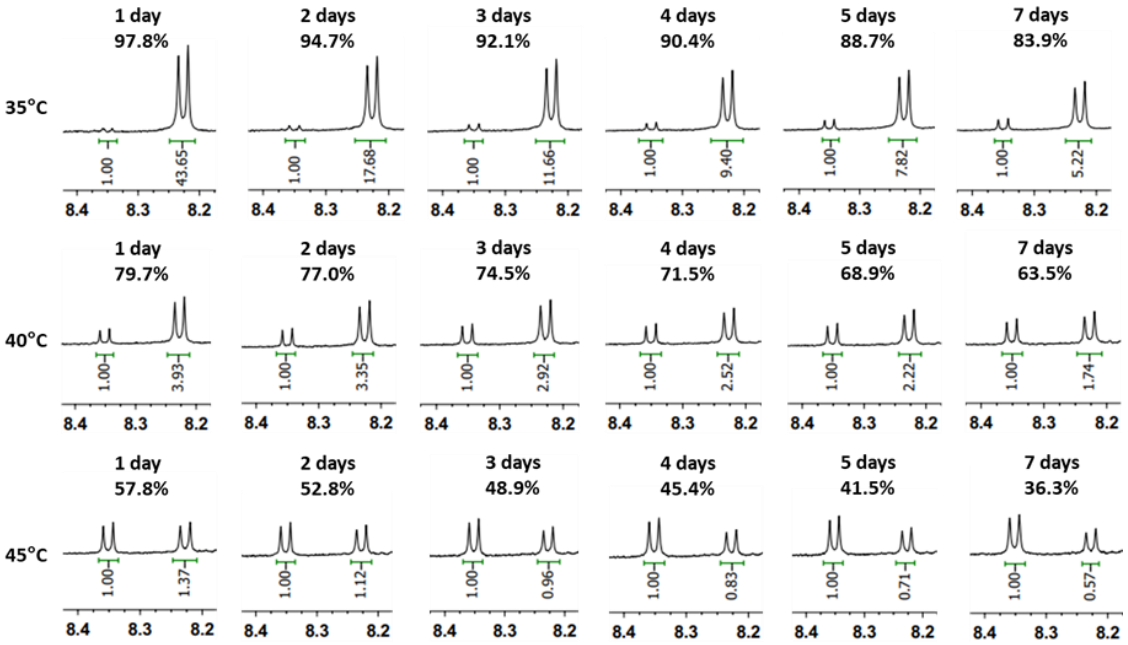

Fig 3.37 Example of ^{1}H-NMR analysis of trial 1 of slippage experiments of **3.17.**

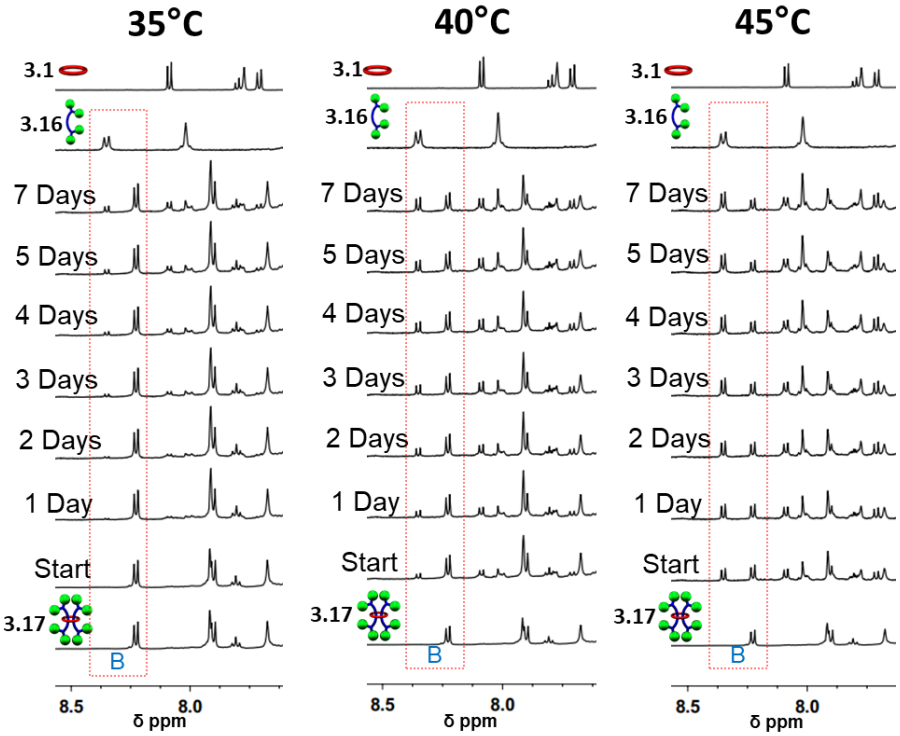

Fig 3.38 Partial ^{1}H-NMR overlay (1mM, 500 MHz, $CDCl_3$, 25°C) of trial 2 of slippage experiments of **3.17**.

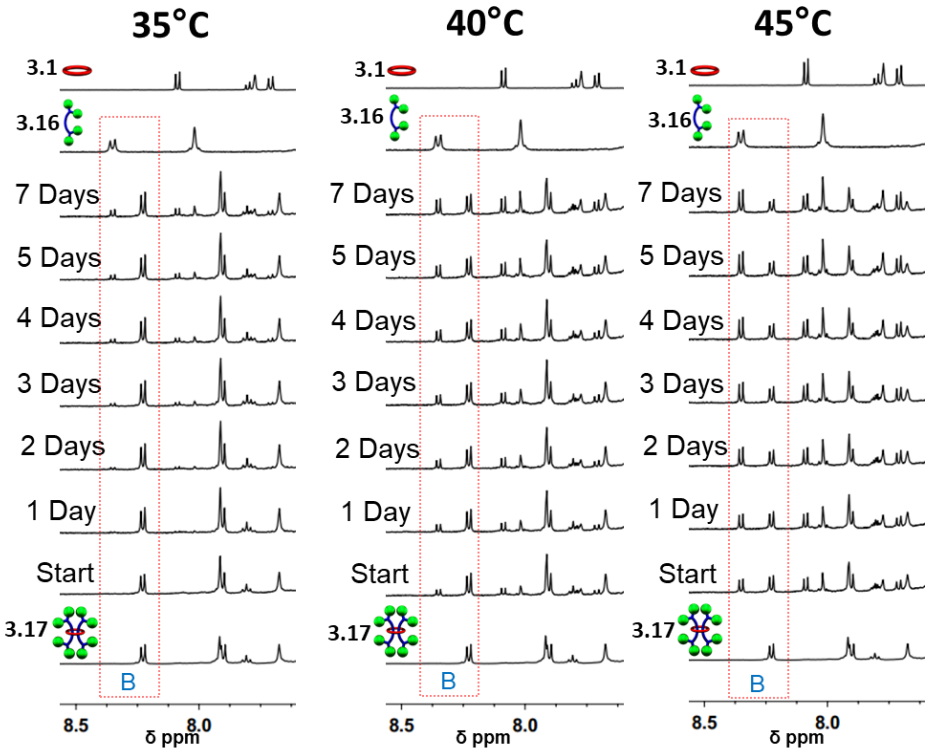

Fig 3.39 Partial ^{1}H-NMR overlay (1mM, 500 MHz, $CDCl_3$, 25°C) of trial 3 of slippage experiments of **3.17**.

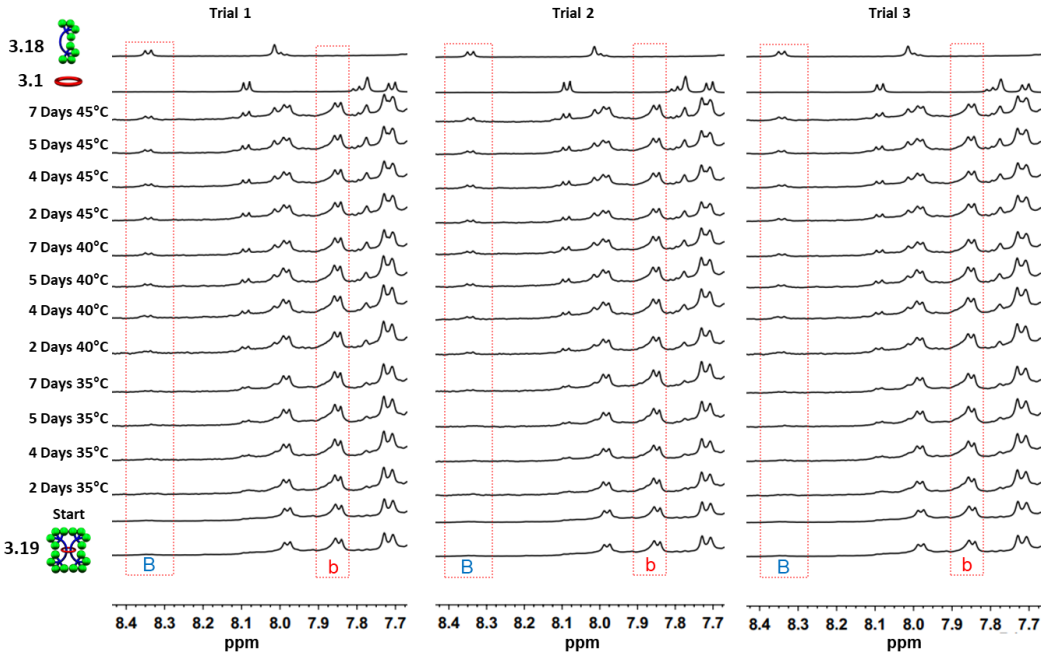

Fig 3.40 Partial ^{1}H-NMR overlay (1mM, 500 MHz, $CDCl_3$, 25°C) of 3 trials of 3-week kinetic slippage experiments of **3.19**. Time and temperature between measurements indicated on left side.

3.8 References

(1) Stoddart, J. F. The Chemistry of the Mechanical Bond. *Chem. Soc. Rev.* **2009**, *38* (6), 1802–1820. https://doi.org/10.1039/b819333a.

(2) Bruns, C. J.; Stoddart, J. F. *The Nature of the Mechanical Bond: From Molecules to Machines*; Wiley: Hoboken, NJ, 2016. https://doi.org/10.1002/9781119044123.

(3) Sauvage, J.-P. From Chemical Topology to Molecular Machines (Nobel Lecture). *Angew. Chemie - Int. Ed.* **2017**, *56* (37), 11080–11093. https://doi.org/10.1002/anie.201702992.

(4) Feringa, B. L. The Art of Building Small: From Molecular Switches to Motors (Nobel Lecture). *Angew. Chemie Int. Ed.* **2017**, *56* (37), 11060–11078. https://doi.org/10.1002/anie.201702979.

(5) Stoddart, J. F. Mechanically Interlocked Molecules (MIMs)-Molecular Shuttles, Switches, and Machines (Nobel Lecture). *Angew. Chemie Int. Ed.* **2017**, *56* (37), 11094–11125. https://doi.org/10.1002/anie.201703216.

(6) McGonigal, P. R. Multiply Threaded Rotaxanes. *Supramol. Chem.* **2018**, *30* (9), 782–794. https://doi.org/10.1080/10610278.2018.1433832.

(7) Xue, M.; Yang, Y.; Chi, X.; Yan, X.; Huang, F. Development of Pseudorotaxanes and Rotaxanes: From Synthesis to Stimuli-Responsive Motions to Applications. *Chem. Rev.* **2015**, *115* (15), 7398–7501. https://doi.org/10.1021/cr5005869.

(8) Erbas-Cakmak, S.; Leigh, D. A.; McTernan, C. T.; Nussbaumer, A. L. Artificial Molecular Machines. *Chem. Rev.* **2015**, *115* (18), 10081–10206. https://doi.org/10.1021/acs.chemrev.5b00146.

(9) Zhou, H. Y.; Han, Y.; Chen, C. F. PH-Controlled Motions in Mechanically Interlocked Molecules. *Mater. Chem. Front.* **2020**, *4* (1), 12–28. https://doi.org/10.1039/c9qm00546c.

(10) Dattler, D.; Fuks, G.; Heiser, J.; Moulin, E.; Perrot, A.; Yao, X.; Giuseppone, N. Design of Collective Motions from Synthetic Molecular Switches, Rotors, and Motors. *Chem. Rev.* **2020**, *120* (1), 310–433. https://doi.org/10.1021/acs.chemrev.9b00288.

(11) Fernandez, A.; Ferrando-Soria, J.; Pineda, E. M.; Tuna, F.; Vitorica-Yrezabal, I. J.; Knappke, C.; Ujma, J.; Muryn, C. A.; Timco, G. A.; Barran, P. E.; Ardavan, A.; Winpenny, R. E. P. Making Hybrid [n]-Rotaxanes as Supramolecular Arrays of Molecular Electron Spin Qubits. *Nat. Commun.* **2016**, *7*, 1–6. https://doi.org/10.1038/ncomms10240.

(12) Heath, J. R. Wires, Switches, and Wiring. A Route toward a Chemically Assembled Electronic Nanocomputer. *Pure Appl. Chem.* **2000**, *72* (1–2), 11–20. https://doi.org/10.1351/pac200072010011.

(13) Jamieson, E. M. G.; Modicom, F.; Goldup, S. M. Chirality in Rotaxanes and Catenanes. *Chem. Soc. Rev.* **2018**, *47* (14), 5266–5311. https://doi.org/10.1039/c8cs00097b.

(14) Lewis, J. E. M.; Galli, M.; Goldup, S. M. Properties and Emerging Applications of Mechanically Interlocked Ligands. *Chem. Commun.* **2017**, *53* (2), 298–312.

https://doi.org/10.1039/C6CC07377H.

(15) Cotí, K. K.; Belowich, M. E.; Liong, M.; Ambrogio, M. W.; Lau, Y. A.; Khatib, H. A.; Zink, J. I.; Khashab, N. M.; Stoddart, J. F. Mechanised Nanoparticles for Drug Delivery. *Nanoscale* **2009**, *1* (1), 16–39. https://doi.org/10.1039/b9nr00162j.

(16) Harrison, I. T.; Harrison, S. Synthesis of a Stable Complex of a Macrocycle and a Threaded Chain. *J. Am. Chem. Soc.* **1967**, *89* (22), 5723–5724.

(17) Taghavi Shahraki, B.; Maghsoudi, S.; Fatahi, Y.; Rabiee, N.; Bahadorikhalili, S.; Dinarvand, R.; Bagherzadeh, M.; Verpoort, F. The Flowering of Mechanically Interlocked Molecules: Novel Approaches to the Synthesis of Rotaxanes and Catenanes. *Coord. Chem. Rev.* **2020**, *423*, 213484. https://doi.org/10.1016/j.ccr.2020.213484.

(18) Zhou, H. Y.; Zong, Q. S.; Han, Y.; Chen, C. F. Recent Advances in Higher Order Rotaxane Architectures. *Chem. Commun.* **2020**, *56* (69), 9916–9936. https://doi.org/10.1039/d0cc03057k.

(19) Hart, L. F.; Hertzog, J. E.; Rauscher, P. M.; Rawe, B. W.; Tranquilli, M. M.; Rowan, S. J. Material Properties and Applications of Mechanically Interlocked Polymers. *Nat. Rev. Mater.* **2021**, *6*, 508–530. https://doi.org/10.1038/s41578-021-00278-z.

(20) Mena-Hernando, S.; Pérez, E. M. Mechanically Interlocked Materials. Rotaxanes and Catenanes beyond the Small Molecule. *Chem. Soc. Rev.* **2019**, *48* (19), 5016–5032. https://doi.org/10.1039/c8cs00888d.

(21) Bacljić, J. D.; Balzani, V.; Credi, A.; Silvi, S.; Stoddart, J. F. A Molecular Elevator. *Science (80-.).* **2004**, *303* (5665), 1845–1849. https://doi.org/10.1126/science.1094791.

(22) Yamada, Y.; Okamoto, M.; Furukawa, K.; Kato, T.; Tanaka, K. Switchable Intermolecular Communication in a Four-Fold Rotaxane. *Angew. Chemie - Int. Ed.* **2012**, *51* (3), 709–713. https://doi.org/10.1002/anie.201107104.

(23) Fang, L.; Hmadeh, M.; Wu, J.; Olson, M. A.; Spruell, J. M.; Trabolsl, A.; Yang, Y. W.; Elhablrl, M.; Albrecht-Gary, A. M.; Stoddart, J. F. Acid-Base Actuation of [C2]Daisy Chains. *J. Am. Chem. Soc.* **2009**, *131* (20), 7126–7134. https://doi.org/10.1021/ja900859d.

(24) Du, G.; Moulin, E.; Jouault, N.; Buhler, E.; Giuseppone, N. Muscle-like Supramolecular Polymers: Integrated Motion from Thousands of Molecular Machines. *Angew. Chemie - Int. Ed.* **2012**, *51* (50), 12504–12508. https://doi.org/10.1002/anie.201206571.

(25) Meng, Z.; Chen, C. F. A Molecular Pulley Based on a Triply Interlocked [2]Rotaxane. *Chem. Commun.* **2015**, *51* (39), 8241–8244. https://doi.org/10.1039/c5cc01301a.

(26) Okumura, Y.; Ito, K. The Polyrotaxane Gel: A Topological Gel by Figure-of-Eight Cross-Links. *Adv. Mater.* **2001**, *13* (7), 485–487. https://doi.org/10.1002/1521-4095(200104)13:7<485::AID-ADMA485>3.0.CO;2-T.

(27) Ito, K. Novel Cross-Linking Concept of Polymer Network: Synthesis, Structure, and Properties of Slide-Ring Gels with Freely Movable Junctions. *Polym. J.* **2007**, *39* (6), 489–499. https://doi.org/10.1295/polymj.PJ2006239.

(28) Noda, Y.; Hayashi, Y.; Ito, K. From Topological Gels to Slide-Ring Materials. *J. Appl. Polym. Sci.* **2014**, *131* (15), 40509. https://doi.org/10.1002/app.40509.

(29) Rauscher, P. M.; Schweizer, K. S.; Rowan, S. J.; de Pablo, J. J. Dynamics of Poly[n]Catenane Melts. *J. Chem. Phys.* **2020**, *152* (21), 214901. https://doi.org/10.1063/5.0007573.

(30) Hagita, K.; Murashima, T.; Sakata, N. Mathematical Classification and Rheological Properties of Ring Catenane Structures. *Macromolecules* **2021**. https://doi.org/10.1021/acs.macromol.1c01705.

(31) Yasuda, Y.; Toda, M.; Mayumi, K.; Yokoyama, H.; Morita, H.; Ito, K. Sliding Dynamics of Ring on Polymer in Rotaxane: A Coarse-Grained Molecular Dynamics Simulation Study. *Macromolecules* **2019**, *52* (10), 3787–3793. https://doi.org/10.1021/acs.macromol.9b00118.

(32) Oddy, F. E.; Brovelli, S.; Stone, M. T.; Klotz, E. J. F.; Cacialli, F.; Anderson, H. L. Influence of Cyclodextrin Size on Fluorescence Quenching in Conjugated Polyrotaxanes by Methyl Viologen in Aqueous Solution. *J. Mater. Chem.* **2009**, *19* (18), 2846–2852. https://doi.org/10.1039/b821950h.

(33) Kato, K.; Karube, K.; Nakamura, N.; Ito, K. The Effect of Ring Size on the Mechanical Relaxation Dynamics of Polyrotaxane Gels. *Polym. Chem.* **2015**, *6* (12), 2241–2248. https://doi.org/10.1039/c4py01644k.

(34) Saito, S.; Nakazono, K.; Takahashi, E.; April, R. V. Template Synthesis of [2] Rotaxanes with Large Ring Components and Tris (Biphenyl) Methyl Group as the Blocking Group . The Relationship between the Ring Size and the Stability of the Rotaxanes Our Recent Interest in the Chemistry of Rotaxanes Prompte. *J. Org. Chem.* **2006**, *71* (19), 7477–7480.

(35) Saito, S.; Takahashi, E.; Wakatsuki, K.; Inoue, K.; Orikasa, T.; Sakai, K.; Yamasaki, R.; Mutoh, Y.; Kasama, T. Erratum: Synthesis of Large [2]Rotaxanes. the Relationship between the Size of the Blocking Group and the Stability of the Rotaxane (Journal of Organic Chemistry (2013) 8 (3553-3560)DOI: 10.1021/Jo302800t). *J. Org. Chem.* **2013**, *78* (11), 5816. https://doi.org/10.1021/jo4010052.

(36) Raymo, F. M.; Houk, K. N.; Stoddart, J. F. The Mechanism of the Slippage Approach to Rotaxanes. Origin of the "all- or-Nothing" Substituent Effect. *J. Am. Chem. Soc.* **1998**, *120* (36), 9318–9322. https://doi.org/10.1021/ja9806229.

(37) Affeld, A.; Hühner, G. M.; Seel, C.; Schalley, C. A. Rotaxane or Pseudorotaxane? Effects of Small Structural Variations on the Deslipping Kinetics of Rotaxanes with Stopper Groups of Intermediate Size. *European J. Org. Chem.* **2001**, No. 15, 2877–2890. https://doi.org/10.1002/1099-0690(200108)2001:15<2877::AID-EJOC2877>3.0.CO;2-R.

(38) Linnartz, P.; Bitter, S.; Schalley, C. A. Deslipping of Ester Rotaxanes: A Cooperative Interplay of Hydrogen Bonding with Rotational Barriers. *European J. Org. Chem.* **2003**, No. 24, 4819–4829. https://doi.org/10.1002/ejoc.200300466.

(39) Heim, C.; Affeld, A.; Nieger, M.; Vögtle, F. Size Complementarity of Macrocyclic Cavities and Stoppers in Amide- Rotaxanes. *Helv. Chim. Acta* **1999**, *82* (5), 746–759.

(40) Groppi, J.; Casimiro, L.; Canton, M.; Corra, S.; Jafari-Nasab, M.; Tabacchi, G.; Cavallo, L.; Baroncini, M.; Silvi, S.; Fois, E.; Credi, A. Precision Molecular Threading/Dethreading. *Angew. Chemie - Int. Ed.* **2020**, *59* (35), 14825–14834. https://doi.org/10.1002/anie.202003064.

(41) Händel, M.; Plevoets, M.; Gestermann, S.; Vögtle, F. Synthesis of Rotaxanes by Brief Melting of Wheel and Axle Components. *Angew. Chemie (International Ed. English)* **1997**, *36* (11), 1199–1201. https://doi.org/10.1002/anie.199711991.

(42) Ashton, P. R.; Baxter, I.; Fyfe, M. C. T.; Raymo, F. M.; Spencer, N.; Stoddart, J. F.; White, A. J. P.; Williams, D. J. Rotaxane or Pseudorotaxane? That Is the Question! *J. Am. Chem. Soc.* **1998**, *120* (10), 2297–2307. https://doi.org/10.1021/ja9731276.

(43) Chiu, S.; Rowan, S. J.; Cantrill, S. J.; Glink, P. T.; Garrell, R. L.; Stoddart, J. F. A Rotaxane-Like Complex with Controlled-Release Characteristics. *Org. Lett.* **2000**, *2* (4), 3631–3634.

(44) Cherraben, S.; Scelle, J.; Hasenknopf, B.; Vives, G.; Sollogoub, M. Precise Rate Control of Pseudorotaxane Dethreading by PH-Responsive Selectively Functionalized Cyclodextrins. *Org. Lett.* **2021**, *23* (20), 7938–7942. https://doi.org/10.1021/acs.orglett.1c02940.

(45) Ling, X.; Samuel, E. L.; Patchell, D. L.; Masson, E. Cucurbituril Slippage: Translation Is a Complex Motion. *Org. Lett.* **2010**, *12* (12), 2730–2733. https://doi.org/10.1021/ol1008119.

(46) Qiu, Y.; Song, B.; Pezzato, C.; Shen, D.; Liu, W.; Zhang, L.; Feng, Y.; Guo, Q.-H.; Cai, K.; Li, W.; Chen, H.; Nguyen, M. T.; Shi, Y.; Cheng, C.; Dean Astumian, R.; Li, X.; Fraser Stoddart, J. A Precise Polyrotaxane Synthesizer. *Science (80-.).* **2020**, *368* (June), 1247–1253.

(47) Qiu, Y.; Zhang, L.; Pezzato, C.; Feng, Y.; Li, W.; Nguyen, M. T.; Cheng, C.; Shen, D.; Guo, Q. H.; Shi, Y.; Cai, K.; Alsubaie, F. M.; Astumian, R. D.; Stoddart, J. F. A Molecular Dual Pump. *J. Am. Chem. Soc.* **2019**, *141* (44), 17472–17476. https://doi.org/10.1021/jacs.9b08927.

(48) Cheng, C.; McGonigal, P. R.; Schneebeli, S. T.; Li, H.; Vermeulen, N. A.; Ke, C.; Stoddart, J. F. An Artificial Molecular Pump. *Nat. Nanotechnol.* **2015**, *10* (6), 547–553. https://doi.org/10.1038/nnano.2015.96.

(49) Pezzato, C.; Nguyen, M. T.; Cheng, C.; Kim, D. J.; Otley, M. T.; Stoddart, J. F. An Efficient Artificial Molecular Pump. *Tetrahedron* **2017**, *73* (33), 4849–4857. https://doi.org/10.1016/j.tet.2017.05.087.

(50) Soto, M. A.; Lelj, F.; MacLachlan, M. J. Programming Permanent and Transient Molecular Protection: Via Mechanical Stoppering. *Chem. Sci.* **2019**, *10* (44), 10422–10427. https://doi.org/10.1039/c9sc03744f.

(51) Soto, M. A.; Maclachlan, M. J. Disabling Molecular Recognition through Reversible Mechanical Stoppering. *Org. Lett.* **2019**, *21* (6), 1744–1748. https://doi.org/10.1021/acs.orglett.9b00310.

(52) Hsueh, S. Y.; Lai, C. C.; Liu, Y. H.; Wang, Y.; Peng, S. M.; Chiu, S. H. Protecting a Squaraine Near-IR Dye through Its Incorporation in a Slippage-Derived [2]Rotaxane. *Org. Lett.* **2007**, *9* (22), 4523–4526. https://doi.org/10.1021/ol702050w.

(53) Chiang, T. H.; Tsou, C. Y.; Chang, Y. H.; Lai, C. C.; Cheng, R. P.; Chiu, S. H. Using Slippage to Construct a Prototypical Molecular "Lock & Lock" Box. *Org. Lett.* **2021**, *23* (15), 5787–5792. https://doi.org/10.1021/acs.orglett.1c01945.

(54) Lee, J. J.; White, A. G.; Baumes, J. M.; Smith, B. D. Microwave-Assisted Slipping Synthesis of Fluorescent Squaraine Rotaxane Probe for Bacterial Imaging. *Chem. Commun.* **2010**, *46* (7), 1068–1069. https://doi.org/10.1039/b924350j.

(55) Fan, M. M.; Yu, Z. J.; Luo, H. Y.; Zhang, S.; Li, B. J. Supramolecular Network Based on the Self-Assembly of y-Cyclodextrin with Poly(Ethylene Glycol) and Its Shape Memory Effect. *Macromol. Rapid Commun.* **2009**, *30* (11), 897–903. https://doi.org/10.1002/marc.200800712.

(56) Iijima, K.; Aoki, D.; Otsuka, H.; Takata, T. Synthesis of Rotaxane Cross-Linked Polymers with Supramolecular Cross-Linkers Based on γ-CD and PTHF Macromonomers: The Effect of the Macromonomer Structure on the Polymer Properties. *Polymer (Guildf).* **2017**, *128*, 392–396. https://doi.org/10.1016/j.polymer.2017.01.024.

(57) Yamamoto, K.; Nameki, R.; Sogawa, H.; Takata, T. Macrocyclic Dinuclear Palladium Complex as a Novel Doubly Threaded [3]Rotaxane Scaffold and Its Application as a Rotaxane Cross-Linker. *Angew. Chemie - Int. Ed.* **2020**, *59* (41), 18023–18028. https://doi.org/10.1002/anie.202007866.

(58) Aramoto, H.; Osaki, M.; Konishi, S.; Ueda, C.; Kobayashi, Y.; Takashima, Y.; Harada, A.; Yamaguchi, H. Redox-Responsive Supramolecular Polymeric Networks Having Double-Threaded Inclusion Complexes. *Chem. Sci.* **2020**, *11* (17), 4322–4331. https://doi.org/10.1039/c9sc05589d.

(59) Danon, J. J.; Leigh, D. A.; McGonigal, P. R.; Ward, J. W.; Wu, J. Triply Threaded [4]Rotaxanes. *J. Am. Chem. Soc.* **2016**, *138* (38), 12643–12647. https://doi.org/10.1021/jacs.6b07733.

(60) Klotz, E. J. F.; Claridge, T. D. W.; Anderson, H. L. Homo- and Hetero-[3]Rotaxanes with Two π-Systems Clasped in a Single Macrocycle. *J. Am. Chem. Soc.* **2006**, *128* (48), 15374–15375. https://doi.org/10.1021/ja0665139.

(61) Prikhod'ko, A. I.; Durola, F.; Sauvage, J. P. Iron(II)-Templated Synthesis of [3]Rotaxanes by Passing Two Threads through the Same Ring. *J. Am. Chem. Soc.* **2008**, *130* (2), 448–449. https://doi.org/10.1021/ja078216p.

(62) Prikhod'ko, A. I.; Sauvage, J. P. Passing Two Strings through the Same Ring Using an Octahedral Metal Center as Template: A New Synthesis of [3]Rotaxanes. *J. Am. Chem. Soc.* **2009**, *131* (19), 6794–6807. https://doi.org/10.1021/ja809267z.

(63) Cheng, H. M.; Leigh, D. A.; Maffei, F.; McGonigal, P. R.; Slawin, A. M. Z.; Wu, J. En Route to a Molecular Sheaf: Active Metal Template Synthesis of a [3]Rotaxane with Two Axles Threaded through One Ring. *J. Am. Chem. Soc.* **2011**, *133* (31), 12298–12303.

https://doi.org/10.1021/ja205167e.

(64) Yamashita, Y.; Mutoh, Y.; Yamasaki, R.; Kasama, T.; Saito, S. Synthesis of [3]Rotaxanes That Utilize the Catalytic Activity of a Macrocyclic Phenanthroline-Cu Complex: Remarkable Effect of the Length of the Axle Precursor. *Chem. - A Eur. J.* **2015**, *21* (5), 2139–2145. https://doi.org/10.1002/chem.201405090.

(65) Hayashi, R.; Mutoh, Y.; Kasama, T.; Saito, S. Synthesis of [3]Rotaxanes by the Combination of Copper-Mediated Coupling Reaction and Metal-Template Approach. *J. Org. Chem.* **2015**, *80* (15), 7536–7546. https://doi.org/10.1021/acs.joc.5b01120.

(66) Movsisyan, L. D.; Franz, M.; Hampel, F.; Thompson, A. L.; Tykwinski, R. R.; Anderson, H. L. Polyyne Rotaxanes: Stabilization by Encapsulation. *J. Am. Chem. Soc.* **2016**, *138* (4), 1366–1376. https://doi.org/10.1021/jacs.5b12049.

(67) Meldal, M.; Tomøe, C. W. Cu-Catalyzed Azide - Alkyne Cycloaddition. *Chem. Rev.* **2008**, *108* (8), 2952–3015. https://doi.org/10.1021/cr0783479.

(68) Hänni, K. D.; Leigh, D. A. The Application of CuAAC 'Click' Chemistry to Catenane and Rotaxane Synthesis. *Chem. Soc. Rev.* **2010**, *39* (4), 1240–1251. https://doi.org/10.1039/b901974j.

(69) Enamullah, M.; Linert, W. Substituent- and Solvent-Effects on the Stability of Iron(II)-4-x-2,6-Bis-(Benzimidazol-2′-YL)Pyridine Complexes Showing Spin-Crossover in Solution. *J. Coord. Chem.* **1996**, *40* (3), 193–201. https://doi.org/10.1080/00958979608024344.

(70) Wojtecki, R. J.; Wu, Q.; Johnson, J. C.; Ray, D. G.; Korley, L. S. T. J.; Rowan, S. J. Optimizing the Formation of 2,6-Bis(N-Alkyl-Benzimidazolyl)Pyridine-Containing [3]Catenates through Component Design. *Chem. Sci.* **2013**, *4* (12), 4440–4448. https://doi.org/10.1039/c3sc52082j.

(71) Tranquilli, M. M.; Wu, Q.; Rowan, S. J. Effect of Metallosupramolecular Polymer Concentration on the Synthesis of Poly[n]Catenanes . *Chem. Sci.* **2021**. https://doi.org/10.1039/d1sc02450g.

(72) Wu, Q.; Rauscher, P. M.; Lang, X.; Wojtecki, R. J.; De Pablo, J. J.; Hore, M. J. A.; Rowan, S. J. Poly[n]Catenanes: Synthesis of Molecular Interlocked Chains. *Science (80-.).* **2017**, *358* (6369), 1434–1439. https://doi.org/10.1126/science.aap7675.

(73) Herrmann, T.; Güntert, P.; Wüthrich, K. Protein NMR Structure Determination with Automated NOE-Identification in the NOESY Spectra Using the New Software ATNOS. *J. Biomol. NMR* **2002**, *24* (3), 171–189. https://doi.org/10.1023/A:1021614115432.

(74) Sibi, M. P.; Petrovic, G. Enantioselective Radical Reactions: The Use of Metal Triflimides as Lewis Acids. *Tetrahedron Asymmetry* **2003**, *14* (19), 2879–2882. https://doi.org/10.1016/S0957-4166(03)00543-3.

(75) McKenzie, B. M.; Miller, A. K.; Wojtecki, R. J.; Johnson, J. C.; Burke, K. A.; Tzeng, K. A.; Mather, P. T.; Rowan, S. J. Improved Synthesis of Functionalized Mesogenic 2,6-Bisbenzimidazolylpyridine Ligands. *Tetrahedron* **2008**, *64* (36), 8488–8495.

Chapter 4: Influencing the [3]Rotaxane Stability Further Through Stopper Arm Length Modification

4.1 Introduction

Chapter 3 was a significant step forward towards synthetically realizing doubly threaded poly[3]rotaxanes. Multiple metastable doubly threaded [3]rotaxanes that varied in stopper group size through changing the number of tris(p-t-butylbiphenyl)methyl moieties, were able to be prepared in high byield.[1] By doing this, it was possible to tune the interlocked stability of the [3]rotaxane with a resultant half-life in deuterated chloroform from <1 minute to *ca*. 6 months at room temperature. This validated the Bip ligand[2] as an effective framework for making rotaxane structures and proved there is potential for a synthetic path to other classes of interlocked polymers besides the poly(n)catenane[3,4] using it. It also demonstrated that the concept of component design[5] (increasing stopper group size) could be used to impact the stability of the [3]rotaxane.

Realizing a fully stable [3]rotaxane structure using this Bip ligand was crucial for the incorporation of this rotaxane motif into interlocked polymers. Towards this end, efforts were now turned to how the [3]rotaxane structure could be changed to fully stabilize its interlocked structure. Each isolated [3]rotaxane described in chapter 3 takes anywhere from 19-23 total synthetic steps from commercial starting materials. As such, there are plenty of opportunities to incorporate synthetic variation along the pathway to [3]rotaxane formation.

Chapter 3 also demonstrated that more careful thought than simply adding more stopper groups would be necessary to stabilize the [3]rotaxane. Following dendrimer chemistry[6,7] and going further than 4 stopper groups (to 8 each side) would make the [3]rotaxane greater than 90%

stopper group by mass which would be less practical for incorporation into polymeric materials. In order to think more critically about this slippage process and gain more insight about what structural features to change that could influence stability, all-atom molecular dynamics simulations[8,9] were conducted to investigate the mechanism of slippage of [3]rotaxane **3.17**, by a collaborator, Dr. Phillip Rauscher. Unfortunately, using this exact chemical structure for the [3]rotaxane during the simulations did not allow for slippage to be observed as the relatively small simulation timescale (40 ns) was not long enough to physically observe the dethreading process. As such, simulations were conducted on a singly stoppered [2]rotaxane with a slightly larger ring. This system is more analogous to **3.15** in which the slippage process was too rapid to physically isolate the compound. During these simulations an interesting observation was made. The ditopic Bip containing macrocycle rotated around both pyridine rings while the linker simultaneously pinched in order to lengthen the ring (Fig 4.1).

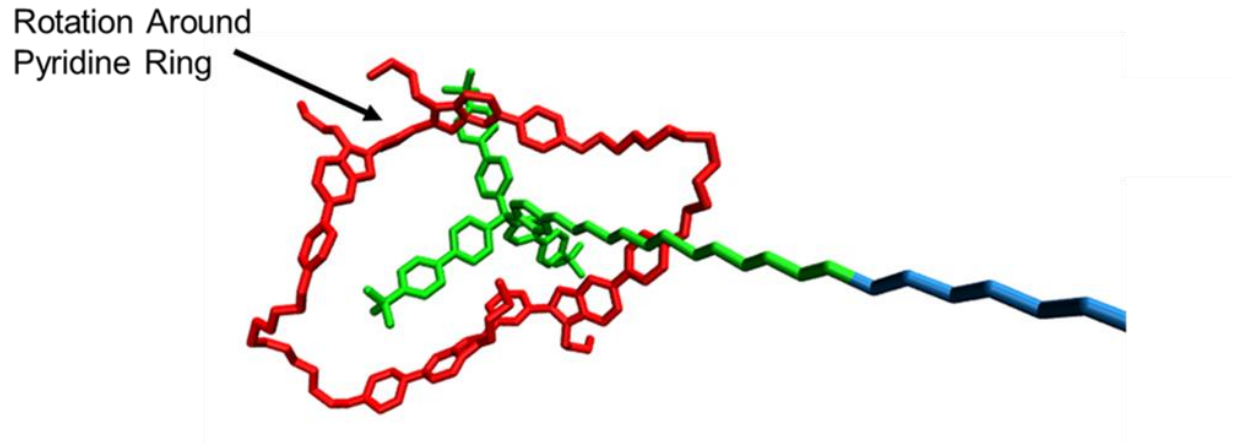

Fig 4.1 All-atom implicit-solvent model render of simulated [3]rotaxane.

Following the simulation for ~30ns shows that once the rings elongates it then sequentially wraps around each branch of the stopper group one at a time (Fig 4.2a-d) allowing the macrocycle to eventually leave the stopper group completely.

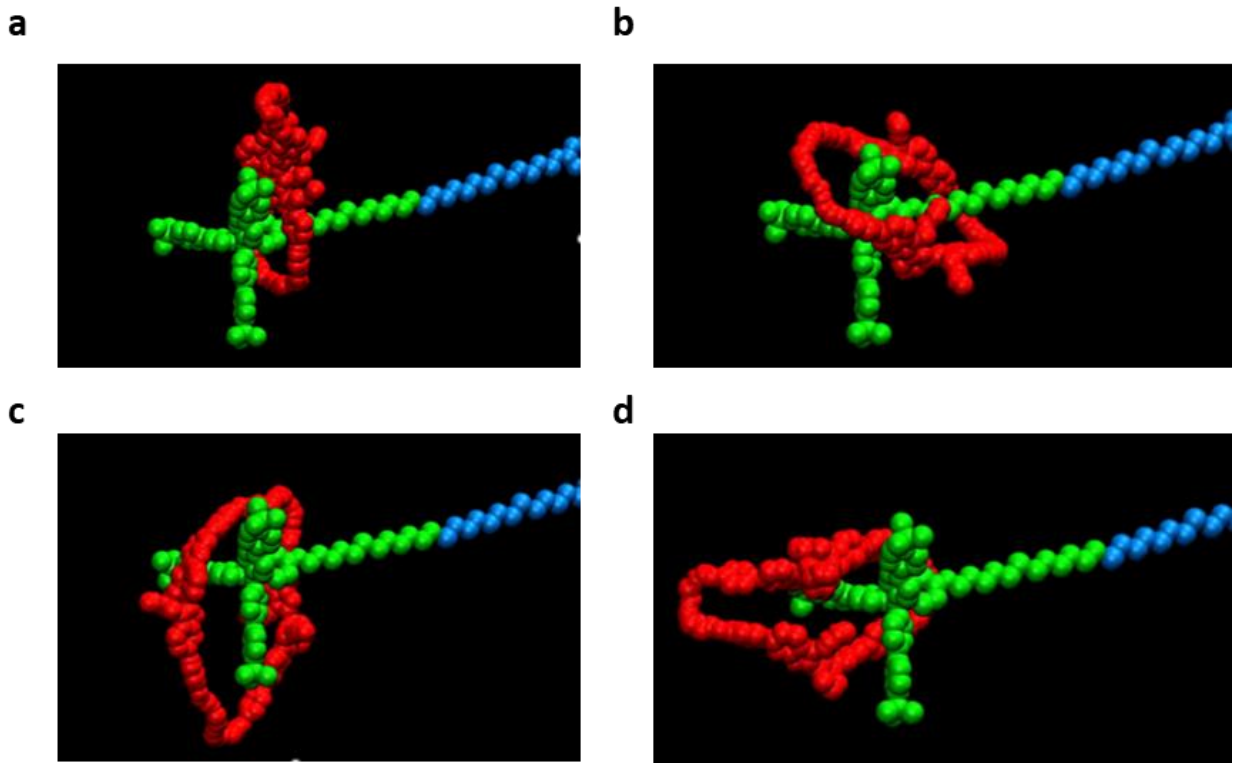

Fig 4.2 All-atom implicit-solvent model snapshots of the simulated [3]rotaxane a) approaching stopper group, b) looping around first arm, c) looping around second arm, and finally d) looping around the last arm to dissociate from the interlocked complex.

Hypothesizing that if a similar mechanism occurs to a much slower extent in the double stoppered system, then the macrocycle must at some point stretch around the full arm connecting each individual stopper group together. As such, the length of the stopper group connecting arm in the doubly threaded [3rotaxane **3.17** (Fig 4.3a) should be a tunable parameter to affect the slippage rate. It was then hypothesized that increasing its length (Fig 4.2b) should result in a more stable [3]rotaxane and as such two arm extensions were considered to the original system (**3.15**) as seen in Figure 4.3c.

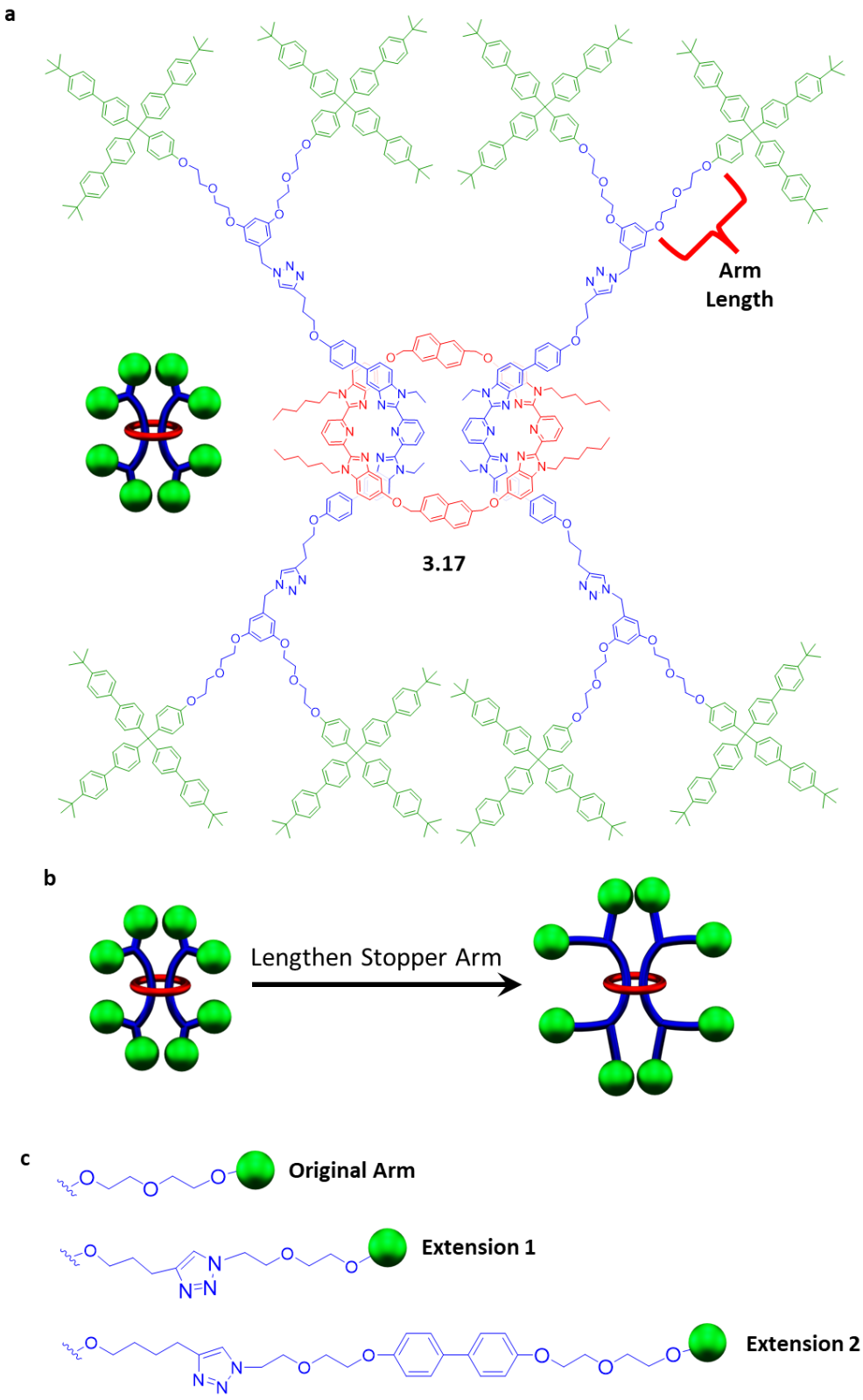

Fig 4.3 a) Chemical structure with labeled connecting arm length of **3.17**, b) Cartoon scheme describing increasing the [3]rotaxane arm length, c) Chemical structure of arm extensions considered in this chapter.

The original arm is a 7 atom long diethylene glycol fragment (Fig 4.3a-c). The first extension adds an alkyl fragment and a triazole connection increasing this arm to 13 atoms long. The second extension adds another diethylene glycol fragment in addition to a rigid biphenyl linker making it 29 atoms long. The goal of this to chapter is to understand if these structural changes impact the stability of the [3]rotaxane, and if so, are the extensions long enough to result in a stable [3]rotaxane.

4.2 Component Synthesis

No additional new components need to be synthesized to make the first stopper arm extension beyond those described in Chapter 3 (stopper **3.1**:**3.3**$_2$:Fe(II)$_2$ with **3.10**). The synthesis of the second extension requires the synthesis of a new longer stopper group **4.1** (Fig 4.4).

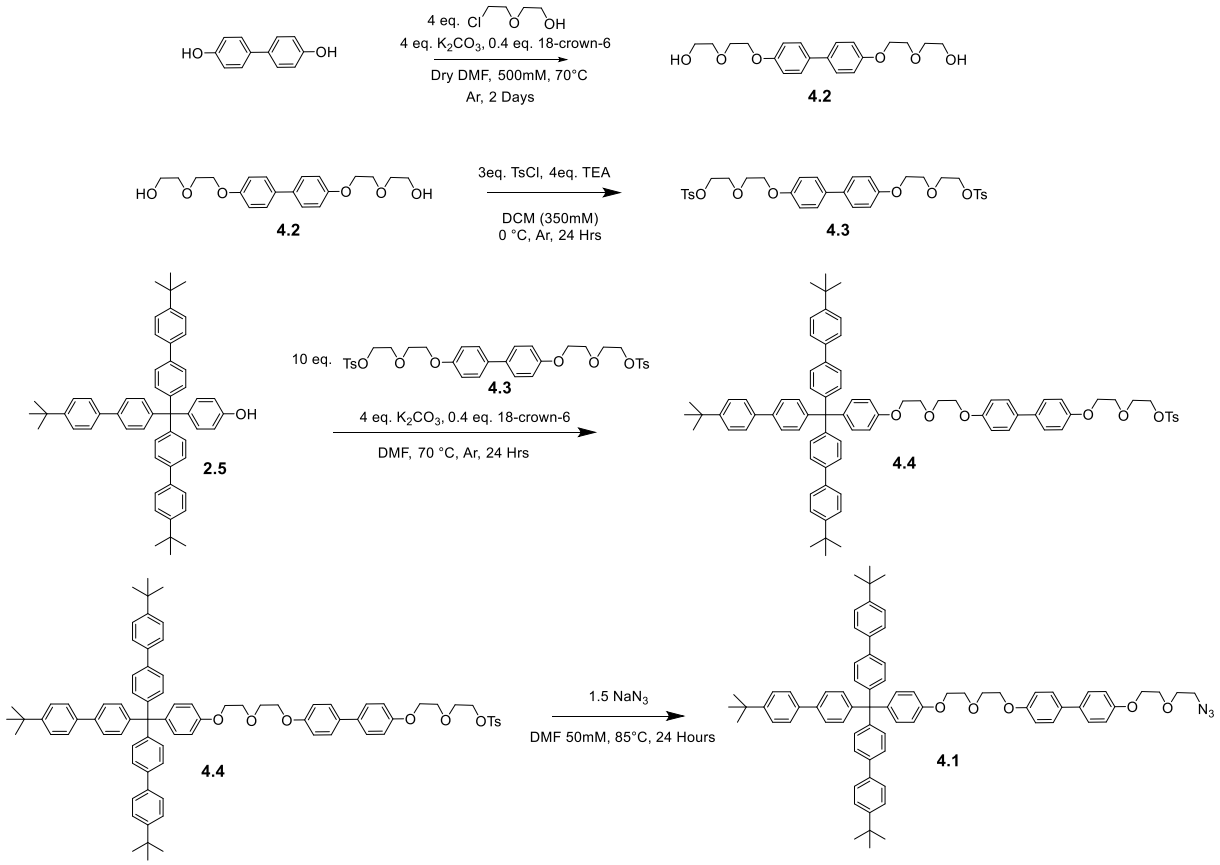

Fig 4.4 Synthesis of stopper component **4.1**.

Briefly, 4,4'-Dihydroxybiphenyl was functionalized at both ends with 2-(2-chloroethoxy)ethanol via standard Williamson ether[10] conditions to give **4.2**. This product was converted to the ditosylate **4.3** using standard tosylation conditions. **4.3** was then attached to stopper group **2.5** via Williamson ether conditions to give a tosylated version of the newly extended stopper group **4.4**. This could then be easily converted to the azide stopper group **4.1** via standard azidation conditions with a minimal amount of NaN_3. (See experimental for full details of all steps**).**

4.3 [3]Rotaxane Synthesis and Characterization

The first extended [3]rotaxane was made by stoppering the previously described pseudo[3]rotaxane **3.1**:**3.3**$_2$:Fe(II)$_2$ with the previously described mono stopper **3.10** (Fig 4.5, see experimental for full details including the synthesis of the corresponding new free dumbbell **4.5**) to yield the new doubly threaded [3]rotaxane **4.6**.

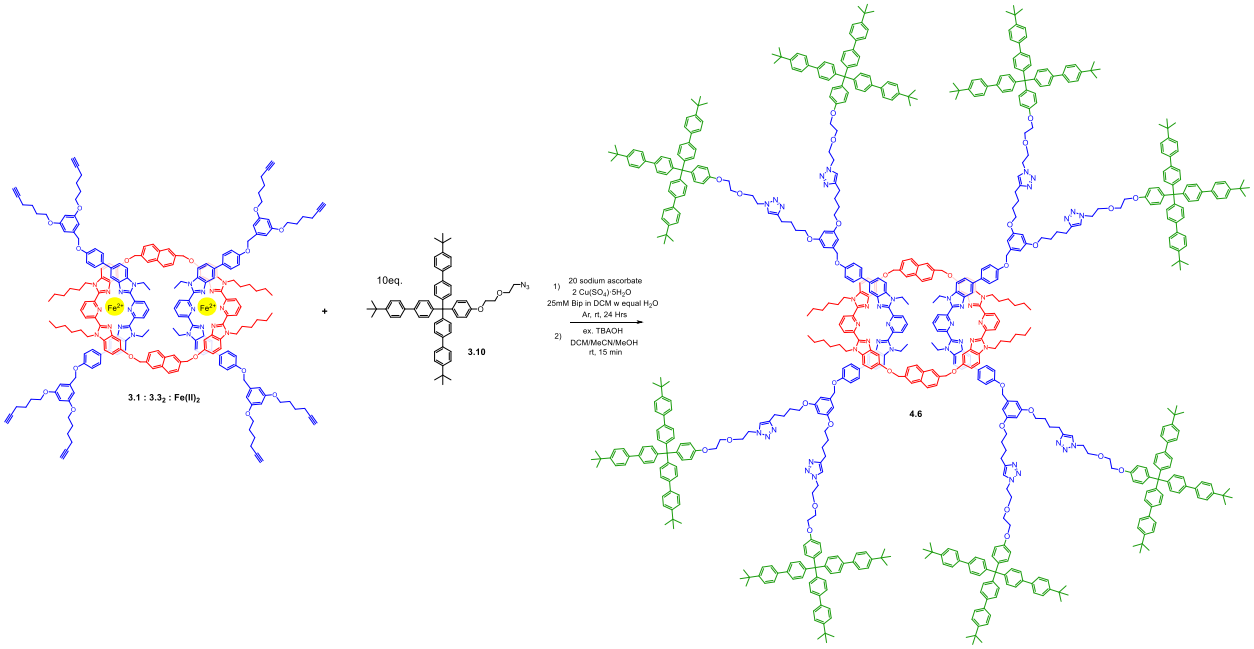

Fig 4.5 Scheme showing synthesis and chemical structure of [3]rotaxane **4.6**.

After stoppering with similar copper-catalyzed azide-alkyne cycloaddition (CuACC)[11,12] conditions to those developed in Chapter 3, a large lower Rf spot was seen via thin layer

chromatography (TLC, 6% MeOH in $CHCl_3$) of the crude demetallated mixture relative to the noninterlocked components indicative of [3]rotaxane product. In addition, crude ^{1}H-NMR spectroscopy revealed upfield shifted peaks relative to the noninterlocked components also indicative of interlocked product (Fig 4.6).

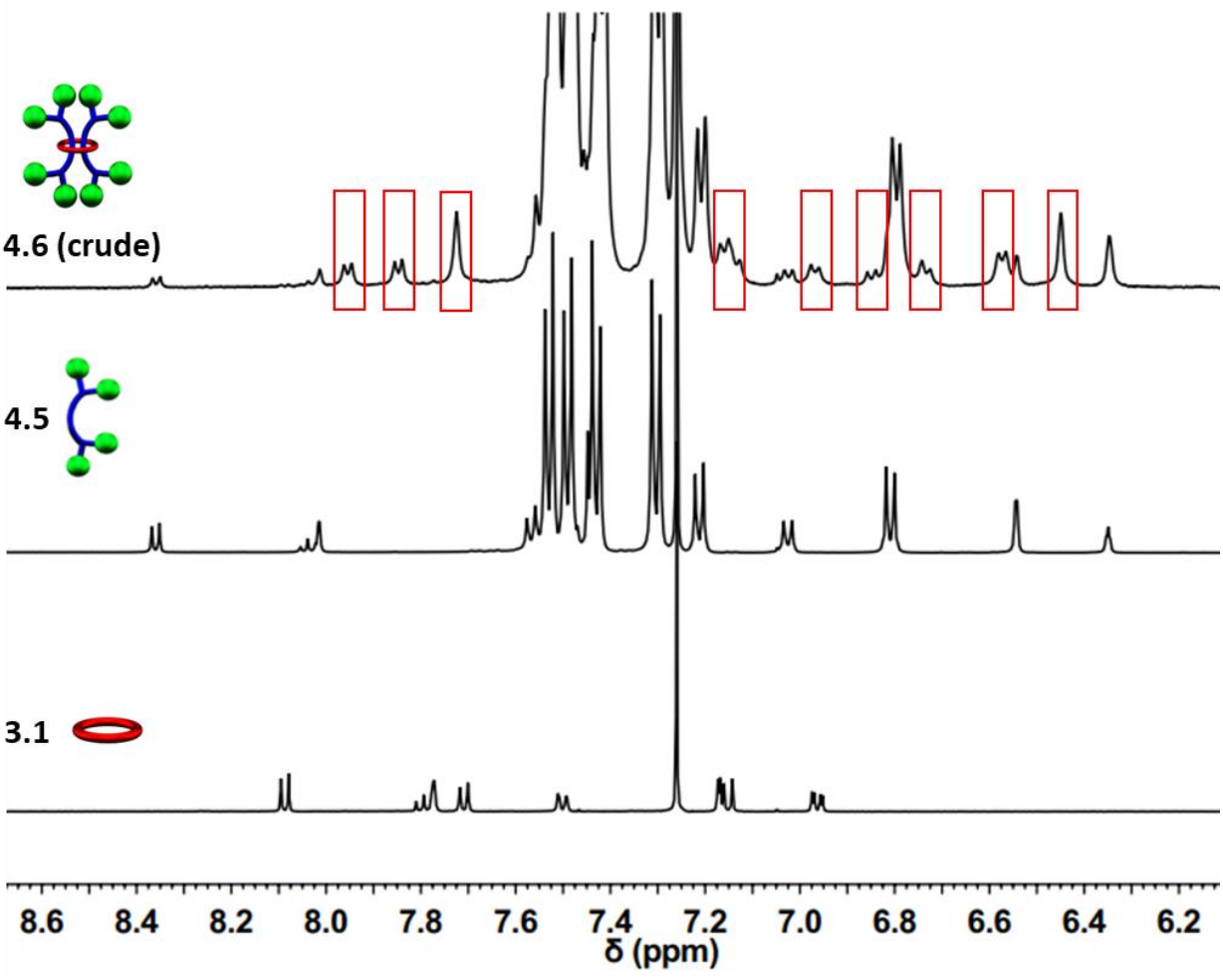

Fig 4.6 Partial ^{1}H-NMR overlay (500 MHz, 25°C, $CDCl_3$) of crude **4.6** relative to its components, red boxes indicate interlocked product.

Preparative thin layer chromatography was used to isolate the [3]rotaxane **4.6** in 65% yield. Comparison to the previously assigned spectra of [3]rotaxanes **3.17** and **3.19** and the noninterlocked components **4.5** and **3.1** combined with ^{1}H-^{1}H COSY NMR of **4.6** allowed the ^{1}H-

NMR of **4.6** to be fully assigned (See Fig 4.7 and 4.8 for the diagnostic aromatic region and experimental for full details).

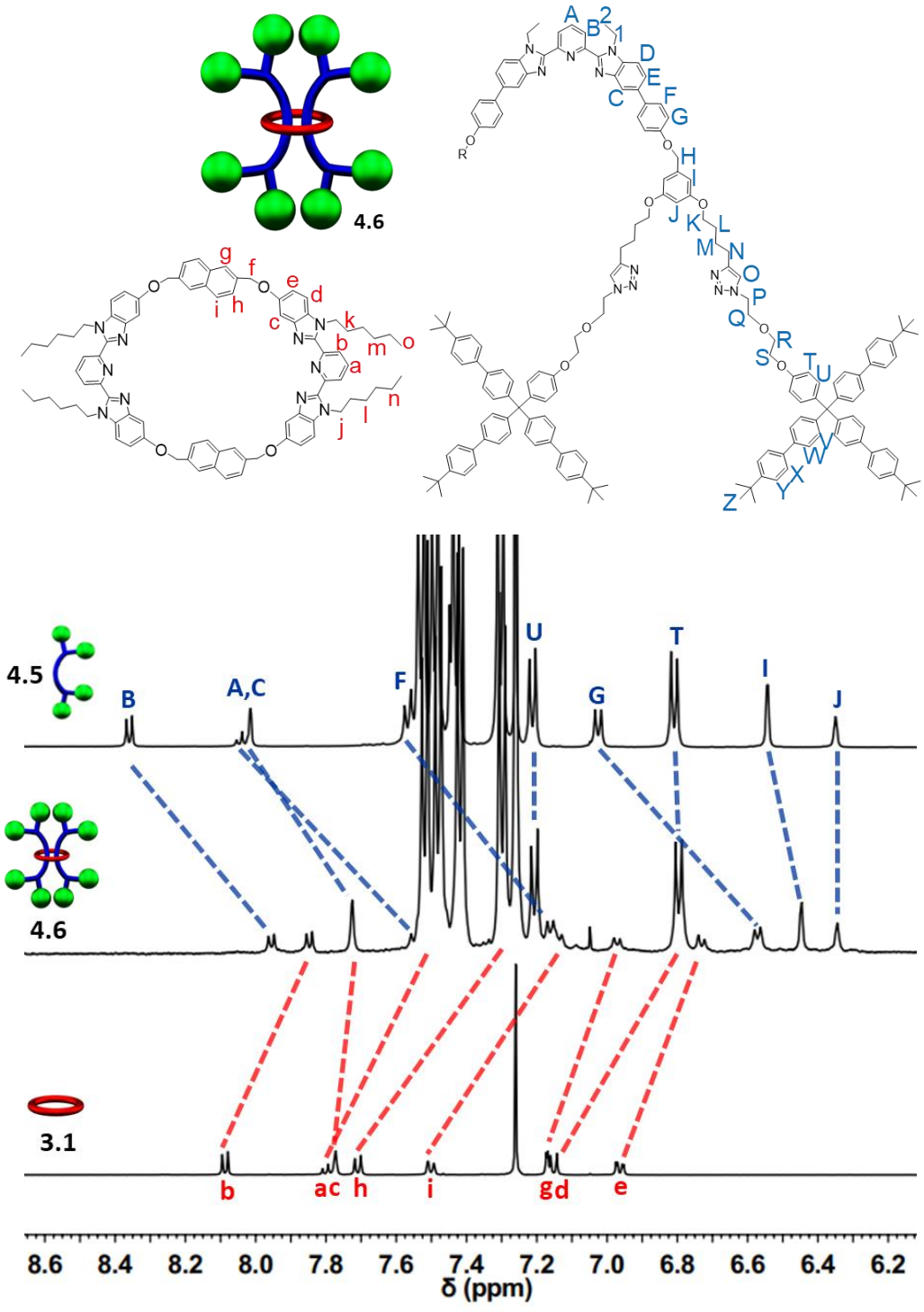

Fig 4.7 Partial ^{1}H-NMR overlay (500 MHz, 25°C, $CDCl_3$) of purified **4.6** relative to its components **4.5** and **3.1**, ^{1}H assignments at top of figure.

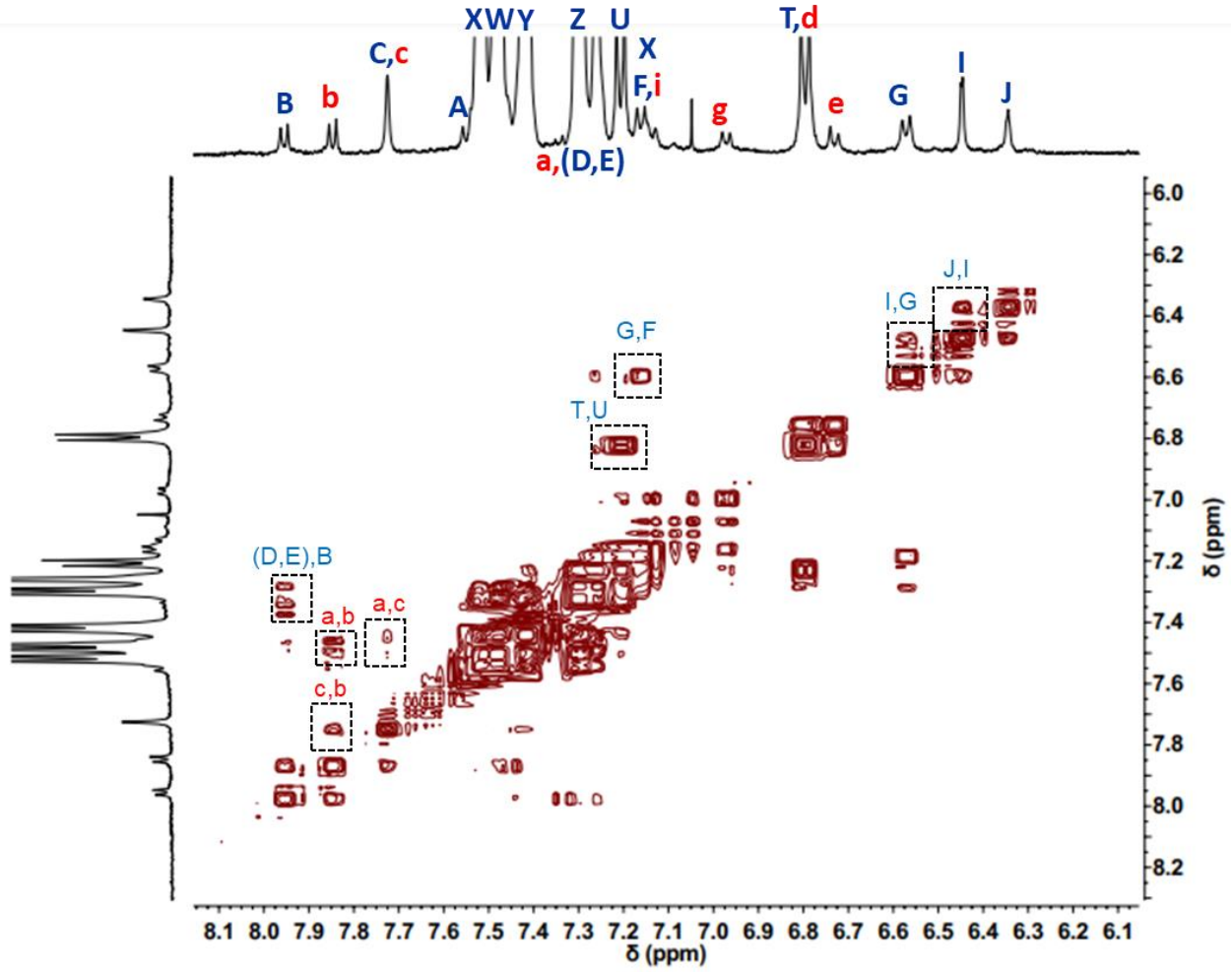

Fig 4.8 Partial ^{1}H-^{1}H COSY (5mM, 500 MHz, 25°C, $CDCl_3$) of doubly threaded [3]rotaxane **4.6**. Peak assignments correspond to those given in Figure 4.7.

Further characterization of **4.6** using size exclusion chromatography revealed a single lower retention time product for the [3]rotaxane relative to its noninterlocked components **4.**5 and **3.**1 as expected (Fig 4.9a). In addition, MALDI-TOF MS displayed the expected fragmentation pattern of the interlocked structure (Fig 4.9b).

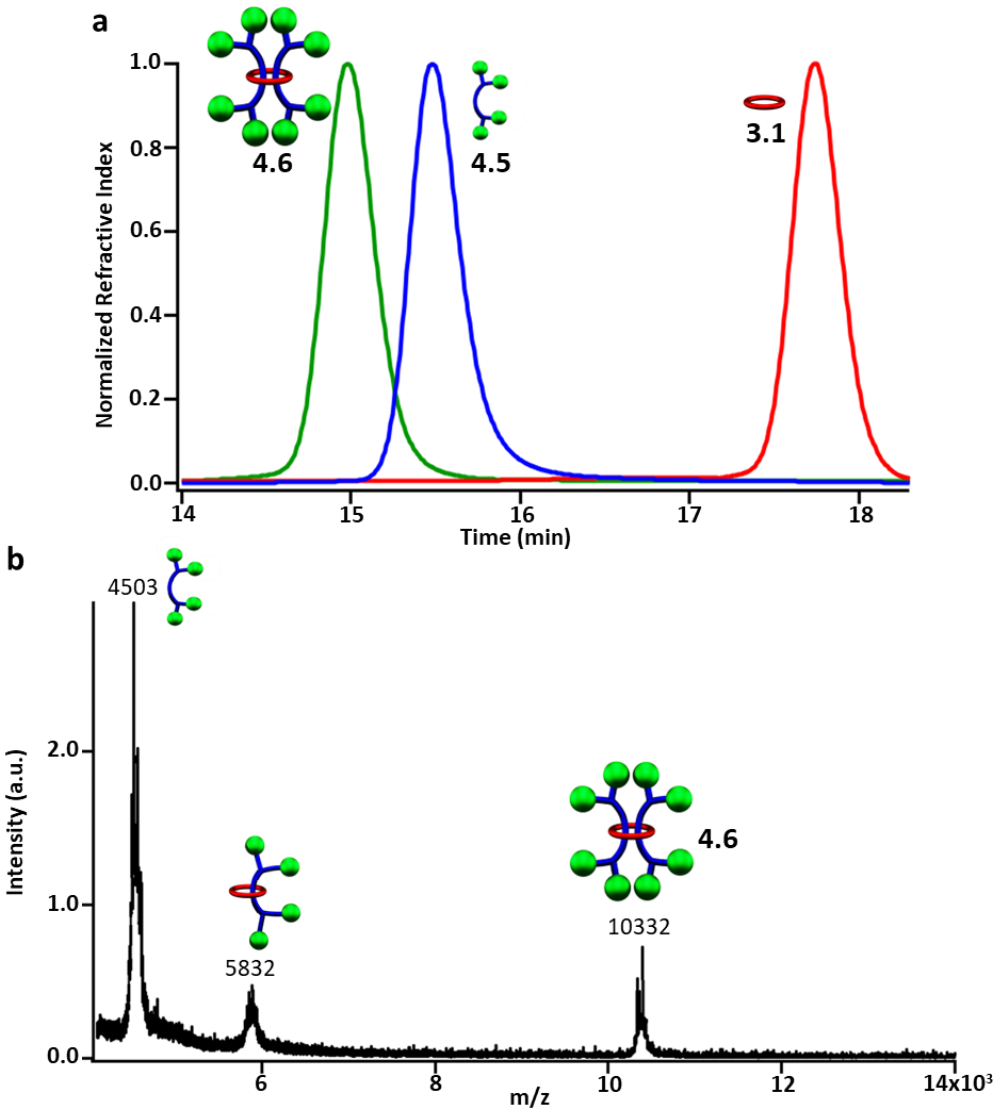

Fig 4.9 a) GPC chromatogram of (3:1 THF:DMF as eluent) purified **4.6**, **4.5**, and **3.1** at 298K, and b) MALDI-TOF MS (Dithranol, no salt) of purified **4.6.**

The second extended [3]rotaxane was made by stoppering the previously described **3.1**:**3.3**$_2$:Fe(II)$_2$ with the newly synthesized stopper group **4.1** (Fig 4.9, see experimental for full details including the synthesis of the corresponding new free dumbbell **4.7**) to yield the new doubly threaded [3]rotaxane **4.8** (Fig 4.10).

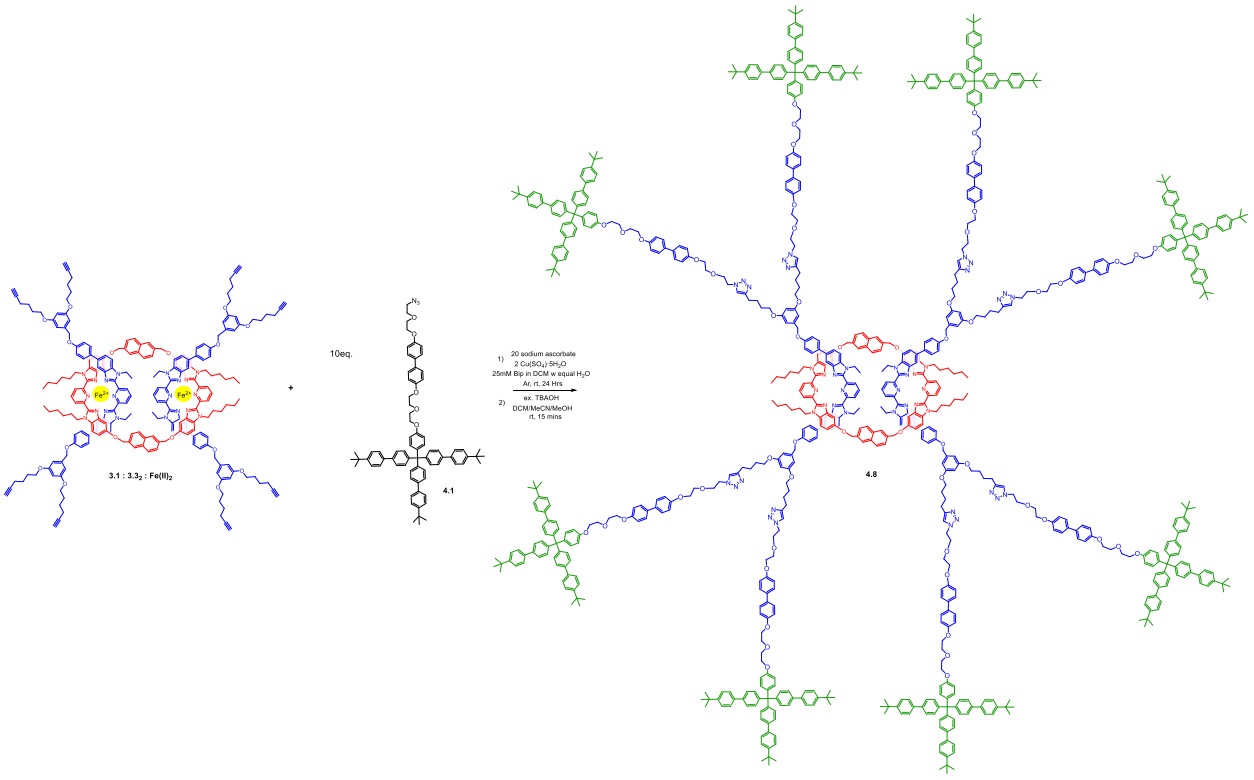

Fig 4.10 Scheme showing synthesis and chemical structure of [3]rotaxane **4.8**.

Again, after stoppering and demetallating, an intense lower Rf spot was seen via TLC (6% MeOH in $CHCl_3$) of the crude mixture relative to its noninterlocked components indicative of [3]rotaxane product. In addition, ^{1}H-NMR spectroscopy revealed upfield shifted peaks relative to the noninterlocked components (Fig 4.11) in the typical regions seen in this thesis confirming that the [3]rotaxane had been successfully formed. Preparative thin layer chromatography was used to isolate the lower Rf [3]rotaxane **4.8** in 55% yield from its noninterlocked components.

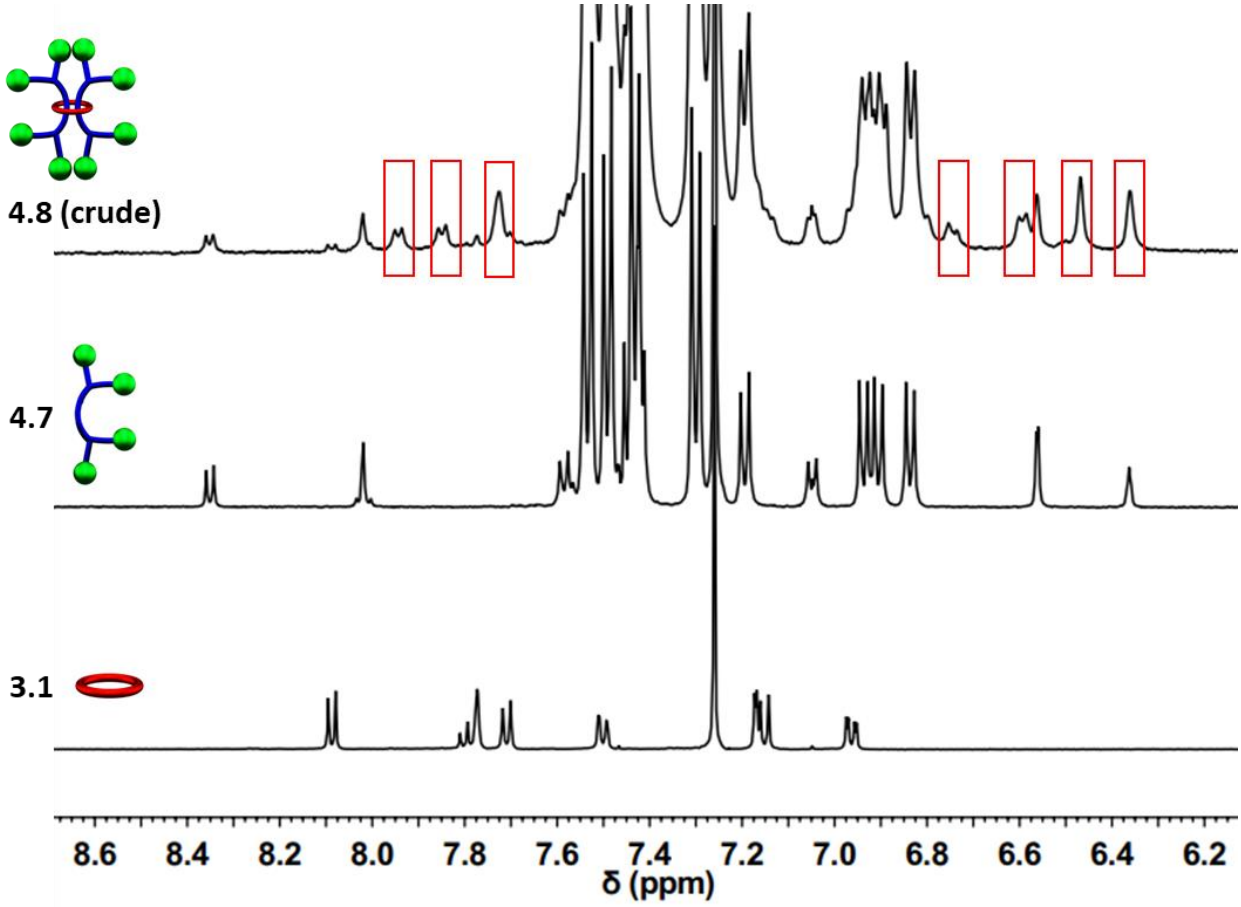

Fig 4.11 Partial ^{1}H-NMR overlay (500 MHz, 25°C, $CDCl_3$) of crude **4.8** relative to its components, red boxes indicate interlocked product.

Comparison to the previously assigned ^{1}H-NMR spectra of [3]rotaxanes **3.17**, **3.19**, and **4.6** and the noninterlocked components **4.7** and **3.1** combined with ^{1}H-^{1}H COSY NMR of **4.8** allowed the ^{1}H-NMR of **4.8** to be fully assigned (See Fig 4.12 and 4.13 for the diagnostic aromatic region and experimental for full details). Both [3]rotaxanes **4.8** and **4.6** show an average upfield shift of ~0.3ppm of their aromatic ^{1}H peaks relative to their noninterlocked components. This is a bit larger than the shift seen in **3.17** and is more akin to the tetra stoppered system **3.19**. In addition, similar downfield shifted B, b, C, and c environments are seen in **4.8** and **4.6** as in **3.19**. This suggests the use of thread component **3.2** (as opposed to **3.1**) is likely responsible for this increase in upfield shifting due to this slightly shorter thread length between the DHBA linkers.

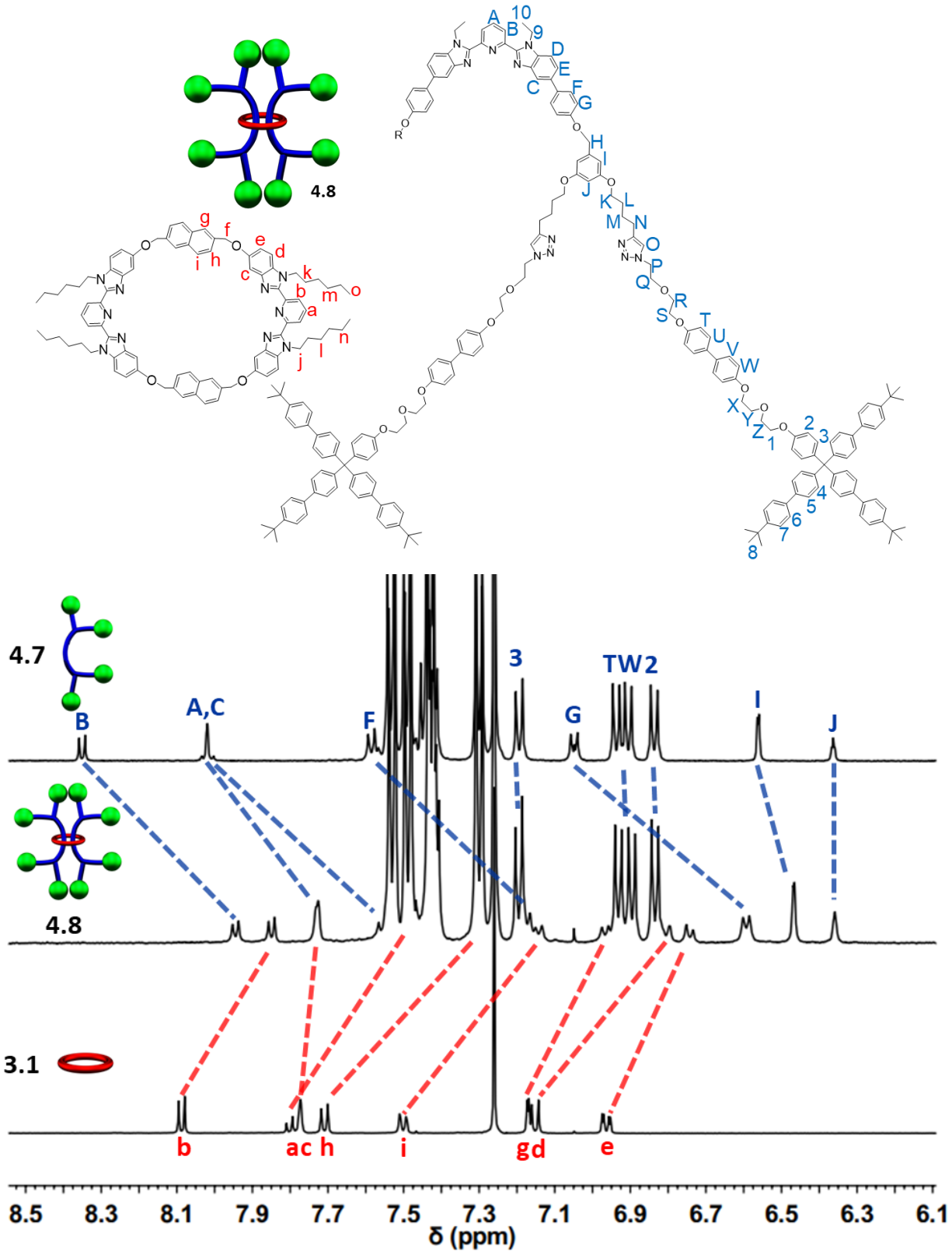

Fig 4.12 Partial ^{1}H-NMR overlay (500 MHz, 25°C, $CDCl_3$) of purified **4.8** relative to its components **4.7** and **3.1**, ^{1}H assignments at top of figure.

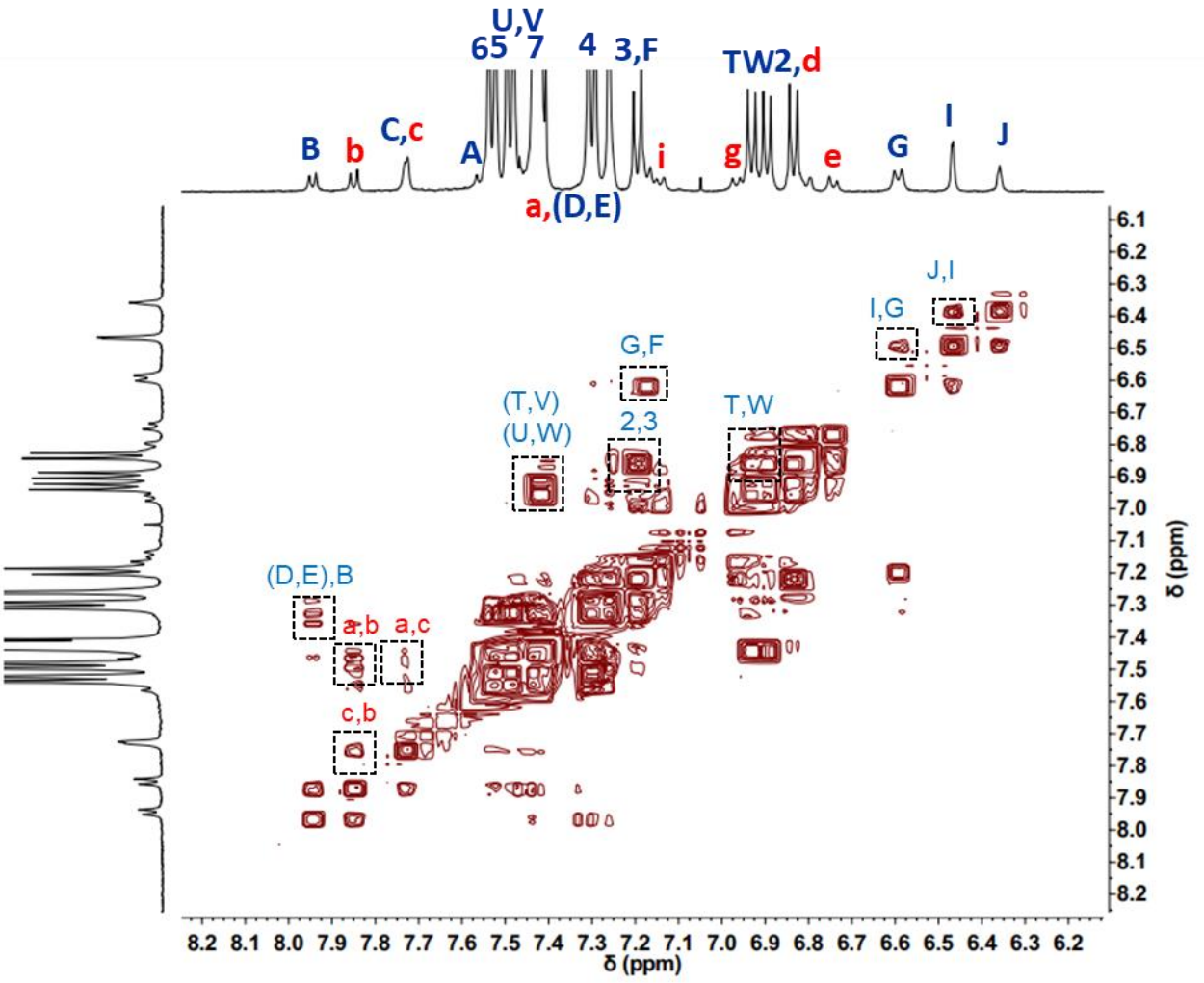

Fig 4.13 Partial ^{1}H-^{1}H COSY (5mM, 500 MHz, 25°C, $CDCl_3$) of doubly threaded [3]rotaxane **4.6**. Peak assignments correspond to those given in Figure 4.12.

Further characterization of **4.8** to confirm its structure using size exclusion chromatography revealed a single lower retention time product for the [3]rotaxane relative to its noninterlocked components as expected (Fig 4.14a). In addition, MALDI-TOF MS displayed the expected fragmentation pattern of the interlocked structure (Fig 4.14b).

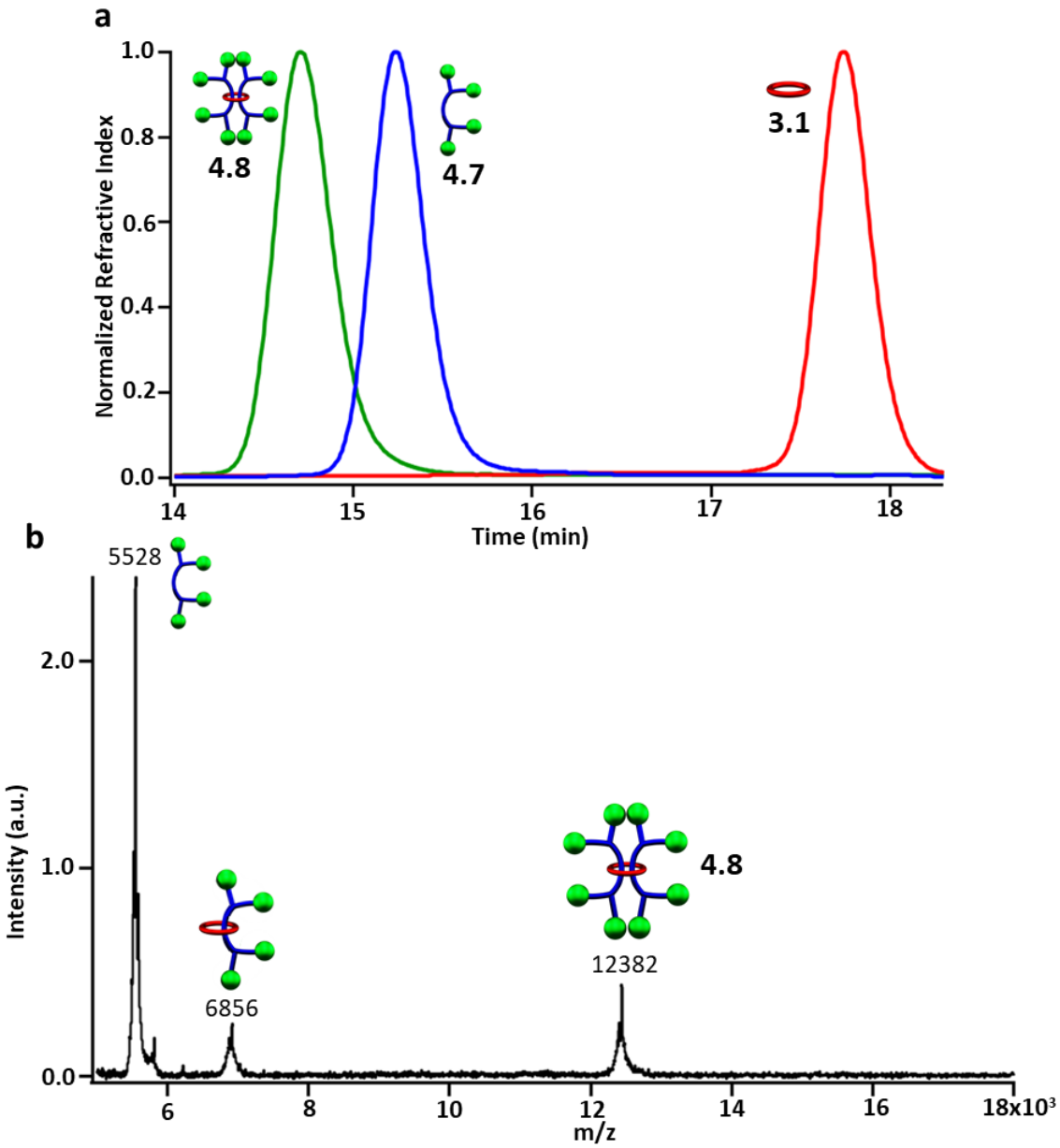

Fig 4.14 a) GPC chromatogram of (3:1 THF:DMF as eluent) purified **4.8**, **4.7**, and **3.1** at 298K, and b) MALDI-TOF MS (Dithranol, no salt) of purified **4.8.**

Combined GPC analysis of the [3]rotaxanes **4.8**, **4.6**, and **3.17** with the corresponding dumbbells **4.7**, **4.5**, and **3.16** shows a clear decrease in retention time corresponding to an increased size (hydrodynamic radius) of the [3]rotaxane and dumbbells as the arm length is increased (Fig 4.15). The first extension is relatively close in size to the original [3]rotaxane and the second extension shows a significantly larger retention time shift.

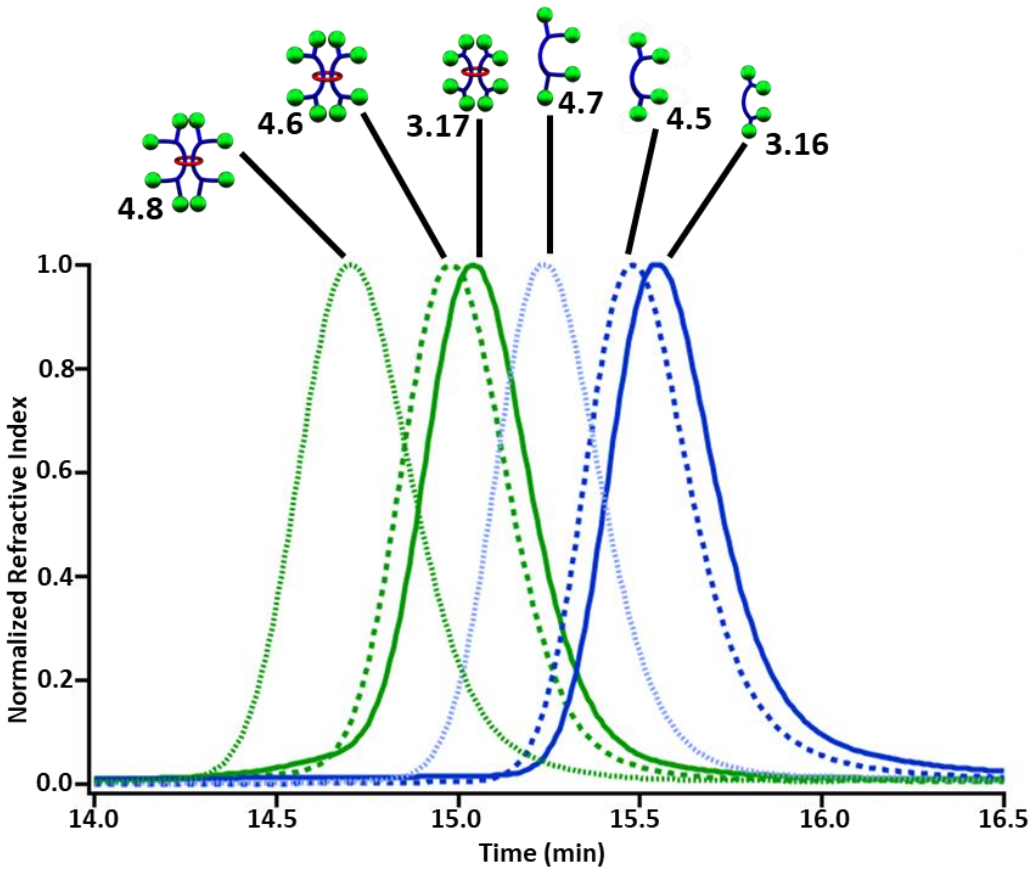

Fig 4.15 GPC chromatogram of (3:1 THF:DMF as eluent) purified **4.8**, **4.6**, **3.17**, **4.7**, **4.5**, and **3.16** at 298K**.**

4.4 [3]Rotaxane Slippage Analysis

As stated in the introduction the key goal was to understand if the [3]rotaxane arm length was a tunable parameter for affecting the slippage rate and if these extensions were long enough to achieve a stable [3]rotaxane. Towards this end, the same kinetic experiment described in Chapter 3[1,13] was applied to doubly threaded [3]rotaxanes **4.6** and **4.8**. Freshly prepared 1mM solutions of both were monitored at 35 °C for one week followed by 40 °C for another week, and finally 45 °C for a final week with their ^{1}H-NMR spectra recorded after 2 days, 4 days, 5 days, and 7 days each week. From this it can be seen that both rotaxanes undergo slippage of the 46 atom ring **3.1** over the extended dumbbells. (Fig 4.16 and 4.17) tracking the diagnostic meta-pyridyl “B” peak (Fig 4.7+4.12 for labels).

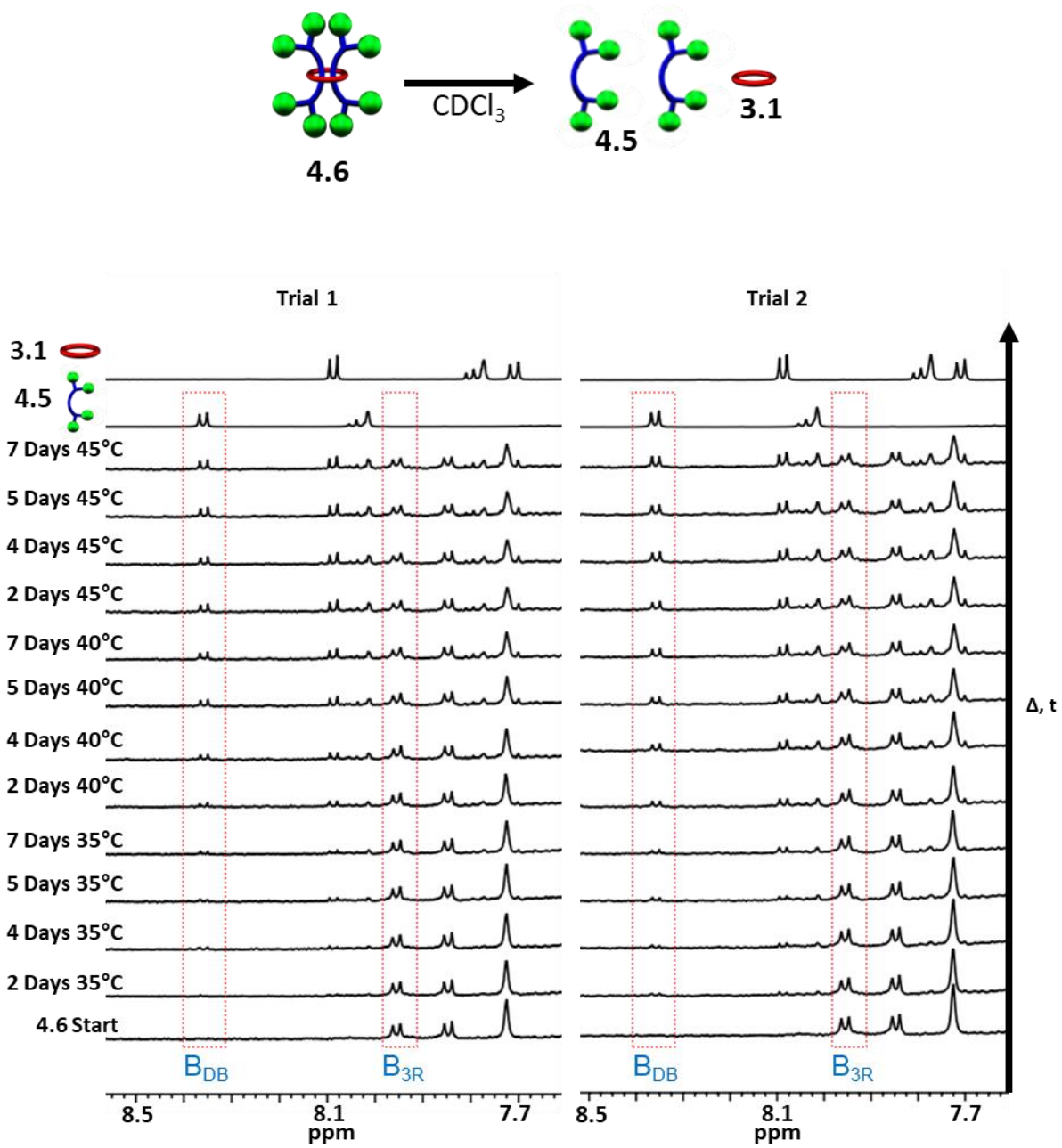

Fig 4.16 Partial ^{1}H-NMR overlay (500 MHz, $CDCl_3$) of slippage trials of **4.6**, time and temperature indicated at side of figure with cartoon describing slippage process at top of figure.

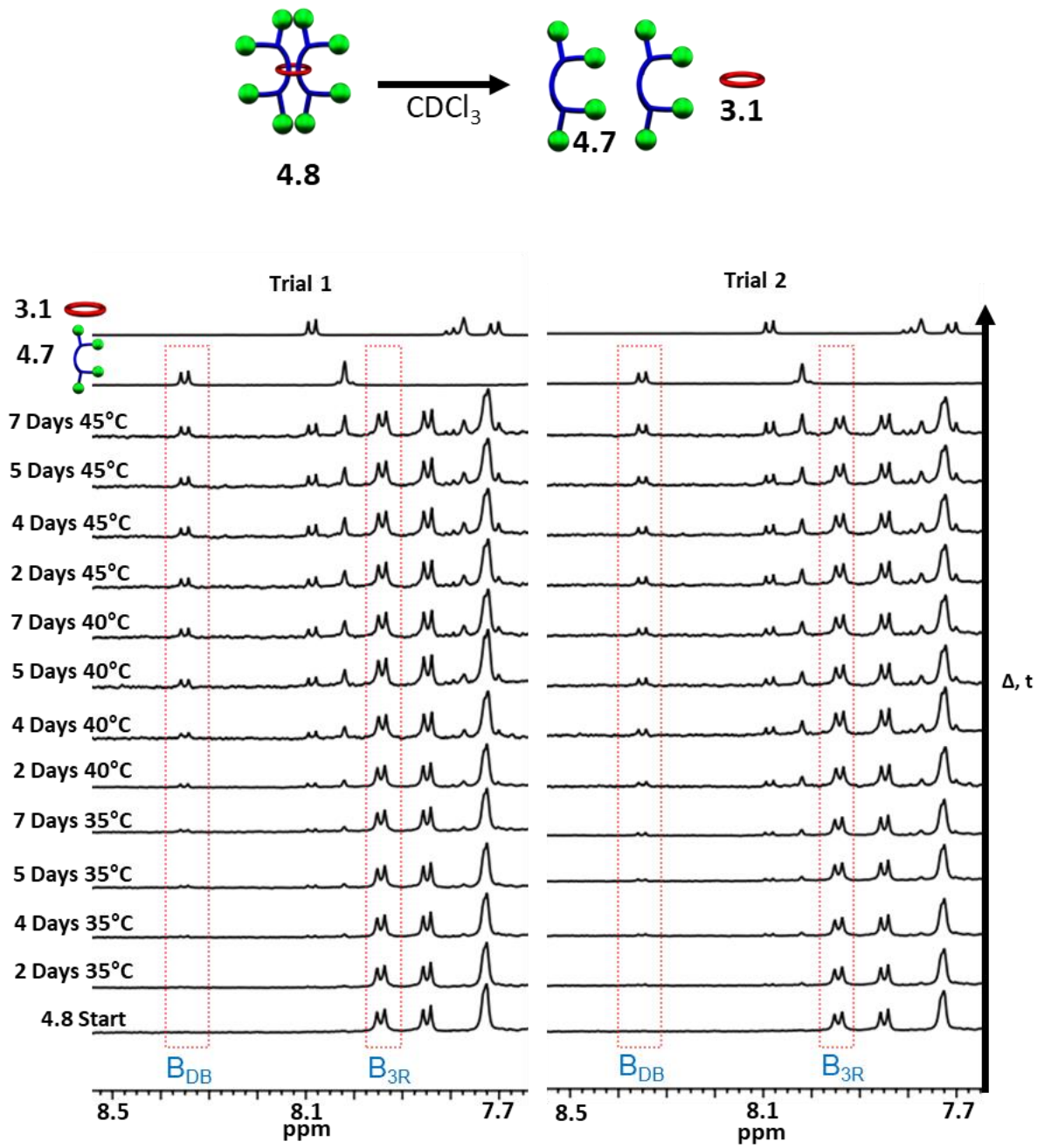

Fig 4.17 Partial ^{1}H-NMR overlay (500 MHz, $CDCl_3$) of slippage trials of **4.8**, time and temperature indicated at side of figure with cartoon describing slippage process at top of figure.

In addition, as with all of the slippage processes in Chapter 3, no [2]rotaxane intermediate was observed in any appreciable scale during the slippage of either **4.6** or **4.8** suggesting that any corresponding [2]rotaxane using either extended dumbbell with the 46 atom ring **3.1** is not stable

at all. Applying standard first-order kinetics and Eyring/Arrhenius methods allows the kinetic and thermodynamic parameters of both slippage processes to be determined (See Fig 4.18 and the Experimental for full details).

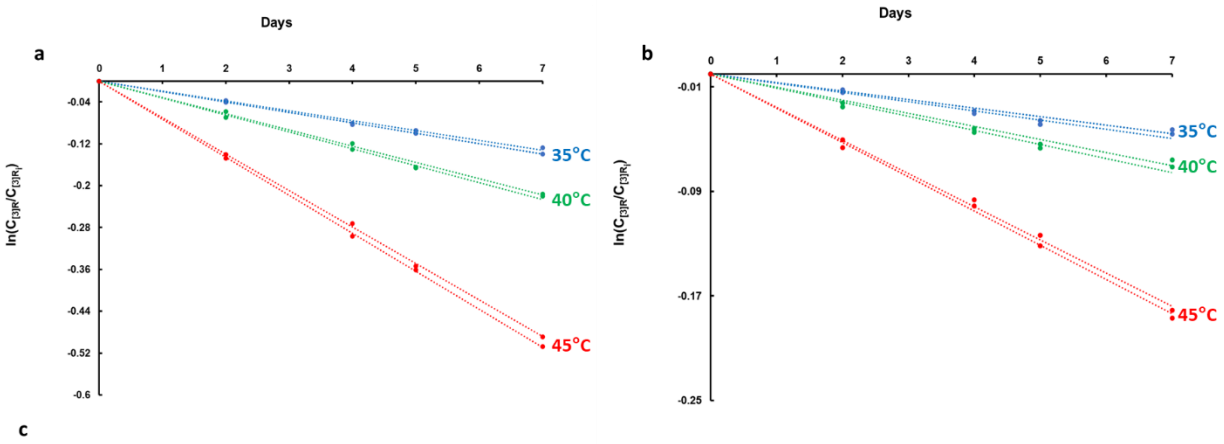

c

[3]R	$t_{1/2}$ (days, 308K)	$t_{1/2}$ (days, 313K)	$t_{1/2}$ (days, 318K)	E_a (kJ/mol)	$\Delta H^{\ddagger}$ (kJ/mol)	$\Delta S^{\ddagger}$ (J/mol*K)	$\Delta G^{\ddagger 298K}$ (kJ/mol)
3.17	27 ± 1	17 ± 1	8.5 ± 2	98 ± 4	95 ± 3	-61 ± 8	113 ± 6
4.6	35 ± 4	22 ± 3	10 ± 2	101 ± 4	99 ± 4	-47 ± 9	113 ± 5
4.8	105 ± 7	65 ± 5	28 ± 4	117 ± 8	111 ± 6	-20 ± 5	120 ± 10

Fig 4.18 Kinetic first-order plot of two trials of slippage at three different temperatures of a) **4.6**, b) **4.8**, and c) obtained thermodynamic and kinetic parameters for both slippage processes.

From this data, the first extension from 7 to 13 atoms provides a relatively small increase to the barrier to dethreading while the second extension to 29 atoms provides a much larger stability increase (Fig 4.18c). Specifically, upon the first arm increase from **3.17** to **4.6**, the activation energy barrier to slippage slightly changes from 98±4 kJ/mol to 101±4 kJ/mol (within error of one another), $\Delta G^{\ddagger 298K}$ is unchanged at 113±5/6 kJ/mol, and the kinetic half-lives show a minimal increase (Fig 4.18c). The arm length increase from **3.17** (or **4.6**) to **4.8** has a much more dramatic effect on the stability of the [3]rotaxane. The activation energy for slippage is increased significantly to 117±8 kJ/mol while the $\Delta G^{\ddagger 298K}$ increases to 120±10 kJ/mol. From a kinetic

standpoint the half-life for slippage is nearly quadrupled in value to 105±7 days at 35°C, 65±5 days at 40°C, and 28±4 days at 45°C (Fig 4.18c). The dramatic stability increase seen here may be in part a result of the bulkiness added from the biphenyl linker in this second arm extension. Overall, this data clearly shows that the stopper group arm length connecting each bulky tris(p-t-butylbiphenyl)methyl moiety in this [3]rotaxane structure is a tunable parameter that can impact the slippage rate to dethreading. However, the two extensions considered in this chapter were not long enough to result in a fully stable interlocked molecule.

4.5 Conclusions and Future Directions

Motivated by preliminary all-atom molecular dynamics simulations results, this chapter explored the effect of increasing the stopper group arm length on the kinetic stability of the [3]rotaxane structure. Specifically, two new doubly threaded [3]rotaxanes **4.6** and **4.8** containing differing size stopper group arms were synthesized, characterized, and their kinetic stability was tested. The first arm increase from 7 to 13 atoms resulted in a very minor increase in the stability of the [3]rotaxane. The second arm increase to 29 atoms had a much more significant impact on the barrier to dethreading for the interlocked structure. These results imply that longer and more rigid arms connecting the stopper group may result in a stable [3]rotaxane structure.

Based on the results in this chapter, the easiest path forward for this specific component design parameter is to incorporate polymeric stoppers to easily access long and controllable lengths of the stopper group arm. Specifically, the easiest envisioned synthetic pathway to this would involve atom transfer radical polymerization (ATRP)[14,15] and one possible structure is seen in Figure 4.19.

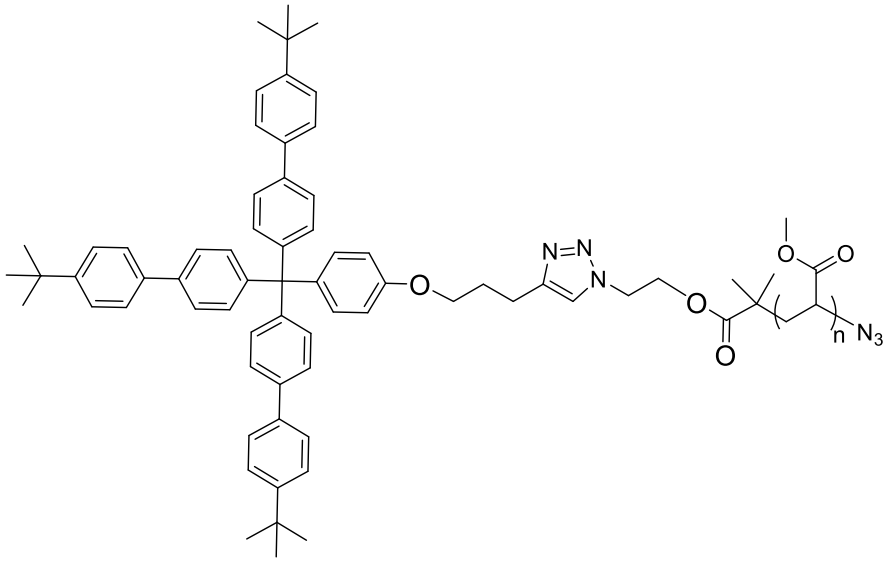

Fig 4.19 Chemical structure of proposed stopper group with easy synthetic variation of stopper group arm.

This stopper group structure could be made easily in three steps from commercially available starting materials. In addition, ATRP has been well explored, and many polymers including styrenes, acrylates, methacrylates, acrylamides, and more have been used allowing for the potential to build an easy synthetic library of differing arms. Additional parameters to the stopper arm beyond length such as arm thickness and polarity could also be experimentally varied using this synthetic platform.

4.6 Experimental

4.6.1 Materials and Methods

Materials. All reagents were purchased from Sigma-Aldrich unless otherwise stated. All chemicals were used as received without further purification unless otherwise stated. Solvents for chromatography were purchased from Fisher-Scientific. Deuterated solvents and 3,5-dihydroxybenzyl alcohol were purchased from ACROS Organics. 4-Bromo-4'-tert-butylbiphenyl

was purchased from TCI chemicals. *p*-Toluenesulfonyl chloride was purchased from Alfa Aesar. Iron(II) bistriflimide[16] and 2,6-bisbenzimidazolylpyridine ligands[2] were prepared following literature procedures. Tetrahydrofuran (THF) was dried over sodium and benzophenone. Dichloromethane was distilled over calcium hydride before use. Dimethylformamide (DMF) was dried with activated molecular sieves before use. Thin layer chromatography plates (1000 micron) were purchased from Analtech.

Matrix Assisted Laser Desorption/Ionization Mass Spectrometry (MALDI-MS). MALDI-TOF was measured by a Bruker Ultraflextreme MALDI-TOF-TOF spectrometer in linear (or reflectance) mode using dithranol as matrix and sodium trifluoroacetate or silver trifluoroacetate as ionizer (or no ionizer).

Nuclear Magnetic Resonance Spectroscopy (NMR). Room Temperature Nuclear Magnetic Resonance Spectroscopy was performed using a Bruker Ascend Avance III 500 MHz spectrometer, a Bruker Avance II+ 500 MHz spectrometer, or a Bruker DRX 400 MHz spectrometer at the University of Chicago NMR facilities. ^{1}H NMR spectra were referenced to the residual protonated solvent signal and ^{13}C{^{1}H} NMR spectra were referenced to the deuterated solvent carbon resonance signal.

NMR Slippage Kinetic Experiments. Kinetic experiments were performed in Shigemi Tubes purchased from Wilmad-Labglass in $CDCl_3$ (1mM) using a Bruker AVANCE III HD 500 MHz spectrometer at the NMR facilities at the University of Chicago.

Gel Permeation Chromatography (GPC). GPC measurements were performed utilizing the Soft Matter Characterization Facility at the University of Chicago. Measurements were conducted at 25^{o}C using 3:1 THF:DMF as eluent (flow rate = 1 mL/min), using a Shimadzu

autosampler, Shimadzu HPLC LC20-AD pump, 2 Agilent PLgel 5 um MIXED-D + guard SEC columns, and a Wyatt Optilab T-rEX differential refractive index detector.

4.6.2 Synthesis of 4.2

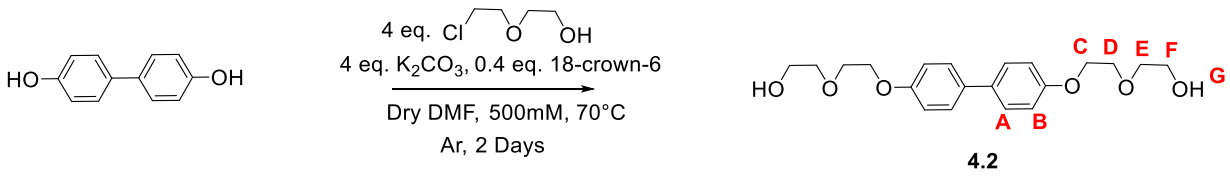

4.2

4,4'-Dihydroxybiphenyl (5.0g, 26.8mmol), K_2CO_3 (14.84g, 107mmol), and 18-crown-6 (2.83g, 2.7mmol) were added to a 100mL RBF. The reaction chamber was purged with argon and DMF (54mL) was added via cannula. The reaction mixture was heated to 70°C and 2-(2-chloroethoxy)ethanol (8.5mL, 80.4mmol) was injected via syringe. The reaction mixture was allowed to stir at 70°C overnight and another portion of 2-(2-chloroethoxy)ethanol (2.8mL, 26.8mmol) was injected via syringe. The following day the reaction mixture was cooled to room temperature and the solvent was removed under reduced pressure resulting in an off-white solid that was washed with hot $CHCl_3$ (4 × 150 mL) and filtered. The filtrate was collected and the solvent removed under reduced pressure resulting in an off-white residue. Purification from recrystallization in 3:1 methanol:chloroform resulted in a white solid, **4.2**, in 75% yield. ^{1}H NMR (400 MHz, $CDCl_3$) δ 7.47 (d, *J* = 8.6Hz, 4H, A), 6.97 (d, *J* = 8.6Hz, 4H, B), 4.17 (m, 4H, C), 3.90 (m, 4H, D), 3.78 (m, 4H, E), 3.70 (m, 4H, F), 2.11 (t, *J* = 6.0Hz, 2H, G). ^{13}C NMR (101 MHz, $CDCl_3$) δ 157.95, 133.78, 127.89, 115.03, 72.72, 69.87, 67.66, 61.96. MALDI-MS: 385.2 ($[M]+Na^+$).

4.6.3 Synthesis of 4.3

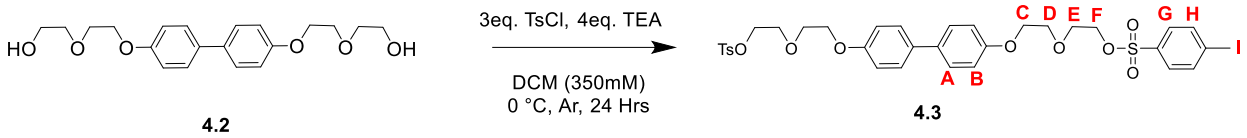

A 100 mL RBF was charged with **4.2** (3.0 g, 8.2 mmol), *p*-toluenesulfonyl chloride (4.73 g, 24.6mmol) and DCM (24mL, reaction conc. = 350mM). The reaction was stirred, cooled with an ice bath and NEt_3 (4.61mL, 32.8 mmol) was added dropwise and the reaction was allowed to warm to RT. After 18h the reaction mixture was diluted with 50mL CH_2Cl_2 and washed once with 1M HCl (50mL) and twice with H_2O (100 mL). The organic layer was removed and dried with $MgSO_4$, filtered and the solvent reduced under reduced pressure. The product **4.3** was purified using recrystallization from 88:12 $CHCl_3$:MeOH as a white solid in 75% yield. ^{1}H NMR (400 MHz, $CDCl_3$) δ 7.80 (d, *J* = 8.2Hz, 4H, H), 7.46 (d, *J* = 8.7Hz, 4H, A), 7.30 (d, *J* = 8.2Hz, 4H, G), 6.94 (d, *J* = 8.7Hz, 4H, B), 4.20 (m, 4H, C), 4.08 (m, 4H, D), 3.81 (m, 4H, E), 3.78 (m, 4H, F), 2.41 (s, 6H, I). ^{13}C{^{1}H} NMR (101 MHz, $CDCl_3$) δ 157.92, 144.93, 133.79, 133.09, 129.93, 128.11, 127.83, 115.00, 70.05, 69.39, 69.04, 67.62, 21.76. MALDI-MS: 693.8 ([M]+Na^+).

4.6.4 Synthesis of 4.4

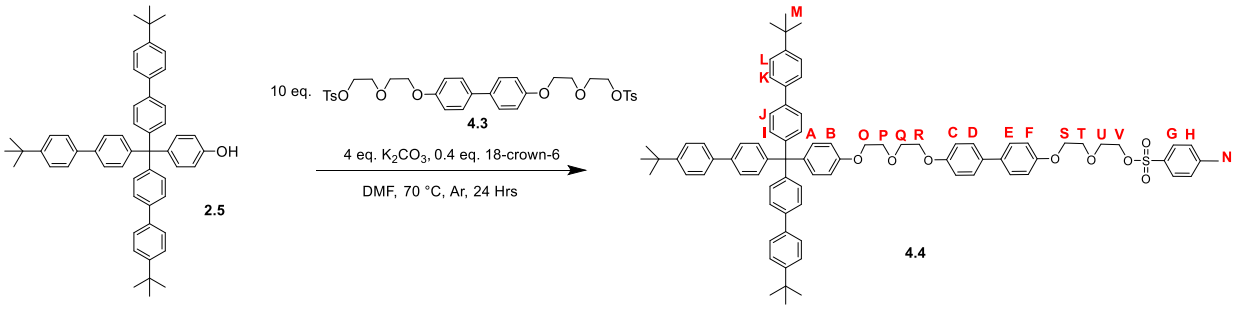

2.5 (396mg, 0.54mmol), K_2CO_3 (300mg, 2.1mmol), **4.3** (3.6g, 5.4mmol), and 18-crown-6 (56mg, 0.21mmol) were added to a 100mL RBF. The reaction chamber was purged with argon and DMF

(11mL) was added via cannula. The reaction mixture was allowed to stir at 70°C overnight. The following day the reaction mixture was cooled to room temperature and the solvent was removed under reduced pressure resulting in an off-white solid that was washed with hot $CHCl_3$ (4 × 50 mL) and filtered. The filtrate was collected and the solvent removed under reduced pressure resulting in an off-white residue. Purification was achieved by column chromatography (silica gel, $CHCl_3$) resulting in a white solid, **4.4**, in 55% yield. ^{1}H NMR (400 MHz, $CDCl_3$) δ 7.80 (d, *J* = 8.4Hz, 2H, H), 7.55 (d, *J* = 8.5Hz, 6H, J), 7.50 (d, *J* = 8.5Hz, 6H, L), 7.47-7.42 (m, 10H, D+E+I), 7.33-7.26 (m, 8H, G+K), 7.20 (d, *J* = 8.9Hz, 2H, A), 6.97 (d, *J* = 8.8Hz, 2H, C), 6.92 (d, *J* = 8.8Hz, 2H, F), 6.86 (d, *J* = 8.9Hz, 2H, B), 4.21-4.16 (m, 6H, Q+R+S), 4.08-4.05 (m, 2H, T), 3.97-3.93 (m, 4H, O+P), 3.81-3.75 (m, 4H, U+V), 2.40 (s, 3H, N), 1.35 (s, 27H, M). ^{13}C NMR (101 MHz, $CDCl_3$) δ 156.91, 150.26, 145.93, 144.89, 138.48, 137.80, 133.84, 132.33, 131.57, 129.92, 128.10, 127.82, 127.79, 126.70, 126.03, 125.79, 115.07, 114.96, 113.61, 70.11, 70.06, 70.02, 69.37, 69.01, 67.71, 67.57, 67.49, 63.77, 34.64, 31.49, 21.74. MALDI-MS: 1339.7 ([M]+Ag^+).

4.6.5 Synthesis of 4.1

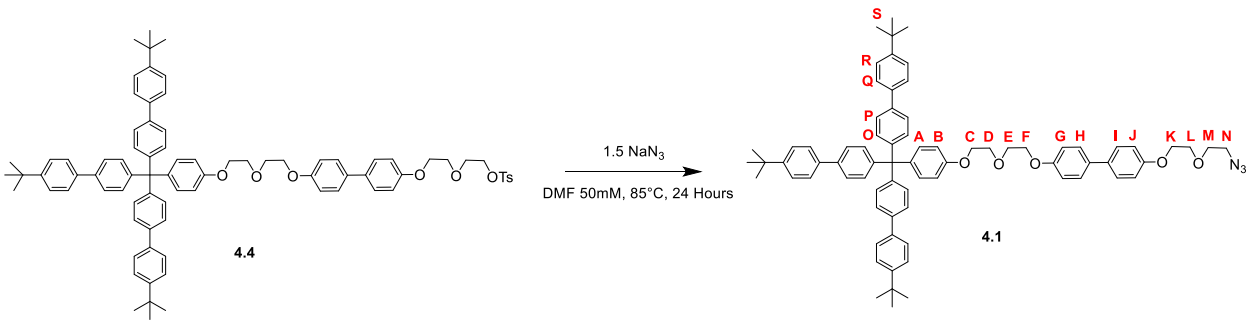

An Ar-filled 50 mL RBF was charged with **4.4** (320mg, 0.26mmol), NaN_3 (24mg, 0.39mmol) and DMF (5.2mL, reaction concentration 50mM). The reaction mixture was heated at 85 °C and stirred for 18h. After this time the solvent was removed under reduced pressure resulting in an off-white solid that was washed with hot DCM (4 × 15mL) and filtered. The filtrate was collected and the

solvent removed under reduced pressure resulting in an off-white residue. Purification using column chromatography (standard silica gel, eluent gradient 1:1 $CHCl_3$:Hexanes to 100 % $CHCl_3$) resulted in a white solid, **4.1**, in 65% yield. ^{1}H NMR (500 MHz, $CDCl_3$) δ 7.55 (d, *J* = 8.4Hz, 6H, P), 7.50 (d, *J* = 8.4Hz, 6H, R), 7.45-7.42 (m, 10H, O+H+I), 7.31 (d, *J* = 8.4Hz, 6H, Q), 7.20 (d, *J* = 8.8Hz, 2H, A), 6.96 (m, 4H, G+J), 6.86 (d, *J* = 8.8Hz, 2H, B), 4.21-4.15 (m, 6H, C+F+K), 3.97-3.95 (m, 4H, D+E), 3.89-3.87 (m, 2H, L), 3.78-3.75 (m, 2H, M), 3.44-3.41 (m, 2H, N), 1.35 (s, 27H, S). ^{13}C{^{1}H} NMR (101 MHz, $CDCl_3$) δ 158.03, 157.93, 156.93, 150.27, 145.94, 139.34, 138.50, 137.83, 133.86, 133.74, 132.35, 131.59, 127.84, 126.72, 126.04, 125.81, 115.10, 115.07, 115.04, 113.62, 70.40, 70.13, 70.09, 69.95, 67.73, 67.68, 67.52, 63.79, 50.87, 34.66, 31.51. MALDI-MS: 1210.5 ([M]+Ag^+) and 1182.4 ([M]+Ag^+ -N_2).

4.6.6 Synthesis of Dumbbell Component 4.5

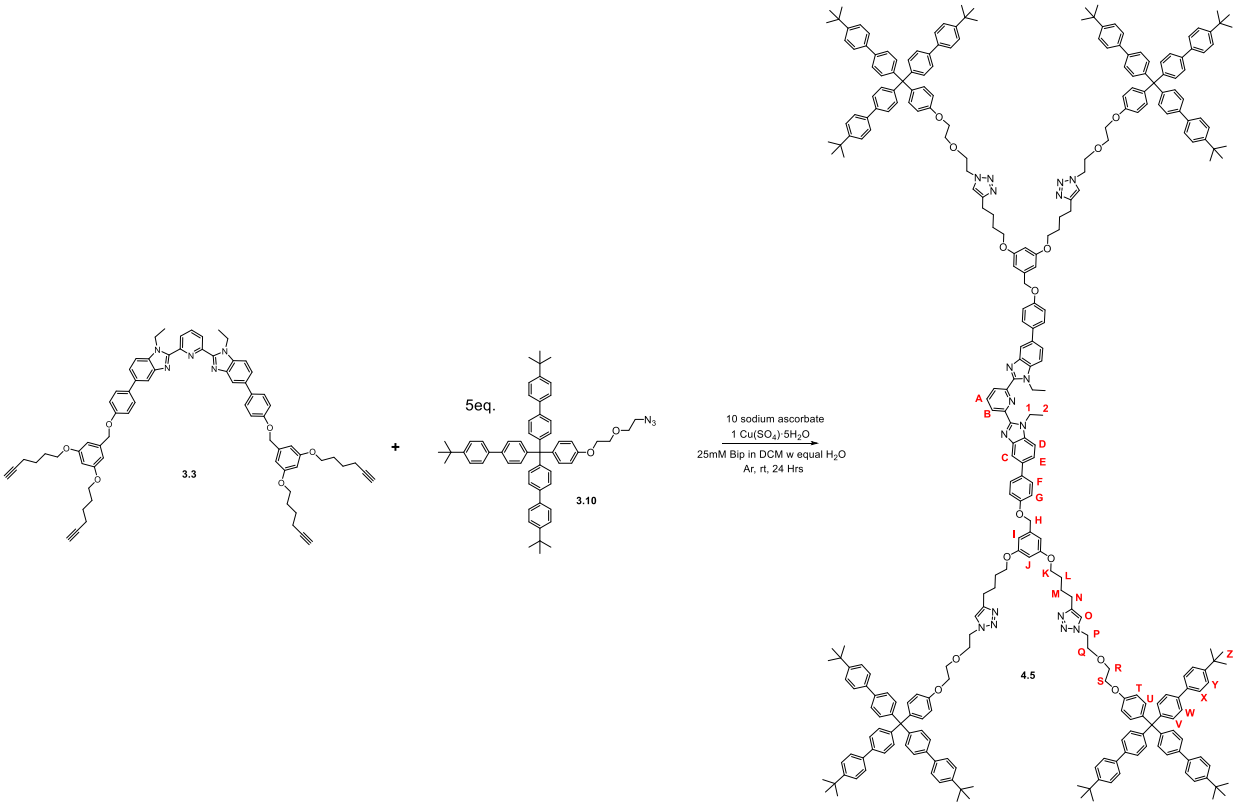

3.10 (112mg, 0.110mmol) was added to a 4mL glass vial followed by **3.3** (24.8mg, 0.022mmol), sodium ascorbate (43.5mg, 0.22mmol), and the reaction chamber was purged with Ar. 880µL DCM (25mM **3**), 780µL H_2O, and finally 100µL of stock $Cu(SO_4)\cdot 5H_2O$ in H_2O solution (5.5mg, 0.0222mmol, (25mol% per alkyne)) were added to the reaction mixture. The reaction mixture was left to stir overnight and then diluted with 10mL DCM and 10mL H_2O. The organic layer was isolated and washed with 2x5mL H_2O before the organic solvent was removed under reduced pressure resulting in a light brown crude solid. The solid was purified using preparative thin layer chromatography (5% MeOH in $CHCl_3$ as eluent) followed by recrystallization (chloroform/methanol layering) resulting in **4.5** as white solid in 88% yield. ^{1}H NMR (500 MHz, $CDCl_3$) δ 8.36 (d, *J* = 7.9Hz, 2H, B), 8.03 (m, 3H, A+C), 7.58–7.48 (m, 56H, W+Y+D+E+F), 7.46-7.40 (m, 26H, V+O), 7.30 (d, *J* = 8.5Hz, 24H, X), 7.21 (d, *J* = 8.9Hz, 8H, U), 7.03 (d, *J* = 8.9Hz, 4H, G), 6.81 (d, *J* = 8.8Hz, 8H, T), 6.54 (s, 2H, J), 6.35 (d, *J* = 2.0Hz, 4H, I), 4.96 (s, 4H), 4.80 (q, *J* = 7.1Hz, 4H, 1), 4.49 (t, *J* = 5.0Hz, 8H, K), 4.10–4.04 (m, 8H, S), 3.95–3.87 (m, 16H, R+Q), 3.81–3.75 (m, 8H, P), 2.74 (t, *J* = 7.1Hz, 8H, N), 1.86–1.74 (m, 16H, L+M), 1.37 (t, *J* = 7.2 Hz, 6H, 2), 1.34 (s, 108H, Z). ^{13}C NMR (126 MHz, $CDCl_3$) δ 160.52, 158.22, 156.72, 150.47, 150.29, 150.10, 149.80, 147.88, 145.86, 143.65, 139.55, 139.42, 138.51, 138.22, 137.75, 136.31, 135.28, 134.61, 132.40, 131.54, 128.50, 126.69, 126.05, 125.81, 123.32, 122.08, 118.23, 115.37, 113.51, 110.45, 105.78, 100.83, 77.26, 70.20, 69.92, 67.70, 67.26, 63.77, 50.23, 40.06, 34.64, 31.49, 29.84, 28.86, 26.10, 25.48, 15.63, MALDI-MS: 4,503.1 ([M]+H^+).

4.6.7 Synthesis of [3]Rotaxane 4.6

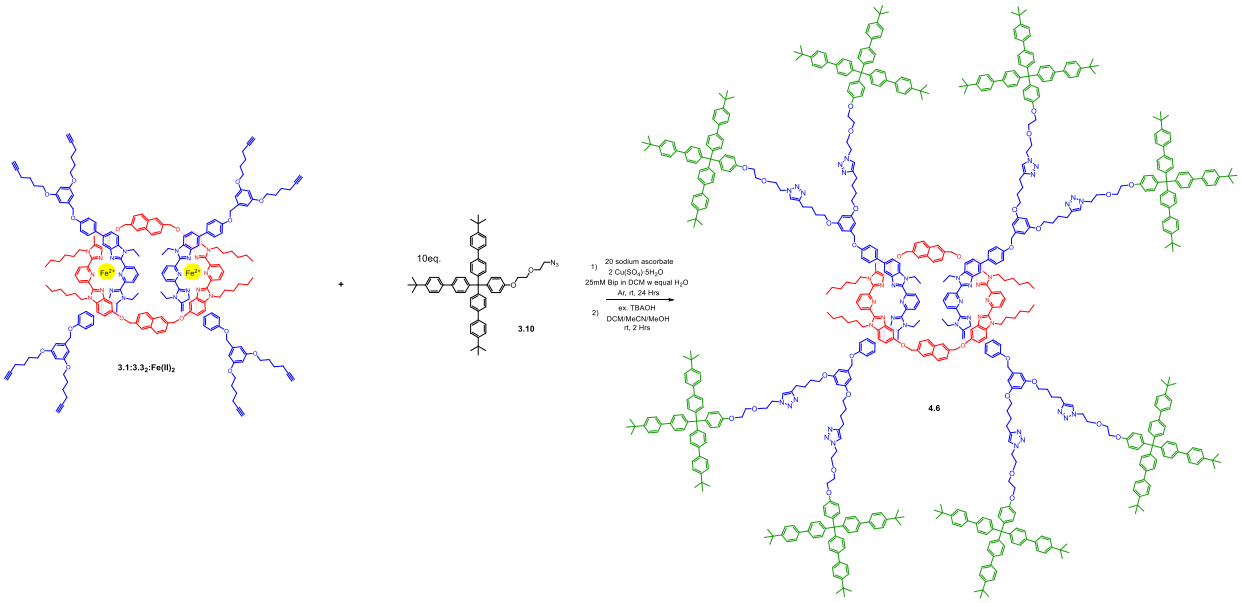

3.1:**3.3**$_2$:Fe(II)$_2$ (15.1mg, 0.0038mmol), **3.10** (32mg, 0.038 mmol) and sodium ascorbate (12.3mg, 0.076mmol) were added to a 4mL glass vial purged with Ar. To this mixture was added CH_2Cl_2 (0.50mL, conc of alkyne = 25 mM), H_2O (0.40mL), and 100µL of an aqueous stock solution of $Cu(SO_4)\cdot 5H_2O$ (76mM, 0.0076mmol, 2eq, (25mol% per alkyne)). The reaction was stirred vigorously for 18 h at RT. After this time the reaction mixture was diluted with CH_2Cl_2 and H_2O (5 mL each). The organic layer was taken and washed with H_2O (2 × 5 mL). Removed organic solvent and redissolved crude purple in 5mL of 50:50 dichloromethane and acetonitrile and stirred slowly at room temperature. 1mL of tetrabutylammonium hydroxide solution (1M in MeOH) was added dropwise to the stirring solution resulting in a rapid color change from purple to light brown and precipitation of the demetallated product. After 15 minutes of stirring, the off-white solid was filtered off and washed with methanol (2x 10mL). The frit was then washed with 5mL of $CHCl_3$ to redissolve the demetallated product and washed once with 5mL water. Solvent was removed under reduced pressure resulting in an off-white residue. Purification of **4.6** was achieved using

preparative thin layer chromatography (SiO_2, eluent = 94:6 $CHCl_3$:MeOH, lowest Rf band taken (R_f=0.15-0.3) as [3]R product, macrocycle byproduct R_f=0.35, dumbbell byproduct R_f=0.70-0.80) followed by precipitation from cold methanol resulting in an off-white solid, **4.6** in 65% isolated yield. ^{1}H NMR (500 MHz, $CDCl_3$, ^{1}H-Assignments in Figure 4.5) δ 7.96 (d, *J* = 7.7Hz, 4H, B), 7.85 (d, *J* = 7.8Hz, 4H, b), 7.73 (s, 8H, C+c), 7.57–7.45 (m, 102H, A+Y+W+D), 7.45 –7.39 (m, 62H, a+E+V+O), 7.30 (m, 52H, X+h), 7.21 (d, *J* = 8.9Hz, 16H, U), 7.18-7.14 (m, 12H, i+F), 6.97 (d, *J* = 8.5Hz, 4H, g), 6.83-6.78 (m, 20H, T+d), 6.73 (d, *J* = 8.9Hz, 4H, e), 6.57 (d, *J* = 8.4Hz, 8H, G), 6.45 (s, 8H, I), 6.34 (s, 4H, J), 5.34 (bs, 8H, h), 4.57 (s, 8H, H), 4.46 (t, *J* = 5.1Hz, 16H, K), 4.31 (bq, 8H, 1), 4.11 (bt, 8H, j), 4.04 (t, *J* = 4.7Hz, 16H, S), 3.93 – 3.82 (m, 32H, R+Q), 3.75 (t, *J* = 4.6Hz, 16H, P), 2.72 (t, *J* = 7.1Hz, 16H, N), 1.79 (m, 32H, L+M), 1.37 (bt, 12H, 2), 1.33 (s, 216H, Z), 0.78 – 0.61 (m, 32H, k+l+m+n), 0.45 (t, *J* = 7.1Hz, 12H, o). MALDI-MS: 10,332.3 ([M]+H^+), 5,832.2 ([M]+H^+-DB(**4.5**)), 4,503.8 ([M]+H^+-MC(**3.1**)-DB(**4.5**)).

4.6.8 Synthesis of Dumbbell Component 4.7

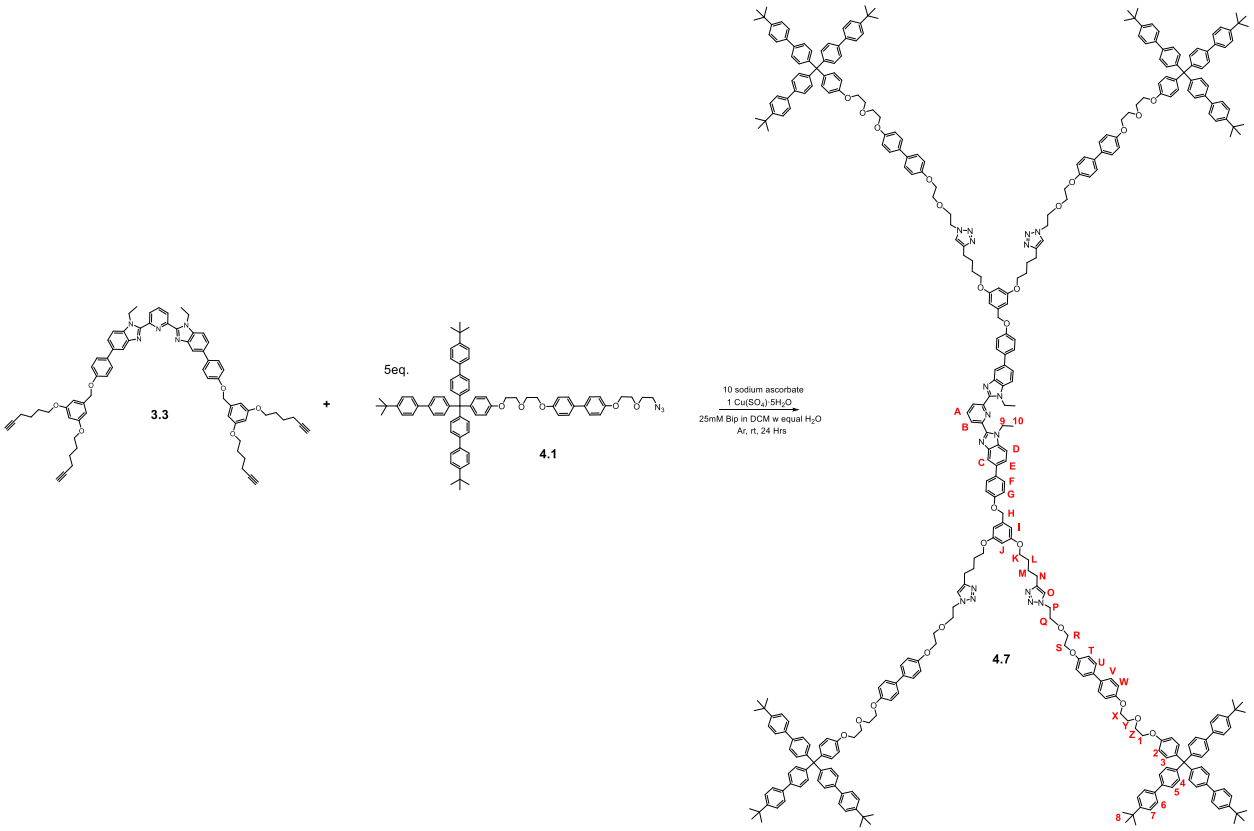

4.1 (33.4mg, 0.03mmol) was added to a 4mL glass vial followed by **3.3** (6.8mg, 0.0060mmol), sodium ascorbate (11.9mg, 0.06mmol), and the reaction chamber was purged with Ar. 250µL DCM (25mM **3**), 150µL H_2O, and finally 100µL of stock $Cu(SO_4)\cdot 5H_2O$ in H_2O solution (1.5mg, 0.006mmol, (25mol% per alkyne)) were added to the reaction mixture. The reaction mixture was left to stir overnight and then diluted with 10mL DCM and 10mL H_2O. The organic layer was isolated and washed with 2x5mL H_2O before the organic solvent was removed under reduced pressure resulting in a light brown crude solid. The solid was purified using preparative thin layer chromatography (5% MeOH in $CHCl_3$ as eluent) followed by recrystallization (chloroform/methanol layering) resulting in **4.7** as white solid in 86% yield. ^{1}H NMR (500 MHz, $CDCl_3$) δ 8.35 (d, *J* = 7.9Hz, 2H,B), 8.04–8.00 (m, 3H, A+C), 7.57 (d, *J* = 8.8Hz, 4H, F), 7.53 (d,

J = 8.5Hz, 24H, 7), 7.50-7.47 (m, 28H, 5+D+E), 7.46 – 7.39 (m, 42H, 4+O+U+V), 7.30 (d, *J* = 8.5Hz, 24H, 6), 7.19 (d, *J* = 8.9Hz, 8H, 3), 7.05 (d, *J* = 8.8Hz, 4H, G), 6.96-6.90 (m, 16H, T+W), 6.84 (d, *J* = 9.0Hz, 8H, 2), 6.56 (bd, *J* = 2.1Hz, 4H, I), 6.36 (bt, 2H, J), 4.99 (s, 4H, H), 4.79 (q, *J* = 6.9Hz, 4H, 9), 4.50 (t, *J* = 5.0Hz, 8H, K), 4.18 – 4.11 (m, 16H, 1+X), 4.10 – 4.06 (m, 8H, S), 3.95 – 3.88 (m, 32H, Y+Z+R+Q), 3.81 – 3.76 (m, 8H, P), 2.75 (t, *J* = 6.9Hz, 8H, N), 1.86 – 1.75 (m, 16H, L+M), 1.37 (t, *J* =7.2 Hz, 6H, 2), 1.34 (s, 108H, 8). MALDI-MS: 5,528.1 ([M]+H^+).

4.6.9 Synthesis of [3]Rotaxane 4.8

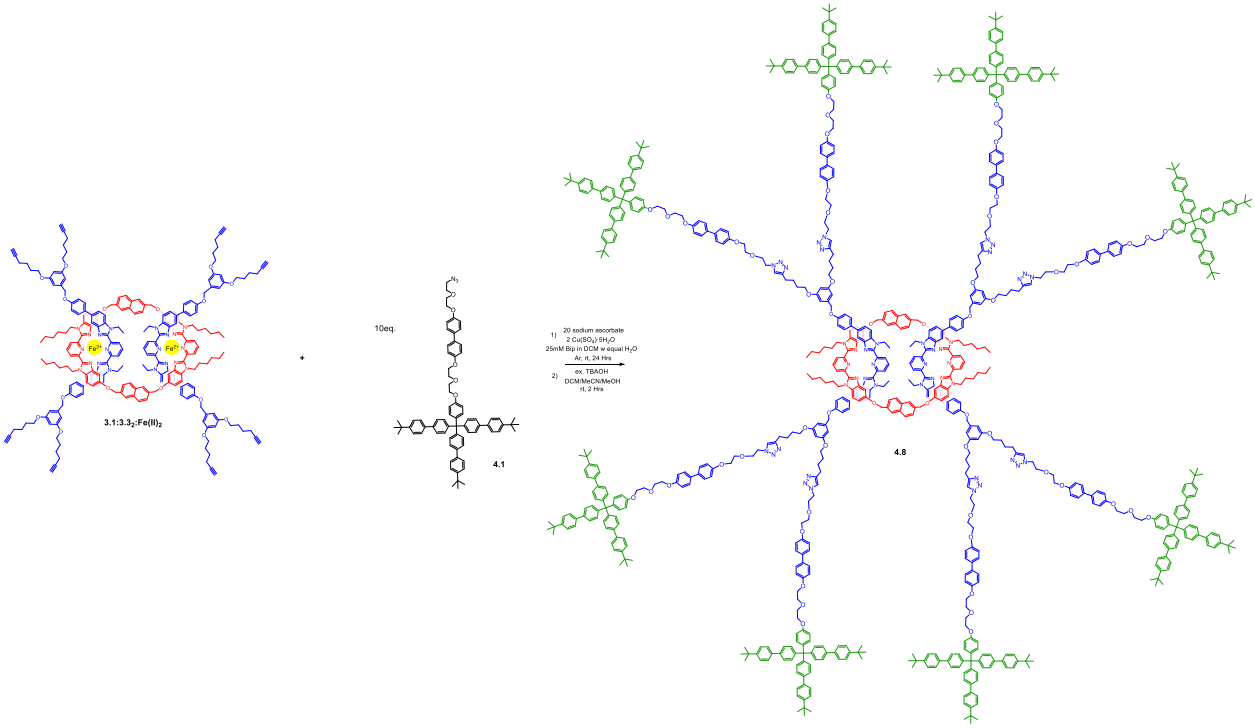

3.1:**3.3**$_2$:Fe(II)$_2$ (17.5mg, 0.0036mmol), **4.1** (40.2mg, 0.036mmol) and sodium ascorbate (14.3mg, 0.072mmol) were added to a 4mL glass vial purged with Ar. To this mixture was added CH_2Cl_2 (0.59mL, conc of alkyne = 25 mM), H_2O (0.49mL), and 100µL of an aqueous stock solution of $Cu(SO_4)\cdot 5H_2O$ (72mM, 0.0072mmol, 2eq, (25mol% per alkyne)). The reaction was stirred vigorously for 18 h at RT. After this time the reaction mixture was diluted with CH_2Cl_2 and H_2O

(5 mL each). The organic layer was taken and washed with H_2O (2 × 5 mL). Removal of the organic solvent resulted in a purple solid that was redissolved in 5mL of 50:50 dichloromethane and acetonitrile and stirred slowly at room temperature. 1mL of tetrabutylammonium hydroxide solution (1M in MeOH) was added dropwise to the stirring solution resulting in a rapid color change from purple to light brown and precipitation of the demetallated product. After 15 minutes of stirring, the off-white solid was filtered off and washed with methanol (2x 10mL). The frit was then washed with 5mL of $CHCl_3$ to redissolve the demetallated product and washed once with 5mL water. Solvent was removed under reduced pressure resulting in an off-white residue. Purification of **4.8** was achieved using preparative thin layer chromatography (SiO_2, eluent = 94:6 $CHCl_3$:MeOH, lowest Rf band taken (R_f=0.15-0.3) as [3]R product, macrocycle byproduct R_f=0.35, dumbbell byproduct R_f=0.70-0.80) followed by precipitation from cold methanol resulting in an off-white solid, **4.8** in 55% isolated yield. ^{1}H NMR (500 MHz, $CDCl_3$, ^{1}H-Assignments in Figure 4.10) δ 7.95 (d, *J* = 7.7Hz, 4H, B), 7.85 (d, *J* = 7.8Hz, 4H, b), 7.73 (s, 8H, C+c), 7.57–7.45 (m, 102H, A+5+7+D), 7.45 –7.39 (m, 94H, a+E+4+O+U+V), 7.30 (m, 52H, 6+h), 7.21 (d, *J* = 8.8Hz, 16H, 3), 7.20-7.16 (m, 12H, i+F), 6.97-6.87 (m, 4H, g+T+W), 6.83-6.79 (m, 20H, 2+d), 6.74 (d, *J* = 9.0Hz, 4H, e), 6.59 (d, *J* = 8.3Hz, 8H, G), 6.47 (s, 8H, I), 6.36 (s, 4H, J), 5.34 (bs, 8H, h), 4.60 (s, 8H, H), 4.47 (t, *J* = 5.1Hz, 16H, K), 4.30 (bq, 8H, 9), 4.15-4.07 (m, 56H, 1+X+S+j), 3.95–3.85 (m, 64H, Y+Z+R+Q), 3.75 (t, *J* = 4.6Hz, 16H, P), 2.74 (t, *J* = 7.1Hz, 16H, N), 1.81 (m, 32H, L+M), 1.37 (bt, 12H, 10), 1.33 (s, 216H, 8), 0.78 – 0.61 (m, 32H, k+l+m+n), 0.45 (t, *J* = 7.1Hz, 12H, o). MALDI-MS: 12,382.4 ([M]+H^+), 6,856.1 ([M]+H^+-DB(**4.7**)), 5,528.4 ([M]+H^+-MC(**3.1**)-DB(**4.7**)).

4.6.10 Kinetic Slippage Experimental Details

The same procedure was done for both [3]rotaxanes. A 1mM sample of fresh [3]rotaxane was prepared in a 5 mm Bruker Shigemi NMR tube. This tube was placed in an oil bath at 35°C and the ^{1}H-NMR spectrum was recorded after 2 days, 4 days, 5 days, and 7 days. The tube was then heated to 40°C and the same ^{1}H-NMR acquisition process was repeated. The tube was then heated to 45°C and the same ^{1}H-NMR acquisition process was repeated. In total, the [3]rotaxane was heated for three weeks. This process was repeated once for both rotaxanes. The resulting kinetic data was analyzed according to the following method. The downfield doublet corresponding to the proton labeled B in the dumbbell of the [3]rotaxane (Fig 4.6) was used to determine the amount of [3]R left in each sample as the shift between free and interlocked species was diagnostic and clean of other peaks. The free B doublet is in the region 8.34-8.38ppm and the interlocked B doublet is in the region 7.96-8.00ppm. Let C_0 be the initial concentration of [3]rotaxane and C be the concentration of [3]rotaxane at timepoint *t*. The absolute integral intensity of B that is interlocked ($I_{3[R]}$) divided by the sum of the absolute integral intensities of B that is free and interlocked (I_{DB} + $I_{3[R]}$) multiplied by 100% gives the percent of [3]R remaining in the sample. Dividing this percent rotaxane remaining by the initial rotaxane percent present is equivalent to C/C_0 for each timepoint of slippage. Following first-order kinetics and standard Eyring/Arrhenius methods the thermodynamic and kinetic parameters were determined. See Fig 4.20-21 for the appropriate Eyring/Arrhenius plots and Fig 4.22 for example of ^{1}H-NMR integrations.

.

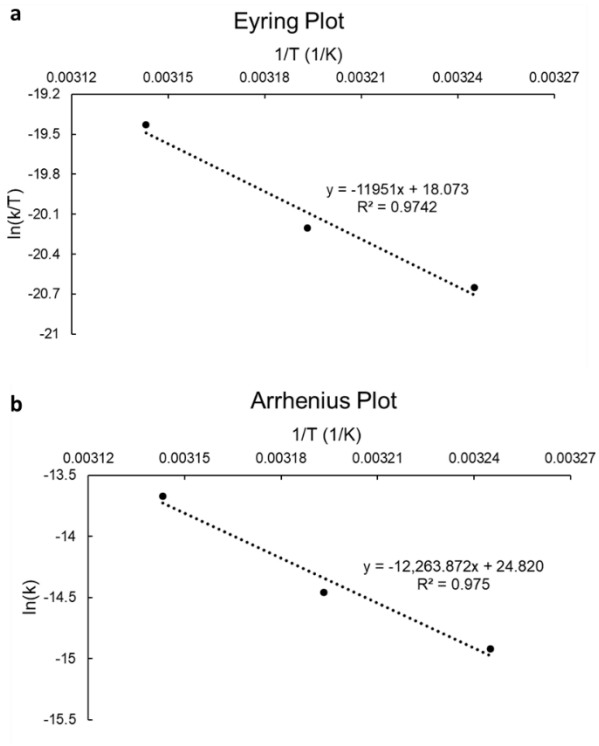

Fig 4.20 a) Eyring and b) Arrhenius plot of the slippage of **4.6**.

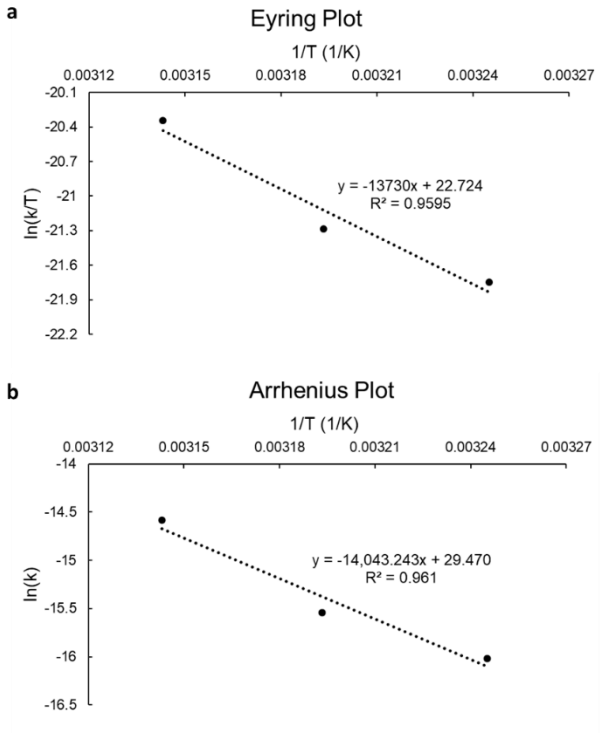

Fig 4.21 a) Eyring and b) Arrhenius plot of the slippage of **4.8**.

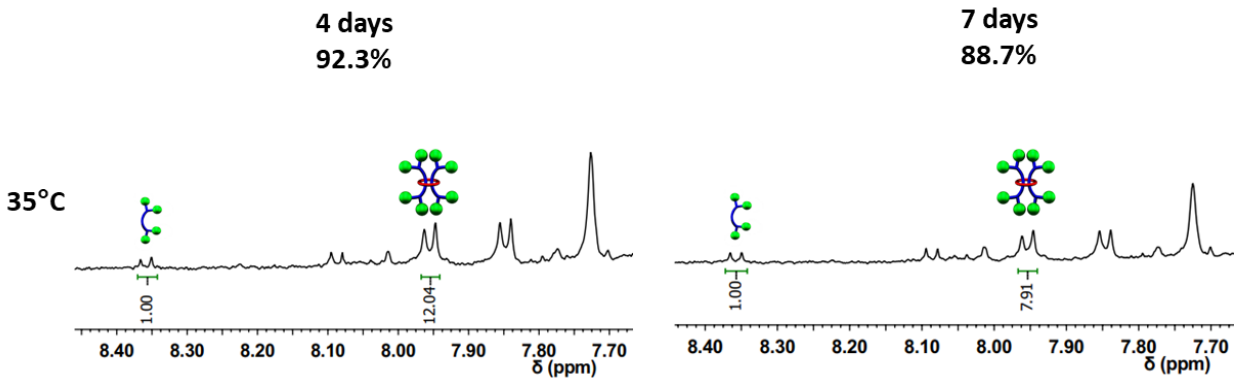

Fig 4.22 Example of ^{1}H-NMR analysis of trial 1 of slippage experiments of **4.6**.

4.7 References

(1) Hertzog, J. E.; Maddi, V. J.; Hart, L. F.; Rawe, B. W.; Rauscher, P. M.; Herbert, K. M.; Bruckner, E. P.; de Pablo, J. J.; Rowan, S. J. Metastable Doubly Threaded [3]Rotaxanes with a Large Macrocycle. *Chem. Sci.* **2022**, 5333–5344. https://doi.org/10.1039/d2sc01486f.

(2) McKenzie, B. M.; Miller, A. K.; Wojtecki, R. J.; Johnson, J. C.; Burke, K. A.; Tzeng, K. A.; Mather, P. T.; Rowan, S. J. Improved Synthesis of Functionalized Mesogenic 2,6-Bisbenzimidazolylpyridine Ligands. *Tetrahedron* **2008**, *64* (36), 8488–8495. https://doi.org/10.1016/j.tet.2008.05.075.

(3) Wu, Q.; Rauscher, P. M.; Lang, X. L.; Wojtecki, R. J.; de Pablo, J. J.; Hore, M. J. A.; Rowan, S. J. Poly[n]Catenanes: Synthesis of Molecular Interlocked Chains. *Science (80-.).* **2017**, *358* (6369), 1434–1439. https://doi.org/10.1126/science.aap7675.

(4) Tranquilli, M. M.; Wu, Q.; Rowan, S. J. Effect of Metallosupramolecular Polymer Concentration on the Synthesis of Poly[n]Catenanes . *Chem. Sci.* **2021**. https://doi.org/10.1039/d1sc02450g.

(5) Wojtecki, R. J.; Wu, Q.; Johnson, J. C.; Ray, D. G.; Korley, L. S. T. J.; Rowan, S. J. Optimizing the Formation of 2,6-Bis(N-Alkyl-Benzimidazolyl)Pyridine-Containing [3]Catenates through Component Design. *Chem. Sci.* **2013**, *4* (12), 4440–4448. https://doi.org/10.1039/c3sc52082j.

(6) Matthews, O. A.; Shipway, A. N.; Stoddart, J. F. Dendrimers - Branching out from Curiosities into New Technologies. *Prog. Polym. Sci.* **1998**, *23* (1), 1–56. https://doi.org/10.1016/S0079-6700(97)00025-7.

(7) Abbasi, E.; Aval, S. F.; Akbarzadeh, A.; Milani, M.; Nasrabadi, H. T.; Joo, S. W.; Hanifehpour, Y.; Nejati-Koshki, K.; Pashaei-Asl, R. Dendrimers: Synthesis, Applications, and Properties. *Nanoscale Res. Lett.* **2014**, *9* (1), 1–10. https://doi.org/10.1186/1556-276X-9-247.

(8) Rauscher, P. M.; Rowan, S. J.; de Pablo, J. J. Topological Effects in Isolated Poly[n]Catenanes: Molecular Dynamics Simulations and Rouse Mode Analysis. *ACS*

Macro Lett. **2018**, *7* (8), 938–943. https://doi.org/10.1021/acsmacrolett.8b00393.

(9) Rauscher, P. M.; Schweizer, K. S.; Rowan, S. J.; de Pablo, J. J. Dynamics of Poly[n]Catenane Melts. *J. Chem. Phys.* **2020**, *152* (21), 214901. https://doi.org/10.1063/5.0007573.

(10) Alexander, W. Theory of AEtherification. *Philisophical Mag.* **1850**, *37* (251), 350–356.

(11) Meldal, M.; Tomøe, C. W. Cu-Catalyzed Azide - Alkyne Cycloaddition. *Chem. Rev.* **2008**, *108* (8), 2952–3015. https://doi.org/10.1021/cr0783479.

(12) Hänni, K. D.; Leigh, D. A. The Application of CuAAC "click" Chemistry to Catenane and Rotaxane Synthesis. *Chem. Soc. Rev.* **2010**, *39* (4), 1240–1251. https://doi.org/10.1039/b901974j.

(13) Prikhod'ko, A. I.; Durola, F.; Sauvage, J. P. Iron(II)-Templated Synthesis of [3]Rotaxanes by Passing Two Threads through the Same Ring. *J. Am. Chem. Soc.* **2008**, *130* (2), 448–449. https://doi.org/10.1021/ja078216p.

(14) Li, Q.; Zhang, L.; Bai, L.; Miao, J.; Cheng, Z.; Zhu, X. Atom Transfer Radical Polymerization. *Prog. Chem.* **2010**, *22* (11), 2079–2088. https://doi.org/10.1002/9783527809080.cataz01278.

(15) Matyjaszewski, K. Atom Transfer Radical Polymerization (ATRP): Current Status and Future Perspectives. *Macromolecules* **2012**, *45* (10), 4015–4039. https://doi.org/10.1021/ma3001719.

(16) Sibi, M. P.; Petrovic, G. Enantioselective Radical Reactions: The Use of Metal Triflimides as Lewis Acids. *Tetrahedron Asymmetry* **2003**, *14* (19), 2879–2882. https://doi.org/10.1016/S0957-4166(03)00543-3.

Chapter 5: Fully Stabilizing The [3]Rotaxane Structure Through Macrocycle Size Variation

* Chapter adapted from: Hertzog, J. E., Liu, G., Rawe, B. W., Hart, L. F., Maddi, V. M., Dolinski, N. D. and Rowan, S. J. "Effect of Macrocycle Size Variation on the Structure of Doubly Threaded [3]Rotaxanes With Big Rings" *In prep.*

5.1 Introduction

Mechanically interlocked molecules (MIMs) are molecules comprised of multiple components that are connected as a result of their topology as opposed to a standard covalent bond.[1] This unusual connectivity has been exploited by scientists over the past few decades resulting in the use of MIMs in a wide range of applications including catalysis,[2,3] drug and gene delivery,[4,5] switchable surfaces,[6,7] molecular machines[8,9] and more.[10,11] Specifically, their use as molecular machines received international acclaim with the awarding of the 2016 Nobel Prize in Chemistry to Sauvage,[12] Feringa,[13] and Stoddart.[14] Key to this wide-ranging application of MIMs is building a thorough understanding of how the individual components interact and are able to move relative to one another, dictating the MIMs function.[15] To this end, the majority of MIMs contain at least one macrocyclic component which is typically key to their structure and function.

Rotaxanes specifically are a class of interlocked molecules comprised of ring and dumbbell components. The most elementary version is a singly threaded [2]rotaxane comprised of one macrocycle component kinetically trapped between the stopper groups of a second dumbbell component.[16,17] Matching the correctly sized ring to stopper group is critical for achieving a stable interlocked molecule.[18–20] The resulting interlocked structure allows for the rotation and translation of the ring along the dumbbell axle which chemists have been able to control using stimuli such

as acid/base,[21,22] heat,[23] light,[24] and more[25] which gives researchers control of the molecular movement of the system.[26] Careful design and chemical consideration must be given to both components in order to ensure a stable rotaxane that can perform useful function. As such, an important design parameter that has emerged in rotaxane synthesis and application is macrocycle size variation.[27–36] Specifically, control over the size of the ring(s) employed in rotaxane structures has allowed researchers to influence their ring mobility,[28] impact their electrochemical properties,[31] use them to develop molecular shuttles,[32] develop means of programmable chemical protection[33] and more. In these studies, relatively small changes (1-2 atoms) in macrocycle size results in a dramatic effect in the resulting rotaxane function.

The rotaxanes discussed above are all based on a simple singly threaded [2]rotaxane motif. As the rotaxane field continues to progress, there is a growing interest in looking towards higher order rotaxanes[37] such as multiply threaded[38] ones in addition to their corresponding mechanically interlocked polymers (MIPs)[39,40] in order to achieve more complicated function and amplify the molecular motions of rotaxanes into bulk materials. However, the synthesis of doubly threaded [3]rotaxanes remains a challenging task.[38] In addition, the effect of macrocycle size variation has been far less explored in doubly threaded systems, but initial experiments have shown that 1-2 atom size changes can slightly alter the yield of doubly threaded [3]rotaxane obtained.[41–43]

The synthesis and characterization of a series of metastable doubly threaded [3]rotaxanes that vary in stopper group size with one of the largest macrocycles reported to date (46 atoms) in rotaxane synthesis has been reported recently.[44] By changing the stopper group size through varying the number of tris(p-t-butylbiphenyl)methyl moieties it was possible to tune the interlocked stability of the [3]rotaxane with a resultant half-life in deuterated chloroform from <1 minute to *ca*. 6 months at room temperature. As macrocycle size variation has emerged as an

important design parameter in rotaxane synthesis, it was then envisioned that this ditopic 2,6-bis(N-alkyl-benzimidazolyl)pyridine[45] (Bip) framework[44] should allow synthetic access to a systematic study on how ring size affects doubly threaded [3]rotaxane structure (Figure 1a-c). Specifically, five different macrocycles in the large size window of 40-48 atoms were synthesized and tested for their ability to form doubly threaded [3]rotaxanes (Fig 1d). Overall, a large size

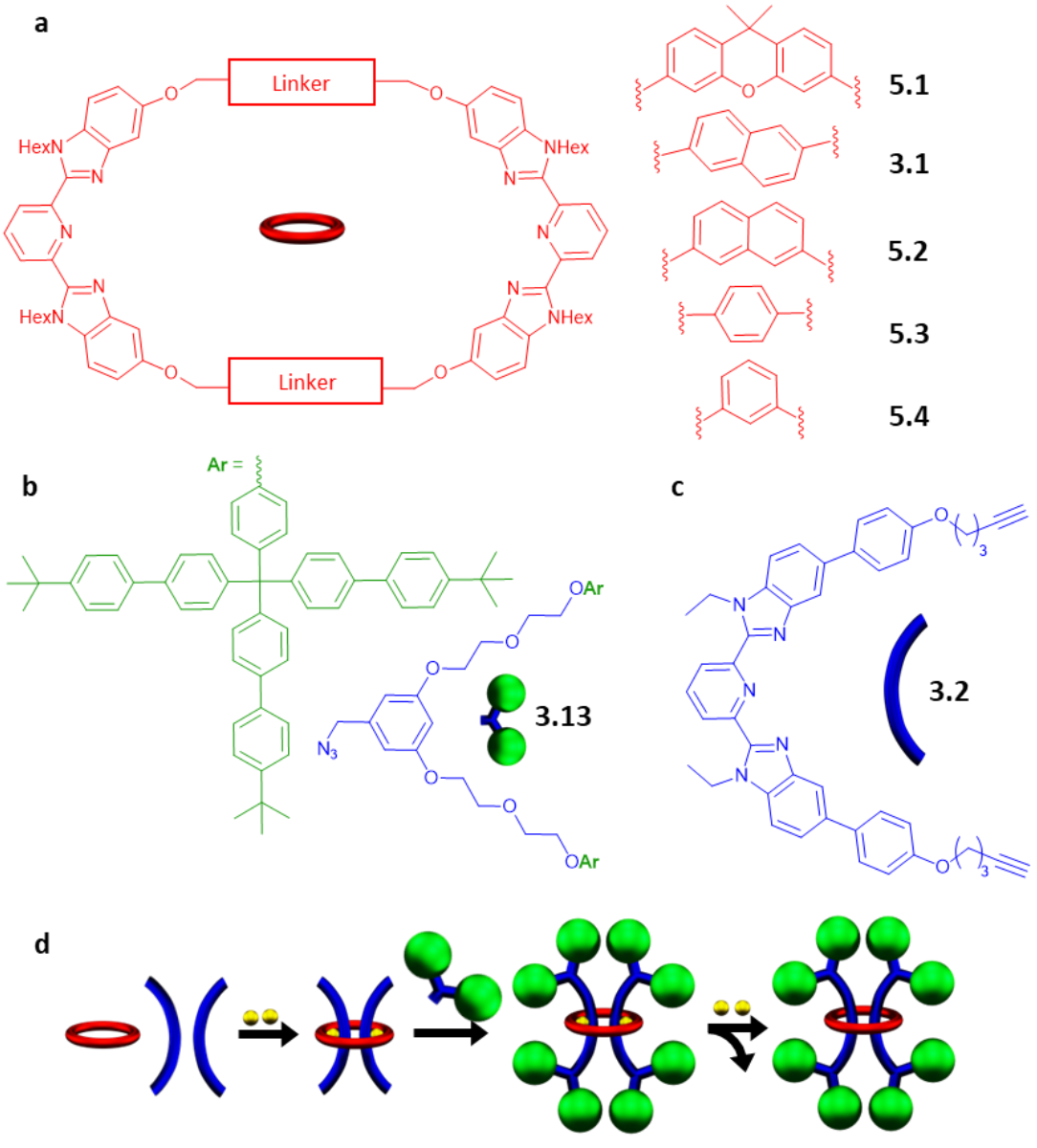

Fig 5.1 Chemical structure of a) rings, b) stopper group, and c) thread used in this chapter. d) Scheme of the proposed three-step doubly threaded [3]rotaxane synthesis.

range for successful [3]rotaxane formation was established and a dramatic effect of macrocycle size variation on the rotaxane structure was seen via kinetic stability tests, ^{1}H–^{1}H NOESY ^{1}H-NMR measurements, and steady-state and time-resolved fluorescence experiments which will be detailed in this work.

5.2 Component Synthesis

To conduct the proposed study, four new ring components **5.1**-**5.4** were synthesized and fully characterized (Fig 5.2, See Experimental for full details and characterization).

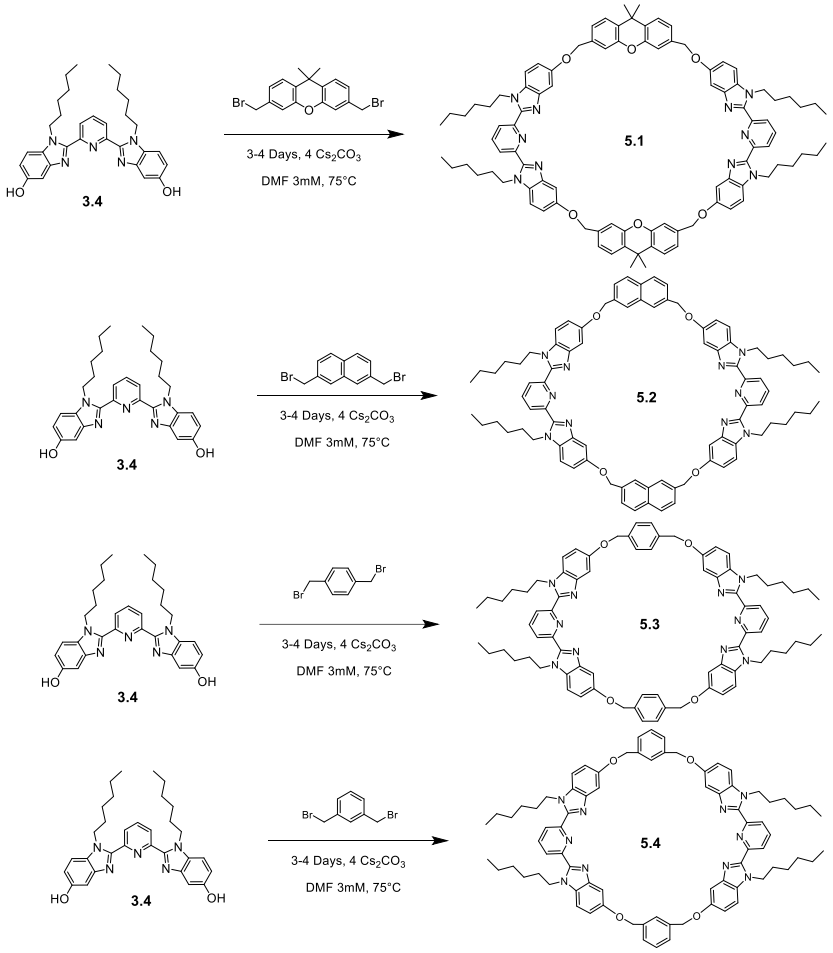

Fig 5.2 Scheme summarizing synthesis of four new macrocycle components for this chapter.

A dilute ring closing reaction using standard Williamson Ether conditions was used to synthesize the four rings. One important observation is that the isolated yields of ditopic ring decrease sharply

with smaller ring sizes. Specifically, the three 48-44 atom rings all have a yield of about ~20% which is reasonable given the relatively uncontrolled reaction employed. The 42-atom ring **5.3** decreases to 11% and the 40-atom ring **5.4** is only a 5% yield. These observations suggest that more targeted syntheses may be necessary to scale up future procedures with these macrocycles.

5.3 Establishing Ring Size Ceiling

One initial question before reducing the size of the ring was whether a larger ring than 46 atoms could be accessed in a metastable [3]rotaxane using the developed Bip framework. Thus, the 48-atom ring **5.1** was first explored. The rigidity present from the xanthene linker in the macrocycle was designed to prevent self-binding of both Bip ligands in the macrocycle to a single metal. This was confirmed by a UV metal titration of **5.1** which shows visible absorption changes upon metal addition at 378nm until 2 metal equivalents (relative to **5.1**) are reached (Fig 5.3).

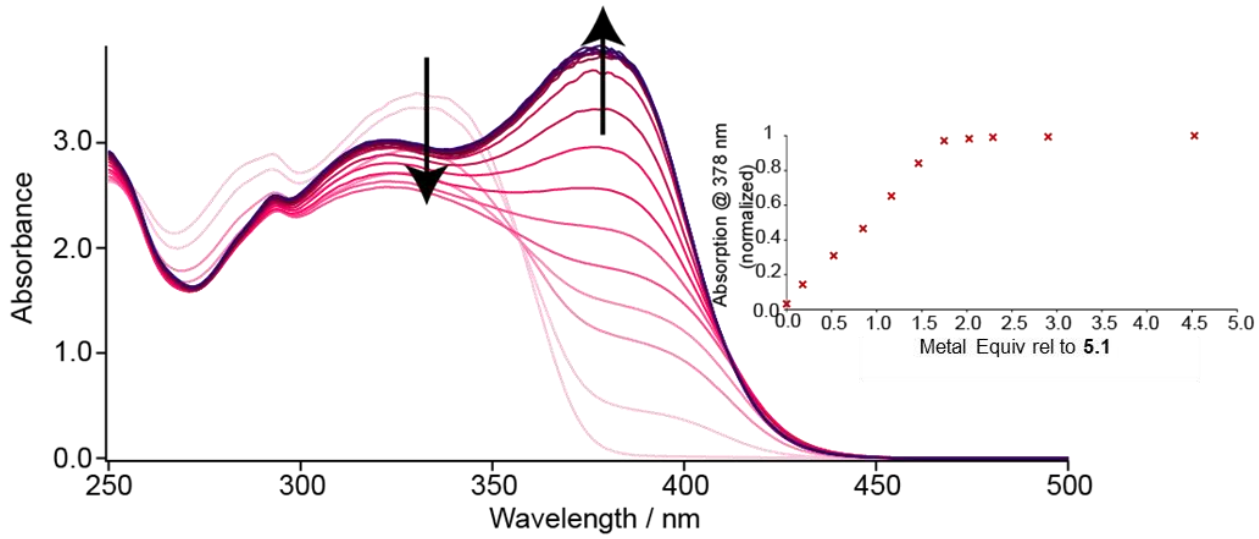

Fig 5.3 UV/Vis titration of **5.1** with Zn(II), inset shows absorbance at 378nm.

Further metal addition results in negligible absorption increase. Once the proper metal-binding capabilities of **5.1** were confirmed, then the doubly threaded pseudo[3]rotaxane **5.1:3.2$_2$:**Fe(II)$_2$ was targeted based on similar metal-templating procedures described in the last two chapters (Fig 5.4, see Experimental for full details on assembly procedures).

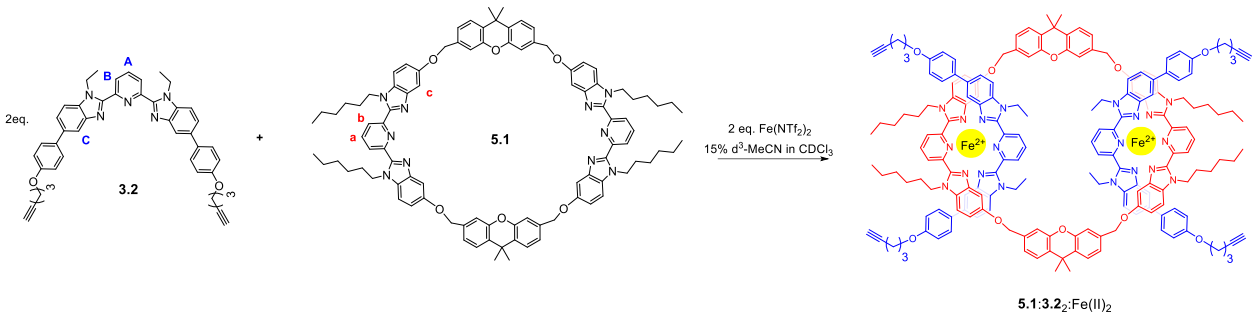

Fig 5.4 Scheme showing formation of **5.1:3.2**$_2$**:**Fe(II)$_2$ from its components**.**

Tracking the metal addition and equilibration process via ^{1}H-NMR spectroscopy reveals similar diagnostic downfield shifting of the pyridinyl Bip protons (Fig 5.5) confirming the successful formation of **5.1:3.2**$_2$**:**Fe(II)$_2$.

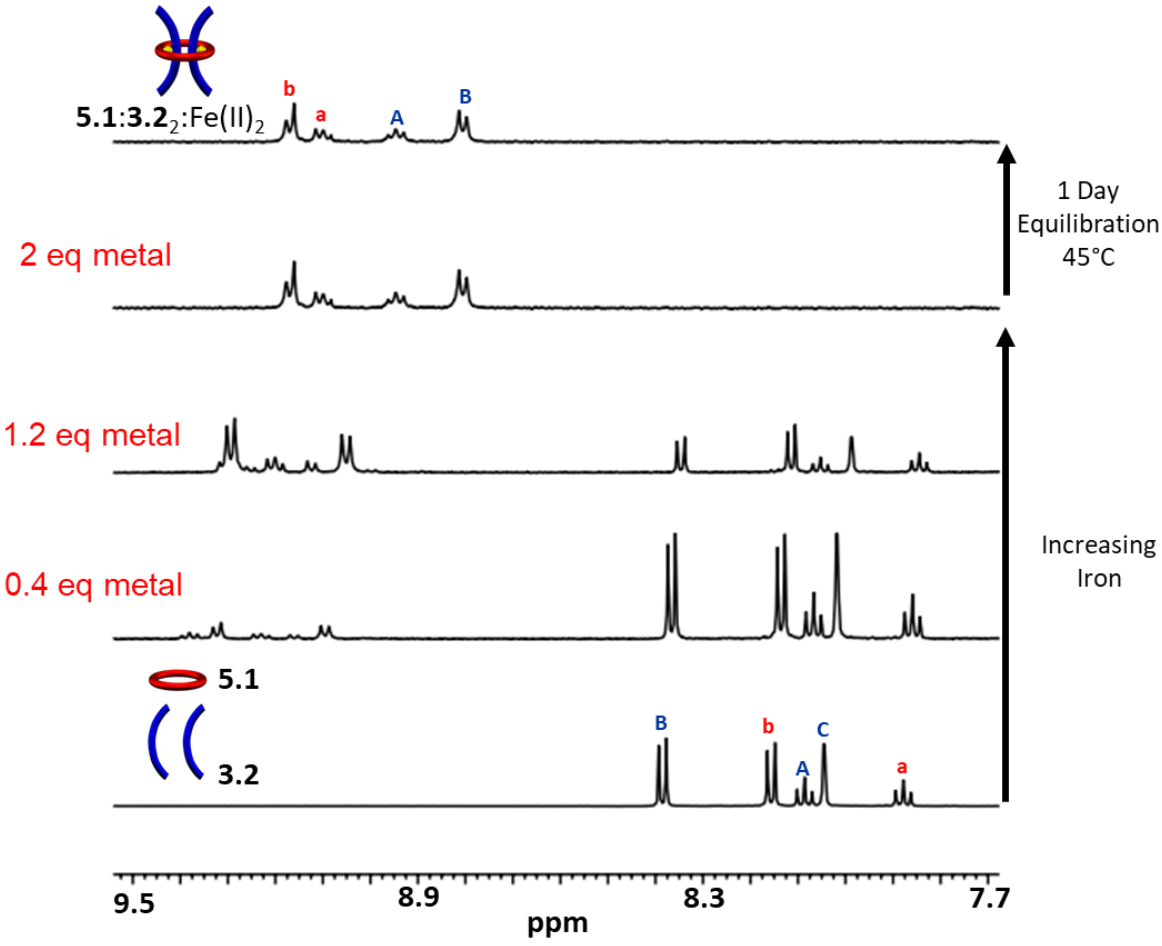

Fig 5.5 Partial ^{1}H-NMR overlay (500 MHz, 25°C, Solvent: 0, 3, 9, 15, 15% d_3-MeCN in $CDCl_3$ increasing upwards) of Fe(II) addition and 1 day equil. ^{1}H assignments in Fig 5.4.

Next, a similar stoppering and demetallation procedure to that described in the past two chapters was used to target the doubly threaded [3]rotaxane **5.5** (Fig 5.6).

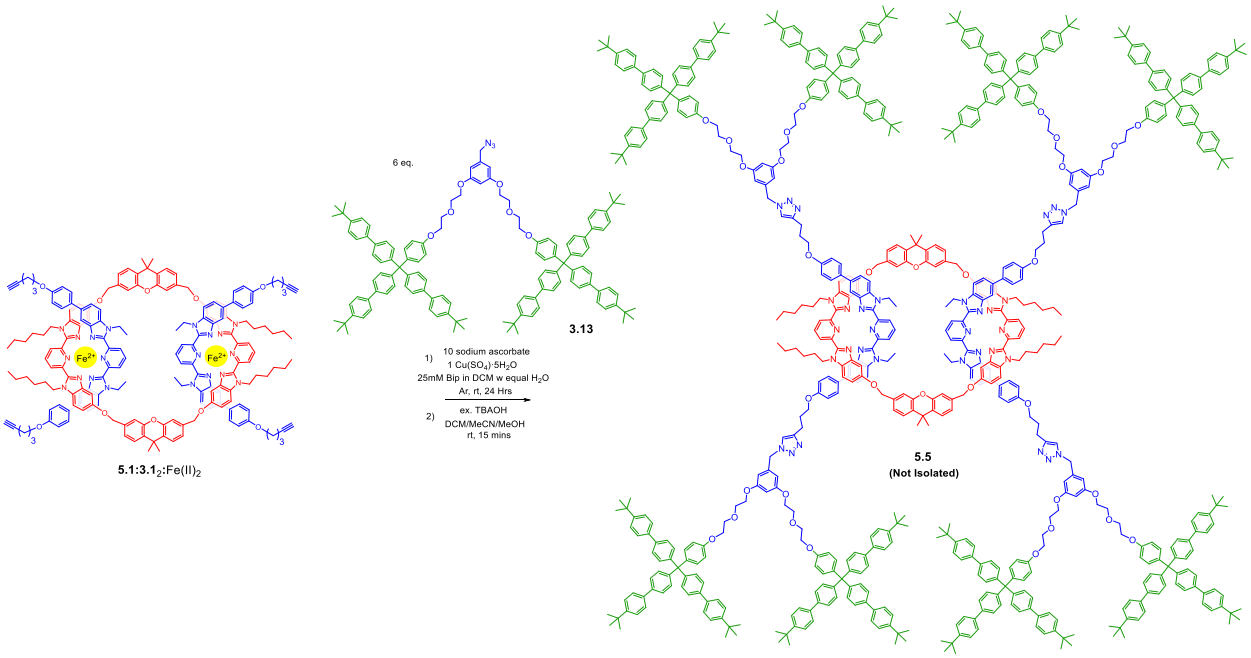

Fig 5.6 Scheme showing proposed synthesis of doubly threaded [3]rotaxane **5.5.**

Upon demetallation, the crude product was analysed immediately via ^{1}H-NMR spectroscopy and MALDI-TOF mass spectrometry. This initial analysis revealed only the free dumbbell **3.16** and macrocycle **5.1** in the crude analysis of **5.5** (Fig 5.7 and 5.8).

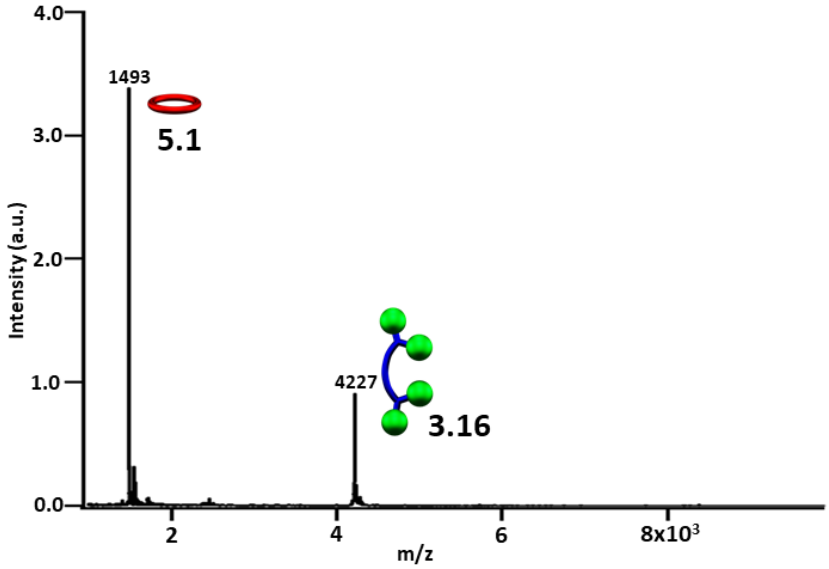

Fig 5.7 MALDI-TOF analysis (Dithranol, no salt) of the of the crude attempt of **5.5.**

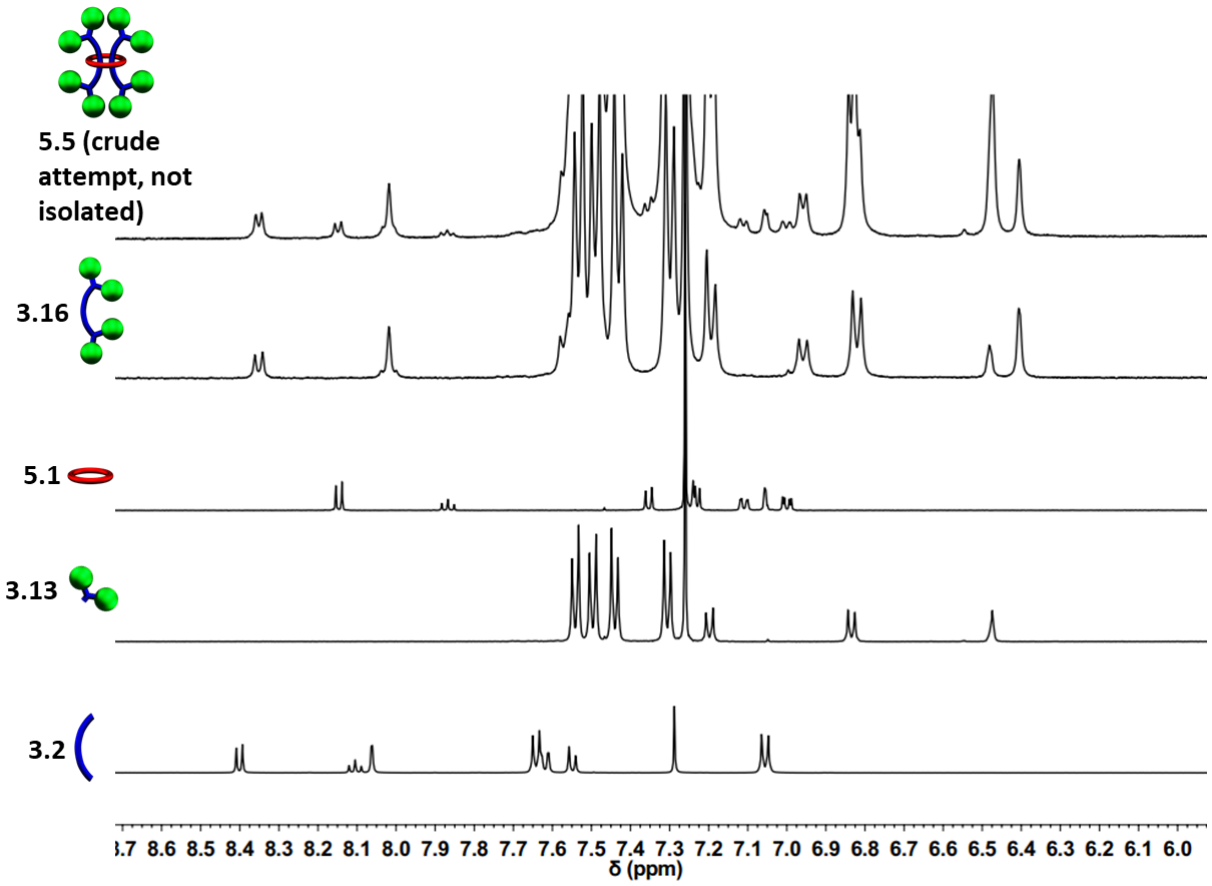

Fig 5.8 Partial ^{1}H-NMR overlay (500 MHz, 25°C, $CDCl_3$) of the demetallated crude reaction mixture from the stoppering of **5.1**:**3.2**$_2$:Fe(II)$_2$ with **3.13** compared to starting materials and free components.

Further attempts to repeat or optimize the synthesis of **5.5** were all met with the same result suggesting that the larger ring size of **5.1** (48 atoms) is too large for the stopper group **3.13** to successfully stabilize the [3]rotaxane on any appreciable timescale (Fig 5.9).

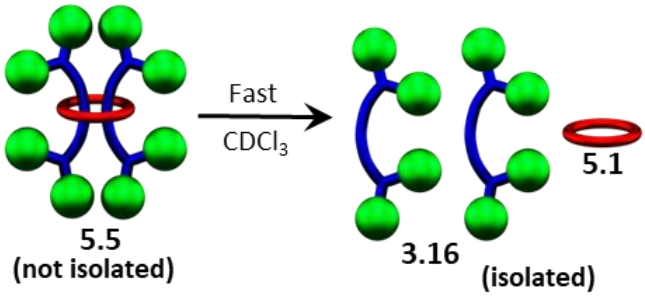

Fig 5.9 Cartoon scheme depicting the rapid dethreading of **5.5** hypothesized

This relatively abrupt cutoff between no isolatable doubly threaded [3]rotaxane product using a 48 atom ring and a relatively long-lived metastable [3]rotaxane species with a 46 atom ring[44] is consistent with other reported multiply threaded systems[41,46] and seems reasonable given the substantially larger sizes of rings being considered in this study relative to the majority of macrocycles in rotaxane literature.

5.4 [3]Rotaxane Results With a 44 and 42 Atom Ring

With the first two ring sizes (48 and 46 atoms) well understood, efforts were then turned to the two smaller rings **5.2** (44 atoms) and **5.3** (42 atoms, see Fig 5.2). Both macrocycles were designed using a rigid linker between the Bips, and a UV metal titration was conducted on both to confirm that no self-binding to a single metal ion occurs upon metal addition (Fig 5.10a-b).

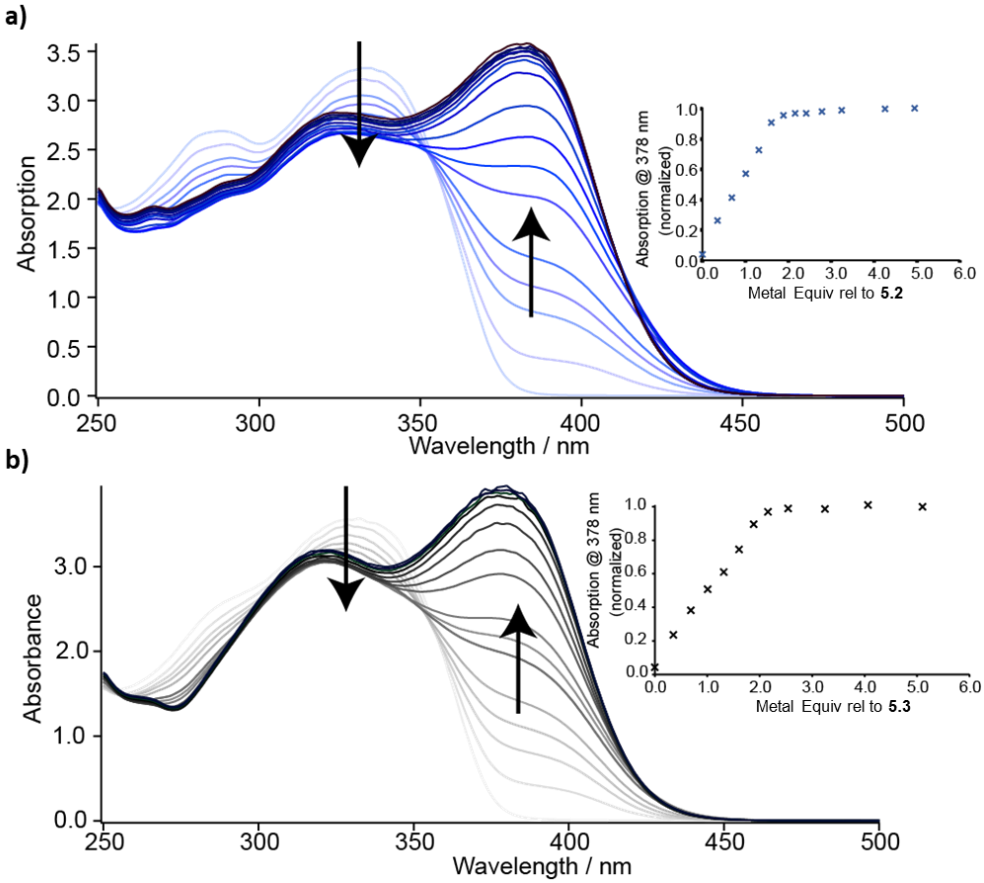

Fig 5.10 UV/Vis titration of a) **5.2** and b) **5.3** with Zn(II), insets shows absorbance at 378nm.

Next, the pseudo[3]rotaxanes **5.2:3.2$_2$:**Fe(II)$_2$ and **5.3:3.2$_2$:**Fe(II)$_2$ were targeted based on similar metal-templating procedures described in the last two chapters and similar diagnostic downfield shifting of the pyridinyl Bip protons were seen via ^{1}H-NMR spectroscopy (Fig 5.11 and 5.12, see Experimental for full details on assembly procedures).

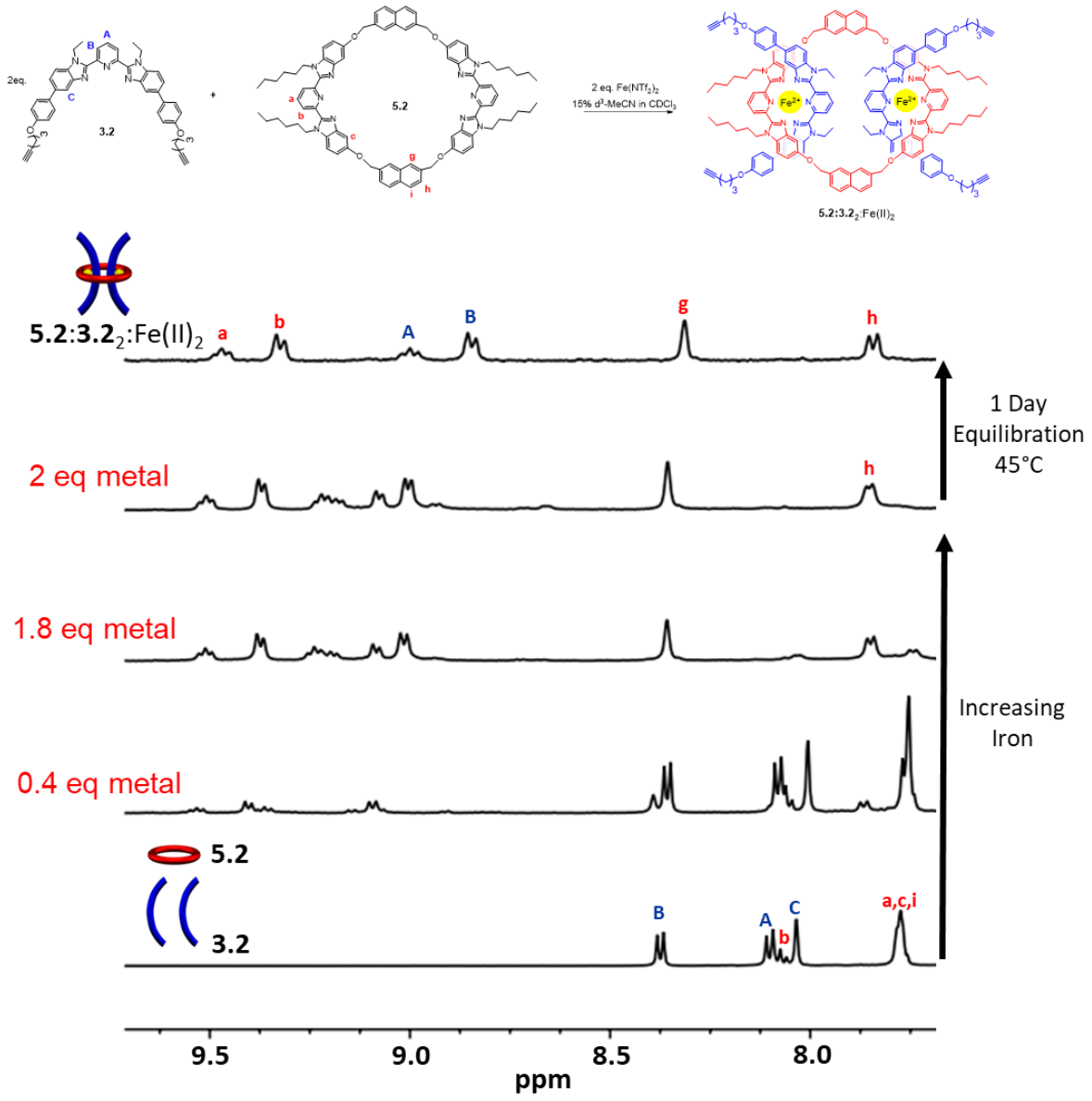

Fig 5.11 Partial ^{1}H-NMR overlay (500 MHz, 25°C, Solvent: 0, 3, 13.5, 15, 15% d_3-MeCN in $CDCl_3$ increasing upwards) of Fe(II) addition and 1 day equilibration. ^{1}H assignments at top of figure in scheme depicting assembly of **5.2:3.2$_2$:**Fe(II)$_2$.

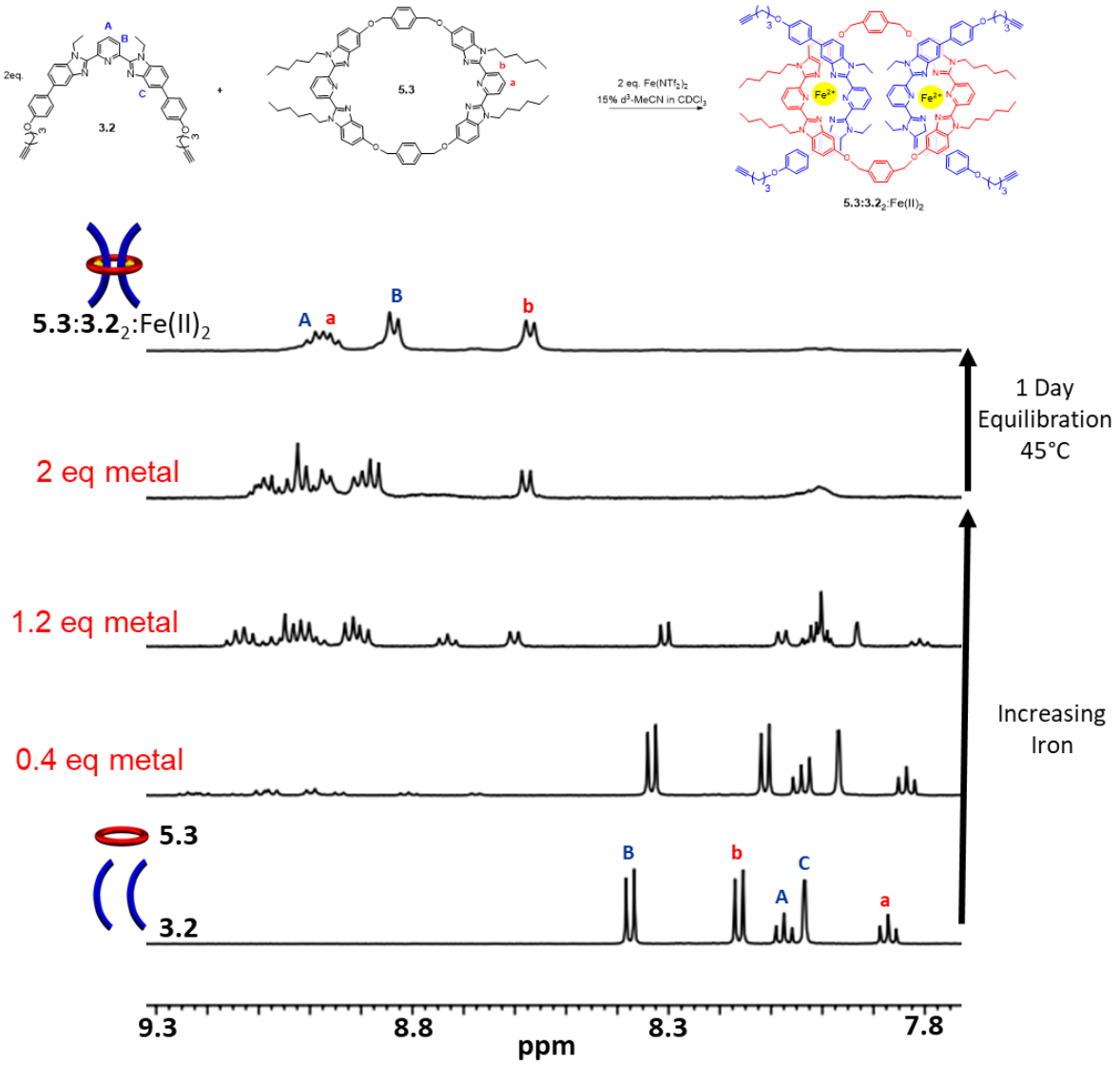

Fig 5.12 Partial ^{1}H-NMR overlay (500 MHz, 25°C, Solvent: 0, 3, 9, 15, 15% d_3-MeCN in $CDCl_3$ increasing upwards) of Fe(II) addition and 1 day equilibration. ^{1}H assignments at top of figure in scheme depicting assembly of **5.3:3.2**$_2$**:**Fe(II)$_2$.

Once the assembly of the pseudo[3]rotaxanes **5.2:3.2**$_2$**:**Fe(II)$_2$ and **5.3:3.2**$_2$**:**Fe(II)$_2$ was confirmed, both were stoppered and demetallated according to similar conditions described previously to target the [3]rotaxanes **5.6** and **5.7** (Fig 5.13-5.14, see Experimental for full details on stoppering and demetallation procedures).

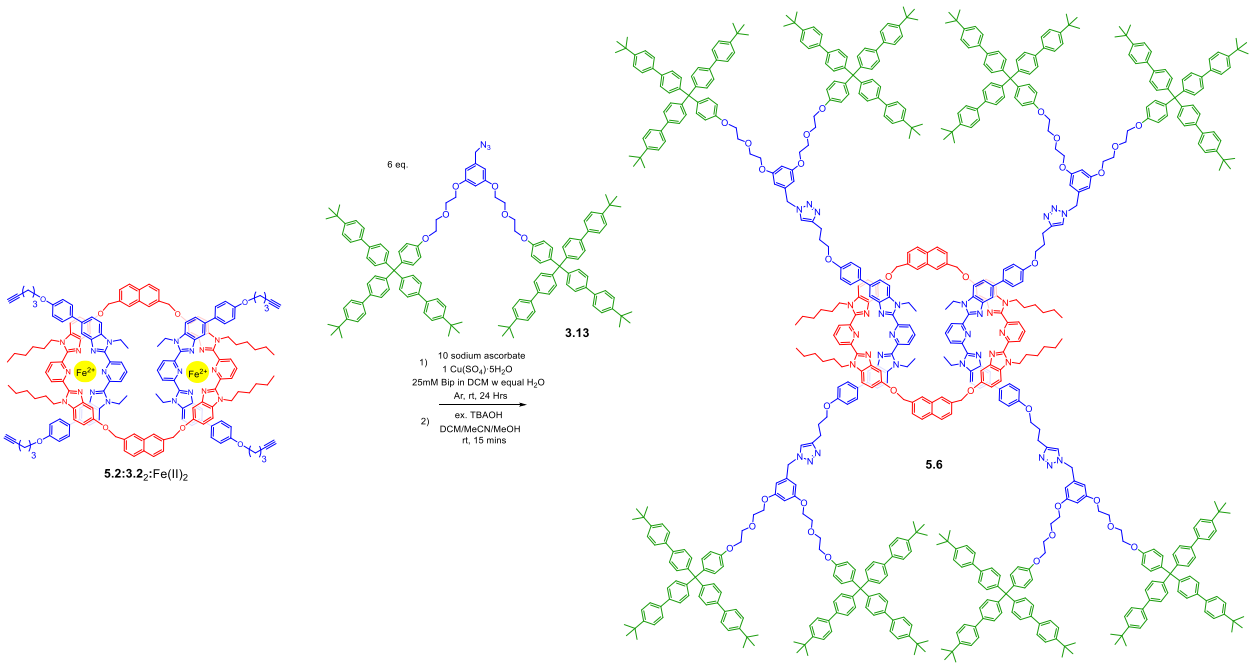

Fig 5.13 Scheme showing synthesis of doubly threaded [3]rotaxane **5.6.**

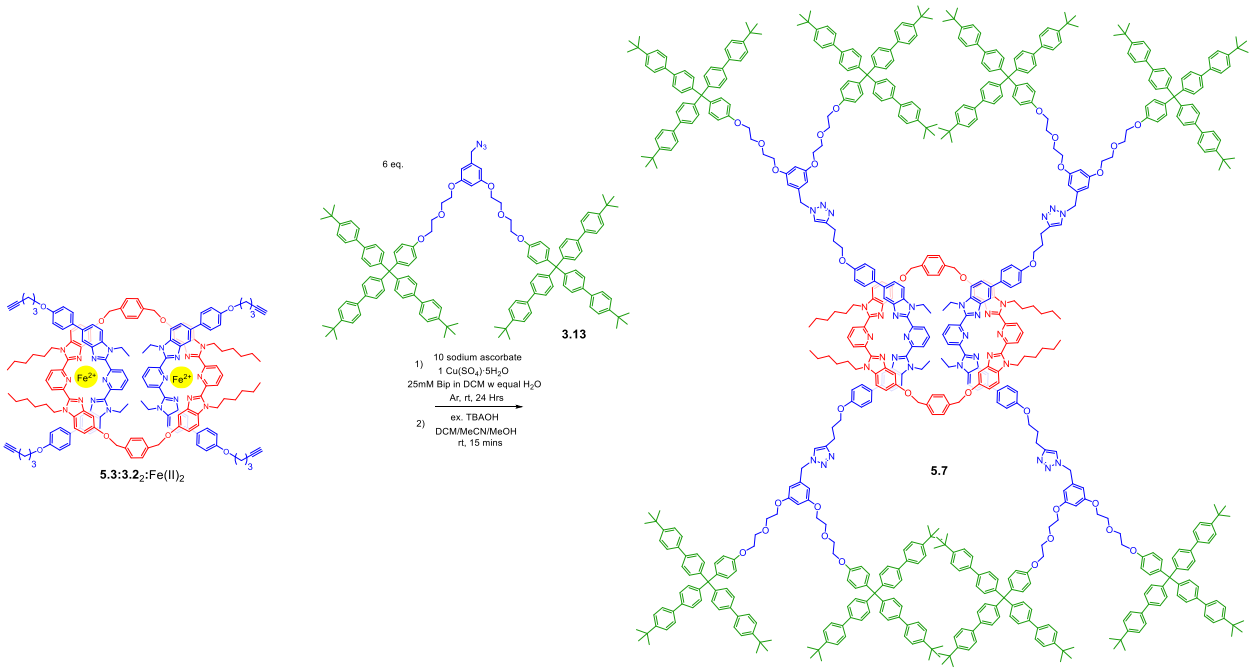

Fig 5.14 Scheme showing synthesis of doubly threaded [3]rotaxane **5.7.**

Both crude [3]rotaxane products were analysed immediately via ^{1}H-NMR spectroscopy upon demetallation. This analysis revealed dominant upfield shifted peaks in the regions consistent with interlocked [3]rotaxane product that have been identified in the past two chapters (See Fig 5.15 a-b, interlocked product boxed in red).

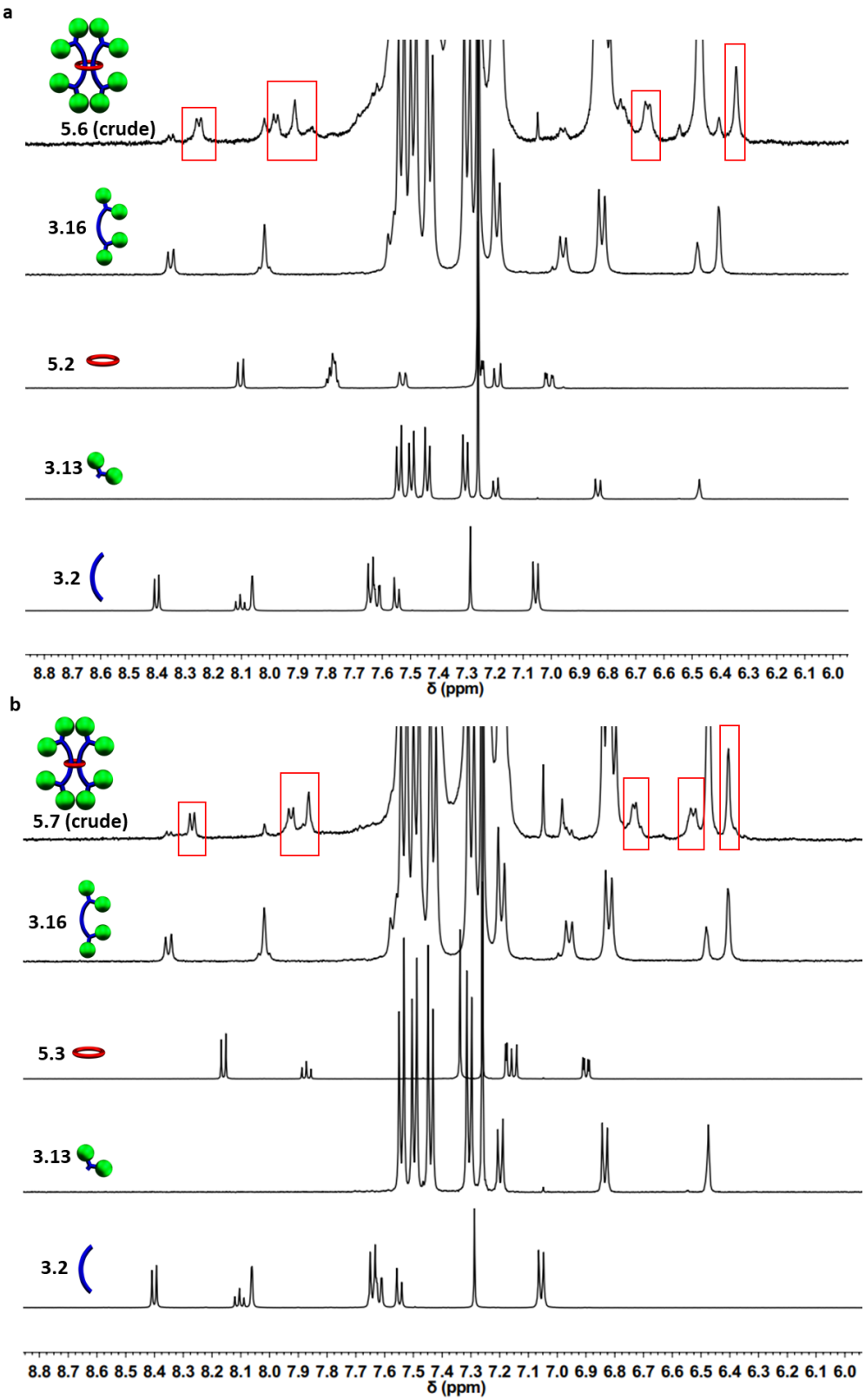

Fig 5.15 Partial ^{1}H-NMR overlay (500 MHz, 25°C, $CDCl_3$) of the demetallated crude reaction mixture of a) **5.6**, and b) **5.7** compared to starting materials and free components. Interlocked product is boxed in red.

In both cases the noninterlocked byproduct was estimated to be ca. 15% via ^{1}H-NMR integration (85% [3]R product). Using preparative thin layer chromatography both [3]rotaxanes **5.6** and **5.7** were isolated in ~ 75% yield consistent with the previously described [3]rotaxane **3.17**. GPC analysis of the purified **5.6** and **5.7** revealed a single monodisperse lower retention time peak relative to each [3]rotaxane's noninterlocked components as expected (Fig 5.16).

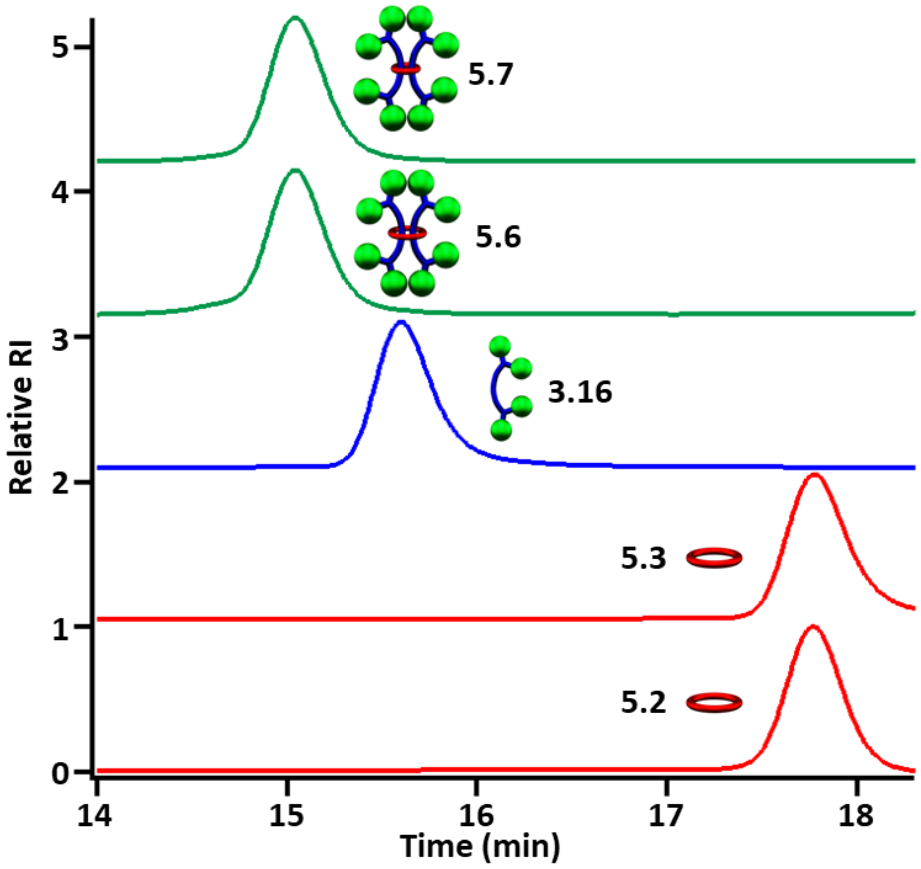

Fig 5.16 GPC chromatogram of (3:1 THF:DMF) purified **5.7**, **5.6**, **3.16**, **5.3**, and **5.2** at 25°C.

To obtain further characterization of the [3]rotaxane structure, MALDI-TOF mass spectrometry was used to confirm the expected fragmentation pattern of the interlocked [3]rotaxane structure as well as the expected isotopic distribution of the high molecular weight [3]rotaxane peak for both [3]rotaxanes (Fig 5.17 a-b, $C_{676}H_{696}N_{32}O_{32}$ for **5.6** and $C_{668}H_{692}N_{32}O_{32}$ for **5.7**).

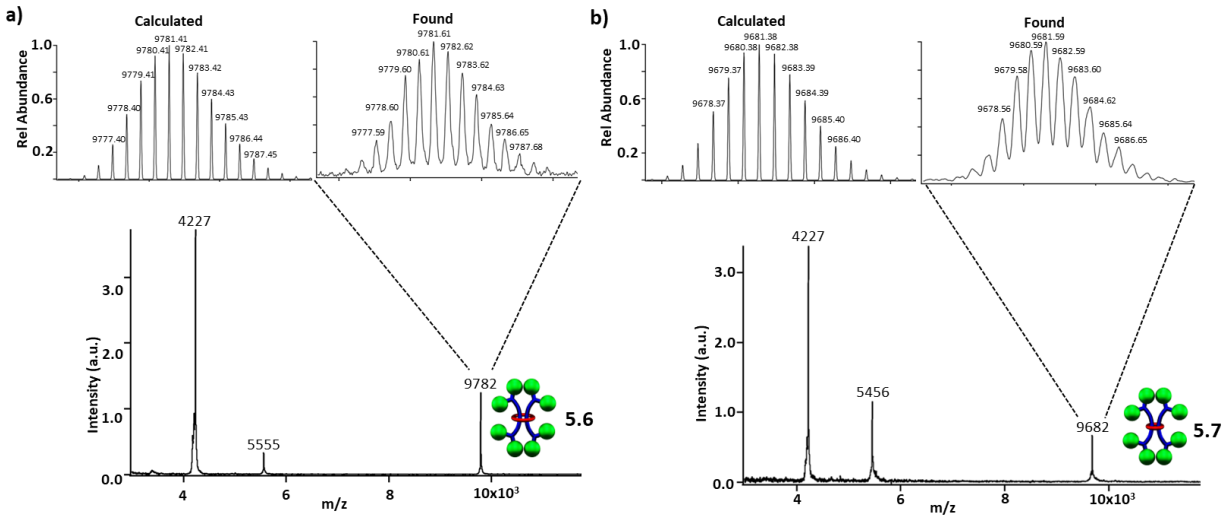

Fig 5.17 a) MALDI-TOF MS of **5.6** with expansion showing isotopic distribution of the 9782 m/z peak ($C_{676}H_{696}N_{32}O_{32}$ (MH^+)) and b) MALDI-TOF MS of **5.7** with expansion showing isotopic distribution of the 9682 m/z peak ($C_{668}H_{692}N_{32}O_{32}$ (MH^+)).

^{1}H-NMR and ^{1}H-^{1}H COSY analysis of both **5.6** and **5.7** combined with comparison to each [3]rotaxane's noninterlocked components and the previously published **3.17**[44] allows the full ^{1}H-NMR spectrum of **5.6** and **5.7** to be assigned (See Fig 5.18-5.19 for the diagnostic aromatic comparison to components and Fig 5.20-5.21 for the full ^{1}H and ^{1}H-^{1}H COSY NMR spectra).

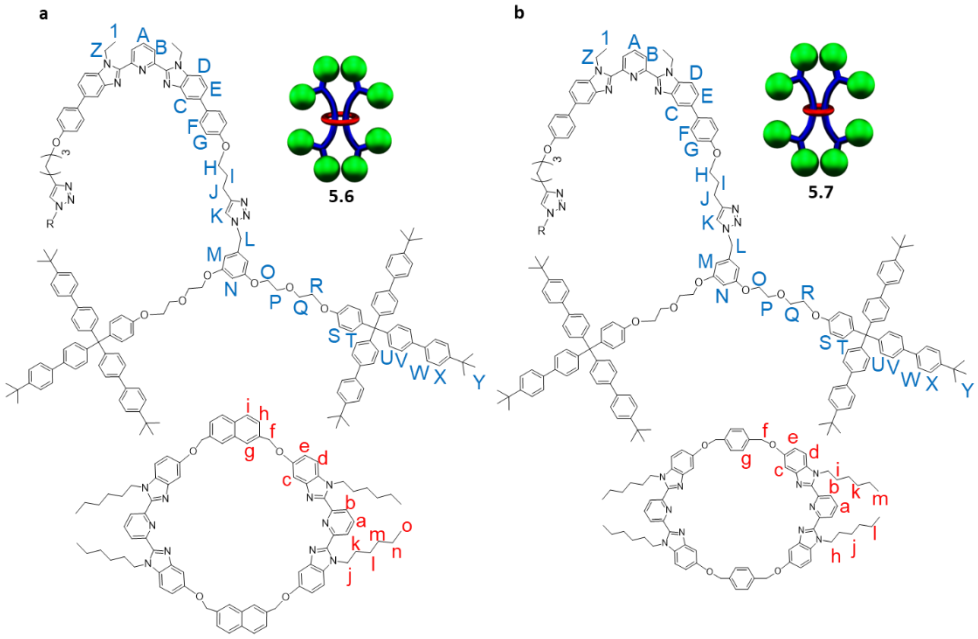

Fig 5.18 ^{1}H-NMR labeling schemes for a) **5.6** and b) **5.7**.

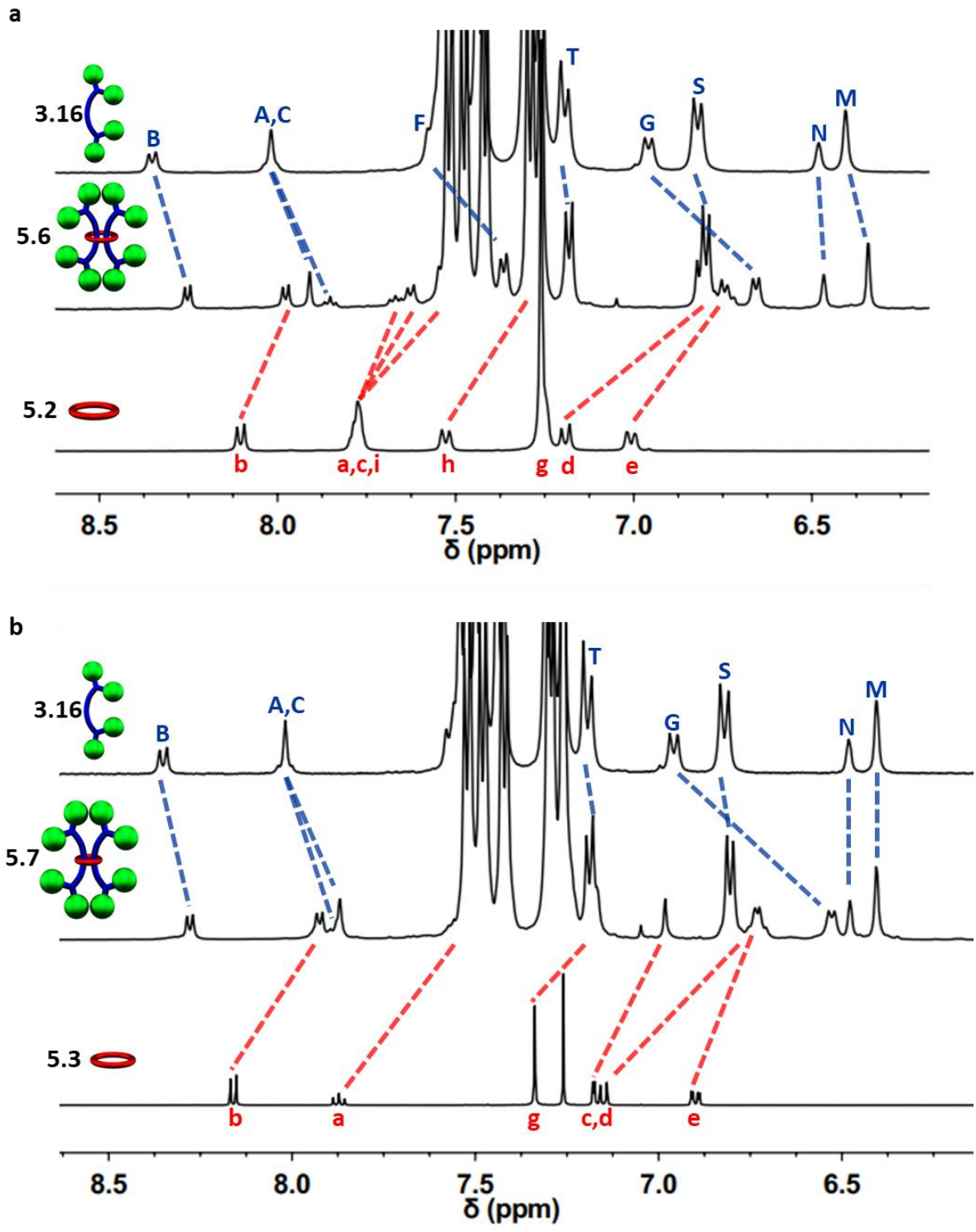

Fig 5.19 a) Partial ^{1}H-NMR overlay (500 MHz, 25°C, $CDCl_3$) of purified **5.6** relative to its components **3.16** and **5.2**, and b) Partial ^{1}H-NMR overlay (500 MHz, 25°C, $CDCl_3$) of purified **5.7** relative to its components **3.16** and **5.3**, all ^{1}H assignments in Fig 5.18.

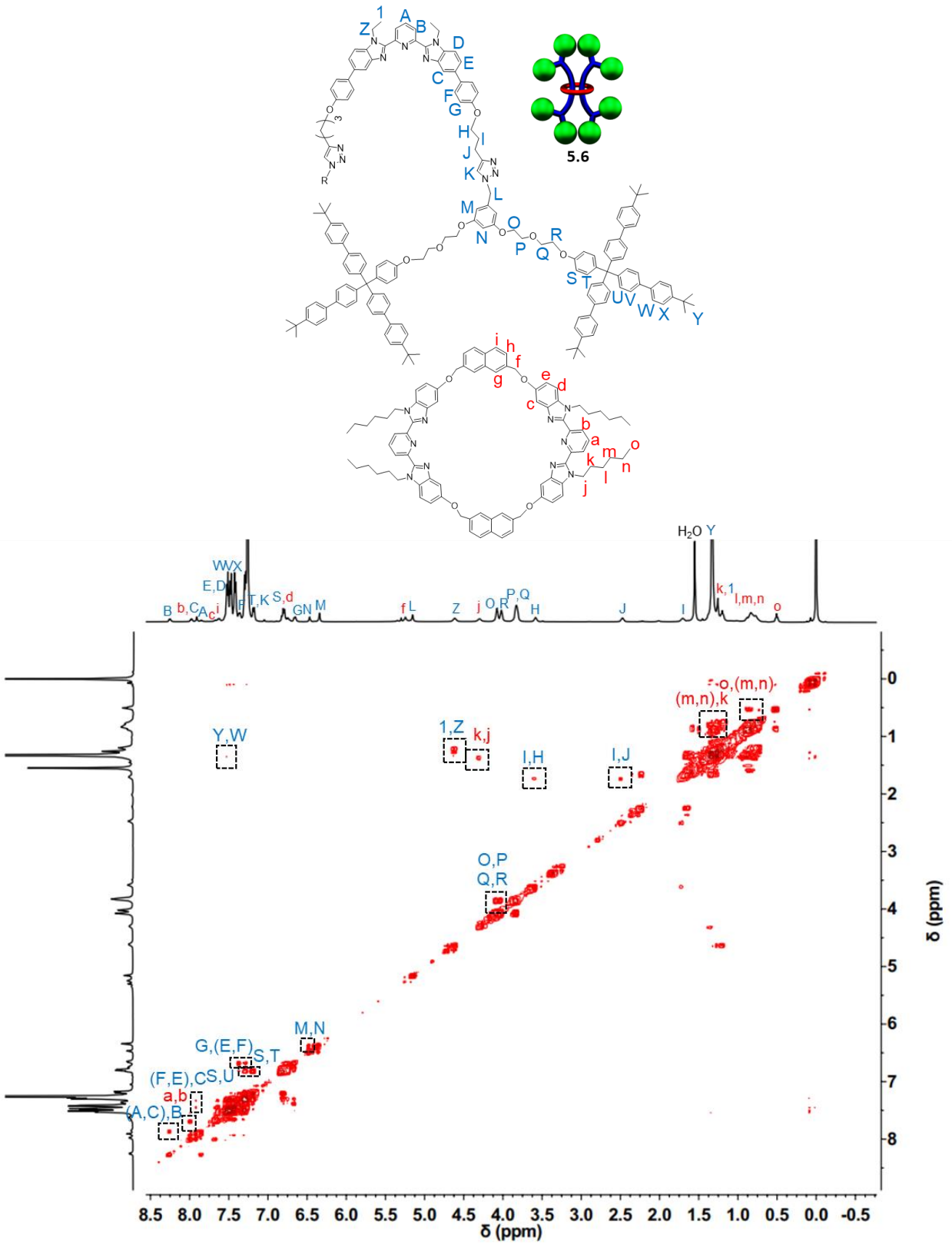

Fig 5.20 Full ^{1}H-^{1}H COSY (5mM, 500 MHz, 25°C, $CDCl_3$) of **5.6**. Select ^{1}H annotations correspond to labels at top of figure.

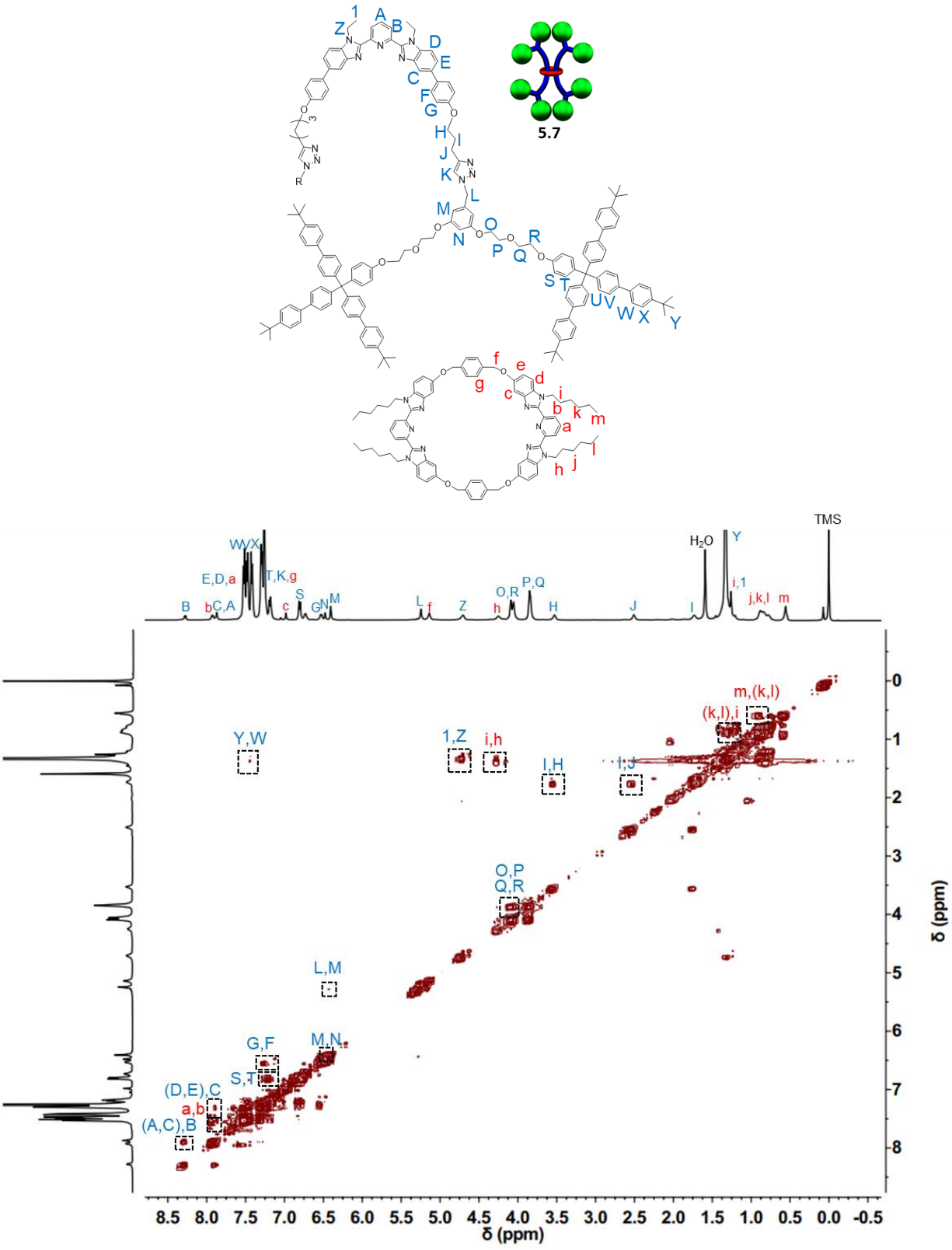

Fig 5.21 Full ^{1}H-^{1}H COSY (5mM, 500 MHz, 25°C, $CDCl_3$) of **5.7**. Select ^{1}H annotations correspond to labels at top of figure.

In both [3]rotaxanes, similar upfield shifting of the aromatic peaks via ^{1}H-NMR is seen upon interlocking relative to their respective noninterlocked components (Fig 5.19). In particular, the farthest downfield shifted aromatic pyridinyl resonances shift accordingly with ring size. As the ring is tightened from 46 atoms in **3.17** to 44 atoms in **5.6** to 42 atoms in **5.7** the labelled A and B peaks shift downfield incrementally while the C singlet shifts upfield (Fig 5.22).

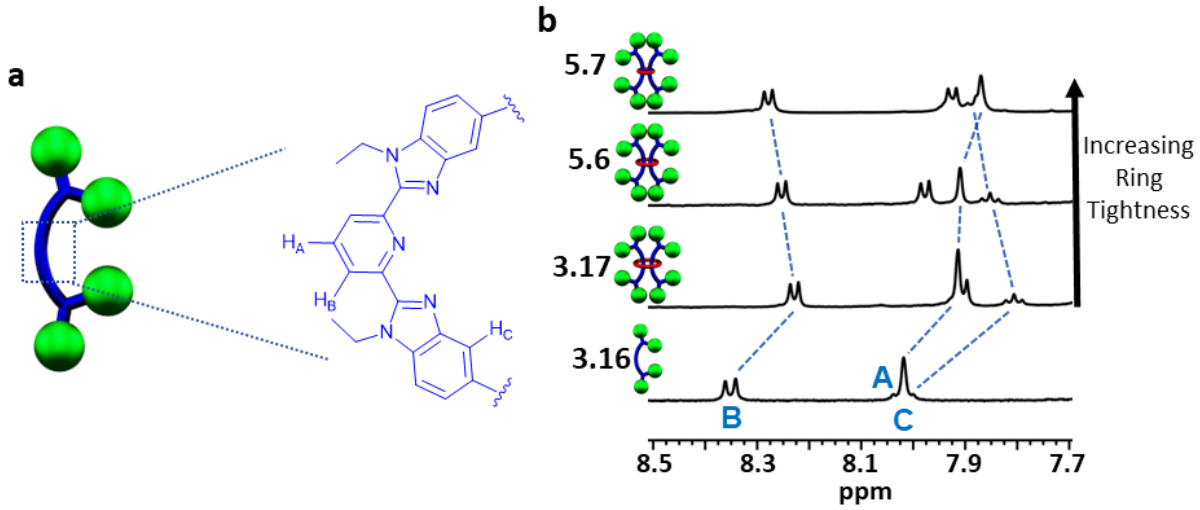

Fig 5.22 a) Labelling scheme for selected pyridinyl resonances on the dumbbell **3.17**. b) Partial ^{1}H-NMR overlay of [3]rotaxanes **3.17**, **5.6**, **5.7** and the corresponding dumbbell **3.16**.

As [3]rotaxane **5.5** was not able to be isolated on any appreciable timescale and [3]rotaxane **3.17** is known to be metastable (half-life = 5 weeks at room temp)[44], the first major structural analysis conducted was to investigate the kinetic stability of **5.6** and **5.7**. A preliminary room temperature experiment was conducted by monitoring freshly prepared solutions (1mM [3]R, $CDCl_3$) of [3]rotaxanes **5.6** and **5.7** every 2 weeks via ^{1}H-NMR spectroscopy for 6 weeks. This initial analysis revealed that in **5.6** the upfield shifted peaks assigned to interlocked product slowly decreased while signals corresponding to the free noninterlocked components slowly increased implying a slippage process and in [3]rotaxane **5.7** no slippage was observed (Fig 5.23).

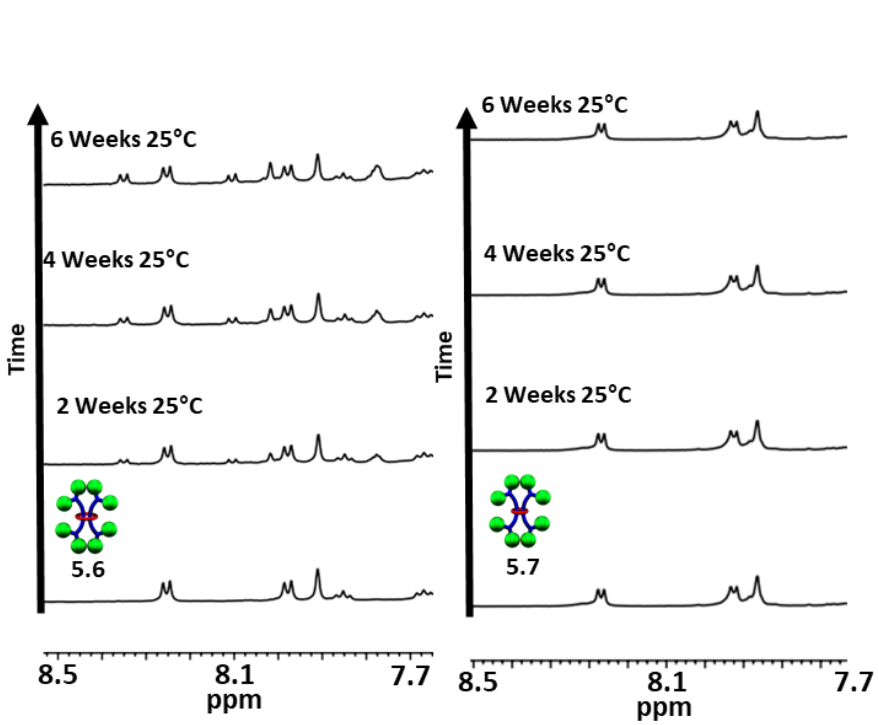

Fig 5.23 Partial ^{1}H-NMR overlay (1mM, 500 MHz, 25°C, $CDCl_3$) of initial room temperature slippage observations of **5.6** (left) and **5.7** (right).

This preliminary analysis implied a half-life of slippage of ~9 weeks for **5.6** at room temperature and indicated that the smaller 42 atom ring in **5.7** was able to fully stabilize the [3]rotaxane system. Taken together, it can be seen that the entire kinetic window of slippage is accessible by varying the ring from 42 to 48 atoms (Fig 5.24) at room temperature highlighting the dramatic effect that ring size can have on the doubly threaded [3]rotaxane structure.

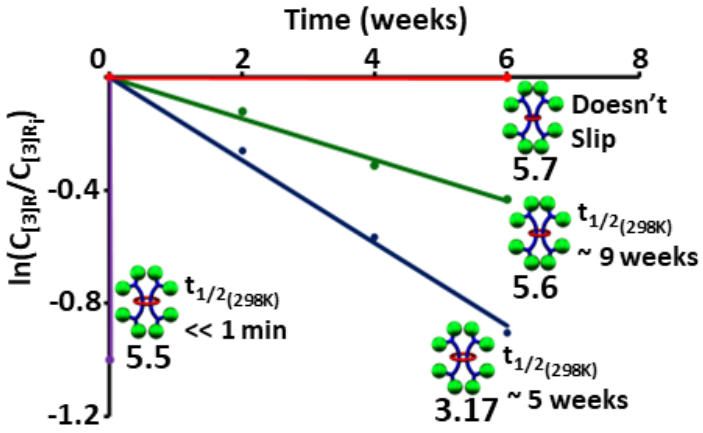

Fig 5.24 Kinetic first-order plot of slippage (25°C) of **5.5** (48-atom ring), **3.17** (46-atom ring), **5.6 (**44-atom ring), and **5.7** (42-atom ring).

In order to further probe the stability, a more detailed kinetic study similar to those described in Chapters 3 and 4 was performed. Both [3]rotaxanes were individually monitored at 35°C for one week followed by 40°C for another week and 45°C for a third week with their ^{1}H-NMR spectra recorded at regular time intervals. From this kinetic experiment it can again be seen that **5.7** shows no slippage during the 3-week experiment at moderate temperatures while **5.6** slowly disassembles to its free components and using the same downfield shifted pyridinyl "B" ^{1}H-NMR peak (Fig 5.22) a full first-order kinetic and thermodynamic analysis can be conducted (See Fig 5.25-5.27 for the corresponding analysis and the Experimental for full slippage details).

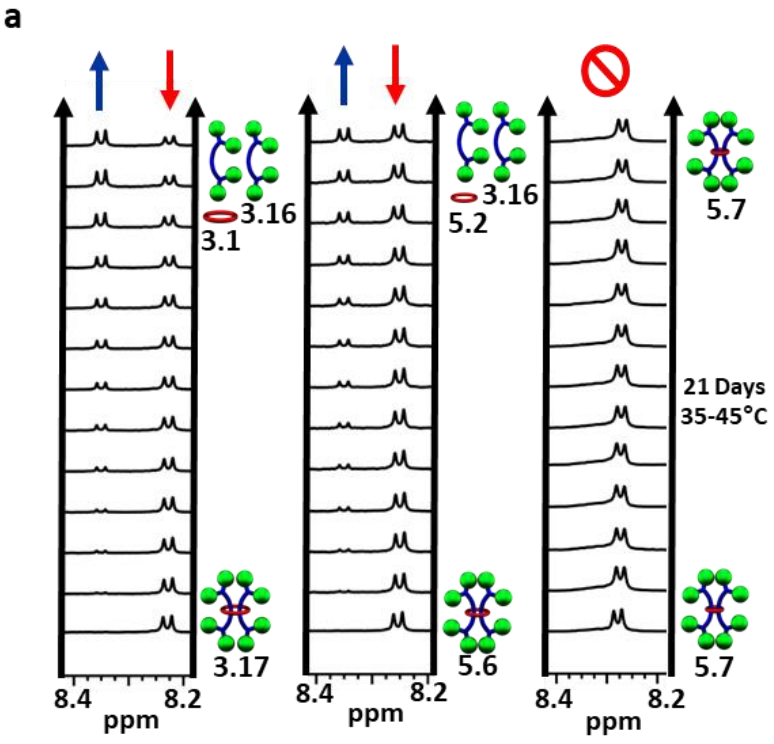

b

[3]R	E_a (kJ/mol)	$\Delta H^{\ddagger}$ (kJ/mol)	$\Delta S^{\ddagger}$ (J/mol*K)	$\Delta G^{\ddagger 298K}$ (kJ/mol)
3.17	98 ± 4	95 ± 3	-61 ± 8	113 ± 6
5.6	107 ± 3	104 ± 5	-36 ± 9	116 ± 5

Fig 5.25 a) Partial ^{1}H-NMR overlay of 3-week slippage experiment at 35-45°C of **3.17**, **5.6**, and **5.7**. b) Obtained thermodynamic parameters for slippage of **3.17** and **5.6**.

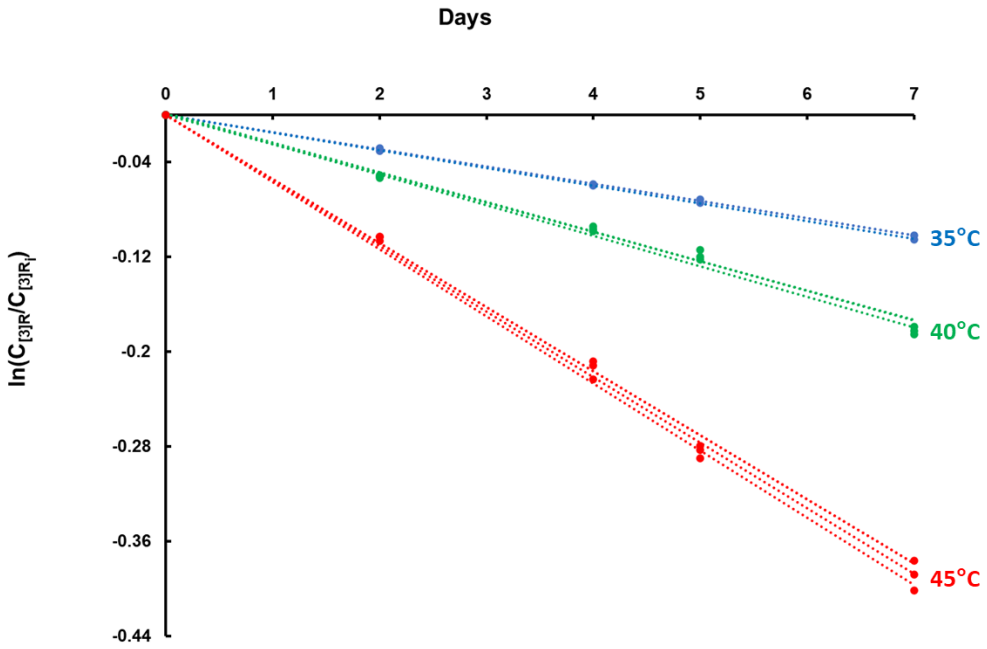

Fig 5.26 Kinetic first-order plot of three trials of slippage of **5.6** at three different temperatures.

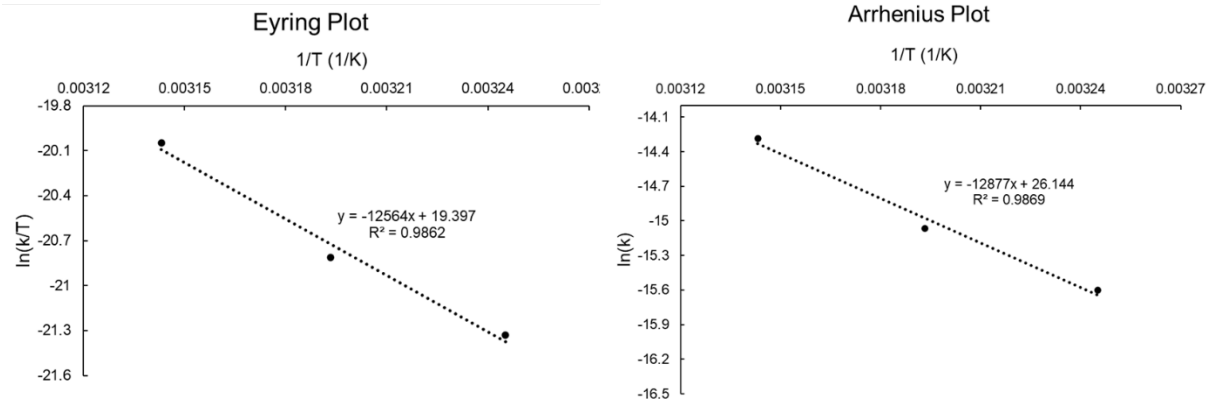

Fig 5.27 Eyring and Arrhenius plot of the slippage of **5.6**.

Applying standard Arrhenius and Eyring analysis to the slippage data of **5.6** allows the thermodynamic parameters to both slippage processes to be easily calculated which can be directly compared to the analogous 46 atom ring system **3.17**. Overall, a modest increase in the activation energy (98 ± 4 kJ mol^{-1} to 107 ± 3 kJ mol^{-1}) and Gibbs free energy change of the transition state (113 ± 6 kJ mol^{-1} to 116 ± 5 kJ mol^{-1}) of slippage was seen by tightening the ring from 46 atoms in **3.17** to 44 atoms in **5.6**.

As noted in the introduction, a particularly unique aspect of doubly threaded [3]rotaxanes compared to the general body of rotaxane literature is their ability to enforce the close spatial proximity of the two dumbbell components within the ring component.[38] As such, by varying the ring from 46 atoms in **3.17** to 44 atoms in **5.6** to 42 atoms in **5.7**, the two dumbbell components should be pushed closer and closer together as the ring tightens. Efforts then turned to characterization methods that could attempt to elucidate this effect. ^{1}H-^{1}H NOESY NMR has proven diagnostic in demonstrating the close proximity of differing components in interlocked molecules based on the Bip ligand and the [3]rotaxane **9**.[44,47,48] As such, a full ^{1}H-^{1}H NOESY NMR analysis of **5.6** and **5.7** and their corresponding noninterlocked controls (2:1 solution of free dumbbell:macrocycle at same concentration) was conducted at the slightly reduced temperature of 278K used in Chapter 3 (to enhance the NOE interactions) to understand better the effect of tightening the noose. ^{1}H-^{1}H NOESY NMR analysis of doubly threaded [3]rotaxane **3.16** shows 10 different intercomponent NOEs that are not present in the noninterlocked control (2:1 solution of **3.16**:**3.1**) of **3.17** which was described in Chapter 3.[44] When the ring is tightened once to 44 atoms in **5.6**, 19 different intercomponent NOEs are observed. When the ring is tightened again to 42 atoms in **5.7**, 31 different intercomponent NOEs now become visible demonstrating the significant

effect that the 4 atom tightening causes (Fig 5.28-5.30 for full spectra and 5.31 for a summary of the observed NOEs).

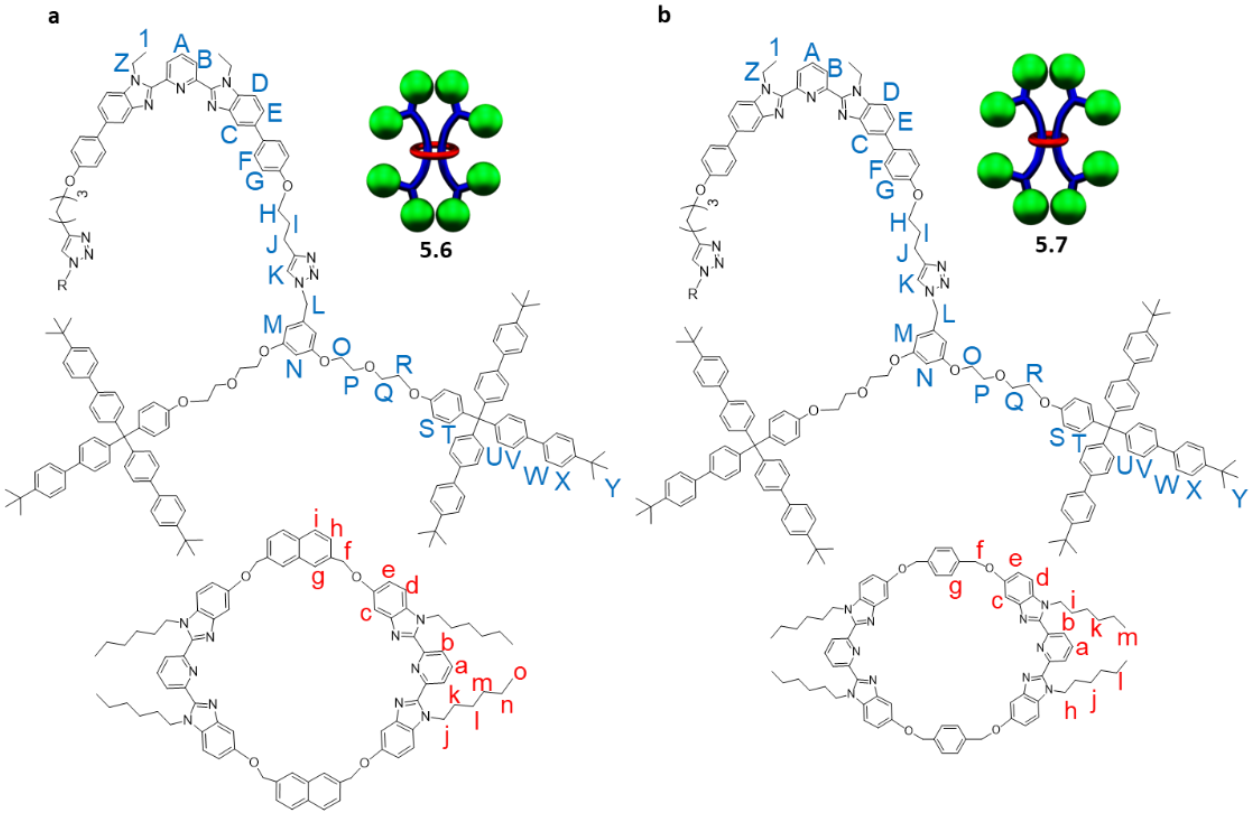

Fig 5.28 ^{1}H-NMR labeling schemes for a) **5.6** and b) **5.7** used for NOE spectra.

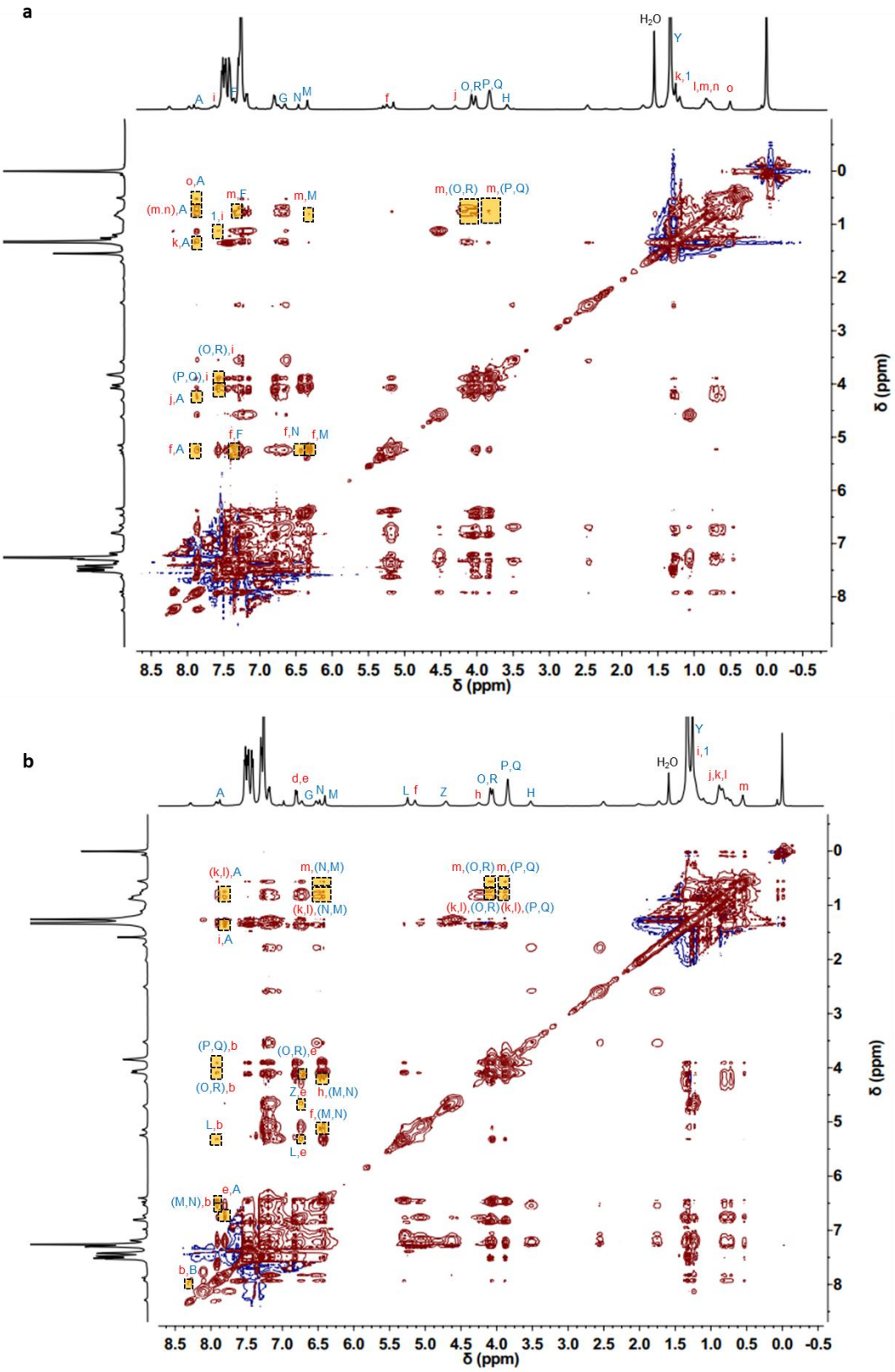

Fig 5.29 Full ^{1}H-^{1}H NOESY (5mM, 500 MHz, 5°C, $CDCl_3$) of a) **5.6** and b) **5.7**. Select ^{1}H annotations correspond to Fig 5.28. Intercomponent cross peaks boxed in yellow.

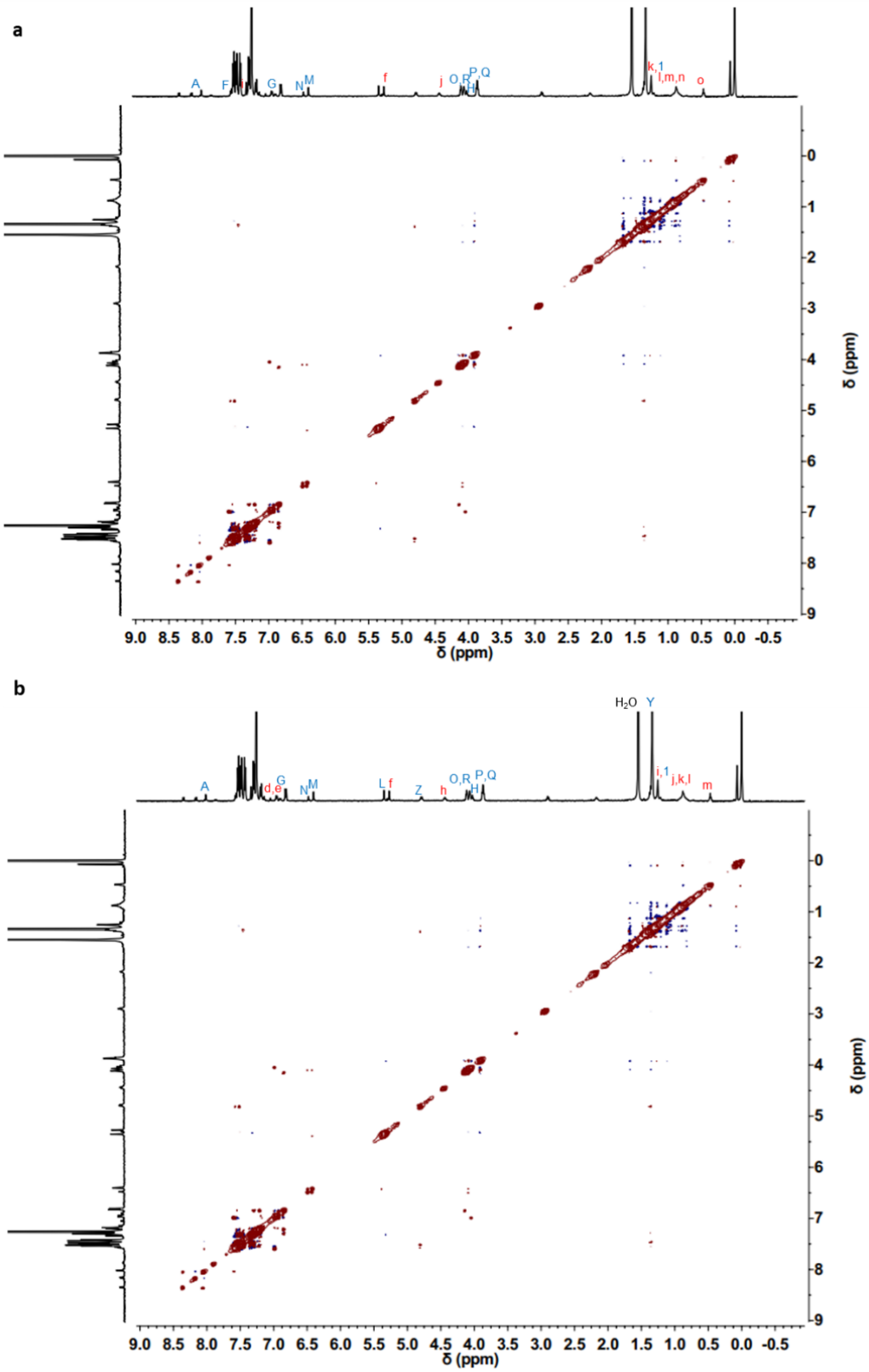

Fig 5.30 Full ^{1}H-^{1}H NOESY (5mM, 500 MHz, 5°C, $CDCl_3$) of 2:1 mixture of a) **3.17**:**5.2** and b) **3.17**:**5.3**. Select ^{1}H annotations correspond to Fig 5.28.

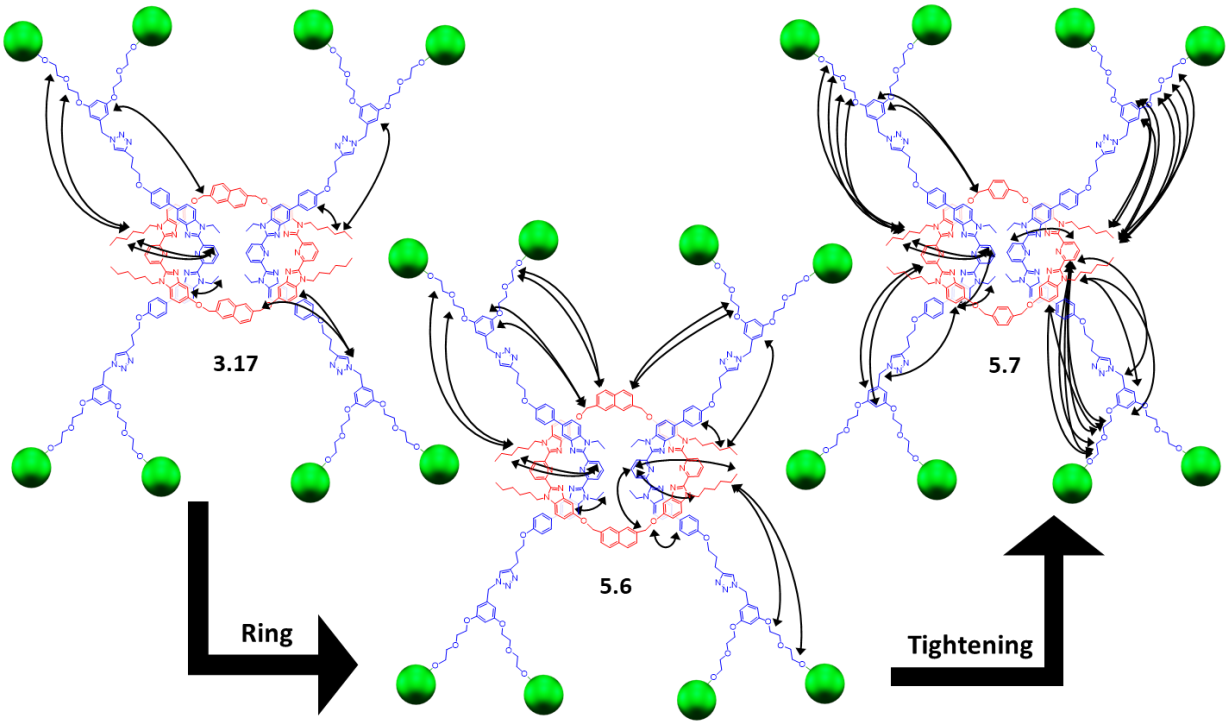

Fig 5.31 Schematic describing increase in intercomponent NOEs seen upon tightening the ring in the doubly threaded [3]rotaxane structure.

Closer examination of the specific NOE increases with ring size reduction reveal that the majority of the NOES added interact with the dumbbell component near the middle pyridine ring of the dumbbell and the end diethylene glycol linker near the stopper. This is consistent with previously described all-atom molecular dynamics simulations of **3.17**[44] that suggest an asymmetric orientation of the two dumbbells where the ring assumes a position near a stopper group of one dumbbell and in the middle of the other (Fig 5.32).

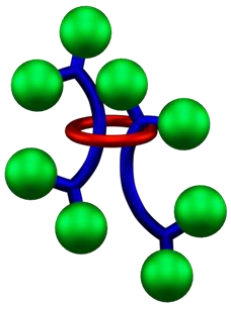

Fig 5.32 Cartoon representation of asymmetric dumbbell orientation.

To further probe the close proximity of the interlocked components and this possible asymmetric dumbbell orientation, steady-state fluorescence and ultraviolet-visible (UV-Vis) spectroscopy measurements were conducted on [3]rotaxanes **3.17**, **5.6**, and **5.7** and their corresponding noninterlocked controls and components. The obtained absorption and emission spectra can be seen in Figure 5.33 (See Experimental for full details).

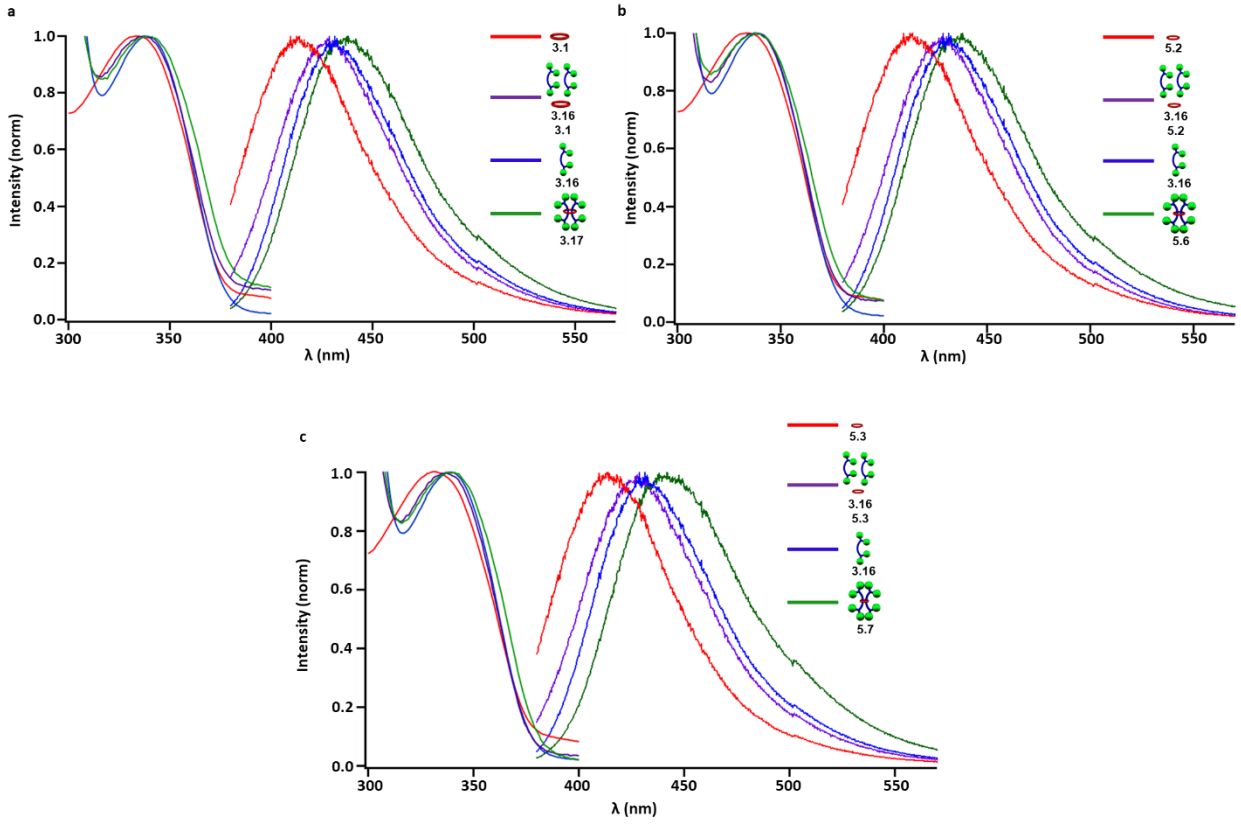

d

	3.1	5.2	5.3	3.16	3.16 + 3.1	3.16 + 5.2	3.16 + 5.3	3.17	5.6	5.7
λ_{Abs} (nm)	333	334	334	338	337	337	337	338	338	338
λ_{Em} (nm)	413	413	414	431	428	428	428	437	438	442

Fig 5.33 Absorption and emission spectra (1μM, DCM) for the corresponding [3]rotaxane, 2:1 dumbbell:macrocycle mixture, free dumbbell, and free macrocycle for the a) 46-atom ring system, b) 44-atom ring system, c) 42-atom ring system, and d) Table summarizing obtained spectral properties of [3]rotaxanes and their noninterlocked controls and components for all three ring sizes.

In addition, time-correlated single photon counting techniques were used to examine the fluorescence lifetimes of the same assortment of [3]rotaxanes and controls/components (Fig 5.34, See Experimental for full details).

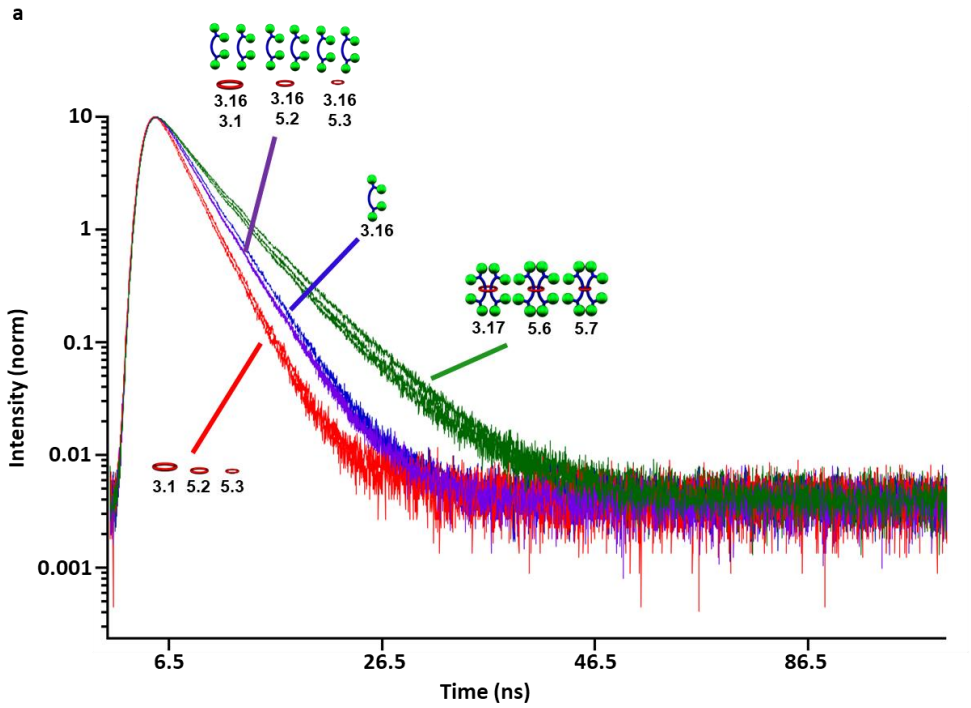

b

	3.1	5.2	5.3	3.16	3.16 + 3.1	3.16 + 5.2	3.16 + 5.3	3.17	5.6	5.7
τ_1 (ns)	2.19	2.20	2.26	2.82	2.71	2.72	2.71	2.69	2.62	2.38
τ_2 (ns)	-	-	-	-	-	-	-	4.59	4.46	4.66
f_1 (%)	100	100	100	100	100	100	100	45.3	45.9	31.1
f_2 (%)	-	-	-	-	-	-	-	54.7	54.1	68.9

Fig 5.34 a) Fluorescence decay profiles (1μM, DCM) for the corresponding [3]rotaxane, 2:1 dumbbell:macrocycle mixture, free dumbbell, and free macrocycle for all three ring sizes, and b) Table summarizing obtained fluorescence lifetime properties of [3]rotaxanes and their noninterlocked controls and components for all three ring sizes.

From this analysis it can be seen that all three [3]rotaxanes relative to their 2:1 dumbbell:macrocycle controls show a slight broadening and 1 nm (337 to 338nm) red shift of their absorption band (assignable to the $\pi \rightarrow \pi^*$ transition of the Bip ligand[49]). Red-shifting has been

reported in [2]rotaxane systems relative to their free components before[50–53], and could be consistent with rotaxination restricting the dumbbells local motion and vibrational relaxation modes resulting in a slight decreases in the energy difference of the transition. More interestingly, similar red-shifting occurs in the emission spectra (λ_{exc}=365nm) of all [3]rotaxanes but to a varying extent with ring size. All three dumbbell:macrocycle control mixtures have a consistent maximum at 337nm (which appears to be a weighted average of the free dumbbell and ring). The largest ring [3]rotaxane **3.16** red-shifts 9nm to 437nm, **5.6** shifts 10nm to 438nm, and the tightest 42 atom ring system **5.7** shifts 14nm to 442nm (Fig 5.33).

The observed fluorescent lifetime profiles displayed a similar effect as the decay curves of the [3]rotaxanes are all significantly shifted to longer times (Fig 5.34a). Specifically, all 2:1 dumbbell:macrocycle control mixtures were fit with a consistent τ_1 of ~2.71ns. On the other hand, the [3]rotaxanes were fit better with a standard bifunctional decay curve leading to one lifetime of a similar magnitude (2.4-2.7ns) as the free dumbbell and a second lifetime significantly slower (4.4-4.7ns). In addition, the population of this slower lifetime increases from ~55% in **3.17** and **5.6** to ~69% in the tightest ring system **5.7**. Longer lifetimes of main-chain polyrotaxanes compared to their unthreaded counterparts have been reported before[54,55] and is in part a result of the entrapped rings leading to more extended, near-planar conformations of the threaded backbone.[56,57] The interpretation of the results for this specific [3]rotaxane system are still premature but may be a result of the interlocked ring causing both dumbbell components to be in a more planar confirmation that hinders free rotation around the Bip ligand of both leading to the longer observed lifetimes. The effect may also be caused by the rigidification of the interlocked structure slowing down nonradiative decay. Quantum yield measurements and further analysis are currently underway to help explain these results.

5.5 Preliminary [3]Rotaxane Results With a 40 Atom Ring

With the size range of 48-42 atoms well understood for this [3]rotaxane system, efforts were then turned to the next step smaller using the 40 atom ring **5.4**. First, the pseudo[3]rotaxane **5.4:3.2**$_2$**:**Fe(II)$_2$ was targeted using similar metal-templating procedures to those described previously (Fig 5.35).

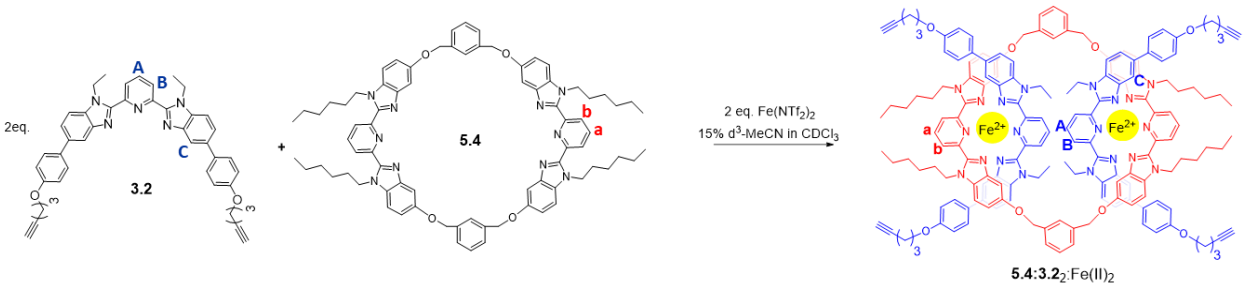

Fig 5.35 Scheme showing formation of **5.4:3.2**$_2$**:**Fe(II)$_2$ from its components**.**

Similar diagnostic downfield shifting of the pyridinyl Bip protons were seen via ^{1}H-NMR spectroscopy upon metal addition an equilibration (Fig 5.36, see Experimental for full details on assembly procedures). Careful examination of the ^{1}H-NMR spectrum of the equilibrated pseudo[3]rotaxane reveals a second minor product in addition to the desired pseudo[3]rotaxane (Fig 5.36, desired product is two labelled doublets and triplets, extra peaks marked by red arrows). The extra peaks are also not consistent with metallated thread complex (i.e. **3.2**$_2$:Fe(II)) suggesting they could be some sort of singly threaded pseudorotaxane structure. This observation requires further attention but may indicate that the tighter 40 atom ring requires slightly elevated conditions to reach full equilibration. Nevertheless, this pseudo[3]rotaxane was carried forward with this knowledge and stoppered with **3.13** using similar conditions to those described previously to target the [3]rotaxane **5.8** (Fig 5.37, see Experimental for full details).

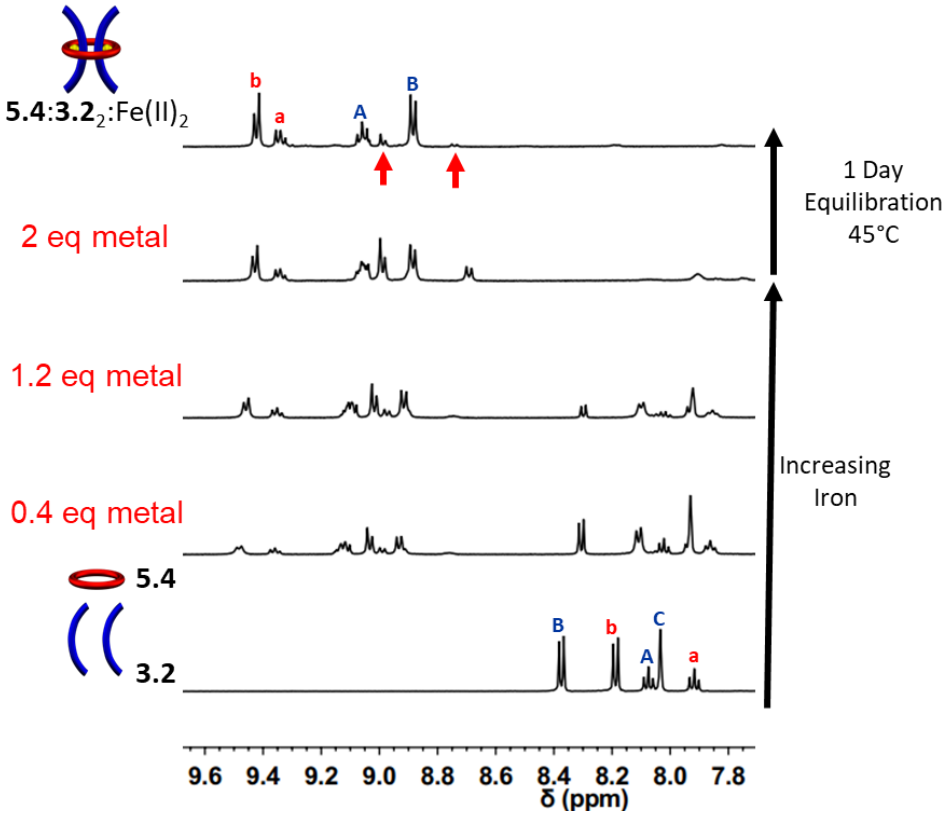

Fig 5.36 Partial ^{1}H-NMR overlay (500 MHz, 25°C, Solvent: 0, 3, 9, 15, 15% d_3-MeCN in $CDCl_3$ increasing upwards) of Fe(II) addition and equilibration. ^{1}H assignments in Fig 5.38.

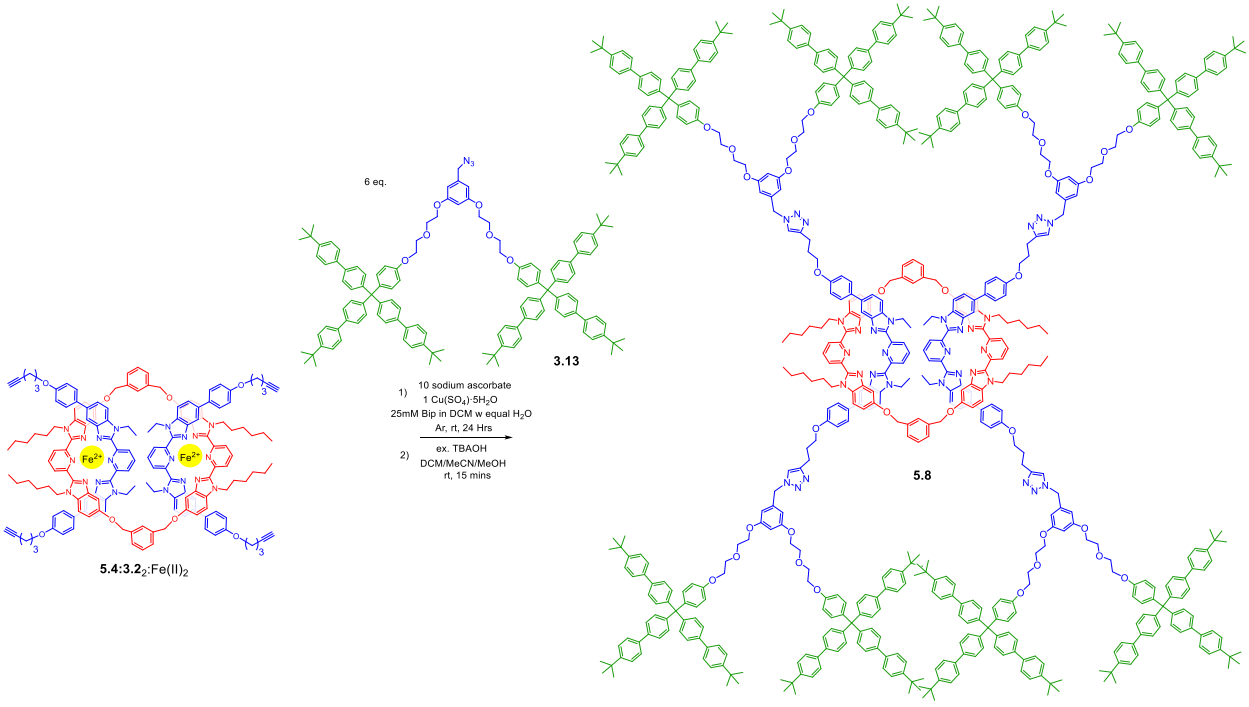

Fig 5.37 Scheme showing synthesis of doubly threaded [3]rotaxane **5.8.**

The crude [3]rotaxane product **5.8** was analysed immediately via ^{1}H-NMR spectroscopy upon demetallation. This analysis revealed upfield shifted peaks in the regions consistent with interlocked [3]rotaxane product that have been identified in the past two chapters (See Fig 5.38, interlocked product boxed in red).

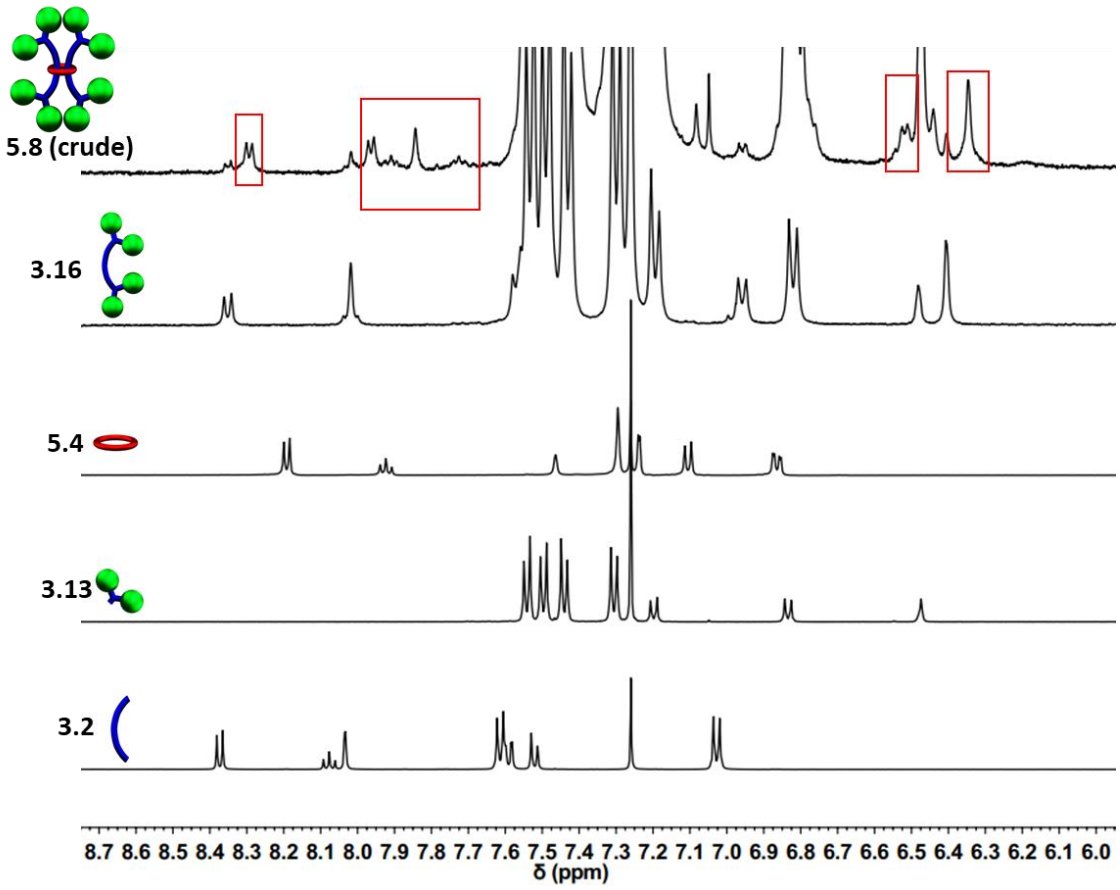

Fig 5.38 Partial ^{1}H-NMR overlay (500 MHz, 25°C, $CDCl_3$) of the demetallated crude reaction mixture from the stoppering of **5.4**:**3.2**$_2$:Fe(II)$_2$ with **3.13** compared to starting materials and free components. Interlocked product is boxed in red.

The noninterlocked byproduct was estimated at ~20% via ^{1}H-NMR integration (80% interlocked product). Using preparative thin layer chromatography, the [3]rotaxane product was isolated in 65% yield and characterized via ^{1}H-NMR spectroscopy, MALDI-TOF MS, and GPC. The ^{1}H-NMR spectrum again shows similar upfield shifting of **5.8** relative to its noninterlocked components (Figure 5.39).

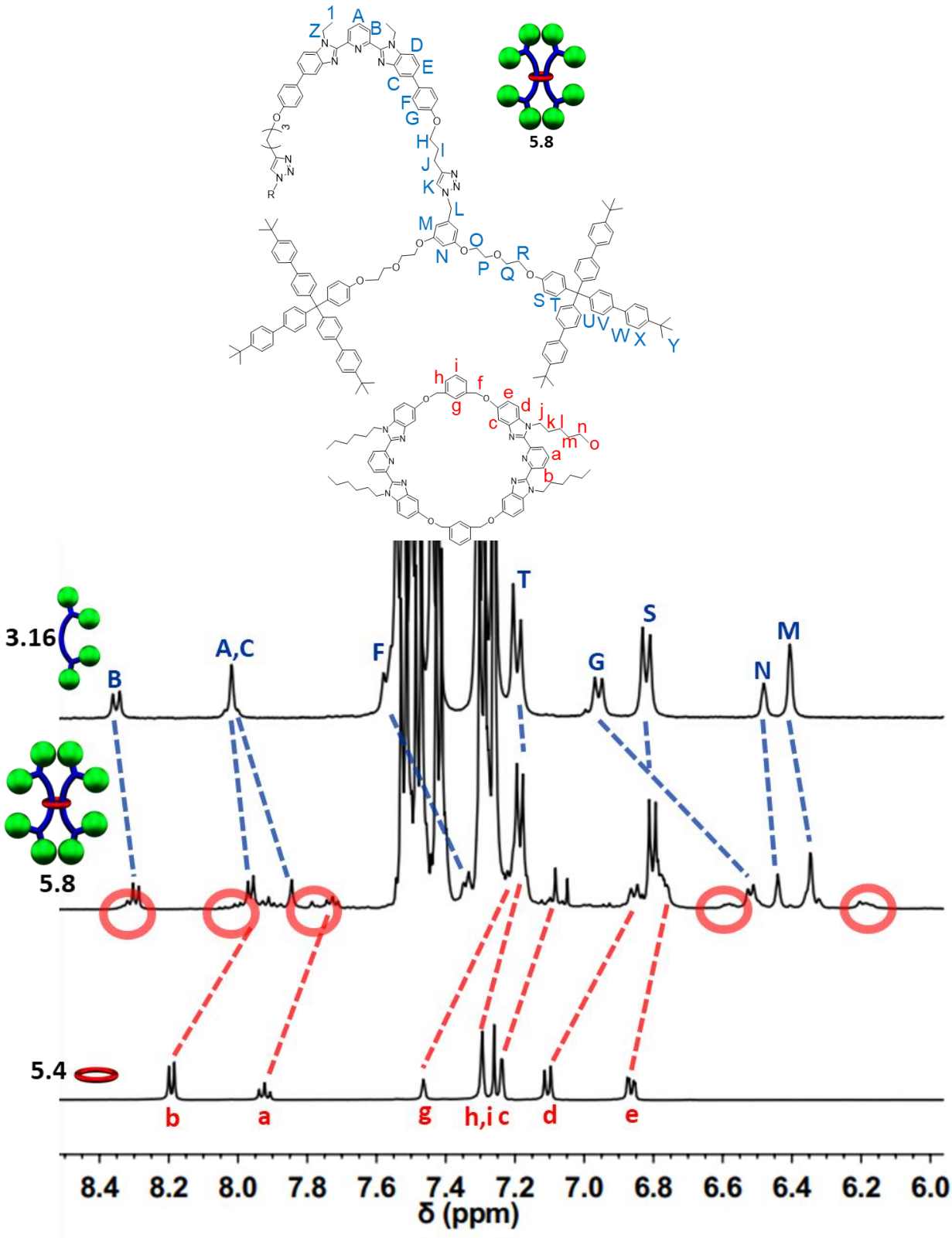

Fig 5.39 Partial ^{1}H-NMR overlay (500 MHz, 25°C, $CDCl_3$) of purified **5.8** relative to its components **5.4** and **3.16**, ^{1}H assignments at top of figure.

In addition to the expected [3]rotaxane peaks, there are minor additional signals observed in the ^{1}H-NMR spectrum that are also shifted upfield from the free components (Fig 5.39a red circles). The MALDI-TOF MS spectrum and GPC trace also both confirm the expected [3]rotaxane product as the major product and similarly an additional minor product not assignable to the free components (Fig 5.40 red circles).

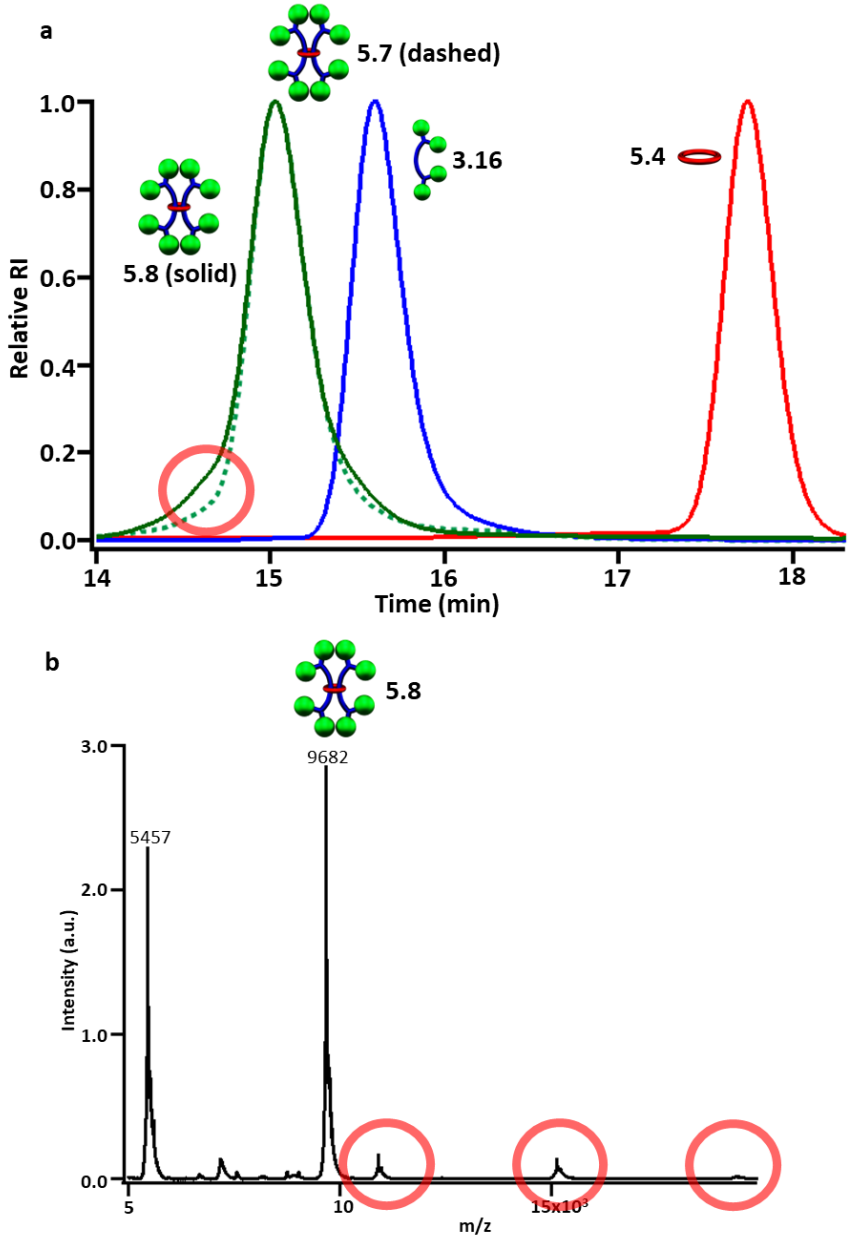

Fig 5.40 a) GPC chromatogram of (3:1 THF:DMF) purified **5.8**, **5.7**, **3.16**, and **5.4** at 25°C. b) MALDI-TOF MS of **5.8**.

The most probable explanations for this observation are that either the tightest fitting 40 atom ring tightens the dumbbells so much that two different confirmations become possible or a small amount of another interlocked molecule has been made (either a singly threaded [2]rotaxane or something higher order). In order to determine this, detailed GPC-MALS and HPLC analysis, fractionation studies, kinetic stability studies, and closer examination of the metal-binding capabilities of the 40-atom ring **5.4** are currently underway.

5.6 Conclusions

In conclusion, the successful synthesis of a series of Bip-containing doubly threaded [3]rotaxanes varying in macrocycle size from 40-48 atoms has been achieved in good yield. The size of the ring was found to have a profound effect on the [3]rotaxane structure as evidenced by NMR spectroscopy and steady-state and time-resolved fluorescence spectroscopy techniques. In particular, the entire kinetic window of slippage from not stable on any appreciable timescale to metastable to fully stable could be observed by tightening the ring from 48 to 42 atoms. Steady-state fluorescence measurements revealed red shifting in the emission spectra upon rotaxination varying with ring size and fluorescence lifetime measurements confirmed the existence of slower lifetimes in all the studied [3]rotaxanes.

The large range of macrocycle size variation available in this system is currently being extending to the corresponding polyrotaxanes and slide-ring materials (Fig 5.41).

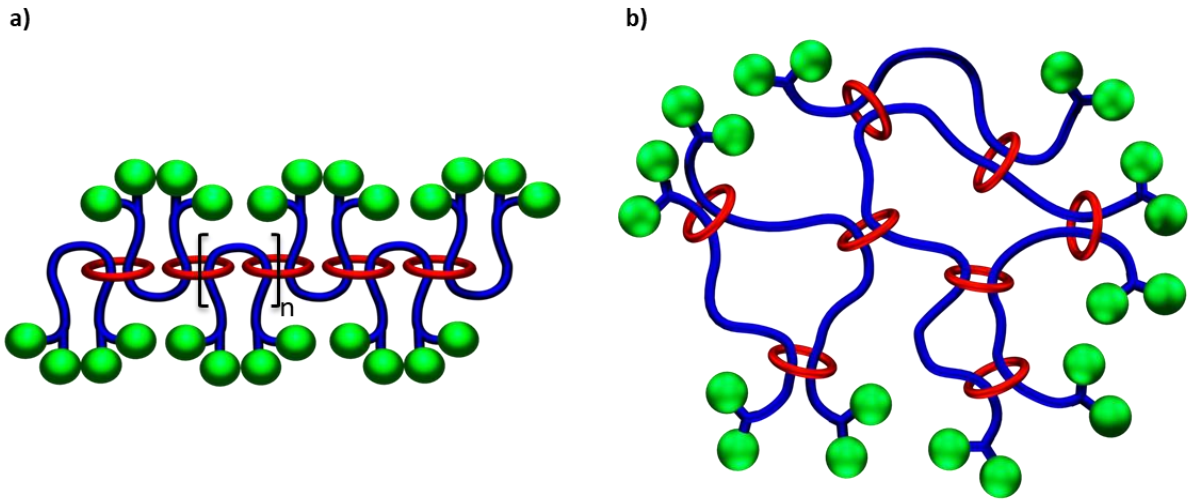

Fig 5.41 Cartoon representation of doubly threaded a) poly[3]rotaxane and b) slide-ring materials.

The wide 6-atom range for isolatable materials that has been established in this chapter is very desirable from a materials standpoint and will allow future researchers access to two differing metastable ring sizes and two fully stable ring sizes. The effect of macrocycle size variation and tightening the noose in these doubly threaded polymers can then be easily probed.

5.7 Experimental

5.7.1 Materials and Methods

Materials. All reagents were purchased from Sigma-Aldrich unless otherwise stated. All chemicals were used as received without further purification unless otherwise stated. Solvents for chromatography were purchased from Fisher-Scientific. Deuterated solvents and 3,5-dihydroxybenzyl alcohol were purchased from ACROS Organics. 4-Bromo-4'-tert-butylbiphenyl was purchased from TCI chemicals. *p*-Toluenesulfonyl chloride was purchased from Alfa Aesar. Iron(II) bistriflimide[58] and 2,6-bisbenzimidazolylpyridine ligands[45] were prepared following literature procedures. Tetrahydrofuran (THF) was dried over sodium and benzophenone.

Dichloromethane was distilled over calcium hydride before use. Dimethylformamide (DMF) was dried with activated molecular sieves before use. Thin layer chromatography plates (1000 micron) were purchased from Analtech.

Matrix Assisted Laser Desorption/Ionization Mass Spectrometry (MALDI-MS). MALDI-TOF was measured by a Bruker Ultraflextreme MALDI-TOF-TOF spectrometer in linear (or reflectance) mode using dithranol as matrix and sodium trifluoroacetate or silver trifluoroacetate as ionizer (or no ionizer).

Nuclear Magnetic Resonance Spectroscopy (NMR). Room Temperature Nuclear Magnetic Resonance Spectroscopy was performed using a Bruker Ascend Avance III 500 MHz spectrometer, a Bruker Avance II+ 500 MHz spectrometer, or a Bruker DRX 400 MHz spectrometer at the University of Chicago NMR facilities. ^{1}H NMR spectra were referenced to the residual protonated solvent signal and $^{13}C\{^{1}H\}$ NMR spectra were referenced to the deuterated solvent carbon resonance signal.

NMR Slippage Kinetic Experiments. Kinetic experiments were performed in Shigemi Tubes purchased from Wilmad-Labglass in $CDCl_3$ (1mM) using a Bruker AVANCE III HD 500 MHz spectrometer at the NMR facilities at the University of Chicago.

Gel Permeation Chromatography (GPC). GPC measurements were performed utilizing the Soft Matter Characterization Facility at the University of Chicago. Measurements were conducted at 25°C using 3:1 THF:DMF as eluent (flow rate = 1 mL/min), using a Shimadzu autosampler, Shimadzu HPLC LC20-AD pump, 2 Agilent PLgel 5 um MIXED-D + guard SEC columns, and a Wyatt Optilab T-rEX differential refractive index detector.

UV-Vis Spectrometry. UV-Vis spectrometry was measured using a Shimadzu UV-3600 Plus UV-Vis-NIR spectrophotometer and a 1 cm width quartz cuvette.

Steady-State Fluorescence Measurements. Standard emission spectra were obtained using a HORIBA Fluorolog-3 Spectrofluorometer at an excitation wavelength of 365nm using a Synapse OE-CCD detector.

Time-Correlated Single Photon Counting (TCPSC) Methods. Fluorescence lifetime measurements were conducted on an ISS ChronosBH Lifetime Fluorometer using a 345nm pulsed LED excitation source coupled to a hybrid PMT detector.

5.7.2 Synthesis of 5.1

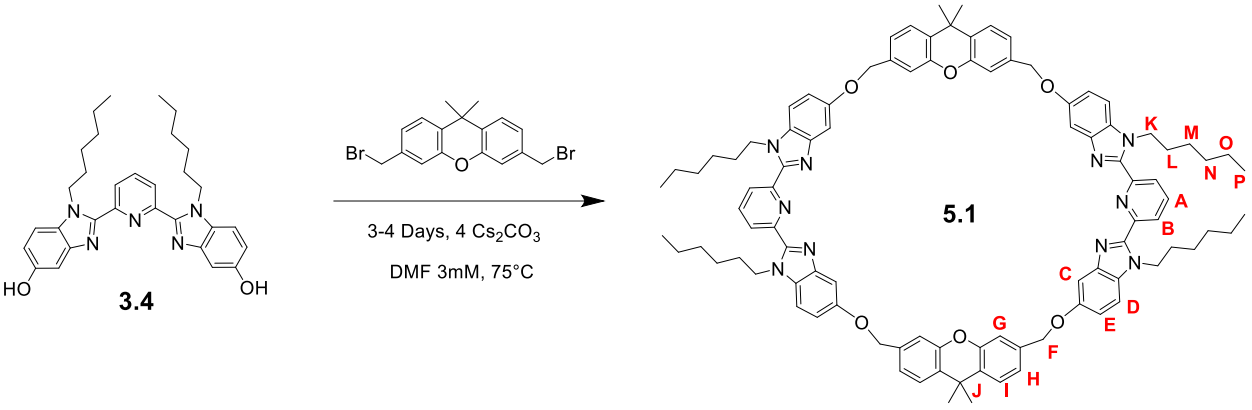

A 2-necked 1 L RBF was charged with **3.4**[44] (1.5 g, 2.94 mmol), Cs_2CO_3 (3.82 g, 11.8 mmol) and DMF (620mL) under an Ar atmosphere. The mixture was heated to 75 °C and stirred while a DMF (310 mL) solution of 3,6-bis(bromomethyl)-9,9-dimethyl-9H-xanthene[47] (1.16g, 2.94 mmol) was added dropwise (at an approximate rate of one drop every 10 s) over 3 d. When all the solution was added the reaction was stirred for a further 24 h at 75 °C. After this time (total reaction time 4 d) the reaction mixture was cooled to RT and the solvent was removed under reduced pressure. The residue was washed in hot $CHCl_3$ (4 × 100 mL) and the insoluble material (salts) was removed

by filtration. The filtrate was collected and the solvent removed under reduced pressure. The resulting material was purified using column chromatography (TEA treated silica gel, chloroform/methanol gradient as eluent) followed by recrystallization (chloroform/methanol mixture) to yield white crystals of **5.1** in 21% yield. ^{1}H NMR (500 MHz, $CDCl_3$) δ 8.15 (d, *J* = 7.9 Hz, 4H, B), 7.87 (t, *J* = 7.9 Hz, 2H, A), 7.35 (d, *J* = 8.0 Hz, 4H, H), 7.25-7.21 (m, 8H, C+I), 7.11 (d, *J* = 8.1 Hz, 4H, D), 7.06 (s, 4H, G), 7.00 (dd, *J* = 8.9, 2.3 Hz, 4H, E), 5.24 (s, 8H, F), 4.54 (t, *J* = 7.5 Hz, 8H, K), 1.62 (m, 8H, L), 1.00 (m, 24H, M+N+O), 0.54 (m, 12H, P). ^{13}C NMR (126 MHz, $CDCl_3$) δ 155.07, 150.55, 150.31, 150.06, 143.47, 137.86, 137.47, 131.24, 129.28, 126.60, 125.16, 121.39, 114.81, 114.77, 110.74, 104.42, 70.00, 44.95, 33.90, 32.61, 31.19, 30.10, 26.36, 22.42, 13.82. MALDI-MS: 1599.6 ([M]+Ag^+).

5.7.3 Synthesis of 5.2

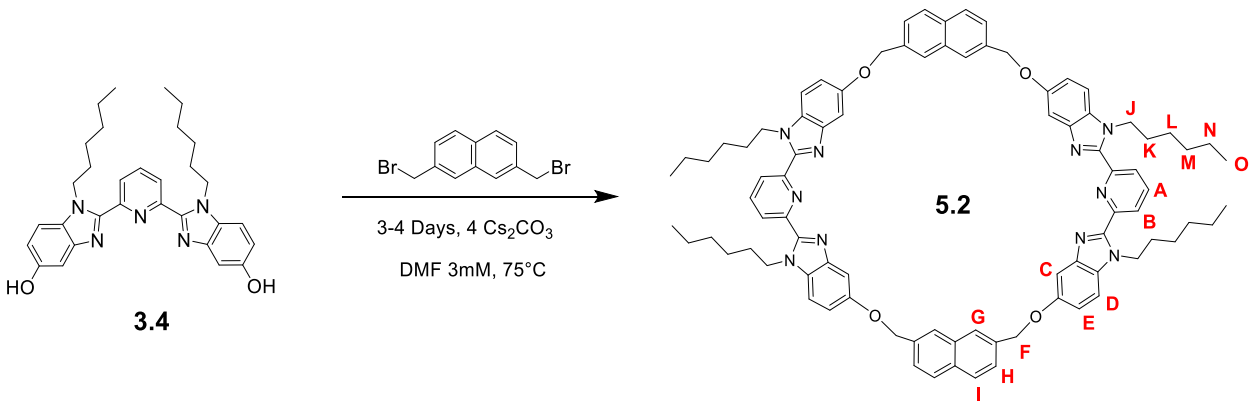

A 2-necked 1 L RBF was charged with **3.4**[44] (1.0 g, 1.95 mmol), Cs_2CO_3 (2.6 g, 7.8 mmol) and DMF (440 mL) under an Ar atmosphere. The mixture was heated to 75 °C and stirred while a DMF (220 mL) solution of 2,7-bis(bromomethyl)naphthalene (0.61g, 1.95 mmol) was added dropwise (at an approximate rate of one drop every 10 s) over 3 d. When all the solution was added the reaction was stirred for a further 24 h at 75 °C. After this time (total reaction time 4 d) the

reaction mixture was cooled to RT and the solvent was removed under reduced pressure. The residue was washed in hot $CHCl_3$ (4 × 100 mL) and the insoluble material (salts) was removed by filtration. The filtrate was collected and the solvent removed under reduced pressure. The resulting material was purified using column chromatography (TEA treated silica gel, chloroform/methanol gradient as eluent) followed by recrystallization (chloroform/methanol mixture) to yield white crystals of **5.2** in 20% yield. ^{1}H NMR (400 MHz, $CDCl_3$) δ 8.10 (d, *J* = 7.9 Hz, 4H, B), 7.81-7.75 (m, 10H, A+C+I), 7.53 (d, *J* = 8.0 Hz, 4H, H), 7.24 (s, 4H, G), 7.19 (d, *J* = 8.9 Hz, 4H, D), 7.01 (dd, *J* = 8.9, 2.3 Hz, 4H, E), 5.42 (s, 8H), F, 4.48 (t, *J* = 7.5 Hz, 8H, J), 1.55 (m, 8H, K), 0.89 (m, 24H, L+M+N), 0.49 (m, 12H, O). ^{13}C NMR (101 MHz, $CDCl_3$) δ 154.97, 150.20, 149.98, 143.41, 137.73, 135.83, 133.38, 132.64, 131.26, 128.45, 125.66, 125.22, 124.76, 114.70, 110.78, 104.72, 70.72, 44.89, 31.18, 29.85, 26.35, 22.43, 13.79. MALDI-MS: 1436.1 ([M]+Ag^+).

5.7.4 Synthesis of 5.3

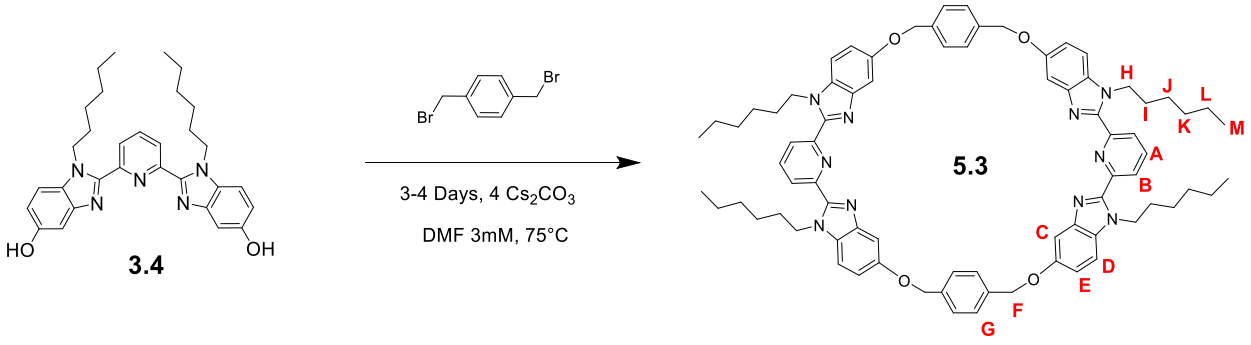

1 L RBF was charged with **3.4**[44] (1.0 g, 1.95 mmol), Cs_2CO_3 (2.6 g, 7.8 mmol) and DMF (440 mL) under an Ar atmosphere. The mixture was heated to 75 °C and stirred while a DMF (220 mL) solution of α,α′-Dibromo-p-xylene (0.51g, 1.95 mmol) was added dropwise (at an approximate rate of one drop every 10 s) over 3 d. When all the solution was added the reaction was stirred for a further 24 h at 75 °C. After this time (total reaction time 4 d) the reaction mixture was cooled to

RT and the solvent was removed under reduced pressure. The residue was washed in hot $CHCl_3$ (4 × 100 mL) and the insoluble material (salts) was removed by filtration. The filtrate was collected and the solvent removed under reduced pressure. The resulting material was purified using column chromatography (TEA treated silica gel, chloroform/methanol gradient as eluent) followed by recrystallization (chloroform/methanol mixture) to yield white crystals of **5.3** in 11% yield. ^{1}H NMR (400 MHz, $CDCl_3$) δ 8.19 (d, *J* = 7.9 Hz, 4H, B), 7.90 (t, *J* = 7.9 Hz, 2H, A), 7.37 (s, 8H, G), 7.21-7.15 (m, 8H, C+D), 6.93 (dd, *J* = 8.8, 2.4 Hz, 4H, E), 5.30 (s, 8H, F), 4.48 (t, *J* = 7.5 Hz, 8H, H), 1.55 (m, 8H, I), 0.89 (m, 24H, J+K+L), 0.49 (m, 12H, M). ^{13}C NMR (101 MHz, $CDCl_3$) δ 154.65, 150.16, 150.04, 143.41, 137.85, 137.28, 131.27, 126.99, 125.15, 114.72, 110.70, 104.79, 70.07, 44.87, 31.17, 29.86, 26.37, 22.46, 13.75. MALDI-MS: 1228.9 ([M]+H^+).

5.7.5 Synthesis of 5.4

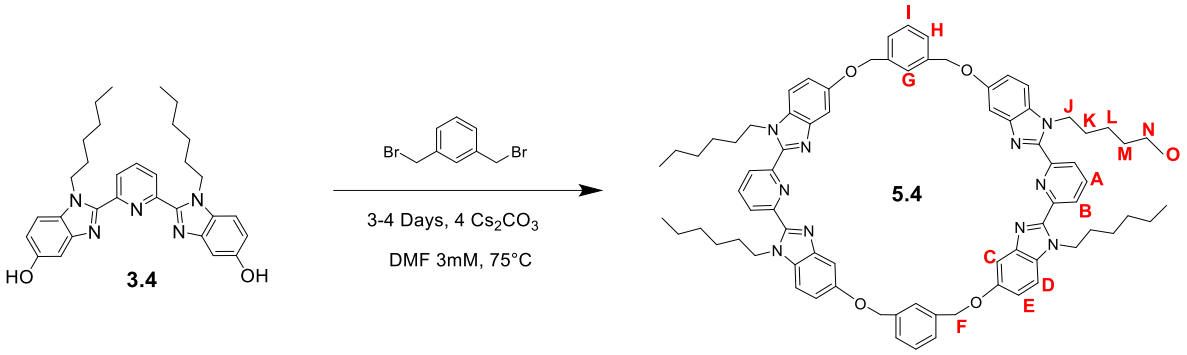

1 L RBF was charged with **3.4**[44] (1.0 g, 1.95 mmol), Cs_2CO_3 (2.6 g, 7.8 mmol) and DMF (440 mL) under an Ar atmosphere. The mixture was heated to 75 °C and stirred while a DMF (220 mL) solution of α,α′-Dibromo-m-xylene (0.51g, 1.95 mmol) was added dropwise (at an approximate rate of one drop every 10 s) over 3 d. When all the solution was added the reaction was stirred for a further 24 h at 75 °C. After this time (total reaction time 4 d) the reaction mixture was cooled to RT and the solvent was removed under reduced pressure. The residue was washed in hot $CHCl_3$

(4 × 100 mL) and the insoluble material (salts) was removed by filtration. The filtrate was collected and the solvent removed under reduced pressure. The resulting material was purified using column chromatography (TEA treated silica gel, chloroform/methanol gradient as eluent) followed by recrystallization (chloroform/methanol mixture) to yield white crystals of **5.4** in 5% yield. ^{1}H NMR (500 MHz, $CDCl_3$) δ 8.19 (d, *J* = 7.9Hz, 4H, B), 7.92 (t, *J* = 7.9Hz, 2H, A), 7.46 (s, 2H, G), 7.29 (m, 6H, H+I), 7.24 (bs, 4H, C), 7.11 (d, *J* = 8.8Hz, 4H, D), 6.86 (dd, *J* = 8.8, 2.1Hz, 4H, E), 5.24 (s, 8H, F), 4.42 (t, *J* = 7.2Hz, 8H, J), 1.52 (bm, 8H, K), 0.88 (bm, 24H, L+M+N), 0.51 (d, *J* = 6.7Hz, 12H, O). ^{13}C NMR (125 MHz, $CDCl_3$) δ 154.94, 150.20, 150.17, 143.40, 138.17, 137.90, 131.37, 128.95, 126.40, 126.00, 125.09, 115.17, 110.57, 105.66, 77.27, 71.09, 44.84, 31.20, 30.05, 26.29, 22.40, 13.78. MALDI-MS: 1228.7 ([M]+H^+).

5.7.6 Assembly of 5.1:3.2$_2$:Fe(II)$_2$

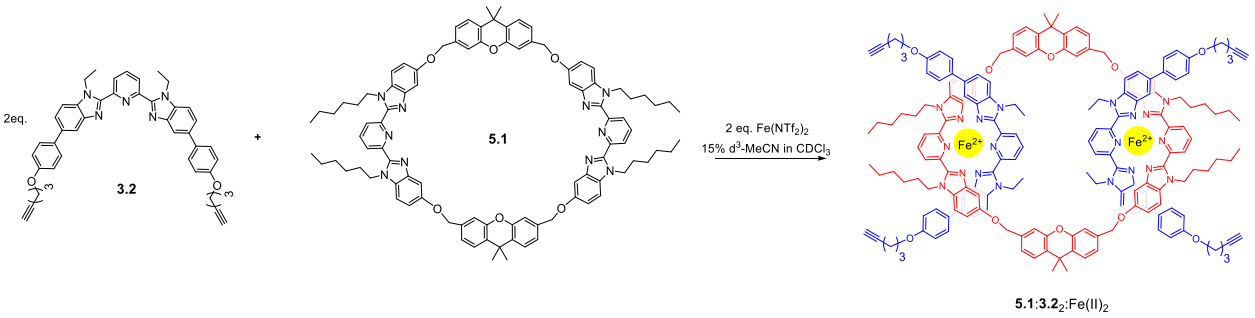

Dissolved 25.1mg of **5.1** in 1.5mL $CDCl_3$**.** Titrated thread stock solution (30mM) of **3.2** into solution of **5.1** until an exact 2:1 (**3.2**:**5.1**) ratio was formed (done by monitoring both the N-CH_2 peaks on the alkyl groups of the bip ligands). The mixture was then diluted to a total volume to 3.5mL $CDCl_3$ (5 mM **5.1**). A stock solution of $Fe(NTF_2)_2$ (30mM in 1:1 $CDCl_3$:d_3-MeCN) was added until no free Bip peak appeared at ~2 equiv. of metal ion. The solvent was removed under vacuum resulting in a dark purple solid that was redissolved in 2mL dry 15% MeCN in $CHCl_3$,

bubbled with argon for 1 min, and allowed to stir under Ar at 45°C for 1 day to allow equilibration. Solvent was then removed under vacuum and ^{1}H-NMR was recorded using 15% d_3-MeCN in $CDCl_3$.

5.7.7 Assembly of 5.2:3.2$_2$:Fe(II)$_2$

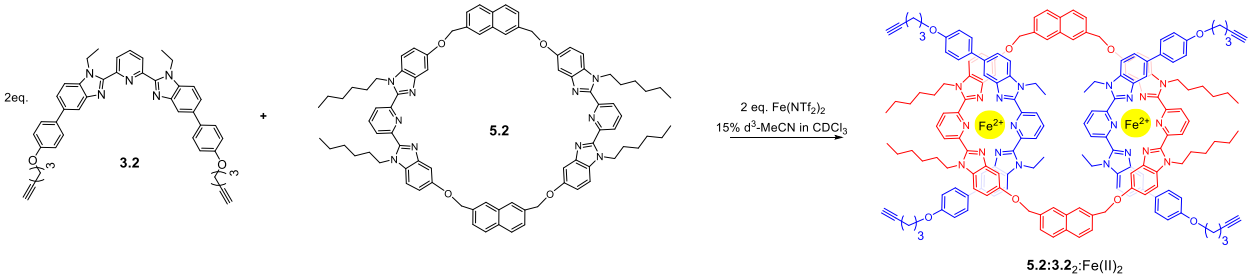

Dissolved 26.5mg of **5.2** in 1.5mL $CDCl_3$**.** Titrated thread stock solution (30mM) of **3.2** into solution of **5.2** until an exact 2:1 (**3.2**:**5.2**) ratio was formed (done by monitoring both the N-CH_2 peaks on the alkyl groups of the bip ligands). The mixture was then diluted to a total volume to 4mL $CDCl_3$ (5 mM **5.2**). A stock solution of $Fe(NTF_2)_2$ (30mM in 1:1 $CDCl_3$:d_3-MeCN) was added until no free Bip peak appeared at ~2 equiv. of metal ion. The solvent was removed under vacuum resulting in a dark purple solid that was redissolved in 2mL dry 15% MeCN in $CHCl_3$, bubbled with argon for 1 min, and allowed to stir under Ar at 45°C for 1 day to allow equilibration. Solvent was then removed under vacuum and ^{1}H-NMR was recorded using 15% d_3-MeCN in $CDCl_3$.

5.7.8 Assembly of 5.3:3.2$_2$:Fe(II)$_2$

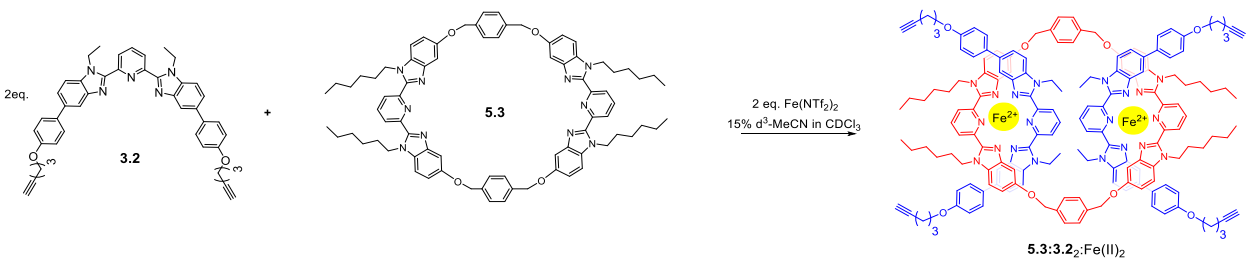

Dissolved 24.8mg of **5.3** in 1.5mL $CDCl_3$**.** Titrated thread stock solution (30mM) of **3.2** into solution of **5.3** until an exact 2:1 (**3.2**:**5.3**) ratio was formed (done by monitoring both the N-CH_2 peaks on the alkyl groups of the bip ligands). The mixture was then diluted to a total volume to 4mL $CDCl_3$ (5 mM **5.3**). A stock solution of $Fe(NTF_2)_2$ (30mM in 1:1 $CDCl_3$:d_3-MeCN) was added until no free Bip peak appeared at ~2 equiv. of metal ion. The solvent was removed under vacuum resulting in a dark purple solid that was redissolved in 2mL dry 15% MeCN in $CHCl_3$, bubbled with argon for 1 min, and allowed to stir under Ar at 45°C for 1 day to allow equilibration. Solvent was then removed under vacuum and ^{1}H-NMR was recorded using 15% d_3-MeCN in $CDCl_3$.

5.7.9 Assembly of 5.4:3.2$_2$:Fe(II)$_2$

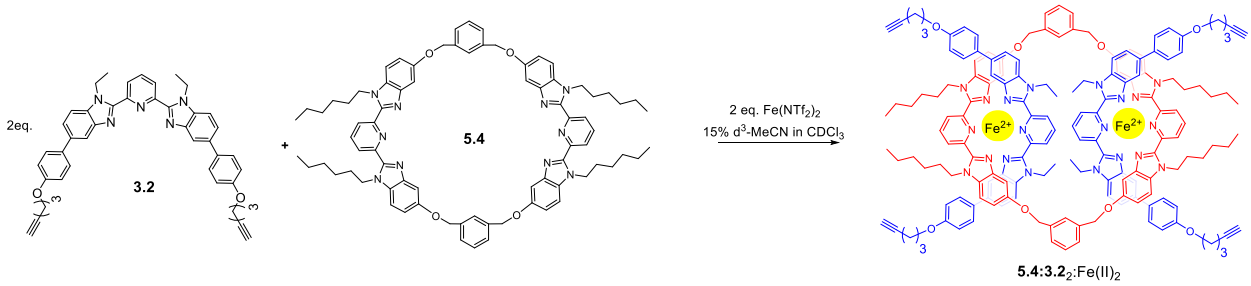

Dissolved 13.2mg of **5.4** in 0.8mL $CDCl_3$**.** Titrated thread stock solution (30mM) of **3.2** into solution of **5.4** until an exact 2:1 (**3.2**:**5.4**) ratio was formed (done by monitoring both the N-CH_2 peaks on the alkyl groups of the bip ligands). The mixture was then diluted to a total volume to 2mL $CDCl_3$ (5 mM **5.4**). A stock solution of $Fe(NTF_2)_2$ (30mM in 1:1 $CDCl_3$:d_3-MeCN) was added until no free Bip peak appeared at ~2 equiv. of metal ion. The solvent was removed under vacuum resulting in a dark purple solid that was redissolved in 2mL dry 15% MeCN in $CHCl_3$, bubbled with argon for 1 min, and allowed to stir under Ar at 45°C for 1 day to allow equilibration. Solvent was then removed under vacuum and ^{1}H-NMR was recorded using 15% d_3-MeCN in $CDCl_3$.

5.7.10 Attempting Synthesis of [3]Rotaxane 5.5

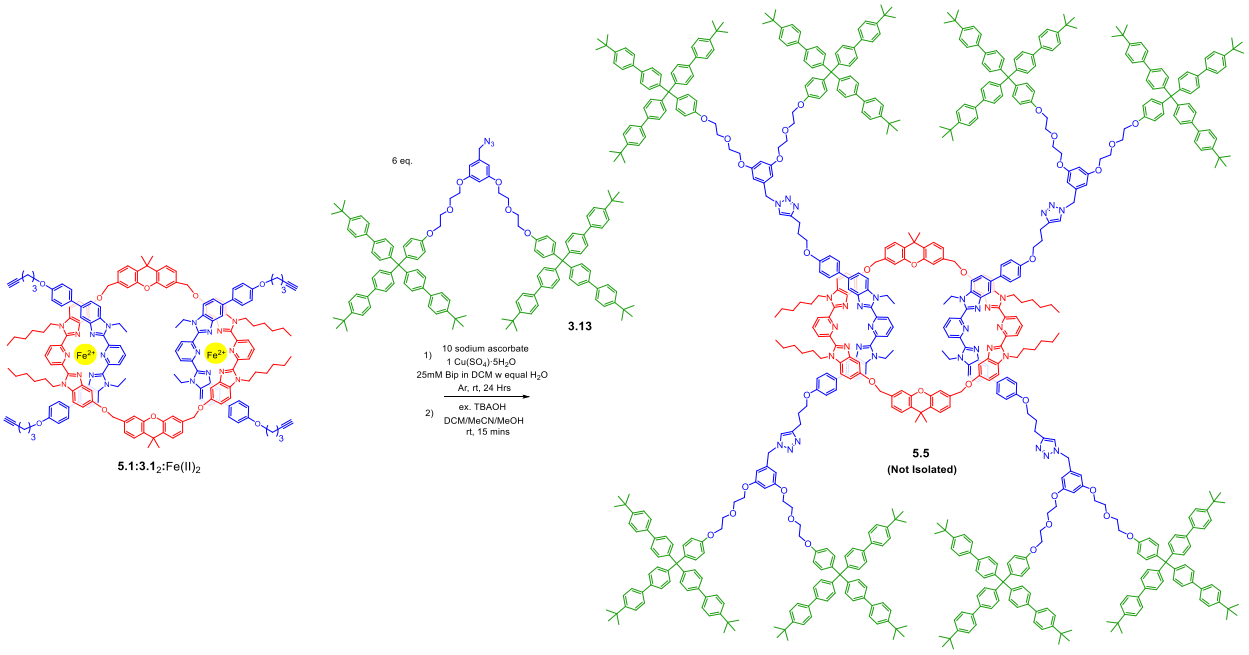

5.1:3.2$_2$:Fe(II)$_2$ (11.0 mg, 0.0027 mmol), **3.13** (28.6 mg, 0.016 mmol, 6eq) and sodium ascorbate (5.2 mg, 0.027 mmol, 10 eq) were added to a 4mL glass vial purged with Ar. To this mixture was added CH_2Cl_2 (0.43 mL, conc of alkyne = 25 mM), H_2O (0.33 mL), and 100µL of an aqueous stock solution of $Cu(SO_4)\cdot 5H_2O$ (27mM, 0.0027mmol, 1eq, (25mol% per alkyne)). The reaction was stirred vigorously for 18 h at RT. The reaction mixture was then diluted with CH_2Cl_2 and H_2O (5 mL each). The organic layer was collected and washed with H_2O (2 × 5 mL). Removal of organic solvent resulted in a purple solid that was washed 3x with 5mL of 10% chloroform in hexanes to help remove leftover stopper group. The crude purple solid was redissolved in 3mL of 50:50 dichloromethane and acetonitrile and stirred slowly at room temperature. 0.5mL of tetrabutylammonium hydroxide solution (1M in MeOH) was added dropwise to the stirring solution resulting in a rapid color change from purple to light brown and precipitation of demetallated product. After 15 minutes of stirring, an off-white solid was filtered off and washed

with methanol (2x 10mL). The frit was then washed with 2mL of $CDCl_3$ to redissolve the demetallated product and analyzed immediately via 1H-NMR spectroscopy and MALDI-TOF mass spectrometry.

5.7.11 Synthesis of [3]Rotaxane 5.6

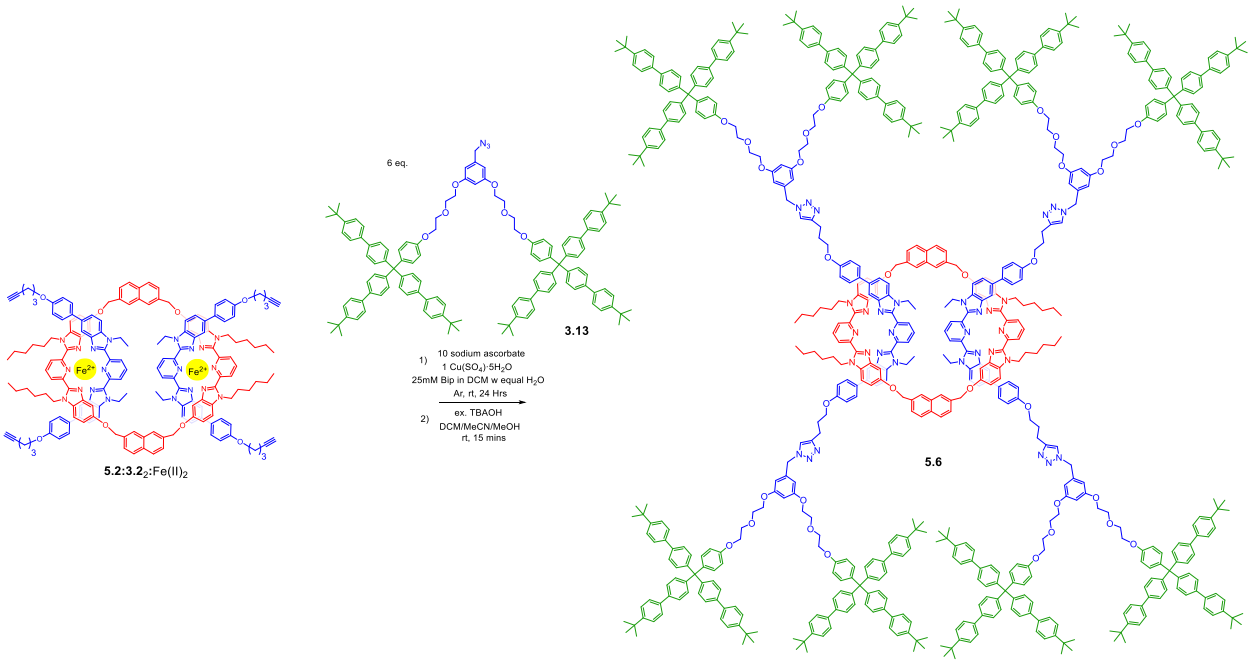

5.2:3.2$_2$:Fe(II)$_2$ (20.0 mg, 0.0051 mmol), **3.13** (54.2 mg, 0.030 mmol, 6eq) and sodium ascorbate (10.1 mg, 0.051 mmol, 10 eq) were added to a 4mL glass vial purged with Ar. To this mixture was added CH_2Cl_2 (0.82 mL, conc of alkyne = 25 mM), H_2O (0.72 mL), and 100µL of an aqueous stock solution of $Cu(SO_4)\cdot 5H_2O$ (51mM, 0.0051mmol, 1eq, (25mol% per alkyne)). The reaction was stirred vigorously for 18 h at RT. The reaction mixture was then diluted with CH_2Cl_2 and H_2O (5 mL each). The organic layer was collected and washed with H_2O (2 × 5 mL). Removal of organic solvent resulted in a purple solid that was washed 3x with 5mL of 10% chloroform in hexanes to help remove leftover stopper group. The crude purple solid was redissolved in 5mL of 50:50 dichloromethane and acetonitrile and stirred slowly at room temperature. 1mL of

tetrabutylammonium hydroxide solution (1M in MeOH) was added dropwise to the stirring solution resulting in a rapid color change from purple to light brown and precipitation of demetallated product. After 15 minutes of stirring, an off-white solid was filtered off and washed with methanol (2x 10mL). The frit was then washed with 5mL of $CHCl_3$ to redissolve the demetallated product and washed once with 5mL water. Solvent was removed under reduced pressure resulting in an off-white residue. Purification of **5.6** was achieved using preparative thin layer chromatography (SiO_2, eluent = 94:6 $CHCl_3$:MeOH, lowest Rf band taken (R_f=0.1-0.3) as [3]R product, macrocycle byproduct R_f=0.4, dumbbell byproduct R_f=0.65-0.75) followed by precipitation from cold methanol to result in an off-white solid, **5.6** in 75% isolated yield (37.4 mg). ^{1}H NMR (500 MHz, $CDCl_3$) ^{1}H NMR (500 MHz, $CDCl_3$) δ 8.25 (d, *J* = 7.8Hz, 4H), 7.98 (d, *J* = 7.8Hz, 4H), 7.91 (s, 4H), 7.85 (t, *J* = 7.9Hz, 2H), 7.67 (t, *J* = 7.9Hz, 2H), 7.63 (d, *J* = 8.5Hz, 4H), 7.55-7.45 (m, 108H), 7.42 (d, *J* = 8.5Hz, 48H), 7.37 (d, *J* = 8.6 Hz, 8H), 7.31-7.28 (m, 52H), 7.21-7.15 (m, 20H), 6.84-6.70 (m, 28H), 6.66 (d, *J* = 8.6 Hz, 8H), 6.47 (bs, 4H), 6.34 (bd, 8H), 5.29 (bs, 4H), 5.15 (s, 4H), 4.62 (bq, *J* = 7.2 Hz, 8H), 4.30 (bt, 8H) 4.12-4.00 (m, 32H), 3.88-3.76 (m, 32H), 3.58 (bt, 8H), 2.47 (bt, 8H), 1.70 (bt, 8H), 1.36 (m, 8H), 1.33 (s, 216H), 1.18 (t, *J* = 7.2Hz, 12H), 0.89 -0.69 (m, 24H), 0.50 (t, *J* = 7.0Hz, 12H). MALDI-MS: 9,782.5 ([M]+H^+), 5,554.3 ([M]+H^+-DB(**3.16**)), 4,226.9 ([M]+H^+-MC(**5.2**)-DB(**3.16**)).

5.7.12 Synthesis of [3]Rotaxane 5.7

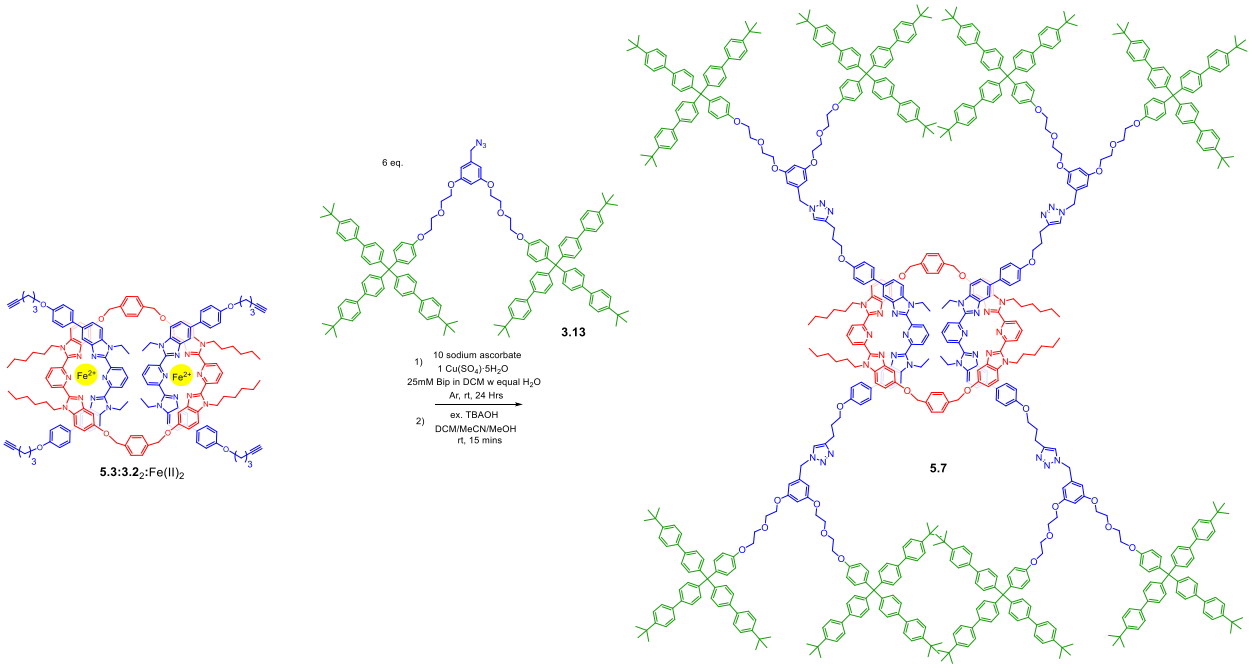

5.3:3.2$_2$:Fe(II)$_2$ (18.2 mg, 0.0047 mmol), **3.13** (50.1 mg, 0.029 mmol, 6eq) and sodium ascorbate (9.3 mg, 0.047 mmol, 10 eq) were added to a 4mL glass vial purged with Ar. To this mixture was added CH_2Cl_2 (0.76 mL, conc of alkyne = 25 mM), H_2O (0.66 mL), and 100µL of an aqueous stock solution of $Cu(SO_4)\cdot 5H_2O$ (51mM, 0.0051mmol, 1eq, (25mol% per alkyne)). The reaction was stirred vigorously for 18 h at RT. The reaction mixture was then diluted with CH_2Cl_2 and H_2O (5 mL each). The organic layer was collected and washed with H_2O (2 × 5 mL). Removal of organic solvent resulted in a purple solid that was washed 3x with 5mL of 10% chloroform in hexanes to help remove leftover stopper group. The crude purple solid was redissolved in 5mL of 50:50 dichloromethane and acetonitrile and stirred slowly at room temperature. 1mL of tetrabutylammonium hydroxide solution (1M in MeOH) was added dropwise to the stirring solution resulting in a rapid color change from purple to light brown and precipitation of demetallated product. After 15 minutes of stirring, an off-white solid was filtered off and washed

with methanol (2x 10mL). The frit was then washed with 5mL of $CHCl_3$ to redissolve the demetallated product and washed once with 5mL water. Solvent was removed under reduced pressure resulting in an off-white residue. Purification of **5.7** was achieved using preparative thin layer chromatography (SiO_2, eluent = 94:6 $CHCl_3$:MeOH, lowest Rf band taken (R_f=0.1-0.3) as [3]R product, macrocycle byproduct R_f=0.4, dumbbell byproduct R_f=0.65-0.75) followed by precipitation from cold methanol to result in an off-white solid, **5.7** in 74% isolated yield. ^{1}H NMR (500 MHz, $CDCl_3$) δ 8.28 (d, *J* = 7.8Hz, 4H), 7.92 (d, *J* = 7.8Hz, 4H), 7.90-7.84 (m, 6H), 7.56-7.44 (m, 106H), 7.42 (d, *J* = 8.5 Hz, 48H), 7.32-7.28 (m, 56H), 7.22-7.18 (m, 28H), 6.98 (s, 4H), 6.81 (d, *J* = 8.9 Hz, 16H), 6.76-6.70 (m, 8H), 6.53 (d, *J* = 8.2 Hz, 8H), 6.48 (bs, 4H), 6.41 (bd, *J* = 2.0 Hz, 8H), 5.25 (bs, 4H), 5.14 (bs, 4H), 4.71 (bq, 8H), 4.25 (bt, 8H), 4.12-4.02 (m, 32H), 3.89-3.79 (m, 32H), 3.53(bt, 8H), 2.49 (bt, 8H), 1.73 (bt, 8H), 1.36 (m, 8H), 1.33 (s, 216H), 1.26 (t, *J* = 7.2H, 12H), 0.90-0.70 (m, 24H), 0.47 (t, *J* = 6.9Hz, 12H). MALDI-MS: 9,682.1 ([M]+H^+), 5,455.8 ([M]+H^+-DB(**3.16**)), 4,226.8 ([M]+H^+-MC(**5.3**)-DB(**3.16**)).

5.7.13 Synthesis of [3]Rotaxane 5.8

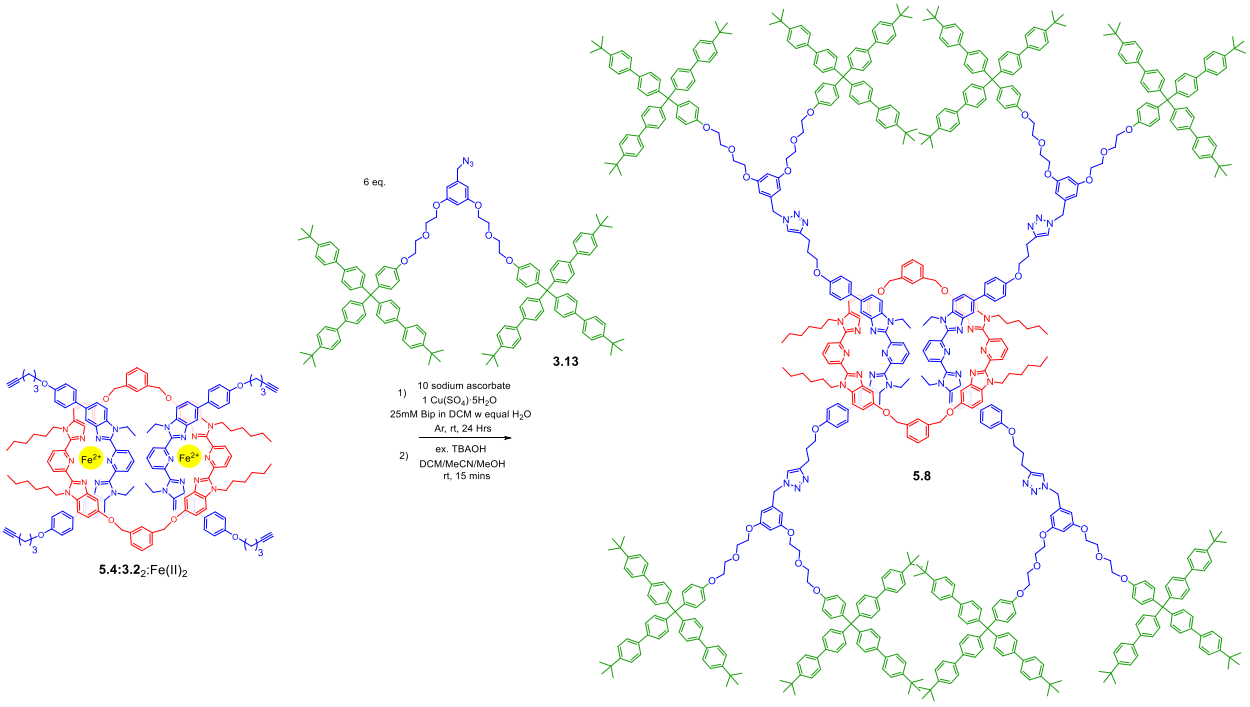

5.4:3.2$_2$:Fe(II)$_2$ (17.2 mg, 0.0044 mmol), **3.13** (49.1 mg, 0.026 mmol, 6eq) and sodium ascorbate (9.0 mg, 0.044 mmol, 10 eq) were added to a 4mL glass vial purged with Ar. To this mixture was added CH_2Cl_2 (0.68 mL, conc of alkyne = 25 mM), H_2O (0.56 mL), and 100μL of an aqueous stock solution of $Cu(SO_4)\cdot 5H_2O$ (44mM, 0.0044mmol, 1eq, (25mol% per alkyne)). The reaction was stirred vigorously for 18 h at RT. The reaction mixture was then diluted with CH_2Cl_2 and H_2O (5 mL each). The organic layer was collected and washed with H_2O (2 × 5 mL). Removal of organic solvent resulted in a purple solid that was washed 3x with 5mL of 10% chloroform in hexanes to help remove leftover stopper group. The crude purple solid was redissolved in 5mL of 50:50 dichloromethane and acetonitrile and stirred slowly at room temperature. 1mL of tetrabutylammonium hydroxide solution (1M in MeOH) was added dropwise to the stirring solution resulting in a rapid color change from purple to light brown and precipitation of demetallated product. After 15 minutes of stirring, an off-white solid was filtered off and washed with methanol (2x 10mL). The frit was then washed with 5mL of $CHCl_3$ to redissolve the demetallated product and washed once with 5mL water. Solvent was removed under reduced pressure resulting in an off-white residue. Purification of **5.7** was achieved using preparative thin layer chromatography (SiO_2, eluent = 94:6 $CHCl_3$:MeOH, lowest Rf band taken (R_f=0.1-0.3) as partially purified [3]rotaxane product.

5.7.14 Kinetic Slippage Experimental Details

The same procedure was done for both [3]rotaxanes **5.6** and **5.7**. A 1mM sample of fresh [3]rotaxane was prepared in a 5 mm Bruker Shigemi NMR tube. This tube was placed in an oil bath at 35°C and the ^{1}H-NMR spectrum was recorded after 2 days, 4 days, 5 days, and 7 days. The tube was then heated to 40°C and the same ^{1}H-NMR acquisition process was repeated. The tube was then heated to 45°C and the same ^{1}H-NMR acquisition process was repeated. In total, the

[3]rotaxane was heated for three weeks. This process was repeated once for both rotaxanes. The resulting kinetic data was analyzed according to the following method. The downfield doublet corresponding to the proton labeled B in the dumbbell of the [3]rotaxane (Fig 5.22) was used to determine the amount of [3]R left in each sample as the shift between free and interlocked species was diagnostic and clean of other peaks. The free B doublet is in the region 8.34-8.38ppm and the interlocked B doublet is in the region 8.24-8.26ppm. Let C_0 be the initial concentration of [3]rotaxane and C be the concentration of [3]rotaxane at timepoint *t*. The absolute integral intensity of B that is interlocked ($I_{3[R]}$) divided by the sum of the absolute integral intensities of B that is free and interlocked ($I_{DB} + I_{3[R]}$) multiplied by 100% gives the percent of [3]R remaining in the sample. Dividing this percent rotaxane remaining by the initial rotaxane percent present is equivalent to C/C_0 for each timepoint of slippage. Following first-order kinetics and standard Eyring/Arrhenius methods the thermodynamic and kinetic parameters were determined. See Fig 5.42 for example of ^{1}H-NMR integrations and Fig 5.43-5.44 for additional slippage trials.

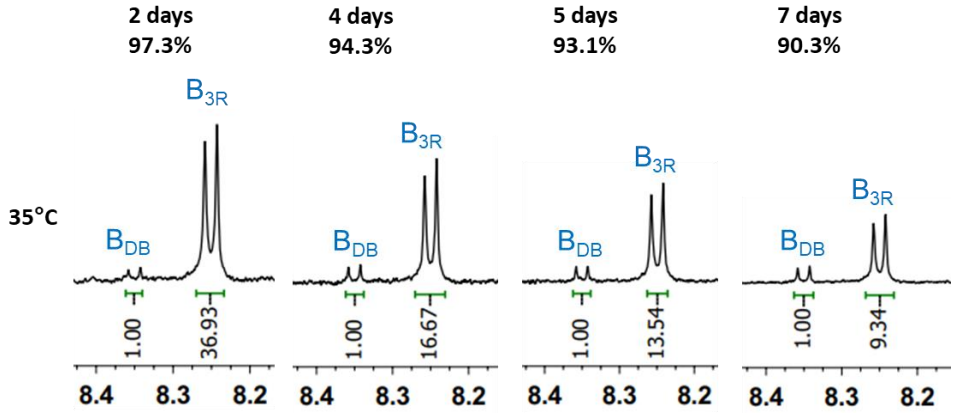

Fig 5.42 Example of integral calculations involved with ^{1}H-NMR analysis of week 1 of trial 1 of slippage experiments of **5.6.**

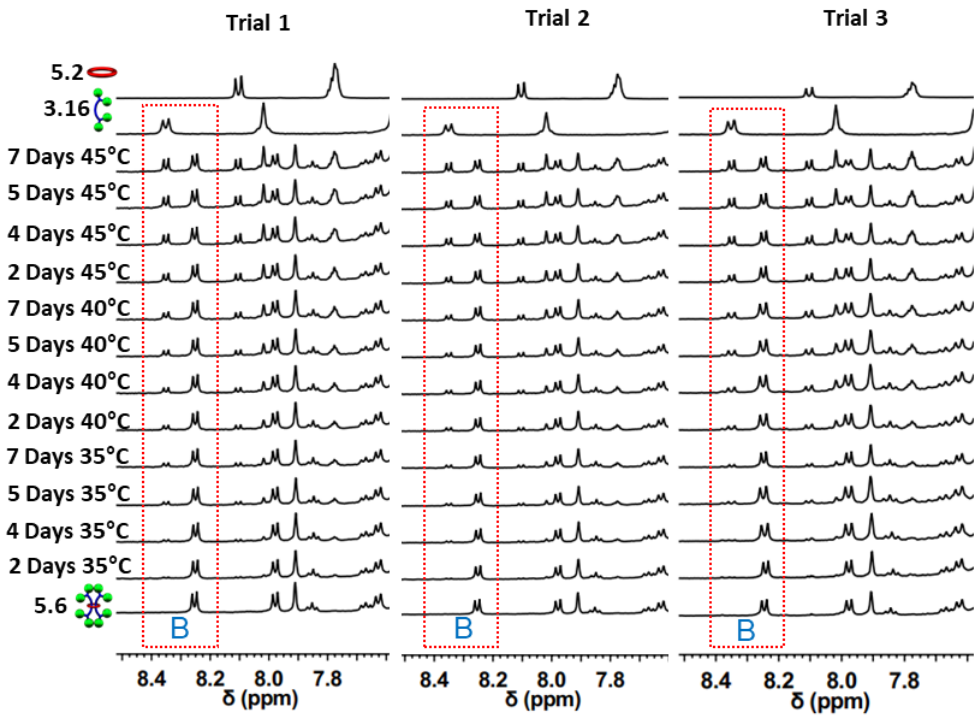

Fig 5.43 Partial ^{1}H-NMR overlay (1mM, 500 MHz, $CDCl_3$, 25°C) of 3 trials of 3-week kinetic slippage experiments of **5.6**. Time and temperature between measurements indicated on left side. Diagnostic meta-pyridinyl dumbbell peak area outlined in red box.

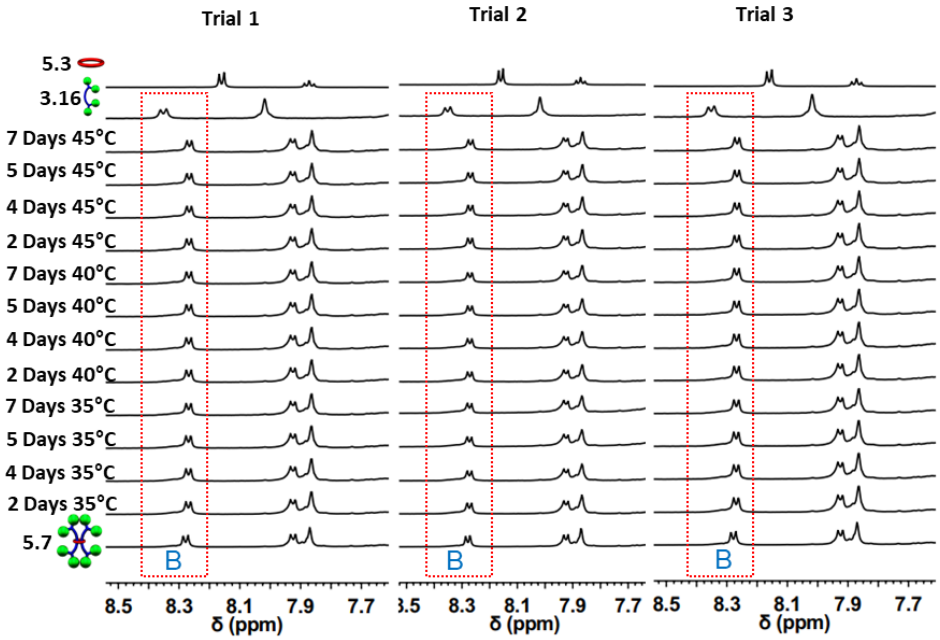

Fig 5.44 Partial ^{1}H-NMR overlay (1mM, 500 MHz, $CDCl_3$, 25°C) of 3 trials of 3-week kinetic slippage experiments of **5.7**. Time and temperature between measurements indicated on left side. Diagnostic meta-pyridinyl dumbbell peak area outlined in red box.

5.8 References

(1) Stoddart, J. F. The Chemistry of the Mechanical Bond. *Chem. Soc. Rev.* **2009**, *38* (6), 1802–1820. https://doi.org/10.1039/b819333a.

(2) Lewis, J. E. M.; Galli, M.; Goldup, S. M. Properties and Emerging Applications of Mechanically Interlocked Ligands. *Chem. Commun.* **2017**, *53* (2), 298–312. https://doi.org/10.1039/C6CC07377H.

(3) Jamieson, E. M. G.; Modicom, F.; Goldup, S. M. Chirality in Rotaxanes and Catenanes. *Chem. Soc. Rev.* **2018**, *47* (14), 5266–5311. https://doi.org/10.1039/c8cs00097b.

(4) Cotí, K. K.; Belowich, M. E.; Liong, M.; Ambrogio, M. W.; Lau, Y. A.; Khatib, H. A.; Zink, J. I.; Khashab, N. M.; Stoddart, J. F. Mechanised Nanoparticles for Drug Delivery. *Nanoscale* **2009**, *1* (1), 16. https://doi.org/10.1039/b9nr00162j.

(5) Tamura, A.; Yui, N. Threaded Macromolecules as a Versatile Framework for Biomaterials. *Chem. Commun.* **2014**, *50* (88), 13433–13446. https://doi.org/10.1039/C4CC03709J.

(6) Davis, J. J.; Orlowski, G. A.; Rahman, H.; Beer, P. D. Mechanically Interlocked and Switchable Molecules at Surfaces. *Chem. Commun.* **2010**, *46* (1), 54–63. https://doi.org/10.1039/b915122b.

(7) Takata, T. Switchable Polymer Materials Controlled by Rotaxane Macromolecular Switches. *ACS Cent. Sci.* **2020**, *6* (2), 129–143. https://doi.org/10.1021/acscentsci.0c00002.

(8) Erbas-Cakmak, S.; Leigh, D. A.; McTernan, C. T.; Nussbaumer, A. L. Artificial Molecular Machines. *Chem. Rev.* **2015**, *115* (18), 10081–10206. https://doi.org/10.1021/acs.chemrev.5b00146.

(9) Bruns, C. J.; Stoddart, J. F. *The Nature of the Mechanical Bond: From Molecules to Machines*; Wiley: Hoboken, NJ, 2016. https://doi.org/10.1002/9781119044123.

(10) Van Dongen, S. F. M.; Cantekin, S.; Elemans, J. A. A. W.; Rowan, A. E.; Nolte, R. J. M. Functional Interlocked Systems. *Chemical Society Reviews*. 2014. https://doi.org/10.1039/c3cs60178a.

(11) Sluysmans, D.; Stoddart, J. F. The Burgeoning of Mechanically Interlocked Molecules in Chemistry. *Trends Chem.* **2019**, *1* (2), 185–197. https://doi.org/10.1016/j.trechm.2019.02.013.

(12) Sauvage, J.-P. From Chemical Topology to Molecular Machines (Nobel Lecture). *Angew. Chemie - Int. Ed.* **2017**, *56* (37), 11080–11093. https://doi.org/10.1002/anie.201702992.

(13) Feringa, B. L. The Art of Building Small: From Molecular Switches to Motors (Nobel Lecture). *Angew. Chemie Int. Ed.* **2017**, *56* (37), 11060–11078. https://doi.org/10.1002/anie.201702979.

(14) Stoddart, J. F. Mechanically Interlocked Molecules (MIMs)-Molecular Shuttles, Switches,

and Machines (Nobel Lecture). *Angew. Chemie Int. Ed.* **2017**, *56* (37), 11094–11125. https://doi.org/10.1002/anie.201703216.

(15) Kay, E. R.; Leigh, D. A.; Zerbetto, F. *Synthetic Molecular Motors and Mechanical Machines*; 2007; Vol. 46. https://doi.org/10.1002/anie.200504313.

(16) Harrison, I. T.; Harrison, S. Synthesis of a Stable Complex of a Macrocycle and a Threaded Chain. *J. Am. Chem. Soc.* **1967**, *89* (22), 5723–5724. https://doi.org/10.1021/ja00998a052.

(17) Xue, M.; Yang, Y.; Chi, X.; Yan, X.; Huang, F. Development of Pseudorotaxanes and Rotaxanes: From Synthesis to Stimuli-Responsive Motions to Applications. *Chem. Rev.* **2015**, *115* (15), 7398–7501. https://doi.org/10.1021/cr5005869.

(18) Raymo, F. M.; Houk, K. N.; Stoddart, J. F. The Mechanism of the Slippage Approach to Rotaxanes. Origin of the "all- or-Nothing" Substituent Effect. *J. Am. Chem. Soc.* **1998**, *120* (36), 9318–9322. https://doi.org/10.1021/ja9806229.

(19) Affeld, A.; Hühner, G. M.; Seel, C.; Schalley, C. A. Rotaxane or Pseudorotaxane? Effects of Small Structural Variations on the Deslipping Kinetics of Rotaxanes with Stopper Groups of Intermediate Size. *European J. Org. Chem.* **2001**, No. 15, 2877–2890. https://doi.org/10.1002/1099-0690(200108)2001:15<2877::AID-EJOC2877>3.0.CO;2-R.

(20) Heim, C.; Affeld, A.; Nieger, M.; Vögtle, F. Size Complementarity of Macrocyclic Cavities and Stoppers in Amide- Rotaxanes. *Helv. Chim. Acta* **1999**, *82* (5), 746–759. https://doi.org/10.1002/(SICI)1522-2675(19990505)82:5<746::AID-HLCA746>3.0.CO;2-C.

(21) Mock, W. L.; Pierpont, J. A Cucurbituril-Based Molecular Switch. *J. Chem. Soc. Chem. Commun.* **1990**, No. 21, 1509–1511. https://doi.org/10.1039/C39900001509.

(22) Im Jun, S.; Wook Lee, J.; Sakamoto, S.; Yamaguchi, K.; Kim, K. Rotaxane-Based Molecular Switch with Fluorescence Signaling. *Tetrahedron Lett.* **2000**, *41* (4), 471–475. https://doi.org/10.1016/S0040-4039(99)02094-8.

(23) Abe, Y.; Okamura, H.; Nakazono, K.; Koyama, Y.; Uchida, S.; Takata, T. Thermoresponsive Shuttling of Rotaxane Containing Trichloroacetate Ion. *Org. Lett.* **2012**, *14* (16), 4122–4125. https://doi.org/10.1021/ol301771w.

(24) Wang, Y.; Wang, J.; Li, G. X.; He, G.; Chen, G. Halogen-Bond-Promoted Photoactivation of Perfluoroalkyl Iodides: A Photochemical Protocol for Perfluoroalkylation Reactions. *Org. Lett.* **2017**, *19* (6), 1442–1445. https://doi.org/10.1021/acs.orglett.7b00375.

(25) Zhou, H. Y.; Han, Y.; Chen, C. F. PH-Controlled Motions in Mechanically Interlocked Molecules. *Mater. Chem. Front.* **2020**, *4* (1), 12–28. https://doi.org/10.1039/c9qm00546c.

(26) Dattler, D.; Fuks, G.; Heiser, J.; Moulin, E.; Perrot, A.; Yao, X.; Giuseppone, N. Design of Collective Motions from Synthetic Molecular Switches, Rotors, and Motors. *Chem. Rev.* **2020**, *120* (1), 310–433. https://doi.org/10.1021/acs.chemrev.9b00288.

(27) Harrison, I. T. The Effect of Ring Size on Threading Reactions of Macrocycles. *J. Chem. Soc. Chem. Commun.* **1972**, *0* (4), 231–232. https://doi.org/10.1039/C39720000231.

(28) Hirose, K.; Ishibashi, K.; Shiba, Y.; Doi, Y.; Tobe, Y. Control of Rocking Mobility of Rotaxanes by Size Change of Stimulus-Responsive Ring Components. *Chem. Lett.* **2007**, *36* (6), 810–811. https://doi.org/10.1246/cl.2007.810.

(29) Dasgupta, S.; Wu, J. Formation of [2]Rotaxanes by Encircling [20], [21] and [22]Crown Ethers onto the Dibenzylammonium Dumbbell. *Chem. Sci.* **2012**, *3* (2), 425–432. https://doi.org/10.1039/c1sc00613d.

(30) Sugino, H.; Kawai, H.; Umehara, T.; Fujiwara, K.; Suzuki, T. Effects of Axle-Core, Macrocycle, and Side-Station Structures on the Threading and Hydrolysis Processes of Imine-Bridged Rotaxanes. *Chem. - A Eur. J.* **2012**, *18* (43), 13722–13732. https://doi.org/10.1002/chem.201200837.

(31) Tokunaga, Y.; Iwamoto, T.; Nakashima, S.; Shoji, E.; Nakata, R. Electrochemical Properties of 3,5-Diphenylaniline Units Encapsulated within a Crown Ether. Effects of the Macrocycle's Aromatic Functionality and Ring Size. *Tetrahedron Lett.* **2011**, *52* (2), 240–243. https://doi.org/10.1016/j.tetlet.2010.11.043.

(32) Zhu, K.; Baggi, G.; Loeb, S. J. Ring-through-Ring Molecular Shuttling in a Saturated [3]Rotaxane. *Nat. Chem.* **2018**, *10* (6), 625–630. https://doi.org/10.1038/s41557-018-0040-9.

(33) Soto, M. A.; Lelj, F.; MacLachlan, M. J. Programming Permanent and Transient Molecular Protection: Via Mechanical Stoppering. *Chem. Sci.* **2019**, *10* (44), 10422–10427. https://doi.org/10.1039/c9sc03744f.

(34) Naito, M.; Fujino, T.; Tajima, S.; Miyagawa, S.; Yoshida, K.; Inoue, H.; Takagawa, H.; Kawasaki, T.; Tokunaga, Y. Ring Size Affects the Kinetic and Thermodynamic Formation of [2]Rotaxanes Featuring an Unsymmetric Bis-Crown Ether Component. *Mater. Chem. Front.* **2019**, *3* (12), 2702–2706. https://doi.org/10.1039/c9qm00441f.

(35) Hoshino, S.; Ono, K.; Kawai, H. Ring-Over-Ring Deslipping From Imine-Bridged Heterorotaxanes. *Front. Chem.* **2022**, *10* (May), 1–10. https://doi.org/10.3389/fchem.2022.885939.

(36) Gaedke, M.; Hupatz, H.; Witte, F.; Rupf, S. M.; Douglas, C.; Schröder, H. V.; Fischer, L.; Malischewski, M.; Paulus, B.; Schalley, C. A. Sequence-Sorted Redox-Switchable Hetero[3]Rotaxanes. *Org. Chem. Front.* **2022**, *9* (1), 64–74. https://doi.org/10.1039/d1qo01553b.

(37) Zhou, H. Y.; Zong, Q. S.; Han, Y.; Chen, C. F. Recent Advances in Higher Order Rotaxane Architectures. *Chem. Commun.* **2020**, *56* (69), 9916–9936. https://doi.org/10.1039/d0cc03057k.

(38) McGonigal, P. R. Multiply Threaded Rotaxanes. *Supramol. Chem.* **2018**, *30* (9), 782–794. https://doi.org/10.1080/10610278.2018.1433832.

(39) Mena-Hernando, S.; Pérez, E. M. Mechanically Interlocked Materials. Rotaxanes and Catenanes beyond the Small Molecule. *Chem. Soc. Rev.* **2019**, *48* (19), 5016–5032. https://doi.org/10.1039/C8CS00888D.

(40) Hart, L. F.; Hertzog, J. E.; Rauscher, P. M.; Rawe, B. W.; Tranquilli, M. M.; Rowan, S. J.

Material Properties and Applications of Mechanically Interlocked Polymers. *Nat. Rev. Mater.* **2021**, *6*, 508–530. https://doi.org/10.1038/s41578-021-00278-z.

(41) Danon, J. J.; Leigh, D. A.; McGonigal, P. R.; Ward, J. W.; Wu, J. Triply Threaded [4]Rotaxanes. *J. Am. Chem. Soc.* **2016**, *138* (38), 12643–12647. https://doi.org/10.1021/jacs.6b07733.

(42) Hayashi, R.; Mutoh, Y.; Kasama, T.; Saito, S. Synthesis of [3]Rotaxanes by the Combination of Copper-Mediated Coupling Reaction and Metal-Template Approach. *J. Org. Chem.* **2015**, *80* (15), 7536–7546. https://doi.org/10.1021/acs.joc.5b01120.

(43) Movsisyan, L. D.; Franz, M.; Hampel, F.; Thompson, A. L.; Tykwinski, R. R.; Anderson, H. L. Polyyne Rotaxanes: Stabilization by Encapsulation. *J. Am. Chem. Soc.* **2016**, *138* (4), 1366–1376. https://doi.org/10.1021/jacs.5b12049.

(44) Hertzog, J. E.; Maddi, V. J.; Hart, L. F.; Rawe, B. W.; Rauscher, P. M.; Herbert, K. M.; Bruckner, E. P.; de Pablo, J. J.; Rowan, S. J. Metastable Doubly Threaded [3]Rotaxanes with a Large Macrocycle. *Chem. Sci.* **2022**, 5333–5344. https://doi.org/10.1039/d2sc01486f.

(45) McKenzie, B. M.; Miller, A. K.; Wojtecki, R. J.; Johnson, J. C.; Burke, K. A.; Tzeng, K. A.; Mather, P. T.; Rowan, S. J. Improved Synthesis of Functionalized Mesogenic 2,6-Bisbenzimidazolylpyridine Ligands. *Tetrahedron* **2008**, *64* (36), 8488–8495. https://doi.org/10.1016/j.tet.2008.05.075.

(46) Cheng, H. M.; Leigh, D. A.; Maffei, F.; McGonigal, P. R.; Slawin, A. M. Z.; Wu, J. En Route to a Molecular Sheaf: Active Metal Template Synthesis of a [3]Rotaxane with Two Axles Threaded through One Ring. *J. Am. Chem. Soc.* **2011**, *133* (31), 12298–12303. https://doi.org/10.1021/ja205167e.

(47) Wojtecki, R. J.; Wu, Q.; Johnson, J. C.; Ray, D. G.; Korley, L. S. T. J.; Rowan, S. J. Optimizing the Formation of 2,6-Bis(N-Alkyl-Benzimidazolyl)Pyridine-Containing [3]Catenates through Component Design. *Chem. Sci.* **2013**, *4* (12), 4440–4448. https://doi.org/10.1039/c3sc52082j.

(48) Wu, Q.; Rauscher, P. M.; Lang, X.; Wojtecki, R. J.; De Pablo, J. J.; Hore, M. J. A.; Rowan, S. J. Poly[n]Catenanes: Synthesis of Molecular Interlocked Chains. *Science (80-.).* **2017**, *358* (6369), 1434–1439. https://doi.org/10.1126/science.aap7675.

(49) Kırpık, H.; Kose, M.; Ballı, J. N. Tridentate Benzimidazole Ligand and Its Metal Complexes: Synthesis, Characterization, Photo Physical and Sensor Properties. *Appl. Organomet. Chem.* **2020**, *34* (12), 1–11. https://doi.org/10.1002/aoc.5992.

(50) Deligkiozi, I.; Papadakis, R.; Tsolomitis, A. Synthesis, Characterisation and Photoswitchability of a New [2]Rotaxane of α-Cyclodextrin with a Diazobenzene Containing π-Conjugated Molecular Dumbbell. *Supramol. Chem.* **2012**, *24* (5), 333–343. https://doi.org/10.1080/10610278.2012.660529.

(51) Park, J.; Koh, J. The Synthesis and Spectral Properties of an Encapsulated Aminoazobenzene Dye. *Dye. Pigment.* **2009**, *82* (3), 347–352. https://doi.org/10.1016/j.dyepig.2009.02.005.

(52) Milan, D. C.; Krempe, M.; Ismael, A. K.; Movsisyan, L. D.; Franz, M.; Grace, I.; Brooke, R. J.; Schwarzacher, W.; Higgins, S. J.; Anderson, H. L.; Lambert, C. J.; Tykwinski, R. R.; Nichols, R. J. The Single-Molecule Electrical Conductance of a Rotaxane-Hexayne Supramolecular Assembly. *Nanoscale* **2017**, *9* (1), 355–361. https://doi.org/10.1039/c6nr06355a.

(53) Fu, N.; Baumes, J. M.; Arunkumar, E.; Noll, B. C.; Smith, B. D. Squaraine Rotaxanes with Boat Conformation Macrocycles. *J. Org. Chem.* **2009**, *74* (17), 6462–6468. https://doi.org/10.1021/jo901298n.

(54) Mayumi, K.; Ito, K.; Kato, K. *Polyrotaxane and Slide-Ring Materials*; Monographs in Supramolecular Chemistry; Royal Society of Chemistry: Cambridge, 2015.

(55) Frampton, M. J.; Anderson, H. L. Insulated Molecular Wires. *Angew. Chemie - Int. Ed.* **2007**, *46* (7), 1028–1064. https://doi.org/10.1002/anie.200601780.

(56) Belosludov, R. V.; Mizuseki, H.; Ichinoseki, K.; Kawazoe, Y. Theoretical Study on Inclusion Complex of Polyaniline Covered by Cyclodextrins for Molecular Device. *Jpn. J. Appl. Phys* **2002**, *41* (4 B), 2739–2741. https://doi.org/10.1143/JJAP.41.2739.

(57) Belosludov, R. V.; Sato, H.; Farajian, A. A.; Mizuseki, H.; Ichinoseki, K.; Kawazoe, Y. Molecular Enamel Wires for Electronic Devices: Theoretical Study. *Jpn. J. Appl. Phys.* **2003**, *42* (4 B), 2492–2494. https://doi.org/10.1143/jjap.42.2492.

(58) Sibi, M. P.; Petrovic, G. Enantioselective Radical Reactions: The Use of Metal Triflimides as Lewis Acids. *Tetrahedron Asymmetry* **2003**, *14* (19), 2879–2882. https://doi.org/10.1016/S0957-4166(03)00543-3.

Chapter 6: Initial Synthesis and Component Modifications of Doubly Threaded Poly[3]rotaxanes

6.1 Introduction

Mechanically interlocked polymers[1,2] such as polyrotaxanes[3,4] continue to attract widespread attention from chemists and engineers alike due to their unique wide range of applications including molecular wires[5,6], drug/gene delivery[7,8], glassy materials[9,10], biological targeting[11,12], molecular machines[13,14], their incorporation as a binder in batters[15], and more. All of the polyrotaxanes used in these applications are based on a singly threaded non-topological main-chain polyrotaxane framework (Fig 6.1a).

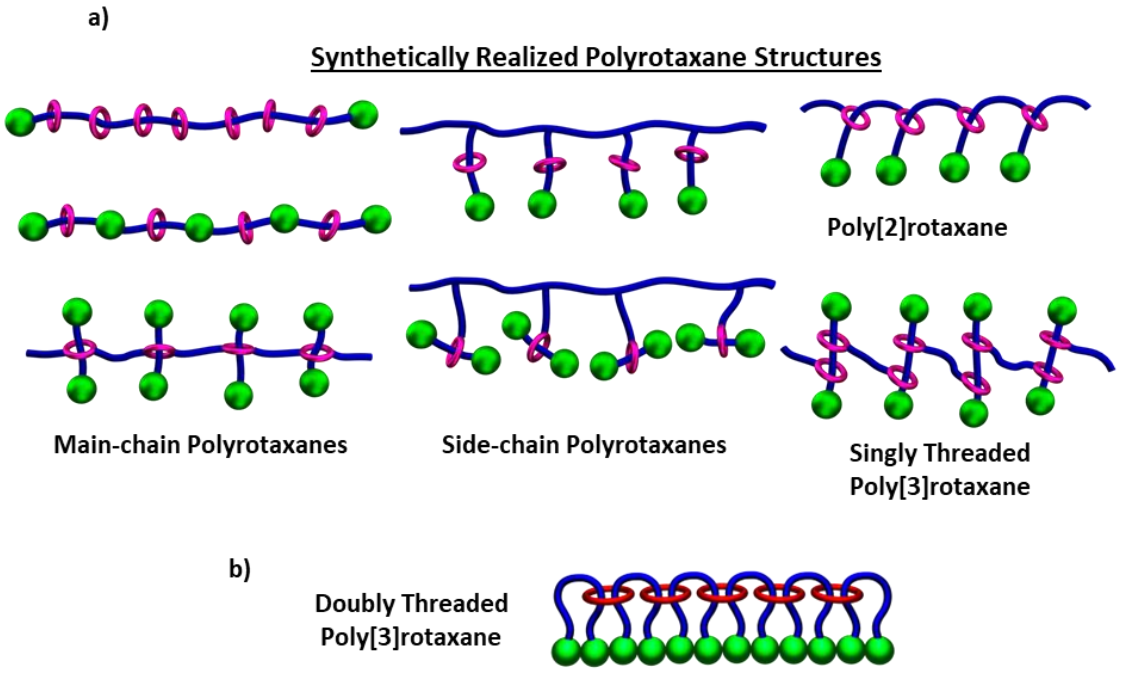

Fig 6.1 Cartoon representations of a) polyrotaxane architectures that have been synthetically made in some capacity and b) the doubly threaded poly[3]rotaxane architecture.

Following the same trend seen in molecular rotaxanes from simple singly threaded [2]rotaxane structures to higher order rotaxanes as the field has progressed[16–18], researchers are now imagining more intricate polyrotaxane structures. Towards this end, doubly threaded polyrotaxane structures have seen minimal synthetic success. Preliminary work has resulted in polymeric networks that do contain doubly threaded ring cross-links.[19–22] However, all of these examples are either held together by noncovalent interactions beyond the mechanical bond (i.e., metal-ligand coordination) or are effectively stoppered by the network architecture. Thus, the rings in these networks do not have free sliding mobility throughout the network. Developing true doubly threaded polyrotaxane materials that are stoppered by a molecular stopper group in the structure without any other noncovalent interactions holding the structure together would allow the rings to slide throughout the entire network making them very desirable from a materials standpoint. In addition, systematically changing the thread backbone by adding length (sliding distance), steric bulk, hydrogen bonding sites, or reactive chemistry sites along it will allow the unique doubly threaded nature of the polymers to be exploited.

Chapters 2-5 of this thesis involved a deep dive into the physical organic chemistry of the [3]rotaxane structure. Initial efforts focused on finding a suitable stoppering chemistry for the metal-bound Bip framework to work effectively. Once appropriate stoppering conditions had been determined, various aspects of the [3]rotaxane structure were systematically probed to determine how a fully stable [3]rotaxane could be realized. In particular, three different series of [3]rotaxanes that varied in stopper group size, stopper group arm length, and ring size were synthesized, characterized, and evaluated for slippage. These tests showed that ultimately macrocycle size was the key parameter examined and that a fully stable [3]rotaxane could be realized with a 42 atom ring or smaller using the Bip framework determined in this thesis. Bip has previously been used to

access metallo-supramolecular polymeric assemblies[23–28] as a framework to synthesize poly(n)catenanes[29,30]. The focus of this chapter is to translate the Bip [3]rotaxane motif developed in Chapters 2-5 to a doubly threaded poly[3]rotaxane framework using a similar metal-templated approach (Fig 6.2).

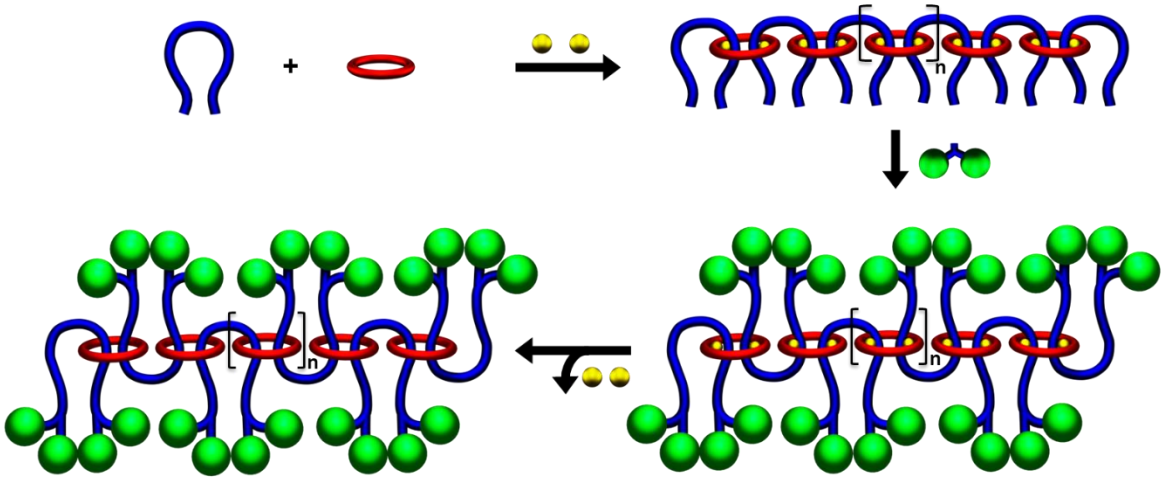

Fig 6.2 Cartoon schematic of proposed poly[3]rotaxane synthesis based on an MSP template.

The first step involves titration of 2 equivalents of metal ion to a 1:1 solution of ditopic macrocycle and ditopic thread to form an MSP. Stopper group is then added to the MSP followed by demetallation of the metal template to yield the proposed doubly threaded poly[3]rotaxane. This chapter will report preliminary studies on this synthesis and initial component modification of the poly[3]rotaxane structure.

6.2 Component Synthesis

In all of the metal-templated [3]rotaxane syntheses reported in Chapters 2-5, a monotopic Bip-derived thread component and ditopic macrocycle component were used to target a

pseudo[3]rotaxane assembly upon metalation. In order to attempt the proposed poly[3]rotaxane synthesis in Fig 6.2, a ditopic, Bip-containing, alkyne functionalized thread must be synthesized. Thus, the thread component **6.1** was synthesized in two steps (Fig 6.3).

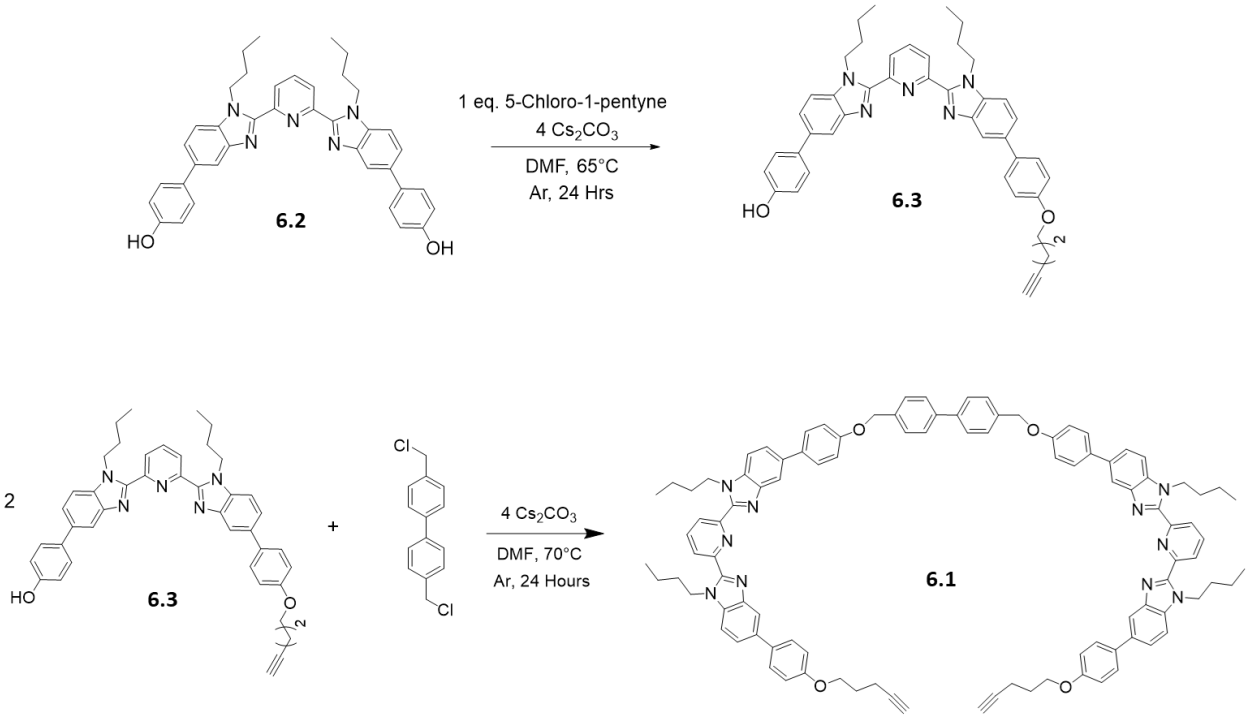

Fig 6.3 Scheme describing synthesis of ditopic thread component **6.1**.

In the first step, one side of the Bip ligand **6.2**[29,31] is functionalized with 5-chloro-1-pentyne to yield **6.3**. Next, the other side can be reacted twice with 4,4'-Bis(chloromethyl)-1-1'-biphenyl using standard Williamson Ether conditions to yield the thread **6.1** (See experimental for full synthetic details and characterization). The butyl functionalized Bip ligand is specifically chosen with this thread in order to aid the solubility of **6.1**. It is important to note that if the same second step is done with the ethyl Bip derivative (compound **3.5** described previously), an insoluble material is obtained.

In addition to **6.1**, another ditopic thread component **6.4** was synthesized containing a different polymeric (PEO M_n~2K) linker instead of the biphenyl linker (Fig 6.4).

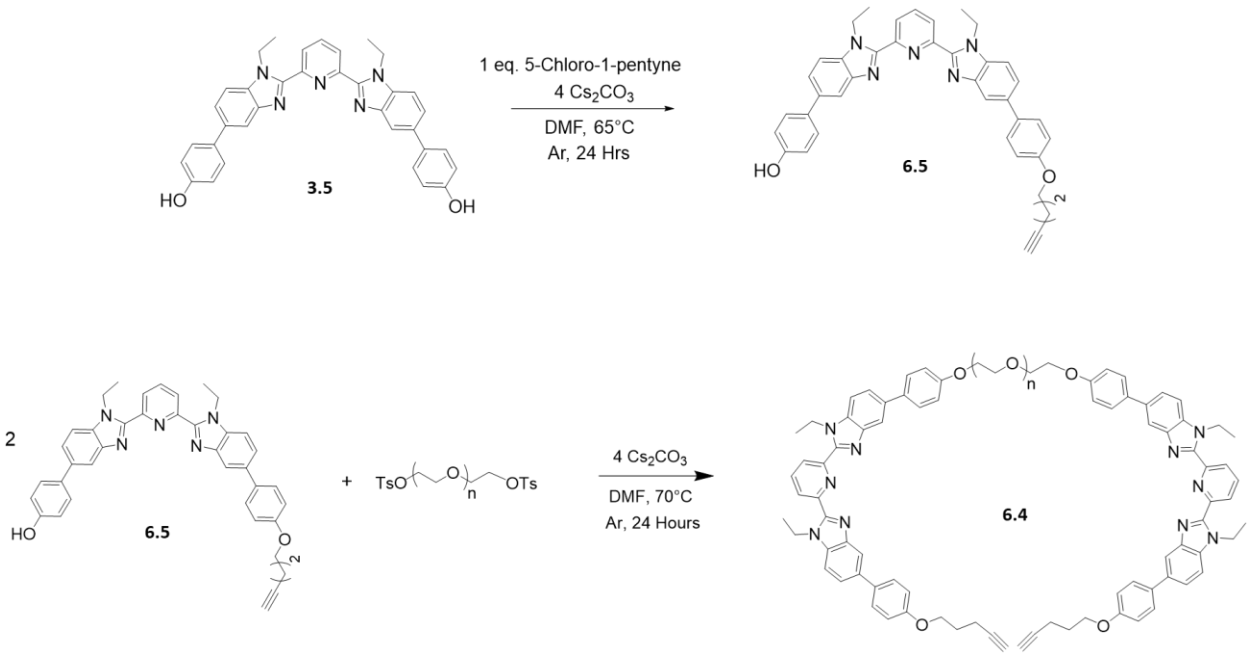

Fig 6.4 Scheme describing synthesis of ditopic thread component **6.4**.

In the first step, one side of the previously described ethyl Bip ligand **3.5** is functionalized with 5-chloro-1-pentyne to yield **6.5**. Next, the other side can be reacted twice with a ditosylated polyethylene glycol linker (Mn~2K, prepared via standard procedure[32] from commercially bought PEG) to yield **6.4** (See Experimental for full synthetic details). The structure of **6.4** was confirmed via MALDI-TOF mass spectrometry and ^{1}H-NMR analysis (Fig 6.5 and 6.6).

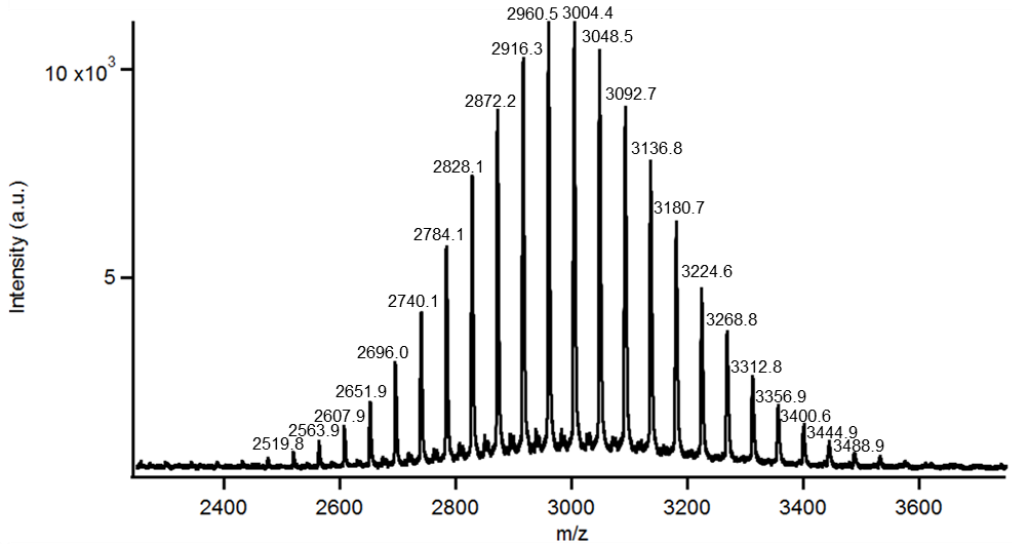

Fig 6.5 MALDI-TOF analysis (Dithranol, no salt) of the of the thread component **6.4**.

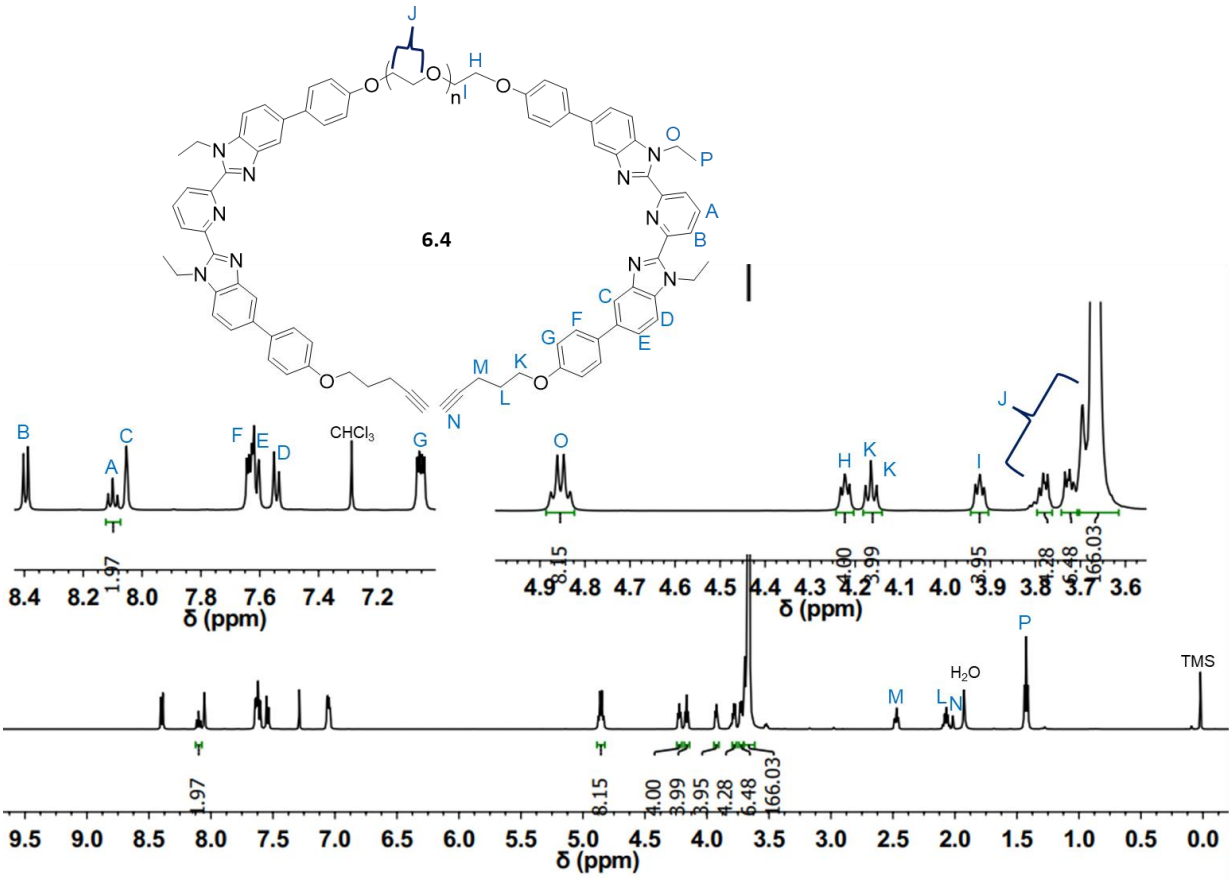

Fig 6.6 Full ^{1}H-NMR (500 MHz, 25°C, $CDCl_3$) of thread component **6.4**.

End-group analysis from the ^{1}H-NMR spectrum (Fig 6.6 integrals (176/4)) implies a DP of 44 and the MALDI-TOF implies a DP of 41 for the PEO segment of **6.4**. This is overall consistent with the slightly lower Mw estimation typical of MALDI-TOF vs ^{1}H-NMR analysis[33] and confirms the presence of a ~2K PEO linker in the ditopic thread component **6.4**.

6.3 Accessing a Metastable Poly[3]rotaxane With Ring 3.1

The first step towards synthesizing doubly threaded poly[3]rotaxane with the thread component **6.1** and ring **3.1** involves the formation of an alternating MSP **6.1**:**3.1**:$Fe(II)_2$ (Fig 6.7).

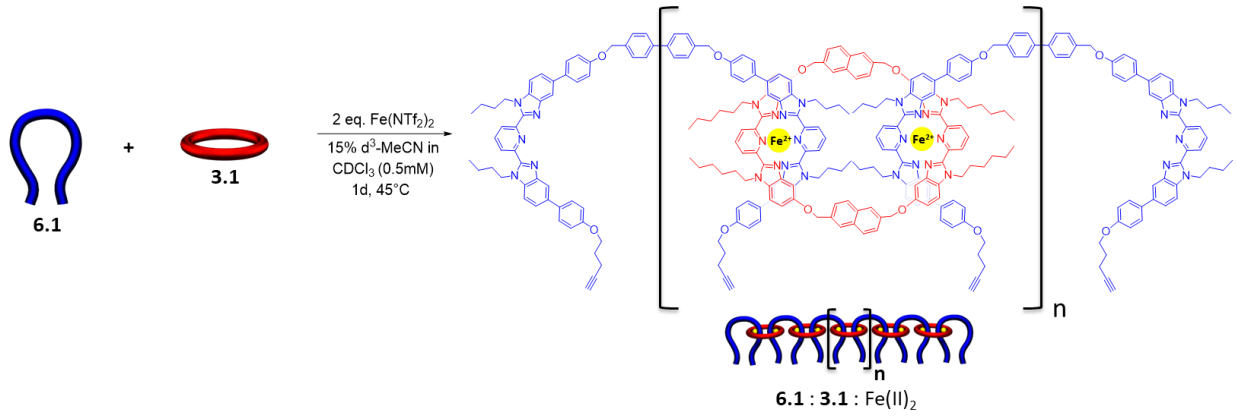

Fig 6.7 Scheme describing assembly of **6.1**:**3.1**:$Fe(II)_2$.

2 equivalents of Fe(II) are added to an exact 1:1 solution of **6.1**:**3.1** followed by a 1-day equilibration period at 45°C to form the MSP **6.1**:**3.1**:$Fe(II)_2$. The alternating polymer is the result of the principle of maximum occupancy[34] and exact stoichiometry used similar to the pseudo[3]rotaxanes formed in Chapter 2-5. As discussed and proven in Chapter 3, both bip ligands in **3.1** cannot self-bind to the same metal ion meaning that the only way for the system to maximize its enthalpic gain is the formation of the alternating MSP. Diagnostic broad downfield shifting of the pyridinyl protons closest to the metal-binding interaction is seen via ^{1}H-NMR spectroscopy upon metal addition (Fig 6.8).

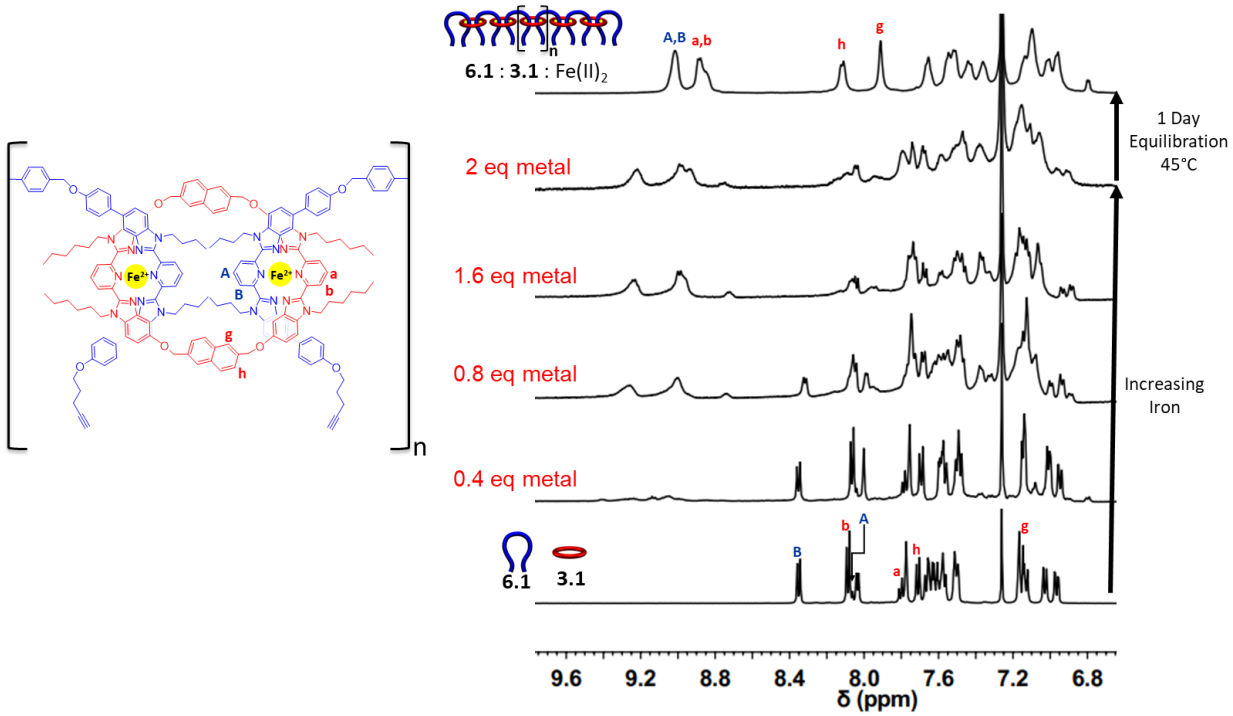

Fig 6.8 Partial ^{1}H-NMR overlay (500 MHz, 25°C, Solvent: 0, 3, 6, 12, 15, 15% d_3-MeCN in $CDCl_3$ increasing upwards) of metal addition and equilibration of 1:1 mixture of **6.1**:**3.1**.

This shifting has been well documented in Bip containing MSPs[24,29,30] and combined with this prior knowledge and comparison to the analogous pseudo[3]rotaxane **3.1**:**3.2**$_2$:Fe(II)$_2$, this shifting can be tentatively assigned (Fig 6.8-6.9) and confirms the successful formation of **6.1**:**3.1**:Fe(II)$_2$.

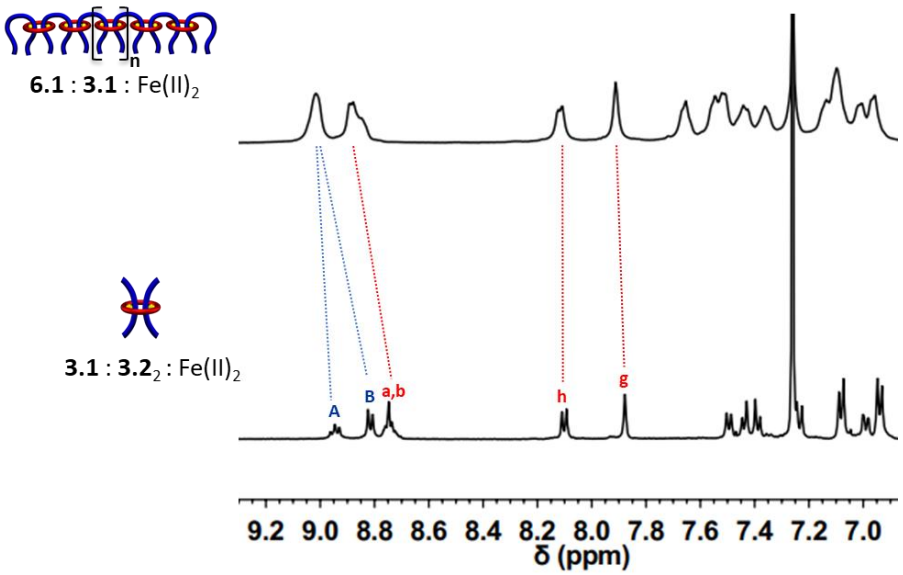

Fig 6.9 Partial ^{1}H-NMR overlay (500 MHz, 25°C, 15% d_3-MeCN in $CDCl_3$) of **6.1**:**3.1**:Fe(II)$_2$ and **3.1**:**3.2**$_2$:Fe(II)$_2$.

After successful MSP formation, the next two steps were stoppering and demetallation of the poly[3]rotaxane. Similar stoppering conditions using azide-alkyne cycloaddition[35,36] were employed to stopper **6.1**:**3.1**:Fe(II)$_2$ with the stopper group **3.13** followed by rapid demetallation using base to convert the Fe(II) to Fe(OH)$_3$ (Fig 6.10, see experimental for full details including the synthesis of the corresponding free dumbbell **6.6**).

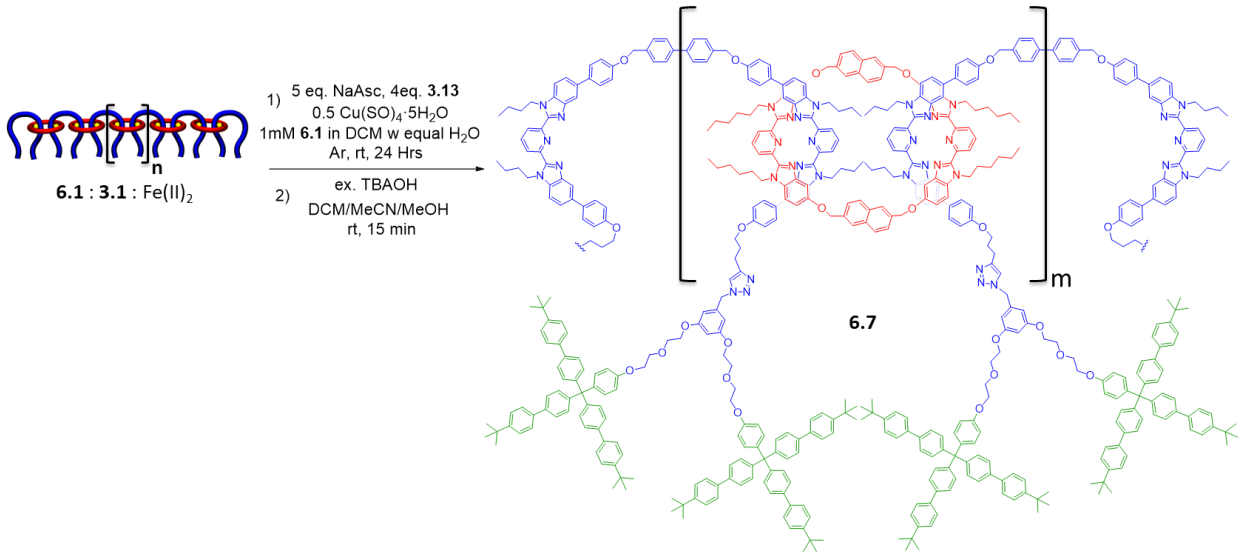

Fig 6.10 Scheme showing synthesis and demetallation of doubly threaded poly[3]rotaxane **6.7**.

Immediately upon demetallation, the crude product was passed through a silica plug ($CHCl_3$ to 5% MeOH in $CHCl_3$) to help remove leftover stopper group and some free macrocycle and dumbbell. ^{1}H-NMR comparison of the partially purified **6.7** to the free components **6.6** and **3.1** revealed broad upfield shifted peaks (Fig 6.11, red boxes indicate interlocked product). These upfield shifted ^{1}H-NMR signals are in the region consistent with interlocked product described in Chapters 3-5 suggesting interlocked polymer had been successfully made. To gain definitive evidence of polymer formation, GPC was employed. Size exclusion chromatography of partially purified **6.**7 shows a dominant broad lower retention time peak consistent with polymer formation in addition to a smaller amount of higher retention time free components and starting materials (Fig 6.12).

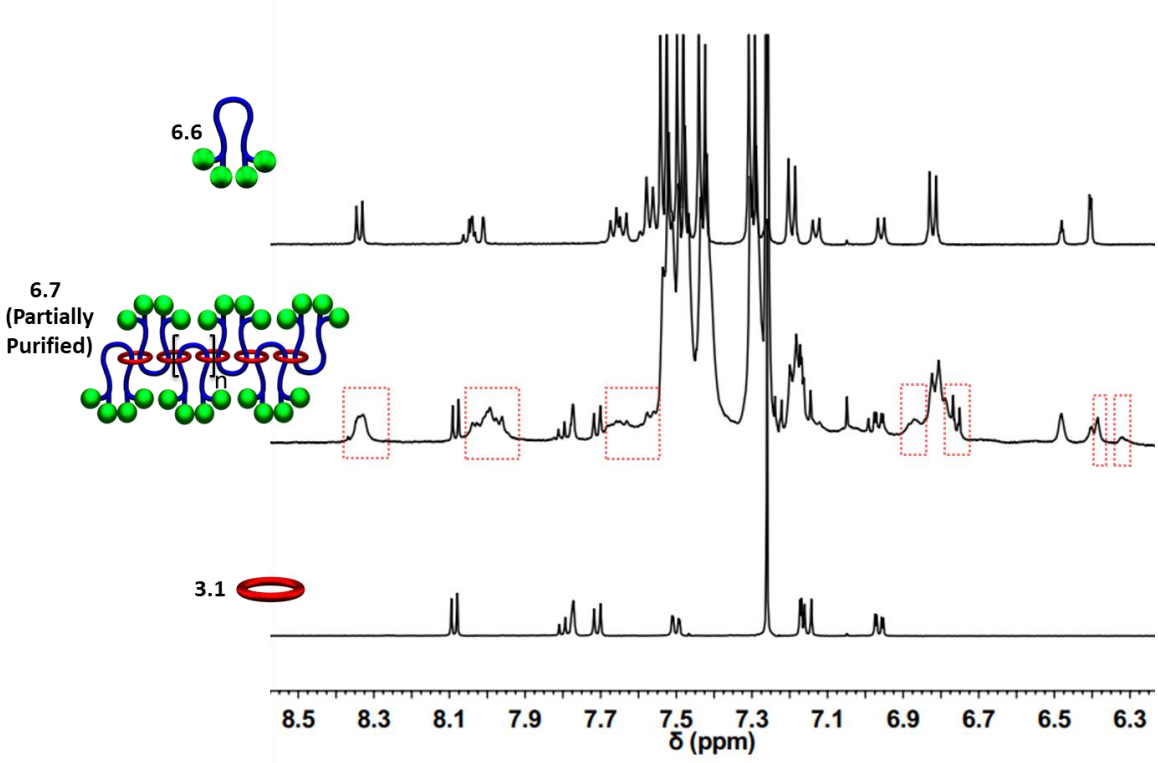

Fig 6.11 Partial ^{1}H-NMR overlay (500 MHz, 25°C, $CDCl_3$) of **6.6**, partially purified **6.7**, and **3.1**.

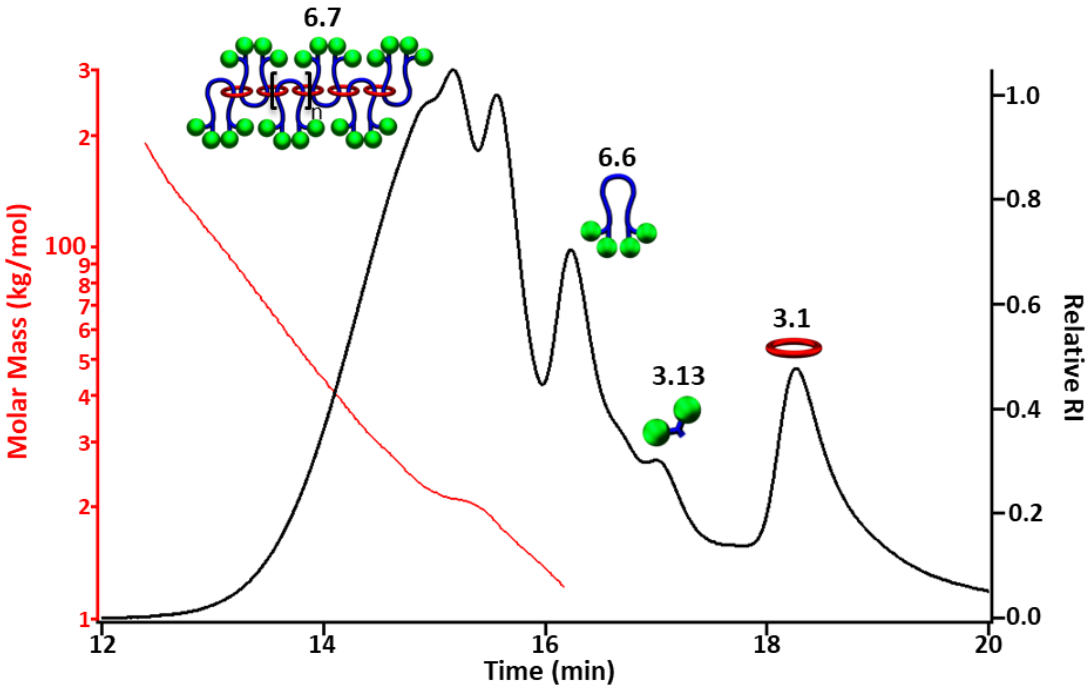

Fig 6.12 GPC chromatogram of (DMF) partially purified **6.7** at 25°C.

The free dumbbell **6.6**, free ring **3.1**, and trace leftover stopper group **3.13** can all be identified by direct comparison to synthesized compounds in chapter 3 and the experimental of this chapter. Standard RI detection was used in addition to a multiangle light scattering (GPC-MALS[37]) detector to measure the absolute molar mass of the interlocked polymer. The specific refractive index increment[38] was roughly estimated for this polymer using the analogous [3]rotaxane **3.17** at 0.150. This analysis gave a M_n ca. 34,100g/mol of the higher molecular weight region (12.3-16.1 mins) for the partially purified poly[3]rotaxane **6.7**. This molecular weight corresponds to roughly 5 interlocked dumbbell and 4 macrocycle components implying an average of 8 mechanical bonds have been formed from this preliminary synthesis. It's important to note this value is highly preliminary in nature, and a more detailed MALS analysis with a calibration curve and the updated GPC conditions (3:1 THF:DMF)[30] is necessary, but this exciting result does confirm the ability of this rotaxane motif to be correlated to a polymeric framework.

An interesting observation is that the higher molecular weight region appears to have multiple broad peaks implying the possibility of multiple polymeric products. Attempts were then made to fully purify the poly[3]rotaxane **6.7** from its noninterlocked components using dialysis to better analyze the interlocked polymer and analyze these peaks (Snakeskin 7k MW cutoff tubing in $CHCl_3$). After sitting for 2.5 weeks at room temperature, ^{1}H-NMR analysis of the higher molecular weight product (in the dialysis tube) revealed the diagnostic broad peaks in the region consistent with interlocked product had been replaced with slightly downfield shifted peaks more consistent with the free components (Fig 6.13, indicated peaks in red boxes).

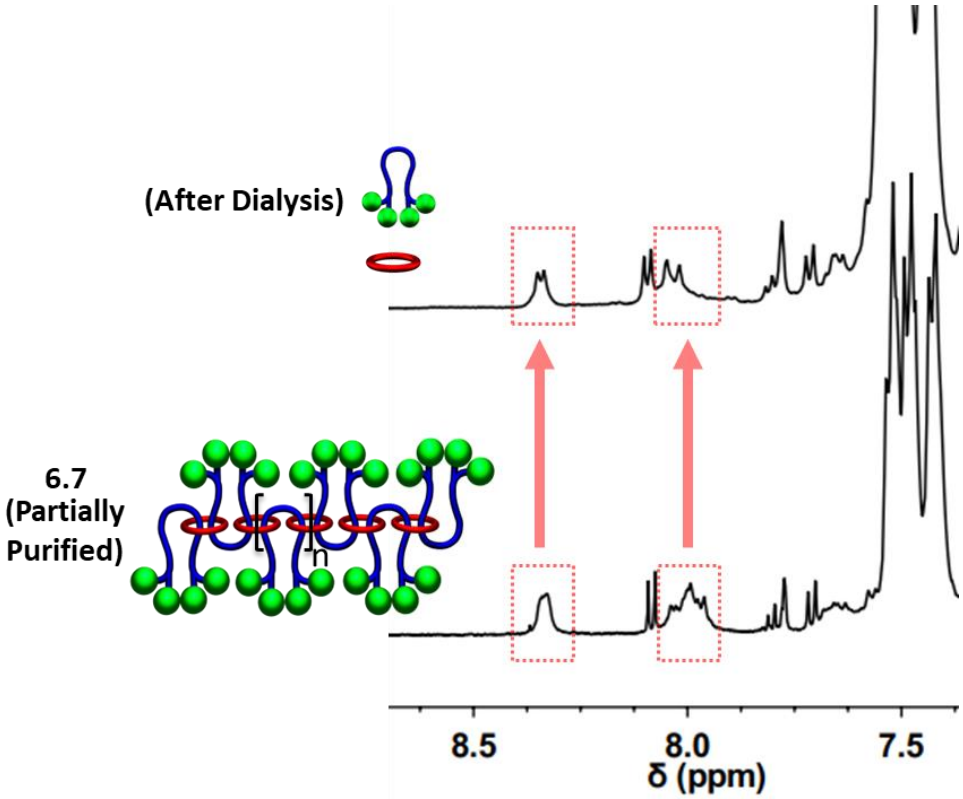

Fig 6.13 Partial ^{1}H-NMR overlay (500 MHz, 25°C, $CDCl_3$) of partially purified **6.7** before (bottom) and after (top) dialysis attempt.

In addition, only the free ring **3.1** was detected in the large volume of $CHCl_3$ outside the dialysis tubing. These results combined with the studies in Chapters 3-4 with the same ring imply that the poly[3]rotaxane **6.7** is a metastable interlocked structure and that dialysis resulted in the alternating polymer falling apart slowly via a slow slippage process. Nevertheless, the results in this section confirm the exciting result of poly[3]rotaxane formation using a Bip ligand system.

6.4 Using Ring 5.3 to Synthesize a Fully Stable Poly[3]rotaxane

As Chapter 5 confirmed the ability to fully stabilize the [3]rotaxane structure with the 42 atom ring **5.3**, efforts were then turned to using this ring for poly[3]rotaxane synthesis. Thus, the MSP **6.1**:**5.3**:$Fe(II)_2$ was targeted (Fig 6.14).

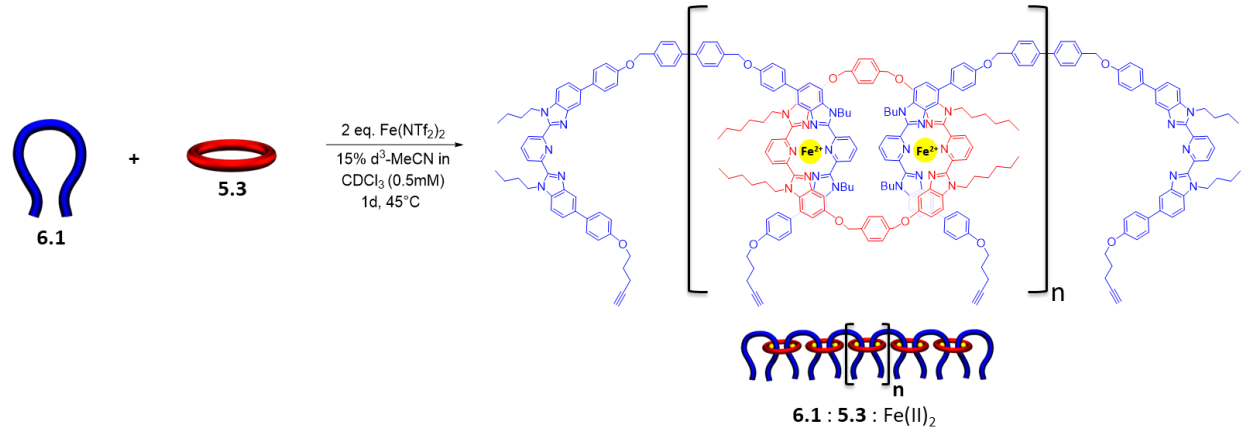

Fig 6.14 Scheme describing assembly of **6.1**:**5.3**:$Fe(II)_2$.

An analogous procedure to that described previously for **6.1**:**5.3**:$Fe(II)_2$ was used and similar broad downfield shifting of the ^{1}H-NMR pyridinyl peaks was seen consistent with successful MSP formation (Fig 6.15, See experimental for full details).

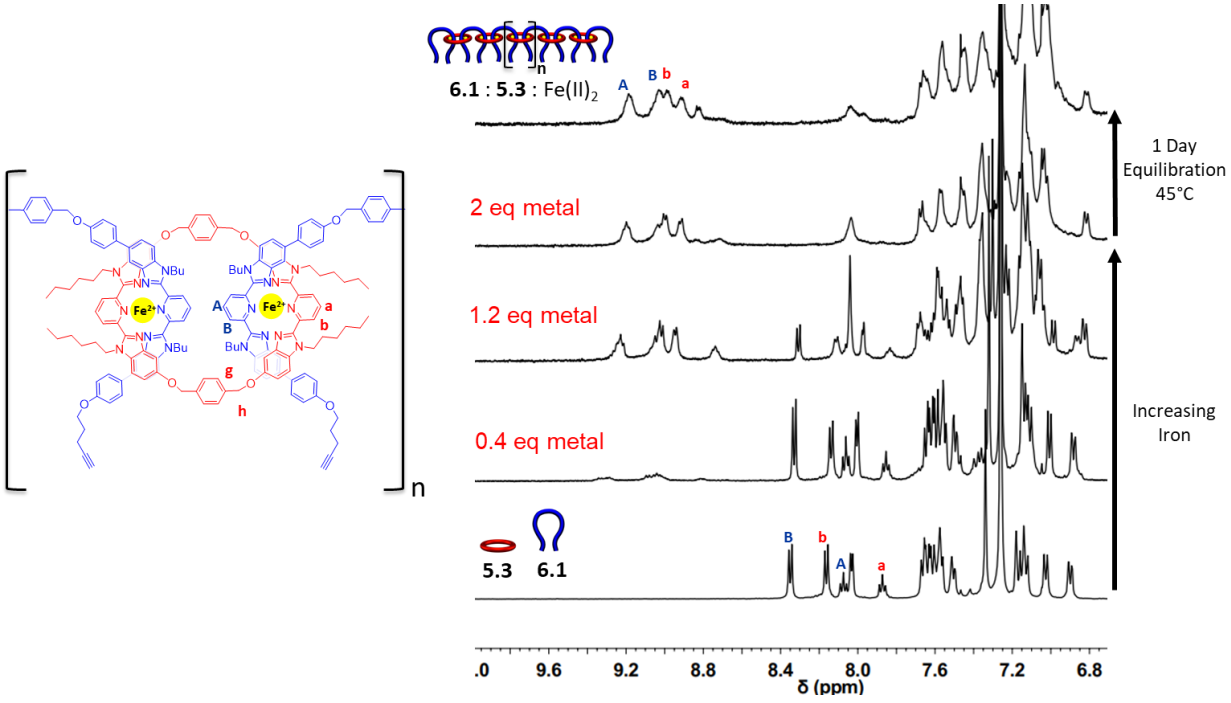

Fig 6.15 Partial ^{1}H-NMR overlay (500 MHz, 25°C, Solvent: 0, 3, 9, 15, 15% d_3-MeCN in $CDCl_3$ increasing upwards) of metal addition and equilibration of 1:1 mixture of **6.1**:**5.3**.

Upon successful assembly of **6.1**:**5.3**:$Fe(II)_2$, similar stoppering conditions to those for **6.7** were used to target the poly[3]rotaxane **6.8** (Fig 6.16, See Experimental for full stoppering procedure).

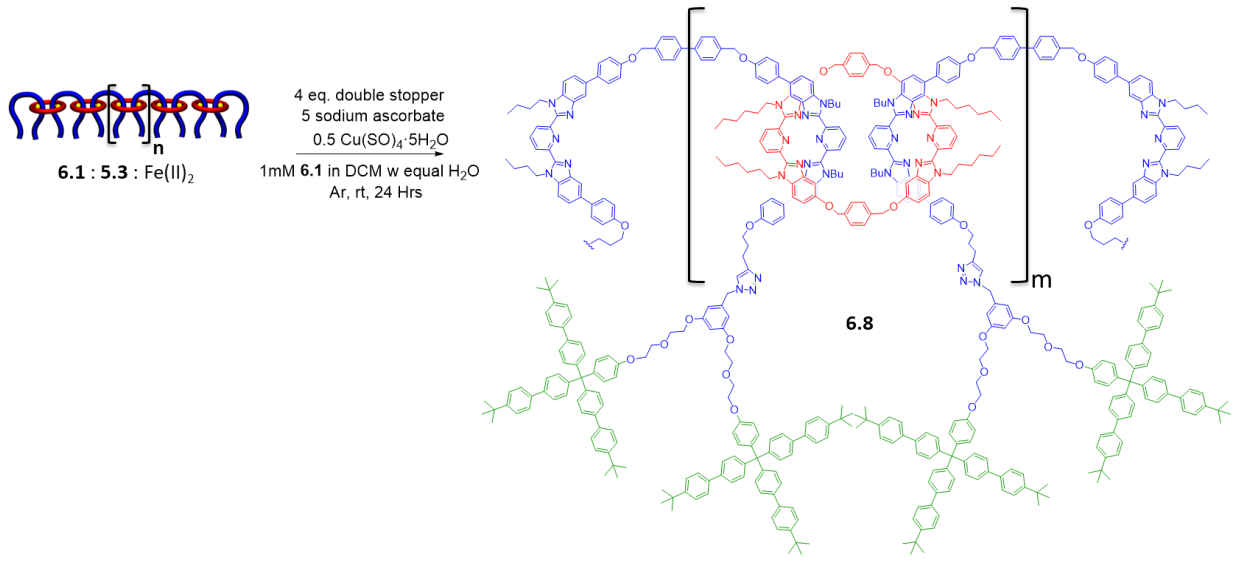

Fig 6.16 Scheme showing synthesis and demetallation of doubly threaded poly[3]rotaxane **6.8**.

Immediately upon demetallation a dominant lower R_f product was observed via TLC (6% MeOH in $CHCl_3$) relative to the free dumbbell **6.6** and ring **5.3** confirming the presence of interlocked product. Preparative thin layer chromatography was used to isolate the lower R_f (0.15-0.35) interlocked product in 55% isolated yield from its noninterlocked components and excess stopper group (Note: This yield is based on 4.5mg of **6.8** being isolated and it is anticipated that scaling up this procedure will increase this interlocked yield closer to the ~75-80% seen in the rest of this thesis, see Experimental for full details). Comparing the ^{1}H-NMR of purified **6.8** relative to its noninterlocked components **6.6** and **5.3** and the corresponding [3]rotaxane based on a 42 atom macrocycle **5.8** allows the ^{1}H-NMR to be tentatively assigned (See Fig 6.17 for diagnostic aromatic region and Experimental for full details).

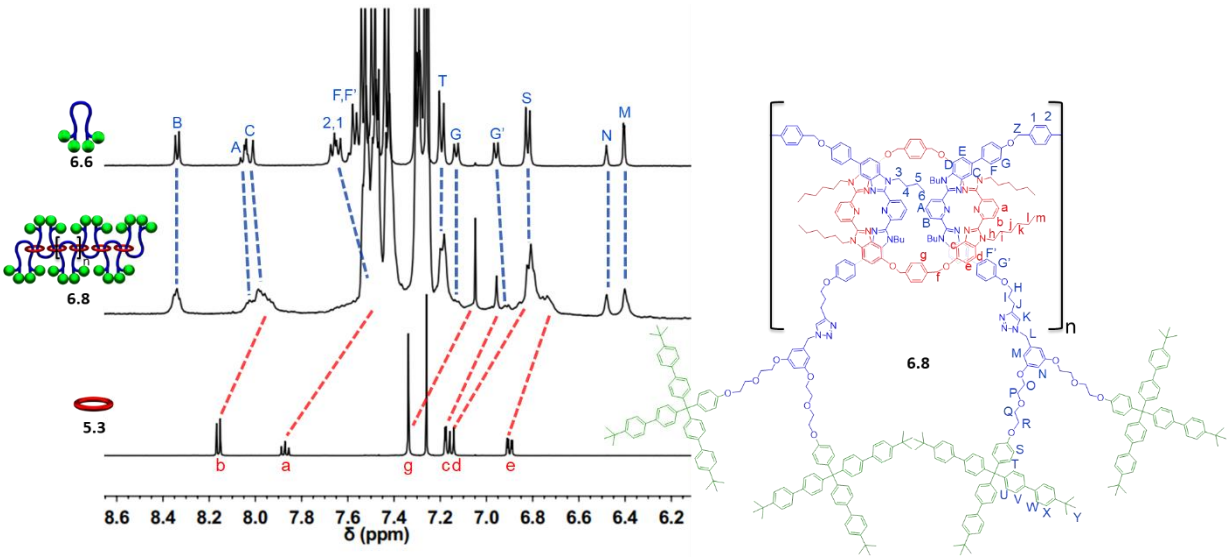

Fig 6.17 Partial ^{1}H-NMR overlay (500 MHz, 25°C, $CDCl_3$) of purified **6.8** relative to its components **6.6** and **5.3**, ^{1}H assignments at side of figure.

As can be seen, the isolated poly[3]rotaxane displays broad upfield shifted peaks relative to its noninterlocked components indicative of interlocked product. The increased broadness and asymmetric nature of the peaks displayed are more reminiscent of the ^{1}H-NMR of interlocked poly[n]catenanes[29,30] based on the Bip ligand and not the symmetric [3]rotaxanes discussed primarily in this thesis[39]. This is consistent with interlocked poly[3]rotaxane being formed where an irregular polymeric structure would be expected leading to the observed peaks. Size exclusion chromatography using RI and MALS detection was then used to estimate the absolute molar mass of the interlocked polymer. The specific refractive index increment[38] was estimated for **6.8** using the analogous [3]rotaxane **5.8** at 0.148. This preliminary analysis gave a M_n ca. 43,700g/mol with a $Đ$ of 1.30 of poly[3]rotaxane **6.8** (Fig 6.18a). This molecular weight would correspond to roughly 7 interlocked dumbbell and 6 macrocycle components implying an average of 12 mechanical bonds have been formed per polymer from this preliminary synthesis with a 42 atom ring. To better understand these results a GPC deconvolution using 4 Gaussian peaks was applied to the RI trace

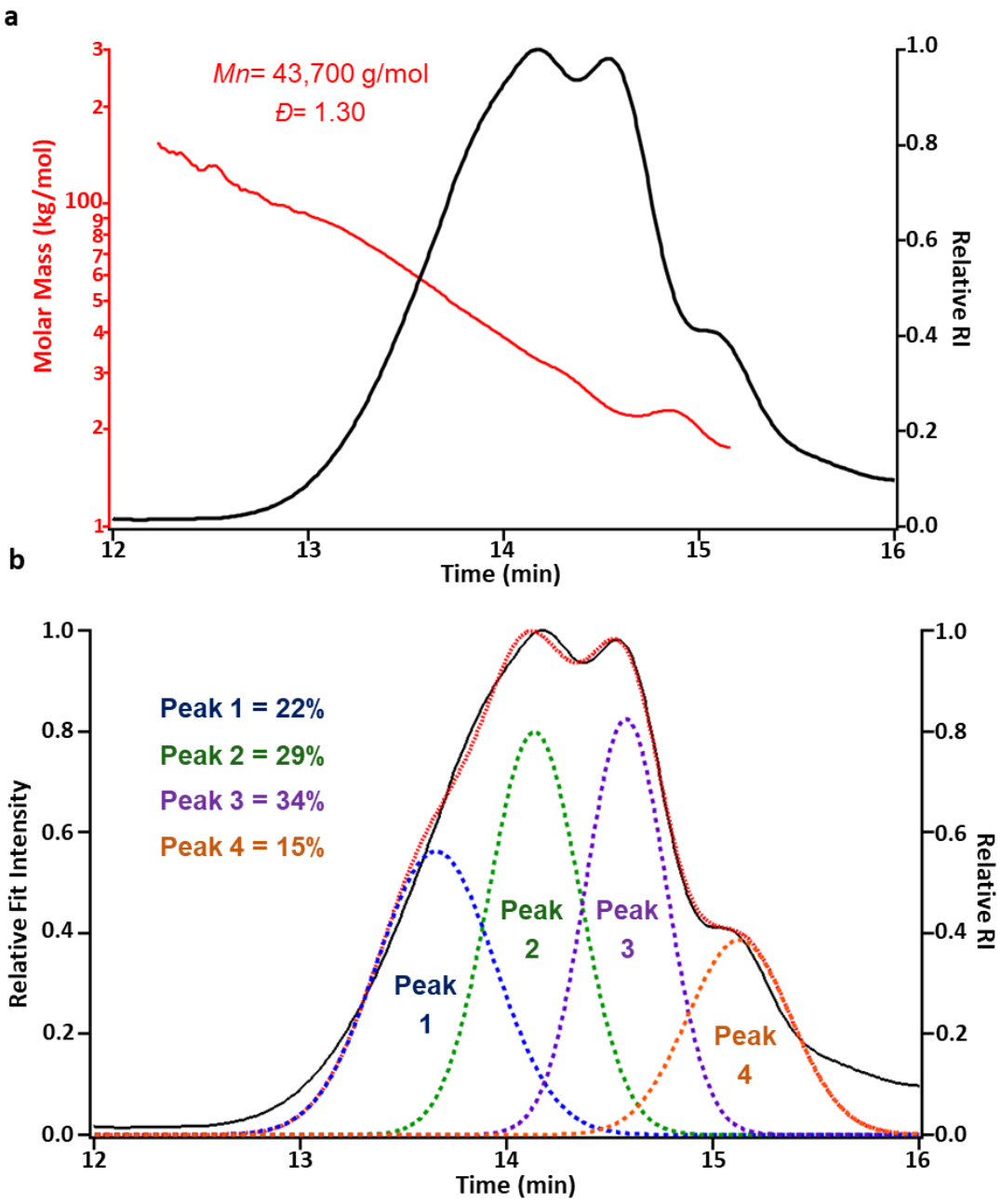

Fig 6.18 a) GPC chromatogram (3:1 THF:DMF) of purified **6.8** at 25°C and b) Gaussian deconvolution using 4 peaks of RI trace.

of **6.8** (Fig 6.18b).[30] From this, Peak 3 can be seen to be the major component of the overall polymeric product and its relatively low M_n (~25K, 4DBs and 4MC components) may be consistent with cyclic poly[3]rotaxane species. Another important parameter to note is that the

equilibration (0.5mM) and stoppering (1.0mM) procedures were both done at relatively low concentrations due to the small scale both reactions were done at which would favor the cyclic MSP species before stoppering (based on understanding of similar poly(n)catenane systems[30]). Scaling this up to a ~250mg scale and doing both assembly and stoppering procedures at the highest concentration possible is necessary to access the true potential of this MSP template to target high molecular weight linear poly[3]rotaxane.

The stability of **6.8** to dethreading was then examined. A freshly purified solution of **6.8** (1mM in $CDCl_3$) was allowed to sit in solution at the elevated temperature of 50°C for one week with its ^{1}H-NMR spectrum recorded at various timepoints. Comparing the compiled spectra to the free ring **5.3** reveals that no macrocycle is observed to slip from the polymer during the experiment confirming that **6.8** is a fully interlocked poly[3]rotaxane (Fig 6.19).

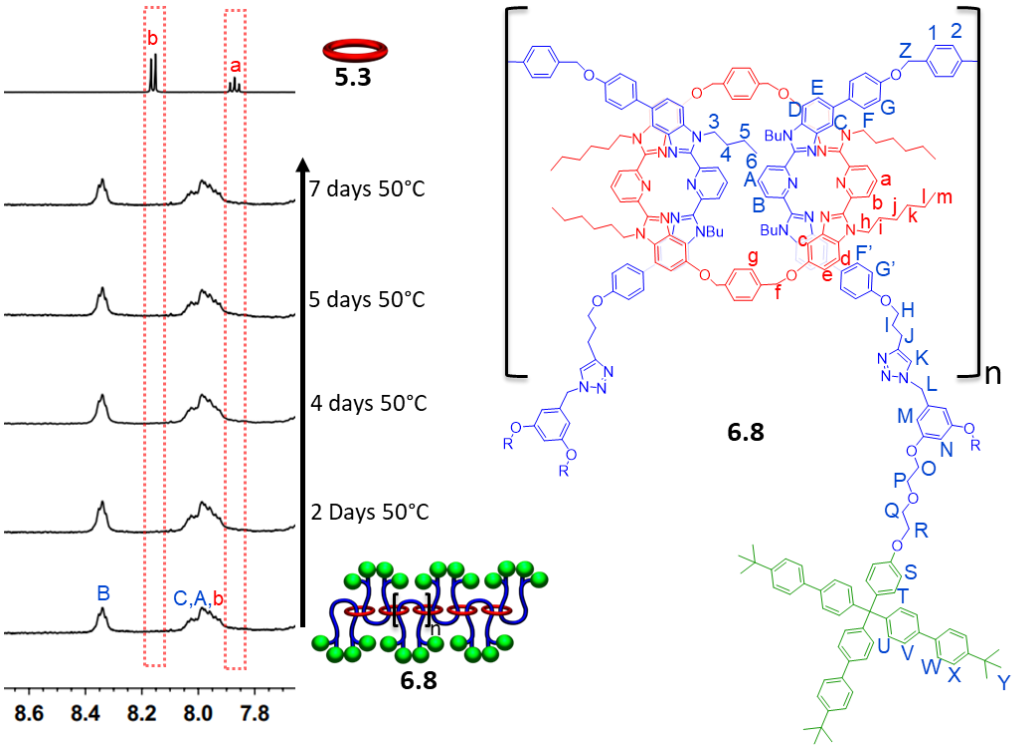

Fig 6.19 Partial ^{1}H-NMR overlay (500 MHz, 25°C, $CDCl_3$) of purified **6.8** during 1-week slippage experiment, time and temperature between measurements indicated on right side with ^{1}H-assignments.

This exciting result confirms the ability to correlate the stability increase upon tightening the ring from 46 atoms to 42 atoms seen in the molecular [3]rotaxane to the interlocked poly[3]rotaxane (Fig 6.20). Further studies are needed involving higher temperatures and the solid state for the interlocked stability during melt processing techniques and other materials preparation techniques to be evaluated.

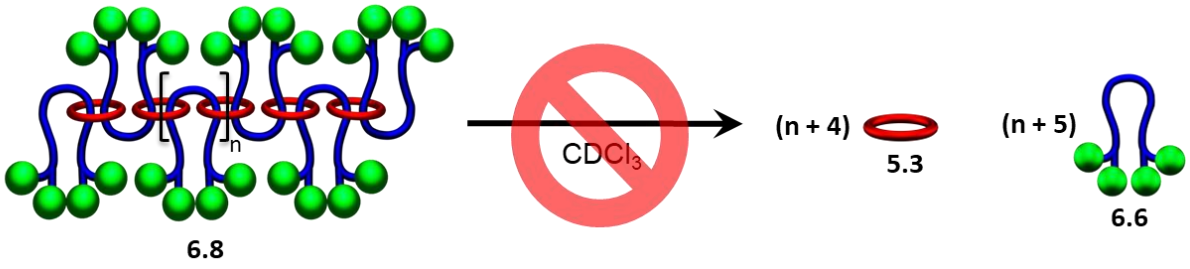

Fig 6.20 Scheme describing observed stability of **6.8**.

6.5 Preliminary Extension Using a Polymeric Thread Component 6.4

One of the most challenging aspects to accessing functional interlocked materials using this approach is to synthesize them on a scale and appropriate form factor that mechanical testing and materials characterization can be performed on. One way to help alleviate these issues and increase the scalability is the incorporation of more bulk material into the structure (i.e., add more mass to the "non-Bip" part of the architecture). As such, this section details the use of the thread component **6.4** (Fig 6.21, See section 2 and experimental for full synthetic details).

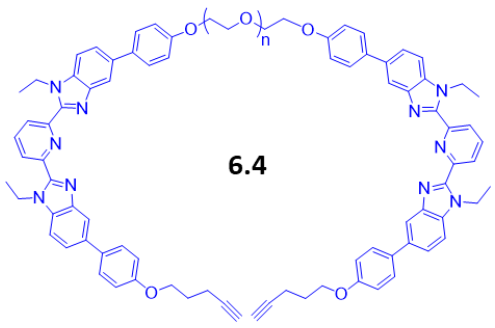

Fig 6.21 Chemical structure of polymeric thread component **6.4**.

6.4 contains a ~2K Mw PEO backbone between two Bip ligands. A similar metal-templated MSP assembly procedure to those described in the previous sections was employed to form **6.4**:**3.1**:$Fe(II)_2$ (Fig 6.22).

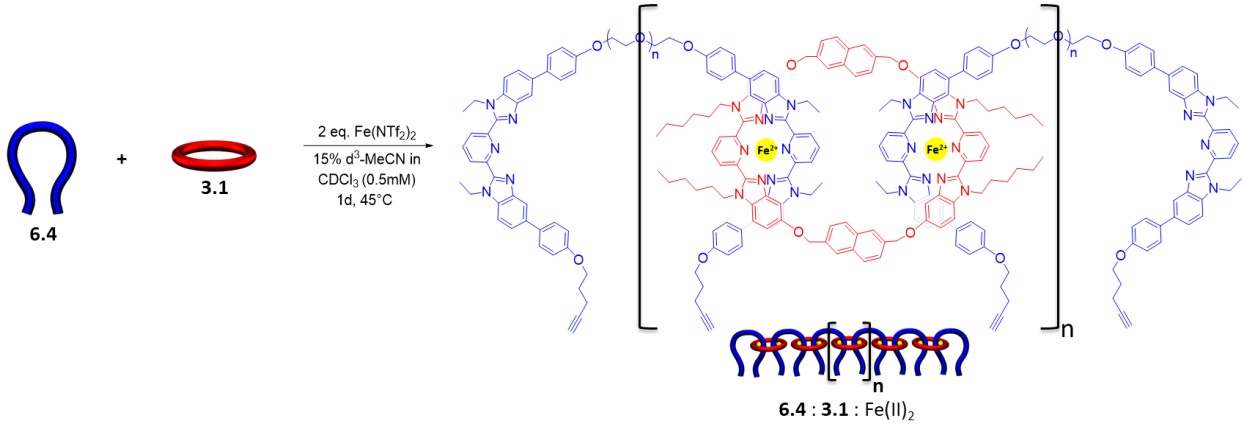

Fig 6.22 Scheme describing assembly of **6.4**:**3.1**:$Fe(II)_2$.

Similar broad downfield shifting of the diagnostic ^{1}H-NMR pyridinyl peaks closest to the metal binding interaction was seen that was consistent with the previously described MSP **6.1**:**3.1**:$Fe(II)_2$ and pseudo[3]rotaxane **3.1**:$\mathbf{3.2}_2$:$Fe(II)_2$ (Fig 6.23).

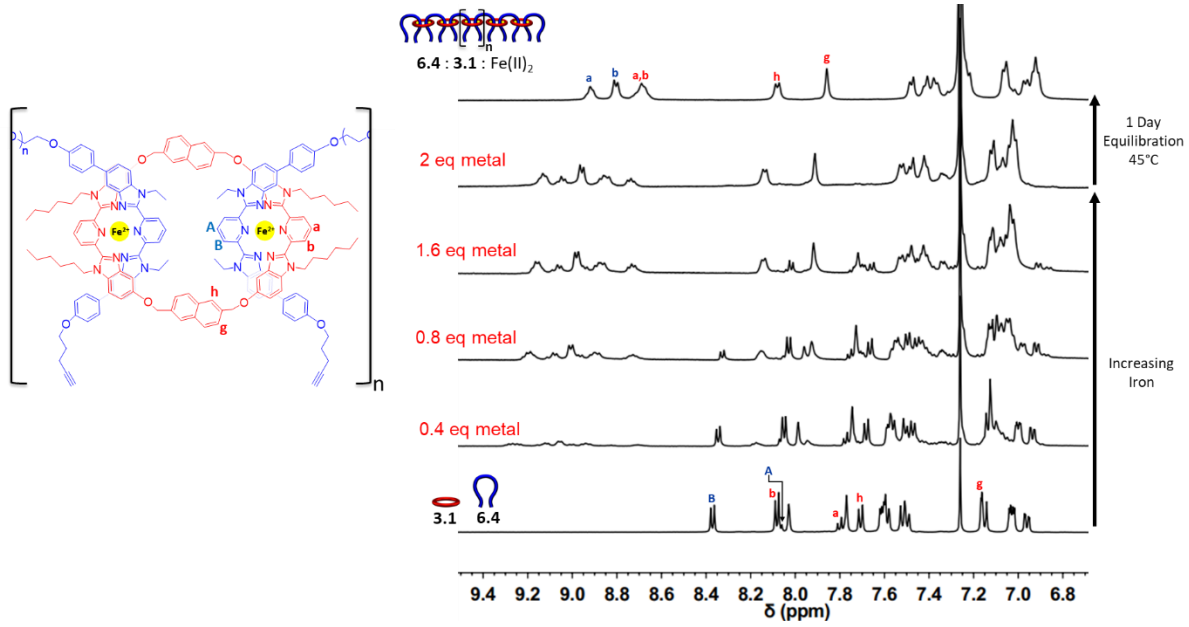

Fig 6.23 Partial ^{1}H-NMR overlay (500 MHz, 25°C, Solvent: 0, 3, ,6, 9, 15, 15% d_3-MeCN in $CDCl_3$ increasing upwards) of metal addition and equilibration of 1:1 mixture of **6.4**:**3.1**.

After successfully assembling **6.4**:**3.1**:$Fe(II)_2$, similar stoppering and demetallation conditions to those for **6.7** and **6.8** were employed to synthesize the doubly threaded poly[3]rotaxane **6.9** (Fig 6.24, See Experimental for full stoppering procedure).

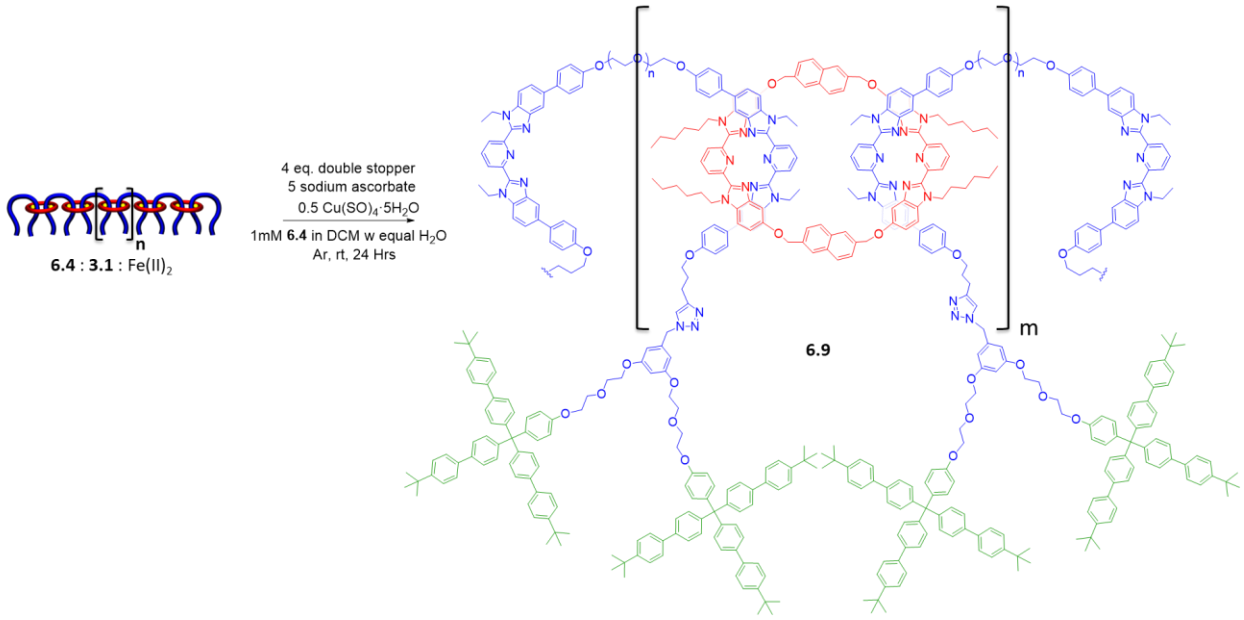

Fig 6.24 Scheme showing synthesis and demetallation of doubly threaded poly[3]rotaxane **6.9**.

Immediately upon demetallation a dominant lower R_f product was observed via TLC, and the crude material was passed through a silica plug ($CHCl_3$ + 2% MeOH) to help remove leftover stopper group followed by multiple precipitations from methanol which partially removed free macrocycle. ^{1}H-NMR comparison of the partially purified **6.9** to the free macrocycle **3.1** revealed broad upfield shifted peaks (Fig 6.25a, red boxes indicate potential interlocked product, note the free corresponding dumbbell was not synthesized) consistent with interlocked product. In addition, size exclusion chromatography confirms the existence of a higher molecular weight product in a similar region to **6.8** (Fig 6.25b, 12.3-16.1 mins). This preliminary crude analysis confirms the ability to incorporate polymeric components into the synthetic approach developed in this thesis to target doubly threaded poly[3]rotaxanes.

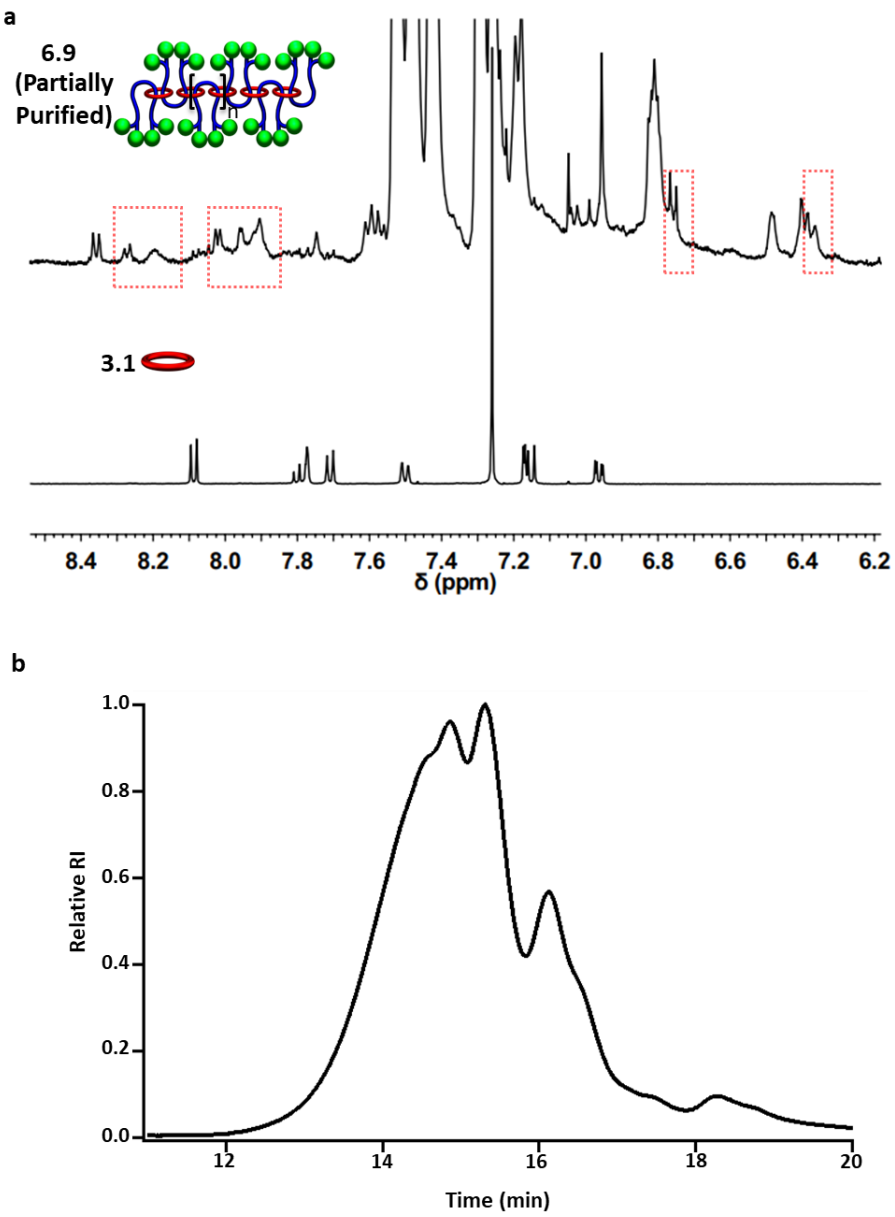

Fig 6.25 a) Partial ^{1}H-NMR overlay (500 MHz, 25°C, $CDCl_3$) of partially purified **6.9** and **3.1** and b) GPC chromatogram of (DMF) partially purified **6.9** at 25°C.

6.6 Conclusions

This chapter has detailed the first few synthetic examples of the interlocked doubly threaded poly[3]rotaxane architecture. First, the [3]rotaxane motif developed in Chapter 3 with a 46 atom ring was used to synthesize the corresponding metastable poly[3]rotaxane **6.7**.

Purification attempts with dialysis resulted in this interlocked polymer dethreading. Based on the results in Chapter 5, the corresponding 42 atom macrocycle poly[3]rotaxane **6.8** was synthesized and its kinetic stability to dethreading at moderate temperatures was confirmed. Finally, initial attempts to incorporate a polymeric thread component to access more scalable materials resulted in the successful synthesis of poly[3]rotaxane **6.9** containing a 2K PEO thread backbone.

These initial results confirm the ability to incorporate the doubly threaded [3]rotaxane motif that was developed in Chapters 2-5 into a polymeric system. All of the synthesized poly[3]rotaxanes in this chapter were done so at relatively low MSP equilibration (<1mM) and stoppering concentrations (0.5mM). These low concentrations more than likely favor smaller cyclic interlocked species which would be consistent with the observed results. The only products possible from stoppering MSP are cyclic or linear poly[3]rotaxane as the branching side product seen in the poly(n)catenane synthesis is not possible due to the excess of mono-functionalized stopper group used. Thus, scaling up all of these poly[3]rotaxane synthetic procedures (>250mg) at the highest concentration possible (>1M) should result in the longest linear poly[3]rotaxane possible via this approach and should be an immediate task. The demonstration of the use of a polymeric thread component is the starting point for a systematic study on how the thread backbone (polymer length, composition, thickness, etc.) impacts the material properties of the poly[3]rotaxane. Due to the synthetic approach a wide variety of polymers could be chosen for the ditopic thread. In addition, adding the polymeric stopper group described at the end of Chapter 4 would allow for two different polymers (one on the stopper group arm and one on the thread backbone) to be incorporated into the interlocked polymeric system at once. This would essentially result in highly tunable copolymeric networks that are cross-linked with doubly threaded movable Bip cross-links.

Potentially one of the most exciting future directions is the use of this [3]rotaxane motif to access doubly threaded slide-ring materials (Figure 6.26). These novel slide-ring materials offer significant advantages in tunability parameters compared to current published singly threaded ones as ring size, thread thickness, backbone composition, and the presence of additional singly threaded rings can all be fine-tuned easily using this framework.

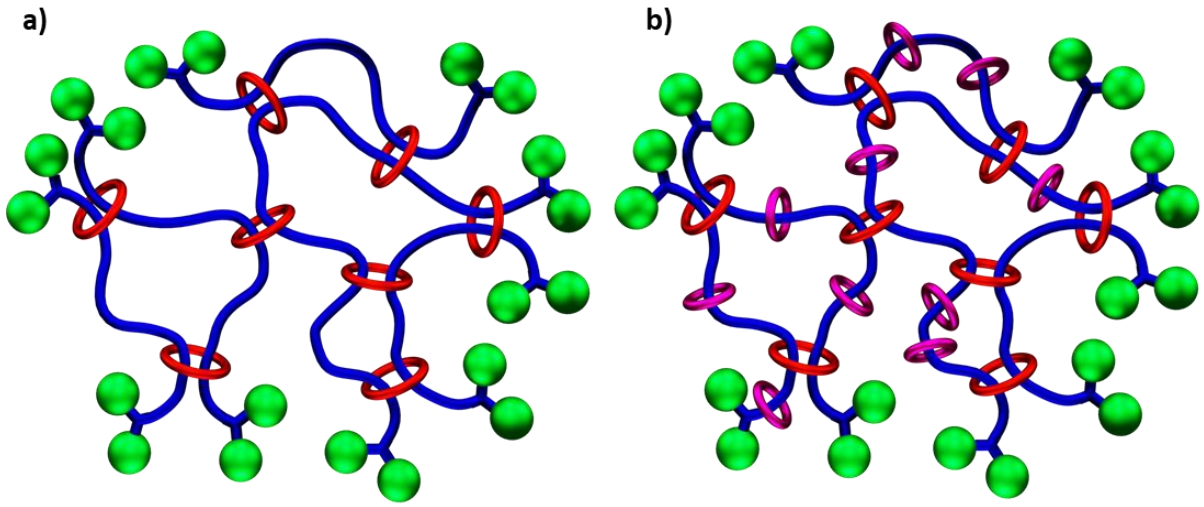

Fig 6.26 Cartoon representation of doubly threaded slide-ring gels with (a) only doubly threaded rings and (b) added singly threaded rings.

6.7 Experimental

6.7.1 Materials and Methods

Materials. All reagents were purchased from Sigma-Aldrich unless otherwise stated. All chemicals were used as received without further purification unless otherwise stated. Solvents for chromatography were purchased from Fisher-Scientific. Deuterated solvents and 3,5-dihydroxybenzyl alcohol were purchased from ACROS Organics. 4-Bromo-4'-tert-butylbiphenyl was purchased from TCI chemicals. *p*-Toluenesulfonyl chloride was purchased from Alfa Aesar.

Iron(II) bistriflimide[40] and 2,6-bisbenzimidazolylpyridine ligands[31] were prepared following literature procedures. Tetrahydrofuran (THF) was dried over sodium and benzophenone. Dichloromethane was distilled over calcium hydride before use. Dimethylformamide (DMF) was dried with activated molecular sieves before use. Thin layer chromatography plates (1000 micron) were purchased from Analtech.

Matrix Assisted Laser Desorption/Ionization Mass Spectrometry (MALDI-MS). MALDI-TOF was measured by a Bruker Ultraflextreme MALDI-TOF-TOF spectrometer in linear (or reflectance) mode using dithranol as matrix and sodium trifluoroacetate or silver trifluoroacetate as ionizer (or no ionizer).

Nuclear Magnetic Resonance Spectroscopy (NMR). Room Temperature Nuclear Magnetic Resonance Spectroscopy was performed using a Bruker Ascend Avance III 500 MHz spectrometer, a Bruker Avance II+ 500 MHz spectrometer, or a Bruker DRX 400 MHz spectrometer at the University of Chicago NMR facilities. ^{1}H NMR spectra were referenced to the residual protonated solvent signal and $^{13}C\{^{1}H\}$ NMR spectra were referenced to the deuterated solvent carbon resonance signal.

NMR Slippage Kinetic Experiments. Kinetic experiments were performed in Shigemi Tubes purchased from Wilmad-Labglass in $CDCl_3$ (1mM) using a Bruker AVANCE III HD 500 MHz spectrometer at the NMR facilities at the University of Chicago.

Gel Permeation Chromatography (GPC). GPC measurements were performed utilizing the Soft Matter Characterization Facility at the University of Chicago. Measurements were conducted at 25°C using 3:1 THF:DMF as eluent (flow rate = 1 mL/min), using a Shimadzu autosampler, Shimadzu HPLC LC20-AD pump, 2 Agilent PLgel 5 um MIXED-D + guard SEC

columns, and a Wyatt Optilab T-rEX differential refractive index detector with an additional MALS detector.

Dialysis Purification. Dialysis was conducted using Snakeskin dialysis tubing (Mw cutoff 7K purchased from Thermofisher and ACS reagent grade $CHCl_3$). Poly[3]rotaxane sample was dissolved in 2mL $CHCl_3$ inside the tubing and the surrounding 1200mL of $CHCl_3$ was changed 10 times over 2.5 weeks at regular intervals.

6.7.2 Synthesis of 6.3

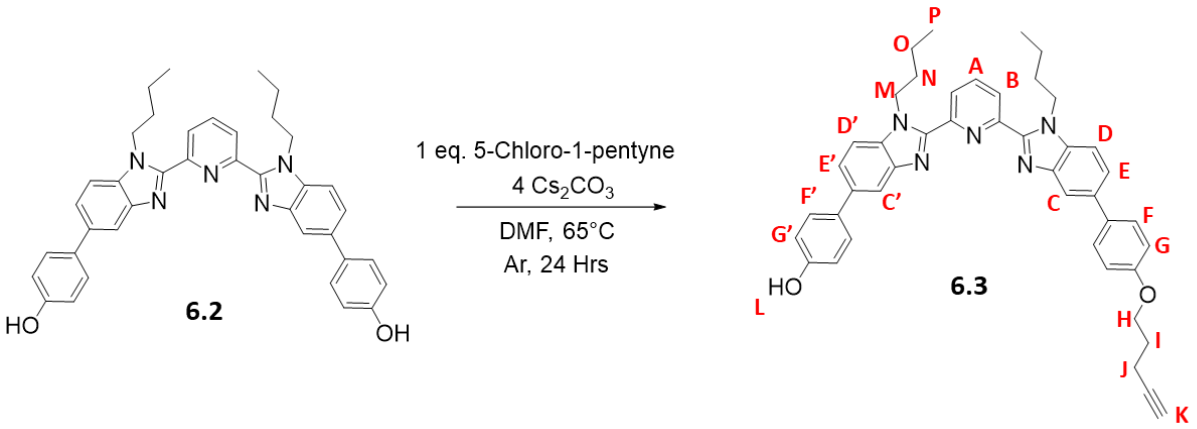

6.2[31,41] (3.0g, 4.9mmol) and Cs_2CO_3 (6.43g, 19.6mmol) were added to a 100mL RBF. The reaction chamber was purged with argon and DMF (49mL) was added via cannula. The reaction mixture was heated to 65°C and 5-Chloro-1-pentyne (0.523mL, 4.9mmol) was injected via syringe. The reaction mixture was allowed to stir at 65°C overnight. The following day the reaction mixture was cooled to room temperature and the solvent was removed under reduced pressure resulting in an off-white solid that was washed with hot $CHCl_3$ (4 × 150 mL) and filtered. The filtrate was collected and the solvent removed under reduced pressure resulting in an off-white residue. Purification using column chromatography (standard silica gel, eluent gradient $CHCl_3$ to 5% MeOH in $CHCl_3$) resulted in a white solid **6.3**, in 34% yield. ^{1}H NMR (500 MHz, $CDCl_3$) δ 8.38

(d, *J* = 7.9Hz, 2H, B), 8.08 (t, *J* = 7.9Hz, 1H, A), 8.06 (s, 1H, C), 8.05 (s, 1H, C'), 7.68 (d, *J* = 8.7Hz, 2H, E+E'), 7.61–7.56 (m, 4H, F+F'), 7.57–7.53 (m, 2H, D+D'), 7.08 (d, *J* = 8.6Hz, 2H, G), 7.00 (d, *J* = 8.6Hz, 2H, G'), 4.90 (t, *J* = 7.4Hz, 4H, M), 4.20 (t, *J* = 6.1Hz, 2H, H), 2.46 (m, 2H, J), 2.10 (m, 2H, I), 2.00 (t, *J* = 2.7Hz, 1H, K), 1.78 (m, 4H, N), 1.16 (m, 4H, O), 0.80 (t, *J* = 7.2Hz, 6H, P). MALDI-MS: 675.1 ([M]+H^+).

6.7.3 Synthesis of 6.1

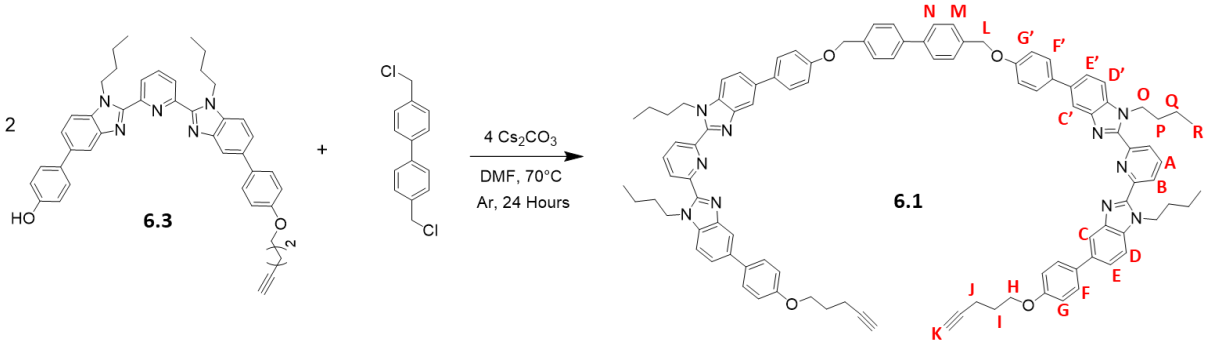

A 50mL RBF was charged with **6.3** (0.68g, 1.0mmol), Cs_2CO_3 (1.31g, 4.0mmol), 4,4'-Bis(chloromethyl)-1-1'-biphenyl (0.12g, 0.5mmol), and DMF (10 mL) under an Ar atmosphere. The mixture was heated to 70°C and stirred overnight. The next day the reaction mixture was cooled to RT and the solvent was removed under reduced pressure. The residue was washed in hot $CHCl_3$ (4 × 100 mL) and the insoluble material (salts) was removed by filtration. The filtrate was collected and the solvent removed under reduced pressure. The resulting material was purified using column chromatography (TEA treated silica gel, eluent gradient $CHCl_3$ to 5% MeOH in $CHCl_3$) followed by recrystallization (chloroform/methanol mixture) to yield white crystals of **6.1** in 68% yield. ^{1}H NMR (500 MHz, $CDCl_3$) δ 8.37 (d, *J* = 7.9Hz, 4H, B), 8.10 (t, *J* = 7.9Hz, 2H, A), 8.06 (s, 1H, C), 8.05 (s, 1H, C'), 7.71–7.56 (m, 20H, E+E'+F+F'+M+N), 7.53 (dd, *J* = 8.5, 2.6Hz, 4H, D+D'), 7.15 (d, *J* = 8.8Hz, 4H, G), 7.05 (d, *J* = 8.8Hz, 4H, G'), 5.21 (s, 4H, L), 4.79 (t, *J* = 7.3Hz, 8H, O), 4.17 (t, *J* = 6.1Hz, 4H, H), 2.47 (m, 4H, J), 2.11–2.03 (m, 4H, I), 2.01 (t, *J*

= 2.6Hz, 2H, K), 1.77 (m, 8H, P), 1.17 (m, 8H, Q), 0.76 (t, *J* = 7.4Hz, 12H, R). MALDI-MS: 1526.4 ([M]+H^+).

6.7.4 Synthesis of 6.5

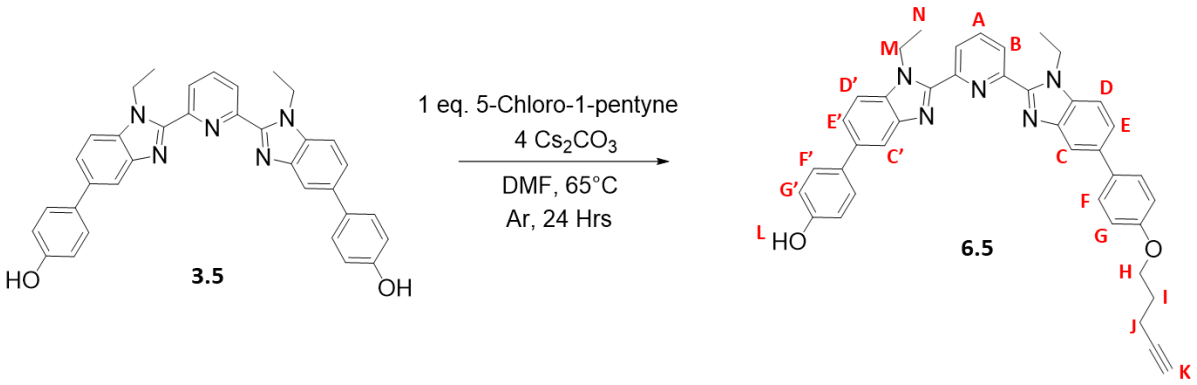

3.5 (3.0g, 5.4mmol) and Cs_2CO_3 (7.67g, 21.6mmol) were added to a 100mL RBF. The reaction chamber was purged with argon and DMF (54mL) was added via cannula. The reaction mixture was heated to 65°C and 5-Chloro-1-pentyne (0.576mL, 5.4mmol) was injected via syringe. The reaction mixture was allowed to stir at 65°C overnight. The following day the reaction mixture was cooled to room temperature and the solvent was removed under reduced pressure resulting in an off-white solid that was washed with hot $CHCl_3$ (4 × 150 mL) and filtered. The filtrate was collected and the solvent removed under reduced pressure resulting in an off-white residue. Purification using column chromatography (standard silica gel, eluent gradient $CHCl_3$ to 5% MeOH in $CHCl_3$) resulted in a white solid **6.5**, in 30% yield. ^{1}H NMR (500 MHz, $CDCl_3$) δ 8.40 (d, *J* = 7.8Hz, 2H, B), 8.10 (t, *J* = 7.8Hz, 1H, A), 8.06 (s, 1H, C), 8.05 (s, 1H, C'), 7.64 (d, *J* = 8.7Hz, 2H, E+E'), 7.62–7.57 (m, 4H, F+F'), 7.57–7.53 (m, 2H, D+D'), 7.06 (d, J = 8.6Hz, 2H, G), 6.99 (d, *J* = 8.6Hz, 2H, G'), 4.86 (q, *J* = 7.2Hz, 4H, M), 4.17 (t, *J* = 6.1Hz, 2H, H), 2.48 (m, 2H, J), 2.08 (m, 2H, I), 2.02 (t, *J* = 2.7Hz, 1H, K), 1.43 (t, *J* = 7.2Hz, 6H, N). MALDI-MS: 619.0 ([M]+H^+).

6.7.5 Synthesis of 6.4

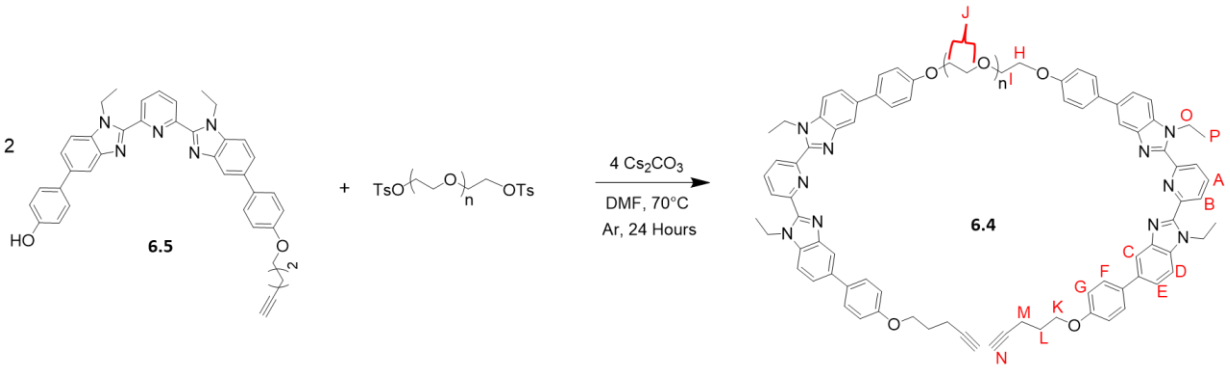

A 25mL RBF was charged with **6.5** (0.25g, 0.4mmol), Cs_2CO_3 (1.31g, 1.6mmol), 2K PEG-ditosylate[32] (0.41g, 0.2mmol), and DMF (5 mL) under an Ar atmosphere. The mixture was heated to 70°C and stirred overnight. The next day the reaction mixture was cooled to RT and the solvent was removed under reduced pressure. The residue was washed in hot $CHCl_3$ (4 × 25 mL) and the insoluble material (salts) was removed by filtration. The filtrate was collected and the solvent removed under reduced pressure. The resulting material was purified using column chromatography (TEA treated silica gel, eluent gradient $CHCl_3$ to 8% MeOH in $CHCl_3$) followed by precipitation from methanol to yield a white solid, **6.4** in 64% yield. ^{1}H NMR (500 MHz, $CDCl_3$) δ 8.40 (d, *J* = 7.9 Hz, 4H, B), 8.10 (t, *J* = 7.9 Hz, 2H, A), 8.06 (s, 4H, C), 7.66-7.59 (m, 12H, E+F), 7.54 (d, *J* = 8.4 Hz, 4H, D), 7.05 (m, 8H, G), 4.85 (q, *J* = 7.2 Hz, 8H, O), 4.22 (t, *J* = 4.9 Hz, 4H, H), 4.16 (t, *J* = 6.1 Hz, 4H, K), 3.92 (d, J = 4.8 Hz, 4H, I), 3.81 – 3.76-3.65 (bs, 176H, J), 2.47 (m, 4H, M), 2.10 – 2.04 (m, 4H, L), 2.02 (t, *J* = 2.6 Hz, 2H, N), 1.43 (t, *J* = 7.2 Hz, 12H, P). MALDI-MS: 2519.8, 2563.9, 2607.9, 2651.9, 2696.0, 2740.1, 2784.1, 2828.1, 2872.2, 2916.3, 2960.5, 3004.4, 3048.5, 3092.7, 3136.8, 3180.7, 3224.6, 3268.8, 3312.8, 3356.9, 3400.6, 3444.9, 3488.9 ([M]+H^+).

6.7.6 Assembly of 6.1:3.1:Fe(II)$_2$

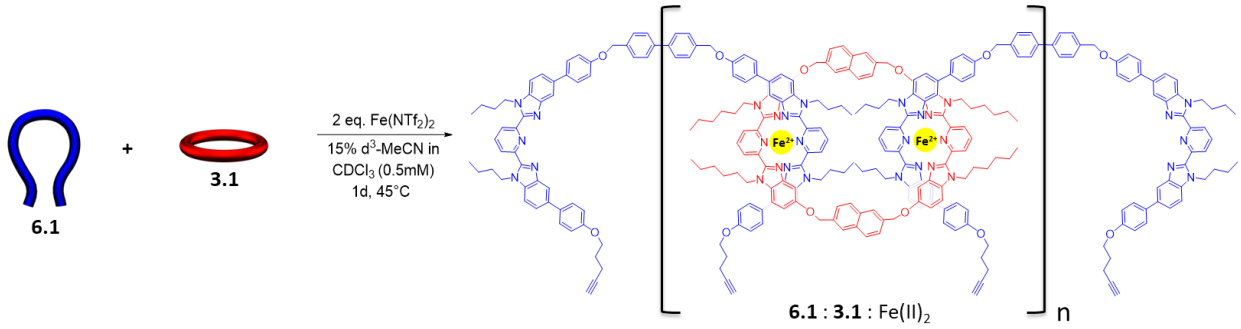

Dissolved 5.2mg of **3.1** in 1mL $CDCl_3$**.** Titrated thread stock solution (30mM) of **6.1** into solution of **3.1** until an exact 1:1 (**6.1**:**3.1**) ratio was formed (done by monitoring both the N-CH_2 peaks on the alkyl groups of the bip ligands). The mixture was then diluted to a total volume to 3.5mL $CDCl_3$ (1 mM **3.1**). A stock solution of $Fe(NTF_2)_2$ (30mM in 1:1 $CDCl_3$:d_3-MeCN) was added until no free Bip peak appeared at ~2 equiv. of metal ion. The solvent was removed under vacuum resulting in a dark purple solid that was redissolved in 7mL dry 15% MeCN in $CHCl_3$, bubbled with argon for 2 min, and allowed to stir under Ar at 45°C for 1 day to allow equilibration. Solvent was then removed under vacuum and ^{1}H-NMR was recorded using 15% d_3-MeCN in $CDCl_3$.

6.7.7 Assembly of 6.1:5.3:Fe(II)$_2$

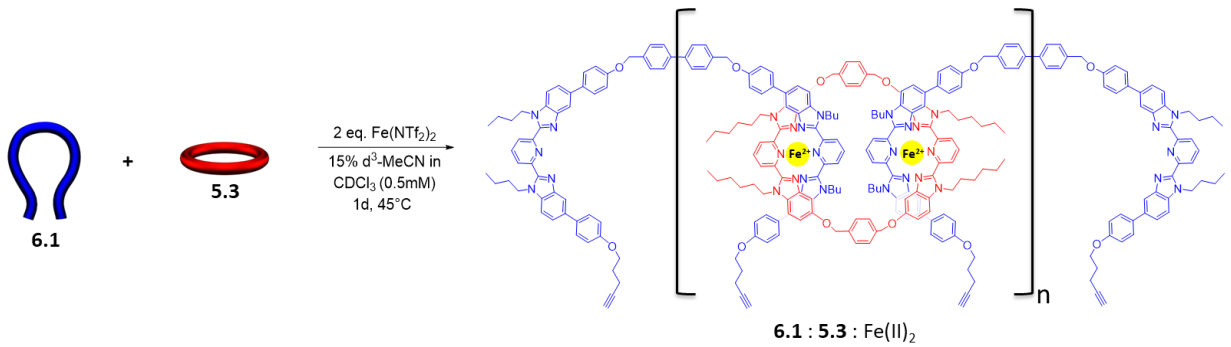

Dissolved 5.4mg of **5.3** in 1mL $CDCl_3$**.** Titrated thread stock solution (30mM) of **6.1** into solution of **5.3** until an exact 1:1 (**6.1**:**5.3**) ratio was formed (done by monitoring both the N-CH_2 peaks on the alkyl groups of the bip ligands). The mixture was then diluted to a total volume to 3.5mL

$CDCl_3$ (1 mM **5.3**). A stock solution of $Fe(NTF_2)_2$ (30mM in 1:1 $CDCl_3$:d_3-MeCN) was added until no free Bip peak appeared at ~2 equiv. of metal ion. The solvent was removed under vacuum resulting in a dark purple solid that was redissolved in 7mL dry 15% MeCN in $CHCl_3$, bubbled with argon for 2 min, and allowed to stir under Ar at 45°C for 1 day to allow equilibration. Solvent was then removed under vacuum and ^{1}H-NMR was recorded using 15% d_3-MeCN in $CDCl_3$.

6.7.8 Assembly of 6.4:3.1:Fe(II)$_2$

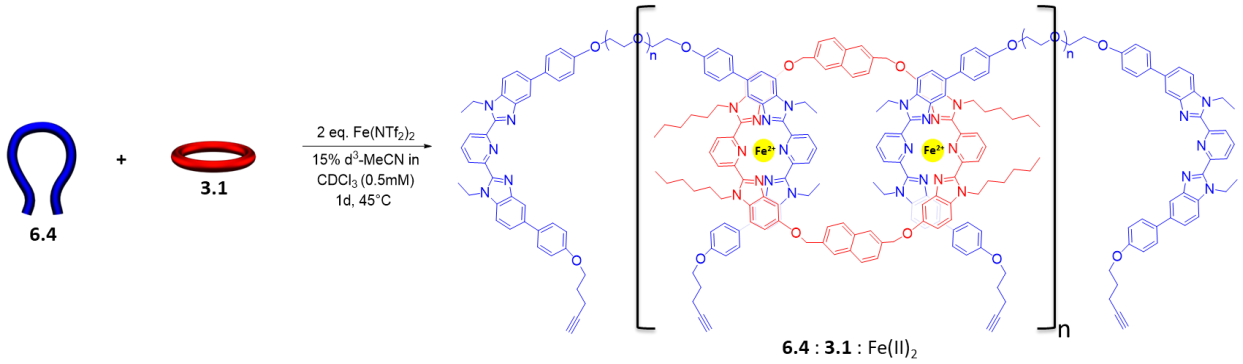

Dissolved 5.1mg of **3.1** in 1mL $CDCl_3$**.** Titrated thread stock solution (30mM) of **6.4** into solution of **3.1** until an exact 1:1 (**6.4**:**3.1**) ratio was formed (done by monitoring both the N-CH_2 peaks on the alkyl groups of the bip ligands). The mixture was then diluted to a total volume to 3.5mL $CDCl_3$ (1 mM **3.1**). A stock solution of $Fe(NTF_2)_2$ (30mM in 1:1 $CDCl_3$:d_3-MeCN) was added until no free Bip peak appeared at ~2 equiv. of metal ion. The solvent was removed under vacuum resulting in a dark purple solid that was redissolved in 7mL dry 15% MeCN in $CHCl_3$, bubbled with argon for 2 min, and allowed to stir under Ar at 45°C for 1 day to allow equilibration. Solvent was then removed under vacuum and ^{1}H-NMR was recorded using 15% d_3-MeCN in $CDCl_3$.

6.7.9 Synthesis of Dumbbell 6.6

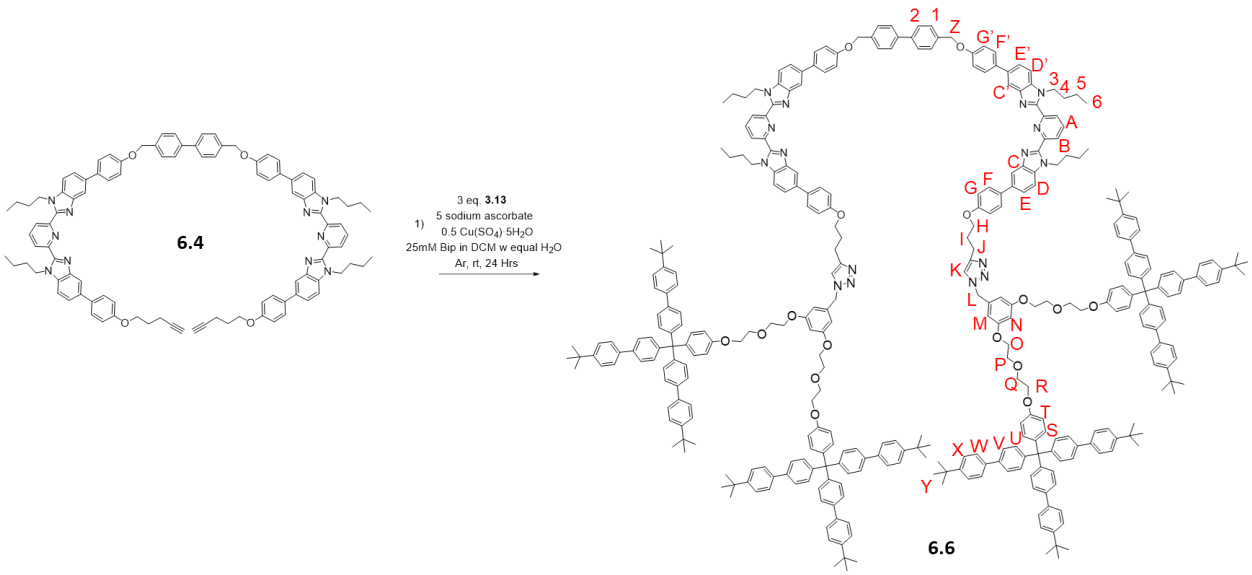

3.13 (39.7mg, 0.033mmol), **6.4** (16.3mg, 0.011 mmol) and sodium ascorbate (10.4mg, 0.055mmol) were added to a 4mL glass vial purged with Ar. To this mixture was added CH_2Cl_2 (0.43 mL, conc of **6.4** = 25 mM), H_2O (0.33 mL), and 100µL of an aqueous stock solution of $Cu(SO_4)\cdot 5H_2O$ (55 mM, 0.0055mmol, 0.5eq, (25mol% per alkyne)). The reaction was stirred vigorously for 18 h at RT. After this time the reaction mixture was diluted with CH_2Cl_2 and H_2O (10 mL each). The organic layer was taken and washed with H_2O (2 × 5 mL). Removal of organic solvent resulted in a light brown crude solid, which was purified using preparative thin layer chromatography (SiO_2, eluent = 95:5 $CHCl_3$:MeOH) followed by recrystallization (chloroform/methanol layering) resulting in a white solid, **6.6** in 85% yield. ^{1}H NMR (500 MHz, $CDCl_3$) δ 8.34 (d, *J* = 7.9Hz, 4H, B), 8.07–7.99 (m, 6H, A+C+C'), 7.69 – 7.62 (m, 8H, 2+1), 7.58-7.45 (m, 66H, D+D'+E+E'+F+F'+V+X), 7.43 (d, *J* = 8.4Hz, 24H, U), 7.30 (d, *J* = 8.5Hz, 24H, W), 7.19 (m, 10H, T+K), 7.13 (d, *J* = 8.7Hz, 4H, G), 6.96 (d, *J* = 8.7Hz, 4H, G'), 6.82 (d, *J* = 8.9Hz, 8H, S), 6.48 (s, 2H, N), 6.40 (d, *J* = 2.0Hz, 4H, M), 5.35 (s, 4H, Z), 5.19 (s, 4H, L), 4.78–4.71 (bq, 8H, 3), 4.13-4.07 (m, 16H, O+R), 4.03 (t, *J* = 6.2Hz, 4H, H), 3.91-3.85 (m, 16H, P+Q),

2.90 (t, *J* = 7.4Hz, 4H, J), 2.17 (t, *J* = 7.3Hz, 4H, I), 1.73 (m, 8H, 4), 1.34 (s, 108H, Y), 1.16–1.09 (m, 8H, 5), 0.72 (t, *J* = 7.2Hz, 12H, 6). MALDI-MS: 5069.9 ([M]+H^+).

6.7.10 Synthesis of Poly[3]rotaxane 6.7

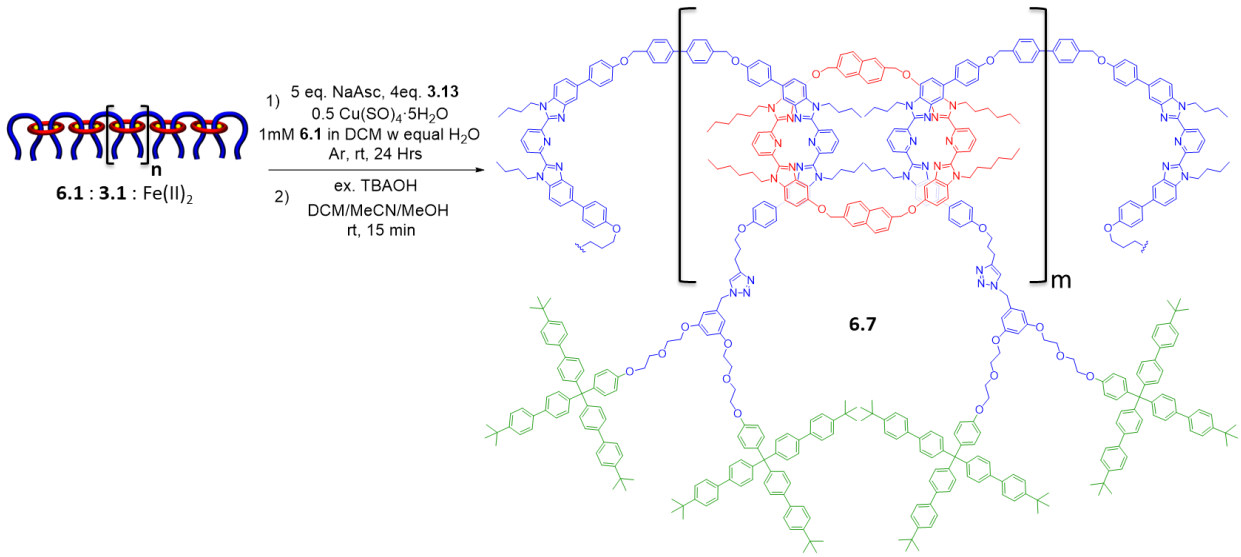

6.1:3.1:Fe(II)$_2$ (6.0mg, 0.0014mmol), **3.13** (10.4mg, 0.0056mmol) and sodium ascorbate (1.4mg, 0.007mmol) were added to a 4mL glass vial purged with Ar. To this mixture was added CH_2Cl_2 (1.25mL, conc of **6.1** = 1 mM), H_2O (1.15mL), and 100µL of an aqueous stock solution of $Cu(SO_4)\cdot 5H_2O$ (7mM, 0.0007mmol, 0.5eq, (25mol% per alkyne)). The reaction was stirred vigorously for 18 h at RT. The reaction mixture was then diluted with CH_2Cl_2 and H_2O (5 mL each). The organic layer was collected and washed with H_2O (2 × 5 mL). The crude purple solid was redissolved in 4mL of 50:50 dichloromethane and acetonitrile and stirred slowly at room temperature. 1mL of tetrabutylammonium hydroxide solution (1M in MeOH) was added dropwise to the stirring solution resulting in a rapid color change from purple to light brown and precipitation of demetallated product. After 15 minutes of stirring, an off-white solid was filtered off and washed with methanol (2x 10mL). The frit was then washed with 5mL of $CHCl_3$ to redissolve the demetallated product and washed once with 5mL water. Solvent was removed under reduced

pressure resulting in an off-white residue that was passed through a silica plug ($CHCl_3$ to 5% MeOH in $CHCl_3$ as eluent) resulting in an off-white solid that was not further purified.

6.7.11 Synthesis of Poly[3]rotaxane 6.8

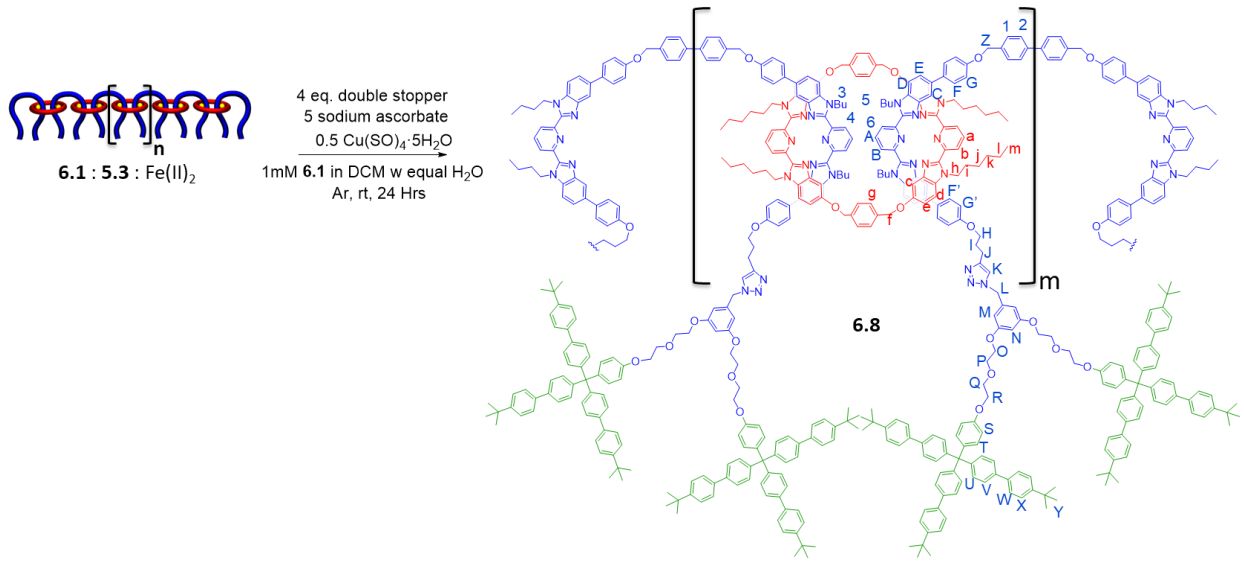

6.1:5.3:$Fe(II)_2$ (5.4mg, 0.0013mmol), **3.13** (9.5mg, 0.0052mmol) and sodium ascorbate (1.3mg, 0.0065mmol) were added to a 4mL glass vial purged with Ar. To this mixture was added CH_2Cl_2 (1.25mL, conc of **6.1** = 1 mM), H_2O (1.15mL), and 100µL of an aqueous stock solution of $Cu(SO_4)\cdot 5H_2O$ (6.5mM, 0.00065mmol, 0.5eq, (25mol% per alkyne)). The reaction was stirred vigorously for 18 h at RT. The reaction mixture was then diluted with CH_2Cl_2 and H_2O (5 mL each). The organic layer was collected and washed with H_2O (2 × 5 mL). The crude purple solid was redissolved in 4mL of 50:50 dichloromethane and acetonitrile and stirred slowly at room temperature. 1mL of tetrabutylammonium hydroxide solution (1M in MeOH) was added dropwise to the stirring solution resulting in a rapid color change from purple to light brown and precipitation of demetallated product. After 15 minutes of stirring, an off-white solid was filtered off and washed with methanol (2x 10mL). The frit was then washed with 5mL of $CHCl_3$ to redissolve the demetallated product and washed once with 5mL water. Solvent was removed under reduced

pressure resulting in an off-white residue. Purification of **6.8** was achieved using preparative thin layer chromatography (SiO_2, eluent = 94:6 $CHCl_3$:MeOH, lowest Rf band taken (R_f=0.15-0.35) as [3]R product, macrocycle byproduct R_f=0.4, dumbbell byproduct R_f=0.70-0.80) followed by precipitation from cold methanol to result in an off-white solid, **6.8** in 55% isolated yield. ^{1}H NMR (500 MHz, $CDCl_3$) δ 8.37-8.32 (bm, 4H, B), 8.06-7.90 (bm, 10H, A+C+b), 7.58-7.34 (bm, 98H, V+X+U+2+1+F+F'+D+D'+E+E'+a), 7.29 (bd, *J* = 6.5Hz, 24H, W), 7.20-7.11 (bm, 14H, T+K+G), 7.05 (s, 8H, g), 6.98 (s, 4H, c), 6.90 (bd, *J* = 4.5Hz, 4H, G'), 6.87–6.67 (m, 16H, S+d+e), 6.48 (bs, 2H, N), 6.40 (bs, 4H, M), 5.25–5.09 (m, 8H, Z+L), 4.80-4.68 (bt, 8H, 3), 4.68-4.66 (bs, 8H, f), 4.16-3.99 (bm, 24H, R+O+h), 3.92-3.80 (bm, 20H, P+Q+H), 2.77 (bm, 4H, J), 2.07 (bm, 4H, I), 1.58 (bm, 8H, 4), 1.46-1.29 (bm, 112H, Y+i), 0.92–0.86 (bm, 8H, 5), 0.78–0.65 (bm, 24H, j+k+l), 0.58-0.50 (bm, 24H, m+6).

6.7.12 Synthesis of Poly[3]rotaxane 6.9

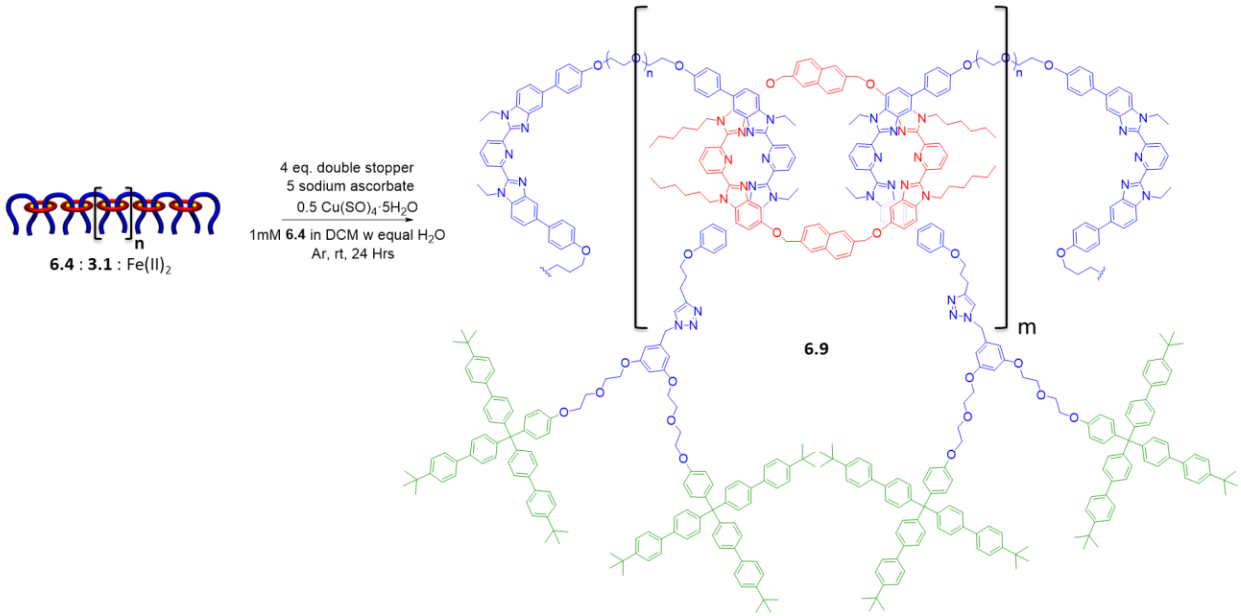

6.4:3.1:Fe(II)$_2$ (8.2mg, 0.0015mmol), **3.13** (10.6mg, 0.0060mmol) and sodium ascorbate (1.5mg, 0.0075mmol) were added to a 4mL glass vial purged with Ar. To this mixture was added CH_2Cl_2 (1.25mL, conc of **6.4** = 1 mM), H_2O (1.15mL), and 100μL of an aqueous stock solution of

$Cu(SO_4)\cdot 5H_2O$ (7.5mM, 0.00075mmol, 0.5eq, (25mol% per alkyne)). The reaction was stirred vigorously for 18 h at RT. The reaction mixture was then diluted with CH_2Cl_2 and H_2O (5 mL each). The organic layer was collected and washed with H_2O (2 × 5 mL). The crude purple solid was redissolved in 4mL of 50:50 dichloromethane and acetonitrile and stirred slowly at room temperature. 1mL of tetrabutylammonium hydroxide solution (1M in MeOH) was added dropwise to the stirring solution resulting in a rapid color change from purple to light brown and precipitation of demetallated product. After 15 minutes of stirring, an off-white solid was filtered off and washed with methanol (2x 10mL). The frit was then washed with 5mL of $CHCl_3$ to redissolve the demetallated product and washed once with 5mL water. Solvent was removed under reduced pressure resulting in an off-white residue that was passed through a silica plug (2% MeOH in $CHCl_3$ as eluent) followed by three precipitations from cold methanol resulting in an off-white solid that was not further purified.

6.8 References

(1) Hart, L. F.; Hertzog, J. E.; Rauscher, P. M.; Rawe, B. W.; Tranquilli, M. M.; Rowan, S. J. Material Properties and Applications of Mechanically Interlocked Polymers. *Nat. Rev. Mater.* **2021**, *6*, 508–530. https://doi.org/10.1038/s41578-021-00278-z.

(2) Mena-Hernando, S.; Pérez, E. M. Mechanically Interlocked Materials. Rotaxanes and Catenanes beyond the Small Molecule. *Chem. Soc. Rev.* **2019**, *48* (19), 5016–5032. https://doi.org/10.1039/c8cs00888d.

(3) Arunachalam, M.; Gibson, H. W. Recent Developments in Polypseudorotaxanes and Polyrotaxanes. *Prog. Polym. Sci.* **2014**, *39* (6), 1043–1073. https://doi.org/10.1016/j.progpolymsci.2013.11.005.

(4) Huang, F. H.; Gibson, H. W. Polypseudorotaxanes and Polyrotaxanes. *Prog. Polym. Sci.* **2005**, *30* (10), 982–1018. https://doi.org/10.1016/j.progpolymsci.2005.07.003.

(5) Akai, T.; Shimomura, T.; Ito, K. HCl-Doping of Insulated Molecular Wire Formed by Emeraldine Base Polyaniline and Molecular Nanotube. *Synth. Met.* **2003**, *135–136*, 777–778. https://doi.org/10.1016/S0379-6779(02)00852-4.

(6) Farcas, A.; Aubert, P. H.; Mohanty, J.; Lazar, A. I.; Cantin, S.; Nau, W. M. Molecular Wire Formation from Poly[2,7-(9,9-Dioctylfluorene)-Alt-(5,5′-

Bithiophene/Cucurbit[7]Uril)] Polyrotaxane Copolymer. *Eur. Polym. J.* **2015**, *62*, 124–129. https://doi.org/10.1016/j.eurpolymj.2014.11.021.

(7) Ooya, T.; Yamashita, A.; Kurisawa, M.; Sugaya, Y.; Maruyama, A.; Yui, N. Effects of Polyrotaxane Structure on Polyion Complexation with DNA. *Sci. Technol. Adv. Mater.* **2004**, *5* (3), 363–369. https://doi.org/10.1016/j.stam.2003.12.014.

(8) Uchida, W.; Yoshikawa, M.; Seki, T.; Miki, R.; Seki, T.; Fujihara, T.; Ishimaru, Y.; Egawa, Y. A Polyrotaxane Gel Using Boronic Acid-Appended γ-Cyclodextrin as a Hybrid Cross-Linker. *J. Incl. Phenom. Macrocycl. Chem.* **2017**, *89* (3–4), 281–288. https://doi.org/10.1007/s10847-017-0755-z.

(9) Kato, K.; Nemoto, K.; Mayumi, K.; Yokoyama, H.; Ito, K. Ductile Glass of Polyrotaxane Toughened by Stretch-Induced Intramolecular Phase Separation. *ACS Appl. Mater. Interfaces* **2017**, *9* (38), 32436–32440. https://doi.org/10.1021/acsami.7b10845.

(10) Kato, K.; Ohara, A.; Yokoyama, H.; Ito, K. Prolonged Glass Transition Due to Topological Constraints in Polyrotaxanes. *J. Am. Chem. Soc.* **2019**, *141* (32), 12502–12506. https://doi.org/10.1021/jacs.9b06063.

(11) Mammen, M.; Choi, S.-K.; Whitesides, G. M. Polyvalent Interactions in Biological Systems: Implications for Design and Use of Multivalent Ligands and Inhibitors. *Angew. Chem. Int.* **1998**, *37* (20), 2754–2794. https://doi.org/10.1002/chin.199909293.

(12) Ooya, T.; Yui, N. Multivalent Interactions between Biotin-Polyrotaxane Conjugates and Streptavidin as a Model of New Targeting for Transporters. *J. Control. Release* **2002**, *80* (1–3), 219–228. https://doi.org/10.1016/S0168-3659(02)00030-5.

(13) Stoddart, J. F. Mechanically Interlocked Molecules (MIMs)-Molecular Shuttles, Switches, and Machines (Nobel Lecture). *Angew. Chemie Int. Ed.* **2017**, *56* (37), 11094–11125. https://doi.org/10.1002/anie.201703216.

(14) Browne, W. R.; Feringa, B. L. Making Molecular Machines Work. *Nat. Nanotechnol.* **2006**, *1* (1), 25–35. https://doi.org/10.1038/nnano.2006.45.

(15) Choi, S.; Kwon, T.; Coskun, A.; Choi, J. W. Highly Elastic Binders Integrating Polyrotaxanes for Silicon Microparticle Anodes in Lithium Ion Batteries. *Science (80-.).* **2017**, *357* (6348), 279–283. https://doi.org/10.1126/science.aal4373.

(16) Zhou, H. Y.; Zong, Q. S.; Han, Y.; Chen, C. F. Recent Advances in Higher Order Rotaxane Architectures. *Chem. Commun.* **2020**, *56* (69), 9916–9936. https://doi.org/10.1039/d0cc03057k.

(17) Beves, J. E.; Blight, B. A.; Campbell, C. J.; Leigh, D. A.; McBurney, R. T. Strategies and Tactics for the Metal-Directed Synthesis of Rotaxanes, Knots, Catenanes, and Higher Order Links. *Angew. Chemie - Int. Ed.* **2011**, *50* (40), 9260–9327. https://doi.org/10.1002/anie.201007963.

(18) Zhou, H. Y.; Han, Y.; Chen, C. F. PH-Controlled Motions in Mechanically Interlocked Molecules. *Mater. Chem. Front.* **2020**, *4* (1), 12–28. https://doi.org/10.1039/c9qm00546c.

(19) Fan, M. M.; Yu, Z. J.; Luo, H. Y.; Zhang, S.; Li, B. J. Supramolecular Network Based on

the Self-Assembly of y-Cyclodextrin with Poly(Ethylene Glycol) and Its Shape Memory Effect. *Macromol. Rapid Commun.* **2009**, *30* (11), 897–903. https://doi.org/10.1002/marc.200800712.

(20) Iijima, K.; Aoki, D.; Otsuka, H.; Takata, T. Synthesis of Rotaxane Cross-Linked Polymers with Supramolecular Cross-Linkers Based on γ-CD and PTHF Macromonomers: The Effect of the Macromonomer Structure on the Polymer Properties. *Polymer (Guildf).* **2017**, *128*, 392–396. https://doi.org/10.1016/j.polymer.2017.01.024.

(21) Yamamoto, K.; Nameki, R.; Sogawa, H.; Takata, T. Macrocyclic Dinuclear Palladium Complex as a Novel Doubly Threaded [3]Rotaxane Scaffold and Its Application as a Rotaxane Cross-Linker. *Angew. Chemie - Int. Ed.* **2020**, *59* (41), 18023–18028. https://doi.org/10.1002/anie.202007866.

(22) Aramoto, H.; Osaki, M.; Konishi, S.; Ueda, C.; Kobayashi, Y.; Takashima, Y.; Harada, A.; Yamaguchi, H. Redox-Responsive Supramolecular Polymeric Networks Having Double-Threaded Inclusion Complexes. *Chem. Sci.* **2020**, *11* (17), 4322–4331. https://doi.org/10.1039/c9sc05589d.

(23) Burnworth, M.; Tang, L.; Kumpfer, J. R.; Duncan, A. J.; Beyer, F. L.; Fiore, G. L.; Rowan, S. J.; Weder, C. Optically Healable Supramolecular Polymers. *Nature* **2011**, *472* (7343), 334–337. https://doi.org/10.1038/nature09963.

(24) Beck, J. B.; Ineman, J. M.; Rowan, S. J. Metal / Ligand-Induced Formation of Metallo-Supramolecular Polymers. **2005**, 5060–5068.

(25) Rowan, S. J.; Beck, J. B. Metal-Ligand Induced Supramolecular Polymerization: A Route to Responsive Materials. *Faraday Discuss.* **2005**, *128*, 43–53. https://doi.org/10.1039/b403135k.

(26) Kanehara, M.; Kodzuka, E.; Teranishi, T. Self-Assembly of Small Gold Nanoparticles through Interligand Interaction. *J. Am. Chem. Soc.* **2006**, *128* (40), 13084–13094. https://doi.org/10.1021/ja064510q.

(27) Yu, S. C.; Hou, S.; Chan, W. K. Synthesis, Metal Complex Formation, and Electronic Properties of a Novel Conjugate Polymer with a Tridentate 2,6-Bis(Benzimidazol-2-Yl)Pyridine Ligand. *Macromolecules* **1999**, *32* (16), 5251–5256. https://doi.org/10.1021/ma990056h.

(28) Michal, B. T.; McKenzie, B. M.; Felder, S. E.; Rowan, S. J. Metallo-, Thermo-, and Photoresponsive Shape Memory and Actuating Liquid Crystalline Elastomers. *Macromolecules* **2015**, *48* (10), 3239–3246. https://doi.org/10.1021/acs.macromol.5b00646.

(29) Wu, Q.; Rauscher, P. M.; Lang, X. L.; Wojtecki, R. J.; de Pablo, J. J.; Hore, M. J. A.; Rowan, S. J. Poly[n]Catenanes: Synthesis of Molecular Interlocked Chains. *Science (80-.).* **2017**, *358* (6369), 1434–1439. https://doi.org/10.1126/science.aap7675.

(30) Tranquilli, M. M.; Wu, Q.; Rowan, S. J. Effect of Metallosupramolecular Polymer Concentration on the Synthesis of Poly[n]Catenanes . *Chem. Sci.* **2021**. https://doi.org/10.1039/d1sc02450g.

(31) McKenzie, B. M.; Miller, A. K.; Wojtecki, R. J.; Johnson, J. C.; Burke, K. A.; Tzeng, K. A.; Mather, P. T.; Rowan, S. J. Improved Synthesis of Functionalized Mesogenic 2,6-Bisbenzimidazolylpyridine Ligands. *Tetrahedron* **2008**, *64* (36), 8488–8495. https://doi.org/10.1016/j.tet.2008.05.075.

(32) Harris, J. M.; Struck, E. C.; Case, M. G.; Paley, S. M.; Yalpani, M.; Van Alstine, J. M.; Brooks, D. E. Synthesis and Characterization of Poly(Ethylene Glycol) Derivatives. *J. Polym. Sci. Part A Polym. Chem.* **1984**, *22*, 341–352.

(33) Nielen, M. W. F. Maldi Time-of-Flight Mass Spectrometry of Synthetic Polymers. *Mass Spectrom. Rev.* **1999**, *18* (5), 309–344. https://doi.org/10.1002/(SICI)1098-2787(1999)18:5<309::AID-MAS2>3.0.CO;2-L.

(34) Kramer, R.; Lehn, J.; Bel, I. Le; Pasteur, U. L.; Marquis-rigault, A. Self-Recognition in Helicate Self-Assembly: Spontaneous Formation of Helical Metal Complexes from Mixtures of Ligands and Metal Ions. *Proc. Natl. Acad. Sci.* **1993**, *90* (June), 5394–5398.

(35) Meldal, M.; Tomøe, C. W. Cu-Catalyzed Azide - Alkyne Cycloaddition. *Chem. Rev.* **2008**, *108* (8), 2952–3015. https://doi.org/10.1021/cr0783479.

(36) Hänni, K. D.; Leigh, D. A. The Application of CuAAC 'Click' Chemistry to Catenane and Rotaxane Synthesis. *Chem. Soc. Rev.* **2010**, *39* (4), 1240–1251. https://doi.org/10.1039/b901974j.

(37) Wyatt, P. J. Light Scattering and the Absolute Characterization of Macromolecules. *Anal. Chim. Acta* **1993**, *272* (1), 1–40. https://doi.org/10.1016/0003-2670(93)80373-S.

(38) Huglin, M. B. Specific Refractive Index Increments of Polymer Solutions. Part I. Literature Values. *J. Appl. Polym. Sci.* **1965**, *9* (12), 3963–4001. https://doi.org/10.1002/app.1965.070091219.

(39) Hertzog, J. E.; Maddi, V. J.; Hart, L. F.; Rawe, B. W.; Rauscher, P. M.; Herbert, K. M.; Bruckner, E. P.; de Pablo, J. J.; Rowan, S. J. Metastable Doubly Threaded [3]Rotaxanes with a Large Macrocycle. *Chem. Sci.* **2022**, 5333–5344. https://doi.org/10.1039/d2sc01486f.

(40) Sibi, M. P.; Petrovic, G. Enantioselective Radical Reactions: The Use of Metal Triflimides as Lewis Acids. *Tetrahedron Asymmetry* **2003**, *14* (19), 2879–2882. https://doi.org/10.1016/S0957-4166(03)00543-3.

(41) Wu, Q.; Rauscher, P. M.; Lang, X.; Wojtecki, R. J.; De Pablo, J. J.; Hore, M. J. A.; Rowan, S. J. Poly[n]Catenanes: Synthesis of Molecular Interlocked Chains. *Science (80-.).* **2017**, *358* (6369), 1434–1439. https://doi.org/10.1126/science.aap7675.